frontiers | Research Topics

Community series in trends in neuroimmunology: cross-talk between brain-resident and peripheral immune cells in both health and disease, volume II

Edited by
Estela Maris Muñoz, Rajnikant Mishra, Veronica Martinez Cerdeño and Shashank Kumar Maurya

Coordinated by
Janina Edith Borgonovo, Suryanarayan Biswal and Carlos Leandro Freites

Published in
Frontiers in Immunology

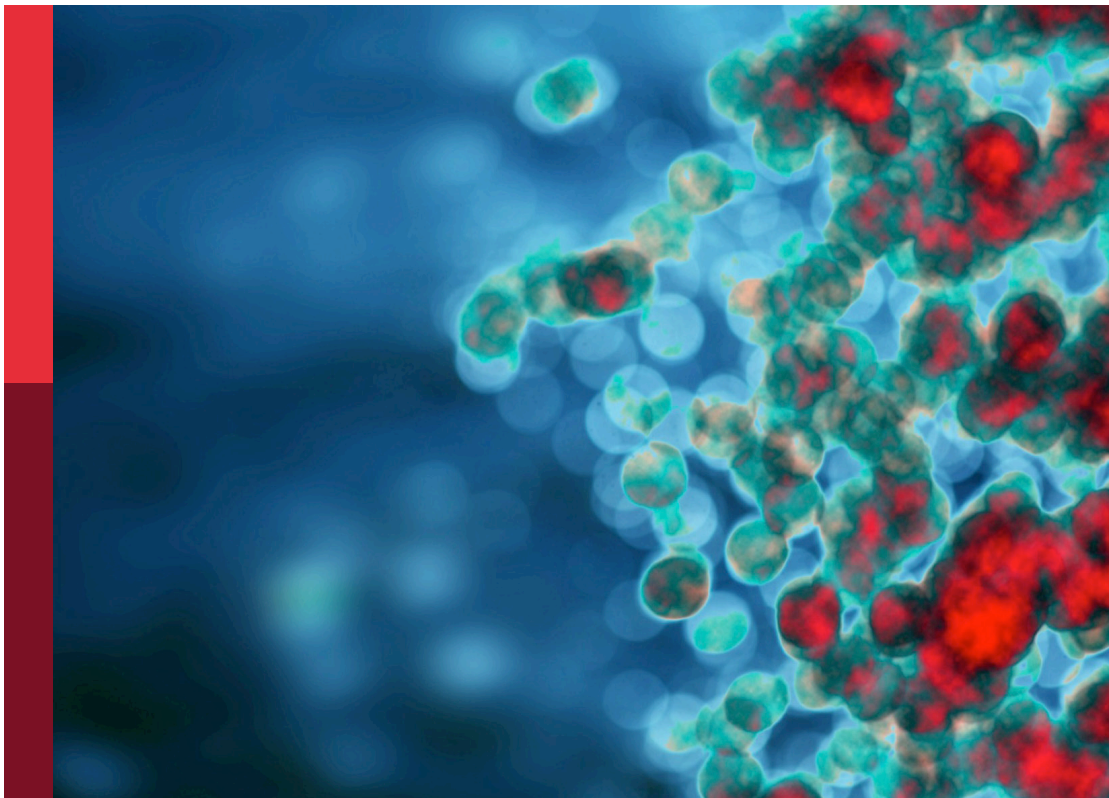

ISSN 1664-8714
ISBN 978-2-8325-6622-0
DOI 10.3389/978-2-8325-6622-0

Generative AI statement
Any alternative text (Alt text) provided alongside figures in the articles in this ebook has been generated by Frontiers with the support of artificial intelligence and reasonable efforts have been made to ensure accuracy, including review by the authors wherever possible. If you identify any issues, please contact us.

About Frontiers

Frontiers is more than just an open access publisher of scholarly articles: it is a pioneering approach to the world of academia, radically improving the way scholarly research is managed. The grand vision of Frontiers is a world where all people have an equal opportunity to seek, share and generate knowledge. Frontiers provides immediate and permanent online open access to all its publications, but this alone is not enough to realize our grand goals.

Frontiers journal series

The Frontiers journal series is a multi-tier and interdisciplinary set of open-access, online journals, promising a paradigm shift from the current review, selection and dissemination processes in academic publishing. All Frontiers journals are driven by researchers for researchers; therefore, they constitute a service to the scholarly community. At the same time, the *Frontiers journal series* operates on a revolutionary invention, the tiered publishing system, initially addressing specific communities of scholars, and gradually climbing up to broader public understanding, thus serving the interests of the lay society, too.

Dedication to quality

Each Frontiers article is a landmark of the highest quality, thanks to genuinely collaborative interactions between authors and review editors, who include some of the world's best academicians. Research must be certified by peers before entering a stream of knowledge that may eventually reach the public - and shape society; therefore, Frontiers only applies the most rigorous and unbiased reviews. Frontiers revolutionizes research publishing by freely delivering the most outstanding research, evaluated with no bias from both the academic and social point of view. By applying the most advanced information technologies, Frontiers is catapulting scholarly publishing into a new generation.

What are Frontiers Research Topics?

Frontiers Research Topics are very popular trademarks of the *Frontiers journals series*: they are collections of at least ten articles, all centered on a particular subject. With their unique mix of varied contributions from Original Research to Review Articles, Frontiers Research Topics unify the most influential researchers, the latest key findings and historical advances in a hot research area.

Find out more on how to host your own Frontiers Research Topic or contribute to one as an author by contacting the Frontiers editorial office: frontiersin.org/about/contact

Community series in trends in neuroimmunology: cross-talk between brain-resident and peripheral immune cells in both health and disease, volume II

Topic editors

Estela Maris Muñoz — Institute of Histology and Embryology of Mendoza Dr. Mario H. Burgos (IHEM)-UNCuyo-CONICET, Argentina

Rajnikant Mishra — Banaras Hindu University, India

Veronica Martinez Cerdeño — University of California, Davis, United States

Shashank Kumar Maurya — University of Delhi, India

Topic coordinators

Janina Edith Borgonovo — University of Chile, Chile

Suryanarayan Biswal — Central University of Punjab, India

Carlos Leandro Freites — Autonomous University of Barcelona, Spain

Citation

Muñoz, E. M., Mishra, R., Martinez Cerdeño, V., Maurya, S. K., Borgonovo, J. E., Biswal, S., Freites, C. L., eds. (2025). *Community series in trends in neuroimmunology: cross-talk between brain-resident and peripheral immune cells in both health and disease, volume II*. Lausanne: Frontiers Media SA.

doi: 10.3389/978-2-8325-6622-0

Table of contents

05 Editorial: Community series in trends in neuroimmunology: cross-talk between brain-resident and peripheral immune cells in both health and disease, volume II
Suryanarayan Biswal, Janina E. Borgonovo, Carlos L. Freites, Verónica Martínez-Cerdeño, Rajnikant Mishra, Shashank K. Maurya and Estela M. Muñoz

12 Interferon-gamma ameliorates experimental autoimmune encephalomyelitis by inducing homeostatic adaptation of microglia
Juan E. Tichauer, Gabriel Arellano, Eric Acuña, Luis F. González, Nirmal R. Kannaiyan, Paola Murgas, Concepción Panadero-Medianero, Jorge Ibañez-Vega, Paula I. Burgos, Eileah Loda, Stephen D. Miller, Moritz J. Rossner, Peter J. Gebicke-Haerter and Rodrigo Naves

34 Sustained effects on immune cell subsets and autoreactivity in multiple sclerosis patients treated with oral cladribine
Rikke Holm Hansen, Marina Rode von Essen, Mie Reith Mahler, Stefan Cobanovic and Finn Sellebjerg

47 Emergence of the brain-border immune niches and their contribution to the development of neurodegenerative diseases
Li Yang Tan, Grace Cunliffe, Michael Patrick Hogan, Xin Yi Yeo, Chansik Oh, Bohwan Jin, Junmo Kang, Junho Park, Min-Soo Kwon, MinYoung Kim and Sangyong Jung

67 Single-cell profiling indicates a high similarity between immune cells in the cerebrospinal fluid and in meningeal ectopic lymphoid tissue in experimental autoimmune encephalomyelitis
Tanya Georgieva, Jolien Diddens, Verena Friedrich, Gildas Lepennetier, Rosa Margareta Brand and Klaus Lehmann-Horn

81 Dysregulated C1q and CD47 in the aging monkey brain: association with myelin damage, microglia reactivity, and cognitive decline
Sarah A. DeVries, Christina Dimovasili, Maria Medalla, Tara L. Moore and Douglas L. Rosene

95 Stimulation of microneedles alleviates pathology of Parkinson's disease in mice by regulating the CD4+/CD8+ cells from the periphery to the brain
Jin Hee Kim, Yujin Choi, Jin Se Kim, Hanbyeol Lee, In Gyoung Ju, Na Young Yoo, Sookie La, Do Hyeon Jeong, Changsu Na, Hi-Joon Park and Myung Sook Oh

108 Extracorporeal photopheresis in stiff person syndrome
Yandy Marx Castillo-Aleman and Pierre Christophe Krystkowiak

115 Tregs levels and phenotype modifications during Amyotrophic Lateral Sclerosis course
Elisabetta Zucchi, Federico Banchelli, Cecilia Simonini, Sara De Biasi, Ilaria Martinelli, Giulia Gianferrari, Domenico Lo Tartaro, Andrea Cossarizza, Roberto D'Amico and Jessica Mandrioli on behalf of RAPALS study group

129 Blood immunophenotyping of multiple sclerosis patients at diagnosis identifies a classical monocyte subset associated to disease evolution
Stéphane Rodriguez, Laura Couloume, Juliette Ferrant, Nicolas Vince, Marion Mandon, Rachel Jean, Celine Monvoisin, Simon Leonard, Simon Le Gallou, Nayane S. B. Silva, Sonia Bourguiba-Hachemi, David Laplaud, Alexandra Garcia, Romain Casey, Helene Zephir, Anne Kerbrat, Gilles Edan, Emmanuelle Lepage, Eric Thouvenot, Aurelie Ruet, Guillaume Mathey, Pierre-Antoine Gourraud, Karin Tarte, Celine Delaloy, Patricia Amé, Mikael Roussel and Laure Michel on behalf of OFSEP investigators

147 Immune conversations at the border: meningeal immunity in health and disease
Preya U. Patel, Aryan Regmi, Angelina I. Dass and Olga L. Rojas

frontiers | Frontiers in Immunology

TYPE Editorial
PUBLISHED 03 July 2025
DOI 10.3389/fimmu.2025.1644278

OPEN ACCESS

EDITED AND REVIEWED BY
Robert Weissert,
University of Regensburg, Germany

*CORRESPONDENCE
Suryanarayan Biswal
suryanarayan.biswal@cup.edu.in;
surya08bio@gmail.com
Shashank K. Maurya
smaurya1@zoology.du.ac.in;
maurya.shashankkumar@gmail.com
Estela M. Muñoz
munoz.estela@fcm.uncu.edu.ar;
emunoz@mendoza-conicet.gob.ar

†These authors have contributed equally to this work

RECEIVED 10 June 2025
ACCEPTED 18 June 2025
PUBLISHED 03 July 2025

CITATION
Biswal S, Borgonovo JE, Freites CL, Martínez-Cerdeño V, Mishra R, Maurya SK and Muñoz EM (2025) Editorial: Community series in trends in neuroimmunology: cross-talk between brain-resident and peripheral immune cells in both health and disease, volume II. *Front. Immunol.* 16:1644278. doi: 10.3389/fimmu.2025.1644278

Editorial: Community series in trends in neuroimmunology: cross-talk between brain-resident and peripheral immune cells in both health and disease, volume II

Suryanarayan Biswal[1*†], Janina E. Borgonovo[2†], Carlos L. Freites[3†], Verónica Martínez-Cerdeño[4], Rajnikant Mishra[5], Shashank K. Maurya[6*] and Estela M. Muñoz[7*]

[1]Department of Human Genetics and Molecular Medicine, Central University of Punjab, Bathinda, India, [2]Integrative Biology Program, Institute of Biomedical Sciences, Faculty of Medicine, University of Chile, Santiago, Chile, [3]Department of Cell Biology, Physiology and Immunology, Institute of Neurosciences (INc), Autonomous University of Barcelona (UAB), Bellaterra, Spain, [4]Department of Pathology and Laboratory Medicine, Institute for Pediatric Regenerative Medicine, Shriners Hospitals for Children of Northern California, and MIND Institute at the UC Davis Medical Center, University of California, Davis School of Medicine, Sacramento, CA, United States, [5]Biochemistry and Molecular Biology Laboratory, Department of Zoology, Institute of Science, Banaras Hindu University, Varanasi, India, [6]Biochemistry and Molecular Biology Laboratory, Department of Zoology, Faculty of Science, University of Delhi, Delhi, India, [7]Institute of Histology and Embryology of Mendoza (IHEM), National University of Cuyo (UNCuyo), National Scientific and Technical Research Council (CONICET), Mendoza, Argentina

KEYWORDS

neuroinflammation, neurodegeneration, microglia, t cells, b cells, immunoregulation, meninges

Editorial on the Research Topic

Community series in trends in neuroimmunology: cross-talk between brain-resident and peripheral immune cells in both health and disease, volume II

The intricate interplay between the central nervous system (CNS) and the immune system is increasingly recognized as fundamental to both neurological health and disease (1, 2). This second volume of the Community Series in Trends in Neuroimmunology continues to spotlight emerging insights into how brain-resident and peripheral immune cells communicate across anatomical and functional borders, shaping responses in both homeostatic and pathological contexts. Ten peer-reviewed manuscripts, including seven original articles, two reviews, and one opinion, encompass this special volume. Ninety-five authors from research laboratories located in twelve countries: Brazil, Canada, Chile, Denmark, France, Germany, Italy, United Arab Emirates, United Kingdom, United States, Republic of Korea, and Singapore, took part in this initiative. The featured articles collectively deepen our understanding of how immune surveillance, modulation, and dysfunction at CNS interfaces—such as the meninges, choroid plexus, and perivascular

spaces—contribute to neurodevelopmental, autoimmune, infectious, and degenerative processes. From the dynamic roles of meningeal immunity and ectopic lymphoid tissues in neuroinflammation, to the surprising effects of peripheral interventions like extracorporeal photopheresis (ECP) or microneedle stimulation in disorders such as stiff person syndrome (SPS) and Parkinson's disease (PD), respectively, this Research Topic emphasizes the permeability and responsiveness of the brain-immune interface. Novel mechanistic insights into immune cell plasticity, such as interferon-gamma (IFN-γ)–induced homeostatic microglia reprogramming and sustained immunomodulation by cladribine, highlight the therapeutic potential of immune-targeted strategies. Additionally, the exploration of aging-related myelin degradation and immune dysregulation offers promising new directions for understanding cognitive decline. Together, these contributions expand the conceptual framework of neuroimmunology and underscore the translational relevance of immune-CNS cross-talk. As research unravels the bidirectional communication between the brain and the immune system, targeting these interactions may redefine therapeutic landscapes for neurological diseases.

Among the featured contributions, Patel et al. provided a comprehensive review about meningeal immunity in health and disease. The meninges, consisting of three layers (dura mater, arachnoid mater, and pia mater), were once thought to serve primarily as a physical barrier for the CNS. However, recent research has revealed that the meninges play a crucial role in immune function and CNS homeostasis (3). The review discusses details of the anatomy of the meninges and their contribution to immune cell mobilization. It describes the various immune cell populations present in the meninges during steady-state conditions, including T cells, B cells, border-associated macrophages, dendritic cells, neutrophils, mast cells, innate lymphoid cells, and natural killer cells. Each of these cell types has specific functions in maintaining CNS health and responding to pathological conditions (4). The review also discusses the spatial organization of immune cells in the dura mater, particularly the recently discovered dural-associated lymphoid tissues (DALT) (5). The review then explores the role of meningeal immunity in various pathologies, including multiple sclerosis (MS), infections [such as ZIKV (Zika virus), human immunodeficiency virus (HIV), and Toxoplasma gondii], stroke, traumatic brain injury, and neurodegenerative contexts like those in Alzheimer's disease (AD) and PD. The authors highlighted how meningeal immune responses can contribute to pathology and provide protection in these conditions (6). One of the most intriguing insights from this review is the emerging understanding of the meninges as a dynamic immunological interface rather than a simple physical barrier. The discovery of meningeal lymphatic vessels and organized lymphoid structures within the meninges has challenged previous notions of CNS immune privilege (7). Additionally, the authors also highlighted the connections between meningeal immunity and cognitive function, with certain immune cells and cytokines influencing learning, memory, and social behavior. These suggest a complex interplay between the immune and nervous systems that goes beyond traditional concepts of neuroimmunology. The potential for targeting meningeal immune cells as a novel therapeutic approach for various neurological disorders opens new avenues for research and treatment strategies (8). Overall, the review emphasizes the complex and dynamic nature of meningeal immunity and its significance in both CNS health and disease, highlighting the need for further research to fully understand and potentially manipulate this system for therapeutic purposes.

Tan et al. reviewed the contribution of the brain-border immune niches to the pathogenesis of neurodegenerative disorders. Under non-homeostatic conditions, the immune cells of choroid plexus, meninges, and perivascular spaces can infiltrate the CNS, exacerbating neuroinflammation and neuronal death in pathologies such as AD, PD and MS (9–11). Similarly, cranial bone marrow (CBM) can be a source of lymphoid and myeloid cells for the brain during inflammatory events (12, 13). There is also evidence that obstruction of lymphatic flow delays the clearance of protein aggregates in proteinopathies (14–16). In this review, the authors provided an overview of the different brain-border immune niches, followed by a summary of current knowledge about how their immune cells play a role in the progression of diseases. A special section presented approaches and tools available for monitoring the immune niches such as functional and structural imaging techniques, as well as future research directions in this field (17, 18). Finally, Tan et al. provided a framework for thinking about strategies to target brain-border immune niches in neurological disorders with inflammatory scenarios.

Extracorporeal photopheresis (ECP) is proposed by Castillo-Aleman and Krystkowiak as a potential treatment for SPS, a rare neuroimmunological disorder characterized by progressive muscle rigidity and painful spasms (19). In their opinion article, the authors explained the etiopathophysiology of SPS, which involves autoantibodies targeting various antigens present in inhibitory synapses, particularly anti-GAD65 (glutamic acid decarboxylase) antibodies, and the participation of B cells and GAD65-specific T cells (20). These alter γ-aminobutyric acid (GABA) synthesis and release on synaptic neuronal junctions within the CNS, resulting in impaired neurotransmission and neuronal dysfunction. The authors outlined current therapies for SPS, including symptomatic treatments with diazepam or other benzodiazepines (GABA agonists), and immunotherapies such as corticosteroids, intravenous and subcutaneous immunoglobulins (IVIg and SCIg, respectively), and plasma exchange. They also discussed newer approaches like anti-B cell therapies, autologous anti-CD19 chimeric antigen receptor (CAR) T cells, and hematopoietic stem cell transplantation. However, these treatments have limitations, including heterogeneous clinical responses and potential adverse effects (21). The authors proposed ECP as a rational approach for treating SPS, particularly its classical form. They explained the mechanisms of ECP, which involves exposure of autologous leukocytes to a photosensitizing agent and ultraviolet-A irradiation before reinfusion. This process induces apoptosis in a cell type-dependent manner [T and B cells are more susceptible than monocytes and regulatory T (Treg) cells] and triggers a

cascade of immunomodulatory effects (22). Potential benefits of ECP in SPS include its ability to induce tolerance to GAD65-expressing neurons, restore inhibitory signals, and stabilize neuron membranes (23). A unique insight was given by the authors to the investigational use of ECP in SPS, despite the presence of the blood-brain barrier (BBB). They argued that although the BBB may diminish the effects of ECP, the trafficking of immune cells between the periphery and the CNS, and the systemic production of anti-GAD65 antibodies justify exploring ECP as a potential treatment. This perspective challenges the conventional view of the CNS as an immune-privileged site and suggests that peripheral immunomodulation could have significant effects on neurological autoimmune disorders like SPS (24). The authors also proposed a pilot clinical trial (OPTION study; NCT06703333) to evaluate the safety and efficacy of ECP in patients with classical SPS, demonstrating a concrete step towards translating this theoretical approach into clinical practice.

Anti-CD20 monoclonal antibodies (aCD20 mAbs) effectively deplete B cells and are widely used in treating certain forms of MS. Disease progression may persist, suggesting additional mechanisms beyond B cell-mediated pathology (25). The role of B cells in meningeal ectopic lymphoid tissue (mELT) and mELT formation and potential contribution to MS progression even in the absence of B cells, remain unclear (26). Georgieva et al. conducted an original study to compare gene expression profiles of immune cells from cerebrospinal fluid (CSF) and mELT in a spontaneous 2D2xTh EAE (experimental autoimmune encephalomyelitis) murine model of MS. The researchers also applied single-cell RNA sequencing to study the effects of aCD20 mAbs on these compartments. The study found that the immune cell compositions in CSF and mELT were very similar, with both compartments predominantly consisting of B cells and $CD4^+$ T lymphocytes. The gene expression profile and pathway enrichment analysis revealed no striking differences between the two compartments. When treated with aCD20 mAbs, the murine CSF showed a complete depletion of B cells, a reduction in naïve $CD4^+$ T cells, and a marked increase in macrophages. However, no remarkable differences in regulated genes or pathways were observed between the treated and untreated groups. This study provides several unique insights. Firstly, it suggests that CSF immune cells may serve as a surrogate for studying mELT in EAE, which could potentially be applied to MS research in humans. This is particularly valuable as mELT is not easily accessible in living MS patients (27). Secondly, the observed increase in macrophages in B-cell depleted CSF is a novel finding that warrants further investigation in MS patients treated with aCD20 mAbs. Lastly, the study highlights the complexity of B-cell depletion effects, as it did not significantly alter the inflammatory state of remaining immune cells, despite changing the overall cellular composition. This and other limitations of the study were pointed out by the authors. Nevertheless, their findings contribute to our understanding of the mechanisms underlying MS and the effects of B cell-depleting therapies, potentially informing future treatment strategies for MS and other autoimmune diseases.

Tichauer at al. exposed further evidence on the dynamic balance between pro-inflammatory and anti-inflammatory microglial phenotypes in pathological contexts. The authors investigated the effect of 5-day systemic administration of IFN-γ on infiltrating myeloid cells (MC) and microglial cells (MG) during the peak of EAE, a widely used model of MS (28, 29). IFN-γ treatment markedly decreased the absolute number of $CD11b^+$ MC, infiltrated inflammatory cells ($CD11b^+$ $Ly6G^-$), and demyelination levels within the spinal cord (SC) of EAE mice compared to PBS-treated EAE mice. Moreover, IFN-γ-treated EAE mice displayed a reduced number of activated MC/MG cells alongside an increase in resting MG. Immunofluorescence staining of SC sections from IFN-γ-treated EAE animals, using Iba1 as a microglial marker, revealed cells with a ramified morphology, in contrast to the amoeboid-like shapes observed in control EAE animals. While the authors used the now outdated term 'resting' to describe ramified MG, current evidence demonstrates that ramified microglia are highly dynamic, actively extending their processes to continuously monitor and sense the surrounding microenvironment (30–32). The study also explored the regulatory and tolerogenic activity of MG cells induced by IFN-γ. Primary MC/MG cultures from SC of IFN-γ-treated EAE animals, when re-stimulated *ex vivo* with low doses of IFN-γ and myelin oligodendrocyte glycoprotein (MOG_{35-55}), showed enhanced induction of $CD4^+$ Treg cells and elevated levels of transforming growth factor-beta (TGF-β). In addition, the treated cultures exhibited reduced nitrite production following lipopolysaccharide (LPS) stimulation compared to controls. *In vivo* stimulation of EAE mice with IFN-γ upregulated the expression of the microglial marker CX3CR1 (fractalkine receptor) while downregulating the coinhibitory molecule PD-L1 in MC/MG populations. These MG cells were highly reactive for canonical microglial markers, such as Tmem119, P2ry12, and Hexb, but not for MC, oligodendrocyte, or astrocyte markers, suggesting the presence of a distinct microglial subpopulation ($CX3CR1^{high}PD\text{-}L1^{low}$ MG). This phenotype was shown to be induced via STAT-1 (signal transducer and activator of transcription 1) signaling, involved in proinflammatory molecules expression (33). Transcriptional profiling of $CX3CR1^{high}PD\text{-}L1^{low}$ MG cells revealed that *in vivo* IFN-γ stimulation upregulated tolerogenic and anti-inflammatory genes, and downregulated pro-inflammatory genes. Collectively, these findings highlight the dual modulatory effects of IFN-γ on microglial phenotypes and their potential relevance in the context of autoimmune neuroinflammation.

Patients with MS often experience exacerbations of clinical symptoms followed by periods of recovery, known as relapsing-remitting MS (RRMS), where infiltrating blood monocytes play a significant role in neuroinflammation (34). In this context, Rodriguez et al. conducted a comprehensive phenotypic characterization of the monocyte population in MS patients at diagnosis. Peripheral blood mononuclear cells (PBMCs) from early RRMS patients (N=69) were analyzed using mass cytometry, revealing a significant increase in two subsets of $CD14^+$ monocytes (Mo) expressing high and intermediate levels of CD206 and CD209 ($CD206^{high}$ $CD209^{high}$ and $CD206^{int}$ $CD209^{int}$, respectively) compared to age- and sex-matched healthy controls (N=29). These molecules are typically expressed

in tissue-infiltrating monocyte-derived cells (35–38). Notably, $CD206^{high}$ $CD209^{high}$ Mo exhibited elevated expression of markers such as HLA-DR, CD86, CD45RA, CCR5, CCR2, and CD106 compared to classical monocytes (cMo), indicating an active proinflammatory and migratory phenotype (39–42). The study also found that only 22% of MS patients showed an enrichment of $CD206^{high}$ $CD209^{high}$ Mo, and these individuals presented greater disability than MS patients lacking this subset. Moreover, 75% of patients with $CD206^{high}$ $CD209^{high}$ Mo carried the HLA-DRB1*15:01 allele, a well-known genetic risk factor for MS (43, 44). A second allele, HLA-DQB1*06:02, was also frequent among $CD206^{high}$ $CD209^{high}$ subjects included in this study. Furthermore, single-cell RNA sequencing of $CD206^{high}$ $CD209^{high}$ Mo-like cells isolated from CSF of RRMS patients revealed that they were enriched in monocytic lineage genes, distinct from microglial or macrophage signatures. These CSF-infiltrating cells displayed a characteristic antigen presentation profile and enhanced proinflammatory capacity, suggesting that circulating $CD206^{high}$ $CD209^{high}$ Mo-like cells adopt a pathological phenotype once reaching the CNS. Although the listed limitations of this study, the authors propose that the $CD206^{high}$ $CD209^{high}$ Mo subset may contribute to MS progression, and targeting their polarization, trafficking to the CNS, and antigen presentation process could serve as potential therapeutic strategies.

Holm Hansen et al. contributed to this Research Topic with a case-control exploratory study aimed to evaluate the long-term effects of oral cladribine treatment in patients with MS. There are currently several disease-modifying therapies approved by the US Food and Drug Administration for the RRMS (45–47). Among the high-efficacy therapies, oral administration of cladribine induces temporary immune suppression followed by lymphocyte repopulation and reconstitution of the immune system and its effector functions (48–51). Although cladribine appears to be a therapeutic option, most of the clinical evidence comes from short-term studies. In their article, Holm Hansen et al. presented a longitudinal analysis of the sustained effects of cladribine tablet therapy on the dynamics of circulating immune cell subsets and autoreactivity, during the second year of treatment in patients with RRMS. PBMCs from untreated patients and RRMS patients treated chronically for 52, 60, 72 and 96 weeks (W) were subjected to flow cytometry and FluoroSpot antigen reactivity assay. The authors reported that the therapy has long-term effects and still maintains its ability to modulate immune responses in a cell subset- and time-dependent manner. Mainly, chronic cladribine administration induced significant reductions in circulating memory B cells and proinflammatory B cell responses. It also impaired T and B cell cross-talk, reducing T cell responses to autoantigens possibly presented by B cells, including RAS guanyl releasing protein 2 (RASGRP2), a-B crystallin (CRYAB), myelin basic protein (MBP), and MOG, in a time-dependent fashion. The study by Holm Hansen et al. provides important information for better defining prolonged therapeutic strategies for treating RRMS patients.

Aging is one of the most significant risk factors for cognitive decline, with white matter deterioration playing a crucial role in age-related cognitive impairment, even in the absence of neurodegenerative pathologies like AD (52). Despite evidence linking myelin degeneration to cognitive decline, the interplay between the signals in aging white matter remains unexplored, leaving a critical gap in understanding how microglia-mediated myelin degradation contributes to cognitive impairment. DeVries et al. investigated the role of the immune proteins C1q and CD47 in age-related myelin damage, microglia reactivity, and cognitive decline in rhesus monkeys. These proteins act as 'eat me' and 'don't eat me' signals, respectively, regulating in opposition microglial phagocytosis. The study examines changes in C1q and CD47 within the monkey cingulum bundle, a white matter tract in the brain, across normal aging. The researchers used various techniques including immunofluorescence, RNAscope, and ELISA, to analyze the expression and colocalization of C1q and CD47 in relation to MBP and microglia phenotypes. The findings reveal that with age, there is a significant increase in C1q protein in the cingulum bundle, particularly colocalized with myelin. This increase correlated with cognitive impairment in the monkeys. Conversely, CD47 showed a decrease in middle age but paradoxically increased in old age (53). The study also found that microglia become more reactive with age, exhibiting more phagocytic and inflammatory phenotypes. These changes in microglia are associated with increased cognitive impairment (54). A unique insight from this study is the potential role of the balance between 'eat me' (C1q) and 'don't eat me' (CD47) signals in age-related myelin damage. The dysregulation of these signals may contribute to an increased vulnerability of myelin to be phagocytized by microglia, potentially leading to cognitive decline (55). This study also highlights the complex and dynamic nature of CD47 expression throughout the aging process, suggesting that its role in myelin maintenance may change at different stages of life. These findings provide a new perspective on the mechanisms underlying age-related cognitive decline and suggest potential targets for therapeutic interventions aimed at preserving cognitive function in aging.

The study by Kim et al. provides insights into how regulation of the peripheral immune system can affect the progression of a neurodegenerative process associated with inflammation. In the search for alternative therapies for PD, acupuncture and moxibustion have emerged as complementary interventions to medications to relieve patients' motor and non-motor symptoms (56–58). Although it is not known how these types of treatments exert these actions, it has been shown in a PD murine model that acupuncture promotes the clearance of alpha-synuclein aggregates through autophagy (59). Furthermore, acupuncture has a neuromodulatory effect, which is especially relevant in chronic diseases with an inflammatory basis (60–62). Various evidence shows that acupuncture can regulate the function of cellular components of the innate and adaptive immune systems, including mast cells, macrophages, natural killer cells, and $CD4^+$ and $CD8^+$ lymphocytes (63–66). Kim et al. showed that the attachment of microneedle patches (MPs) to the acupoints GB20 and GB34 in a 6-OHDA (6-hydroxydopamine)-induced PD murine

model led to an improvement in the motor and neurodegenerative phenotypes. This improvement was associated with a recovery of the $CD4^+/CD8^+$ ratio at the peripheral and cerebral levels, and a concomitant suppression of both neuroinflammation and damage of dopaminergic neurons in the brain. Therefore, the authors proposed that MPs restore the immune dysfunction in the PD murine model from the periphery to the brain, with significant impact on PD pathology. Despite the limitations of this study listed by the authors, the results open the opportunity to consider acupuncture as a non-invasive complementary therapy for patients with neurological diseases associated with immune alterations, including PD.

Amyotrophic lateral sclerosis (ALS) is a progressive neurological disorder that primarily affects motor neurons. Interestingly, peripheral $CD4^+$-expressing Treg cells have been found to inversely correlate with disease progression (67, 68). Zucchi et al. conducted a longitudinal study to evaluate the levels and phenotypes of Tregs in ALS patients, and the potential correlation with ALS progression measured via the ALS functional rating scale (ALSFRS-r) or forced vital capacity (FVC). The study included 21 participants, both men and women, from the placebo arm of the RAP-ALS trial (69, 70). Blood samples were collected at five time points over a period of 54 weeks (8W, 18W, 30W, 42, and 54W). The findings revealed that Treg levels did not exhibit significant changes on average throughout the study. However, specific subpopulations of Tregs may tend to show dynamic alterations: the percentage of $PD1^+$ Tregs may decrease, while $CD39^+$ Tregs may increase over time. Regarding diverse variables, Zucchi et al. found a positive association between total cholesterol and Tregs, that was particularly evident for $CD38^+$ and $CXCR3^+$ subsets, suggesting a switch to a more metabolically active profile. Additionally, monocyte counts were positively associated with Treg cell numbers. A modest association and no association between Treg concentrations with FVC and ALSFRS-r declines, respectively, were found in this exploratory study. Due to the lack of significant variation in overall Treg numbers throughout the disease course, the authors cautioned that using Treg numbers alone as a pharmaco-dynamic biomarker for ALS trials may have limited value. Nonetheless, the observed changes in specific Treg phenotypes throughout the ASL course, including $PD1^+$ Tregs (71, 72), may merit further investigation for their potential role in ALS progression and therapeutic targeting.

These diverse arrays of articles underscore the intricate and evolving dialogue between the central nervous and immune systems, both at the brain borders and within the parenchyma. The contributions offer cutting-edge insights into how peripheral and brain-resident immune cells influence neurological health, disease progression, and therapeutic responsiveness across conditions like MS, PD, SPS, and age-related cognitive decline. By bridging experimental and clinical perspectives, these studies challenge long-held paradigms of CNS immune privilege and lay critical groundwork for future immunomodulatory strategies in neurodegenerative and neuroinflammatory diseases.

Author contributions

SB: Writing – original draft, Writing – review & editing. JB: Writing – original draft, Writing – review & editing. CF: Writing – original draft, Writing – review & editing. VM: Writing – review & editing. RM: Writing – review & editing. SM: Writing – original draft, Writing – review & editing. EM: Writing – original draft, Writing – review & editing.

Funding

The author(s) declare that financial support was received for the research and/or publication of this article. SB is an Assistant Professor in the Department of Human Genetics and Molecular Medicine, Central University of Punjab, Bathinda, India. Supported by grants from the Indian Council of Medical Research (India; ICMR; EMDR/IG/9-2023-0001025; https://www.icmr.gov.in). SKM is an Assistant Professor in the Department of Zoology, University of Delhi, New Delhi, India. Supported by grants from the Indian Council of Medical Research (India; ICMR; EMDR/SG/11/2023-1452; https://www.icmr.gov.in), and the Institution of Eminence, University of Delhi (India; IOE/2021/12/FRP; https://www.ioe.du.ac.in). EMM is a member of the CONICET scientific career at IHEM-UNCuyo-CONICET, Mendoza, Argentina. Supported by grants from ANPCyT (Argentina; PICT 2021-314; http://www.agencia.mincyt.gob.ar), and CONICET (Argentina; PIP 2023–2025 GI: 112-202201-00410; http://www.conicet.gov.ar).

Acknowledgments

We thank Philipp Albrecht (Heinrich Heine University of Düsseldorf, Germany), Wassim Elyaman (Columbia University, United States), Mahsa Ghajarzadeh (Johns Hopkins University, United States), Marija Mostarica-Stojkovic (University of Belgrade, Serbia), James W. Neal (Swansea University Medical School, United Kingdom), and Luc Vallieres (Laval University, Canada), who edited six of the ten articles included in this RT.

Conflict of interest

The authors declare that the research was conducted in the absence of any commercial or financial relationships that could be construed as a potential conflict of interest.

The author(s) declared that they were an editorial board member of Frontiers, at the time of submission. This had no impact on the peer review process and the final decision.

Generative AI statement

The author(s) declare that no Generative AI was used in the creation of this manuscript.

Publisher's note

References

1. Maurya SK, Borgonovo JE, Biswal S, Martínez-Cerdeño V, Mishra R, Muñoz EM. Editorial: Trends in neuroimmunology: cross-talk between brain-resident and peripheral immune cells in both health and disease. *Front Immunol*. (2024) 15:1442322. doi: 10.3389/fimmu.2024.1442322

2. Muñoz EM, Mishra R, Martínez-Cerdeño V, Borgonovo JE, Maurya SK, Biswal S eds. *E-Book: Trends in neuroimmunology: Cross-talk between brain-resident and peripheral immune cells in both health and disease*. Lausanne: Frontiers Media S.A (2024). doi: 10.3389/978-2-8325-5082-3

3. Su Y, Zheng H, Shi C, Li X, Zhang S, Guo G, et al. Meningeal immunity and neurological diseases: new approaches, new insights. *J Neuroinflammation*. (2023) 20:125. doi: 10.1186/s12974-023-02803-z

4. Matejuk A, Vandenbark AA, Offner H. Cross-talk of the CNS with immune cells and functions in health and disease. *Front Neurol*. (2021) 12:672455. doi: 10.3389/fneur.2021.672455

5. Fitzpatrick Z, Ghabdan Zanluqui N, Rosenblum JS, Tuong ZK, Lee CYC, Chandrashekhar V, et al. Venous-plexus-associated lymphoid hubs support meningeal humoral immunity. *Nature*. (2024) 628:612–9. doi: 10.1038/s41586-024-07202-9

6. Ma T, Wang F, Xu S, Huang JH. Meningeal immunity: Structure, function and a potential therapeutic target of neurodegenerative diseases. *Brain Behav Immun*. (2021) 93:264–76. doi: 10.1016/j.bbi.2021.01.028

7. Da Mesquita S, Fu Z, Kipnis J. The meningeal lymphatic system: A new player in neurophysiology. *Neuron*. (2018) 100:375–88. doi: 10.1016/j.neuron.2018.09.022

8. Zhang X, Liu L, Chai Y, Zhang J, Deng Q, Chen X. Reimagining the meninges from a neuroimmune perspective: a boundary, but not peripheral. *J Neuroinflammation*. (2024) 21:299. doi: 10.1186/s12974-024-03286-2

9. Da Mesquita S, Louveau A, Vaccari A, Smirnov I, Cornelison RC, Kingsmore KM, et al. Functional aspects of meningeal lymphatics in ageing and Alzheimer's disease. *Nat vol*. (2018) 560:185–91. doi: 10.1038/s41586-018-0368-8

10. Schonhoff AM, Figge DA, Williams GP, Jurkuvenaite A, Gallups NJ, Childers GM, et al. Border-associated macrophages mediate the neuroinflammatory response in an alpha-synuclein model of Parkinson disease. *Nat Commun*. (2023) 14:3754. doi: 10.1038/s41467-023-39060-w

11. Zenaro E, Pietronigro E, Della Bianca V, Piacentino G, Marongiu L, Budui S, et al. Neutrophils promote Alzheimer's disease-like pathology and cognitive decline via LFA-1 integrin. *Nat Med*. (2015) 21:880–6. doi: 10.1038/nm.3913

12. Li B, Li J, Li B, Ouchi T, Li L, Li Y, et al. A single-cell transcriptomic atlas characterizes age-related changes of murine cranial stem cell niches. *Aging Cell*. (2023) 22:e13980. doi: 10.1111/acel.13980

13. Shi K, Li H, Chang T, He W, Kong Y, Qi C, et al. Bone marrow hematopoiesis drives multiple sclerosis progression. *Cell*. (2022) 185:2234–2247.e17. doi: 10.1016/j.cell.2022.05.020

14. Ding XB, Wang XX, Xia DH, Liu H, Tian HY, Fu Y, et al. Impaired meningeal lymphatic drainage in patients with idiopathic Parkinson's disease. *Nat Med*. (2021) 27:411–8. doi: 10.1038/s41591-020-01198-1

15. Iliff JJ, Wang M, Liao Y, Plogg BA, Peng W, Gundersen GA, et al. A paravascular pathway facilitates CSF flow through the brain parenchyma and the clearance of interstitial solutes, including amyloid β. *Sci Trans Med*. (2012) 4(147):147ra111. doi: 10.1126/scitranslmed.3003748

16. Lee Y, Choi Y, Park EJ, Kwon S, Kim H, Lee JY, et al. Improvement of glymphatic-lymphatic drainage of beta-amyloid by focused ultrasound in Alzheimer's disease model. *Sci Rep*. (2020) 10:16144. doi: 10.1038/s41598-020-73151-8

17. Kolabas ZI, Kuemmerle LB, Perneczky R, Forstera B, Ulukaya S, Ali M, et al. Distinct molecular profiles of skull bone marrow in health and neurological disorders. *Cell*. (2023) 186:3706–3725.e29. doi: 10.1016/j.cell.2023.07.009

18. Shen T, Yue Y, Ba F, He T, Tang X, Hu X, et al. Diffusion along perivascular spaces as marker for impairment of glymphatic system in Parkinson's disease. *NPJ Parkinson's Dis*. (2022) 8:174. doi: 10.1038/s41531-022-00437-1

19. Baizabal-Carvallo JF, Jankovic J. Stiff-person syndrome: insights into a complex autoimmune disorder. *J Neurol Neurosurg Psychiatry*. (2015) 86:840–8. doi: 10.1136/jnnp-2014-309201

20. Ciccotto G, Blaya M, Kelley RE. Stiff person syndrome. *Neurol Clin*. (2013) 31:319–28. doi: 10.1016/j.ncl.2012.09.005

21. Vlad B, Wang Y, Newsome SD, Balint B. Stiff person spectrum disorders-an update and outlook on clinical, pathophysiological and treatment perspectives. *Biomedicines*. (2023) 11:2500. doi: 10.3390/biomedicines11092500

22. Buchele V, Hackstein H. A simplified extracorporeal photopheresis procedure based on single high-dose ultraviolet A light irradiation shows similar *in vitro* efficacy. *Transfusion*. (2021) 61:883–93. doi: 10.1111/trf.16209

23. Newsome SD, Johnson T. Stiff person syndrome spectrum disorders; more than meets the eye. *J Neuroimmunol*. (2022) 369:577915. doi: 10.1016/j.jneuroim.2022.577915

24. Rakocevic G, Floeter MK. Autoimmune stiff person syndrome and related myelopathies: understanding of electrophysiological and immunological processes. *Muscle Nerve*. (2012) 45:623–34. doi: 10.1002/mus.23234

25. Frisch ES, Pretzsch R, Weber MS. A milestone in multiple sclerosis therapy: monoclonal antibodies against CD20-yet progress continues. *Neurotherapeutics*. (2021) 18:1602–22. doi: 10.1007/s13311-021-01048-z

26. Brand RM, Friedrich V, Diddens J, Pfaller M, Romana de Franchis F, Radbruch H, et al. Anti-CD20 depletes meningeal B cells but does not halt the formation of meningeal ectopic lymphoid tissue. *Neurol Neuroimmunol Neuroinflamm*. (2021) 8:e1012. doi: 10.1212/NXI.0000000000001012

27. Negron A, Stüve O, Forsthuber TG. Ectopic lymphoid follicles in multiple sclerosis: centers for disease control? *Front Neurol*. (2020) 11:607766. doi: 10.3389/fneur.2020.607766

28. Voskuhl RR, MacKenzie-Graham A. Chronic experimental autoimmune encephalomyelitis is an excellent model to study neuroaxonal degeneration in multiple sclerosis. *Front Mol Neurosci*. (2022) 15:1024058. doi: 10.3389/fnmol.2022.1024058

29. Diebold M, Fehrenbacher L, Frosch M, Prinz M. How myeloid cells shape experimental autoimmune encephalomyelitis: At the crossroads of outside-in immunity. *Eur J Immunol*. (2023) 53:e2250234. doi: 10.1002/eji.202250234

30. Nimmerjahn A, Kirchhoff F, Helmchen F. Resting microglial cells are highly dynamic surveillants of brain parenchyma *in vivo*. *Science*. (2005) 308:1314–8. doi: 10.1126/science.1110647

31. Davalos D, Grutzendler J, Yang G, Kim JV, Zuo Y, Jung S, et al. ATP mediates rapid microglial response to local brain injury in *vivo*. *Nat Neurosci*. (2005) 8:752–8. doi: 10.1038/nn1472

32. Petry P, Oschwald A, Kierdorf K. Microglial tissue surveillance: The never-resting gardener in the developing and adult CNS. *Eur J Immunol*. (2023) 53:e2250232. doi: 10.1002/eji.202250232

33. Ivashkiv LB, Donlin LT. Regulation of type I interferon responses. *Nat Rev Immunol*. (2014) 14:36–49. doi: 10.1038/nri3581

34. Zhang G, Yao Q, Long C, Yi P, Song J, Wu L, et al. Infiltration by monocytes of the central nervous system and its role in multiple sclerosis: reflections on therapeutic strategies. *Neural Regen. Res*. (2025) 20:779–93. doi: 10.4103/NRR.NRR-D-23-01508

35. Silva R, Sideris-Lampretsas G, Fox S, Zeboudj L, Malcangio M. CD206+/MHCII-macrophage accumulation at nerve injury site correlates with attenuation of allodynia in TASTPM mouse model of Alzheimer's disease. *Brain Behav Immun Health*. (2022) 26:100548. doi: 10.1016/j.bbih.2022.100548

36. Riew TR, Hwang JW, Jin X, Kim HL, Lee MY. Infiltration of meningeal macrophages into the Virchow-Robin space after ischemic stroke in rats: Correlation with activated PDGFR-β-positive adventitial fibroblasts. *Front Mol Neurosci*. (2022) 15:1033271. doi: 10.3389/fnmol.2022.1033271

37. Ifergan I, Kebir H, Bernard M, Wosik K, Dodelet-Devillers A, Cayrol R, et al. The blood-brain barrier induces differentiation of migrating monocytes into Th17-polarizing dendritic cells. *Brain*. (2008) 131:785–99. doi: 10.1093/brain/awm295

38. Wright PB, McDonald E, Bravo-Blas A, Baer HM, Heawood A, Bain CC, et al. The mannose receptor (CD206) identifies a population of colonic macrophages in health and inflammatory bowel disease. *Sci Rep*. (2021) 11:19616. doi: 10.1038/s41598-021-98611-7

39. Mcgill RB, Steyn FJ, Ngo ST, Thorpe KA, Heggie S, Henderson RD, et al. Monocyte CD14 and HLA-DR expression increases with disease duration and severity in amyotrophic lateral sclerosis. *Amyotroph Lateral Scler Frontotemporal Degener*. (2022) 23:430–7. doi: 10.1080/21678421.2021.1964531

40. Nguyen CTH, Kambe N, Yamazaki F, Ueda-Hayakawa I, Kishimoto I, Okamoto H. Up-regulated expression of CD86 on circulating intermediate monocytes correlated

with disease severity in psoriasis. *J Dermatol Sci*. (2018) 90:135–43. doi: 10.1016/j.jdermsci.2018.01.005

41. Kim JY, Kim J, Huang M, Kosonen R, Lee JE. CCR4 and CCR5 involvement in monocyte-derived macrophage migration in neuroinflammation. *Front Immunol*. (2022) 13:876033. doi: 10.3389/fimmu.2022.876033

42. Xu J, Ganguly A, Zhao J, Ivey M, Lopez R, Osterholzer JJ, et al. CCR2 signaling promotes brain infiltration of inflammatory monocytes and contributes to neuropathology during cryptococcal meningoencephalitis. *mBio*. (2021) 12:e0107621. doi: 10.1128/mBio.01076-21

43. Mosca L, Mantero V, Penco S, La Mantia L, De Benedetti S, Marazzi MR, et al. HLA-DRB1*15 association with multiple sclerosis is confirmed in a multigenerational Italian family. *Funct Neurol*. (2017) 32:83–8. doi: 10.11138/fneur/2017.32.2.083

44. Barcellos LF, Sawcer S, Ramsay PP, Baranzini SE, Thomson G, Briggs F, et al. Heterogeneity at the HLA-DRB1 locus and risk for multiple sclerosis. *Hum Mol Genet*. (2006) 15:2813–24. doi: 10.1093/hmg/ddl223

45. Freeman L, Longbrake EE, Coyle PK, Hendin B, Vollmer T. High-efficacy therapies for treatment-naïve individuals with relapsing-remitting multiple sclerosis. *CNS Drugs*. (2022) 36:1285–99. doi: 10.1007/s40263-022-00965-7

46. Montalban X, Gold R, Thompson AJ, Otero-Romero S, Amato MP, Chandraratna D, et al. ECTRIMS/EAN Guideline on the pharmacological treatment of people with multiple sclerosis. *Multiple sclerosis (Houndmills Basingstoke England)*. (2018) 24:96–120. doi: 10.1177/1352458517751049

47. Śladowska K, Kawalec P, Holko P, Osiecka O. Comparative safety of high-efficacy disease-modifying therapies in relapsing-remitting multiple sclerosis: a systematic review and network meta-analysis. *Neurological Sci*. (2022) 43:5479–500. doi: 10.1007/s10072-022-06197-3

48. Comi G, Cook S, Giovannoni G, Rieckmann P, Sorensen PS, Vermersch P, et al. Effect of cladribine tablets on lymphocyte reduction and repopulation dynamics in patients with relapsing multiple sclerosis. *Multiple sclerosis related Disord*. (2019) 29:168–74. doi: 10.1016/j.msard.2019.01.038

49. Leist TP, Weissert R. Cladribine: mode of action and implications for treatment of multiple sclerosis. *Clin neuropharmacology*. (2011) 34:28–35. doi: 10.1097/WNF.0b013e318204cd90

50. Moser T, Schwenker K, Seiberl M, Feige J, Akgun K, Haschke-Becher E, et al. Long-term peripheral immune cell profiling reveals further targets of oral cladribine in MS. *Ann Clin Trans Neurol*. (2020) 7:2199–212. doi: 10.1002/acn3.51206

51. Stuve O, Soelberg Soerensen P, Leist T, Giovannoni G, Hyvert Y, Damian D, et al. Effects of cladribine tablets on lymphocyte subsets in patients with multiple sclerosis: an extended analysis of surface markers. *Ther Adv neurological Disord*. (2019) 12:1756286419854986. doi: 10.1177/1756286419854986

52. Gonzales MM, Garbarino VR, Pollet E, Palavicini JP, Kellogg DL Jr, Kraig E, et al. Biological aging processes underlying cognitive decline and neurodegenerative disease. *J Clin Invest*. (2022) 132:e158453. doi: 10.1172/JCI158453

53. Cham LB, Torrez Dulgeroff LB, Tal MC, Adomati T, Li F, Bhat H, et al. Immunotherapeutic blockade of CD47 inhibitory signaling enhances innate and adaptive immune responses to viral infection. *Cell Rep*. (2020) 31:107494. doi: 10.1016/j.celrep.2020.03.058

54. Costa J, Martins S, Ferreira PA, Cardoso AMS, Guedes JR, Peca J, Cardoso AL, et al. The old guard: Age-related changes in microglia and their consequences. *Mech Ageing Dev*. (2021) 197:111512. doi: 10.1016/j.mad.2021.111512

55. Wang K, Li J, Zhang Y, Huang Y, Chen D, Shi Z, et al. Central nervous system diseases related to pathological microglial phagocytosis. *CNS Neurosci Ther*. (2021) 27:528–39. doi: 10.1111/cns.13619

56. Doo K-H, Lee JH, Cho SY, Jung WS, Moon SK, Park JM, et al. A prospective open-label study of combined treatment for idiopathic parkinson's disease using acupuncture and bee venom acupuncture as an adjunctive treatment. *J Altern complementary Med (New York N.Y.)*. (2015) 21:598–603. doi: 10.1089/acm.2015.0078

57. Eng ML, Lyons KE, Greene MS, Pahwa R. Open-label trial regarding the use of acupuncture and yin tui na in Parkinson's disease outpatients: a pilot study on efficacy, tolerability, and quality of life. *J Altern complementary Med (New York N.Y.)*. (2006) 12:395–9. doi: 10.1089/acm.2006.12.395

58. Shulman LM, Wen X, Weiner WJ, Bateman D, Minagar A, Duncan R, et al. Acupuncture therapy for the symptoms of Parkinson's disease. *Movement Disord*. (2002) 17:799–802. doi: 10.1002/mds.10134

59. Tian T, Sun Y, Wu H, Pei J, Zhang J, Zhang Y, et al. Acupuncture promotes mTOR-independent autophagic clearance of aggregation-prone proteins in mouse brain. *Sci Rep*. (2016) 6:19714. doi: 10.1038/srep19714

60. Li N, Guo Y, Gong Y, Zhang Y, Fan W, Yao K, et al. The anti-inflammatory actions and mechanisms of acupuncture from acupoint to target organs via neuro-immune regulation. *J Inflammation Res*. (2021) 14:7191–224. doi: 10.2147/JIR.S341581

61. Wang M, Liu W, Ge J, Liu S. The immunomodulatory mechanisms for acupuncture practice. *Front Immunol*. (2023) 14:1147718. doi: 10.3389/fimmu.2023.1147718

62. Zhao H, Dong F, Li Y, Ren X, Xia Z, Wang Y, et al. Inhibiting ATG5 mediated autophagy to regulate endoplasmic reticulum stress and CD4+ T lymphocyte differentiation: Mechanisms of acupuncture's effects on asthma. *Biomedicine pharmacotherapy = Biomedecine pharmacotherapie*. (2021) 142:112045. doi: 10.1016/j.biopha.2021.112045

63. Yin N, Yang H, Yao W, Xia Y, Ding G. Mast cells and nerve signal conduction in acupuncture. *Evidence-Based complementary Altern Med*. (2018) 2018:3524279. doi: 10.1155/2018/3524279

64. Zhang K, Zhao X, Ding S, Liu Y, Xu Y, Yan Y, et al. Applying complex network and cell-cell communication network diagram methods to explore the key cytokines and immune cells in local acupoint involved in acupuncture treating inflammatory pain. *Evidence-Based complementary Altern Med*. (2020) 2020:2585960. doi: 10.1155/2020/2585960

65. Huang Z, Hu Z, Ouyang J, Huang C. Electroacupuncture regulates the DREAM/NF-κB signalling pathway and ameliorates cyclophosphamide-induced immunosuppression in mice. *Acupuncture Med*. (2019) 37:292–300. doi: 10.1136/acupmed-2017-011593

66. Watanabe M, Kainuma E, Tomiyama C. Repetitive manual acupuncture increases markers of innate immunity in mice subjected to restraint stress. *Acupuncture Med*. (2015) 33:312–8. doi: 10.1136/acupmed-2014-010660

67. Sheean RK, McKay FC, Cretney E, McKay FC, Cretney E, Bye CR, Perera ND, Tomas D, et al. Association of regulatory T-cell expansion with progression of amyotrophic lateral sclerosis: A study of humans and a transgenic mouse model. *JAMA Neurol*. (2018) 75:681–9. doi: 10.1001/jamaneurol.2018.0035

68. Yazdani S, Seitz C, Cui C, Lovik A, Pan L, Piehl F, et al. T cell responses at diagnosis of amyotrophic lateral sclerosis predict disease progression. *Nat Commun*. (2022) 13:6733. doi: 10.1038/s41467-022-34526-9

69. Mandrioli J, D'Amico R, Zucchi E, De Biasi S, Banchelli F, Martinelli I, et al. Randomized, double-blind, placebo-controlled trial of rapamycin in amyotrophic lateral sclerosis. *Nat Commun*. (2023) 14:4970. doi: 10.1038/s41467-023-40734-8

70. Mandrioli J, D'Amico R, Zucchi E, Gessani A, Fini N, Fasano A, et al. Rapamycin treatment for amyotrophic lateral sclerosis: Protocol for a phase II randomized, double-blind, placebo-controlled, multicenter, clinical trial (RAP-ALS trial). *Med (Baltimore)*. (2018) 97:e11119. doi: 10.1097/MD.0000000000011119

71. Manenti S, Orrico M, Masciocchi S, Mandelli A, Finardi A, Furlan R. PD-1/PD-L axis in neuroinflammation: new insights. *Front Neurol*. (2022) 13:877936. doi: 10.3389/fneur.2022.877936

72. Nguyen LT, Ohashi PS. Clinical blockade of PD1 and LAG3–potential mechanisms of action. *Nat Rev Immunol*. (2015) 15:45–56. doi: 10.1038/nri3790

frontiers | Frontiers in Immunology

TYPE Original Research
PUBLISHED 02 June 2023
DOI 10.3389/fimmu.2023.1191838

OPEN ACCESS

EDITED BY
Luc Vallieres,
Laval University, Canada

REVIEWED BY
Roland S. Liblau,
Institut National de la Santé et de la Recherche Médicale (INSERM), France
Giacomo Casella,
Thomas Jefferson University, United States

*CORRESPONDENCE
Rodrigo Naves
rodrigonaves@uchile.cl

†These authors have contributed equally to this work and share first authorship

RECEIVED 22 March 2023
ACCEPTED 16 May 2023
PUBLISHED 02 June 2023

CITATION
Tichauer JE, Arellano G, Acuña E, González LF, Kannaiyan NR, Murgas P, Panadero-Medianero C, Ibañez-Vega J, Burgos PI, Loda E, Miller SD, Rossner MJ, Gebicke-Haerter PJ and Naves R (2023) Interferon-gamma ameliorates experimental autoimmune encephalomyelitis by inducing homeostatic adaptation of microglia. *Front. Immunol.* 14:1191838. doi: 10.3389/fimmu.2023.1191838

Interferon-gamma ameliorates experimental autoimmune encephalomyelitis by inducing homeostatic adaptation of microglia

Juan E. Tichauer[1†], Gabriel Arellano[1,2†], Eric Acuña[1], Luis F. González[1], Nirmal R. Kannaiyan[3], Paola Murgas[4], Concepción Panadero-Medianero[4], Jorge Ibañez-Vega[1], Paula I. Burgos[5], Eileah Loda[2], Stephen D. Miller[2], Moritz J. Rossner[3], Peter J. Gebicke-Haerter[1,6] and Rodrigo Naves[1*]

[1]Program of Immunology, Institute of Biomedical Sciences, Faculty of Medicine, Universidad de Chile, Santiago, Chile, [2]Department of Microbiology-Immunology, Feinberg School of Medicine, Northwestern University, Chicago, IL, United States, [3]Molecular Neurobiology, Department of Psychiatry & Psychotherapy, Ludwig-Maximilians-University of Munich, Munich, Germany, [4]Center for Integrative Biology, Faculty of Science, Universidad Mayor, Santiago, Chile, [5]Department of Clinical Immunology and Rheumatology , School of Medicine, Pontificia Universidad Católica de Chile, Santiago, Chile, [6]Central Institute of Mental Health, Faculty of Medicine, University of Heidelberg, Mannheim, Germany

Compelling evidence has shown that interferon (IFN)-γ has dual effects in multiple sclerosis and in its animal model of experimental autoimmune encephalomyelitis (EAE), with results supporting both a pathogenic and beneficial function. However, the mechanisms whereby IFN-γ may promote neuroprotection in EAE and its effects on central nervous system (CNS)-resident cells have remained an enigma for more than 30 years. In this study, the impact of IFN-γ at the peak of EAE, its effects on CNS infiltrating myeloid cells (MC) and microglia (MG), and the underlying cellular and molecular mechanisms were investigated. IFN-γ administration resulted in disease amelioration and attenuation of neuroinflammation associated with significantly lower frequencies of CNS $CD11b^+$ myeloid cells and less infiltration of inflammatory cells and demyelination. A significant reduction in activated MG and enhanced resting MG was determined by flow cytometry and immunohistrochemistry. Primary MC/MG cultures obtained from the spinal cord of IFN-γ-treated EAE mice that were *ex vivo* re-stimulated with a low dose (1 ng/ml) of IFN-γ and neuroantigen, promoted a significantly higher induction of $CD4^+$ regulatory T (Treg) cells associated with increased transforming growth factor (TGF)-β secretion. Additionally, IFN-γ-treated primary MC/MG cultures produced significantly lower nitrite in response to LPS challenge than control MC/MG. IFN-γ-treated EAE mice had a significantly higher frequency of $CX3CR1^{high}$ MC/MG and expressed lower levels of program death ligand 1 (PD-L1) than PBS-treated mice. Most $CX3CR1^{high}PD\text{-}L1^{low}CD11b^+Ly6G^-$ cells expressed MG

markers (Tmem119, Sall2, and P2ry12), indicating that they represented an enriched MG subset (CX3CR1^{high}PD-L1^{low} MG). Amelioration of clinical symptoms and induction of CX3CR1^{high}PD-L1^{low} MG by IFN-γ were dependent on STAT-1. RNA-seq analyses revealed that *in vivo* treatment with IFN-γ promoted the induction of homeostatic CX3CR1^{high}PD-L1^{low} MG, upregulating the expression of genes associated with tolerogenic and anti-inflammatory roles and down-regulating pro-inflammatory genes. These analyses highlight the master role that IFN-γ plays in regulating microglial activity and provide new insights into the cellular and molecular mechanisms involved in the therapeutic activity of IFN-γ in EAE.

KEYWORDS

multiple sclerosis, experimental autoimmune encephalomyelitis, interferon-gamma, microglia, myeloid cells, neuroinflammation, neurodegenerative disease, immune tolerance.

1 Introduction

Multiple Sclerosis (MS) is a disease of the central nervous system (CNS) characterized by chronic inflammation and demyelination. It is the most common autoimmune disease in the brain and the leading cause of non-traumatic neurological disability in young adults (1). Experimental autoimmune encephalomyelitis (EAE) remains the animal model most widely used to study disease mechanisms and therapeutic approaches for MS (2). EAE is actively induced by immunization with myelin-derived antigens associated with adjuvant and consists of an induction phase and an effector phase (3). The induction phase involves the priming of myelin epitope-specific CD4$^+$ T cells in the periphery. The effector phase is characterized by innate and adaptive immune cell migration from the periphery into the CNS and their re-activation by CNS resident cells such as microglia (MG) or immigrating antigen-presenting cells (APC) (2, 3). Both MS and EAE are characterized by inflammatory lesions in the CNS that mainly contain cells expressing the CD11b cell marker (4). This CD11b$^+$ cell population includes peripheral myeloid cells (MC) such as neutrophils, monocytes, dendritic cells, and macrophages as well as CNS resident MG.

MG constitute about 5-20% of all cells in the CNS (5) and their primary role is the support and maintenance of CNS as well as to perform important surveillance functions (6). MG are characterized by a prominent expression of the fractalkine receptor CX3CR1, which is not expressed in astrocytes, oligodendrocytes, or neurons (7, 8). Indeed, CX3CR1 promotor activity has been used for the visualization, genetic manipulation, and the study of the function of MG in the CNS (9). In addition, CX3CR1 is considered a microglial homeostatic marker (10, 11) and lack of this receptor results in exacerbation of inflammation and increased expression of MHC class II molecules in MG (12–14). During early stages of demyelination, active lesions present increased numbers of MG expressing pro-inflammatory markers associated with phagocytosis, antigen presentation and T cell co-stimulation. In later stages, MG develop an intermediate phenotype between pro- and anti-inflammatory activation. Interestingly, loss of homeostatic microglial signature observed in active lesions of MS patients is restored during disease inactivity (15, 16). Therefore, MG have the capability of producing a wide variety of molecules that allow them to exert both inflammatory/detrimental and anti-inflammatory/protective functions in EAE and MS (16).

Interferon gamma (IFN-γ), the only member of the type II IFN family, is a cytokine that has been historically considered the hallmark of Th1 cells driving inflammation in EAE and MS (17, 18). However, compelling evidence has challenged the notion that IFN-γ is strictly pathogenic and has been ascribed a protective role as well [reviewed in (19–21)]. Several studies analyzing EAE development in mice either deficient in the IFN-γ gene, lacking the IFN-γ receptor, or treated with neutralizing antibodies against IFN-γ, demonstrate that endogenous IFN-γ plays a disease-limiting role in EAE (22–33). Likewise, EAE symptoms are ameliorated in response to IFN-γ administered systemically (i.p.) (29, 30) or directly into the CNS (33). Therefore, IFN-γ has opposite effects in EAE, which can be explained, at least in part, through its dose-dependent dual action on MG. Low doses of IFN-γ enable MG to perform neuroprotective functions, whereas high doses of IFN-γ polarize MG toward an inflammatory state [reviewed in (20)]. In EAE, we and other investigators have found that IFN-γ is detrimental during the induction phase but protective during the early effector phase (acute phase) (26, 32, 34, 35), indicating that opposing effects of IFN-γ depend on the stage of the disease. However, the mechanisms whereby IFN-γ is able to exert protection in EAE and its role at the peak of EAE remain unresolved. Moreover, most studies concerning the role of IFN-γ in the pathogenesis and progression of EAE and MS have primarily focused on peripheral lymphoid cells while its action on CNS-infiltrating myeloid cells and CNS-resident cells such as MG has been largely ignored, despite their critical role in regulating autoimmune neuroinflammation. This study aims to elucidate the impact of systemic administration of IFN-γ at the peak of EAE, its effects on CNS infiltrating MC and MG, and the underlying cellular and molecular mechanisms.

2 Material and methods

2.1 Mice

C57BL/6 mice and the Signal Transducer and Activation Transcription (Stat)-1$^{-/-}$ (B6.129S(Cg)-Stat1tm1Dlv/J, stock #012606) mice were obtained from The Jackson Laboratory. C57BL/6J MOG_{35-55}-specific TCR transgenic (2D2) mouse strain was kindly provided by Dr. R Pacheco (Fundación Ciencia & Vida, Chile). All mice were maintained under specific pathogen-free (SPF) conditions. All experimental procedures complied with the Helsinki Declaration of animal experiments and were approved by the Institutional Animal Care and Use Committee (IACUC) of the University of Chile and Northwestern University.

2.2 Induction of EAE and treatment

EAE was induced in 8- to 12-week-old mice with a s.c. injection of 150 µg myelin oligodendrocyte glycoprotein-derived 35-55 peptide (MOG_{35-55}, MEVGWYRSPFSRVVHLYRNGK, CPC Scientific, California, US), emulsified in Incomplete Freund's adjuvant containing 500 µg *Mycobacterium tuberculosis* (BD Difco, Detroit, Michigan, US) followed by an i.p. injection with 500 ng *Bordetella pertussis* toxin (List Biological, Campbell, California, US) on the day of immunization and 48 h later. Body weight and clinical symptoms were monitored daily using a standard clinical score of 0-6 as previously described (36). For treatment with IFN-γ, 1 µg/mouse/day of recombinant murine IFN-γ (Biolegend, San Diego, California, US) was administered i.p. for 5 days starting at the peak of EAE. Non-immunized (NI) mice (without EAE) and EAE mice injected with phosphate-buffered saline (PBS) (Gibco, Grand Island, New York, US) were used as control groups (Figure 1A).

2.3 Histological analysis

Mice were deeply anesthetized and intracardially perfused with PBS (0.1 M) followed by 4% paraformaldehyde (pH=7.4). Thoracic and lumbar spinal cord (SC) sections were removed, post-fixed in 4% paraformaldehyde, and embedded in paraffin. Serial sections with 6 µm thickness were cut, followed by hematoxylin and eosin (H&E) and luxol fast blue (LFB) staining. All reagents were purchased from Sigma (Saint Louis, Missouri, USA). LFB images were captured on an Olympus BX51 multichannel light/epifluorescence microscope (Olympus, Tokyo, Japan). H&E images were captured on a NanoZoomer XR slide scanner (Hamamatsu Photonics, Japan) employing the NanoZoomer Digital Pathology scan software v3.0 (Hamamatsu Photonics,

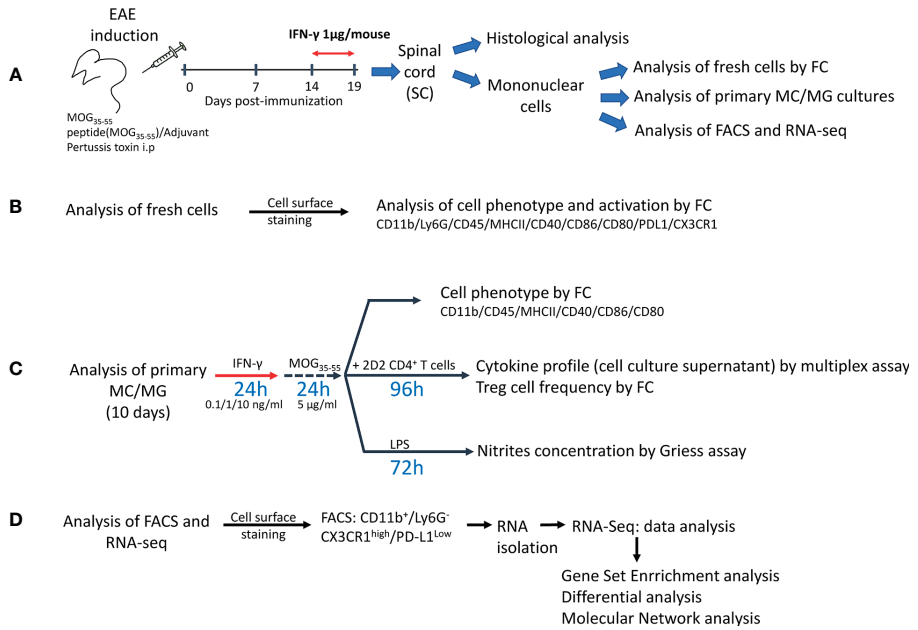

FIGURE 1
Experimental design. **(A)** Mice were immunized with myelin oligodendrocyte protein peptide (MOG_{35-55}) to induce experimental autoimmune encephalomyelitis (EAE). Mice were treated daily with 1 µg/mouse of mrIFN-γ or PBS for 5 days at the peak of EAE. SC were collected for histological analysis or to isolate mononuclear cells, which were used for analysis of fresh cells by multiparametric flow cytometry (FC), primary myeloid cells/microglia (MC/MG) cultures, fluorescence activated cell sorting (FACS), and RNAseq analysis. **(B)** Fresh isolated cells were used to determine the cell phenotype by FC analysis using the markers described in the figure. **(C)** Primary MC/MG cultures were established and then cells were pre-conditioned with low doses of IFN-γ (0.1, 1, and 10 ng/ml) for 24 h and then pulsed with MOG_{35-55} (5 µg/ml) for an additional 24 h. Cells were analyzed for tolerogenic phenotype by FC or were co-cultured with $1x10^6$ $CD4^+$ T cells obtained by negative selection from spleens of 2D2 mice. After 4 days of co-culture, supernatants were collected for further cytokine analysis by multiplex assay or ELISA and the cells were analyzed for Treg cell frequency ($CD4^+CD25^{high}Foxp3^+$) by FC. In other assays, pre-conditioned MC/MG cultures were challenged with 1 µg/ml LPS for 72 h. Cell culture supernatant was collected and nitrite was determined by Griess reaction. **(D)** Fresh isolated cells were stained with antibodies against CD11b, LY6G, CD45, CX3CR1 and PD-L1, and immediately sorted on a FACSAria™ III. RNA was isolated using RNAeasy Micro kit and used for RNAseq analysis.

Japan). Density of infiltrating inflammatory cells was determined as the number of cell nuclei per 10.000 μm^2. The extent of demyelination was evaluated by measuring the percentage of demyelinated area over the total white matter area for each SC section. Quantifications were performed using ImageJ software (NIH, USA).

2.4 Immunohistochemistry

For immunostaining, thoracic SC sections were deparaffinized and rehydrated. Heat-induced antigen retrieval was performed in citrate buffer (pH=6.0) for 30 min. Sections were washed in 1X Tris-buffered saline (TBS), permeabilized, and blocked for 1 h at room temperature (RT) in blocking buffer [5% bovine serum albumin (BSA), 0.5% Triton-X 100 in 1X TBS)]. Tissues were incubated with the primary antibody polyclonal rabbit anti-ionized-calcium binding adaptor protein (Iba) 1 diluted in blocking buffer (1:300, FujiFilm Wako, Osaka, Japan) overnight at 4°C. The next day, slides were washed with 1X TBS and incubated with Alexa Fluor 555-labeled secondary antibody anti-rabbit (1:200, Invitrogen, Waltham, MA, US) for 3 h at RT (Table 1). Slides were washed with 1X TBS, and cell nuclei were stained with 4',6-diamidino-2-phenylindole (DAPI). Finally, slides were rinsed with 1X TBS, mounted with an anti-fade mounting media, and visualized in a Leica DMI8 inverted fluorescence microscope. Image J-assisted analysis was used to evaluate density of $Iba1^+$ cells, determined as the number of $Iba1^+$ cells per 100.000 μm^2; average $Iba1^+$ cell size, determined as cell area of $Iba1^+$ cells; and percentage Iba1 coverage, determined as the percentage of the total section area occupied by $Iba1^+$ cells (μm^2).

2.5 Cell cultures and ex vivo re-stimulation

Mononuclear cells were isolated from SC of EAE mice treated with PBS or IFN-γ at day 19 post-immunization as previously described (37). Briefly, spinal cord homogenates were obtained and incubated with 0.5 mg/ml collagenase (Roche, Manheim, Germany) and 10 units/ml DNAse I (New England Biolabs, Ipswich,

TABLE 1 List of antibodies used for immunofluorescence and flow cytometry.

Specificity	Fluorochrome	Dilution	Source	Clone/ID
Neutrophil				
LY6G	BV605	1:500	BIOLEGEND	1A8
Microglia				
TMEM119	Unconjugated (Rabbit)	1:100	ABCAM	106-6
	anti-rabbit Alexa fluor 555	1:1000	INVITROGEN	AB_2535849
Myeloid cells/Microglia				
Iba1	Unconjugated (Rabbit)	1:300	WACO	Polyclonal
	anti-rabbit Alexa fluor 555	1:200	INVITROGEN	AB_2535849
CD11b	FITC/PE	1:300	BIOLEGEND	M1/70
CD45	APC	1:500	BIOLEGEND	30-F11
CX3CR1	PE/Cy7	1:500	BIOLEGEND	SA011F11
PD-L1 (CD274; B7-H1)	BV711	1:400	BIOLEGEND	10F.9G2
MHCII	Alexa Fluor700	1:600	EBIOSCIENCE	MS/114.15.2
CD86	APC/Cy7	1:400	BIOLEGEND	GL-1
CD80	PE	1:200	BIOLEGEND	16-10A1
CD40	PerCP	1:300	BIOLEGEND	3/23
$CD4^+$ Treg cells				
CD4	FITC	1:200	BIOLEGEND	RM4-5
CD25	APC	1:200	BIOLEGEND	PC61
FoxpP3	PE	1:200	BIOLEGEND	150D
Myelin				
MBP1	Unconjugated (Mouse)	1:70	BIOLEGEND	SMI99
	anti-mouse Alexa fluor 555	1:500	INVITROGEN	AB_2535844

APC, allophycocyanin; BV,brilliant violet; Cy, cyanine; FITC, fluorescein isothiocyanate; PE, phycoerythrin; PERCP, Peridinin Chlorophyll Protein Complex.

Massachusetts, US) at 37°C for 1 h. Mononuclear cells were purified using 40%/70% discontinuous Percoll gradients (Amersham, Piscataway, New Jersey, US), and total cell numbers were determined using a hemocytometer with viability assessed by trypan blue exclusion. In some assays, fresh cells were immediately analyzed by flow cytometry (Figure 1B). In other experiments, primary cell cultures were established; seeding cells in 24-well plates at a density of $2x10^5$ cells per well in 1 ml Iscove´s Modified Dulbecco´s Medium (IMDM) supplemented with 10% fetal calf serum (FCS), 100U/ml penicillin plus 100 µg/ml streptomycin, 1 mM sodium pyruvate, 50 µM beta-mercaptoethanol, 2 mM glutamine, and non-essential amino acids (all from Gibco, Carlsbad, California, US) (Figure 1C). Primary cell cultures usually contained 80-90% of adherent $CD11b^+$ myeloid/microglia (MC/MG) (Supplementary Figure 1). For nitric oxide (NO) determination, MC/MG were re-stimulated with 1 ng/ml IFN-γ for 24 h and then pulsed with 5 µg/ml MOG_{35-55} for an additional 24 h. Then, re-stimulated MC/MG cultures were challenged with 1 µg/ml bacterial lipopolysaccharide (LPS) for 72 h in IMDM culture media. Thereafter, the medium was collected, and nitrite, a stoichiometric and stable metabolite of NO, was determined from supernatants by Griess reaction (Promega, Madison, Wisconsin, US). For cell co-culture experiments, MC/MG were re-stimulated with varying amounts of IFN-γ (0.1-1-10 ng/ml) for 24 h, washed, and then pulsed with MOG_{35-55} (5 µg/ml) for an additional 24 h. After washing, cells were co-cultured with $1x10^6$ $CD4^+$ T cells previously purified by negative selection from spleens of 2D2 mice using a $CD4^+$ T cell isolation kit (Miltenyi Biotec, Bergisch Gladbach, Germany). After 4 days of co-culture, cell culture supernatant was collected for further cytokine analysis, and the cells were analyzed for Treg cell frequency ($CD4^+CD25^{high}Foxp3^+$) by flow cytometry (Figure 1C).

2.6 Immune staining, flow cytometry, and FACS Sorting.

For cell surface staining, isolated cells were immediately fixed with fixation buffer (eBioscience, San Diego California, US) overnight at 4°C. For blocking non-specific Fc receptor-mediated antibody binding, cells were incubated with anti-FcγR III/II antibody for 15 min at 4°C in 2% fetal calf serum (FCS) PBS. Then, cells were stained with antibodies against CD11b, lymphocyte antigen 6 complex locus G (LY6G), CD45, CX3C chemokine Receptor 1 (CX3CR1), programmed death ligand 1 (PD-L1), CD86, CD80, CD40, MHC class II (MHC-II) molecules, and transmembrane protein (TMEM) 119 for 30 minutes at 4°C (Table 1). For intracellular staining, cells were permeabilized with Permeabilization kit (eBioscience, San Diego California, US) for 30 minutes at RT and then incubated with antibodies against forkhead box P3 (FoxP3) (Biolegend, USA) for 30 minutes at RT. Next, cells were resuspended in PBS and analyzed using a Fortessa Flow Cytometer (BD Biosciences, USA) and FlowJo software (Tree Star, USA). Flow cytometry gating strategies are described in Supplementary Figure 2.

For FACS (Figure 1D), freshly isolated SC cells of 5-6 mice were incubated with anti-FcγR III/II antibody for 15 min at 4°C in 2% FCS PBS and immune stained with antibodies against CD11b, LY6G, CD45, CX3CR1, PD-L1, for 30 minutes at 4°C. Cells were immediately sorted on a FACSAria™ III (BD Biosciences, US), collected in tubes containing 2.4 ml of RLT lysis buffer (Qiagen, Hilden, Germany), and frozen at -80°C until RNA-Seq analysis. Usually, $6x10^4$ to $1x10^5$ cells were obtained, and cell viability was higher than 97% (not shown). Post sorting analysis confirmed that >97.5% of sorted cells were $CD11b^+LY6G^-CX3CR1^{high}PD\text{-}L1^{low}$.

2.7 Cytokine analysis

The concentration of IFN-γ, IL-1β, tumor necrosis factor (TNF)-α, granulocyte macrophage colony-stimulating factor (GM-CSF), IL-2, IL-4, and IL-10 in cell co-culture supernatants was determined by a multiplex assay using Luminex technology (Merck Millipore, Darmstadt, Germany) according to manufacturer´s instructions. Total and active transforming growth factor (TGF)-β production was determined by ELISA (Invitrogen, Vienna, Austria). The standard curve was diluted in medium containing 10% fetal calf serum, so TGF-β production was calculated over the basal level contained in the fetal calf serum (Figure 1C).

2.8 RNA sequencing analysis

2.8.1 Library preparation and sequencing

RNA was isolated from $CD11b^+Ly6G^-CX3CR1^{high}PD\text{-}L1^{low}$cells obtained from SC of EAE mice treated with either IFN-γ or PBS using RNAeasy Micro kit (Qiagen, Hilden, Germany) (Figure 1D). 1 µl of ERCC RNA Spike-In Mix (ThermoFisher, Carlsbad, California, US) diluted 1:5000 was added to the isolated RNA as an external control. cDNA was synthesized using Ovation RNA-Seq System V2 (NuGen, Groningen, Netherlands). 100 ng of cDNA was used as input for fragmentation and followed by library preparation using the IonXpress plus gDNA and Amplicon Library preparation kit (ThermoFisher, Carlsbad, California, US) as described by the manufacturer. The library was then size selected on a 2% E-Gel (ThermoFisher, Carlsbad, California, US). Sample specific barcodes were then added and amplified. Individual sample libraries were quantified using a Kapa Library Quantification Kit (Kapa, Wilmington, Massachusetts, US) using samples diluted 1:200. Equal quantities of individual samples were then pooled and sequenced on an Ion Proton Sequencer.

2.8.2 Data analysis

The raw reads (Fastq) were split into sample-specific reads based on the barcodes. The reads were then checked for sequence quality and sequence repeats. Low-quality bases and short reads were removed from further analysis. The reads were subsequently mapped to the Mus musculus genome (mm10) using TMAP Aligner and quantified using Ensembl annotation 86 using Partek Flow. Genes with a minimum of 5 reads in at least 80% of the samples were considered for further analysis. Differentially expressed genes (DEGs) were determined in R with the DESeq2 package (38). Genes with at least one-fold change and corrected p-Value of less than 0.05 were considered as differentially expressed between IFN-γ-treated and PBS control mice. Gene set enrichment

analysis (GSEA) was performed using the gene sets from the Molecular Signatures Database-MsigDB. Overrepresentation analysis was performed using Reactome database (a database of reactions, pathways, and biological processes) (39, 40).

2.8.3 Construction of a molecular network of protein interactions

In order to search for molecular connections between selected genes, each gene was subjected to a nearest neighbor or cluster analysis using the STRING platform (https://string-db.org/). The setting of 100 interactions (custom value) and a minimum score of 0.400 (medium confidence) was chosen. The lists for each gene were entered into "genes.R " available in "R" (https://cran.r-project.org/bin/windows/base/) and turned into a graphical display by using "igraph", a network analysis R package (http://igraph.org/r/).

2.9 Statistical analysis

Results were analyzed using a Mann–Whitney nonparametric test or one-way ANOVA using GraphPad Prism v.5.0 (GraphPad Software). P values <0.05 were considered statistically significant.

3 Results

3.1 IFN-γ treatment induces amelioration of the clinical symptoms and attenuation of neuroinflammation at the peak of EAE

First, we determined the effect of systemic administration of IFN-γ for 5 days starting at the peak of EAE. The results showed that IFN-γ significantly decreased the severity of clinical symptoms and body weight loss compared to PBS-treated mice (Figure 2A). After cessation of treatment, disease severity returned to levels similar to PBS-treated mice (Supplementary Figure 3). Histological analyses showed that thoracic and lumbar SC sections from IFN-γ-treated EAE mice had significantly less infiltration of inflammatory cells and fewer demyelinated areas compared to PBS-treated-EAE mice (Figures 2B, C). Interestingly, flow cytometry analysis revealed that *in vivo* IFN-γ-treatment resulted in a significantly lower absolute number of mononuclear cells and lower frequency and absolute numbers of $CD11b^+$ cells and non-neutrophil MC/MG ($CD11b^+Ly6G^-$) compared to SC from PBS-treated EAE mice; however, levels were still higher than the non-immunized (NI) group (Figure 3A–C). There was no significant difference in the frequency and absolute number of neutrophils ($CD11b^+Ly6G^+$) between the PBS- and IFN-γ-treated mice (Figure 3D). Similar total number of cells was determined in draining lymph nodes (dLN) and spleen from IFN-γ-treated EAE mice and control mice. Frequency and absolute number of $CD11b^+$ cells and neutrophils and macrophages in dLN was not affected by IFN-γ treatment. In contrast, a significantly lower frequency and absolute number of $CD11b^+$ cells and neutrophils were found in spleen from IFN-γ-treated EAE mice compared to those from PBS-treated EAE mice; whilst macrophages were not significantly altered (Supplementary Figure 4).

Several studies have reported that in a neuroinflammatory or tumor microenvironment MG are induced to upregulate CD45 expression (5, 41–49). Consequently, an increase in the frequency of $CD45^{hi}$ cells would reflect the activation of $CD45^{low}$ MG into $CD45^{hi}$ cells resembling peripheral infiltrating MC (44–46). Our results showed that IFN-γ-treatment resulted in a significantly lower frequency and absolute number of activated MC/MG cells ($CD11b^+Ly6G^-CD45^{high}$) compared to PBS-treatment. In addition, IFN-γ-treatment induced a significant increase in the percentage of resting MG compared to PBS-treated EAE mice; but was still lower than NI mice (Figure 3E, F). Consistent with the activation status of these cell populations, activated MC/MG ($CD11b^+Ly6G^-CD45^{high}$) obtained from both IFN-γ- and PBS-treated EAE mice showed a significantly higher expression of MHC-II molecules, CD80, CD40, and PD-L1 than resting MG ($CD11b^+Ly6G^-CD45^{low}$) (Supplementary Figure 5).

Resting MG are also characterized by a ramified cell morphology with numerous thin processes that upon activation are drawn back into the soma, resulting in a rounded amoeboid-like appearance. In order to evaluate morphological changes associated with microglial activation, thoracic SC sections from NI mice and IFN-γ- and PBS-treated EAE mice were immunostained for Iba1, a known cell marker used to evaluate MC/MG morphology and activation (50–54). SC from PBS-treated mice were characterized by extensive Iba1 staining and amoeboid-shaped $Iba1^+$ cells. Instead, IFN-γ-treated mice had predominantly ramified-shaped, Iba1-stained cells similar to NI mice (Figure 4A). In addition, SC from IFN-γ-treated EAE mice showed the density of $Iba1^+$ cells, average $Iba1^+$ cell area (indicative of cell size), and percentage Iba1 coverage (indicative of simultaneous alterations in cell density and morphology) significantly reduced in comparison to PBS-treated mice, but similar to NI mice (Figure 4B–D).

IFN-γ also plays a protective role in preventing hindbrain neuroinflammation, an effect dependent on the interaction between IFN-γ and CNS cells (55–57). Therefore, changes in MG and myelination in the cerebellum obtained from EAE mice treated with IFN-γ or PBS by immunofluorescence were examined. A significantly higher expression of TMEM119, a recently described homeostatic marker for MG (11, 58), and of MBP staining was observed in response to IFN-γ compared to control treatment (Supplementary Figure 6; Method S1). Taken together, these results indicate that *in vivo* IFN-γ-treatment starting at the peak of EAE induces amelioration of clinical symptoms, reduction of body weight loss, attenuation of neuroinflammation associated with significantly less infiltration of inflammatory cells and demyelination, reduced activation of MC/MG, and enhanced expression of homeostatic microglial markers.

3.2 Ex vivo re-stimulation with low doses of IFN-γ and MOG_{35-55} induces tolerogenic and anti-inflammatory activity in MC/MG from IFN-γ-treated EAE mice

It has been reported that low concentrations of IFN-γ induce a tolerogenic phenotype in MG from neonatal mice capable of inducing regulatory T (Treg) cells (59). Thus, we were interested in determining the tolerogenic activity and phenotype of primary MC/MG cultures established from EAE-induced mice treated with

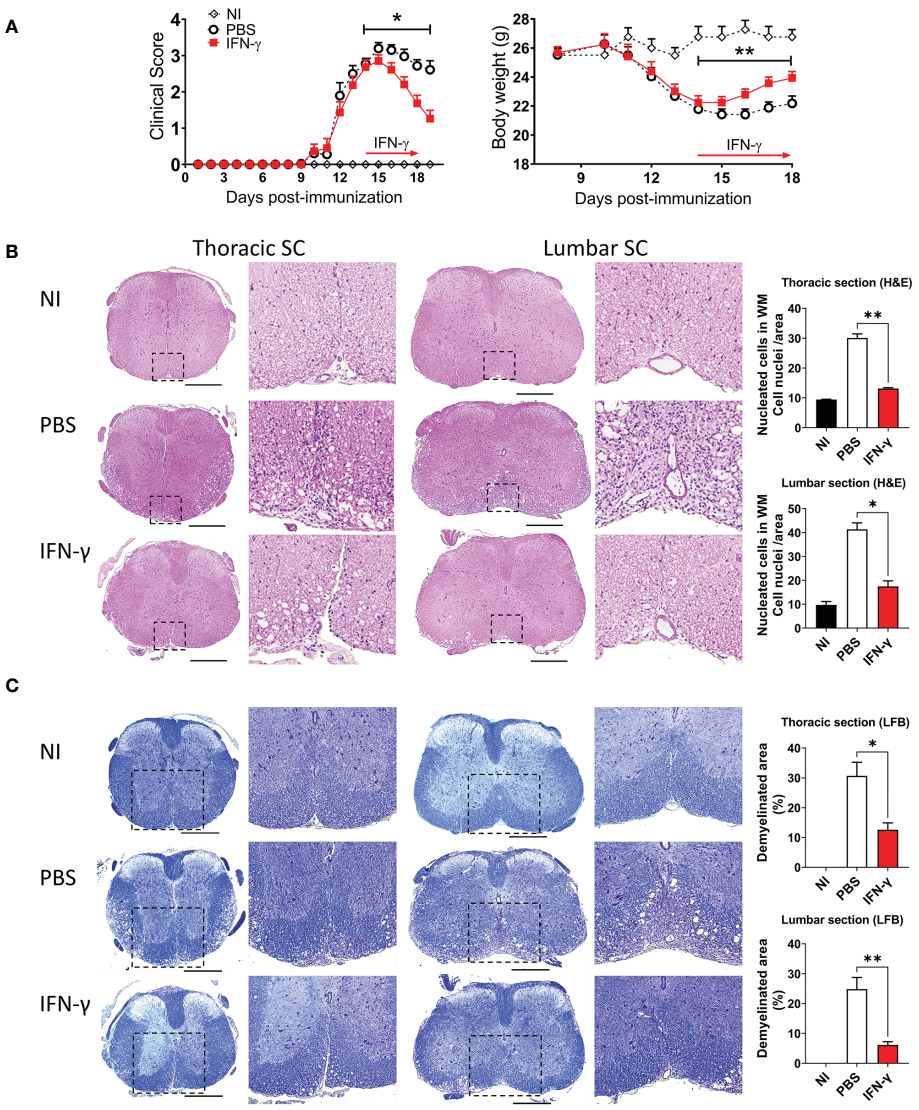

FIGURE 2
IFN-γ treatment induces disease amelioration and attenuation of neuroinflammation at the peak of EAE. **(A)** Clinical progression and body weight were monitored daily in non-immunized (NI) mice (white diamonds) and mice developing EAE treated with either PBS (black circles) or 1 µg IFN-γ (red squares) for 5 days at the peak of EAE. n= 5 mice per group; 5 independent experiments. **(B, C)** Thoracic and lumbar SC sections from NI, PBS-treated EAE, and IFN-γ-treated EAE mice were analyzed by histochemical staining for **(B)** H&E and **(C)** luxol fast blue. Representative microphotographs are shown. Scale bar is 500 µm. Dashed boxes show magnified image of infiltrated and demyelinated area. Infiltration of inflammatory cells and demyelination area was quantified as described in Methods. All measurements were performed on 3 serial sections per animal (n=5 mice per group). Results are shown as the mean ± SEM. *P <0.05; **P <0.01.

IFN-γ or PBS. First, cell cultures were *ex vivo* pre-conditioned with low doses (0.1, 1, and 10 ng/ml) of IFN-γ and MOG_{35-55}, and then co-cultured with $CD4^+$ T cells obtained from transgenic 2D2 mice for 96 h (Figure 1C). The results showed that MC/MG obtained from IFN-γ-treated EAE mice and *ex vivo* stimulated with 0.1 and 1 ng/ml IFN-γ induced a significantly higher frequency of Treg cells compared to untreated cells. Interestingly, *ex vivo* re-stimulation with 1 ng/ml IFN-γ and MOG_{35-55} induced a significantly higher frequency and absolute number of Treg cells in co-cultures containing MC/MG obtained from IFN-γ-treated EAE mice than in co-cultures containing MC/MG from PBS-treated EAE mice (Figure 5A). No differences in the expression of MHC-II, CD86, CD80, and CD40 in primary MC/MG obtained from either IFN-γ-treated EAE mice or PBS-treated mice and stimulated with low doses of IFN-γ and MOG_{35-55} were detected prior to culture with 2D2 $CD4^+$ T cells (Figure 5B). Cell culture supernatants obtained at the end of the co-cultures of pre-conditioned MC/MG and 2D2 $CD4^+$ T cells were analyzed by immunoassays. Cell co-cultures containing MC/MG obtained from IFN-γ-treated EAE mice had lower production of IFN-γ, TNF-α, and GM-CSF than conditioned cell co-cultures containing MC/MG obtained from PBS-treated EAE mice. However, only the secretion of IFN-γ in co-cultures containing MC/MG from IFN-γ-treated EAE mice and pre-conditioned with 10 ng/ml IFN-γ and MOG_{35-55} was statistically lower than in those from control mice. Interestingly, cell co-cultures containing MC/MG isolated from IFN-γ-treated EAE mice and *ex*

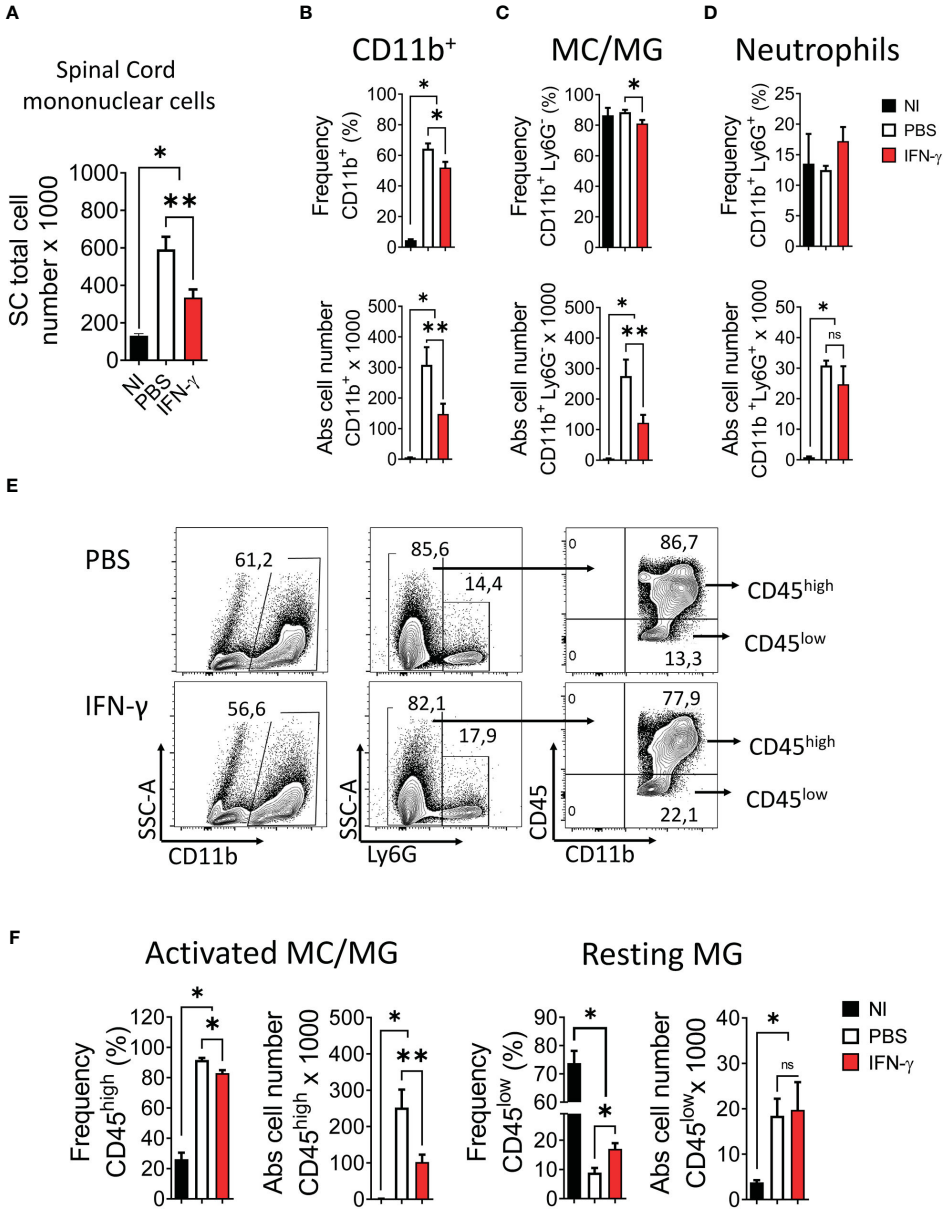

FIGURE 3
IFN-γ treatment induces a decrease in the number of spinal cord mononuclear cells, a reduction of activated myeloid cell/microglia, and an increase of resting microglia. SC from non-immunized (NI) mice (black bar) and mice developing EAE treated with either PBS (white bar) or 1 µg IFN-γ (red bar) were used to determine **(A)** number of mononuclear cells. **(B-D)** Frequency (top panel) and absolute cell number (bottom panel) of **(B)** $CD11b^+$ cells, **(C)** myeloid cell/microglia (MC/MG) ($CD11b^+Ly6G^-$), and **(D)** neutrophils ($CD11b^+Ly6G^+$) were determined by flow cytometry. **(E)** Flow cytometry gating for the determination of activated MC/MG ($CD11b^+Ly6G^-CD45^{high}$) and resting MG ($CD11b^+Ly6G^-CD45^{low}$). **(F)** Frequency and absolute cell number of activated MC/MG and resting MG were determined by flow cytometry. Values In flow cytometry plots indicate the percentage of positive cells in each gate or quadrant. n= 5 mice per group; 5 independent experiments. Results are shown as the mean ± SEM. *P <0.05; **P <0.01.

vivo pre-conditioned with 1 ng/ml IFN-γ and MOG_{35-55} showed a significantly higher production of total TGF-β than control co-cultures (Figure 5C). Furthermore, active TGF-β production was higher in co-cultures containing MC/MG isolated from IFN-γ-treated EAE mice and *ex vivo* conditioned with 1 and 10 ng/ml IFN-γ and MOG_{35-55} than control co-cultures (Figure 5C). In contrast, cell co-cultures containing MC/MG obtained from PBS-treated EAE mice and stimulated *ex vivo* with low doses of MOG_{35-55} alone or in combination with IFN-γ produced significantly lower levels of active TGF-β than unstimulated cell co-cultures. There was no difference in the production of IL-4, IL-10, IL-2, and IL-1β between both groups of co-cultures. These results suggest that *ex vivo* re-stimulation with low doses of IFN-γ and MOG_{35-55} endow MC/MG with the capacity to induce conversion of $CD4^+$ T cells into Treg cells in association with high secretion of TGF-β.

Since nitric oxide (NO) is recognized as an important effector molecule produced by macrophages and microglia in response to inflammation (60), we evaluated NO production. Pre-conditioned MC/MG cultures obtained from IFN-γ-treated EAE mice produced significantly lower nitrite in response to LPS stimulation than those

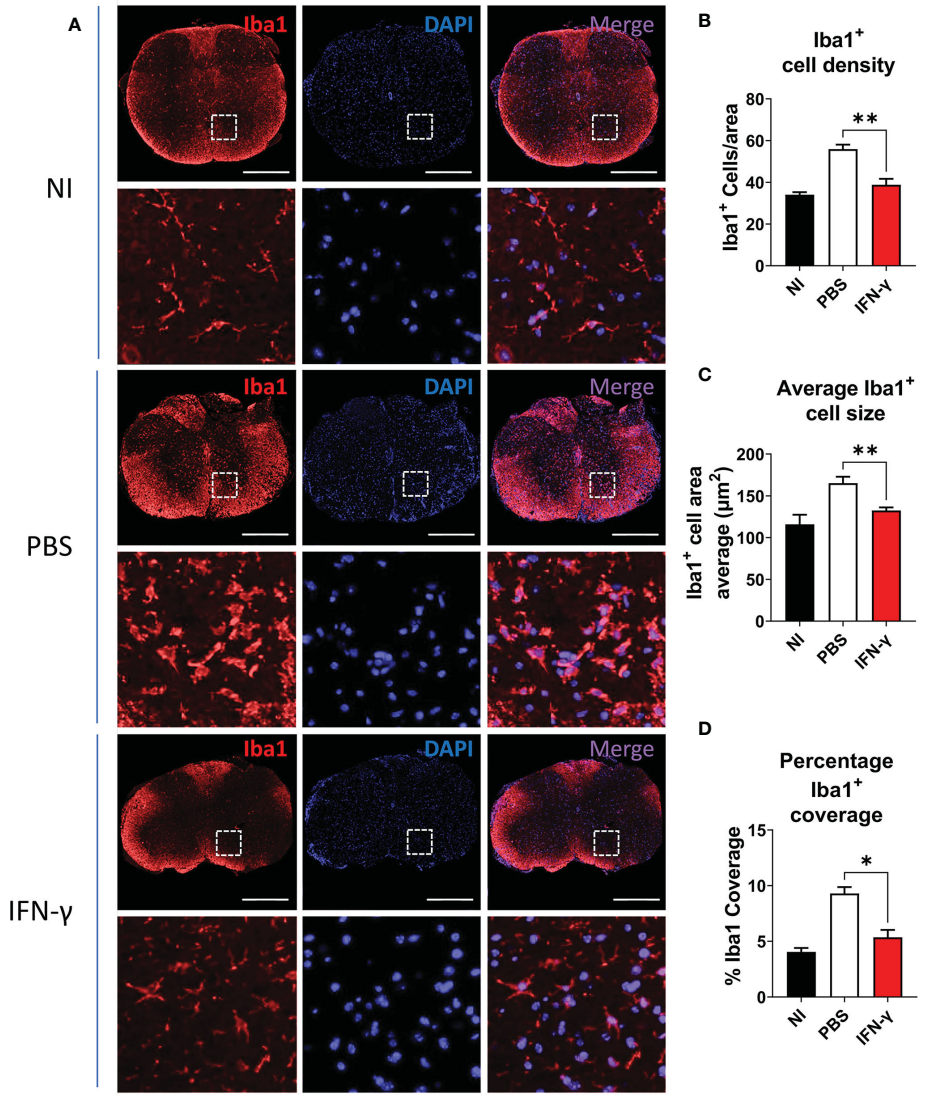

FIGURE 4
IFN-γ treatment reduces myeloid cell/microglia activation in EAE mice. **(A)** Representative microphotographs of thoracic SC sections from non-immunized (NI) mice, PBS-treated EAE mice (PBS), and IFN-γ-treated EAE mice (IFN-γ) immunostained for Iba1 (red). Cell nuclei were labeled with DAPI (blue). **(B–D)** Determination of **(B)** density of Iba1$^+$ cells (number of Iba1$^+$ cells per area), **(C)** average Iba1$^+$ cell area, and **(D)** percentage Iba1 coverage (percentage of the total section area occupied by Iba1$^+$ cells). All measurements were performed on 3 serial sections per animal (n=5 mice per group). Scale bar is 500 μm. Results are shown as the mean ± SEM. *P <0.05; **P <0.01.

from PBS-treated EAE mice (Figure 5D). Taken together, these results show that *ex vivo* re-stimulation with low doses of IFN-γ and MOG_{35-55} induces tolerogenic and anti-inflammatory activity in MC/MG.

3.3 In vivo IFN-γ-treatment induces increased frequency of CX3CR1^{high}PD-L1^{low} MG in a STAT-1-dependent manner

Next, we examined the expression of MHC class II molecules, costimulatory molecules (CD80, CD86, CD40), coinhibitory molecules (PD-L1), and a microglial marker (CX3CR1) in MC/MG obtained from IFN-γ and PBS-treated EAE mice by flow cytometry (Supplementary Figure 7A). Interestingly, we found that *in vivo* IFN-γ treatment induced a significantly higher expression of CX3CR1 in MC/MG cells than in control cells (Figure 6A). In turn, an analysis of CX3CR1^{high}CD11b$^+$Ly6G$^-$ cells showed that IFN-γ treatment induced a significantly higher frequency of these cells expressing low PD-L1 (Figure 6B; Supplementary Figure 7B). There was no difference in the absolute number of CX3CR1^{high}PD-L1^{low}CD11b$^+$Ly6G$^-$ cells from mice treated with IFN-γ or PBS. However, the total number of live mononuclear cells isolated from the SC of IFN-γ-treated EAE mice was almost half of PBS-treated EAE mice (Figure 3A). These CX3CR1^{high}PD-L1^{low}CD11b$^+$Ly6G$^-$ cells were 75-85% TMEM119$^+$ (Supplementary Figure 8A). In addition, CX3CR1^{high}PD-L1^{low}CD11b$^+$Ly6G$^-$ cells showed a strong expression of gene markers for MG and weak expression for MC, oligodendrocytes, and astrocytes (Supplementary Figure 8B). Therefore, these results strongly suggest that this cell subpopulation is an enriched subset of CX3CR1^{high} MG expressing low PD-L1

10.3389/fimmu.2023.1191838

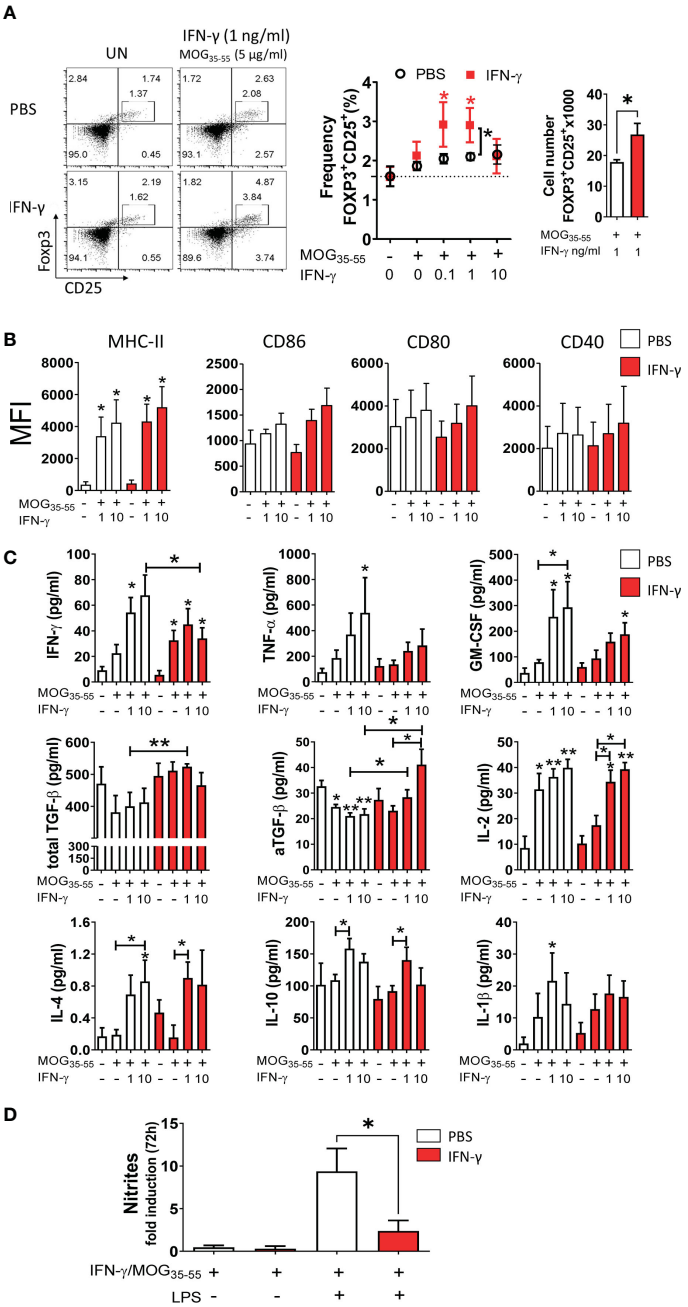

FIGURE 5
Ex vivo re-stimulation with low doses of IFN-γ and MOG_{35-55} induces tolerogenic activity in myeloid cell/microglia from IFN-γ-treated EAE mice. **(A)** Primary MC/MG culture from EAE mice treated with IFN-γ (red squares) or PBS (white circles) were *ex vivo* pre-conditioned with low concentrations of IFN-γ (0.1, 1, and 10 ng/ml) for 24 h, incubated with 5 μg/ml MOG_{35-55} for an additional 24 h, and then co-cultured with purified $CD4^+$ T cells obtained from spleens of transgenic 2D2 mice for 96 h. The frequency of Treg cells ($CD4^+CD25^{high}FoxP3^+$) was determined by flow cytometry. Representative flow cytometry plots and frequency and cell number of Tregs in co-cultures containing untreated (UN) or pre-conditioned MC/MG with 1 ng/ml IFN-γ and 5 μg/ml MOG_{35-55} is shown. **(B)** The cell surface expression, shown as median fluorescence intensity (MFI), of MHC-II molecules, CD86, CD80, and CD40 was determined by flow cytometry in primary MC/MG obtained from EAE mice treated with IFN-γ (red bars) or PBS (white bars) and pre-conditioned with 1 or 10 ng/ml IFN-γ and 5 μg/ml MOG_{35-55} prior to culture with 2D2 $CD4^+$ T cells. **(C)** Secretion of IFN-γ, TNF-α, GM-CSF, IL-2, IL-4, IL-10, and IL-1β was determined by multiplex assay and the production of TGF-β by ELISA in cell culture supernatants from co-cultures between 2D2 $CD4^+$ T cells and pre-conditioned MC/MG. **(D)** Production of nitrites was determined by Griess assay in primary MC/MG obtained from EAE mice treated with IFN-γ (red bars) or PBS (white bars) pre-conditioned with 1 ng/ml IFN-γ and 5 μg/ml MOG_{35-55} (IFN-γ/MOG_{35-55}) and challenged with 1 μg/ml LPS for 72 h. Results are shown as mean ± SEM of five independent experiments. *Comparison between unstimulated cell cultures and cell cultures stimulated with IFN-γ. Other relevant comparisons are shown with brackets. *P <0.05; **P <0.01. aTGF-β: active transforming growth factor.

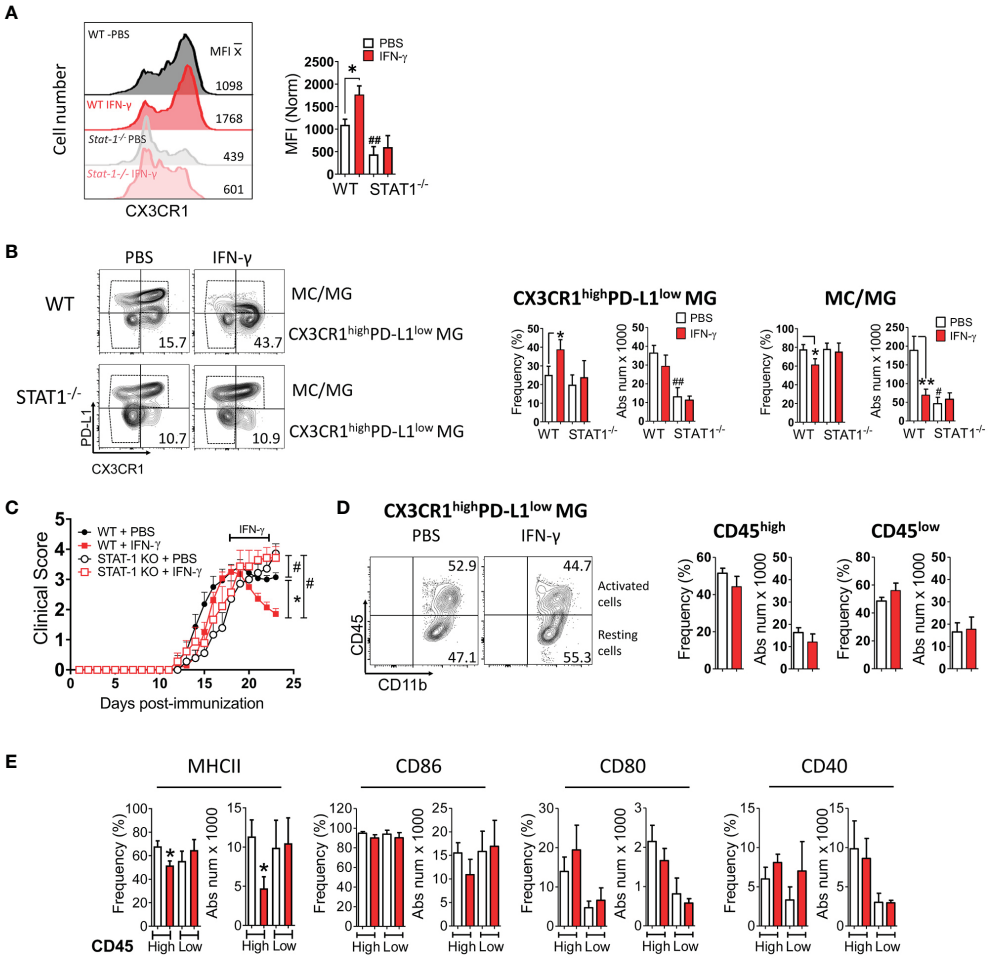

FIGURE 6
In vivo IFN-γ-treatment induces increased frequency of CX3CR1^{high}PD-L1^{low} MG in a STAT-1-dependent manner. Mononuclear cells from SC of EAE WT and STAT-1$^{-/-}$ mice treated with IFN-γ or PBS for 5 days at the peak of EAE were analyzed by flow cytometry. **(A)** The expression level of CX3CR1. **(B)** Frequency and absolute cell number of CX3CR1^{high} PD-L1^{low} MG and MC/MG in WT and STAT-1$^{-/-}$ mice treated with IFN-γ or PBS. **(C)** EAE progression in WT (filled symbols) and STAT-1$^{-/-}$ (empty symbols) mice treated with IFN-γ (red line) or PBS (black line) for 5 days at the peak of EAE. **(D)** Frequency and absolute cell number of activated (CD11b^{+}CD45^{high}) and resting (CD11b^{+}CD45^{low}) CX3CR1^{high}PD-L1^{low} MG and **(E)** their expression of MHC-II, CD86, CD80, and CD40 molecules. *Comparison between mice or cells obtained from IFN-γ-treated EAE mice and control cells obtained from PBS-treated EAE mice. *P <0.05; **P <0.01. $^{\#}$Comparison between mice or cells obtained from WT and STAT1$^{-/-}$ mice. $^{\#}$P <0.05; $^{\#\#}$P <0.01. MFI, median fluorescence intensity.

(CX3CR1^{high}PD-L1^{low} MG). The remaining cells were 47-52% TMEM119^{+} (Supplementary Figure 8A) and were considered MC/MG. A significantly lower frequency and absolute number of MC/MG was observed in SC from IFN-γ-treated EAE mice than in SC from PBS-treated EAE mice (Figure 6B). Interestingly, NI mice exhibited a significantly higher frequency and absolute number of CX3CR1^{high}PD-L1^{low} MG (60.2% ± 5.4%) than MC/MG (39.5% ± 5.6%) (Supplementary Figure 9A).

To determine whether the increase in CX3CR1^{high}PD-L1^{low} MG induced by IFN-γ is due to proliferation, mice treated with IFN-γ or PBS received a simultaneous i.p. injection of 5-bromo-2´-deoxyuridine (BrdU) starting at the peak of EAE. After 5 days, mononuclear cells were isolated from SC, and the frequency of proliferating CX3CR1^{high}PD-L1^{low} MG was analyzed by flow cytometry. The results showed that there was no difference in the frequency of proliferating CX3CR1^{high}PD-L1^{low} MG between EAE mice treated with IFN-γ or PBS, suggesting that enhanced CX3CR1^{high}PD-L1^{low} MG induced by IFN-γ might be explained by microglial plasticity (Supplementary Figure 9; Method S2).

To obtain mechanistic insight into the induction of CX3CR1^{high}PD-L1^{low} MG by IFN-γ, mice lacking STAT-1, the major STAT activated in response to engagement of IFN-γ receptor, were induced with EAE and then treated with IFN-γ for 5 days starting at the peak of disease. IFN-γ treatment had no effect on disease progression in EAE-induced *Stat-1*$^{-/-}$ mice (Figure 6C). Furthermore, the lack of STAT-1 inhibited the IFN-γ-induced expression of CX3CR1 in MC/MG cells (Figure 6A), suppressed the increase of CX3CR1^{high}PD-L1^{low} MG, and reversed the decreased frequency of MC/MG induced by IFN-γ in WT mice (Figure 6B). We thus conclude that the IFN-γ/STAT-1 signaling axis is involved in symptom amelioration and induction of CX3CR1^{high}PD-L1^{low} MG in EAE.

Next, we analyzed the impact of IFN-γ-treatment on the activation state and the expression of MHC-II molecules and costimulatory molecules in CX3CR1^{high}PD-L1^{low} MG from EAE-

10.3389/fimmu.2023.1191838

induced WT mice treated with IFN-γ or PBS. A similar frequency of activated (51.5 ± 6%) and resting (44.2 ± 12%) CX3CR1^{high}PD-L1^{low} MG was found in SC from IFN-γ- and PBS-treated EAE mice (Figure 6D). However, activated CX3CR1^{high}PD-L1^{low} MG from IFN-γ-treated EAE mice exhibited a significantly lower frequency and absolute number of cells expressing MHC-II molecules than cells from PBS-treated EAE mice (Figure 6E). There was no significant difference in the frequency or absolute number of cells expressing CD80, CD86, or CD40 between CX3CR1^{high}PD-L1^{low} MG from IFN-γ- and PBS-treated EAE mice. Interestingly, in NI mice most of CX3CR1^{high}PD-L1^{low} MG (91.9% ± 4.2%) were in a resting state and had significantly lower frequency of cells expressing CD40 compared to activated cells, whereas the expression of MHC-II molecules, CD86, and CD80 were not statistically significant (Supplementary Figure 9B).

3.4 Differential gene expression profile of MG isolated from IFN-γ or PBS-treated EAE mice

We next wanted to identify genes and signaling pathways in which IFN-γ may be differentially regulating the activity of CX3CR1^{high}PD-L1^{low} MG in EAE by analyzing the transcriptional profile of these cells. CX3CR1^{high}PD-L1^{low} MG were isolated from IFN-γ- and PBS-treated EAE mice for FACS sorter (97.5% purity), and the transcriptional profile was analyzed by RNAseq. A total of 12,524 genes were detected above the threshold (see Methods), with 336 genes upregulated and 188 down-regulated after IFN-γ treatment (Figure 7A). Using more stringent criteria, lowering the p-value to 0.01, setting the Log2 Fold change to a minimum of 1.0, and raising the threshold of minimum expression to 40 read units,

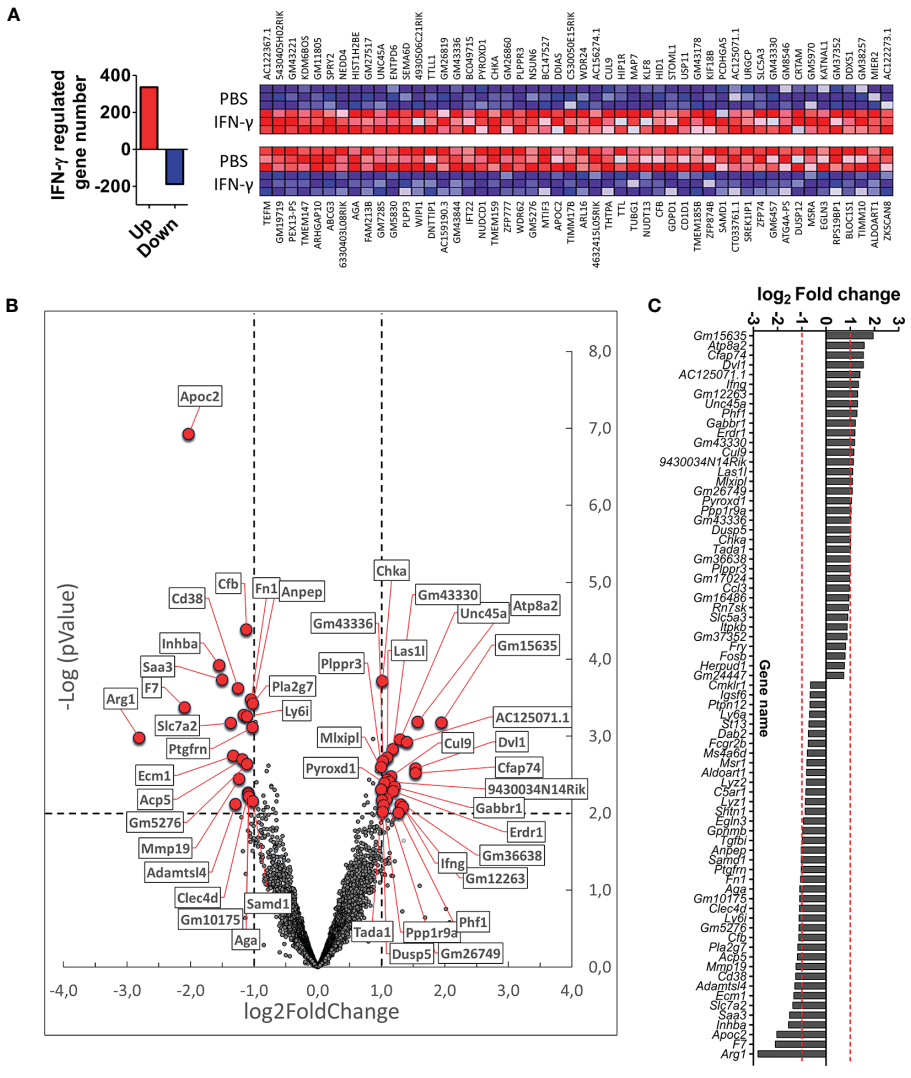

FIGURE 7
Differential gene expression profile in CX3CR1^{high}PD-L1^{low} MG in response to *in vivo* IFN-γ-treatment. Gene expression profile was analyzed on RNA obtained from CX3CR1^{high} MG expressing low PD-L1 purified from SC of IFN-γ or PBS-treated EAE mice by RNA sequencing (RNA-seq). **(A)** Left panel, total number of genes up (red bar)- and down (blue bar)-regulated by IFN-γ treatment; right panel, heat map showing the top 100 up (red squares)- and down (blue squares)-regulated genes in CX3CR1^{high}PD-L1^{low} MG from IFN-γ-treated mice versus those cells from PBS-treated mice. **(B)** Volcano plot showing up- and down-regulated genes induced by IFN-γ in CX3CR1^{high}PD-L1^{low} MG from IFN-γ-treated mice. **(C)** Gene expression analysis using more stringent criteria by lowering the p-value to 0.01, setting the Log2 Fold change to a minimum of 1.0, and by raising the threshold of minimum expression to 40 units. n= 3 independent samples per group.

resulted in 25 upregulated and 22 down-regulated genes in response to IFN-γ (Figures 7B, C). Interestingly, the gene expression of *ATPase phospholipid transporting 8A2* (*Atp8a2*), a selective microglial gene marker, and several genes associated with anti-inflammatory processes such as *dual-specificity phosphatase 5* (*Dusp5*), *MLX interacting protein-like* (*Mlxipl*, *ChREBP*), *dishevelled segment polarity protein 1* (*Dvl1*) and *gamma-aminobutyric acid type B receptor subunit 1* (*Gabbr1*), were upregulated in IFN-γ-treated EAE CX3CR1^{high}PD-L1^{low} MG (Figures 7B, C; Table 2). Several genes associated with M1 inflammatory activity such as the *cd38 molecule* (*Cd38*), *complement factor B* (*Cfb*), *inhibin subunit Beta A* (*Inhba*), *serum amyloid A3* (*Saa3*), *and* APN-like peptidase cytosolic alanyl-aminopeptidase *(Anpep)* were down-regulated in IFN-γ-treated EAE CX3CR1^{high}PD-L1^{low} MG (Figures 7B, C; Table 2). Unexpectedly, *arginase 1* (*Arg1*), a M2 classic gene, was down-regulated in CX3CR1^{high}PD-L1^{low} MG from IFN-γ-treated EAE mice. However, the cationic amino acid transporter 2 (*Slc7a2*), a gene involved in the uptake of arginine, was also down-regulated, suggesting a decreased substrate availability for NO production in these cells (Figures 7B, C; Table 2).

3.5 IFN-γ-treatment induces an anti-inflammatory profile in MG

To determine if any molecular pathways were differentially regulated in CX3CR1^{high}PD-L1^{low} MG by IFN-γ, changes in the

TABLE 2 Role of genes regulated by IFN-γ.

Up	Name	Activity	Role	Ref
Atp8a2	ATPase Phospholipid Transporting 8A2	Lipid flipping: generating and maintaining asymmetry in membrane lipid	Selective microglial marker	(117)
Dusp5	Dual specificity phosphatase 5	Mitogen-activated protein kinase phosphatase	Inhibits production of TNF-α and IL-6 by inactivating ERK 1/2 pathway	(61, 62)
Mixipl (ChREBP)	Carbohydrate-responsive element binding protein	Transcription factor involved in regulation and maintenance of macrophages redox status	Prevents macrophage inflammatory responses	(63)
Dvl1	Dishevelled Segment Polarity Protein 1	Cytoplasmic phosphoprotein	Participates in the Wnt/β-catenin signaling pathway inducing tolerogenic DC	(64, 65)
Gabbr1	Gamma-Aminobutyric Acid Type B Receptor Subunit 1	Metabotropic GABAB inhibitory G-coupled receptor	Inhibits LPS-induced IL-6 and IL-12p40 expression in microglia	(66, 67)
Ifn-y	Interferon-y	Cytokine	Pro- and anti-inflammatory role	(19)
Down	**Name**	**Activity**	**Role**	**Ref**
Cd38	CD38	Transmembrane enzyme that synthesizes and hydrolyzes cADP-ribose	Associated to M1 macrophages activity inducing activation of iNOS and production of TNF-α, IL-6 and IL-1β. EAE mice lacking CD38 showed ameliorated disease.	(68–71)
Cfb	Complement Factor B	Component of the alternative pathway complement activation	Associated to M1 macrophages activity. Enhanced expression of Cfb in microglia is associated with late stages of neurodegeneration. Inhibition of alternative complement pathway in EAE attenuated the chronic phase of disease.	(72)
Inhba	Inhibin Subunit Beta A (Activin A)	Member of TGF-β- superfamily proteins	Induces M1 macrophage polarization and is considered a canonical M1 marker. Blocking anti-Activin A antibody reduced M1 macrophage polarization	(73, 74)
Saa3	Serum amyloid A3	Acute phase lipoprotein	Associated to M1 macrophage activity. Considered a pro-inflammatory biomarker involved in releasing active IL-1β by the activation of the NLRP3 inflammasome in LPS-induced microglia	(75–77)
Anpep	Alanyl Aminopeptidase, membrane (CD13)	aminopeptidase	Involved in adhesion of monocytes to endothelial cells and trafficking toward inflammation. Pharmacological inhibition of ANPEP induced amelioration of EAE.	(110–111)
Slc7a2	Solute Carrier Family 7 Member 2 (CAT2)	Cationic amino acid transporter	Responsible for the cellular uptake of arginine, lysine, and ornithine. Controls critical aspects of macrophage activation	(78)
Arg 1	Arginase 1	Catalyzes the hydrolysis of arginine to ornithine	A canonical M2 marker	(73)

transcriptional profile were analyzed by gene set enrichment analysis (GSEA) using different reference databases. Using Gene Ontology (GO) biological processes and Reactome databases, we found that gene sets corresponding to RNA transcription and nucleus-cytoplasmatic transporter activity were highly and significantly upregulated in CX3CR1^{high}PD-L1^{low} MG from IFN-γ-treated EAE mice, compared to the control group ($p< 0.001$); indicating enhanced transcriptional and translational activities in response to IFN-γ stimulation (Figure 8A). The Kyoto Encyclopedia of Genes and Genomes (KEGG) analysis showed that the top enriched gene set induced by IFN-γ were related to signaling transduction pathways (MAPK and RIG I like receptor), transcription factors (Basal transcription factors), and metabolism (Methionine and Glycerolipids metabolism), which might be

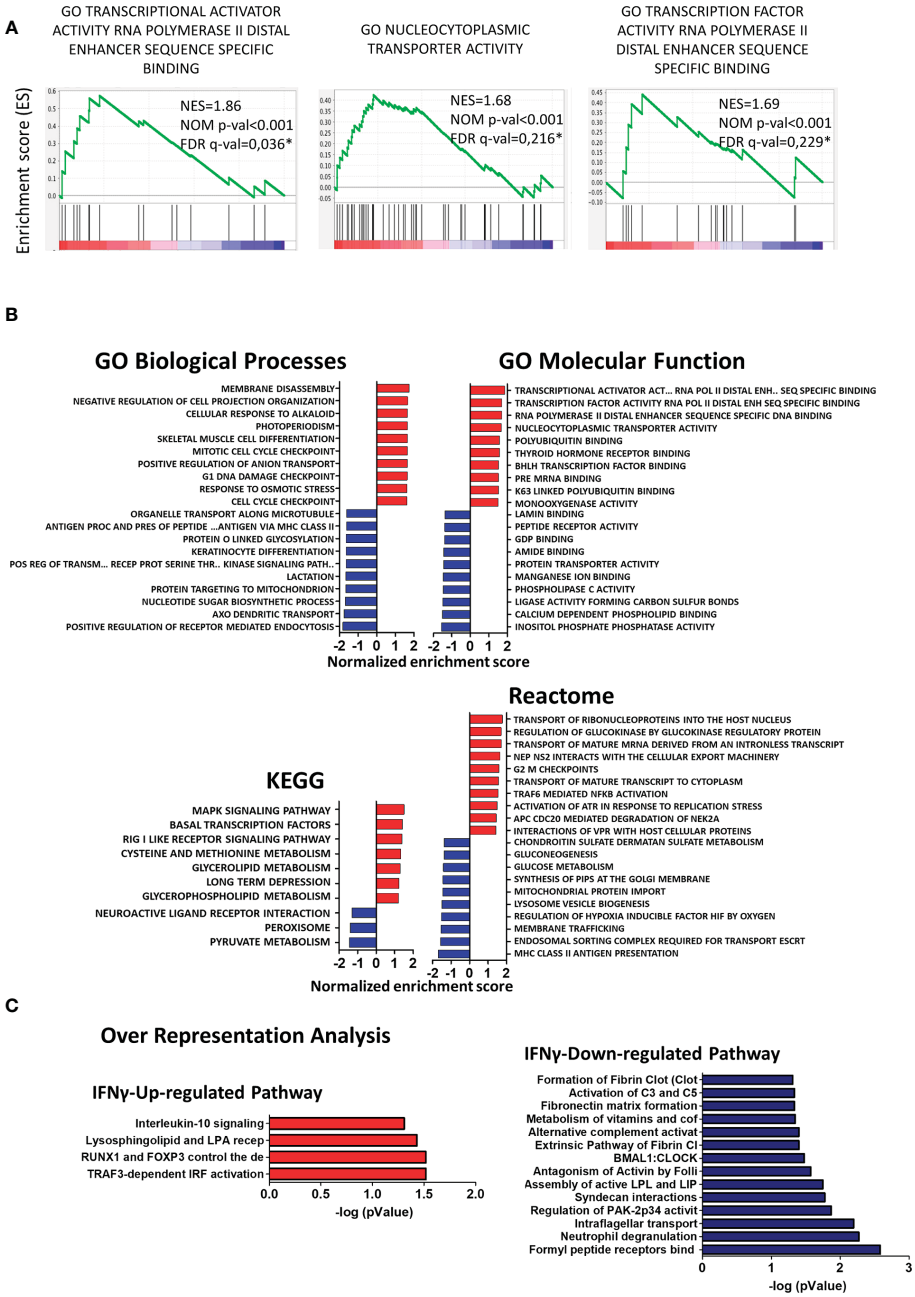

FIGURE 8
Gene set enrichment analysis (GSEA) and over-representation analysis in CX3CR1^{high}PD-L1^{low} MG in response to *in vivo* IFN-γ-treatment. GSEA enrichment score plots show **(A)** up-regulation of gene sets corresponding to RNA transcription and to nucleus-cytoplasmatic transporter activity in CX3CR1^{high}PD-L1^{low} MG from IFN-γ-treated EAE mice compared to those cells from PBS-treated EAE mice. Each bar at the bottom of each panel represents a member gene of the respective pathway and shows its relative location in the ranked list. **(B)** Normalized enrichment scores indicate the distribution of Gene Ontology categories across a list of genes ranked by hypergeometrical score (HGS). Higher enrichment scores indicate a shift of genes belonging to certain GO, KEGG, or Reactome categories toward either end of the ranked list, representing up or down-regulation (positive or negative values, respectively). **(C)** Over-representation analysis showing significantly up- and down-regulated cellular pathways in MG from IFN-γ-treated EAE mice compared to MG from PBS-treated EAE mice. n=3 independent samples per group.

10.3389/fimmu.2023.1191838

related to a change in the activation pattern, oxidative status and lipid-related metabolism associated with a decreased inflammatory profile. Instead, downregulated enriched gene sets in CX3CR1^{high}PD-L1^{low} MG from IFN-γ-treated EAE mice were associated with oxidative metabolism (pyruvate metabolism), lipid metabolism, nitric oxide induction (peroxisome), and G-protein coupled receptor-associated to a neuroantigen response (neuroactive ligand-receptor interaction) (Figure 8B). Remarkably, over-representation analysis using the Reactome database showed that IFN-γ significantly induced an anti-inflammatory profile in EAE MG. Regarding immune cell function, genes in the TRAF3-dependent IRF activation pathway and Interleukin-10 signaling pathway were upregulated, while neutrophil degranulation, alternative complement activation, and activation of C3 and C5 pathways were down-regulated in CX3CR1^{high}PD-L1^{low} MG from IFN-γ-treated EAE mice (Figure 8C). Taken together, these results confirm that IFN-γ is a key inducer of anti-inflammatory pathways and suppressor of inflammatory mechanisms in EAE MG.

Because our results indicate the importance of IFN-γ/STAT-1 axis in the induction of CX3CR1^{high}PD-L1^{low} MG in EAE, STAT-1 target genes were analyzed in our RNAseq database using the Harmonizome database ($p< 0.05$) (79). The analysis revealed that 8 genes (*Cfb, Dusp5, Anxa4, Neurl1b, C3, Naca, Anxa11, Slc15a2*) were regulated by STAT-1. Using more stringent criteria ($p< 0.01$), Cfb and Dusp5 were functionally associated with STAT-1.

3.6 IFN-γ establishes tight connections with clusters of down-regulated inflammatory genes and with upregulated anti-inflammatory genes

In order to search for molecular connections among genes regulated by IFN-γ-treatment, a molecular network of protein-protein interactions has been constructed based on the known interactions between the gene products of the 25 up- and 22 down-regulated genes by IFN-γ using the STRING database. Some regulated genes could not be considered because no interacting proteins were found in the STRING database. This resulted in 31 regulated gene products (primary nodes), 13 up-regulated, and 18 down-regulated by IFN-γ-treatment, with various numbers – up to 100 – of interacting proteins (secondary nodes) with each primary node. All secondary nodes were then searched for their occurrence in columns of at least two regulated gene products (Figure 9A). Inserting edges (connections) of all primary nodes with secondary nodes identified in their respective columns gave rise to the molecular network displayed in Figure 9. As expected, *Ifn-γ* interacted with secondary nodes associated with inflammation, such as TNF-α, IL-6, IL-4, TGF-β1, or IL-10 (Figure 9A). Interestingly, we also found that *Ifn-γ* associated with secondary nodes interacting with three clusters of down-regulated inflammatory genes (cluster 1: *Inhba, Cfb, and F7; cluster 2: Saa3, Cd38, and Anpep; cluster 3: acid phosphatase 5, tartrate resistant* (*Acp5*), *c-type lectin domain family 4 member d* (*Clec4d*), *and Arg1*) and with secondary nodes interacting with up-regulated genes associated with anti-inflammatory roles (*Dusp5, Mlxipl, and Gabbr1*) (Figures 9A, B; Table 2).

4 Discussion

The role of IFN-γ in EAE and MS is still controversial, with evidence supporting both a pathogenic and beneficial function. Some studies have suggested that IFN-γ may have dual activity in these diseases depending on the dose, target cell, and stage of the disease [reviewed in (19–21)]. However, the neuroprotective mechanisms of IFN-γ in EAE remain largely unclear. It is shown here, for the first time, that IFN-γ has therapeutic activity at the peak of EAE by suppressing neuroinflammation and inducing tolerogenic activity of MC/MG and STAT-1-dependent homeostatic adaptation of MG.

Our results showed that IFN-γ-treatment resulted in a significant amelioration of clinical symptoms and reduction of body weight loss. Consistently, SC from IFN-γ-treated EAE mice had significantly less infiltration of inflammatory cells and fewer demyelinated areas. Furthermore, dampening of neuroinflammation by IFN-γ was associated with decreased frequency of CNS infiltrating CD11b$^+$ cells and activated MC/MG and increased frequency of resting MG. Decrease of absolute cell number of CD11b$^+$ cells was associated with a selective decrease in the absolute cell number of activated CD45^{high} cells without changes in the absolute cell number of resting CD45^{low} cells. This effect could reflect a decreased infiltration of peripheral MC, a deactivation of CD45^{high} activated MC/MG or both processes induced by treatment with IFN-γ. We have found no significant difference in the total numbers of cells in lymph nodes and spleen from IFN-γ- and PBS-treated EAE mice. However, splenic CD11b$^+$ cells and neutrophils were significantly reduced in EAE mice treated with IFN-γ; whilst macrophages were not significantly altered. Further studies will be necessary to determine if other peripheral subsets of CD11b$^+$ cells are influenced by IFN-γ. In addition, we have found a similar number of cells and frequencies of CD4$^+$ T cells, Th1, and Th17 cells in the periphery and the CNS of IFN-γ- and PBS-treated EAE mice (unpublished data). Although IFN-γ did not affect macrophages, these results suggest that IFN-γ might also have a protective role in EAE decreasing the abundance of neutrophils and some other peripheral subset of CD11b$^+$ cells, which might indirectly contribute to downregulate MG activation. However, induction of tolerogenic and anti-inflammatory activity in primary MC/MG cultures from the spinal cord of IFN-γ-treated EAE mice by *ex vivo* re-stimulation with low doses of IFN-γ and MOG_{35-55} argues for a direct regulatory role of IFN-γ on these cells. Supporting this view, several studies have demonstrated a direct protective role of IFN-γ in the CNS as well as on MG. Intracerebroventricular (i.c.v.) administration of IFN-γ or intrathecal delivery of an IFN-γ expression system in EAE mice resulted in suppression of clinical symptoms (33, 34). *In vitro* assays have shown that IFN-γ treatment enabled MG to restore homeostasis by promoting neuroprotection, neurogenesis and glutamate clearance (80–82). In turn, i.c.v. injection of IFN-γ-treated MG during the inductive phase of EAE significantly delayed the onset of the disease compared to control mice (83). Remarkably, silencing IFN-γ signaling in MG significantly enhanced EAE severity accompanied by a significant increase in the total number mononuclear cells and in the absolute number of CD11b$^+$, CD11b$^+$CD45^{lo}, CD11b$^+$CD45^{high}, CD11c$^+$, Gr-1$^+$, CD4$^+$, Th1, and

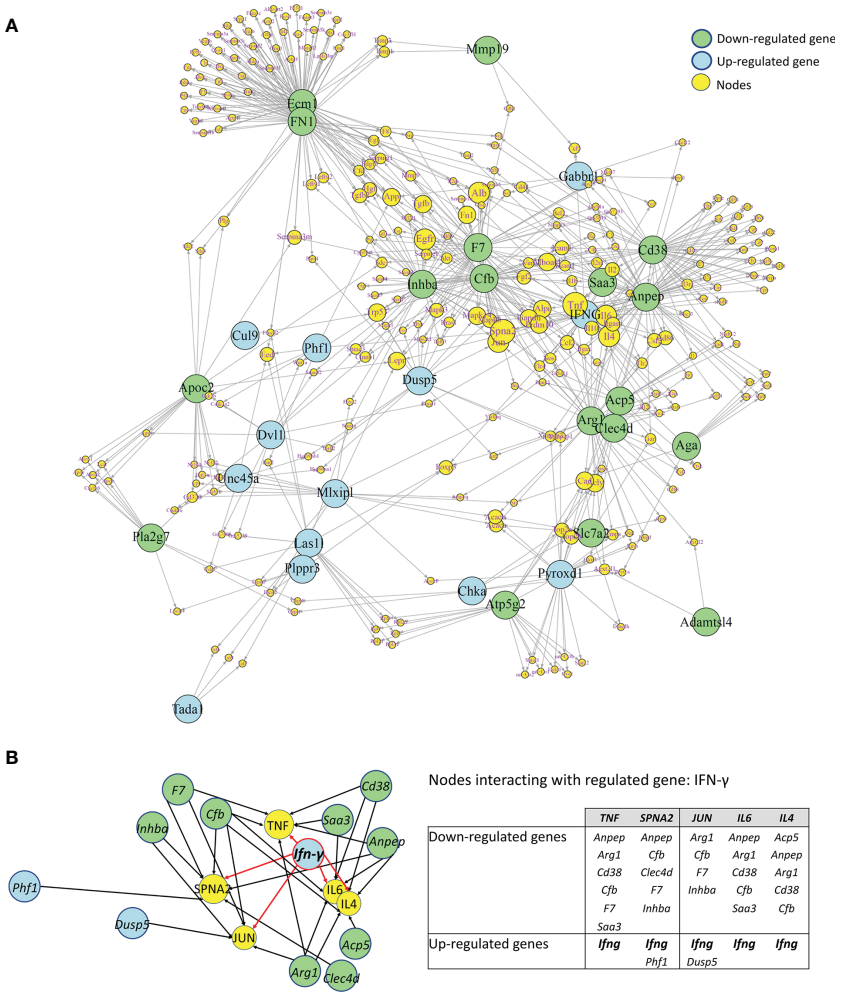

	TNF	SPNA2	JUN	IL6	IL4
Down-regulated genes	Anpep Arg1 Cd38 Cfb F7 Saa3	Anpep Cfb Clec4d F7 Inhba	Arg1 Cfb F7 Inhba	Anpep Arg1 Cd38 Cfb Saa3	Acp5 Anpep Arg1 Cd38 Cfb
Up-regulated genes	**Ifng**	**Ifng** Phf1	**Ifng** Dusp5	**Ifng**	**Ifng**

FIGURE 9
Molecular Network of differentially regulated genes by IFN-γ in CX3CR1^{high}PD-L1^{low} MG. **(A)** A molecular network of protein-protein interactions based on the known interactions between the gene products of 31 regulated genes regulated by IFN-γ in an enriched subset of CX3CR1^{high}PD-L1^{low} MG. Blue and green circles show down- and upregulated genes by IFN-γ, respectively. Yellow circles represent secondary nodes (connector genes), and their size represents the number of connections with regulated genes. Lines indicate the interaction of regulated genes with connector genes. **(B)** An enlarged area of the molecular network showing that *Ifn-γ* associated with connectors (yellow circles) interacting with three clusters of down-regulated inflammatory genes (green circles) as well as with connectors interacting with upregulated genes (blue circles) associated with anti-inflammatory roles. The table summarizes the up- and down-regulated genes by IFN-γ that interact with each connector.

Th17 cells in both spinal cords and brainstems (84). These findings are consistent with our results showing that IFN-γ treatment significantly reduces the total number of mononuclear cells and CD11b$^+$ cells in spinal cord of EAE mice and demonstrate that IFN-γ signaling in MG plays an important role in controlling CNS cell infiltration and MG activation. On the other hand, a previous report using bone marrow chimeras showed that the protective effect of IFN-γ in EAE is mediated by an increased production of nitric oxide (NO) at the level of both the periphery and the CNS. Peripheral mononuclear cells were identified as cells producing NO in the periphery whereas the authors suggested that microglia and astrocytes could be involved in the IFN-γ-driven NO production in the CNS (85). Taken together, the evidence suggests that IFN-γ can exert protective effects both in the periphery as in the CNS.

Importantly, immunohistochemistry analysis confirmed a significant increase in the percentage of resting microglia, characterized by a ramified morphology and reduced density and cell size, in response to IFN-γ. Furthermore, high expression of TMEM119, a homeostatic marker of MG, and of MBP1 was observed in the cerebellum from IFN-γ-treated EAE mice, supporting the notion that IFN-γ induces a shift of activated MG to a homeostatic profile. These results are in line with previous observations showing that IFN-γ plays an important role in EAE; regulating inflammation of specific regions of the CNS (55–57, 86).

Ex vivo re-stimulation with low doses of IFN-γ (1 ng/ml) and MOG_{35-55} of primary MC/MG cultures obtained from IFN-γ-treated EAE mice resulted in conversion of CD4$^+$ T cells into Treg cells associated with higher secretion of TGF-β. Consistently, we have found a significant increase of Treg cells in spinal cord from IFN-γ-treated EAE mice compared to that of the PBS-treated EAE mice (unpublished data). In line with our results, low concentrations of IFN-γ induce a tolerogenic phenotype in MG

from neonatal mice, characterized by the expression of intermediate levels of MHC-II and increased secretion of IL-10, capable of inducing Treg cells (59). Supporting our results, a recent study showed that microglia require IFN-γ-signaling to shape the Treg cell compartment in relapsing-remitting EAE and that the absence of microglial IFN-γ-receptor results in worse disease (87). Another study showed that the administration of the microparticle MIS416 in EAE mice induced an IFN-γ-dependent expansion and suppressive function of Treg cells (88). Additionally, a direct role of IFN-γ on the conversion of $CD4^+CD25^-$ T cells to $CD4^+$ Treg cells has been reported in EAE (89). Taken together, these results suggest that IFN-γ exerts a tolerogenic role in EAE acting on Treg cells either directly or indirectly through MC/MG.

The contribution of Treg cells to the mechanisms that actively regulate the neuroinflammatory process in EAE has been unequivocally demonstrated (90, 91). Different treatments such as glatiramer acetate, indoleamine 2,3-dioxygenase (IDO), and IL-10 administration, suppress EAE progression promoting an increase in Treg cells (92, 93). In contrast, other treatments such as atorvastatin and trichostatin A suppress EAE progression in a Treg cell-independent manner, suggesting that Treg cells may not always be necessary for the protective effects of some treatments for EAE (94–96). In addition, Korn et al. reported that Treg cells expand in the periphery and accumulate in the CNS but are unable to suppress the proliferation of MOG_{35-55}-specific T effector cells from the CNS. Intrinsic resistance of CNS-derived T effector cells to suppression was associated with high production of IL-6 and TNF (97, 98). However, a subsequent report combining targeted depletion of Treg cells with intravital two-photon microscopy concluded that Treg cells mediate recovery from EAE by controlling cytokine production, proliferation, and motility of effector T cells in the CNS (99). Therefore, the activity of Treg cells can be understood as a dynamic process that would depend on the balance between Treg cells and effector T cells as well as the local inflammatory cytokine milieu (90). Additionally, crosstalk between Treg cells and local APC might be critical in modulating effector T cell pathogenicity (100). Our results showing a higher production of TGF-β and conversion of Treg cells in IFN-γ-treated primary MC/MG cultures obtained from IFN-γ-treated EAE mice are consistent with that model of regulation.

We found that MC/MG from EAE mice treated with IFN-γ had a higher expression of CX3CR1, in support of a recent study showing high expression of CX3CR1 in MG at the peak of EAE (10). CX3CR1 is highly expressed in MG (101, 102) as an alert receptor "sensing" the ligand CX3CL1 released by dying neurons. Importantly, lack of this receptor exacerbates inflammation and increases the expression of MHC class II molecules in microglial cells (12–14). In addition, we found that IFN-γ induced a higher frequency of MG with high expression of CX3CR1 and low expression of PD-L1, compared to MG obtained from PBS-treated EAE mice. Although PD-L1 is involved in maintaining immune tolerance and homeostasis through the regulation of T cell activation and differentiation in MS and EAE (103), low expression or absence of PD-L1 has also been related to a tolerogenic effect of APC. Consistent with our findings, low doses of IFN-γ were required to obtain optimal activation of type II macrophages, a subset of macrophages that have been shown to induce a Th2-type anti-inflammatory response after initial activation in an inflammatory environment. Interestingly, IFN-γ-primed type II-macrophages are characterized by an enhanced production of IL-10, reduced expression of IL-12, and low expression of PD-L1, CD40, and CD80. Furthermore, mice receiving IFN-γ-primed type II-activated macrophages were protected from EAE whereas those receiving classically activated macrophages developed EAE (104). In another study, TNF-treated semi-mature DC deficient in PD-L1 showed a stronger tolerogenic capacity in EAE protection compared to wild-type DC. PD-$L1^{-/-}$DC-treated EAE mice presented lower numbers of MOG-specific IFN-γ and IL-17 producing cells in the CNS whereas an increased production of the protective cytokines IL-10, IL-13, and IL-4, and reduced levels of IFN-γ and IL-17 were detected in the periphery. Therefore, absence of PD-L1 expression on semi-mature DC enhanced their tolerogenic activity in EAE mice (105).

Bulk RNAseq analysis and recent single-cell RNAseq studies of MG have revealed that unique MG subpopulations, characterized by a distinct signature, emerge during development and homeostasis in the healthy brain as well as during demyelination and remyelination in models of demyelinating and neurodegenerative diseases, including EAE and MS (106–108). These results confirm the ability of MG to shift into different functional states in response to a variety of environmental challenges. Accordingly, our results uncover a new mechanism whereby IFN-γ enables a subset of MG to adapt the transcriptional program into a tolerogenic and anti-inflammatory profile at the peak of EAE. Transcriptional profile analysis of $CX3CR1^{high}PD\text{-}L1^{low}$ MG isolated from IFN-γ- and PBS-treated EAE mice revealed that genes with a pro-inflammatory role in MC, MG and EAE such as *Cd38* (68–71, 109), *Cfb* (72, 108), *Saa3* (75, 76), *Inhba*, *Anpep* (110, 111), and *Apoc2* (112) were down-regulated by IFN-γ. From these genes, *Cd38, Cfb, Saa3, and Inhba* are considered canonical M1 pro-inflammatory genes in macrophages (73, 74). Transcriptional analysis of MG have showed that genes encoding for apoliprotein C1 and C2 (*Apoc1* and *Apoc2*) were up-regulated during the process of demyelination in the mouse cuprizone model and brain samples from MS patients (107, 112). Interestingly, IFN-γ treatment induced a down-regulation of *Apoc2* in $CX3CR1^{high}PD\text{-}L1^{low}$ MG. Taken together, these results highlight lipid and lipoprotein metabolism as a key mechanism in the modulation of microglial inflammatory status and as a modifiable target for the treatment of MS (113). A significantly lower frequency and absolute number of activated $CX3CR1^{high}PD\text{-}L1^{low}$ MG expressing MHC-II molecules was found in IFN-γ-treated EAE mice but not in MG from PBS-treated EAE mice. In addition, a decreased expression of MHC class II antigen presentation gene set was observed in $CX3CR1^{high}PD\text{-}L1^{low}$ MG from IFN-γ-treated EAE mice compared with $CX3CR1^{high}PD\text{-}L1^{low}$ MG from control mice; although this difference did not reach statistical significance. Also, *Cfb*, a component of the alternative pathway of complement activation, was downregulated in $CX3CR1^{high}PD\text{-}L1^{low}$ MG from IFN-γ-treated EAE mice. Consistent with our results, single-cell RNAseq analysis revealed decreased gene expression of the MHC-II antigen presentation

pathway both in peripheral APC (dendritic cells, macrophages and B cells) as in microglia in EAE mice treated at the peak of disease with an antigen-specific dual microparticle system (Ag-dMP). In addition, a set of complement genes were downregulated in the microglia from Ag-dMP-treated EAE mice (114). Consequently, EAE mice treated with a monoclonal antibody directed against Cfb significantly attenuated the chronic phase of disease, resulting in reduced cellular infiltration, inflammation and demyelination (72). In line with these results, upregulation in the expression of complement components, including Cfb and MHC-II pathway was determined by single-cell RNAseq analysis in MG isolated during the later stages of neurodegeneration in an Alzheimer's disease-like animal model (108). Arginase 1 (Arg-1) is an enzyme dominantly expressed in M2 macrophages that hydrolyzes arginine to ornithine and urea, limiting bioavailability of intracellular arginine to be metabolized to NO by the enzyme nitric oxide synthase (NOS), resulting in dampening of inflammation (115, 116). Surprisingly, we found that *Arg1*, encoding arginase 1, was down-regulated in CX3CR1^{high}PD-L1^{low} MG by IFN-γ treatment. However, *Nos2*, encoding inducible NOS, was slightly decreased. In addition, *Slc7a2*, which encodes inducible cationic amino acid transporter, and is involved in the uptake of arginine (78), was significantly down-regulated. Consequently, decreased availability of arginine could be expected in response to IFN-γ treatment. Therefore, although *Arg1* is down-regulated in CX3CR1^{high}PD-L1^{low} MG, the net result would be an anti-inflammatory effect due to a decrease in the uptake of arginine and decreased *Nos2* expression. This hypothesis is supported by the decreased secretion of nitrites induced by LPS in primary MC/MG cell cultures obtained from IFN-γ-treated EAE mice (Figure 5D). On the other hand, *Atp8a2* gene, a selective microglial marker (117), and other genes related to tolerogenic and anti-inflammatory processes in MG and EAE such as DVL-1 (64, 65) and Dusp5 (61, 62) were up-regulated by IFN-γ in CX3CR1^{high}PD-L1^{low} MG. Importantly, raising the Log2 Fold change to 1.5, a set of key genes (*Saa3, Inhba*, *Apoc2*, *Atp8a2, and* DVL-1) maintains differential expression in response to IFN-γ treatment.

Our results show that IFN-γ is unable to promote amelioration of EAE symptoms and induction of CX3CR1^{high}PD-L1^{low} MG in the absence of STAT-1, indicating that STAT-1 is critical in the protective effects mediated by IFN-γ in EAE. In line with these results, we found that from all up- and down-regulated genes in CX3CR1^{high}PD-L1^{low} MG by IFN-γ, 8 of them (*Cfb, Dusp5, Anxa4, Neurl1b, C3, Naca, Anxa11, Slc15a2*) are also regulated by STAT-1, suggesting that the IFN-γ/STAT-1 signaling axis would be involved in suppressing neuroinflammation in EAE regulating the expression of a set of genes involved in microglial activation. Supporting this potential mechanism, previous studies have reported that the IFN-γ/STAT-1 axis regulates the expression of indoleamine 2,3-dioxygenase (IDO), a tryptophan catabolizing enzyme involved in immune tolerance and suppression of EAE (118, 119), in microglia (120). Similarly, the IFN-γ/STAT-1 axis also regulates the tolerogenic activity of IDO in dendritic cells in a mouse model of prediabetes (121).

To obtain more detailed insights into the molecular interactions between the differentially expressed genes in MG in response to IFN-γ, we created a molecular network of protein-protein interactions based on the known interactions between the products of the genes targeted by IFN-γ. In this analysis, the number of interacting genes depended on the existing knowledge available from the STRING database and does not necessarily reflect the actual number of biological interactions. Therefore, this model is biased as some genes have been widely studied by many investigators, others less so. Despite this, the model reveals molecules physiologically interacting with those identified by expression profiling and delivers a more complete understanding of their connectedness. These analyses highlight the master role that IFN-γ plays in regulating microglial activity and provide new insights into the cellular and molecular mechanisms involved in the therapeutic activity of IFN-γ in EAE.

5 Conclusions

Our findings show that IFN-γ exerts therapeutic activity in EAE by regulating myeloid cell infiltration and inducing attenuation of neuroinflammation and a shift from activated MG to resting MG. In addition, IFN-γ promotes the induction of homeostatic CX3CR1^{high}PD-L1^{low} MG, characterized by a homeostatic and anti-inflammatory transcriptional signature. The amelioration of clinical symptoms and the induction of CX3CR1^{high}PD-L1^{low} MG were dependent on STAT-1. Also, our analyses reveal that IFN-γ plays a master role in regulating a network of genes involved in microglial activation. Taken together, our findings uncover a novel cellular and molecular mechanism whereby IFN-γ exerts therapeutic activity in EAE and contribute to clarify the complex role that IFN-γ plays in EAE and MS.

Data availability statement

The RNA sequencing datasets generated for this study have been deposited in the NCBI GEO database under accession number GSE231833.

Ethics statement

The animal study was reviewed and approved by the Institutional Animal Care and Use Committee (IACUC) of the University of Chile and Northwestern University.

Author contributions

JT and RN conceived the project. JT, EA, GA, LG, PM, CP, JI-V, and EL performed the experiments and analysis of the data. MR and NK performed RNA-seq analysis. PG-H performed molecular network analysis and its interpretation. RN, JT, PG-H, PIB, SM discussed the results and wrote the manuscript. All authors contributed to the article and approved the submitted version.

Funding

This work was supported by Fondo Nacional de Desarrollo Científico y Tecnológico (FONDECYT/ANID 1191874 and 1231672 RN, FONDECYT/ANID postdoc 3150133 JT, and FONDECYT/ANID 11190258 PM, National Doctoral scholarship CONICYT-CHILE 21130452 and MECESUP UCH 1304 GA). MED.UCHILE-FACS Laboratory is supported by CONICYT-CHILE through grants FONDEQUIP140032 (BD LSR Fortessa X-20, Special Order) and AIC-08 (BD FACSAria III) and by the Institute of Biomedical Sciences (ICBM), School of Medicine, Universidad de Chile, Chile. SPP Neuroglia by the Deutsche Forschungsgemeinschaft (MJR) RO 4076/3-1.

Acknowledgments

We thank Dr. Rodrigo Pacheco for providing 2D2 mice and Maria A. Espinoza for technical assistance (Neuroimmunology Laboratory, Fundación Ciencia & Vida, Chile). We thank Dr. Bárbara Pesce for helpful assistance with flow cytometry analysis and FACS sorting (MED.UCHILE-FACS Laboratory at Institute of Biomedical Sciences (ICBM), School of Medicine, Universidad de Chile, Chile).

Conflict of interest

The authors declare that the research was conducted in the absence of any commercial or financial relationships that could be construed as a potential conflict of interest.

Publisher's note

Supplementary material

The Supplementary Material for this article can be found online at: https://www.frontiersin.org/articles/10.3389/fimmu.2023.1191838/full#supplementary-material

References

1. Dendrou CA, Fugger L, Friese MA. Immunopathology of multiple sclerosis. *Nat Rev Immunol* (2015) 15(9):545–58. doi: 10.1038/nri3871

2. Constantinescu CS, Farooqi N, O'Brien K, Gran B. Experimental autoimmune encephalomyelitis (Eae) as a model for multiple sclerosis (Ms). *Br J Pharmacol* (2011) 164(4):1079–106. doi: 10.1111/j.1476-5381.2011.01302.x

3. Miller SD, Karpus WJ. Experimental autoimmune encephalomyelitis in the mouse. *Curr Protoc Immunol* (2007) 77:15.1.1-15.1.18. doi: 10.1002/0471142735.im1501s77

4. Robinson AP, Harp CT, Noronha A, Miller SD. The experimental autoimmune encephalomyelitis (Eae) model of Ms: utility for understanding disease pathophysiology and treatment. *Handb Clin Neurol* (2014) 122:173–89. doi: 10.1016/b978-0-444-52001-2.00008-x

5. Greter M, Lelios I, Croxford AL. Microglia versus myeloid cell nomenclature during brain inflammation. *Front Immunol* (2015) 6:249. doi: 10.3389/fimmu.2015.00249

6. London A, Cohen M, Schwartz M. Microglia and monocyte-derived macrophages: functionally distinct populations that act in concert in cns plasticity and repair. *Front Cell Neurosci* (2013) 7:34. doi: 10.3389/fncel.2013.00034

7. Cardona AE, Pioro EP, Sasse ME, Kostenko V, Cardona SM, Dijkstra IM, et al. Control of microglial neurotoxicity by the fractalkine receptor. *Nat Neurosci* (2006) 9 (7):917–24. doi: 10.1038/nn1715

8. Jung S, Aliberti J, Graemmel P, Sunshine MJ, Kreutzberg GW, Sher A, et al. Analysis of fractalkine receptor Cx(3)Cr1 function by targeted deletion and green fluorescent protein reporter gene insertion. *Mol Cell Biol* (2000) 20(11):4106–14. doi: 10.1128/mcb.20.11.4106-4114.2000

9. Wolf Y, Yona S, Kim KW, Jung S. Microglia, seen from the Cx3cr1 angle. *Front Cell Neurosci* (2013) 7:26. doi: 10.3389/fncel.2013.00026

10. Mrdjen D, Pavlovic A, Hartmann FJ, Schreiner B, Utz SG, Leung BP, et al. High-dimensional single-cell mapping of central nervous system immune cells reveals distinct myeloid subsets in health, aging, and disease. *Immunity* (2018) 48(3):599. doi: 10.1016/j.immuni.2018.02.014

11. Keren-Shaul H, Spinrad A, Weiner A, Matcovitch-Natan O, Dvir-Szternfeld R, Ulland TK, et al. A unique microglia type associated with restricting development of alzheimer's disease. *Cell* (2017) 169(7):1276–90 e17. doi: 10.1016/j.cell.2017.05.018

12. Breen KT, Anderson SR, Steele MR, Calkins DJ, Bosco A, Vetter ML. Loss of fractalkine signaling exacerbates axon transport dysfunction in a chronic model of glaucoma. *Front Neurosci* (2016) 10:526. doi: 10.3389/fnins.2016.00526

13. Feng X, Szulzewsky F, Yerevanian A, Chen Z, Heinzmann D, Rasmussen RD, et al. Loss of Cx3cr1 increases accumulation of inflammatory monocytes and promotes gliomagenesis. *Oncotarget* (2015) 6(17):15077–94. doi: 10.18632/oncotarget.3730

14. Mai W, Liu X, Wang J, Zheng J, Wang X, Zhou W. Protective effects of Cx3cr1 on autoimmune inflammation in a chronic eae model for Ms through modulation of antigen-presenting cell-related molecular mhc-ii and its regulators. *Neurological Sci* (2019) 40(4):779–91. doi: 10.1007/s10072-019-3721-2

15. Zrzavy T, Hametner S, Wimmer I, Butovsky O, Weiner HL, Lassmann H. Loss of 'Homeostatic' microglia and patterns of their activation in active multiple sclerosis. *Brain* (2017) 140(7):1900–13. doi: 10.1093/brain/awx113

16. Plastini MJ, Desu HL, Brambilla R. Dynamic responses of microglia in animal models of multiple sclerosis. *Front Cell Neurosci* (2020) 14:269. doi: 10.3389/fncel.2020.00269

17. Deczkowska A, Baruch K, Schwartz M. Type I/Ii interferon balance in the regulation of brain physiology and pathology. *Trends Immunol* (2016) 37(3):181–92. doi: 10.1016/j.it.2016.01.006

18. Lowther DE, Chong DL, Ascough S, Ettorre A, Ingram RJ, Boyton RJ, et al. Th1 not Th17 cells drive spontaneous Ms-like disease despite a functional regulatory T cell response. *Acta neuropathologica* (2013) 126(4):501–15. doi: 10.1007/s00401-013-1159-9

19. Arellano G, Ottum PA, Reyes LI, Burgos PI, Naves R. Stage-specific role of interferon-gamma in experimental autoimmune encephalomyelitis and multiple sclerosis. *Front Immunol* (2015) 6:492. doi: 10.3389/fimmu.2015.00492

20. Ottum PA, Arellano G, Reyes LI, Iruretagoyena M, Naves R. Opposing roles of interferon-gamma on cells of the central nervous system in autoimmune neuroinflammation. *Front Immunol* (2015) 6:539. doi: 10.3389/fimmu.2015.00539

21. Sanvito L, Constantinescu CS, Gran B, t`Hart B. The multifaceted role of interferon-gamma in central nervous system autoimmune demyelination. *Open Autoimmun J* (2010) 2:151–9. doi: 10.2174/1876894601002040151

22. Krakowski M, Owens T. Interferon-gamma confers resistance to experimental allergic encephalomyelitis. *Eur J Immunol* (1996) 26(7):1641–6. doi: 10.1002/eji.1830260735

23. Sabatino JJJr., Shires J, Altman JD, Ford ML, Evavold BD. Loss of ifn-gamma enables the expansion of autoreactive Cd4+ T cells to induce experimental autoimmune encephalomyelitis by a nonencephalitogenic myelin variant antigen. *J Immunol* (2008) 180(7):4451–7. doi: 10.4049/jimmunol.180.7.4451

24. Ferber IA, Brocke S, Taylor-Edwards C, Ridgway W, Dinisco C, Steinman L, et al. Mice with a disrupted ifn-gamma gene are susceptible to the induction of experimental autoimmune encephalomyelitis (Eae). *J Immunol* (1996) 156(1):5–7. doi: 10.4049/jimmunol.156.1.5

25. Willenborg DO, Fordham S, Bernard CC, Cowden WB, Ramshaw IA. Ifn-gamma plays a critical down-regulatory role in the induction and effector phase of myelin oligodendrocyte glycoprotein-induced autoimmune encephalomyelitis. *J Immunol* (1996) 157(8):3223–7. doi: 10.4049/jimmunol.157.8.3223

26. Naves R, Singh SP, Cashman KS, Rowse AL, Axtell RC, Steinman L, et al. The interdependent, overlapping, and differential roles of type I and ii ifns in the

pathogenesis of experimental autoimmune encephalomyelitis. *J Immunol* (2013) 191 (6):2967–77. doi: 10.4049/jimmunol.1300419

27. Xiao BG, Ma CG, Xu LY, Link H, Lu CZ. Il-12/Ifn-Gamma/No axis plays critical role in development of Th1-mediated experimental autoimmune encephalomyelitis. *Mol Immunol* (2008) 45(4):1191–6. doi: 10.1016/j.molimm.2007.07.003

28. Billiau A, Heremans H, Vandekerckhove F, Dijkmans R, Sobis H, Meulepas E, et al. Enhancement of experimental allergic encephalomyelitis in mice by antibodies against ifn-gamma. *J Immunol* (1988) 140(5):1506–10. doi: 10.4049/jimmunol.140.5.1506

29. Lublin FD, Knobler RL, Kalman B, Goldhaber M, Marini J, Perrault M, et al. Monoclonal anti-gamma interferon antibodies enhance experimental allergic encephalomyelitis. *Autoimmunity* (1993) 16(4):267–74. doi: 10.3109/08916939309014645

30. Heremans H, Dillen C, Groenen M, Martens E, Billiau A. Chronic relapsing experimental autoimmune encephalomyelitis (Creae) in mice: enhancement by monoclonal antibodies against interferon-gamma. *Eur J Immunol* (1996) 26 (10):2393–8. doi: 10.1002/eji.1830261019

31. Duong TT, Finkelman FD, Singh B, Strejan GH. Effect of anti-Interferon-Gamma monoclonal antibody treatment on the development of experimental allergic encephalomyelitis in resistant mouse strains. *J neuroimmunology* (1994) 53(1):101–7. doi: 10.1016/0165-5728(94)90069-8

32. Dungan LS, McGuinness NC, Boon L, Lynch MA, Mills KHG. Innate ifn-gamma promotes development of experimental autoimmune encephalomyelitis: a role for nk cells and M1 macrophages. *Eur J Immunol* (2014) 44(10):2903–17. doi: 10.1002/eji.201444612

33. Voorthuis JA, Uitdehaag BM, De Groot CJ, Goede PH, van der Meide PH, Dijkstra CD. Suppression of experimental allergic encephalomyelitis by intraventricular administration of interferon-gamma in Lewis rats. *Clin Exp Immunol* (1990) 81(2):183–8. doi: 10.1111/j.1365-2249.1990.tb03315.x

34. Furlan R, Brambilla E, Ruffini F, Poliani PL, Bergami A, Marconi PC, et al. Intrathecal delivery of ifn-gamma protects C57bl/6 mice from chronic-progressive experimental autoimmune encephalomyelitis by increasing apoptosis of central nervous system-infiltrating lymphocytes. *J Immunol* (2001) 167(3):1821–9. doi: 10.4049/jimmunol.167.3.1821

35. Tanuma N, Shin T, Kogure K, Matsumoto Y. Differential role of tnf-alpha and ifn-gamma in the brain of rats with chronic relapsing autoimmune encephalomyelitis. *J neuroimmunology* (1999) 96(1):73–9. doi: 10.1016/s0165-5728(99)00018-1

36. Rowse AL, Naves R, Cashman KS, McGuire DJ, Mbana T, Raman C, et al. Lithium controls central nervous system autoimmunity through modulation of ifn-Γ signaling. *PloS One* (2012) 7(12):e52658. doi: 10.1371/journal.pone.0052658

37. Sedgwick JD, Schwender S, Imrich H, Dörries R, Butcher GW, ter Meulen V. Isolation and direct characterization of resident microglial cells from the normal and inflamed central nervous system. *Proc Natl Acad Sci United States America* (1991) 88 (16):7438–42. doi: 10.1073/pnas.88.16.7438

38. Love MI, Huber W, Anders S. Moderated estimation of fold change and dispersion for rna-seq data with Deseq2. *Genome Biol* (2014) 15(12):550. doi: 10.1186/s13059-014-0550-8

39. Wang J, Vasaikar S, Shi Z, Greer M, Zhang B. Webgestalt 2017: a more comprehensive, powerful, flexible and interactive gene set enrichment analysis toolkit. *Nucleic Acids Res* (2017) 45(W1):W130–W7. doi: 10.1093/nar/gkx356

40. Croft D, O'Kelly G, Wu G, Haw R, Gillespie M, Matthews L, et al. Reactome: a database of reactions, pathways and biological processes. *Nucleic Acids Res* (2011) 39 (Database issue):D691–7. doi: 10.1093/nar/gkq1018

41. Ford AL, Goodsall AL, Hickey WF, Sedgwick JD. Normal adult ramified microglia separated from other central nervous system macrophages by flow cytometric sorting. phenotypic differences defined and direct ex vivo antigen presentation to myelin basic protein-reactive Cd4+ T cells compared. *J Immunol* (1995) 154(9):4309–21. doi: 10.4049/jimmunol.154.9.4309

42. Martin E, El-Behi M, Fontaine B, Delarasse C. Analysis of microglia and monocyte-derived macrophages from the central nervous system by flow cytometry. *J visualized experiments JoVE* (2017) 124). doi: 10.3791/55781

43. Sedgwick JD, Ford AL, Foulcher E, Airriess R. Central nervous system microglial cell activation and proliferation follows direct interaction with tissue-infiltrating T cell blasts. *J Immunol* (1998) 160(11):5320–30. doi: 10.4049/jimmunol.160.11.5320

44. Muller A, Brandenburg S, Turkowski K, Muller S, Vajkoczy P. Resident microglia, and not peripheral macrophages, are the main source of brain tumor mononuclear cells. *Int J Cancer* (2015) 137(2):278–88. doi: 10.1002/ijc.29379

45. Mathur V, Burai R, Vest RT, Bonanno LN, Lehallier B, Zardeneta ME, et al. Activation of the sting-dependent type I interferon response reduces microglial reactivity and neuroinflammation. *Neuron* (2017) 96(6):1290–302 e6. doi: 10.1016/j.neuron.2017.11.032

46. Ponomarev ED, Shriver LP, Dittel BN. Cd40 expression by microglial cells is required for their completion of a two-step activation process during central nervous system autoimmune inflammation. *J Immunol* (2006) 176(3):1402–10. doi: 10.4049/jimmunol.176.3.1402

47. Mizutani M, Pino PA, Saederup N, Charo IF, Ransohoff RM, Cardona AE. The fractalkine receptor but not Ccr2 is present on microglia from embryonic development throughout adulthood. *J Immunol* (2012) 188(1):29–36. doi: 10.4049/jimmunol.1100421

48. Bennett ML, Bennett FC, Liddelow SA, Ajami B, Zamanian JL, Fernhoff NB, et al. New tools for studying microglia in the mouse and human cns. *Proc Natl Acad Sci United States America* (2016) 113(12):E1738–46. doi: 10.1073/pnas.1525528113

49. Ponomarev ED, Shriver LP, Maresz K, Dittel BN. Microglial cell activation and proliferation precedes the onset of cns autoimmunity. *J Neurosci Res* (2005) 81(3):374–89. doi: 10.1002/jnr.20488

50. Rooney S, Sah A, Unger MS, Kharitonova M, Sartori SB, Schwarzer C, et al. Neuroinflammatory alterations in trait anxiety: modulatory effects of minocycline. *Trans Psychiatry* (2020) 10(1):256. doi: 10.1038/s41398-020-00942-y

51. Gentile A, Rossi S, Studer V, Motta C, De Chiara V, Musella A, et al. Glatiramer acetate protects against inflammatory synaptopathy in experimental autoimmune encephalomyelitis. *J Neuroimmune Pharmacol* (2013) 8(3):651–63. doi: 10.1007/s11481-013-9436-x

52. Kozlowski C, Weimer RM. An automated method to quantify microglia morphology and application to monitor activation state longitudinally in vivo. *PloS One* (2012) 7(2):e31814. doi: 10.1371/journal.pone.0031814

53. Hovens IB, Nyakas C, Schoemaker RG. A novel method for evaluating microglial activation using ionized calcium-binding adaptor protein-1 staining: cell body to cell size ratio. *Neuroimmunology Neuroinflamm* (2014) 1:82–8. doi: 10.4103/2347-8659.139719

54. Sloka S, Metz LM, Hader W, Starreveld Y, Yong VW. Reduction of microglial activity in a model of multiple sclerosis by dipyridamole. *J Neuroinflamm* (2013) 10:89. doi: 10.1186/1742-2094-10-89

55. Wensky AK, Furtado GC, Marcondes MC, Chen S, Manfra D, Lira SA, et al. Ifn-gamma determines distinct clinical outcomes in autoimmune encephalomyelitis. *J Immunol* (2005) 174(3):1416–23. doi: 10.4049/jimmunol.174.3.1416

56. Stromnes IM, Cerretti LM, Liggitt D, Harris RA, Goverman JM. Differential regulation of central nervous system autoimmunity by T(H)1 and T(H)17 cells. *Nat Med* (2008) 14(3):337–42. doi: 10.1038/nm1715

57. Lees JR, Iwakura Y, Russell JH. Host T cells are the main producers of il-17 within the central nervous system during initiation of experimental autoimmune encephalomyelitis induced by adoptive transfer of Th1 cell lines. *J Immunol* (2008) 180(12):8066–72. doi: 10.4049/jimmunol.180.12.8066

58. Krasemann S, Madore C, Cialic R, Baufeld C, Calcagno N, El Fatimy R, et al. The Trem2-apoe pathway drives the transcriptional phenotype of dysfunctional microglia in neurodegenerative diseases. *Immunity* (2017) 47(3):566–81 e9. doi: 10.1016/j.immuni.2017.08.008

59. Ebner F, Brandt C, Thiele P, Richter D, Schliesser U, Siffrin V, et al. Microglial activation milieu controls regulatory T cell responses. *J Immunol* (2013) 191(11):5594–602. doi: 10.4049/jimmunol.1203331

60. Tripathi P, Tripathi P, Kashyap L, Singh V. The role of nitric oxide in inflammatory reactions. *FEMS Immunol Med Microbiol* (2007) 51(3):443–52. doi: 10.1111/j.1574-695X.2007.00329.x

61. Ham JE, Oh EK, Kim DH, Choi SH. Differential expression profiles and roles of inducible dusps and Erk1/2-specific constitutive Dusp6 and Dusp7 in microglia. *Biochem Biophys Res Commun* (2015) 467(2):254–60. doi: 10.1016/j.bbrc.2015.09.180

62. Habibian JS, Jefic M, Bagchi RA, Lane RH, McKnight RA, McKinsey TA, et al. Dusp5 functions as a feedback regulator of tnfalpha-induced Erk1/2 dephosphorylation and inflammatory gene expression in adipocytes. *Sci Rep* (2017) 7(1):12879. doi: 10.1038/s41598-017-12861-y

63. Sarrazy V, Sore S, Viaud M, Rignol G, Westerterp M, Ceppo F, et al. Maintenance of macrophage redox status by chrebp limits inflammation and apoptosis and protects against advanced atherosclerotic lesion formation. *Cell Rep* (2015) 13(1):132–44. doi: 10.1016/j.celrep.2015.08.068

64. Manoharan I, Hong Y, Suryawanshi A, Angus-Hill ML, Sun Z, Mellor AL, et al. Tlr2-dependent activation of beta-catenin pathway in dendritic cells induces regulatory responses and attenuates autoimmune inflammation. *J Immunol* (2014) 193(8):4203–13. doi: 10.4049/jimmunol.1400614

65. Suryawanshi A, Manoharan I, Hong Y, Swafford D, Majumdar T, Taketo MM, et al. Canonical wnt signaling in dendritic cells regulates Th1/Th17 responses and suppresses autoimmune neuroinflammation. *J Immunol* (2015) 194(7):3295–304. doi: 10.4049/jimmunol.1402691

66. Kuhn SA, van Landeghem FK, Zacharias R, Farber K, Rappert A, Pavlovic S, et al. Microglia express Gaba(B) receptors to modulate interleukin release. *Mol Cell Neurosci* (2004) 25(2):312–22. doi: 10.1016/j.mcn.2003.10.023

67. Crowley T, Cryan JF, Downer EJ, O'Leary OF. Inhibiting neuroinflammation: the role and therapeutic potential of gaba in neuro-immune interactions. *Brain behavior Immun* (2016) 54:260–77. doi: 10.1016/j.bbi.2016.02.001

68. Mayo L, Jacob-Hirsch J, Amariglio N, Rechavi G, Moutin MJ, Lund FE, et al. Dual role of Cd38 in microglial activation and activation-induced cell death. *J Immunol* (2008) 181(1):92–103. doi: 10.4049/jimmunol.181.1.92

69. Wang YM, Liu ZY, Ai YH, Zhang LN, Zou Y, Peng QY. Blocking the Cd38/Cadpr pathway plays a double-edged role in lps stimulated microglia. *Neuroscience* (2017) 361:34–42. doi: 10.1016/j.neuroscience.2017.08.010

70. Bahri R, Bollinger A, Bollinger T, Orinska Z, Bulfone-Paus S. Ectonucleotidase Cd38 demarcates regulatory, memory-like Cd8+ T cells with ifn-Gamma-Mediated suppressor activities. *PloS One* (2012) 7(9):e45234. doi: 10.1371/journal.pone.0045234

71. Herrmann MM, Barth S, Greve B, Schumann KM, Bartels A, Weissert R. Identification of gene expression patterns crucially involved in experimental autoimmune encephalomyelitis and multiple sclerosis. *Dis Models Mech* (2016) 9 (10):1211–20. doi: 10.1242/dmm.025536

72. Hu X, Holers VM, Thurman JM, Schoeb TR, Ramos TN, Barnum SR. Therapeutic inhibition of the alternative complement pathway attenuates chronic eae. *Mol Immunol* (2013) 54(3-4):302–8. doi: 10.1016/j.molimm.2012.12.018

73. Jablonski KA, Amici SA, Webb LM, Ruiz-Rosado Jde D, Popovich PG, Partida-Sanchez S, et al. Novel markers to delineate murine M1 and M2 macrophages. *PloS One* (2015) 10(12):e0145342. doi: 10.1371/journal.pone.0145342

74. Sierra-Filardi E, Puig-Kroger A, Blanco FJ, Nieto C, Bragado R, Palomero MI, et al. Activin a skews macrophage polarization by promoting a proinflammatory phenotype and inhibiting the acquisition of anti-inflammatory macrophage markers. *Blood* (2011) 117(19):5092–101. doi: 10.1182/blood-2010-09-306993

75. Niemi K, Teirila L, Lappalainen J, Rajamaki K, Baumann MH, Oorni K, et al. Serum amyloid a activates the Nlrp3 inflammasome *Via* P2x7 receptor and a cathepsin b-sensitive pathway. *J Immunol* (2011) 186(11):6119–28. doi: 10.4049/jimmunol.1002843

76. Madeddu S, Woods TA, Mukherjee P, Sturdevant D, Butchi NB, Peterson KE. Identification of glial activation markers by comparison of transcriptome changes between astrocytes and microglia following innate immune stimulation. *PloS One* (2015) 10(7):e0127336. doi: 10.1371/journal.pone.0127336

77. Boutej H, Rahimian R, Thammisetty SS, Beland LC, Lalancette-Hebert M, Kriz J. Diverging mrna and protein networks in activated microglia reveal Srsf3 suppresses translation of highly upregulated innate immune transcripts. *Cell Rep* (2017) 21 (11):3220–33. doi: 10.1016/j.celrep.2017.11.058

78. Sans-Fons MG, Yeramian A, Pereira-Lopes S, Santamaria-Babi LF, Modolell M, Lloberas J, et al. Arginine transport is impaired in C57bl/6 mouse macrophages as a result of a deletion in the promoter of Slc7a2 (Cat2), and susceptibility to leishmania infection is reduced. *J Infect Dis* (2013) 207(11):1684–93. doi: 10.1093/infdis/jit084

79. Rouillard AD, Gundersen GW, Fernandez NF, Wang Z, Monteiro CD, McDermott MG, et al. The harmonizome: a collection of processed datasets gathered to serve and mine knowledge about genes and proteins. *Database (Oxford)* (2016) 2016. doi: 10.1093/database/baw100

80. Butovsky O, Talpalar AE, Ben-Yaakov K, Schwartz M. Activation of microglia by aggregated β-amyloid or lipopolysaccharide impairs mhc-ii expression and renders them cytotoxic whereas ifn-Γ and il-4 render them protective. *Mol Cell Neurosci* (2005) 29(3):381–93. doi: 10.1016/j.mcn.2005.03.005

81. Butovsky O, Ziv Y, Schwartz A, Landa G, Talpalar AE, Pluchino S, et al. Microglia activated by il-4 or ifn-Γ differentially induce neurogenesis and oligodendrogenesis from adult Stem/Progenitor cells. *Mol Cell Neurosci* (2006) 31 (1):149–60. doi: 10.1016/j.mcn.2005.10.006

82. Shaked I, Tchoresh D, Gersner R, Meiri G, Mordechai S, Xiao X, et al. Protective autoimmunity: interferon-Γ enables microglia to remove glutamate without evoking inflammatory mediators. *J Neurochemistry* (2005) 92(5):997–1009. doi: 10.1111/j.1471-4159.2004.02954.x

83. Butovsky O, Landa G, Kunis G, Ziv Y, Avidan H, Greenberg N, et al. Induction and blockage of oligodendrogenesis by differently activated microglia in an animal model of multiple sclerosis. *J Clin Invest* (2006) 116(4):905–15. doi: 10.1172/JCI26836

84. Ding X, Yan Y, Li X, Li K, Ciric B, Yang J, et al. Silencing ifn-Γ Binding/Signaling in astrocytes versus microglia leads to opposite effects on central nervous system autoimmunity. *J Immunol* (2015) 194(9):4251–64. doi: 10.4049/jimmunol.1303321

85. Willenborg DO, Fordham SA, Staykova MA, Ramshaw IA, Cowden WB. Ifn-gamma is critical to the control of murine autoimmune encephalomyelitis and regulates both in the periphery and in the target tissue: a possible role for nitric oxide. *J Immunol* (1999) 163(10):5278–86. doi: 10.4049/jimmunol.163.10.5278

86. Pierson E, Simmons SB, Castelli L, Goverman JM. Mechanisms regulating regional localization of inflammation during cns autoimmunity. *Immunol Rev* (2012) 248(1):205–15. doi: 10.1111/j.1600-065X.2012.01126.x

87. Haimon Z, Frumer GR, Kim J-S, Trzebanski S, Haffner-Krausz R, Ben-Dor S, et al. Cognate microglia–T cell interactions shape the functional regulatory T cell pool in experimental autoimmune encephalomyelitis pathology. *Nat Immunol* (2022) 23 (12):1749–62. doi: 10.1038/s41590-022-01360-6

88. White MPJ, Webster G, Leonard F, La Flamme AC. Innate ifn-gamma ameliorates experimental autoimmune encephalomyelitis and promotes myeloid expansion and pdl-1 expression. *Sci Rep* (2018) 8(1):259. doi: 10.1038/s41598-017-18543-z

89. Wang Z, Hong J, Sun W, Xu G, Li N, Chen X, et al. Role of ifn-gamma in induction of Foxp3 and conversion of Cd4+ Cd25- T cells to Cd4+ tregs. *J Clin Invest* (2006) 116(9):2434–41. doi: 10.1172/jci25826

90. Venken K, Hellings N, Liblau R, Stinissen P. Disturbed regulatory T cell homeostasis in multiple sclerosis. *Trends Mol Med* (2010) 16(2):58–68. doi: 10.1016/j.molmed.2009.12.003

91. Liu R, Du S, Zhao L, Jain S, Sahay K, Rizvanov A, et al. Autoreactive lymphocytes in multiple sclerosis: pathogenesis and treatment target. *Front Immunol* (2022) 13:996469. doi: 10.3389/fimmu.2022.996469

92. Kwilasz AJ, Grace PM, Serbedzija P, Maier SF, Watkins LR. The therapeutic potential of interleukin-10 in neuroimmune diseases. *Neuropharmacology* (2015) 96(Pt A):55–69. doi: 10.1016/j.neuropharm.2014.10.020

93. Beebe AM, Cua DJ, de Waal Malefyt R. The role of interleukin-10 in autoimmune disease: systemic lupus erythematosus (Sle) and multiple sclerosis (Ms). *Cytokine Growth Factor Rev* (2002) 13(4-5):403–12. doi: 10.1016/s1359-6101(02)00025-4

94. Weber MS, Prod'homme T, Youssef S, Dunn SE, Steinman L, Zamvil SS. Neither T-helper type 2 nor Foxp3+Regulatory T cells are necessary for therapeutic benefit of atorvastatin in treatment of central nervous system autoimmunity. *J Neuroinflamm* (2014) 11(1):29. doi: 10.1186/1742-2094-11-29

95. Jayaraman A, Soni A, Prabhakar BS, Holterman M, Jayaraman S. The epigenetic drug trichostatin a ameliorates experimental autoimmune encephalomyelitis *Via* T cell tolerance induction and impaired influx of T cells into the spinal cord. *Neurobiol Dis* (2017) 108:1–12. doi: 10.1016/j.nbd.2017.07.015

96. Danikowski KM, Jayaraman S, Prabhakar BS. Regulatory T cells in multiple sclerosis and myasthenia gravis. *J Neuroinflamm* (2017) 14(1):117. doi: 10.1186/s12974-017-0892-8

97. Korn T, Reddy J, Gao W, Bettelli E, Awasthi A, Petersen TR, et al. Myelin-specific regulatory T cells accumulate in the cns but fail to control autoimmune inflammation. *Nat Med* (2007) 13(4):423–31. doi: 10.1038/nm1564

98. Korn T, Mitsdoerffer M, Croxford AL, Awasthi A, Dardalhon VA, Galileos G, et al. Il-6 controls Th17 immunity in vivo by inhibiting the conversion of conventional T cells into Foxp3+ regulatory T cells. *Proc Natl Acad Sci United States America* (2008) 105(47):18460–5. doi: 10.1073/pnas.0809850105

99. Koutrolos M, Berer K, Kawakami N, Wekerle H, Krishnamoorthy G. Treg cells mediate recovery from eae by controlling effector T cell proliferation and motility in the cns. *Acta Neuropathologica Commun* (2014) 2(1):163. doi: 10.1186/s40478-014-0163-1

100. Li R, Li H, Yang X, Hu H, Liu P, Liu H. Crosstalk between dendritic cells and regulatory T cells: protective effect and therapeutic potential in multiple sclerosis. *Front Immunol* (2022) 13:970508. doi: 10.3389/fimmu.2022.970508

101. Boddeke EW, Meigel I, Frentzel S, Biber K, Renn LQ, Gebicke-Harter P. Functional expression of the fractalkine (Cx3c) receptor and its regulation by lipopolysaccharide in rat microglia. *Eur J Pharmacol* (1999) 374(2):309–13. doi: 10.1016/S0014-2999(99)00307-6

102. Leonardi-Essmann F, Emig M, Kitamura Y, Spanagel R, Gebicke-Haerter PJ. Fractalkine-upregulated milk-fat globule egf factor-8 protein in cultured rat microglia. *J neuroimmunology* (2005) 160(1-2):92–101. doi: 10.1016/j.jneuroim.2004.11.012

103. Ibañez-Vega J, Vilchez C, Jimenez K, Guevara C, Burgos PI, Naves R. Cellular and molecular regulation of the programmed death-1/Programmed death ligand system and its role in multiple sclerosis and other autoimmune diseases. *J Autoimmun* (2021) 123:102702. doi: 10.1016/j.jaut.2021.102702

104. Tierney JB, Kharkrang M, La Flamme AC. Type ii-activated macrophages suppress the development of experimental autoimmune encephalomyelitis. *Immunol Cell Biol* (2009) 87(3):235–40. doi: 10.1038/icb.2008.99

105. Brandl C, Ortler S, Herrmann T, Cardell S, Lutz MB, Wiendl H. B7-H1-Deficiency enhances the potential of tolerogenic dendritic cells by activating Cd1d-restricted type ii nkt cells. *PloS One* (2010) 5(5):e10800. doi: 10.1371/journal.pone.0010800

106. Vainchtein ID, Alsema AM, Dubbelaar ML, Grit C, Vinet J, van Weering HRJ, et al. Characterizing microglial gene expression in a model of secondary progressive multiple sclerosis. *Glia* (2023) 71(3):588–601. doi: 10.1002/glia.24297

107. Masuda T, Sankowski R, Staszewski O, Böttcher C, Amann L, Sagar, et al. Spatial and temporal heterogeneity of mouse and human microglia at single-cell resolution. *Nature* (2019) 566(7744):388–92. doi: 10.1038/s41586-019-0924-x

108. Mathys H, Adaikkan C, Gao F, Young JZ, Manet E, Hemberg M, et al. Temporal tracking of microglia activation in neurodegeneration at single-cell resolution. *Cell Rep* (2017) 21(2):366–80. doi: 10.1016/j.celrep.2017.09.039

109. Zocchi E, Daga A, Usai C, Franco L, Guida L, Bruzzone S, et al. Expression of Cd38 increases intracellular calcium concentration and reduces doubling time in hela and 3t3 cells. *J Biol Chem* (1998) 273(14):8017–24. doi: 10.1074/jbc.273.14.8017

110. Subramani J, Ghosh M, Rahman MM, Caromile LA, Gerber C, Rezaul K, et al. Tyrosine phosphorylation of Cd13 regulates inflammatory cell-cell adhesion and monocyte trafficking. *J Immunol* (2013) 191(7):3905–12. doi: 10.4049/jimmunol.1301348

111. Reinhold D, Bank U, Entz D, Goihl A, Stoye D, Wrenger S, et al. Petir-001, a dual inhibitor of dipeptidyl peptidase iv (Dp iv) and aminopeptidase n (Apn), ameliorates experimental autoimmune encephalomyelitis in Sjl/J mice. *Biol Chem* (2011) 392(3):233–7. doi: 10.1515/BC.2011.024

112. Olah M, Amor S, Brouwer N, Vinet J, Eggen B, Biber K, et al. Identification of a microglia phenotype supportive of remyelination. *Glia* (2012) 60(2):306–21. doi: 10.1002/glia.21266

113. Loving BA, Bruce KD. Lipid and lipoprotein metabolism in microglia. *Front Physiol* (2020) 11:393. doi: 10.3389/fphys.2020.00393

114. Kwiatkowski AJ, Helm EY, Stewart JM, Drashansky TT, Cho JJ, Avram D, et al. Treatment with an antigen-specific dual microparticle system reverses advanced multiple sclerosis in mice. *Proc Natl Acad Sci United States America* (2022) 119(43): e2205417119. doi: 10.1073/pnas.2205417119

115. Yang Z, Ming XF. Functions of arginase isoforms in macrophage inflammatory responses: impact on cardiovascular diseases and metabolic disorders. *Front Immunol* (2014) 5:533. doi: 10.3389/fimmu.2014.00533

116. Rath M, Müller I, Kropf P, Closs EI, Munder M. Metabolism *Via* arginase or nitric oxide synthase: two competing arginine pathways in macrophages. *Front Immunol* (2014) 5:532. doi: 10.3389/fimmu.2014.00532

117. Butovsky O, Jedrychowski MP, Moore CS, Cialic R, Lanser AJ, Gabriely G, et al. Identification of a unique Tgf-β–dependent molecular and functional signature in microglia. *Nat Neurosci* (2014) 17(1):131–43. doi: 10.1038/nn.3599

118. Kwidzinski E, Bunse J, Aktas O, Richter D, Mutlu L, Zipp F, et al. Indolamine 2,3-dioxygenase is expressed in the cns and down-regulates autoimmune inflammation. *FASEB J* (2005) 19(10):1347–9. doi: 10.1096/fj.04-3228fje

119. Platten M, Ho PP, Youssef S, Fontoura P, Garren H, Hur EM, et al. Treatment of autoimmune neuroinflammation with a synthetic tryptophan metabolite. *Science* (2005) 310(5749):850–5. doi: 10.1126/science.1117634

120. Yadav MC, Burudi EM, Alirezaei M, Flynn CC, Watry DD, Lanigan CM, et al. Ifn-Gamma-Induced ido and wrs expression in microglia is differentially regulated by il-4. *Glia* (2007) 55(13):1385–96. doi: 10.1002/glia.20544

121. Grohmann U, Fallarino F, Bianchi R, Orabona C, Vacca C, Fioretti MC, et al. A defect in tryptophan catabolism impairs tolerance in nonobese diabetic mice. *J Exp Med* (2003) 198(1):153–60. doi: 10.1084/jem.20030633

frontiers | Frontiers in Immunology

TYPE Original Research
PUBLISHED 16 February 2024
DOI 10.3389/fimmu.2024.1327672

OPEN ACCESS

EDITED BY
Marija Mostarica-Stojkovic,
University of Belgrade, Serbia

REVIEWED BY
Alice Mariottini,
University of Florence, Italy
Mirjana Dimitrijević,
University of Belgrade, Serbia

*CORRESPONDENCE
Rikke Holm Hansen
rikke.holm.hansen@regionh.dk

RECEIVED 25 October 2023
ACCEPTED 22 January 2024
PUBLISHED 16 February 2024

CITATION
Holm Hansen R, von Essen MR, Reith Mahler M, Cobanovic S and Sellebjerg F (2024) Sustained effects on immune cell subsets and autoreactivity in multiple sclerosis patients treated with oral cladribine. *Front. Immunol.* 15:1327672. doi: 10.3389/fimmu.2024.1327672

Sustained effects on immune cell subsets and autoreactivity in multiple sclerosis patients treated with oral cladribine

Rikke Holm Hansen[1*], Marina Rode von Essen[1], Mie Reith Mahler[1], Stefan Cobanovic[1] and Finn Sellebjerg[1,2]

[1]Danish Multiple Sclerosis Center, Department of Neurology, Copenhagen University Hospital - Rigshospitalet, Glostrup, Denmark, [2]Department of Clinical Medicine, Faculty of Health and Medical Sciences, University of Copenhagen, Copenhagen, Denmark

Introduction: Cladribine tablet therapy is an efficacious treatment for multiple sclerosis (MS). Recently, we showed that one year after the initiation of cladribine treatment, T and B cell crosstalk was impaired, reducing potentially pathogenic effector functions along with a specific reduction of autoreactivity to RAS guanyl releasing protein 2 (RASGRP2). In the present study we conducted a longitudinal analysis of the effect of cladribine treatment in patients with RRMS, focusing on the extent to which the effects observed on T and B cell subsets and autoreactivity after one year of treatment are maintained, modulated, or amplified during the second year of treatment.

Methods: In this case-control exploratory study, frequencies and absolute counts of peripheral T and B cell subsets and B cell cytokine production from untreated patients with relapsing-remitting MS (RRMS) and patients treated with cladribine for 52 (W52), 60 (W60), 72 (W72) and 96 (W96) weeks, were measured using flow cytometry. Autoreactivity was assessed using a FluoroSpot assay.

Results: We found a substantial reduction in circulating memory B cells and proinflammatory B cell responses. Furthermore, we observed reduced T cell responses to autoantigens possibly presented by B cells (RASGRP2 and a-B crystallin (CRYAB)) at W52 and W96 and a further reduction in responses to the myelin antigens myelin basic protein (MBP) and myelin oligodendrocyte glycoprotein (MOG) after 96 weeks.

Conclusion: We conclude that the effects of cladribine observed after year one are maintained and, for some effects, even increased two years after the initiation of a full course of treatment with cladribine tablets.

KEYWORDS

immune reconstitution, multiple sclerosis, cladribine tablets, autoreactive T cell responses, autoreactive B cells

Introduction

Multiple sclerosis (MS) is an immune-mediated disease characterized by inflammation, demyelination and neuroaxonal damage in the central nervous system (CNS) (1). The etiology of MS remains unknown; however, T (2) and B (3) cells have been implicated in the pathogenesis (4). Specifically, follicular helper T (Tfh) cells, a subset of $CD4^+$ T cells expressing CD127, CXCR5, and PD-1, play a critical role in B cell differentiation and antibody production (5–7). In normal immune homeostasis, Tfh cells interact with follicular regulatory T (Tfr) cells, which regulate immune responses induced by Tfh cells (8–10).

Alterations in the balance between Tfh and Tfr cells, favoring Tfh cells (11, 12) and lower Tfr activity (13), have been reported in MS. Additionally, a recent study demonstrated the active recruitment of Tfh cells to the cerebrospinal fluid in MS patients, presumably mediated by the CXC motif chemokine ligand CXCL13, which is associated with intrathecal immunoglobulin synthesis (14).

Tfh cells can be further categorized based on their expression of CXCR3 and CCR6 into Tfh1 ($CXCR3^+CCR6^-$), Tfh17 ($CXCR3^-CCR6^+$), Tfh2 ($CXCR3^-CCR6^-$) (15) and Tfh17.1 ($CXCR3^+CCR6^+$) cells (16), each possessing distinct cytokine production profiles and B cell helper capacities. Furthermore, phenotypically and functionally distinct $CD25^-$ and $CD25^{int}$ Tfh cell populations with predominantly Tfh1-like and Tfh17-like phenotypes, respectively, have been identified (14).

In addition to alterations in T cell subsets, abnormalities in circulating B cells have been observed in MS patients. These include increased production of proinflammatory cytokines (17–19) and reduced activity of regulatory B cells (20–22).

The treatment strategy for relapsing-remitting MS (RRMS) includes immune reconstitution therapies, e.g. cladribine tablets (23, 24). Cladribine selectively accumulates in immune cells, where it is phosphorylated to its active form 2-chlorodeoxyadenosine triphosphate (Cd-ATP) by deoxycytidine kinase (DCK), thereby inducing apoptosis (25). The selective effect on lymphocytes is attributed to their high DCK concentrations and low levels of the enzyme 5′-Nucleotidase which inactivates Cd-ATP (25).

Cladribine tablets have demonstrated efficacy as immune reconstitution treatment for RRMS, offering long-term benefits with few treatment cycles (26). Treatment results in reductions of circulating T and B cells, particularly within the memory compartment, without affecting immunoglobulin levels (27–34). Recently, a study from our laboratory showed that one year after the initiation of cladribine treatment, T and B cell crosstalk was impaired in a manner that likely reduced their ability to mediate pathogenic effector functions (35). Additionally, there was a specific reduction of autoreactivity to the autoantigen RASGRP2 which is highly expressed in B cells and brain tissue (35).

Studies of the effect of cladribine on immune cell subsets in year two after treatment initiation are limited. With this study we performed a longitudinal analysis of the effect of cladribine treatment in patients with RRMS, focusing on the extent to which the effects observed on T and B cell subsets and autoreactivity after one year of treatment are maintained, modulated, or amplified during the second year of treatment.

Methods

Study participants

In this exploratory case-control study, a total of 30 untreated patients with relapsing-remitting multiple sclerosis (RRMS) and 20 RRMS patients treated with oral cladribine tablets were included. Blood samples were obtained from these patients, which were subsequently used for both *ex vivo* and *in vitro* analysis.

The diagnosis of MS was based on the McDonald 2017 criteria (36). The untreated patients with RRMS were newly diagnosed and had not received any disease-modifying therapy. They were included in the study at least one month after their last steroid treatment.

The administration of a complete cladribine treatment course comprised oral intake of 3.5 mg/kg in two annual courses, each consisting of two treatment weeks, with a four-week interval between. Patients who received cladribine tablets (Mavenclad®, Merck KGaA, Darmstadt, Germany) were included in the study at week 52 (W52), i.e., one year after their first annual course. Additionally, they were included at W60, W72, and W96, i.e., 8, 20 and 44 weeks after the beginning of second annual course.

Study protocols approval, registrations, and patient consent

All participants provided informed, written consent to participate in the study, and the research protocol was approved by the regional scientific ethics committee (protocol number H-16047666).

Blood samples

Peripheral blood mononuclear cells (PBMCs) were obtained from freshly collected venous blood using a density gradient centrifugation technique (Lymphoprep; Axis-Shield, Oslo, Norway). After isolation, PBMCs underwent two consecutive washes in cold phosphate-buffered saline (PBS) supplemented with 2-mM-ethylenediaminetetraacetic-acid (EDTA). Freshly isolated PBMCs were used for flow cytometry phenotyping, and excess PBMCs were cryopreserved in fetal bovine serum (FBS) with 10% dimethyl sulfoxide (DMSO) for subsequent *in vitro* analysis.

Flowcytometry analysis of freshly isolated cells

A minimum of 350,000 freshly isolated PBMCs were incubated with an Fc receptor-blocking reagent (Miltenyi Biotec, Bergisch Gladbach, Germany) and the cells were stained with fluorochrome-conjugated antibodies specific for the surface molecules of interest. For B cells the following antibodies were used: CD19 (PerCP/Cy5.5; HIB19), CD27 (FITC; 323), CD38 (BV421, HIT2) and CD11c (PE/Cy7; Bu15), all from BioLegend (San Diego, CA, USA). For T cells,

the following antibodies were used: CD3 (APC/Cy7; HIT3a), CD4 (PerCP/Cy5.5; RPA-T4), CD25 (PE; M-A251), CD127 (APC; A019D5), CXCR5 (AF488; J252D4), PD-1 (BV605; EH12.2H7), CXCR3 (PE/Cy7; G025H7) and CCR6 (BV421; G034E3) from BioLegend. Where applicable, corresponding isotype controls were used. Absolute counts of T and B cell subpopulations were measured using TruCount beads (BD Biosciences, Franklin Lakes, NJ, USA). Flow cytometry data acquisition was performed using a FACS Canto II flow cytometer (BD Biosciences), and data analysis was conducted using FlowJo software (Tree Star, Inc., Ashland, OR, USA).

PBMC stimulation and intracellular staining

Cryopreserved PBMCs from 20 of the untreated patients with RRMS, 20 cladribine-treated patients at W52, 20 cladribine-treated patients at W96, and an additional 20 healthy controls were thawed and cultured for 48 hours in RPMI 1640 medium supplemented with penicillin and streptomycin (50 U/ml Gibco, Waltham, MA, USA) and 10% human AB serum (Invitrogen, Carlsbad, CA, USA). Cells were either left unstimulated or stimulated with CpG-ODN 2006 TLR9 agonist (InvivoGen, San Diego, CA, USA) at a concentration of 2.5 µg/ml. To assess B cell cytokine production, the CpG-stimulated and unstimulated PBMCs were subsequently incubated with phorbol-myristate-acetate (PMA; Sigma-Aldrich, St. Louis, MO, USA) at a concentration of 10 ng/ml, 0.5 µg/ml ionomycin (Sigma-Aldrich), and 5 µg/ml brefeldin A (Sigma-Aldrich), at 37°C and 5% CO_2 for 4 hours. Following incubation, cells were surface stained with fluorochrome-conjugated anti-CD19 antibody (PE/Cy7; HIB19) and a live/dead stain. Subsequently, cells were fixed, permeabilized, and stained with anti-IL-10 (APC; JES3-19F1), anti-TGF-β (BV421; TW7-16B4) and anti-LTα (PE; 359-81-11) all from BioLegend. Flow cytometry data acquisition was performed using a FACS Canto II flow cytometer and analyzed using FlowJo software.

FluoroSpot antigen reactivity assay

Low fluorescent PVDF FluoroSpot plates (Mabtech AB, Nacka Strand, Sweden) were activated with 35% ethanol for 1 minute and washed with sterile water. Plates were then coated with a dilution of 15 µg/ml IFN-γ, IL-13, IL-17 and IL-21 capture antibodies in sterile PBS supplied in Mabtech FluoroSpot kits (#3654-1-1) and incubated for 24 h at 4°C. After incubation, plates were washed in sterile PBS and blocked for 2 h at RT with RPMI-1640/5% human serum (Invitrogen). 250,000 PBMCs from each of 20 untreated patients with RRMS, 20 cladribine-treated patients with RRMS at W52, 20 cladribine-treated patients with RRMS at W96, and 20 healthy controls were added to each well in RPMI-1640/5% human serum with 30 µg/ml myelin basic protein (MBP; HyTest, Turku, Finland), 10 µg/ml myelin oligodendrocyte glycoprotein (MOG; AnaSpec, Fremont, CA, USA), 0.3 µg/ml RAS guanyl releasing protein 2 (RASGRP2; OriGene Technologies Inc., Rockville, MD, USA), 10 µg/ml alpha B crystallin (CRYAB; Abcam, Cambridge, United Kingdom), $5x10^6$ cells/ml heat-killed Candida albicans (HKCA; InvivoGen) or medium alone. A costimulatory monoclonal anti-CD28 antibody (Mabtech) was added to the wells in a concentration of 0.1 µg/ml and plates were incubated for 48 h at 37°C, 5% CO_2. Subsequently, cells were removed, and plates were washed with PBS and biotinylated-detection antibody in PBS/0.1% bovine serum albumin (BSA) was added for 2 h, at RT. Plates were washed and incubated for 1 h at RT with fluorophore-conjugated antibodies in PBS/0.1% BSA according to manufacturer (Mabtech AB). Subsequently plates were incubated with fluorescence enhancer for 15 minutes and afterwards emptied and left to dry protected from daylight for a minimum of 45 minutes. Analysis of spots was performed using the Mabtech IRIS reader system equipped with Apex™ software (Mabtech AB).

The included untreated patients with RRMS and HC were selected to match the group of cladribine treated patients with RRMS. There were no statistically significant differences in age or sex between any of the included groups.

Statistics

Statistical analyses were performed using GraphPad Prism 7 software (GraphPad software Inc, La Jolla, CA, USA). Mann Whitney U test was applied for comparison of B and T cell subpopulations, between untreated patients with RRMS and patients treated with cladribine for 52 weeks. Friedman paired test was applied for comparison of B and T cell subpopulations between W52, W60, W72 and W96 of cladribine treatment. Kruskal-Wallis test was applied for comparison of B cell cytokine production and CNS antigen reactivity between untreated patients with RRMS and W52 and W96 of cladribine treatment where a Mann Whitney U test was applied for comparison between healthy controls and untreated patients with RRMS. A p value <0.005 was considered statistically significant and <0.05 as suggestive of significance (37).

STROBE guidelines

For this manuscript the STROBE reporting guidelines for observational studies was used.

Data availability

Data are available in anonymized form and can be shared by request form any qualified investigator. Sharing requires approval of a data transfer agreement by the Danish Data Protection Agency.

Results

Patient characteristics

We included 30 untreated patients with RRMS, and 20 patients treated with oral cladribine tablets (Table 1). The two groups showed no significant differences in age, sex, or EDSS scores. However, patients in the cladribine group had a longer disease

duration ($p<0.0001$). Among the untreated patients, all had experienced either relapse or magnetic resonance imaging (MRI) activity in the previous year. In the cladribine-treated group, seven had neither relapse nor MRI activity in the year prior to initiating cladribine therapy. These patients had switched from another treatment due to side effects or the development of anti-JC virus antibodies. In the cladribine group, three patients had not received any previous treatment, while 12 had received oral therapies (teriflunomide, dimethyl fumarate, or fingolimod), and five had received monoclonal antibody treatment (natalizumab or rituximab). Before initiating cladribine treatment, all previously treated patients had normal lymphocyte counts, except for one patient previously treated with dimethyl fumarate who had grade 1 lymphopenia.

Cladribine-treatment induces long-term memory B cell suppression

We found no difference in absolute count of $CD19^+$ B cells between 30 untreated patients with RRMS and 20 patients treated with cladribine at W52 (Figures 1A, B). However, at W60, i.e., eight weeks after the initiation of the second treatment cycle we found a significantly lower number of $CD19^+$ B cells, that was partly maintained to W72, but at W96 $CD19^+$ B cell levels were reconstituted to levels comparable to W52 (Figure 1B). When analyzing the specific B cell subsets according to their expression of CD27 and CD38 (Figure 1C) the number of transitional (Figure 1D) and naïve (Figure 1E) B cells were higher in patients treated with cladribine at W52 compared to untreated, and although there was a significant decrease in numbers of transitional B cells at W72 and naïve B cells at W60 and W72, W96 numbers were comparable to W52 numbers.

Conversely, looking at the memory B cell compartment we found a significantly lower number of $CD27^-CD38^-$ (Figure 1F), $CD38^-$ (Figure 1G) and $CD38^+$ memory (Figure 1H) B cells and plasmablasts (Figure 1I) at W52 of cladribine treatment compared to untreated patients. We also found that the number of all memory B cell subsets were significantly lower at W60 and W72 compared to W52, except for $CD27^-CD38^-$ memory B cells that only showed a decrease in numbers at W60 and the $CD38^+$ memory B cells which remained significantly lower at W96 than at W52.

Investigating atypical, $CD11c^+$ memory B cells (Figure 1J) showed that at W52 of cladribine treatment there were significantly lower numbers of $CD11c^+CD38^-$ and $CD38^+$ memory B cells whereas no difference was observed for $CD38^-CD27^-$ B cells compared to untreated patients with RRMS (Figure 1K). In all three $CD11c^+$ B cell memory subpopulations there was a significant decrease in numbers at W60 and for the $CD38^+$ memory B cells the decrease persisted at W70, but at W96 of cladribine treatment $CD11c^+$ memory B cells were reconstituted to levels comparable to W52 (Figure 1K).

TABLE 1 Patient characteristics.

	Untreated RRMS (n = 30)	CLA (n = 20)
Biological sex, male/female	8 (27%), 22 (73%)	8 (40%), 12 (60%)
Age, years	35 [21-62]	41 [27-59]
Disease duration, years	1 [0-25]	9 [1-31]
EDSS Score	1.75 [0-4]	2.5 [0-6]
Relapse previous year	27/30 (90%)	12/24 (50%)
MRI activity without relapse previous year	3/3 (100%)	5/12 (42%)
Previous therapy	None (n=30, 100%)	None (n=3, 15%) Teriflunomide (n=3, 13%) Dimethyl fumarate (n=5, 21%) Fingolimod (n=4, 20%) Natalizumab (n=4, 20%) Rituximab (n=1, 4%)

RRMS, relapsing-remitting multiple sclerosis; CLA, cladribine treated patients with RRMS; EDSS, expanded disability status scale; MRI, magnetic resonance imaging; n, number of individuals.
Data are given as numbers and percentages or median and range.

Long-term cladribine treatment induces a shift in Tfh: Tfr cell ratio

Cladribine treatment induced long-term depletion of $CD4^+$ T cells persisting from W52 to W96 with even lower numbers of circulating cells at W60 and W72 than W52 (Figures 2A, B). We measured the absolute count of Tfh and Tfr cells and non-follicular regulatory T cells (Treg) in order to investigate the B cell activation potential. We defined Tfh cells as $CD4^+CD127^+CXCR5^+$, Tfr cells as $CD4^+CD127^-CD25^{hi}CXCR5^+$, activated Tfh and Tfr cells as PD-1^+ and non-follicular Tregs as $CD4^+CD127^-CD25^{hi}CXCR5^-$ T cells (Figures 2C, D, F). The number of circulating $CD25^-$ and $CD25^{int}$ Tfh cells was significantly lower at W52 compared to untreated patients with RRMS (Figure 2E). While the number of $CD25^-$ Tfh cells was unchanged from W52 to W96, the number of $CD25^{int}$ Tfh cells decreased significantly at W60 and W72 (Figure E). There were no changes in numbers of PD-1^+ Tfh cells between untreated patients with RRMS and W52 of cladribine treatment, but after the second treatment cycle PD-1^+ $CD25^{int}$ Tfh cells were significantly reduced at W60, W72 and W96 compared to W52 (Figure 2E).

Looking at the regulatory potential we found a suggestively significant lower number of Tfr cells at W52 in cladribine-treated patients compared to untreated, and furthermore we found a suggestively significant decrease in the number of Tfr cells at W72 and a significantly lower number after W96 compared to W52 in the cladribine-treated patients (Figure 2G). There were no changes in numbers of PD-1^+ Tfr cells between untreated and W52 of cladribine-treated patients with RRMS. There was a significantly lower number of PD-1^+ Tfr cells at W72 compared to W52 of

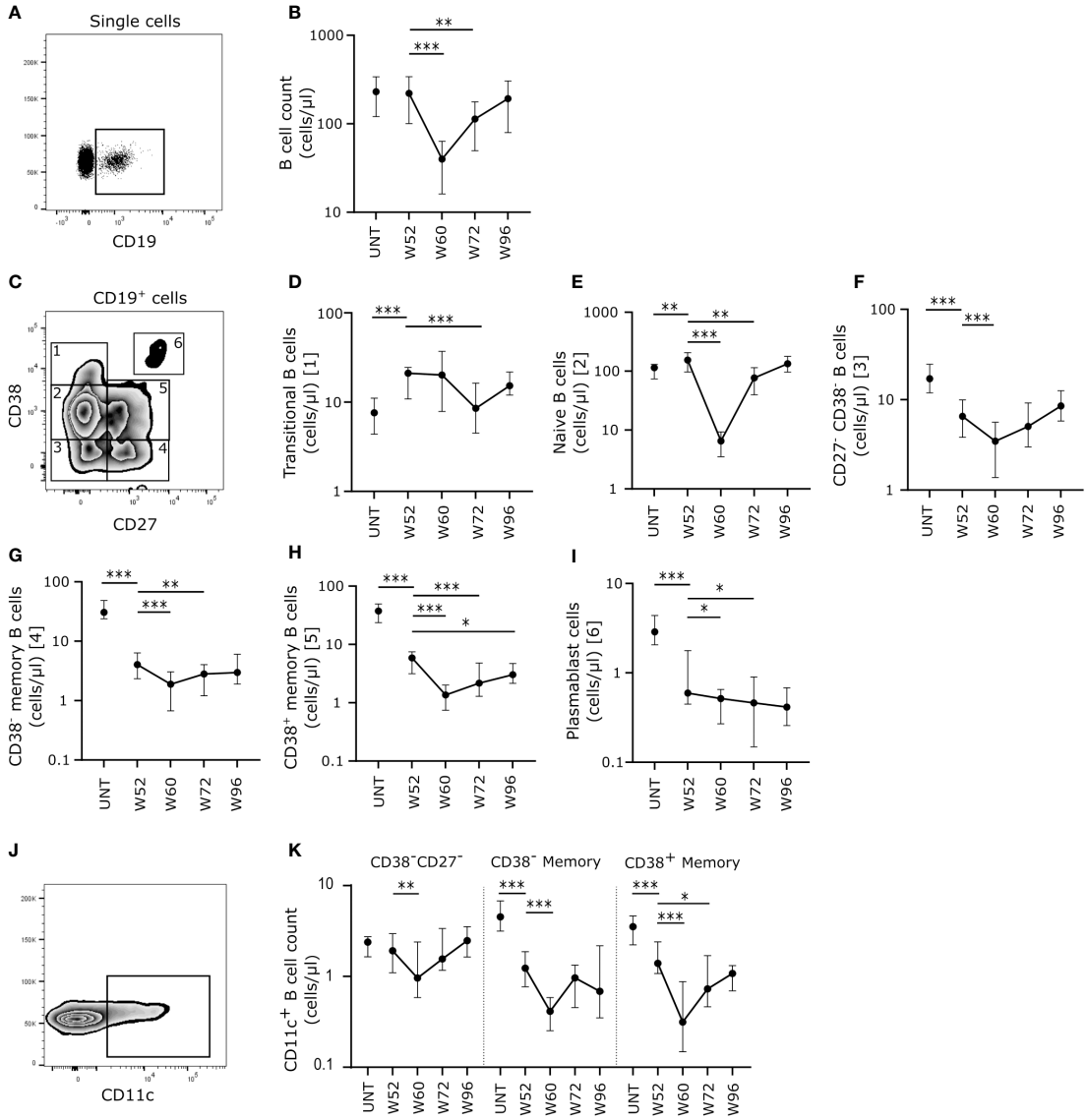

FIGURE 1
Cladribine-treatment induce long-term memory B cell suppression. **(A)** Gating strategy of $CD19^+$ B cells. Gating strategy includes a $CD19^+$ gate in a dot plot of single cell lymphocytes. **(B)** Scatterplots showing absolute counts (cells/µl blood) of total $CD19^+$ B cells. **(C)** Gating strategy of $CD19^+$ B cell substes. Gating strategy includes a CD27/CD38 zebra plot for gating of the six different B cell subtypes in blood; 1: $CD27^-CD38^{++}$ transitional B cells, 2: $CD27^-CD38^+$ naïve B cells, 3: $CD27^-CD38^-$ B cells, 4: $CD27^+CD38^-$ memory B cells, 5: $CD27^+CD38^+$ memory B cells and 6: $CD27^{++}CD38^{++}$ plasmablasts. **(D–I)** Scatterplots showing absolute counts (cells/µl blood) transitional B cells **(D)**, naïve B cells **(E)**, $CD27^-CD38^-$ B cells **(F)**, $CD27^+CD38^-$ memory B cells **(G)**, $CD27^+CD38^+$ memory B cells **(H)** and plasmablasts **(I)** from untreated patients with RRMS (UNT; n=30) and patients treated with cladribine for 52 (W52), 60 (W60), 72 (W72) and 96 (W96) weeks, n=20. **(J)** A flow cytometry zebra-plot example of CD11c gating on memory B cells. **(K)** A scatterplot showing absolute counts (cells/µl blood) of $CD11c^+$ $CD27^-CD38^-$ B cells, $CD27^+CD38^-$ memory B cells and $CD27^+CD38^+$ memory B cells from untreated patients with RRMS (UNT; n=30) and patients treated with cladribine for 52 (W52), 60 (W60), 72 (W72) and 96 (W96) weeks, n=20. The median value is shown for all groups analyzed. ***p < 0.0001; **p < 0.005; *p < 0.05.

cladribine treatment, but at W96 the number of $PD\text{-}1^+$ Tfr cells were reconstituted to levels comparable to W52 (Figure 2G). Total numbers of non-follicular Tregs were lower at W52 in cladribine-treated patients compared to untreated and significantly lower at W72 and W96 of cladribine treatment than at W52 (Figure 2G).

Analyzing the Tfh: Tfr ratio between groups showed increased Tfh: Tfr cell ratios of both $CD25^-$ and $CD25^{int}$ cells at W96 compared to W52 in cladribine-treated patients. Likewise, both $PD\text{-}1^+CD25^-$ and $PD\text{-}1^+CD25^{int}$ Tfh: Tfr cell ratios were higher at W72 compared to W52. However, at W96 of cladribine therapy we found a shift in $PD\text{-}1^+CD25^{int}$ Tfh: Tfr cell ratios with a significantly lower ratio compared to W52 (Figure 2H).

Long-term cladribine treatment induces lower numbers of proinflammatory effector T cells

Analyzing the long-term cladribine-induced effects on non-follicular effector T cells ($CD4^+CD127^+CXCR5^-$), we measured absolute counts of the functionally distinct effector T cells subsets

10.3389/fimmu.2024.1327672

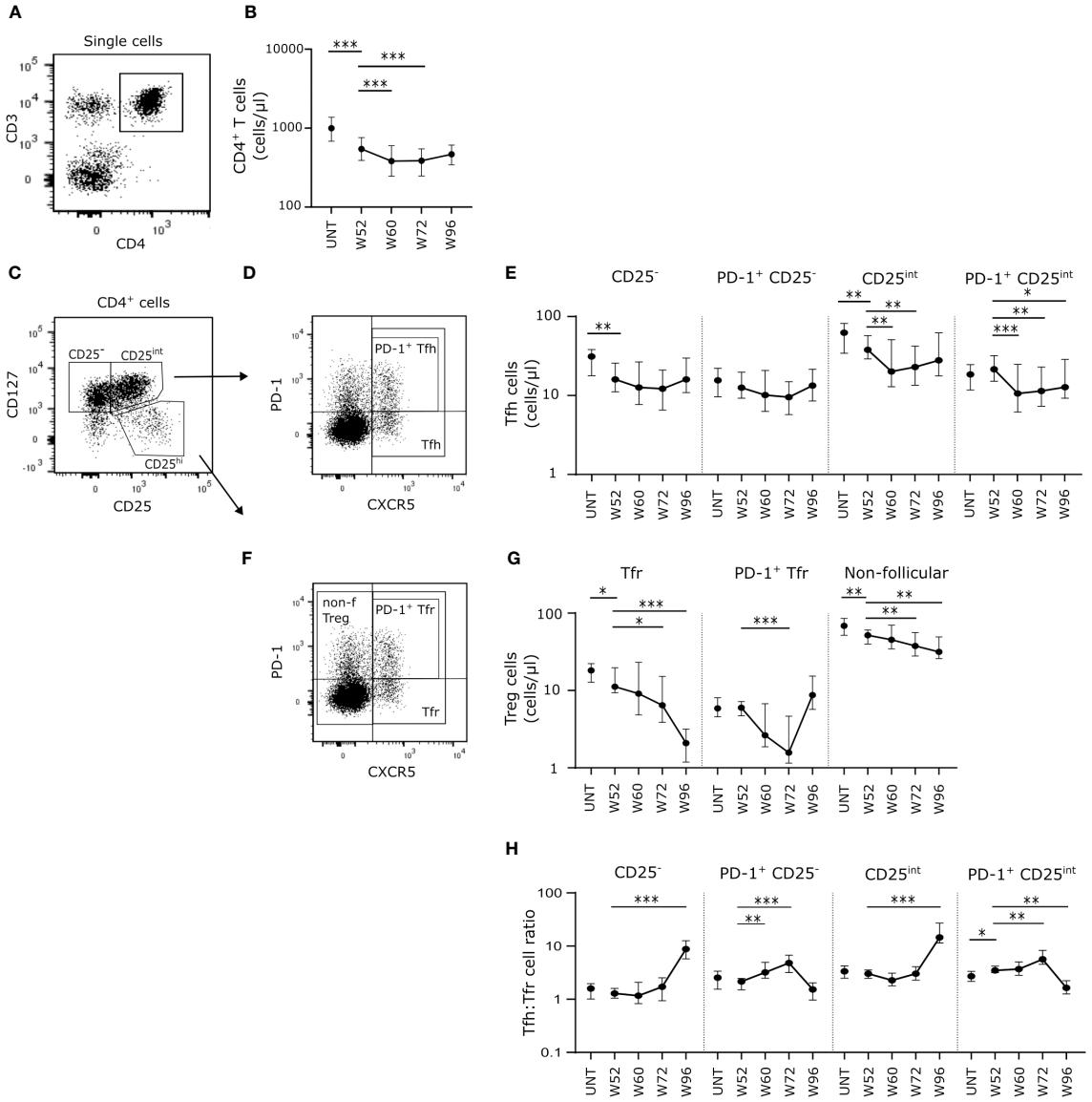

FIGURE 2
Long-term cladribine treatment induces a shift in Tfh: Tfr cell ratio. **(A)** Gating strategy of $CD4^+$ T cells. Gating strategy includes a CD3/CD4 gate in a dot plot of single cell lymphocytes. **(B)** Scatterplots showing absolute counts (cells/µl blood) of total $CD4^+$ T cells. **(C, D, F)** Gating strategy of Tfh, Tfr and non-follicular Treg cells. Gating strategy includes a CD127/CD25 dot plot for gating of $CD127^+CD25^-$, $CD127^+CD25^{int}$ and $CD127^-CD25^{hi}$ **(C)**, and a PD-1/CXCR5 dot plot for PD-$1^{+/-}$Tfh **(D)**, PD-$1^{+/-}$ Tfr and non-follicular Treg cells **(F)**. **(E–G)** Scatterplots showing absolute counts (cells/µl blood) of $CD25^-$ Tfh cells, PD-1^+CD25^- Tfh cells, $CD25^{int}$ Tfh cells and PD-1^+CD25^{int} Tfh cells **(E)** and Tfr cells, PD-1^+ Tfr cells and non-follicular Treg cells **(G)** from untreated patients with RRMS (UNT; n=30) and patients treated with cladribine for 52 (W52), 60 (W60), 72 (W72) and 96 (W96) weeks, n=20. **(H)** Scatterplots showing Tfh: Tfr cell ratios of $CD25^-$, PD-1^+CD25^-, $CD25^{int}$ and PD-1^+CD25^{int} Tfh: Tfr from untreated patients with RRMS (UNT; n=30) and patients treated with cladribine for 52 (W52), 60 (W60), 72 (W72) and 96 (W96) weeks, n=20. The median value is shown for all groups analyzed. ***p < 0.0001; **p < 0.005; *p < 0.05.

Th1, Th17 and Th17.1 characterized according to their expression of CXCR3 and CCR6 (Figure 3A). After W52 of cladribine treatment we found a significant and suggestively significant lower number of Th17 and Th17.1 cells, respectively, compared to untreated patients with RRMS. (Figure 3B). After the second cladribine treatment cycle we found a suggestively significant decrease in Th1 cells at W60 compared to W52, however, at W72 and W96 Th1 cell numbers were comparable to W52. (Figure 3B). Likewise, numbers of Th17.1 were significantly lower at W60 and W72 but reconstituted at W96 to levels comparable to W52 (Figure 3B).

Long-term cladribine treatment induces changes in Tfh subsets

We further subdivided the Tfh cell subsets into the effector subpopulations Tfh1 ($CXCR3^+CCR6^-$), Tfh2 (CXCR3-CCR6-), Tfh17 ($CXCR3^-CCR6^+$) and Tfh17.1 ($CXCR3^+CCR6^+$) (Figure 3A). Here we found that for both $CD25^-$, PD-1^+CD25^- and $CD25^{int}$ Tfh cell populations the number of Tfh1 and Tfh2 cells was significantly lower at W52 in cladribine-treated patients compared to untreated patients (Figures 3C–F). Conversely, numbers of Tfh17 cells were

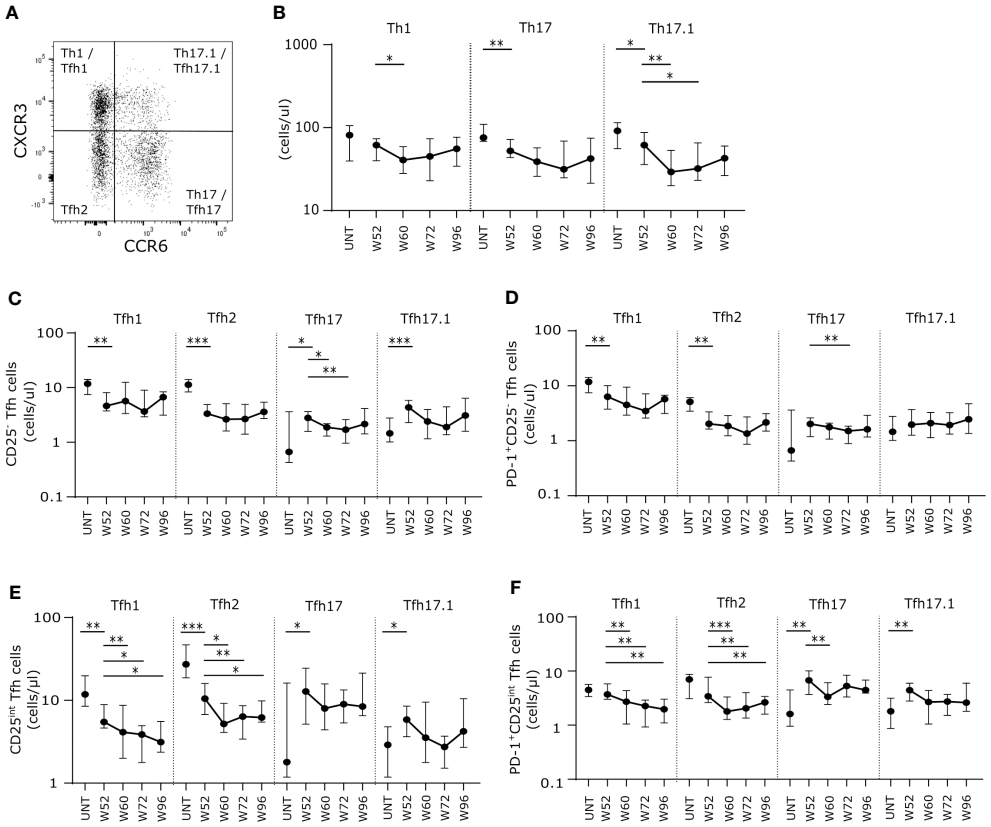

FIGURE 3
Long-term cladribine treatment induce lower numbers of proinflammatory effector T cells and changes in Tfh effector subsets. **(A)** Gating strategy of Th1, Th17, Th17.1, Tfh1, Tfh2, Tfh17 and Tfh17.1. Gating strategy includes a CXCR3/CCR6 gate in a dot plot of $CXCR5^-$ or $CXCR5^+$ $CD4^+CD127^+$ T cells. **(B)** Scatterplots showing absolute counts (cells/µl blood) of non-follicular $CXCR5^-$ Th1, Th17 and Th17.1. **(C–F)** Scatterplots showing absolute counts (cells/µl blood) of Tfh1, Tfh2, Tfh17 and Tfh17.1 cells within $CD25^-$ Tfh cells **(C)**, PD-1^+CD25^- Tfh cells **(D)**, $CD25^{int}$ Tfh cells **(E)** and PD-1^+CD25^{int} Tfh cells **(F)** from untreated patients with RRMS (UNT; n=30) and patients treated with cladribine for 52 (W52), 60 (W60), 72 (W72) and 96 (W96) weeks, n=20. The median value is shown for all groups analyzed. ***p < 0.0001; **p < 0.005; *p < 0.05.

higher in both the $CD25^{int}$ and the PD-1^+CD25^{int} Tfh cell populations, and Tfh17.1 cells were significantly higher in $CD25^-$ and PD-1^+CD25^{int} Tfh cells at W52 in cladribine-treated patients compared to untreated (Figures 3C–F). After the second treatment cycle numbers of $CD25^-$, PD-1^+CD25^- and PD-1^+CD25^{int} Tfh17 cells were lower at W60 or W72 compared to W52 but were reconstituted to levels comparable to W52 at W96 (Figures 3C–F). Conversely, numbers of $CD25^{int}$ and PD-1^+CD25^{int} Tfh1 and Tfh2 cells were significantly lower at both W60, W72 and W96 compared to W52 of cladribine treatment (Figures 3C–F).

Long-term cladribine treatment induces lower frequencies of LTα producing B cells

To analyze the long-term effects of cladribine treatment on B cell cytokine responses, we stimulated cryopreserved PBMCs from 20 healthy controls (median age 42 years; range 24-69 years), 20 untreated patients with RRMS (median age 37 years; range 26-62 years) and 20 patients treated with cladribine at W52 and W96 with or without CpG for 2 days and evaluated the IL-10, TGF-β, and LTα profile (Figures 4A, C, E) of B cells after a short re-stimulation. (Figures 4B, D, F) Without CpG-stimulation we found a significantly lower frequency of IL-10, TGF-β, and LTα producing B cells at W52 compared to untreated patients, however, frequencies of both IL-10 and TGF-β producing B cells were reconstituted to levels comparable to untreated patients at W96. Following CpG stimulation there were no differences between frequencies of IL-10 producing B cells in any of the groups, but frequencies of TGF-β were suggestively significantly decreased compared to untreated at W52 but not at W96 (Figures 4B, D). Conversely, the frequency of LTα producing B cells remained lower in cladribine-treated than in untreated patients at W52 and W96 with and without CpG stimulation (Figure 4F).

Long-term cladribine treatment induces lower reactivity towards MOG, MBP, CRYAB and RASGRP2

Cryopreserved PBMCs from 20 healthy controls, 20 untreated patients with RRMS and 20 patients treated with cladribine at W52 and W96 were stimulated for 48 h with the autoantigens MOG, MBP, CRYAB (for 8 patients from each group), or RASGRP2

10.3389/fimmu.2024.1327672

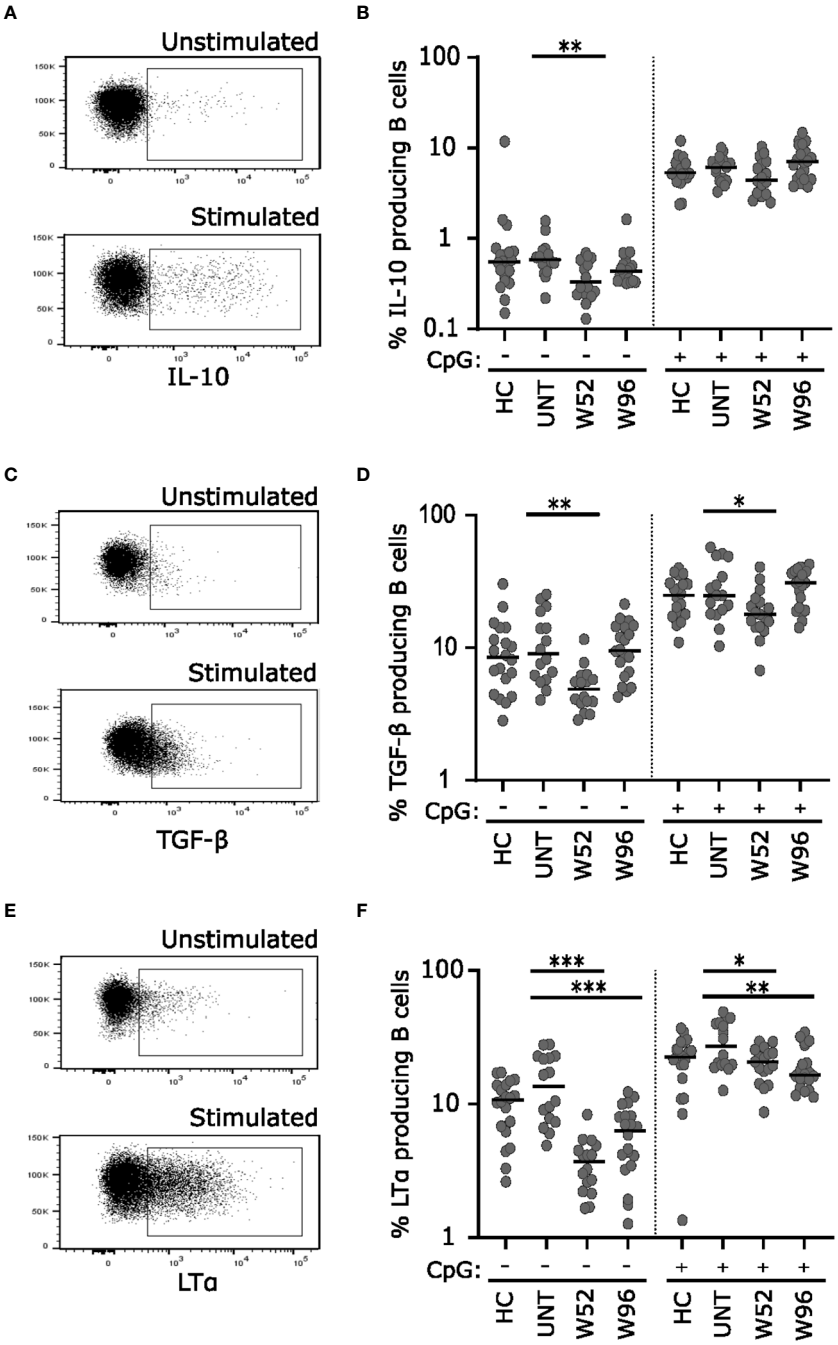

FIGURE 4
Long-term cladribine treatment induces lower frequencies of LTα producing B cells. Dot plot gating examples of intracellular IL-10 **(A)**, TGF-β **(C)** and LTα **(E)** staining of B cells. The *upper* panel shows unstimulated cells and the *lower* panel show cells stimulated for 48 h with CpG followed by a short re-stimulation. Scatterplots showing frequencies of IL-10 **(B)** TGF-β **(D)** and LTα **(F)** producing B cells from healthy controls (HC; n=20), untreated patients with RRMS (UNT; n=20) and patients treated with cladribine for 52 (W52) and 96 (W96) weeks, n=20. The median value is shown for all groups analyzed. ***p < 0.0001; **p < 0.005; *p < 0.05.

together with co-stimulatory anti-CD28 or medium with anti-CD28 alone as control. Following stimulation, IFN-γ, IL-17, IL-13 and IL-21 spot forming units (SFU) at the single cell level were measured. Untreated patients with MS had a suggestively higher number of IL-13 and IL-17 SFUs than healthy controls after stimulation with MOG and CRYAB respectively (Figures 5B, C).

IFN-γ and IL-13 SFUs were lower after stimulation in medium with anti-CD28 at W96 and for IFN-γ SFUs also at W52 compared to untreated patients (Figures 5A, B). IFN-γ SFUs were significantly lower at W96 in response to MBP, MOG and RASGRP2 and the IFN-γ response to RASGRP2 was also suggestively significantly lower at W52 compared to untreated (Figure 5A). IL-17 SFUs were

significantly lover at W96 in response to MOG and CRYAB compared to untreated patients (Figure 5C) IFN-γ^{+}IL-17^{+} SFUs were significantly lower in response to CRYAB at W52 and furthermore suggestively significant lower at W96 in response to both CRYAB and MOG compared to untreated patients (Figure 5E). There were no difference in IL-21 response between groups to any of the autoantigens (Figure 5D).

Discussion

Several studies, including a recent study from our group, have investigated the effects of cladribine on circulating immune cells during the first year of treatment (27–34). In the present study we follow up on 20 of the 24 patients included in our previous study with a detailed analysis of changes in circulating immune cell phenotypes, B cell cytokine production profiles, and autoantigen reactivity during the second year of treatment (35), i.e., after the administration of a full treatment course of 3.5 mg cladribine/kg body weight (23).

In the immune cell phenotype studies, we focused on B cell subsets and function, and confirmed that cladribine treatment has long-term effects on memory B cells. Compared to W52, total B cell counts decreased at W60 and W72 but had returned to normal levels at W96, consistent with the results of other studies investigating cladribine effects over 2 years (28, 30, 32, 33). Numbers of transitional and naïve B cells, memory B cells and plasmablasts decreased at W60 and/or W72 compared with W52. However, whereas numbers of circulating plasmablasts, $CD27^{-}$ $CD38^{-}$ B cells and $CD38^{-}$ and $CD38^{+}$ memory B cells were lower than in untreated patients, numbers of transitional and naïve B cells were higher at W52 and W96. There were no significant differences between B cell reconstitution at W52 and W96, consistent with the results of a previous study (33).

We also found that the numbers of $CD38^{-}$ and $CD38^{+}$ memory B cells expressing CD11c were lower at W52 and W96 than in untreated patients and decreased further from W52 to W60 and/or W72. $CD11c^{+}$ B cell were previously shown to produce proinflammatory cytokines and develop into autoantibody-producing cells (38). We studied induced B cell cytokine production with or without priming with CpG, which stimulates Toll-like receptor 9, before a brief stimulation with PMA and ionomycin (18). At W52 we observed a lower percentage of B cells expressing IL-10 without priming with CpG whereas there was no difference at W96, and there was no difference in the percentage of B cells expressing IL-10 when the cells had been primed with CpG. For B cells expressing TGF-β we found a lower percentage at

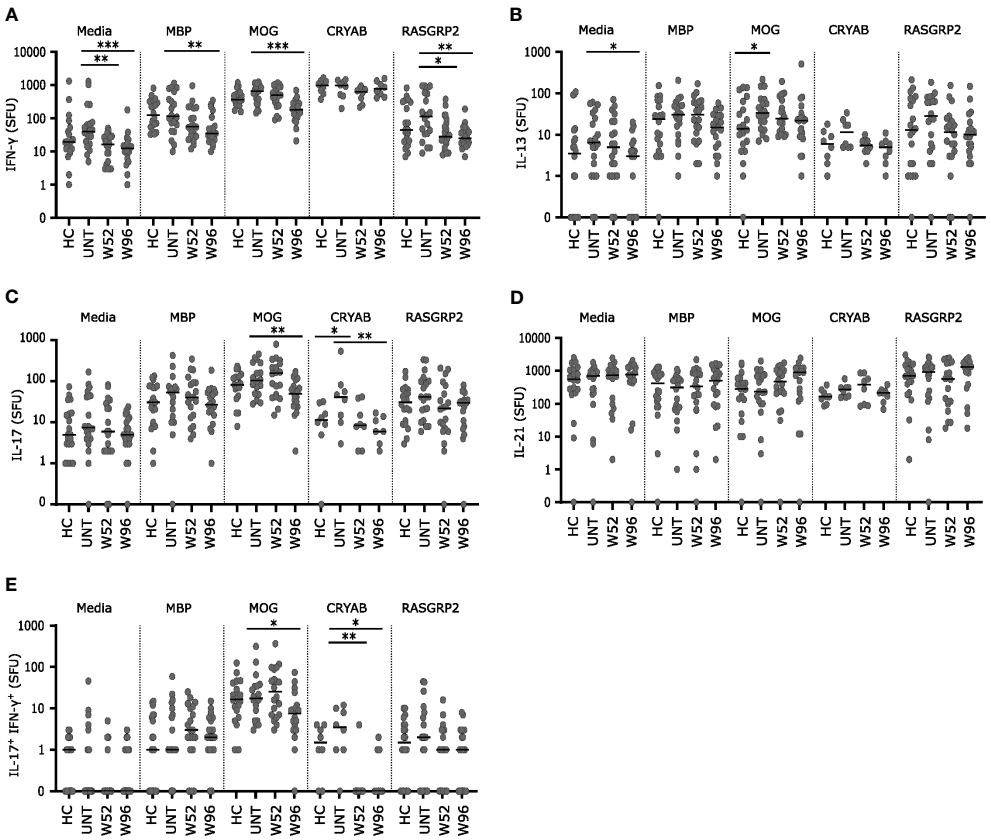

FIGURE 5
Long-term cladribine treatment induce lower reactivity towards MOG, MBP, CRYAB and RASGRP2. **(A–E)** Scatterplots showing spot forming units (SFU) of IFN-γ **(A)**, IL-13 **(B)**, IL-17 **(C)**, IL-21 **(D)** and IL-17^{+}IFN-γ^{+} **(E)** reactivity against media, myelin basis protein (MBP), myelin oligodendrocyte glycoprotein (MOG), alpha B crystallin (CRYAB; n=8 from each group) and RAS guanyl releasing protein 2 (RASGRP2) from PBMCs from healthy controls (HC; n=20), untreated patients with RRMS (UNT; n=20) and patients treated with cladribine for 52 (W52) and 96 (W96) weeks, n=20. The median value is shown for all groups analyzed. ***p < 0.0001; **p < 0.005; *p < 0.05.

W52 both with and without priming with CpG. However, at W96 there was no difference in TGF-β expression between treated and untreated patients. We also found that at W52 and W96 the percentage of B cells producing LT-α was lower both with and without priming with CpG in cladribine-treated patients than in untreated patients. Taken together, these data support the notion that cladribine-treated patients are characterized by long-term depletion of proinflammatory memory B cells and that although a decrease in the production of the immunoregulatory cytokines IL-10 and TGF-β was observed under some culture conditions at W52, this was not observed at W96, whereas a consistent decrease in the production of the proinflammatory cytokine LT-α was observed both at W52 and W96. A dysregulation of IL-10 and LTα has been shown in patients with MS with a higher percentage of B cells producing LTα (18, 19) and a lower percentage of B cells producing IL-10 (17, 19) and these imbalances have been suggested to contribute to exaggerated Th1 and Th17 responses in MS (19).

Consistent with previous studies we find that the depletion of circulating $CD4^+$ T cells is maintained one year after the second treatment cycle (28, 29). We investigated effector T cell subsets involved in the activation of B cells, i.e., follicular helper T (Tfh) cells and follicular regulatory T (Tfr) cells. One year after the first cladribine treatment cycle the total number of Tfh cells was significantly lower than in untreated patients, and this decrease was maintained or even lower in the second year of treatment. We subdivided the Tfh cells into a $CD25^-$ (Th1-like) and a $CD25^{int}$ (Th17-like) subset and used expression of PD-1 as a marker of Tfh activation (15). Numbers of PD-1^-CD25^- Tfh and PD-1^+ and PD-1^- $CD25^{int}$ Tfh cells were lower in patients treated with cladribine, and the number of PD-1^+CD25^{int} Tfh cells decreased even further from W52 to W96. We did, however, also find that the total number of Tfr cells was lower at W52 and although the number of PD-1^+ Tfr cells was higher at W96, the total number of Tfr cells was even lower at W96 than at W52.

A skewing in the Tfh: Tfr cell ratio in favor of Tfh cells has previously been observed in patients with RRMS (11, 39). One year after the first cladribine treatment cycle we found a suggestively significant higher PD-1^+CD25^{int} Tfh: Tfr cell ratio compared to untreated patients, suggesting that the functional activity of Tfh cells is maintained or even increased in cladribine-treated patients. After the second treatment cycle the PD-1^+ Tfh: Tfr cell ratio was initially increased at W72 but at W96 we found a shift in the PD-1^+ $CD25^{int}$ Tfh: Tfr cell ratio with significantly lower ratio compared to W52, suggesting a return of the regulatory function after the second cladribine treatment cycle.

In a separate analysis we used expression of the chemokine receptors CCR6 and CXCR3 to identify Tfh1 ($CXCR3^+CCR6^-$), Tfh2 ($CXCR3^-CCR6^-$), Tfh17 ($CXCR3^-CCR6^+$) and Tfh17.1 ($CXCR3^+CCR6^+$) cells. Tfh17 cells induce naïve human B cells to secrete IgA, IgG and IgM, and Tfh2 cells induce the secretion of IgG, IgA and IgM as well as IgE (15). Both in the $CD25^-$ and the $CD25^{int}$ Tfh subset and in PD-1 positive and negative Tfh cells there was an increase in the absolute number of Tfh17 cells in blood in patients treated with cladribine. Although transient decreases in numbers were observed at W60 or W72 for some subsets, overall Tfh17 cells remained at higher levels than in untreated patients throughout year 2 of cladribine treatment. In contrast, the numbers of Tfh2 cells were lower in all Tfh subsets, and even decreased further from W52 to W96 for some subsets. We hypothesize that the increased number of circulating Tfh17 cells may compensate for the changes in other Tfh subsets and Tfh: Tfr ratios and help explain why patients treated with cladribine maintain normal immunoglobulin levels and preserved humoral responses to vaccination in spite of lower numbers of circulating memory B cells and plasmablasts (27, 31, 34, 40).

Overall, we found lower counts of circulating Tfh1 cells in patients treated with cladribine than in untreated patients and for some subsets the counts were even lower at W96 than at W52. In contrast to Tfh2 and Tfh17 Tfh cells, Tfh1 Tfh cells do not support the differentiation of naïve B cells to immunoglobulin-secreting cells. This may reflect that CXCR3 expression counteracts the retention of Tfh cells in germinal centers (41). We are not aware of studies addressing the Tfh activity of Tfh17.1 cells but since these cells also express CXCR3 they may also have poor Tfh activity, and we found only minor effects on Th17.1 Tfh cells in patients treated with cladribine. The role of changes in Tfh1 and Tfh17.1 cells in patients treated with cladribine therefore remains to be established.

In addition to lower numbers of total $CD4^+$ T cells, there were lower numbers of Th1, Th17 and Th17.1 cells at W52 and W96, and there was a further decrease in Th17.1 cells at W60 and W72 compared with untreated patients. Th1, Th17 and Th17.1 cells have all been implicated in the pathogenesis of MS (2, 42). We did, however, also find that the number of circulating non-follicular Treg cells was lower at W52 and decreased further during the second year of treatment with cladribine. This reduction in Treg cells may help preserve protective T cell responses in patients treated with cladribine.

We also investigated the cytokine responses of circulating immune cells in patients treated with cladribine. When cells were cultured in control medium with anti-CD28 alone there were fewer cells secreting IFN-γ at W52 and 96 and fewer cells secreting IL-13 at W96 compared to untreated patients with RRMS. Using MOG as antigen there were more cells secreting IL-13 in untreated patients with MS than in healthy controls. There was no significant difference in the number of MOG-reactive cells secreting IFN-γ, IL-21 or cells secreting both IFN-γ and IL-17A (Th17.1 cells) between untreated patients and healthy controls, and there were no differences between untreated patients and healthy controls in autoreactive cells after stimulation with MBP, CRYAB or RASGRP2. Increased T cell responses to MBP and RASGRP2 were reported in MS in previous studies (43–46). The use of anti-CD28 for co-stimulation in the present study may at least partly explain this difference, and this may also explain why there was substantial reactivity to all autoantigens even in the control subjects. Furthermore, the results on CRYAB reactivity should be interpreted with caution since insufficient supplies resulted in the antigen only being studied in some of the subjects.

At W52 the IFN-γ response to RASGRP2 was lower than in untreated patients, as also observed in our previous study (35). At W96 the IFN-γ response to RASGRP2 was still reduced and there

were also lower responses to MBP and MOG. We also found that the Th17 and Th17.1 (IL-17A$^+$ and IFN-γ$^+$IL-17A$^+$) response to CRYAB was lower in patients treated with cladribine both at W52 and W96 than in untreated patients. It has been suggested that memory B cells expressing RASGRP2 can initiate and propagate an autoreactive T cell response, leading to CNS migration and causing chronic brain inflammation (43, 45). The autoantigen CRYAB was originally identified as a small heath shock protein present in the cytosol of oligodendrocytes and astrocytes in MS lesions (47). Later it was shown that Epstein Barr virus infection induced CRYAB expression in B cells, and T cells reactive to CRYAB were identified both in healthy controls and patients with MS (47, 48). Our observation of lower Th1 responses to RASGRP2 and lower Th17.1 responses to CRYAB at W52 and W96 is consistent with our hypothesis that lower numbers of circulating memory B cells may lower T cell reactivity to autoantigens expressed in B cells. The lower reactivity to MBP and MOG after 96 weeks does, however, suggest that other mechanisms, including a general decrease in IFN-γ reactivity may contribute. We did, indeed, observe lower numbers of unstimulated cells secreting IFN-γ at W52 and W96, but we only observed lower reactivity to MOG and MBP at W96.This may also, at least partly, explain why patients treated with cladribine are at increased risk of certain viral infections which are generally controlled by IFN-γ-dependent type 1 immune responses (49).

We conclude that the effects of cladribine observed after year one are maintained and, for some effects, even increased two years after the initiation of a full course of treatment with cladribine tablets. The most pronounced effect was a substantial reduction in circulating memory B cells and proinflammatory B cell responses. This is consistent with a reduction of memory B cells being a general feature of disease-modifying MS therapies (50). Furthermore, we observed reduced T cell responses to autoantigens presented by B cells at W52 and a further reduction in responses to the myelin antigens MBP and MOG after 96 weeks. We cannot exclude that the effects of previous treatment could contribute as only few patients in our study were previously untreated but our results compare well with the results of the MAGNIFY-MS study where half of the patients were previously untreated. However, neither the MAGNIFY-MS study nor any other previous studies of which we are aware compared the immunological effects of cladribine in previously treated and untreated patients. Future studies are needed to confirm these observations in independent patient cohorts and address the possible impact of previous treatments on the response to cladribine. Furthermore, it should be addressed whether differences between patients in the magnitude of these effects are associated with the effectiveness of treatment with cladribine tablets.

Data availability statement

The raw data supporting the conclusions of this article will be made available by the authors, without undue reservation.

Ethics statement

The studies involving humans were approved by The regional scientific ethics committee (protocol number H-16047666). The studies were conducted in accordance with the local legislation and institutional requirements. The participants provided their written informed consent to participate in this study.

Author contributions

RH: Conceptualization, Data curation, Formal analysis, Funding acquisition, Investigation, Methodology, Project administration, Resources, Software, Validation, Visualization, Writing – original draft, Writing – review & editing. MV: Conceptualization, Funding acquisition, Supervision, Writing – review & editing. MR: Data curation, Investigation, Writing – review & editing. SC: Data curation, Investigation, Writing – review & editing. FS: Conceptualization, Funding acquisition, Methodology, Project administration, Resources, Supervision, Writing – review & editing.

Funding

The author(s) declare financial support was received for the research, authorship, and/or publication of this article. This study was financially supported by Merck A/S, Søborg, Denmark, an affiliate of Merck KGaA Darmstadt, Germany (CrossRef Funder ID: 10.13039/100009945), however Merck KGaA had no influence on the conduct, analysis, or interpretation of data. FS holds a professorship funded by the Danish Multiple Sclerosis Society.

Acknowledgments

The authors highly acknowledge Lisbeth Stolpe for her excellent technical assistance.

Conflict of interest

RH has received speaker honoraria from Merck KGaA. MV has received speaker honoraria from Merck KGaA. MR has received support for congress participation from Merck KGaA. FS has served on scientific advisory boards for, served as consultant for, received support for congress participation or received speaker honoraria from Alexion, Biogen, Bristol Myers Squibb, Merck KGaA, Novartis, Roche and Sanofi Genzyme. His laboratory has received research support from Biogen, Merck KGaA, Novartis, Roche and Sanofi Genzyme.

The remaining author declares that the research was conducted in the absence of any commercial or financial relationships that could be construed as a potential conflict of interest.

Publisher's note

References

1. Reich DS, Lucchinetti CF, Calabresi PA. Multiple sclerosis. *N Engl J Med* (2018) 378:169–80. doi: 10.1056/NEJMra1401483

2. Kaskow BJ, Baecher-Allan C. Effector T cells in multiple sclerosis. *Cold Spring Harb Perspect Med* (2018) 8(4):a029025. doi: 10.1101/cshperspect.a029025

3. Cencioni MT, Mattoscio M, Magliozzi R, Bar-Or A, Muraro PA. B cells in multiple sclerosis - from targeted depletion to immune reconstitution therapies. *Nat Rev Neurol* (2021) 17:399–414. doi: 10.1038/s41582-021-00498-5

4. Dendrou CA, Fugger L and Friese MA. Immunopathology of multiple sclerosis. *Nat Rev Immunol* (2015) 15:545–58. doi: 10.1038/nri3871

5. Craft JE. Follicular helper T cells in immunity and systemic autoimmunity. *Nat Rev Rheumatol* (2012) 8:337–47. doi: 10.1038/nrrheum.2012.58

6. Weinstein JS, Herman EI, Lainez B, Licona-Limon P, Esplugues E, Flavell R, et al. TFH cells progressively differentiate to regulate the germinal center response. *Nat Immunol* (2016) 17:1197–205. doi: 10.1038/ni.3554

7. Zhang X, Ge R, Chen H, Ahiafor M, Liu B, Chen J, et al. Follicular helper CD4(+) T cells, follicular regulatory CD4(+) T cells, and inducible costimulator and their roles in multiple sclerosis and experimental autoimmune encephalomyelitis. *Mediators Inflammation* (2021) 2021:2058964. doi: 10.1155/2021/2058964

8. Linterman MA, Pierson W, Lee SK, Kallies A, Kawamoto S, Rayner TF, et al. Foxp3+ follicular regulatory T cells control the germinal center response. *Nat Med* (2011) 17:975–82. doi: 10.1038/nm.2425

9. Chung Y, Tanaka S, Chu F, Nurieva RI, Martinez GJ, Rawal S, et al. Follicular regulatory T cells expressing Foxp3 and Bcl-6 suppress germinal center reactions. *Nat Med* (2011) 17:983–8. doi: 10.1038/nm.2426

10. Wollenberg I, Agua-Doce A, Hernandez A, Almeida C, Oliveira VG, Faro J, et al. Regulation of the germinal center reaction by Foxp3+ follicular regulatory T cells. *J Immunol* (2011) 187:4553–60. doi: 10.4049/jimmunol.1101328

11. Puthenparampil M, Zito A, Pantano G, Federle L, Stropparo E, Miante S, et al. Peripheral imbalanced TFH/TFR ratio correlates with intrathecal IgG synthesis in multiple sclerosis at clinical onset. *Mult Scler* (2019) 25:918–26. doi: 10.1177/1352458518779951

12. Dong L, He Y, Cao Y, Wang Y, Jia A, Wang Y, et al. Functional differentiation and regulation of follicular T helper cells in inflammation and autoimmunity. *Immunology* (2021) 163:19–32. doi: 10.1111/imm.13282

13. Dhaeze T, Peelen E, Hombrouck A, Peeters L, Van Wijmeersch B, Lemkens N, et al. Circulating follicular regulatory T cells are defective in multiple sclerosis. *J Immunol (Baltimore Md 1950)* (2015) 195:832–40. doi: 10.4049/jimmunol.1500759

14. Holm Hansen R, Talbot J, Hojsgaard Chow H, Bredahl Hansen M, Buhelt S, Herich S, et al. Increased intrathecal activity of follicular helper T cells in patients with relapsing-remitting multiple sclerosis. *Neurol Neuroimmunol Neuroinflamm* (2022) 9:20220714. doi: 10.1212/NXI.0000000000200009

15. Morita R, Schmitt N, Bentebibel SE, Ranganathan R, Bourdery L, Zurawski G, et al. Human blood CXCR5(+)CD4(+) T cells are counterparts of T follicular cells and contain specific subsets that differentially support antibody secretion. *Immunity* (2011) 34:108–21. doi: 10.1016/j.immuni.2010.12.012

16. Cunill V, Clemente A, Lanio N, Barceló C, Andreu V, Pons J, et al. Follicular T cells from smB(-) common variable immunodeficiency patients are skewed toward a th1 phenotype. *Front Immunol* (2017) 8:174. doi: 10.3389/fimmu.2017.00174

17. Duddy M, Niino M, Adatia F, Hebert S, Freedman M, Atkins H, et al. Distinct effector cytokine profiles of memory and naive human B cell subsets and implication in multiple sclerosis. *J Immunol* (2007) 178:6092–9. doi: 10.4049/jimmunol.178.10.6092

18. McWilliam O, Sellebjerg F, Marquart HV, von Essen MR. B cells from patients with multiple sclerosis have a pathogenic phenotype and increased LTalpha and TGFbeta1 response. *J Neuroimmunol* (2018) 324:157–64. doi: 10.1016/j.jneuroim.2018.09.001

19. Bar-Or A, Fawaz L, Fan B, Darlington PJ, Rieger A, Ghorayeb C, et al. Abnormal B-cell cytokine responses a trigger of T-cell-mediated disease in MS? *Ann Neurol* (2010) 67:452–61. doi: 10.1002/ana.21939

20. Cencioni MT, Ali R, Nicholas R, Muraro PA. Defective CD19+CD24(hi)CD38(hi) transitional B-cell function in patients with relapsing-remitting MS. *Mult Scler* (2021) 27:1187–97. doi: 10.1177/1352458520951536

21. Kim Y, Kim G, Shin HJ, Hyun JW, Kim SH, Lee E, et al. Restoration of regulatory B cell deficiency following alemtuzumab therapy in patients with relapsing multiple sclerosis. *J Neuroinflamm* (2018) 15:300. doi: 10.1186/s12974-018-1334-y

22. Knippenberg S, Peelen E, Smolders J, Thewissen M, Menheere P, Cohen Tervaert JW, et al. Reduction in IL-10 producing B cells (Breg) in multiple sclerosis is accompanied by a reduced naive/memory Breg ratio during a relapse but not in remission. *J Neuroimmunol* (2011) 239:80–6. doi: 10.1016/j.jneuroim.2011.08.019

23. Giovannoni G, Comi G, Cook S, Rammohan K, Rieckmann P, Soelberg Sorensen , et al. A placebo-controlled trial of oral cladribine for relapsing multiple sclerosis. *N Engl J Med* (2010) 362:416–26. doi: 10.1056/NEJMoa0902533

24. Sorensen PS, Sellebjerg F. Pulsed immune reconstitution therapy in multiple sclerosis. *Ther Adv Neurol Disord* (2019) 12:1756286419836913. doi: 10.1177/1756286419836913

25. Baker D, Pryce G, Herrod SS, Schmierer K. Potential mechanisms of action related to the efficacy and safety of cladribine. *Mult Scler Relat Disord* (2019) 30:176–86. doi: 10.1016/j.msard.2019.02.018

26. Giovannoni G, Soelberg Sorensen P, Cook S, Rammohan K, Rieckmann P, Comi G, et al. Safety and efficacy of cladribine tablets in patients with relapsing-remitting multiple sclerosis: Results from the randomized extension trial of the CLARITY study. *Multiple Sclerosis (Houndmills Basingstoke England)* (2018) 24:1594–604. doi: 10.1177/1352458517727603

27. Spiezia AL, Cerbone V, Molinari EA, Capasso N, Lanzillo R, Carotenuto A, et al. Changes in lymphocytes, neutrophils and immunoglobulins in year-1 cladribine treatment in multiple sclerosis. *Mult Scler Relat Disord* (2022) 57:103431. doi: 10.1016/j.msard.2021.103431

28. Baker D, Herrod SS, Alvarez-Gonzalez C, Zalewski L, Albor C, Schmierer K. Both cladribine and alemtuzumab may effect MS *via* B-cell depletion. *Neurol Neuroimmunol Neuroinflamm* (2017) 4:e360. doi: 10.1212/nxi.0000000000000360

29. Ceronie B, Jacobs BM, Baker D, Dubuisson N, Mao Z, Ammoscato F, et al. Cladribine treatment of multiple sclerosis is associated with depletion of memory B cells. *J Neurol* (2018) 265:1199–209. doi: 10.1007/s00415-018-8830-y

30. Comi G, Cook S, Giovannoni G, Rieckmann P, Sorensen PS, Vermersch P, et al. Effect of cladribine tablets on lymphocyte reduction and repopulation dynamics in patients with relapsing multiple sclerosis. *Mult Scler Relat Disord* (2019) 29:168–74. doi: 10.1016/j.msard.2019.01.038

31. Stuve O, Soelberg Soerensen P, Leist T, Giovannoni G, Hyvert Y, Damian D, et al. Effects of cladribine tablets on lymphocyte subsets in patients with multiple sclerosis: an extended analysis of surface markers. *Ther Adv Neurol Disord* (2019) 12:1756286419854986. doi: 10.1177/1756286419854986

32. Rolfes L, Pfeuffer S, Huntemann N, Schmidt M, Su C, Skuljec J, et al. Immunological consequences of cladribine treatment in multiple sclerosis: A real-world study. *Mult Scler Relat Disord* (2022) 64:103931. doi: 10.1016/j.msard.2022.103931

33. Moser T, Schwenker K, Seiberl M, Feige J, Akgün K, Haschke-Becher E, et al. Long-term peripheral immune cell profiling reveals further targets of oral cladribine in MS. *Ann Clin Transl Neurol* (2020) 7:2199–212. doi: 10.1002/acn3.51206

34. Wiendl H, Schmierer K, Hodgkinson S, Derfuss T, Chan A, Sellebjerg F, et al. Specific patterns of immune cell dynamics may explain the early onset and prolonged efficacy of cladribine tablets: A MAGNIFY-MS substudy. *Neurol Neuroimmunol Neuroinflamm* (2023) 10:20221121. doi: 10.1212/nxi.0000000000200048

35. Holm Hansen R, von Essen MR, Mahler MR, Cobanovic S, Binko TS, Sellebjerg F, et al. Cladribine effects on T and B cells and T cell reactivity in multiple sclerosis. . *Ann Neurol* (2023) 94:518–30. doi: 10.1002/ana.26684

36. Thompson AJ, Banwell BL, Barkhof F, Carroll WM, Coetzee T, Comi G, et al. Diagnosis of multiple sclerosis: 2017 revisions of the McDonald criteria. *Lancet Neurol* (2018) 17:162–73. doi: 10.1016/S1474-4422(17)30470-2

37. Benjamin DJ, Berger JO, Johannesson M, Nosek BA, Wagenmakers EJ, Berk R, et al. Redefine statistical significance. *Nat Hum Behav* (2018) 2:6–10. doi: 10.1038/s41562-017-0189-z

38. Portugal S, Obeng-Adjei N, Moir S, Crompton PD, Pierce SK. Atypical memory B cells in human chronic infectious diseases: An interim report. *Cell Immunol* (2017) 321:18–25. doi: 10.1016/j.cellimm.2017.07.003

39. Xu B, Wang S, Zhou M, Huang Y, Fu R, Guo C, et al. The ratio of circulating follicular T helper cell to follicular T regulatory cell is correlated with disease activity in systemic lupus erythematosus. *Clin Immunol (Orlando Fla)* (2017) 183:46–53. doi: 10.1016/j.clim.2017.07.004

40. Achiron A, Mandel M, Dreyer-Alster S, Harari G, Magalashvili D, Sonis P, et al. Humoral immune response to COVID-19 mRNA vaccine in patients with multiple

sclerosis treated with high-efficacy disease-modifying therapies. *Ther Adv Neurol Disord* (2021) 14:17562864211012835. doi: 10.1177/17562864211012835

41. Shi J, Hou S, Fang Q, Liu X, Liu X, Qi H. PD-1 controls follicular T helper cell positioning and function. *Immunity* (2018) 49:264–274.e264. doi: 10.1016/j.immuni.2018.06.012

42. van Langelaar J, van der Vuurst de Vries RM, Janssen M, Wierenga-Wolf AF, Spilt IM, Siepman TA, et al. T helper 17.1 cells associate with multiple sclerosis disease activity: perspectives for early intervention. *Brain* (2018) 141:1334–49. doi: 10.1093/brain/awy069

43. Jelcic I, Al Nimer F, Wang J, Lentsch V, Planas R, Jelcic I, et al. Memory B cells activate brain-homing, autoreactive CD4(+) T cells in multiple sclerosis. *Cell* (2018) 175:85–100:e123. doi: 10.1016/j.cell.2018.08.011

44. von Essen MR, Ammitzbøll C, Börnsen L, Sellebjerg F. Assessment of commonly used methods to determine myelin-reactivity of T cells in multiple sclerosis. *Clin Immunol* (2021) 230:108817. doi: 10.1016/j.clim.2021.108817

45. Wang J, Jelcic I, Muhlenbruch L, Haunerdinger V, Toussaint NC, Zhao Y, et al. HLA-DR15 molecules jointly shape an autoreactive T cell repertoire in multiple sclerosis. *Cell* (2020) 183:1264–81:e1220. doi: 10.1016/j.cell.2020.09.054

46. Elong Ngono A, Pettre S, Salou M, Bahbouhi B, Soulillou JP, Brouard S, et al. Frequency of circulating autoreactive T cells committed to myelin determinants in relapsing-remitting multiple sclerosis patients. *Clin Immunol* (2012) 144:117–26. doi: 10.1016/j.clim.2012.05.009

47. van Sechel AC, Bajramovic JJ, van Stipdonk MJ, Persoon-Deen C, Geutskens SB, van Noort JM. EBV-induced expression and HLA-DR-restricted presentation by human B cells of alpha B-crystallin, a candidate autoantigen in multiple sclerosis. *J Immunol* (1999) 162:129–35. doi: 10.4049/jimmunol.162.1.129

48. van Noort JM, van Sechel AC, Bajramovic JJ, el Ouagmiri M, Polman CH, Lassmann H, et al. The small heat-shock protein alpha B-crystallin as candidate autoantigen in multiple sclerosis. *Nature* (1995) 375:798–801. doi: 10.1038/375798a0

49. Cook S, Leist T, Comi G, Montalban X, Giovannoni G, Nolting , et al. Safety of cladribine tablets in the treatment of patients with multiple sclerosis: An integrated analysis. *Mult Scler Relat Disord* (2019) 29:157–67. doi: 10.1016/j.msard.2018.11.021

50. Baker D, Marta M, Pryce G, Giovannoni G, Schmierer K. Memory B cells are major targets for effective immunotherapy in relapsing multiple sclerosis. *EBioMedicine* (2017) 16:41–50. doi: 10.1016/j.ebiom.2017.01.042

frontiers | Frontiers in Immunology

TYPE Review
PUBLISHED 28 May 2024
DOI 10.3389/fimmu.2024.1380063

OPEN ACCESS

EDITED BY
Mahsa Ghajarzadeh,
Johns Hopkins University, United States

REVIEWED BY
Kalil Alves de Lima,
State University of Campinas, Brazil
Andre Ortlieb Guerreiro Cacais,
Karolinska Institutet (KI), Sweden

*CORRESPONDENCE
Sangyong Jung
jungsy0505@cha.ac.kr

†These authors have contributed equally to this work

RECEIVED 31 January 2024
ACCEPTED 14 May 2024
PUBLISHED 28 May 2024

CITATION
Tan LY, Cunliffe G, Hogan MP, Yeo XY, Oh C, Jin B, Kang J, Park J, Kwon M-S, Kim M and Jung S (2024) Emergence of the brain-border immune niches and their contribution to the development of neurodegenerative diseases. *Front. Immunol.* 15:1380063. doi: 10.3389/fimmu.2024.1380063

Emergence of the brain-border immune niches and their contribution to the development of neurodegenerative diseases

Li Yang Tan[1†], Grace Cunliffe[2†], Michael Patrick Hogan[2], Xin Yi Yeo[1], Chansik Oh[3], Bohwan Jin[3], Junmo Kang[3], Junho Park[4], Min-Soo Kwon[4], MinYoung Kim[5,6,7] and Sangyong Jung[3*]

[1]Department of Psychological Medicine, Yong Loo Lin School of Medicine, National University of Singapore, Singapore, Singapore, [2]Division of Neuroscience, School of Biological Sciences, Faculty of Biology, Medicine and Health, The University of Manchester, Manchester, United Kingdom, [3]Department of Medical Science, College of Medicine, CHA University, Seongnam, Republic of Korea, [4]Department of Pharmacology, Research Institute for Basic Medical Science, School of Medicine, CHA University, Seongnam, Republic of Korea, [5]Rehabilitation and Regeneration Research Center, CHA University School of Medicine, Seongnam, Republic of Korea, [6]Department of Biomedical Science, CHA University School of Medicine, Seongnam, Republic of Korea, [7]Department of Rehabilitation Medicine, CHA Bundang Medical Center, CHA University, Seongnam, Republic of Korea

Historically, the central nervous system (CNS) was regarded as 'immune-privileged', possessing its own distinct immune cell population. This immune privilege was thought to be established by a tight blood-brain barrier (BBB) and blood-cerebrospinal-fluid barrier (BCSFB), which prevented the crossing of peripheral immune cells and their secreted factors into the CNS parenchyma. However, recent studies have revealed the presence of peripheral immune cells in proximity to various brain-border niches such as the choroid plexus, cranial bone marrow (CBM), meninges, and perivascular spaces. Furthermore, emerging evidence suggests that peripheral immune cells may be able to infiltrate the brain through these sites and play significant roles in driving neuronal cell death and pathology progression in neurodegenerative disease. Thus, in this review, we explore how the brain-border immune niches may contribute to the pathogenesis of neurodegenerative disorders such as Alzheimer's disease (AD), Parkinson's disease (PD), and multiple sclerosis (MS). We then discuss several emerging options for harnessing the neuroimmune potential of these niches to improve the prognosis and treatment of these debilitative disorders using novel insights from recent studies.

KEYWORDS

brain-border, neuroimmune, neurodegeneration, Alzheimer's disease, Parkinson's disease, multiple sclerosis

1 Introduction

For over a century, a fundamental principle in neurological research has been the understanding that the central nervous system (CNS) functions as a highly impermeable and immune-privileged organ system. This concept originated from a series of groundbreaking discoveries by Elrich (1885) (1), Bield and Kraus (1898) (2), and Lewandowsky (1900) (3), who showed that arsinine dyes, cholic acids or sodium ferro-cyanide, when administered intravenously, penetrate all organs except the brain. In 1900, Lewandowsky proposed the concept of a blood-brain barrier (BBB) but was met with criticisms regarding the specificity of the injected substrates used, as the substrates were thought to bind to plasma proteins in the blood. However, further evidence for the presence of a BBB was presented in 1913, when Goldmann systemically injected the acidic dye trypan blue into several species, including dogs and monkeys, and found that the brain remained unstained, although the choroid plexuses were stained (4, 5). In contrast, the entire parenchyma was stained when trypan blue was injected directly into the brain ventricles. This led Goldmann to postulate that the CNS is segregated from the blood circulation by a very selective barrier and that the choroid plexus is the host of this barrier that modulates substance entry into the CNS (6). Goldmann further proposed that cerebrospinal fluid (CSF) was the agent of substance transport for the CNS (7).

The concept of an immune privilege in the brain began to gain prominence after the discovery of the physical BBB and blood-cerebrospinal-fluid barrier (BCSFB). In 1921, Japanese scientist Shirai observed that transplanted rat sarcoma cells proliferate when implanted in the mouse brain parenchyma, but not when implanted into the muscles or skin (8). Shortly after in 1923, Murphy and Sturm reported that tumoral growth was inhibited when mouse tumours were co-transplanted into the brain with homologous spleen tissue (9), suggesting that peripheral immune cells were not present within the brain. Around the same time, in 1920–1921, Spanish neuroscientist Rio-Hortega described the brain as containing specialised ramified phagocytes that can self-proliferate (10), indicating that the CNS evolved to have its own unique innate immune system. Nevertheless, the term ‘immune privilege’ was only officially coined in 1948, when Brazilian-British biologist Sir Peter Medawar reported the lack of immune response to skin allografts transplanted to the brain and anterior chamber eyes of rabbits (11). At this time, the consensus was that peripheral immune cells were ‘absolutely’ restricted from the brain parenchyma due to the presence of a tight BBB and BCSFB preventing peripheral immune cell infiltration into the CNS.

However, the perception of this ‘absolute’ barrier between the peripheral system and the CNS began to shift in the 2000s with the discovery that activated peripheral immune cells, such as T cells and B cells, successfully enter and closely localise with the brain parenchyma at the borders of the CNS (12). Meningeal γδ T cells have even been suggested to play pivotal roles in secreting factors to maintain normal neural functions such as synaptic plasticity (13). In addition, it was previously believed that microglial major histocompatibility complex II (MHC-II) was solely responsible for causing neuroinflammation seen in neurodegenerative disease. However, it is becoming increasingly apparent that the microglial MHC-II is not essential for neuroinflammation in various neurodegenerative conditions (14, 15). Moreover, peripheral immune cell types, such as border-associated macrophages (BAMs) at brain-border niches, and infiltrating dendritic cells from the CSF are known to express MHC-II and can migrate to cervical lymph nodes to initiate adaptive responses (14, 16). Collectively, these observations aid in redefining our current understanding of a ‘relative’ immune privilege within the CNS.

Although numerous excellent reviews regarding the brain-border immune niches have been published previously (17, 18), the precise functions of these niches in neurodegenerative diseases remain unknown. Therefore, in this review, we will provide an overview of the immune niches and their functions, before updating the current understanding of the roles of the different niches relating to the progression of Alzheimer’s disease (AD), Parkinson’s disease (PD) and multiple sclerosis (MS) by referencing recent articles. We will discuss how these findings may improve or influence the future direction of the diagnosis, prognosis, and therapy of these progressively debilitating diseases.

2 Brain-border immune niches

2.1 Choroid plexus

The choroid plexus is a highly vascularised tissue that lines the pia mater within each ventricle of the brain, functioning to separate CSF from the blood. The choroid plexus consists of tightly bound epithelial cells with their basolateral surface surrounding a network of fenestrated capillary cores and loose stromal tissues. The apical surfaces of these cells contact the CSF within the brain ventricles and facilitate CSF production and secretion of signalling factors. The choroid plexus epithelium accounts for most of the BCSFB through maintaining tight junctions between epithelial cells (19). Away from the choroid plexus, ependymal cells continuously line the rest of the epithelium on the remaining walls of the CSF cavities. However, unlike choroid plexus epithelial cells, ependymal cells are held more loosely by desmosomes, and thus do not restrict movement between the CSF cavity and the parenchyma (20).

The choroid plexus stroma is a heterogenous, and dynamic immune environment located between the choroid plexus epithelium and the capillaries. It consists primarily of arachnoid cells, reticular fibroblasts, pericytes, and smooth muscle cells (21). Resident lymphoid and myeloid populations such as $CD4^+$ T helper cells (Th1, Th2, Tregs) (22), $CXCR3^+$ dendritic cells, and macrophages (23), are sparsely distributed within the stroma, but still in close proximity to stromal elements. This unique apposition allows the choroid plexus to respond to antigen-presenting cells (APCs) or inflammation factors that may present either from the CSF or the systemic circulation.

Recent research has shed light on the complex immunological interactions within the choroid plexus stroma (Figure 1). In septic mouse models induced by intravenous lipopolysaccharide (LPS) administration, activated APCs such as M1 macrophages can infiltrate the choroid plexus and release interleukin (IL)-1β (21).

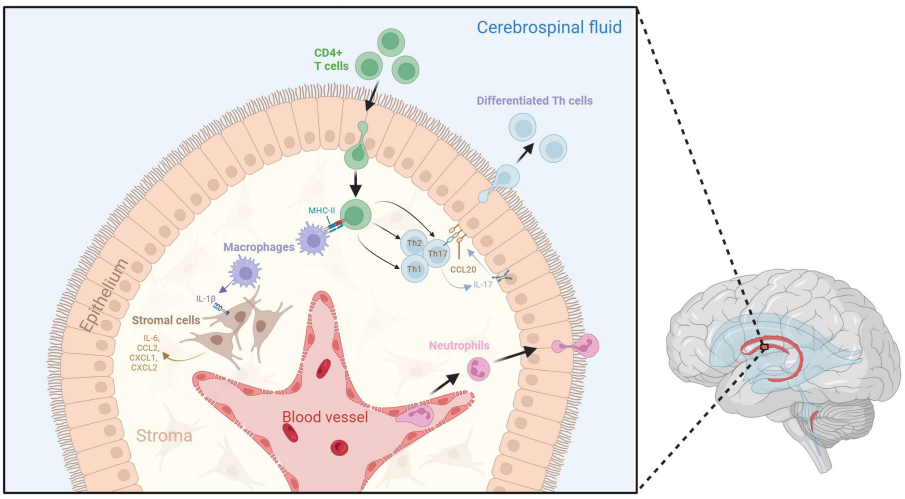

FIGURE 1
Dynamic neuroinflammatory responses at the choroid plexus. The choroid plexus is an active immune niche that monitors immune factors from the blood and the CSF. During the inflammatory response, surveilling CD4+ T cells infiltrate the choroid plexus and are presented with antigen-loaded MHC-II by resident macrophages. This triggers their differentiation into various T helper cell subtypes. Th17 cells secrete IL-17, which promotes choroid plexus epithelial CCL20 expression, therefore allowing for the adhesion of lymphocytes to the choroid plexus epithelium and aiding their transmigration into the CSF. Macrophages within the stroma secrete IL-1β due to interactions with activated $CD4^+$ T cells. IL-1 β interacts with stromal cells, which in turn secrete pro-inflammatory cytokines and chemokines such as IL-6, CCL2, CXCL1, and CXCL2. Tight junctions between choroid plexus epithelial cells become compromised following inflammation, which may lead to increased movement of immune cells across the epithelium. Additionally, neutrophils from the blood stream accumulate in the choroid plexus stroma, allowing them to infiltrate the CSF. Figure created with BioRender.

Stromal cells expressing IL-1 receptor type 1 (IL-1R1) and IL-1 receptor accessory protein (IL-1RAcP) can respond to IL-1β and subsequently secrete proinflammatory factors such as IL-6, CCL2, CXCL1, and CXCL2 (21). Additionally, when stimulated by cytokines such as interferon-gamma (IFN-γ) and IL-17 from $CD4^+$ Th cells, the choroid plexus epithelium expresses unique trafficking molecules and releases chemoattractant ligands such as CCL20, which promote the transmigration of preactivated B cells and T cells into the CSF in experimental autoimmune encephalomyelitis (EAE) mouse models for MS (24, 25). Neutrophils have also been shown to infiltrate the choroid plexus from the bloodstream following traumatic head injury, before accumulating in the CSF around the site of injury (26).

As individuals age, the composition of the choroid plexus stroma undergoes gradual changes due to local and peripheral senescence (27). The tight junctions of the choroid plexus epithelium are greatly compromised (28), and there is an increase in stromal leukocyte proportion, particularly T helper and cytotoxic T cells (29). Consequently, there is a shift in the cytokine profile, marked by elevated levels of inflammatory cytokines such as IL-1β, tumour necrosis factor-alpha (TNF-α), and IFN-γ (22, 27, 30), contributing to a progressively inflammatory brain.

2.2 Meninges

The meninges are a series of membranes covering the brain and spinal cord, forming a continuous barrier between the CNS and periphery. The primary roles of the meninges are to protect the CNS from trauma and to provide structural support for nerves, vasculatures and lymphatics that supply the CNS (31). Conventionally, the meninges are divided into three distinctive structural layers: the outermost dura mater, the arachnoid mater, and the innermost pia mater, which forms direct contact with the brain parenchyma. Fluid-filled cavities between the arachnoid and pia mater are termed subarachnoid spaces and those between the pia mater and parenchyma are called subpial spaces (32). The pia mater, subarachnoid space and arachnoid mater are collectively referred to as the leptomeninges (33).

The thickest and outermost lining of the meninges is known as the dura mater. This fibrous membrane covers the interior of the skull, and receives its own innervation and vascular supply at the apical surface from branches of the external carotid arteries (34). Histologically, the dura mater is further characterised into three major layers: the periosteal layer, which lines the inner surface of the cranium; the meningeal layer, which consists of a dense, fibrous membrane that lies underneath the periosteal layer; and the flattened dural border cell (DBC) layer which attaches to the arachnoid mater. Large cavities between the periosteal and meningeal layers are known as the dural venous sinuses. These provide an avenue for CSF to empty from the subarachnoid space through lymphatic channels into the internal jugular veins. In a healthy brain, there is no subdural space between the dura mater and the arachnoid mater (34).

The arachnoid mater is the middle layer of the meninges and comprises a thin layer of web-like connective tissue. The arachnoid mater is less densely vascularised compared to the dura mater and does not receive any innervation. However, the subarachnoid space that lies beneath the arachnoid mater contains CSF as well as vasculature, including arteries and veins. Lymphatic vessels have

also been reported to reside adjacent to the subarachnoid space (35). Parts of the subarachnoid mater project into the dural venous sinuses as arachnoid granulations, allowing drainage of CSF from the subarachnoid space into the dural sinuses (36).

Though the dura and arachnoid mater can easily be separated from the parenchyma, the pia mater attaches strongly to the convoluted surface of the brain as the innermost layer of flattened cells, forming a thin fibrous tissue (37). Lacking tight junctions, the pia mater is permeable to small solutes such as urea (35), and is highly vascularised, with many vessels permeating the membrane into the brain (38). The pia mater shields the parenchyma from the CSF at the subarachnoid space and, at the cortex, coats the penetrating arterioles (but not venules) of the parenchyma (36). However, as vessels become smaller, the pial lining becomes more discontinuous (39), resulting in capillaries having direct contact with glia limitans. The fluid-filled cavities that form between the vessels and glia limitans of the brain parenchyma are called perivascular spaces, also known as Virchow-Robin spaces. These form the glia-lymphatic (glymphatic) system that drains most of the CSF from the subarachnoid space (40).

Recently, a fourth meningeal layer, defined as the subarachnoid lymphatic-like membrane (SLYM), has been proposed (41). Resembling mesothelium, this comprises only a sparse layer of $Prox1^+$ lymphatic endothelial cells and loosely organised collagen fibres that encase pial vessels, separating the subarachnoid space into two distinct compartments; a superficial and a deep compartment (41, 42). Functionally, the SLYM restricts the passage of molecules smaller than 3 kDa, and therefore serves as a physical filter regulating material exchange between subarachnoid space compartments (41). Furthermore, it facilitates the direct exchange of small solutes between the CSF and venous blood, due to its proximity to the endothelial lining of the meningeal venous sinus (41). Notably, a significant accumulation of $CD45^+$ cells has been observed near the pial vessels on the brain surface, and this increases following the induction of inflammation with LPS, as well as with ageing (41). Macrophages expressing LYVE1, CD206, and CD68, as well as $CD11c^+$ dendritic cells have also been reported to reside in the SLYM (41). The presence of immune populations within this membrane may suggest that the SLYM is an active immune niche that functions as an assembly point for immune cells and regulates immune exchanges between the blood stream and the CSF between superficial and deep compartments of the subarachnoid space. Further investigation is necessary to understand the functional interplay of the SLYM with other meningeal layers, and its modulation of neuroinflammation in the brain parenchyma.

Another recent study unveiled multiple lymphoid-like structures within the dura of mice that closely associate with the infiltrating venous plexus (43). These tissues comprise a rich network of $PV1^+$ fenestrated blood vessels and $LYVE1^+$ lymphatic vessels, intertwined in a stroma of fibroblastic reticular cells. This network harbours germinal centre-like hubs, and contains $CD11c^+$ myeloid cells, $CD3^+$ T cells, B cells, neutrophils, macrophages, dendritic cells and (to varying degrees) their immature progenitors (43). The largest of these clusters was found mainly surrounding the rostral-rhinal confluence of the sinuses, located superior to the olfactory bulb (43). With their proximity to the cranium, these lymphoid tissues, especially those in the rostral-rhinal hubs, are in contact with small, ossified channels through a recess in the bone, and potentially derive their progenitor populations from the cranial bone marrow (CBM) (43). The same study suggested that, in addition to sampling CSF from within the dura, lymphoid hubs can detect antigens and mount responses to infections originating from the olfactory tract, CSF, and peripheral blood circulation. This is due to the presence of fenestrated blood vessels and the proximity of lymphoid hubs to the olfactory tract. When vesicular stomatitis virus (VSV) was introduced intranasally, the cytokine milieu and cellular compositions of dural-associated lymphoid tissues (DALTs) were altered, characterised by increased IL-12 expression and enhanced distribution and activation of B cells into plasma cells (43), thereby triggering a humoral response. Additionally, microbeads were observed to localise within these DALTs following their intravenous injection (43). This evidence indicates that the meningeal hubs actively contribute to preventing external infections from breaching the CNS.

The composition of lymphoid hubs along the dura appears to change with increasing age and disease progression (44, 45). Interestingly, while B cells were found to be derived from the CBM, lineage tracing of the cells did not reveal an increase in $CD4^+$ T cell populations in the CBM, suggesting that the enhanced localisation of $CD4^+$ T cells within the meninges may be derived from systemic circulation (46). An overview of the immune niches within the skull-meninges-brain axis is shown in Figure 2.

2.3 Perivascular spaces

Perivascular spaces are fluid-filled cavities that lie between penetrating arterioles and the brain parenchyma. At the basal section of arterioles, perivascular spaces are continuous with the subarachnoid space (and therefore CSF) of the meninges and separated from the brain parenchyma by the pia mater (47). As vessels enter the cortex through the pia mater, the vascular endothelium and its basal membrane are in direct contact with the end feet of the glia limitans, forming the primary structure of the BBB (48). Perivascular spaces are established between tight junctions of the vascular endothelium and the astrocytic end feet and contain interstitial fluid from the outflow of blood from vessels, and CSF from the subarachnoid space. Although small in diameter, perivascular spaces together form an extensive network of glymphatic channels that function to drain CSF from the subarachnoid space (40) and remove neurometabolic waste from the brain, particularly during sleep (49, 50).

Pericytes and native innate immune cells are the primary cell types found within perivascular spaces. Pericytes play crucial roles in maintaining the structure of the BBB by regulating vascular development, angiogenesis, extending glial limitans end feet, and mediating inflammatory processes associated with immune cells. To fulfil this diverse range of functions, pericytes exhibit stem cell-like properties, enabling them to differentiate into angioblasts, neural

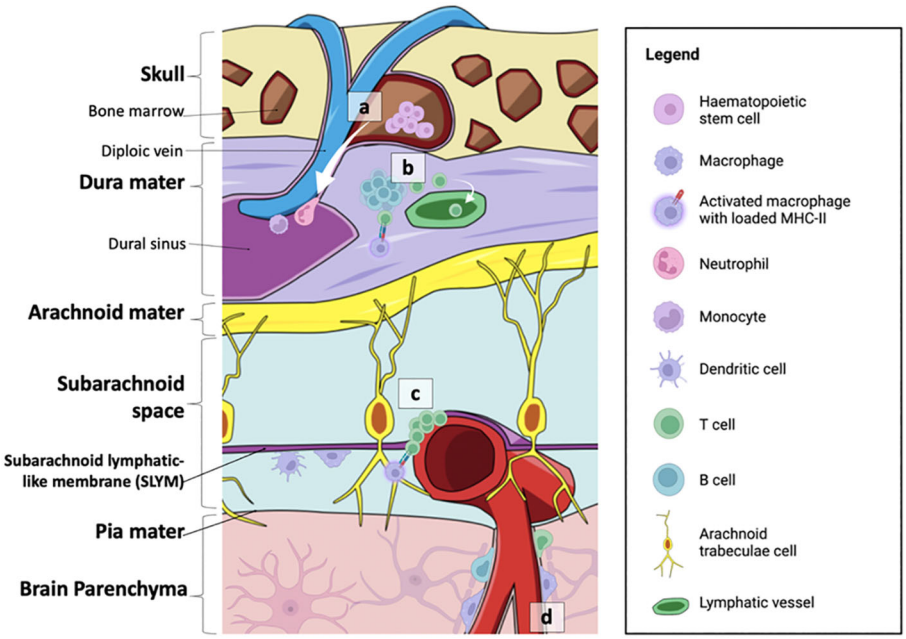

FIGURE 2
Summary of the neuroimmune niches within the skull-meninges-brain axis. **(A)** The cranial bone marrow (CBM) provides a source of haematopoietic stem cells, which supply lymphoid and myeloid cells to the dural sinuses during inflammatory events. **(B)** Germinal-like centres in the dural-associated lymphatic tissues (DALTs) contain lymphocytes. T cell populations in the meninges are most likely derived from the blood or CSF. T helper cells can be activated by MHC-II-presenting macrophages within the dura mater, and subsequently activate B cells and cytotoxic T cells. Immune cell activity within lymphoid hubs may help prevent the entry of external infection into the brain. **(C)** T cell clusters and MHC-II-presenting macrophages are also found at the subarachnoid lymphatic-like membrane (SLYM), closely associated with pial blood vessels. The SLYM may therefore serve as an active immune niche that regulates immune exchanges between the blood stream and the CSF. **(D)** Perivascular spaces house resident immune cells, such as perivascular macrophages, as well as a smaller population of B cells and T cells. Figure created with BioRender.

progenitor cells, endothelial cells, and even microglia-like phenotypes (51, 52).

Regarding perivascular innate immune cells, those found at basal parts of the arterioles have been identified as BAMs (also called perivascular macrophages) positive for CD45, CD11b, CX3CR1, Ly6C and CD38, while $CD119^{+}$ microglia are present in perivascular spaces of capillaries (53). Conversely, lymphocytes such as $CD8^{+}$ tissue resident memory T cells and B cells are typically found in relatively low numbers in the perivascular spaces of the corpus callosum under normal physiological conditions (54), and are likely recruited to these spaces only during pathological states. Interestingly, these observations collectively suggest that perivascular spaces may harbour their own distinct population of self-proliferating immune cells (55).

The identification of perivascular spaces via magnetic resonance imaging (MRI) scans may serve as an important diagnostic and prognostic criterion. In both neonates and adult humans, perivascular spaces that are <2 mm in diameter are considered normal (47). Dilation of perivascular spaces has been associated with various conditions including old age (40), hypertension, vertigo, cysts (56), neuroinflammatory disorders such as dementia, MS (57), secondary PD, mega-encephalopathy, hydrocephalus (58), and autism spectrum disorder (ASD) (59). Currently, the cause of perivascular space dilation is not fully known but may be linked to obstruction of glymphatic flow. Interestingly, sleep (a processes commonly disrupted in old age and neurodegenerative disease) was recently reported to promote glymphatic clearance of metabolic waste by inducing rhythmic oscillations at delta (0.5–4 Hz), theta (6–10Hz), spindle (12–15Hz), and ripple (140–200Hz) wavelengths by synchronising neuronal activity (60). Moreover, aquaporin 4 (AQP4) proteins at astrocytic end feet also appear to have pivotal roles in regulating interstitial fluid pressure at the perivascular spaces (61). Additionally, arterial pulsation (62, 63), and peptide signalling (64), have been suggested to contribute to CSF dynamics and glymphatic clearance. Based on these findings, several hypotheses have been proposed surrounding the cause of perivascular space dilation, and include mechanical stress arising from impaired CSF pulsations (65, 66), increased vascular permeability (67), obstruction of downstream lymphatic drainage, and atrophy of the parenchyma (68, 69), all of which may lead to increased fluid exudation into the perivascular space. In hypertensive rat models, microglia that release inflammatory cytokine IL-1β have been observed to trigger the overexpression of prostaglandin E2 (PGE2) (70) and affect pericyte-endothelial cell interactions, resulting in vascular destabilisation and increased vascular permeability (71). However, the precise extent of immune cell involvement in the dilation of perivascular spaces is not clear.

2.4 Cranial bone marrow

Bone marrows are immune reservoirs for cells of various haematopoietic lineages. In normal physiology, the bone marrows house and deliver cells from myeloid and lymphoid lineages to the peripheral blood and surrounding tissues (72). The CBM is no exception; it has a distinct molecular composition and provides a direct source of immune cells to the CNS, thus shaping neuroimmune responses (73). The proximity of the CBM to the brain allows for the penetration of diploic veins from the meninges into the cranial marrow cavities through small micro-osseous channels, particularly at the frontal, parietal, and occipital cranium (74). These channels establish a route for direct communication between the CBM and the CSF, facilitating the exchange of immune cells, signalling molecules, or even pathogens (75), that may exacerbate wider immune responses.

In healthy mice, the CBM is responsible for maintaining the meningeal lymphocyte populations. For example, early B cells have been suggested to migrate from the CBM through miniature skull-meninges channels into the dural stroma (46), likely settling within DALTs (43). The lack of adaptive immune reactivity in the CBM suggests that clonal selection and full development of B cells could occur within the germinal-like centres in DALTs (43, 46), although this is not yet certain. Interestingly, cells that migrated from the CBM to the dura were not reported to express any T cell markers, suggesting that T cell localisation within the meninges is derived either from the blood or from the CSF (76). This indicates that blood-based or meningeal-based tracing is somewhat specific to lymphocyte populations at the meninges, and that T cells may be important for the prognosis of neurological diseases that arise from peripheral inflammation.

Recently, several groups have attempted to shed light on the conditions required to promote haematopoietic stem cell differentiation and migration from the CBM. CSF has been suggested to transport CSF-derived factors through skull meningeal channels of the cranium (77). This process activates signalling pathways crucial for inducing myelopoiesis and migration to the underlying dura (77). In EAE mice, induction of the CXCL12-CXCL4 axis was shown to promote T cell activation and migration into the CBM, leading to myeloid differentiation of haematopoietic stem cells into $Ly6b^+$ or $Ly6C^+$ macrophages and neutrophils that subsequently invade the CNS (78).

Additionally, the CBM composition appears to change with age (73, 79). Single-cell sequencing has revealed upregulation of senescence markers in mesenchymal cells within cranial stem cell niches and immune cells closely associated with inflammation (79). In adult humans, imaging techniques such as MRI have been utilised to correlate age-related changes with alterations in bone marrow composition. Analysis of apparent diffusion coefficient (ADC) values from MRI scans of five hundred subjects demonstrated significant alterations in the parietal and occipital bone marrow with increasing age (80), indicating changes to cell density (81–83). These inflammatory and age-related changes suggest a potential link between the CBM composition and brain health, although further research is required to determine the relationship between these alterations and age-related neurodegenerative diseases.

2.5 Brain-border lymphatics

In most peripheral tissues, interstitial fluid (ISF) is drained from organs by perforating lymphatic vessels. The lymphatic system also functions as an active immune surveillance system, with downstream lymph nodes housing germinal centres for pathogen recognition, and endothelial cells that secrete specific cytokines and express membrane adhesive factors for leukocytic diapedesis into the surrounding tissues (84). Although the CNS does not possess perforating lymphatics, recent advancements in high-resolution imaging techniques have revealed the presence of lymphatic channels coursing in a specific manner within the dura mater of transgenic Prox1-EGFP-expressing mice stained for LYVE1 (85). Additionally, leptomeningeal lymphatic endothelial cells (LLECs) have been suggested to reside in non-lumenised lymphatic endothelium within the leptomeninges (86). These brain-border lymphatic vessels and LLECs are now being increasingly recognised as crucial players in modulating CNS immunity, by facilitating the drainage of CSF from the meninges and clearance of metabolic waste products, whilst also serving a potential role in immune cell surveillance.

CSF from the brain parenchyma is generally known to flow through one of two different lymphatic routes. At the caudal end of the brain, CSF is drained from the sigmoid sinus through basolateral lymphatics at the dura, passing through the jugular foramen to lateral deep lymphatics, before directly arriving at the lateral cervical lymph nodes (85). In contrast, at the rostral parts of the brain, particularly the cavernous sinus and olfactory bulb, lymphatics pass through the cribriform plate to the olfactory epithelium adjacent to the olfactory neurons (87). From the olfactory epithelium, the fluids are drained into olfactory lymphatics which travel posteriorly to the nasopharynx into the deep medial lymph nodes (87).

A recent study has shown that, in both mice and macaques, the olfactory lymphatics link posteriorly to a lymphatic plexus superior to the nasopharynx bone at the skull base (85). This plexus structure, termed the nasopharyngeal lymphatic plexus (NPLP), subsequently merges with the medial cervical lymphatics, which ultimately connect to the deep cervical lymph nodes (85). Structurally, the plexus consists of a flattened network of unicellular capillaries characterised by button-like and zipper-like junctions, numerous unique valves, as well as the absence of a smooth muscle layer (85). These unique histological features allow the NPLP to be classified as a form of precollecting lymphatics, with extensive valvular structures to ensure the unidirectional flow of CSF towards the deep cervical lymph nodes.

In addition to its role in regulating CSF flow, emerging research suggests that the extensive nasal lymphatic microenvironment responds dynamically to inflammatory signals from the brain. In an induced EAE mouse model, significant lymphangiogenesis and dilation were observed at both the dorsal and ventral ends of the

cribriform plate (88). Furthermore, CD11c-expressing cells and immune cells from the brain parenchyma were found to have drained at the cribriform plate in response to neuroinflammation (88). Notably, atrophy of the NPLP was observed in aged mice, hindering CSF flow and drainage, with transcriptomic profiling revealing elevated expression of genes involved in type I interferon signalling and the leukocyte response, such as *Il3*, *Mcl1* and MHC genes (85). These results suggest an involvement of lymphangiocytes, or the potential accumulation of immune cells within the nasal lymphatics, in modulating neuroimmune responses. Further research is required to characterise the immune profiles within this unique structure, and to determine whether it contains an active immune niche, like the DALTs, which can modulate immune responses in the brain. An overview of the brain-border lymphatics in mouse, alongside the impact of age and inflammatory insult on these processes, is shown in Figure 3.

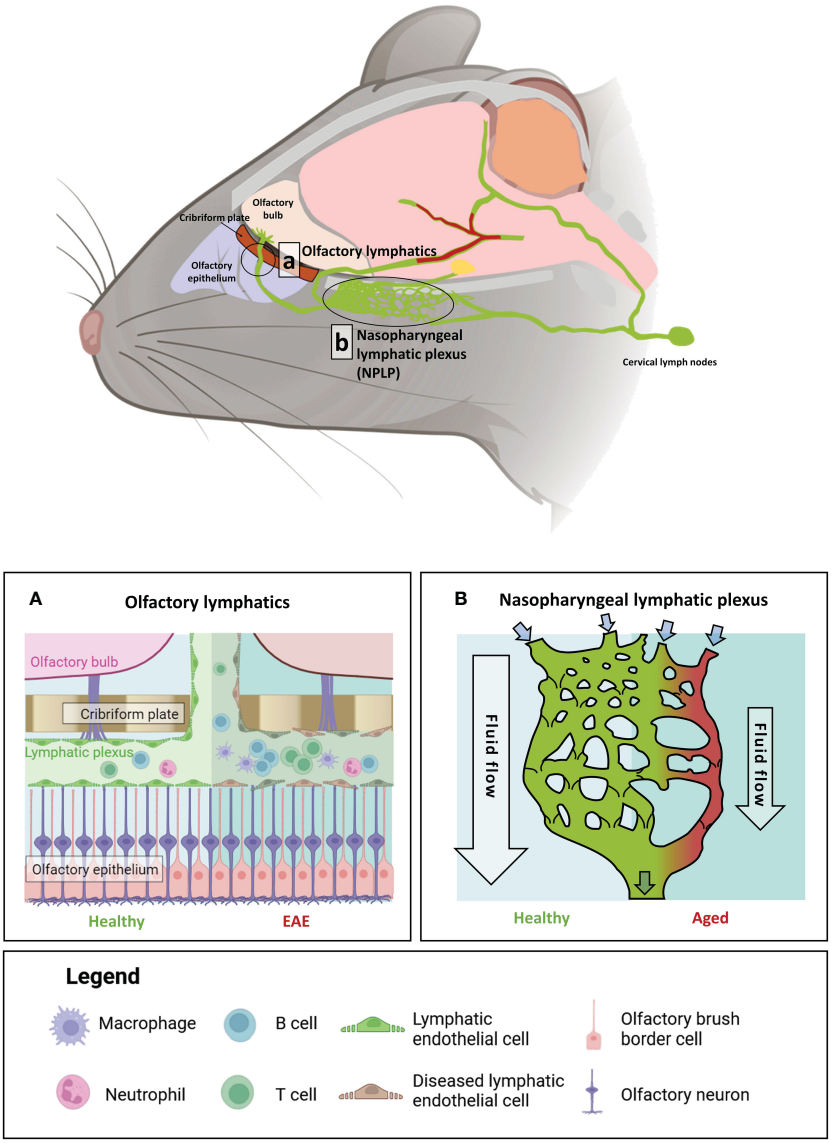

FIGURE 3
The impact of age and auto-immune insult on brain-border lymphatics in *Mus musculus*. Brain-border lymphatics are integral for the removal of metabolic waste and immune cells from the CSF. However, their function can diminish with advancing age or inflammatory insult. Top panel: a schematic of the mouse brain displaying the locations of the olfactory lymphatics **(A)** and nasopharyngeal lymphatic plexus (NPLP) **(B)**. **(A)** In healthy mice (left), lymphatics at the olfactory bulb drain CSF from the meninges and olfactory bulb. Mice with experimental autoimmune encephalomyelitis (EAE) display significant dilation of the lymphatic vessels with increased drainage of immune cells from the CSF (right). **(B)** The NPLP is a recently discovered anastomotic plexus found posterior to the olfactory lymphatics, present in both mice and humans. In healthy mice (left) the NPLP primarily serves to collect CSF that is drained from the ventral regions of the brain, before it is sent to the cervical lymphatics, which travel to deep cervical lymph nodes. During ageing (right), atrophy of the NPLP occurs, which can result in poorer drainage of lymphatic fluid that is likely to impair CSF flow. This age-related impaired lymphatic flow may contribute to the pathology of various neurodegenerative diseases. Figure created with BioRender.

3 Contribution of brain-border immune niches to neurodegenerative diseases

3.1 Alzheimer's disease

AD is the most common neurodegenerative disease, observable by the formation of amyloid beta (Aβ) plaques and tau neurofibrillary tangles (NFTs). During early disease stages, neuronal atrophy is more significant within the temporal brain regions such as the hippocampus, resulting in dementia (89, 90). AD is thought to occur largely because of Aβ misfolding and tau hyperphosphorylation, which result in the accumulation of pathological Aβ plaques and tau NFTs. These are widely regarded as major contributors towards neuronal dysfunction and synaptic loss underlying neurodegeneration (91, 92). Additional hypotheses suggest a role for environmental factors, such as prolonged exposure to heavy metals, pesticides, and air pollution (93–96), in AD presentation, further complicating investigations into disease pathology. The exact underlying aetiology of sporadic AD remains unknown, and thus, current treatment options are limited. First-line treatments (donepezil, galantamine, rivastigmine and memantine) aim to treat cognitive symptoms by increasing cholinergic neurotransmission or, in the case of memantine, reducing glutamatergic neurotransmission to attenuate excitotoxicity. Recently, research has focused more on targeting the clearance of pathological Aβ, which is the mechanism of action of the FDA-approved drugs aducanumab and lecanemab. Although these improve on older treatments by targeting what is believed to be the main driver of pathology, as opposed to downstream effects on cognition, their use remains controversial due to their significant side effects and failure to halt disease progression (97, 98). This is likely due to the complex, multifactorial nature of AD.

Immune system interference has been observed in the AD brain since the disease was first described, when Alois Alzheimer noted reactive gliosis in patient autopsy samples (99–101). Since then, neuroinflammation has been regarded as a key manifestation associated with disease progression. Observations in human patient brain tissue and amyloid mouse models indicate that activated microglia colocalise with Aβ plaques, proposing an important role for glia in the clearance of Aβ from the brain (102–104). Variants of the *Trem2* gene, which encodes for the triggering receptor expressed on myeloid cells-2, have been strongly associated with the presentation of late-onset Alzheimer's disease (LOAD) (105, 106). Studies using cultured neurons and *Trem2* knockout mice have suggested that the activation of TREM2 receptors promotes microglial phagocytosis and proliferation (107, 108), enabling the uptake and degradation of, and thus protection against, Aβ oligomers (109, 110). However, reactive microglia and astrocytes which interact with Aβ have been shown to release inflammatory cytokines, such as IL-1β, IL-6 and TNF-α, across a number of experimental models, including primary mouse microglia culture and APP/PS1 mice, as well as in AD patient brain samples (111–113). These processes have been suggested to seed initial inflammation, triggering a cascade that results in the amplification of the neuroinflammatory response over time. This points to a possible fundamental role for the sustained immune response in the onset of AD (114). Therefore, the precise function of glia, including whether they are protective and the extent to which they contribute to disease progression, remains uncertain, making their targeting for therapeutic advances challenging.

Studies have suggested that dysregulation of the peripheral immune system, in addition to that of the CNS, may also contribute towards AD progression (101), due to the observation that AD patients present with significantly higher levels of peripheral pro-inflammatory cytokines than healthy subjects (115, 116). However, studies that attempt to link peripheral cytokine levels with disease severity in AD patients have so far yielded mixed results (117, 118). Elucidating mechanisms that underlie crosstalk between peripheral and central immune processes throughout disease progression, and specifically the role played by brain-border immune niches in neuroinflammation and pathology progression, is therefore of significant research interest. The presence of Aβ in human cervical lymph nodes suggests that it is cleared via the glymphatic system (119). In mice, CD163- and LYVE1-expressing macrophages in perivascular spaces have been reported to regulate arterial motion which drives the flow of CSF, thereby influencing the rate of Aβ clearance from the brain (70). The glymphatic system is most active during sleep, and its declining function with age has been linked with sleep disturbances and neurodegenerative disease progression (120). The brain-border immune niches and glymphatic system may therefore play an important role in the propagation of late-stage inflammation observed in AD. The increased presence of Aβ aggregates within meningeal vessels and the choroid plexus has been evidenced in AD patients (121), indicating that age-related impairments in meningeal lymphatic vessel drainage may be a key underlying mechanism of Aβ accumulation (122, 123). In addition, an increased number of neutrophils has been found to adhere to the choroid plexus and vasculatures and infiltrate into the hippocampus and cortex of patients (124). Furthermore, in mouse models of AD, neutrophil adhesion to endothelial cells at perivascular spaces has been shown to impair blood flow, resulting in diminished memory function (125). Deficiencies in meningeal lymphatics associated with aging are therefore highly likely to amplify Aβ aggregation in both the meninges and parenchyma, contributing to cognitive dysfunction in AD (126, 127).

Recent studies have identified a potential role for the CBM in enhancing the progression of AD. During neuroinflammation in mice, monocytes and neutrophils from the bone marrow are recruited into the meninges through small osseous channels. A similar role for these channels in humans has been suggested, although this has yet to be confirmed (74, 76, 128). Positron emission tomography (PET) imaging using radioligands for translocator protein (TSPO) signal has revealed significant inflammation, specifically within the frontal and parietal regions of the CBM, in AD patients (73). In the calvaria, TSPO readings were positively correlated with decreased Aβ42 concentration in the CSF, but not decreased Aβ40 concentration. This is particularly significant when considering the specific role of Aβ42 in AD pathogenesis. Aβ40 and Aβ42 are products of the differential

cleavage of Aβ, with 40 and 42 amino acid residues, respectively. Despite being derived from the same precursor, these isoforms possess significant differences in their physicochemical and biological properties. In particular, the Aβ42 isoform is more prone to aggregation, and thus to the formation of Aβ plaques, and is more neurotoxic than Aβ40 (129, 130). As a result, Aβ42 is generally considered to play a greater role in AD pathology. Consequently, the observed correlation between increased TSPO readings in the calvaria and decreased Aβ42 concentration in the CSF suggests a potential link between cranial inflammation and AD pathology, which may contribute towards increased fibrillar Aβ42 deposits in the brain (73). Given these insights it is likely that a dual approach for targeting both immune niches and underlying amyloid plaques may be beneficial for the treatment of AD.

3.2 Parkinson's disease

Like AD, PD is a progressive neurodegenerative disease that is caused by aberrant aggregates of misfolded proteins within the brain. PD is characterised by physical symptoms such as uncontrolled shaking, stiffness, bradykinesia, and a loss of balance. The disease can also present with several psychological symptoms including sleep problems, anxiety and depression and cognitive impairment (131). The main pathological hallmark of PD is the presence of Lewy Body formations, which begins in the substantia nigra of the midbrain and causes dopaminergic neuronal death (132). As the disease progresses, neurodegeneration and tissue damage spread to the rest of the brain. The formation of Lewy bodies is attributed to the misfolding of alpha-synuclein (α-synuclein), resulting in the accumulation of synuclein fibrils (133). The reason for this occurrence in patients with sporadic PD is unclear, but evidence suggests it is likely due to complex interplay between genetic and environmental factors. Multiple gene variants have been linked with the misfolding of α-synuclein and presentation of sporadic PD (134–136), whilst studies have suggested that overexposure to environmental toxins (137) and pesticides (138) could lead to gut microbiota changes that increase PD susceptibility (139). Disease presentation has also been associated with levels of exercise (140), caffeine intake, smoking (141) and traumatic brain injury (142). As with AD, the apparent multifactorial nature of PD makes it extremely difficult to treat effectively. Drugs currently approved for PD treatment include levodopa and dopamine agonists to increase dopaminergic transmission, and monoamine oxidase-B inhibitors to reduce the breakdown of dopamine in the synapse, thereby increasing binding to receptors. Although drugs targeting dopaminergic neurotransmission are initially effective at improving motor symptoms that manifest early in PD presentation, they are known to lose therapeutic efficacy as the disease progresses (143). No drugs currently exist to address the underlying pathology of PD to halt disease advancement.

Multiple inflammation-related genes have been identified as risk factors in the presentation of PD (144), and as such neuroinflammation has been suggested to exacerbate its progression (145, 146). The role of the inflammatory response in PD has been studied since observations that postmortem patient samples contain reactive microglia expressing MHC-II cell surface receptors (147). This leads to the excessive release of proinflammatory cytokines in the striatum, ventricular CSF and spinal CSF (148). The lentiviral-mediated overexpression of α-synuclein in mouse microglia has been reported to result in neurodegeneration of dopaminergic neurons before the aggregation of endogenous α-synuclein, suggesting that microglial activation may be a primary driver of disease pathology in the CNS (149). As well as dopaminergic degeneration, the accumulation of α-synuclein in microglia also leads to the excessive release of pro-inflammatory and oxidative molecules. A proposed mechanism for microglial activation by α-synuclein, characterised in microglial cell lines, primary cultured cells, and mouse models, depends on the binding of the protein to microglial CD11b. This activates NADPH oxidase (NOX2) via the initiation of RhoA pathway signalling (150). The activation of NOX2 increases the production of hydrogen peroxide (H_2O_2), which diffuses into the cytoplasm and directs microglial migration via the activation of Lyn, a tyrosine protein kinase (151). If this mechanism also occurs in human patients, the interaction of α-synuclein with microglia, as opposed to its accumulation in dopaminergic neurons, may be a key component of the initial immune response driving degeneration of the dopaminergic system in PD. The exacerbation of the immune response and excessive release of pro-inflammatory molecules leads to further activation of microglia, in turn contributing towards the increased accumulation of α-synuclein and dopaminergic degeneration in a feedforward cycle of neurodegeneration and inflammation (149, 152).

Braak's hypothesis of PD suggests that the disease arises because of the presence of a pathogen in the gut and nasal cavity, before spreading towards and within the CNS (153–156). Mechanisms of neuroimmune crosstalk and the prevention of PD progression from the periphery into the brain are therefore essential components of research into improved therapeutic outcomes. The progression of the peripheral immune response into the brain during PD occurs due to the damaged integrity of the BBB, which leads to its increased permeability. This may be induced by α-synuclein facilitated by astrocytic signalling (157, 158), or as a result of peripheral inflammation (159). A recent study has shown that the infiltration of lymphocytes into the brain parenchyma is mediated by BAMs residing in the choroid plexus and meninges, indicating a role for brain-border immune niches in facilitating neuroinflammation (14). In mice overexpressing α-synuclein, BAMs were also observed to interact with α-synuclein fibrils, present MHC-II complexes, and to colocalise with $CD4^+$ T cells in the perivascular spaces. These processes have been suggested to initiate T cell antigen recruitment and parenchymal entry, providing a possible mechanism for immune cell entry into the brain during the early stages of PD that precedes neurodegeneration facilitated by α-synuclein. Critically, this study also reported the presence of BAMs in close proximity to T cells in postmortem PD brain samples, suggesting that processes occurring in perivascular spaces are consistent in both animal models of the disease and human patients. Targeting these regions to prevent central neuroinflammation may therefore be a promising route of therapeutic intervention for PD.

Recently, diffusion tensor imaging (DTI) analysis in human PD patients has provided strong evidence that glymphatic system

dysfunction occurs with PD progression (160, 161), and reduced meningeal lymphatic vessel flow has also been observed in idiopathic PD patients via MRI (162). Studies have looked to explore whether these changes to the glymphatic system amplify PD pathology. The accumulation of α-synuclein in human patients has been shown to result in delayed lymphatic drainage, inflammation of the meninges and a reduced concentration of tight junctions between endothelial cells in the meningeal lymphatics system (162). In mice overexpressing α-synuclein, the blocking of meningeal lymphatic drainage indeed exacerbated α-synuclein accumulation, inflammation, and dopaminergic neurodegeneration, which heightened motor deficits (163). These studies highlight a potentially crucial role for immune niches in both the accumulation and clearance of α-synuclein. Therefore, targeting these sites during early-stage PD may be useful in preventing the infiltration of pathology into the brain, whilst similar intervention during the later stages could be harnessed to slow disease progression by increasing the clearance of pathological α-synuclein.

3.3 Multiple sclerosis

MS is a progressive autoimmune demyelinating disorder affecting approximately 36 per 100,000 people (164). Symptoms include extreme fatigue, sensory and visual disturbances, ataxia, and respiratory dysfunction (165). Initial diagnosis of MS is complex, and often requires a thorough examination of the patient's family history, neurological exams, evoked potential tests, lumbar punctures, and MRI for focal white matter lesions, as according to the McDonald criteria (166). There are currently no ways to prevent the progression of the disorder, and patients are expected to relapse without warning. Corticosteroids are acute treatments that hasten recovery from relapse, but long-term corticosteroid treatment does not prevent further relapse (167), prompting the need for better therapeutic alternatives. Typically, MS can be classified into four categories depending on the manner of disease progression: clinically isolated syndrome (CIS), which is diagnosed when patients first experience neurological symptoms for over 24 hours; relapsing-remitting MS (RRMS), the most common diagnosis of MS, characterised by alternating periods of active and inactive disease progression; and the more active, aggressive primary progressive MS (PPMS) and secondary progressive MS (SPMS) subtypes.

The precise cause of MS is not known. However, it is believed that polymorphisms within immune-related genes (168, 169), and genes affecting myelin susceptibility to inflammatory insult (170), along with environmental factors, may cohesively contribute to aberrant lymphocyte activation underlying MS pathology (171, 172). A considerable proportion of MS-associated gene polymorphisms are found within the human leukocyte antigen (HLA-DR2) clusters, which reside within the highly polymorphic MHC-II region. Other reported genes with reported risk alleles include those encoding for interleukin receptor subunits, such as IL2RA and IL7RA (173, 174). Demyelination has also been associated with macrophage and B cell activity, reactive gliosis, altered oligodendrocyte progenitor cell (OPC) recruitment and axonal damage (175).

Compelling evidence suggests that immune cells in the choroid plexus play a role in the early pathogenesis of MS. In EAE mice, the number of $CD4^+$ T cells increases in the choroid plexus and remains elevated throughout disease progression (176). Paracellular diapedesis of $CD4^+$ T-helper 17 (Th17) cells into the brain parenchyma appears particularly crucial in the progression of MS pathogenesis (177), and the infiltration of Th17 cells has been shown to occur from the choroid plexus specifically. The expression of the chemokine receptor CCR6 on Th17 cells is necessary for adherence to $CCL20^+$ choroid plexus epithelial cells, allowing T cells to pass into the CSF (178). This process appears to be facilitated by adenosine signalling; knockdown of adenosine A_{2A} receptors in the choroid plexus has been shown to attenuate diapedesis via inhibition of the NFκB/STAT3 pathway, leading to reduced CCL20 expression in the brain parenchyma (179). However, the diapedesis of effector Th cells (including Th17 cells) *in vitro* appears to be independent of CCR6-CCL20 signalling, suggesting that there might be alternative interactions at play (176). For instance, IFN-γR1 expressed within the choroid plexus has been shown to reduce the local expression of adhesion molecules and chemokines, preventing Th17 cells from infiltrating into the CNS (180). Given the incomplete understanding of this niche, further research is required to identify the precise mechanism facilitating Th17 cell entry into the brain during the pathogenesis of MS.

In addition to the choroid plexus, recent evidence highlights the significance of immune activity within the meninges in the pathogenesis of MS. Lymphoid-like follicular structures, predominantly composed of autoreactive B cells, are frequently observed adjacent to subpial demyelinating cortical lesions within the subarachnoid space of SPMS and PPMS patients (181). These follicular structures tend to be concentrated around the deep cortical sulci (181). Meningeal APCs have been identified as activators of $CD4^+$ T cells within these follicles (182). Furthermore, the depletion of microglia and meningeal macrophages has been shown to reduce MHC-II and CD80 co-stimulatory molecule expressions, diminishing T cell reactivation and proliferation, and consequently halt demyelination events in EAE mice (183), implicating immune cell activity at the meninges in MS pathology.

It has been suggested that glymphatic flow becomes impaired at the perivascular spaces in MS patients. Dilation of the perivascular spaces is observed in some MS patients, although its correlation to severity of MS and the disease progression remains uncertain (184). In a recent study using DTI to analyse fluid diffusion along the perivascular spaces, a negative association between diffusivity index (a proxy for glymphatic function) and disease duration was observed at the onset of disease course, suggesting an early impairment of glymphatic clearance in MS patients (185). Another study has suggested that metabolic dysfunction in perivascular astrocytes may result in the diffused expression of AQP4 in astrocytic end feet, and its expression at lesion sites has

been found to decrease in response to immune elements (186). AQP4 is reported to be an integral component of the glymphatic system and so its reduced expression is likely to lead to alterations in glymphatic clearance (187). However, it is currently unknown if impairment in glymphatic flow and perivascular space dilation are causal factors in the pathology of MS, or consequences arising from a physiological response to MS lesions. Consequently, further investigation is required to determine how glymphatic flow dysfunction contributes to MS pathology.

The CBM may be another brain-border niche that contributes to MS pathogenesis. Indeed, PET scans using radioligands for TPSO have revealed that inflammatory activity tends to be heightened at the skull base in both EAE mice and MS patients (73). This could potentially be explained by autoreactive CXCR4$^+$ myelin-reactive T cells migrating into the bone marrow through ossified skull meningeal channels to augment myelopoiesis through the CCL5-CCR5 axis (78). However, it is not currently known why the skull base specifically is activated, and direct associations between myeloid cells generated from the CBM and the lymphatics also remain to be investigated.

Evidence has also implicated structural changes to the lymphatic system in the pathology of MS. A recent study has reported the occurrence of profound lymphangiogenesis in EAE mice following the proliferation of lymphatic endothelial cells at the nasal lymphatics near the cribriform plate (88). In this study, the lymphatic endothelial cells were found to have proliferated as a response to inflammation, and this proliferation has been shown to depend on vascular endothelial growth factor (VEGF) C signalling (88, 188, 189), although an alternative mechanism for this process has been proposed that requires the transdifferentiation of activated monocytes into lymphatic endothelial cells (190, 191). These findings demonstrate the occurrence of lymphatic vessel remodelling in EAE mice, suggesting a potential role for this process in MS pathology. Indeed, it is feasible that lymphangiogenesis in proximity to the brain could facilitate greater immune cell infiltration into the brain; a known contributor to MS progression (178, 192, 193). Other studies have found evidence that immune activation at specific lymph nodes may also underlie aspects of MS pathology. Lymph nodes are known as 'collecting centres' where APCs come into close contact for priming T cells (194). The medial and lateral cervical lymph nodes receive lymphatic fluids from the brain parenchyma and meninges, and activation of T cells in these regions may contribute to humoral activation during the early stages of MS pathogenesis (195). Accordingly, activated cells from the cervical lymph nodes may re-enter the brain through blood circulation into the dura, perivascular spaces, or choroid plexus. Here they interact with or secrete factors such as IFN-γ to prompt secondary responses within these niches, promoting disease progression (195). Excision of cervical lymph nodes (196) and high-intensity focused ultrasound in cervical lymph nodes for lymphocyte ablation (197), have both been shown to significantly reduce relapse severity in EAE mice, suggesting that this putative disease pathway may be a valid therapeutic target. The contributions of brain-border immune niches to the presentation of neurodegenerative diseases are highlighted in Figure 4.

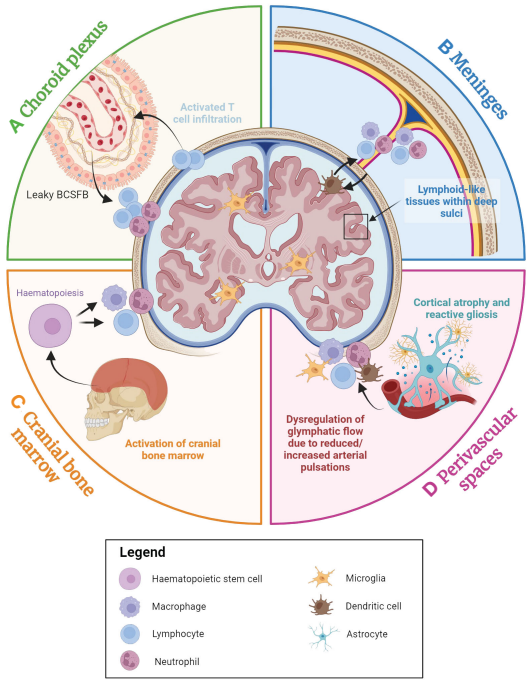

FIGURE 4
An overview of the contributions of the brain-border niches to neurodegenerative diseases. The choroid plexus, cranial bone marrow (CBM), perivascular spaces and meninges all appear to play a role in neurodegenerative disease. **(A)** The choroid plexus serves as the primary brain-cerebrospinal fluid barrier (BCSFB) and actively responds to immune factors from both the CSF and the blood stream. With advancing age and during the inflammatory response, immune cell populations accumulate within the choroid plexus, and the BCSFB becomes leakier due to the loss of tight junctions, potentially facilitating greater peripheral immune cell activation and infiltration into the brain. **(B)** In many age-associated neurodegenerative diseases, high concentrations of inflammatory factors appear to result in the accumulation of myeloid and lymphoid cells in the dura, subarachnoid space, and even within the deep sulci of the cortex, which may perpetuate neurodegeneration. **(C)** The CBM is a brain-border niche containing haematopoietic stem cells, which can differentiate to myeloid and lymphoid cells in response to a range of immune factors. Evidence suggests that immune activation in the CBM is associated with various neurodegenerative diseases. **(D)** Cortical atrophy and gliosis associated with neurodegenerative disease may lead to a leaky blood-brain barrier (BBB), while inflammatory factors from the parenchyma may induce increased immune cell localisation in perivascular spaces. Furthermore, dysregulation of glymphatic flow due to factors such as diminishing arterial pulsations may affect clearance of metabolic waste and immune cells within the brain parenchyma, leading to the build-up of neurotoxic molecules within the brain. Figure created with Biorender.

4 Considerations in the study and clinical use of brain-border immune niches in neurodegenerative diseases

Neurodegenerative diseases are progressive disorders that can be classified into stages depending on the severity of symptoms and histological profiles. While current therapies hold some promise for slowing disease advancement and improving symptoms in initial stages, they have proved less effective for patients diagnosed in intermediate and advanced stages. Moreover, the aetiologies of

these diseases remain elusive, meaning there are limited therapies for preventing or curing them. In AD and PD, neurodegeneration is putatively caused by the introduction of misfolded proteins within the CNS that undergo uncontrolled prion-like propagation and aberrant aggregation, triggering immune responses (198). Microglia and astrocytes form a first-line defence against aggregates. However, this initial neuroinflammatory response from within the parenchyma may trigger a chain reaction in wider brain-border niches, which may contribute to disease progression. Therefore, it is possible that targeting these immune niches could prevent a secondary immune response and slow disease progression in the case of AD and PD. For MS, immunosuppression appears effective as a disease-modifying therapy (DMT), particularly for RRMS and SPMS (199). However, the precise mechanisms and aetiology of MS remain unknown, and treatments are therefore limited, particularly in the case of PPMS. As explained previously, recent findings report the accumulation of immune cells at the brain-borders in MS, which may later infiltrate and release immune factors into the CNS parenchyma (178, 179, 192, 193). Therefore, controlling the immune buildup at the brain-borders may be an efficient acute therapy for MS.

Whilst current literature exploring the brain-border immune system has provided valuable insights, the lack of tools available to isolate the specific role of each brain-associated immune niche in any given neurodegenerative disease poses a significant challenge when attempting to understand their roles in the aetiologies of these conditions. Moreover, although the targeting of immune niches for the treatment of neurological diseases may seem like a promising therapeutic approach, a similar lack of tools to deliver isolated treatment delivery into specific immune niches makes this difficult to achieve at present. Consequently, it is important to consider caveats of current approaches to explore the roles of these immune niches in health and disease, and how we may address these limitations in future investigation and clinical application.

4.1 Challenges associated with the study of immune niches in neurodegenerative disease

To effectively target brain-border immune niches in the treatment of neurodegenerative disease, it is important to understand how these function in health. However, studying these niches in humans is fraught with ethical limitations. Due to the highly invasive nature of biopsies required to access the brain and its bordering regions, investigation of these regions in humans is typically limited to donated post-mortem samples (200, 201). Although valuable, these likely do not represent a true cross-section of healthy tissues across the population, as it is possible that the manner of death may affect the cellular/molecular profile of samples. Similarly, post-mortem diseased tissue is typically only available from late-stage or terminal disease donors, neglecting the dynamical nature of neurodegenerative diseases and the range of immune states they inhabit during their progression. The relatively small sample sizes this issue produces limits the power of findings derived from post-mortem samples. These studies also require strict measures to be undertaken to ensure optimal preservation of DNA, RNA, and protein contained within the brain. However, this can be difficult to achieve due to pre-mortem events, such as hypoxia, and post-mortem delays (202). Because of these difficulties regarding access to and preservation of human tissue, a large proportion of studies in this field rely on animal models, in which tissue is more readily available and experimental conditions are less constrained. However, these studies also come with significant drawbacks. The most apparent limitation of animal models is the differences in neurobiology between model species and humans (203–206). Indeed, rodents, the primary models in this field, lack the full complement of glial complexity seen in humans, and certain vascular and immunological components are also absent (207). Moreover, their short lifespans limit the development of progressive diseases (208), potentially leading to the incomplete development of molecular and cellular pathological hallmarks in brain-associated immune niches. Perhaps because of these reasons, rodent models of neurodegenerative disease are generally considered poor in terms of their predictive validity (209). To utilise these models effectively in the study of immune niche involvement in neurodegenerative disease, it may be valuable to attempt further reverse-translational studies using non-invasive neuroimaging methods, that are currently used in humans, in rodent models (in which high fidelity data is readily available for comparison) to validate their use in humans.

4.2 Monitoring the activity of immune niches through functional and structural imaging

Imaging modalities used for the formulation of diagnoses and prognoses of neurological diseases can provide detailed information about structural or physiological brain changes; due to their non-invasive nature, they are among the most utilised tools to conduct clinical studies and evaluate neurological disease progression. Anatomical imaging techniques such as computed tomography (CT) or MRI may be combined with functional imaging using PET or DTI, respectively, for acute visualisation of aberrant physiological changes in patients. For example, MRI coupled with DTI along the perivascular space (DTI-APS) showed that decreased diffusivity index correlated with increased perivascular burden in both AD and PD patients (161, 210), suggestive of reduced glymphatic flow. On the other hand, the use of CT combined with PET tracers specific to cells of the myeloid lineage is currently being investigated in preclinical studies concerning AD and MS. Examples of promising PET radiotracers include those binding to TSPO (73, 211, 212), GPR84 (213), and triggering receptor expressed on myeloid cells 1 (TREM1) receptor (214), while lymphoid tracers include nanoparticle conjugated CD-19 monoclonal antibodies for B cells (215) and FAraG for T cells in EAE models (216). However, despite their utility, these techniques are not without their limitations. MRI/CT and PET lack the spatial resolution to precisely measure single-cell changes and interactions within these niches triggered by neuroinflammation (217, 218). This makes it challenging to attribute inflammatory functions to

specific cell types and their interactions within immune niches, which likely form an important part of the aetiology of neurodegenerative diseases. Furthermore, whilst PET scanning may be able to provide valuable information about specific disease-relevant cell populations or biomarkers over larger areas, the utility of the tracers used is limited to our understanding of their biology. For example, TSPO, which is one of the most widely utilised PET markers in the study of neuroinflammation, is known to be upregulated by astrocytes and microglia upon their activation and by infiltrating macrophages (219), however, its sources from the periphery are less well understood. This brings into question the source and specificity of TSPO signal in the CNS, in studies using radioligands for this marker (220, 221). Consequently, the lack of specificity and our understanding of the origins of these markers limits our ability to understand the roles and interactions of immune-related molecules or immune cell types in these niches. However, it is expected that with further development of neuroimaging techniques and increased understanding of relevant molecular biomarkers, studies in humans will soon provide more reliable data as to the cellular and molecular makeup of these niches in both disease and health, facilitating their use in disease diagnosis, progression, and clinical study.

4.3 Promoting glymphatic flow and metabolic waste clearance

The obstruction of glymphatic pathways is a common hallmark of neurodegenerative disease that results in failure to clear metabolic waste, thus leading to the accumulation of immune cells within the perivascular spaces. Therefore, it is hypothesised that increasing glymphatic clearance may be a promising therapeutic approach, as it would allow the removal of aggregates and toxic metabolites from the brain parenchyma.

Studies have shown that stiffening of the arteries may lead to impedance of glymphatic flow in a hypertensive rat model (222). Controlling hypertension may therefore be an effective method for treating individuals with glymphatic obstruction associated with neurodegenerative disease, particularly in age-associated dementia, as age is positively correlated with arterial stiffness (223). Non-pharmacological interventions to control hypertension involve lifestyle changes such as weight loss, increased cardiovascular exercise, dietary changes, and reduced salt intake (224). Pharmacological options for treating hypertension include diuretics, angiotensin-II-receptor antagonists (sartans), beta-blockers, and calcium-channel blockers (225).

Current studies have also revealed several other promising agents that may aid in improving glymphatic flow. VEGFC is a lymphangiogenic factor that has been shown to improve glymphatic drainage (126, 226), and therefore potentially enable the clearance of Aβ from the brain parenchyma. Vasoconstrictors, such as α_2-adrenergic agonists, may be used to dilate the glymphatic channels for intrathecal lumbar administration of medications (227), allowing direct delivery of biologics or drugs to the CNS, which may otherwise not be able to cross the BBB or BCSFB.

In addition to using drugs or biologics, clearing obstructed glymphatic channels has also been achieved in animal models using mechanical methods such as focused ultrasound treatment in combination with microbubbles (FUS-MB) (122), and non-invasive neuronal stimulation techniques, such as transcranial magnetic stimulation (TMS) or multisensory stimulation (228, 229). A recent study using the 5xFAD AD mouse model showed that treatment with FUS-MB led to enhanced solute Aβ clearance from the brain, first into the CSF space and then into the deep cervical lymph nodes, which correlated with improved memory functions (122). These findings suggest that non-pharmacological treatment methods, such as transcranial magnetic stimulations at clinics, coupled with multisensory interventions at home, may also be viable therapeutic approaches to promote impaired glymphatic clearance and thus improve disease symptomology in AD patients.

4.4 Preventing immune cell infiltration into the brain parenchyma

The infiltration of immune cells into the brain parenchyma is a significant event associated with neuronal atrophy in numerous neurodegenerative disorders (230, 231). Once within the brain parenchyma, activated lymphocytes release inflammatory cytokines that impair neuronal function, whilst invading myeloid cells are also known to release various cytotoxic and neuroinflammatory factors. Consequently, the specific mechanisms that modulate immune cell invasion into, or egress out of, the brain parenchyma hold promise as potential therapeutic targets.

Neutrophil migration into the brain parenchyma has been observed using PET scans in transgenic AD models (232). Neutrophil depletion or the inhibition of neutrophil trafficking via lymphocyte function-associated antigen 1 (LFA-1) blockade has been shown to reduce AD–like neuropathology and improve memory in mice already showing cognitive dysfunction (124). This indicates that the prevention of neutrophil trafficking to the brain parenchyma may be a valid therapeutic approach for the treatment of AD. Similar approaches, for example, the modulation of α4-integrin-mediated trafficking, have shown promise in the treatment of amyotrophic lateral sclerosis (ALS). α4-integrin is a heterodimeric cell surface marker for leukocytes and is reported to be important in facilitating the migration of leukocytes into the brain parenchyma after neural inflammation or injury (233). Studies have shown that intraperitoneal injection of natalizumab, an anti-α4-integrin monoclonal antibody, is able to block the infiltration of T cells and natural killer cells into the CNS of an ALS mouse model, effectively preventing inflammation and cytokine release in the brain parenchyma and preserving motor function (231). Ultimately, more research is needed to determine the potential of immune-trafficking-modulating therapies in the treatment of human neurodegenerative disease, but initial findings are promising.

4.5 Modulating cranial bone marrow-derived cell populations

In the context of treating neurodegenerative disorders, there have been several significant findings regarding immune activity at the CBM. For example, polymorphonuclear Ly6G$^+$ monocytes and neutrophils derived from the CBM have been observed to modulate the function of other adaptive immune cells, thereby exhibiting an immunoregulatory role, in contrast to infiltrating Ly6G$^+$ cells derived from the blood, which have been reported to display a more inflammatory phenotype (76). These findings therefore provide evidence for the existence, and thus potential manipulation, of immunoregulatory cells from the CBM for therapeutic purposes. What is more, in mice recovering from EAE, Ly6G$^+$ cells have been observed to become recruited to the meninges, where they are converted to myeloid-derived suppressor cells (MDSCs), ultimately suppressing CD138$^+$ B cell accumulation in the meninges (234). This recruitment and conversion process points to the existence of an endogenous mechanism mitigating neuroinflammation in the context of neurodegenerative disease. Indeed, Ly6G$^+$ cells are known to be converted to MDSCs through the activation of the STAT3-dependent signalling pathway (234), therefore providing a precise molecular target for therapeutic intervention in this process. Furthermore, compounds such as cannabidiol and IFN-β have been shown to promote the localisation of MDSCs in the meninges (234), and improve their suppressive functions (235). Furthermore, transcranial application of CXCR4 antagonist AMD3100 into the CBM has been shown to facilitate the migration of Ly6G$^+$ cells into the dura mater (76), indicating that manipulation of MDSCs at the CBM may be a viable strategy for mitigating neuroinflammation in neurodegenerative disorders.

However, specifically modulating CBM-derived cells effectively and precisely may prove to be challenging due to the technical difficulty of accessing the CBM and isolating and targeting specific cell types or molecular targets within this niche. Additionally, the exact routes by which CBM-derived cells are given access to the brain parenchyma have not been fully elucidated, meaning it is unclear how effective the delivery therapeutics via this channel would be (or to precisely where in the brain they would be delivered). Osseous channels have been suggested to display heterogenous plasticity throughout life in a region-dependent manner, although their expression and how this is changed during ageing and neurological disease presentation has not been well-characterised (128). A more comprehensive understanding of these mechanisms is essential to facilitate therapeutic advances associated with targeting of the CBM.

4.6 Directed and intranasal delivery of drugs and biologics

Injections of drugs into the choroid plexus and ventricular system to allow delivery into the brain parenchyma is a promising way of bypassing the BBB, although therapeutic effects are reported to be limited by diffusion distance, particularly during the targeting of deeper tissue regions (236, 237). Studies have suggested that directed drug delivery into the meninges may exert more widespread effects to brain parenchymal regions (123). However, these findings have so far been restricted to rodent models, and it remains to be seen whether their impact will be as effective in human brain tissue (238). Additionally, the way in which CSF flow is disrupted due to neurodegenerative disease is not comprehensively understood, and factors that influence CSF flow have not been fully described (237), therefore limiting the advancement of therapeutics associated with drug delivery into the choroid plexus and meninges.

In recent years, there has been a growing interest in intranasal delivery, using agents such as adeno-associated viruses (AAVs) and nanoparticles, as an alternative, non-invasive method for administering therapeutics to the brain to address neurodegenerative diseases. Notably, the olfactory mucosa in the nasopharynx region serves as a highly accessible region for drug penetrance (85). This approach provides numerous advantages for brain-border-focused treatment: it is non-invasive, and the presence of highly vascularised lymphatic vessels in the nasal mucosa allows the administered agent to swiftly enter the lymphatic system. Additionally, intranasal administration reduces first-pass metabolism at the liver compared to intravenous delivery. Agents administered intranasally can directly affect the lymphatic endothelium and olfactory bulb by modulating the release of inflammatory cytokines (239). Moreover, agents can travel through the lymphatics to reach the cervical lymph nodes, potentially targeting immune cells for gene therapy and precise immunotherapy. In addition to targeting brain-border niches, intranasal applications offer the benefits of either direct or indirect delivery into the brain. Preclinical studies in mice have shown that combining EGFP-AAV delivery with methods like FUS-MB can effectively target specific brain regions with higher efficacy compared to similar treatments via intravenous injections (240, 241).

However, the effectiveness of intranasal delivery is hindered by the rapid clearance of nasal passages due to mucociliary movement, which reduces the bioavailability of administered treatments. To circumvent this limitation, efforts have been made to coat particles with mucoadhesive substances and/or to co-administer enzymes, thus improving drug bioavailability (242, 243). Further research is required to develop novel nanocarriers for improved intranasal drug delivery, whilst ensuring that unintended adaptive responses are not provoked by such techniques.

5 Conclusion

Over the last century, understanding of the barriers surrounding the brain has advanced considerably, from initial beliefs that the brain was encompassed by an absolute, impermeable barrier, to more recent studies revealing the presence of brain-border immune niches. Crucially, modern-day studies have demonstrated a much greater degree of immune

communication between the periphery and CNS than was previously believed. Indeed, peripheral immune cells that accumulate in brain-border regions appear to play an important role in neuroinflammatory processes via the facilitation of immune cell entry into the CNS. This has been reported to occur in several brain-border immune niches, including the choroid plexus, the meninges, and the perivascular spaces. Furthermore, the CBM is also the subject of considerable interest due to the discovery that its immune cells and immature progenitors can enter the brain via ossified channels, whilst the nasal lymphatic system contributes to the control of immune cell drainage from the brain parenchyma. With these findings in mind, it is evident that brain-border immune niches collectively play a significant role in neuroinflammatory processes occurring in the CNS, as well as in the control of neuroimmune interactions between the brain and periphery.

Given these significant findings, research into brain-border immune niches appears to have the potential to advance our understanding of the pathology of numerous brain conditions, in particular neurodegenerative diseases, such as AD, PD and MS. These have all been reported to present with alterations to the inflammatory response in both the brain and periphery, and pathological proteins have been observed to accumulate in brain-border immune niches throughout disease progression. Therefore, activity at the borders of the brain has been proposed to facilitate the infiltration of immune cells into the brain, thereby driving the neuroinflammatory response and thus, contributing to disease progression. Consequently, developing a greater understanding of these niches using both animal models and clinical studies may have significant implications for the diagnosis, prognosis, and development of novel therapeutics for neurodegenerative diseases, which currently remain inadequate.

In the past, the development of drugs that can effectively target the CNS has proven notoriously difficult due to the relative impermeability of the BBB and BCSFB. However, with further research, this may soon change. In the next decade, further investigation into the brain-border niches is expected, with the potential to shed light on the heterogeneity of each niche at single-cell resolution or with spatial transcriptomics. These studies have the potential to reveal the cellular players and immune factors that contribute to the progression of these debilitative diseases, thereby leading to the discovery of specific immune-related biomarkers and potential therapeutic targets. Moreover, continuous advancements in imaging resolution and the development of novel PET radioligands are likely to enable earlier diagnosis of neurodegenerative diseases and be effective in determining disease classification and improving prognosis. Additionally, it is important to note that brain-border niches themselves provide opportunities for therapeutic intervention. Protection against disease-exacerbating neuroinflammation may be achieved by preventing immune cell infiltration from brain-border niches into the parenchyma, or by modulating the function of CBM-derived suppressor cells. Alternatively, evidence also suggests that promoting glymphatic flow may represent another therapeutic avenue, aiding in the removal of pathological proteins from the brain parenchyma and immune niches. Finally, the CBM and nasopharyngeal lymphatic plexus may act as alternative access routes for drugs to enter the brain, for example via intranasal delivery, and thus are beginning to emerge as less-invasive routes of delivery to the CNS for promising new therapeutics.

Author contributions

LT: Writing – review & editing, Writing – original draft, Conceptualization. GC: Writing – review & editing, Writing – original draft, Conceptualization. MH: Writing – review & editing. XY: Writing – original draft, Conceptualization, Writing – review & editing. CO: Writing – review & editing. BJ: Writing – review & editing. JK: Writing – review & editing. JP: Writing – review & editing. M-SK: Writing – review & editing. MK: Writing – review & editing. SJ: Writing – review & editing, Writing – original draft, Supervision, Funding acquisition, Conceptualization.

Funding

The author(s) declare financial support was received for the research, authorship, and/or publication of this article. This work was supported by the industry academic cooperation foundation fund, CHA University Gr ant (CHA-202300230001).

Conflict of interest

The authors declare that the research was conducted in the absence of any commercial or financial relationships that could be construed as a potential conflict of interest.

Publisher's note

References

1. Ehrlich P. Das Sauerstoff-Bedurfnisdes Organismus: eine farbenanalytischeStudie. *Berlin: Hirschward*. (1885).

2. Bield A, Kraus R. U¨ber eine bisherunbekannte toxische Wirkung der Gallensauren auf das Zentralnervensystem. *Zhl Inn Med*. (1898) 19:1185–200.

3. Lewandowsky M. Zur lehre der ze-rebrospinalflussigkeit. *Z Klin Med*. (1900) 40:480–4.

4. Goldmann EE. Die aussere und innere Sekretion des gesunden und kranken Organismus im Liche der "vitalen Farbung". *Beitr Klin Chir*. (1909) 64:192–265.

5. Bentivoglio M, Kristensson K. Tryps and trips: cell trafficking across the 100-year-old blood-brain barrier. *Trends Neurosci*. (2014) 37:325–33. doi: 10.1016/j.tins.2014.03.007

6. Goldmann E. Vitalfarbung am Zen-tralnervensystem: beitrag zur Physiopathologie des plexus chorioideus derHirnhaute. *Abh Preuss Akad WissPhysik-Math*. (1913) 1:1–60.

7. Ribatti D, Nico B, Crivellato E, Artico M. Development of the blood-brain barrier: a historical point of view. *Anat Rec B New Anat*. (2006) 289:3–8. doi: 10.1002/ar.b.20087

8. Shirai Y. On the transplantation of the rat sarcoma in adult heterogenous animals. *Jap Med World*. (1921) 1:14–5.

9. Murphy JB, Sturm E. Conditions determining the transplantability of tissues in the brain. *J Exp Med*. (1923) 38:183–97. doi: 10.1084/jem.38.2.183

10. Rio-Hortega P. THE MICROGLIA. *Lancet*. (1939) 233:1023–6. doi: 10.1016/S0140–6736(00)60571–8

11. Medawar PB. Immunity to homologous grafted skin; the fate of skin homografts transplanted to the brain, to subcutaneous tissue, and to the anterior chamber of the eye. *Br J Exp Pathol*. (1948) 29:58–69.

12. Hickey WF, Hsu BL, Kimura H. T-lymphocyte entry into the central nervous system. *J Neurosci Res*. (1991) 28:254–60. doi: 10.1002/jnr.490280213

13. Ribeiro M, Brigas HC, Temido-Ferreira M, Pousinha PA, Regen T, Santa C, et al. Meningeal γδ T cell–derived IL-17 controls synaptic plasticity and short-term memory. *Sci Immunol*. (2019) 4:eaay5199. doi: 10.1126/sciimmunol.aay5199

14. Schonhoff AM, Figge DA, Williams GP, Jurkuvenaite A, Gallups NJ, Childers GM, et al. Border-associated macrophages mediate the neuroinflammatory response in an alpha-synuclein model of Parkinson disease. *Nat Commun*. (2023) 14:3754. doi: 10.1038/s41467-023-39060-w

15. Wolf Y, Shemer A, Levy-Efrati L, Gross M, Kim J-S, Engel A, et al. Microglial MHC class II is dispensable for experimental autoimmune encephalomyelitis and cuprizone-induced demyelination. *Eur J Immunol*. (2018) 48:1308–18. doi: 10.1002/eji.201847540

16. Hatterer E, Davoust N, Didier-Bazes M, Vuaillat C, Malcus C, Belin M-F, et al. How to drain without lymphatics? Dendritic cells migrate from the cerebrospinal fluid to the B-cell follicles of cervical lymph nodes. *Blood*. (2006) 107:806–12. doi: 10.1182/blood-2005–01-0154

17. Galea I, Bechmann I, Perry VH. What is immune privilege (not)? *Trends Immunol*. (2007) 28:12–8. doi: 10.1016/j.it.2006.11.004

18. Rustenhoven J, Kipnis J. Brain borders at the central stage of neuroimmunology. *Nature*. (2022) 612:417–29. doi: 10.1038/s41586–022-05474–7

19. Wolburg H, Wolburg-Buchholz K, Liebner S, Engelhardt B. Claudin-1, claudin-2 and claudin-11 are present in tight junctions of choroid plexus epithelium of the mouse. *Neurosci Lett*. (2001) 307:77–80. doi: 10.1016/s0304–3940(01)01927–9

20. Hirano A, Matsui T. [Electron microscopic observation of ependyma (author's transl)]. *No Shinkei Geka*. (1975) 3:237–44.

21. Shimada A, Hasegawa-Ishii S. Increased cytokine expression in the choroid plexus stroma and epithelium in response to endotoxin-induced systemic inflammation in mice. *Toxicol Rep*. (2021) 8:520–8. doi: 10.1016/j.toxrep.2021.03.002

22. Kunis G, Baruch K, Rosenzweig N, Kertser A, Miller O, Berkutzki T, et al. IFN-γ-dependent activation of the brain's choroid plexus for CNS immune surveillance and repair. *Brain J Neurol*. (2013) 136:3427–40. doi: 10.1093/brain/awt259

23. Chinnery HR, Ruitenberg MJ, McMenamin PG. Novel characterization of monocyte-derived cell populations in the meninges and choroid plexus and their rates of replenishment in bone marrow chimeric mice. *J Neuropathol Exp Neurol*. (2010) 69:896–909. doi: 10.1097/NEN.0b013e3181edbc1a

24. Kim Y-C, Ahn JH, Jin H, Yang MJ, Hong SP, Yoon J-H, et al. Immaturity of immune cells around the dural venous sinuses contributes to viral meningoencephalitis in neonates. *Sci Immunol*. (2023) 8:eadg6155. doi: 10.1126/sciimmunol.adg6155

25. Haas J, Rudolph H, Costa L, Faller S, Libicher S, Würthwein C, et al. The choroid plexus is permissive for a preactivated antigen-experienced memory B-cell subset in multiple sclerosis. *Front Immunol*. (2020) 11:618544. doi: 10.3389/fimmu.2020.618544

26. Szmydynger-Chodobska J, Strazielle N, Zink BJ, Ghersi-Egea J-F, Chodobski A. The role of the choroid plexus in neutrophil invasion after traumatic brain injury. *J Cereb Blood Flow Metab Off J Int Soc Cereb Blood Flow Metab*. (2009) 29:1503–16. doi: 10.1038/jcbfm.2009.71

27. Baruch K, Ron-Harel N, Gal H, Deczkowska A, Shifrut E, Ndifon W, et al. CNS-specific immunity at the choroid plexus shifts toward destructive Th2 inflammation in brain aging. *Proc Natl Acad Sci*. (2013) 110:2264–9. doi: 10.1073/pnas.1211270110

28. Schwerk C, Rybarczyk K, Essmann F, Seibt A, Mölleken M-L, Zeni P, et al. TNFalpha induces choroid plexus epithelial cell barrier alterations by apoptotic and nonapoptotic mechanisms. *J BioMed Biotechnol*. (2010) 2010:307231. doi: 10.1155/2010/307231

29. Groh J, Knöpper K, Arampatzi P, Yuan X, Lößlein L, Saliba A-E, et al. Accumulation of cytotoxic T cells in the aged CNS leads to axon degeneration and contributes to cognitive and motor decline. *Nat Aging*. (2021) 1:357–67. doi: 10.1038/s43587-021-00049-z

30. Dani N, Herbst RH, McCabe C, Green GS, Kaiser K, Head JP, et al. A cellular and spatial map of the choroid plexus across brain ventricles and ages. *Cell*. (2021) 184:3056–3074.e21. doi: 10.1016/j.cell.2021.04.003

31. Walsh DR, Zhou Z, Li X, Kearns J, Newport DT, Mulvihill JJE. Mechanical properties of the cranial meninges: A systematic review. *J Neurotrauma*. (2021) 38:1748–61. doi: 10.1089/neu.2020.7288

32. Weller RO. Microscopic morphology and histology of the human meninges. *Morphologie*. (2005) 89:22–34. doi: 10.1016/S1286–0115(05)83235–7

33. Pietilä R, Del Gaudio F, He L, Vázquez-Liébanas E, Vanlandewijck M, Muhl L, et al. Molecular anatomy of adult mouse leptomeninges. *Neuron*. (2023) 111:3745–3764.e7. doi: 10.1016/j.neuron.2023.09.002

34. Kekere V, Alsayouri K. *Anatomy, Head and Neck, Dura Mater* (2024). Treasure Island (FL): StatPearls Publishing. Available at: http://www.ncbi.nlm.nih.gov/books/NBK545301/ (Accessed January 23, 2024).

35. Ahn JH, Cho H, Kim J-H, Kim SH, Ham J-S, Park I, et al. Meningeal lymphatic vessels at the skull base drain cerebrospinal fluid. *Nature*. (2019) 572:62–6. doi: 10.1038/s41586–019-1419–5

36. Kiliç T, Akakin A. Anatomy of cerebral veins and sinuses. *Front Neurol Neurosci*. (2008) 23:4–15. doi: 10.1159/000111256

37. Adeeb N, Mortazavi MM, Deep A, Griessenauer CJ, Watanabe K, Shoja MM, et al. The pia mater: a comprehensive review of literature. *Childs Nerv Syst*. (2013) 29:1803–10. doi: 10.1007/s00381–013-2044–5

38. Krahn V. The pia mater at the site of the entry of blood vessels into the central nervous system. *Anat Embryol (Berl)*. (1982) 164:257–63. doi: 10.1007/BF00318509

39. Zhang ET, Inman CB, Weller RO. Interrelationships of the pia mater and the perivascular (Virchow-Robin) spaces in the human cerebrum. *J Anat*. (1990) 170:111–23.

40. Ma Q, Ineichen BV, Detmar M, Proulx ST. Outflow of cerebrospinal fluid is predominantly through lymphatic vessels and is reduced in aged mice. *Nat Commun*. (2017) 8:1434. doi: 10.1038/s41467–017-01484–6

41. Møllgård K, Beinlich FRM, Kusk P, Miyakoshi LM, Delle C, Plá V, et al. A mesothelium divides the subarachnoid space into functional compartments. *Science*. (2023) 379:84–8. doi: 10.1126/science.adc8810

42. Plá V, Bitsika S, Giannetto MJ, Ladron-de-Guevara A, Gahn-Martinez D, Mori Y, et al. Structural characterization of SLYM—a 4th meningeal membrane. *Fluids Barriers CNS*. (2023) 20:93. doi: 10.1186/s12987–023-00500-w

43. Fitzpatrick Z, Ghabdan Zanluqui N, Rosenblum JS, Tuong ZK, Lee CYC, Chandrashekhar V, et al. Venous-plexus-associated lymphoid hubs support meningeal humoral immunity. *Nature*. (2024) 628:612-9. doi: 10.1038/s41586–024-07202–9

44. Rustenhoven J, Pavlou G, Storck SE, Dykstra T, Du S, Wan Z, et al. Age-related alterations in meningeal immunity drive impaired CNS lymphatic drainage. *J Exp Med*. (2023) 220:e20221929. doi: 10.1084/jem.20221929

45. Ransohoff RM. Multiple sclerosis: role of meningeal lymphoid aggregates in progression independent of relapse activity. *Trends Immunol*. (2023) 44:266–75. doi: 10.1016/j.it.2023.02.002

46. Brioschi S, Wang W-L, Peng V, Wang M, Shchukina I, Greenberg ZJ, et al. Heterogeneity of meningeal B cells reveals a lymphopoietic niche at the CNS borders. *Science*. (2021) 373:eabf9277. doi: 10.1126/science.abf9277

47. Kwee RM, Kwee TC. Virchow-robin spaces at MR imaging. *RadioGraphics*. (2007) 27:1071–86. doi: 10.1148/rg.274065722

48. Verkhratsky A, Butt AM. Astroglial physiology. *Neuroglia*. (2023), 89–197. doi: 10.1016/B978–0-12–821565–4.00009–2

49. Vasciaveo V, Iadarola A, Casile A, Dante D, Morello G, Minotta L, et al. Sleep fragmentation affects glymphatic system through the different expression of AQP4 in wild type and 5xFAD mouse models. *Acta Neuropathol Commun*. (2023) 11:16. doi: 10.1186/s40478–022-01498–2

50. Hablitz LM, Plá V, Giannetto M, Vinitsky HS, Stæger FF, Metcalfe T, et al. Circadian control of brain glymphatic and lymphatic fluid flow. *Nat Commun*. (2020) 11:4411. doi: 10.1038/s41467–020-18115–2

51. Özen I, Deierborg T, Miharada K, Padel T, Englund E, Genové G, et al. Brain pericytes acquire a microglial phenotype after stroke. *Acta Neuropathol (Berl)*. (2014) 128:381–96. doi: 10.1007/s00401-014-1295-x

52. Nakagomi T, Kubo S, Nakano-Doi A, Sakuma R, Lu S, Narita A, et al. Brain vascular pericytes following ischemia have multipotential stem cell activity to differentiate into neural and vascular lineage cells. *Stem Cells Dayt Ohio*. (2015) 33:1962–74. doi: 10.1002/stem.1977

53. Van Hove H, Martens L, Scheyltjens I, De Vlaminck K, Pombo Antunes AR, De Prijck S, et al. A single-cell atlas of mouse brain macrophages reveals unique transcriptional identities shaped by ontogeny and tissue environment. *Nat Neurosci*. (2019) 22:1021–35. doi: 10.1038/s41593–019-0393–4

54. Smolders J, Heutinck KM, Fransen NL, Remmerswaal EBM, Hombrink P, Ten Berge IJM, et al. Tissue-resident memory T cells populate the human brain. *Nat Commun*. (2018) 9:4593. doi: 10.1038/s41467–018-07053–9

55. Faraco G, Park L, Anrather J, Iadecola C. Brain perivascular macrophages: characterization and functional roles in health and disease. *J Mol Med Berl Ger*. (2017) 95:1143–52. doi: 10.1007/s00109-017-1573-x

56. Rudie JD, Rauschecker AM, Nabavizadeh SA, Mohan S. Neuroimaging of dilated perivascular spaces: from benign and pathologic causes to mimics. *J Neuroimaging Off J Am Soc Neuroimaging*. (2018) 28:139–49. doi: 10.1111/jon.12493

57. Ineichen BV, Cananau C, Plattén M, Ouellette R, Moridi T, Frauenknecht KBM, et al. Dilated Virchow-Robin spaces are a marker for arterial disease in multiple sclerosis. *eBioMedicine*. (2023) 92:104631. doi: 10.1016/j.ebiom.2023.104631

58. Revel F, Cotton F, Haine M, Gilbert T. Hydrocephalus due to extreme dilation of Virchow-Robin spaces. *BMJ Case Rep*. (2015) 2015:bcr2014207109. doi: 10.1136/bcr-2014–207109

59. Ecker C, Suckling J, Deoni SC, Lombardo MV, Bullmore ET, Baron-Cohen S, et al. Brain anatomy and its relationship to behavior in adults with autism spectrum disorder: a multicenter magnetic resonance imaging study. *Arch Gen Psychiatry*. (2012) 69:195–209. doi: 10.1001/archgenpsychiatry.2011.1251

60. Jiang-Xie L-F, Drieu A, Bhasiin K, Quintero D, Smirnov I, Kipnis J. Neuronal dynamics direct cerebrospinal fluid perfusion and brain clearance. *Nature*. (2024) 627:157–64. doi: 10.1038/s41586–024-07108–6

61. Nagelhus EA, Ottersen OP. Physiological roles of aquaporin-4 in brain. *Physiol Rev*. (2013) 93:1543–62. doi: 10.1152/physrev.00011.2013

62. Mestre H, Tithof J, Du T, Song W, Peng W, Sweeney AM, et al. Flow of cerebrospinal fluid is driven by arterial pulsations and is reduced in hypertension. *Nat Commun*. (2018) 9:4878. doi: 10.1038/s41467–018-07318–3

63. Iliff JJ, Wang M, Zeppenfeld DM, Venkataraman A, Plog BA, Liao Y, et al. Cerebral arterial pulsation drives paravascular CSF-interstitial fluid exchange in the murine brain. *J Neurosci Off J Soc Neurosci*. (2013) 33:18190–9. doi: 10.1523/JNEUROSCI.1592–13.2013

64. Burbach JPH. Neuropetides and cerebrospinal fluid. *Ann Clin Biochem Int J Lab Med*. (1982) 19:269–77. doi: 10.1177/000456328201900416

65. Sawada M, Nishi S, Hashimoto N. Unilateral appearance of markedly dilated Virchow-Robin spaces. *Clin Radiol*. (1999) 54:334–6. doi: 10.1016/s0009–9260(99)90566–4

66. Salzman KL, Osborn AG, House P, Jinkins JR, Ditchfield A, Cooper JA, et al. Giant tumefactive perivascular spaces. *AJNR Am J Neuroradiol*. (2005) 26:298–305. doi: 10.1148/radiol.222559

67. Doubal FN, MacLullich AMJ, Ferguson KJ, Dennis MS, Wardlaw JM. Enlarged perivascular spaces on MRI are a feature of cerebral small vessel disease. *Stroke*. (2010) 41:450–4. doi: 10.1161/STROKEAHA.109.564914

68. Liu X-Y, Ma G-Y, Wang S, Gao Q, Guo C, Wei Q, et al. Perivascular space is associated with brain atrophy in patients with multiple sclerosis. *Quant Imaging Med Surg*. (2022) 12:1004–19. doi: 10.21037/qims-21–705

69. Zhang X, Ding L, Yang L, Qin W, Yuan J, Li S, et al. Brain atrophy correlates with severe enlarged perivascular spaces in basal ganglia among lacunar stroke patients. *PloS One*. (2016) 11:e0149593. doi: 10.1371/journal.pone.0149593

70. Zhang Z-H, Yu Y, Wei S-G, Nakamura Y, Nakamura K, Felder RB. EP_3 receptors mediate PGE_2-induced hypothalamic paraventricular nucleus excitation and sympathetic activation. *Am J Physiol Heart Circ Physiol*. (2011) 301:H1559–1569. doi: 10.1152/ajpheart.00262.2011

71. Perrot CY, Herrera JL, Fournier-Goss AE, Komatsu M. Prostaglandin E2 breaks down pericyte-endothelial cell interaction via EP1 and EP4-dependent downregulation of pericyte N-cadherin, connexin-43, and R-Ras. *Sci Rep*. (2020) 10:11186. doi: 10.1038/s41598-020-68019-w

72. Kondo M. Lymphoid and myeloid lineage commitment in multipotent hematopoietic progenitors. *Immunol Rev*. (2010) 238:37–46. doi: 10.1111/j.1600-065X.2010.00963.x

73. Kolabas ZI, Kuemmerle LB, Perneczky R, Förstera B, Ulukaya S, Ali M, et al. Distinct molecular profiles of skull bone marrow in health and neurological disorders. *Cell*. (2023) 186:3706–3725.e29. doi: 10.1016/j.cell.2023.07.009

74. Herisson F, Frodermann V, Courties G, Rohde D, Sun Y, Vandoorne K, et al. Direct vascular channels connect skull bone marrow and the brain surface enabling myeloid cell migration. *Nat Neurosci*. (2018) 21:1209–17. doi: 10.1038/s41593–018-0213–2

75. Pulous FE, Cruz-Hernández JC, Yang C, Kaya Z, Paccalet A, Wojtkiewicz G, et al. Cerebrospinal fluid can exit into the skull bone marrow and instruct cranial hematopoiesis in mice with bacterial meningitis. *Nat Neurosci*. (2022) 25:567–76. doi: 10.1038/s41593–022-01060–2

76. Cugurra A, Mamuladze T, Rustenhoven J, Dykstra T, Beroshvili G, Greenberg ZJ, et al. Skull and vertebral bone marrow are myeloid cell reservoirs for the meninges and CNS parenchyma. *Science*. (2021) 373:eabf7844. doi: 10.1126/science.abf7844

77. Mazzitelli JA, Smyth LCD, Cross KA, Dykstra T, Sun J, Du S, et al. Cerebrospinal fluid regulates skull bone marrow niches via direct access through dural channels. *Nat Neurosci*. (2022) 25:555–60. doi: 10.1038/s41593–022-01029–1

78. Shi K, Li H, Chang T, He W, Kong Y, Qi C, et al. Bone marrow hematopoiesis drives multiple sclerosis progression. *Cell*. (2022) 185:2234–2247.e17. doi: 10.1016/j.cell.2022.05.020

79. Li B, Li J, Li B, Ouchi T, Li L, Li Y, et al. A single-cell transcriptomic atlas characterizes age-related changes of murine cranial stem cell niches. *Aging Cell*. (2023) 22:e13980. doi: 10.1111/acel.13980

80. Li Q, Pan S, Yin Y, Li W, Chen Z, Liu Y, et al. Normal cranial bone marrow MR imaging pattern with age-related ADC value distribution. *Eur J Radiol*. (2011) 80:471–7. doi: 10.1016/j.ejrad.2010.09.010

81. Harkins KD, Galons J, Secomb TW, Trouard TP. Assessment of the effects of cellular tissue properties on ADC measurements by numerical simulation of water diffusion. *Magn Reson Med*. (2009) 62:1414–22. doi: 10.1002/mrm.22155

82. Surov A, Meyer HJ, Wienke A. Correlation between minimum apparent diffusion coefficient (ADCmin) and tumor cellularity: A meta-analysis. *Anticancer Res*. (2017) 37:3807–10. doi: 10.21873/anticanres.11758

83. Nonomura Y, Yasumoto M, Yoshimura R, Haraguchi K, Ito S, Akashi T, et al. Relationship between bone marrow cellularity and apparent diffusion coefficient. *J Magn Reson Imaging*. (2001) 13:757–60. doi: 10.1002/jmri.1105

84. Carati CJ, Gannon BJ. LYMPHATIC SYSTEM. In: *Encyclopedia of Respiratory Medicine*. Elsevier (2006). p. 643–9. doi: 10.1016/B0–12-370879–6/00227–1

85. Yoon J-H, Jin H, Kim HJ, Hong SP, Yang MJ, Ahn JH, et al. Nasopharyngeal lymphatic plexus is a hub for cerebrospinal fluid drainage. *Nature*. (2024) 1-10. doi: 10.1038/s41586–023-06899–4

86. Shibata-Germanos S, Goodman JR, Grieg A, Trivedi CA, Benson BC, Foti SC, et al. Structural and functional conservation of non-lumenized lymphatic endothelial cells in the mammalian leptomeninges. *Acta Neuropathol (Berl)*. (2020) 139:383–401. doi: 10.1007/s00401-019-02091-z

87. Butler MG, Isogai S, Weinstein BM. Lymphatic development. *Birth Defects Res Part C Embryo Today Rev*. (2009) 87:222–31. doi: 10.1002/bdrc.20155

88. Hsu M, Rayasam A, Kijak JA, Choi YH, Harding JS, Marcus SA, et al. Neuroinflammation-induced lymphangiogenesis near the cribriform plate contributes to drainage of CNS-derived antigens and immune cells. *Nat Commun*. (2019) 10:229. doi: 10.1038/s41467–018-08163–0

89. Bernard C, Helmer C, Dilharreguy B, Amieva H, Auriacombe S, Dartigues J-F, et al. Time course of brain volume changes in the preclinical phase of Alzheimer's disease. *Alzheimers Dement*. (2014) 10:143–151.e1. doi: 10.1016/j.jalz.2013.08.279

90. Berron D, van Westen D, Ossenkoppele R, Strandberg O, Hansson O. Medial temporal lobe connectivity and its associations with cognition in early Alzheimer's disease. *Brain*. (2020) 143:1233–48. doi: 10.1093/brain/awaa068

91. Ballatore C, Lee VM-Y, Trojanowski JQ. Tau-mediated neurodegeneration in Alzheimer's disease and related disorders. *Nat Rev Neurosci*. (2007) 8:663–72. doi: 10.1038/nrn2194

92. Selkoe DJ, Hardy J. The amyloid hypothesis of Alzheimer's disease at 25 years. *EMBO Mol Med*. (2016) 8:595–608. doi: 10.15252/emmm.201606210

93. Yan D, Zhang Y, Liu L, Yan H. Pesticide exposure and risk of Alzheimer's disease: a systematic review and meta-analysis. *Sci Rep*. (2016) 6:32222. doi: 10.1038/srep32222

94. Kilian J, Kitazawa M. The emerging risk of exposure to air pollution on cognitive decline and Alzheimer's disease – Evidence from epidemiological and animal studies. *BioMed J*. (2018) 41:141–62. doi: 10.1016/j.bj.2018.06.001

95. Huat TJ, Camats-Perna J, Newcombe EA, Valmas N, Kitazawa M, Medeiros R. Metal toxicity links to alzheimer's disease and neuroinflammation. *J Mol Biol*. (2019) 431:1843–68. doi: 10.1016/j.jmb.2019.01.018

96. Rahman MA, Rahman MS, Uddin MJ, Mamum-Or-Rashid ANM, Pang M-G, Rhim H. Emerging risk of environmental factors: insight mechanisms of Alzheimer's diseases. *Environ Sci pollut Res*. (2020) 27:44659–72. doi: 10.1007/s11356-020-08243-z

97. Reardon S. FDA approves Alzheimer's drug lecanemab amid safety concerns. *Nature*. (2023) 613:227–8. doi: 10.1038/d41586–023-00030–3

98. Liu KY, Howard R. Can we learn lessons from the FDA's approval of aducanumab? *Nat Rev Neurol*. (2021) 17:715–22. doi: 10.1038/s41582-021-00557-x

99. Alzheimer A. Uber eigenartige Erkrankung der Hirnrinde. *Z Psychiatr*. (1907) 64:146–8.

100. Stelzmann RA, Norman Schnitzlein H, Reed Murtagh F. An english translation of alzheimer's 1907 paper, "über eine eigenartige erkankung der hirnrinde". *Clin Anat*. (1995) 8:429–31. doi: 10.1002/ca.980080612

101. Bettcher BM, Tansey MG, Dorothée G, Heneka MT. Peripheral and central immune system crosstalk in Alzheimer disease — a research prospectus. *Nat Rev Neurol*. (2021) 17:689–701. doi: 10.1038/s41582-021-00549-x

102. Uchihara T, Akiyama H, Kondo H, Ikeda K. Activated microglial cells are colocalized with perivascular deposits of amyloid-β Protein in alzheimer's disease brain. *Stroke*. (1997) 28:1948–50. doi: 10.1161/01.STR.28.10.1948

103. Zhao R, Hu W, Tsai J, Li W, Gan W-B. Microglia limit the expansion of β-amyloid plaques in a mouse model of Alzheimer's disease. *Mol Neurodegener*. (2017) 12:47. doi: 10.1186/s13024–017-0188–6

104. Gerrits E, Brouwer N, Kooistra SM, Woodbury ME, Vermeiren Y, Lambourne M, et al. Distinct amyloid-β and tau-associated microglia profiles in Alzheimer's disease. *Acta Neuropathol (Berl)*. (2021) 141:681–96. doi: 10.1007/s00401-021-02263-w

105. Jonsson T, Stefansson H, Steinberg S, Jonsdottir I, Jonsson PV, Snaedal J, et al. Variant of TREM2 associated with the risk of alzheimer's disease. *N Engl J Med*. (2013) 368:107–16. doi: 10.1056/NEJMoa1211103

106. Gratuze M, Leyns CEG, Holtzman DM. New insights into the role of TREM2 in Alzheimer's disease. *Mol Neurodegener*. (2018) 13:66. doi: 10.1186/s13024–018-0298–9

107. Hsieh CL, Koike M, Spusta SC, Niemi EC, Yenari M, Nakamura MC, et al. A role for TREM2 ligands in the phagocytosis of apoptotic neuronal cells by microglia. *J Neurochem*. (2009) 109:1144–56. doi: 10.1111/j.1471-4159.2009.06042.x

108. Poliani PL, Wang Y, Fontana E, Robinette ML, Yamanishi Y, Gilfillan S, et al. TREM2 sustains microglial expansion during aging and response to demyelination. *J Clin Invest*. (2015) 125:2161–70. doi: 10.1172/JCI77983

109. Wang Y, Ulland TK, Ulrich JD, Song W, Tzaferis JA, Hole JT, et al. TREM2-mediated early microglial response limits diffusion and toxicity of amyloid plaques. *J Exp Med*. (2016) 213:667–75. doi: 10.1084/jem.20151948

110. Zhao Y, Wu X, Li X, Jiang L-L, Gui X, Liu Y, et al. TREM2 is a receptor for β-amyloid that mediates microglial function. *Neuron*. (2018) 97:1023–1031.e7. doi: 10.1016/j.neuron.2018.01.031

111. Combs CK, Karlo JC, Kao S-C, Landreth GE. β-amyloid stimulation of microglia and monocytes results in TNFα-dependent expression of inducible nitric oxide synthase and neuronal apoptosis. *J Neurosci*. (2001) 21:1179–88. doi: 10.1523/JNEUROSCI.21–04-01179.2001

112. Lopez-Rodriguez AB, Hennessy E, Murray CL, Nazmi A, Delaney HJ, Healy D, et al. Acute systemic inflammation exacerbates neuroinflammation in Alzheimer's disease: IL-1β drives amplified responses in primed astrocytes and neuronal network dysfunction. *Alzheimers Dement*. (2021) 17:1735–55. doi: 10.1002/alz.12341

113. Wang W-Y, Tan M-S, Yu J-T, Tan L. Role of pro-inflammatory cytokines released from microglia in Alzheimer's disease. *Ann Transl Med*. (2015) 3:136. doi: 10.3978/j.issn.2305–5839.2015.03.49

114. Kinney JW, Bemiller SM, Murtishaw AS, Leisgang AM, Salazar AM, Lamb BT. Inflammation as a central mechanism in Alzheimer's disease. *Alzheimers Dement Transl Res Clin Interv*. (2018) 4:575–90. doi: 10.1016/j.trci.2018.06.014

115. Lai KSP, Liu CS, Rau A, Lanctôt KL, Köhler CA, Pakosh M, et al. Peripheral inflammatory markers in Alzheimer's disease: a systematic review and meta-analysis of 175 studies. *J Neurol Neurosurg Psychiatry*. (2017) 88:876–82. doi: 10.1136/jnnp-2017–316201

116. Shen X-N, Niu L-D, Wang Y-J, Cao X-P, Liu Q, Tan L, et al. Inflammatory markers in Alzheimer's disease and mild cognitive impairment: a meta-analysis and systematic review of 170 studies. *J Neurol Neurosurg Psychiatry*. (2019) 90:590–8. doi: 10.1136/jnnp-2018–319148

117. Leung R, Proitsi P, Simmons A, Lunnon K, Güntert A, Kronenberg D, et al. Inflammatory proteins in plasma are associated with severity of alzheimer's disease. *PloS One*. (2013) 8:e64971. doi: 10.1371/journal.pone.0064971

118. Saleem M, Herrmann N, Swardfager W, Eisen R, Lanctôt KL. Inflammatory markers in mild cognitive impairment: A meta-analysis. *J Alzheimers Dis*. (2015) 47:669–79. doi: 10.3233/JAD-150042

119. Nauen DW, Troncoso JC. Amyloid-beta is present in human lymph nodes and greatly enriched in those of the cervical region. *Alzheimers Dement*. (2022) 18:205–10. doi: 10.1002/alz.12385

120. Nedergaard M, Goldman SA. Glymphatic failure as a final common pathway to dementia. *Science*. (2020) 370:50–6. doi: 10.1126/science.abb8739

121. Kalaria RN, Premkumar DRD, Pax AB, Cohen DL, Lieberburg I. Production and increased detection of amyloid β protein and amyloidogenic fragments in brain microvessels, meningeal vessels and choroid plexus in Alzheimer's disease. *Mol Brain Res*. (1996) 35:58–68. doi: 10.1016/0169-328X(95)00180-Z

122. Lee Y, Choi Y, Park E-J, Kwon S, Kim H, Lee JY, et al. Improvement of glymphatic–lymphatic drainage of beta-amyloid by focused ultrasound in Alzheimer's disease model. *Sci Rep*. (2020) 10:16144. doi: 10.1038/s41598–020-73151–8

123. Iliff JJ, Wang M, Liao Y, Plogg BA, Peng W, Gundersen GA, et al. A paravascular pathway facilitates CSF flow through the brain parenchyma and the clearance of interstitial solutes, including amyloid β. *Sci Transl Med*. (2012) 4:147ra111. doi: 10.1126/scitranslmed.3003748

124. Zenaro E, Pietronigro E, Bianca VD, Piacentino G, Marongiu L, Budui S, et al. Neutrophils promote Alzheimer's disease–like pathology and cognitive decline via LFA-1 integrin. *Nat Med*. (2015) 21:880–6. doi: 10.1038/nm.3913

125. Cruz Hernández JC, Bracko O, Kersbergen CJ, Muse V, Haft-Javaherian M, Berg M, et al. Neutrophil adhesion in brain capillaries reduces cortical blood flow and impairs memory function in Alzheimer's disease mouse models. *Nat Neurosci*. (2019) 22:413–20. doi: 10.1038/s41593–018-0329–4

126. Da Mesquita S, Louveau A, Vaccari A, Smirnov I, Cornelison RC, Kingsmore KM, et al. Functional aspects of meningeal lymphatics in ageing and Alzheimer's disease. *Nature*. (2018) 560:185–91. doi: 10.1038/s41586–018-0368–8

127. Wang L, Zhang Y, Zhao Y, Marshall C, Wu T, Xiao M. Deep cervical lymph node ligation aggravates AD-like pathology of APP/PS1 mice. *Brain Pathol*. (2019) 29:176–92. doi: 10.1111/bpa.12656

128. Mazzitelli JA, Pulous FE, Smyth LCD, Kaya Z, Rustenhoven J, Moskowitz MA, et al. Skull bone marrow channels as immune gateways to the central nervous system. *Nat Neurosci*. (2023) 26:2052–62. doi: 10.1038/s41593–023-01487–1

129. Snyder SW, Ladror US, Wade WS, Wang GT, Barrett LW, Matayoshi ED, et al. Amyloid-beta aggregation: selective inhibition of aggregation in mixtures of amyloid with different chain lengths. *Biophys J*. (1994) 67:1216–28. doi: 10.1016/S0006–3495(94)80591–0

130. Klein AM, Kowall NW, Ferrante RJ. Neurotoxicity and oxidative damage of beta amyloid 1–42 versus beta amyloid 1–40 in the mouse cerebral cortex. *Ann N Y Acad Sci*. (1999) 893:314–20. doi: 10.1111/j.1749-6632.1999.tb07845.x

131. Sveinbjornsdottir S. The clinical symptoms of Parkinson's disease. *J Neurochem*. (2016) 139:318–24. doi: 10.1111/jnc.13691

132. Wakabayashi K, Mori F, Takahashi H. Progression patterns of neuronal loss and Lewy body pathology in the substantia nigra in Parkinson's disease. *Parkinsonism Relat Disord*. (2006) 12:S92–8. doi: 10.1016/j.parkreldis.2006.05.028

133. Kim WS, Kågedal K, Halliday GM. Alpha-synuclein biology in Lewy body diseases. *Alzheimers Res Ther*. (2014) 6:73. doi: 10.1186/s13195–014-0073–2

134. Mandel SA, Fishman T, Youdim MBH. Gene and protein signatures in sporadic Parkinson's disease and a novel genetic model of PD. *Parkinsonism Relat Disord*. (2007) 13:S242–7. doi: 10.1016/S1353–8020(08)70009–9

135. Romero-Gutiérrez E, Vázquez-Cárdenas P, Moreno-Macías H, Salas-Pacheco J, Tusié-Luna T, Arias-Carrión O. Differences in MTHFR and LRRK2 variant's association with sporadic Parkinson's disease in Mexican Mestizos correlated to Native American ancestry. *NPJ Park Dis*. (2021) 7:1–10. doi: 10.1038/s41531–021-00157-y

136. Wang B, Liu X, Xu S, Liu Z, Zhu Y, Zhang X, et al. Sporadic parkinson's disease potential risk loci identified in han ancestry of chinese mainland. *Front Aging Neurosci*. (2021) 12. doi: 10.3389/fnagi.2020.603793

137. Pan-Montojo F, Reichmann H. Considerations on the role of environmental toxins in idiopathic Parkinson's disease pathophysiology. *Transl Neurodegener*. (2014) 3:10. doi: 10.1186/2047–9158-3–10

138. Priyadarshi A, Khuder SA, Schaub EA, Shrivastava S. A meta-analysis of Parkinson's disease and exposure to pesticides. *Neurotoxicology*. (2000) 21:435–40.

139. Wang H, Yang F, Zhang S, Xin R, Sun Y. Genetic and environmental factors in Alzheimer's and Parkinson's diseases and promising therapeutic intervention via fecal microbiota transplantation. *NPJ Park Dis*. (2021) 7:1–10. doi: 10.1038/s41531–021-00213–7

140. Yang F, Trolle Lagerros Y, Bellocco R, Adami H-O, Fang F, Pedersen NL, et al. Physical activity and risk of Parkinson's disease in the Swedish National March Cohort. *Brain*. (2015) 138:269–75. doi: 10.1093/brain/awu323

141. Hernán MA, Takkouche B, Caamaño-Isorna F, Gestal-Otero JJ. A meta-analysis of coffee drinking, cigarette smoking, and the risk of Parkinson's disease. *Ann Neurol*. (2002) 52:276–84. doi: 10.1002/ana.10277

142. Kenborg L, Rugbjerg K, Lee P-C, Ravnskjær L, Christensen J, Ritz B, et al. Head injury and risk for Parkinson disease. *Neurology*. (2015) 84:1098–103. doi: 10.1212/WNL.0000000000001362

143. Rascol O, Payoux P, Ory F, Ferreira JJ, Brefel-Courbon C, Montastruc J-L. Limitations of current Parkinson's disease therapy. *Ann Neurol*. (2003) 53 Suppl 3:S3–12; discussion S12–15. doi: 10.1002/ana.10513

144. Pierce S, Coetzee GA. Parkinson's disease-associated genetic variation is linked to quantitative expression of inflammatory genes. *PloS One*. (2017) 12:e0175882. doi: 10.1371/journal.pone.0175882

145. Fuzzati-Armentero MT, Cerri S, Blandini F. Peripheral-central neuroimmune crosstalk in parkinson's disease: what do patients and animal models tell us? *Front Neurol*. (2019) 10:232. doi: 10.3389/fneur.2019.00232

146. Tansey MG, Wallings RL, Houser MC, Herrick MK, Keating CE, Joers V. Inflammation and immune dysfunction in Parkinson disease. *Nat Rev Immunol*. (2022) 22:657–73. doi: 10.1038/s41577–022-00684–6

147. McGeer PL, Itagaki S, Boyes BE, McGeer EG. Reactive microglia are positive for HLA-DR in the substantia nigra of Parkinson's and Alzheimer's disease brains. *Neurology*. (1988) 38:1285–5. doi: 10.1212/WNL.38.8.1285

148. Nagatsu T, Mogi M, Ichinose H, Togari A. Cytokines in Parkinson's disease. In: Mizuno Y, Calne DB, Horowski R, Poewe W, Riederer P, Youdim MBH, editors. *Advances in Research on Neurodegeneration*. Springer, Vienna (2000). p. 143–51. doi: 10.1007/978–3-7091–6284-2_12

149. Bido S, Muggeo S, Massimino L, Marzi MJ, Giannelli SG, Melacini E, et al. Microglia-specific overexpression of α-synuclein leads to severe dopaminergic neurodegeneration by phagocytic exhaustion and oxidative toxicity. *Nat Commun*. (2021) 12:6237. doi: 10.1038/s41467-021-26519-x

150. Hou L, Bao X, Zang C, Yang H, Sun F, Che Y, et al. Integrin CD11b mediates α-synuclein-induced activation of NADPH oxidase through a Rho-dependent pathway. *Redox Biol*. (2018) 14:600–8. doi: 10.1016/j.redox.2017.11.010

151. Wang S, Chu C-H, Stewart T, Ginghina C, Wang Y, Nie H, et al. α-Synuclein, a chemoattractant, directs microglial migration via H2O2-dependent Lyn phosphorylation. *Proc Natl Acad Sci*. (2015) 112:E1926–35. doi: 10.1073/pnas.1417883112

152. Zheng T, Zhang Z. Activated microglia facilitate the transmission of α-synuclein in Parkinson's disease. *Neurochem Int*. (2021) 148:105094. doi: 10.1016/j.neuint.2021.105094

153. Braak H, Rüb U, Gai WP, Del Tredici K. Idiopathic Parkinson's disease: possible routes by which vulnerable neuronal types may be subject to neuroinvasion by an unknown pathogen. *J Neural Transm*. (2003) 110:517–36. doi: 10.1007/s00702–002-0808–2

154. Hawkes CH, Del Tredici K, Braak H. Parkinson's disease: a dual-hit hypothesis. *Neuropathol Appl Neurobiol*. (2007) 33:599–614. doi: 10.1111/j.1365-2990.2007.00874.x

155. Hawkes CH, Del Tredici K, Braak H. Parkinson's disease. *Ann N Y Acad Sci*. (2009) 1170:615–22. doi: 10.1111/j.1749-6632.2009.04365.x

156. Rietdijk CD, Perez-Pardo P, Garssen J, van Wezel RJA, Kraneveld AD. Exploring braak's hypothesis of parkinson's disease. *Front Neurol*. (2017) 8:37. doi: 10.3389/fneur.2017.00037

157. Cabezas R, Ávila M, Gonzalez J, El-Bachá RS, Báez E, García-Segura LM, et al. Astrocytic modulation of blood brain barrier: perspectives on Parkinson's disease. *Front Cell Neurosci*. (2014) 8. doi: 10.3389/fncel.2014.00211

158. Lan G, Wang P, Chan RB, Liu Z, Yu Z, Liu X, et al. Astrocytic VEGFA: An essential mediator in blood–brain-barrier disruption in Parkinson's disease. *Glia*. (2022) 70:337–53. doi: 10.1002/glia.24109

159. Huang X, Hussain B, Chang J. Peripheral inflammation and blood–brain barrier disruption: effects and mechanisms. *CNS Neurosci Ther*. (2021) 27:36–47. doi: 10.1111/cns.13569

160. Si X, Guo T, Wang Z, Fang Y, Gu L, Cao L, et al. Neuroimaging evidence of glymphatic system dysfunction in possible REM sleep behavior disorder and Parkinson's disease. *NPJ Park Dis*. (2022) 8:1–9. doi: 10.1038/s41531–022-00316–9

161. Shen T, Yue Y, Ba F, He T, Tang X, Hu X, et al. Diffusion along perivascular spaces as marker for impairment of glymphatic system in Parkinson's disease. *NPJ Park Dis*. (2022) 8:1–10. doi: 10.1038/s41531–022-00437–1

162. Ding X-B, Wang X-X, Xia D-H, Liu H, Tian H-Y, Fu Y, et al. Impaired meningeal lymphatic drainage in patients with idiopathic Parkinson's disease. *Nat Med*. (2021) 27:411–8. doi: 10.1038/s41591–020-01198–1

163. Zou W, Pu T, Feng W, Lu M, Zheng Y, Du R, et al. Blocking meningeal lymphatic drainage aggravates Parkinson's disease-like pathology in mice overexpressing mutated α-synuclein. *Transl Neurodegener*. (2019) 8:7. doi: 10.1186/s40035-019-0147-y

164. Walton C, King R, Rechtman L, Kaye W, Leray E, Marrie RA, et al. Rising prevalence of multiple sclerosis worldwide: Insights from the Atlas of MS, third edition. *Mult Scler Houndmills Basingstoke Engl*. (2020) 26:1816–21. doi: 10.1177/1352458520970841

165. Cosh A, Carslaw H. Multiple sclerosis: symptoms and diagnosis. *InnovAiT Educ Inspir Gen Pract*. (2014) 7:651–7. doi: 10.1177/1755738014551618

166. Thompson AJ, Banwell BL, Barkhof F, Carroll WM, Coetzee T, Comi G, et al. Diagnosis of multiple sclerosis: 2017 revisions of the McDonald criteria. *Lancet Neurol*. (2018) 17:162–73. doi: 10.1016/S1474–4422(17)30470–2

167. Krieger S, Sorrells SF, Nickerson M, Pace TWW. Mechanistic insights into corticosteroids in multiple sclerosis: War horse or chameleon?☆. *Clin Neurol Neurosurg*. (2014) 119:6–16. doi: 10.1016/j.clineuro.2013.12.021

168. Patsopoulos NA. Genetics of multiple sclerosis: an overview and new directions. *Cold Spring Harb Perspect Med*. (2018) 8:a028951. doi: 10.1101/cshperspect.a028951

169. International Multiple Sclerosis Genetics Consortium, Patsopoulos NA, Baranzini SE, Santaniello A, Shoostari P, Cotsapas C, et al. Multiple sclerosis genomic map implicates peripheral immune cells and microglia in susceptibility. *Science*. (2019) 365:eaav7188. doi: 10.1126/science.aav7188

170. Ziaei A, Garcia-Miralles M, Radulescu CI, Sidik H, Silvin A, Bae H-G, et al. Ermin deficiency leads to compromised myelin, inflammatory milieu, and susceptibility to demyelinating insult. *Brain Pathol Zurich Switz*. (2022) 32:e13064. doi: 10.1111/bpa.13064

171. Alfredsson L, Olsson T. Lifestyle and environmental factors in multiple sclerosis. *Cold Spring Harb Perspect Med*. (2019) 9:a028944. doi: 10.1101/cshperspect.a028944

172. Ascherio A. Environmental factors in multiple sclerosis. *Expert Rev Neurother*. (2013) 13:3–9. doi: 10.1586/14737175.2013.865866

173. Buhelt S, Søndergaard HB, Oturai A, Ullum H, von Essen MR, Sellebjerg F. Relationship between multiple sclerosis-associated IL2RA risk allele variants and circulating T cell phenotypes in healthy genotype-selected controls. *Cells*. (2019) 8:634. doi: 10.3390/cells8060634

174. Liu H, Huang J, Dou M, Liu Y, Xiao B, Liu X, et al. Variants in the IL7RA gene confer susceptibility to multiple sclerosis in Caucasians: evidence based on 9734 cases and 10436 controls. *Sci Rep*. (2017) 7:1207. doi: 10.1038/s41598–017-01345–8

175. Jarius S, König FB, Metz I, Ruprecht K, Paul F, Brück W, et al. Pattern II and pattern III MS are entities distinct from pattern I MS: evidence from cerebrospinal fluid analysis. *J Neuroinflamm*. (2017) 14:171. doi: 10.1186/s12974-017-0929-z

176. Lazarevic I, Soldati S, Mapunda JA, Rudolph H, Rosito M, de Oliveira AC, et al. The choroid plexus acts as an immune cell reservoir and brain entry site in experimental autoimmune encephalomyelitis. *Fluids Barriers CNS*. (2023) 20:39. doi: 10.1186/s12987–023-00441–4

177. Langrish CL, Chen Y, Blumenschein WM, Mattson J, Basham B, Sedgwick JD, et al. IL-23 drives a pathogenic T cell population that induces autoimmune inflammation. *J Exp Med*. (2005) 201:233–40. doi: 10.1084/jem.20041257

178. Reboldi A, Coisne C, Baumjohann D, Benvenuto F, Bottinelli D, Lira S, et al. C-C chemokine receptor 6–regulated entry of TH-17 cells into the CNS through the choroid plexus is required for the initiation of EAE. *Nat Immunol*. (2009) 10:514–23. doi: 10.1038/ni.1716

179. Zheng W, Feng Y, Zeng Z, Ye M, Wang M, Liu X, et al. Choroid plexus-selective inactivation of adenosine A2A receptors protects against T cell infiltration and experimental autoimmune encephalomyelitis. *J Neuroinflamm*. (2022) 19:52. doi: 10.1186/s12974-022-02415-z

180. Zheng Y, Hu L, Yang Y, Zheng C, Tu W, Lin H, et al. Blocking the IFN-gamma signal in the choroid plexus confers resistance to experimental autoimmune encephalomyelitis. *FASEB J Off Publ Fed Am Soc Exp Biol*. (2023) 37:e22833. doi: 10.1096/fj.202201767R

181. Howell OW, Reeves CA, Nicholas R, Carassiti D, Radotra B, Gentleman SM, et al. Meningeal inflammation is widespread and linked to cortical pathology in multiple sclerosis. *Brain*. (2011) 134:2755–71. doi: 10.1093/brain/awr182

182. Kivisäkk P, Imitola J, Rasmussen S, Elyaman W, Zhu B, Ransohoff RM, et al. Localizing central nervous system immune surveillance: meningeal antigen-presenting cells activate T cells during experimental autoimmune encephalomyelitis. *Ann Neurol*. (2009) 65:457–69. doi: 10.1002/ana.21379

183. Montilla A, Zabala A, Er-Lukowiak M, Rissiek B, Magnus T, Rodriguez-Iglesias N, et al. Microglia and meningeal macrophages depletion delays the onset of experimental autoimmune encephalomyelitis. *Cell Death Dis*. (2023) 14:16. doi: 10.1038/s41419–023-05551–3

184. Vivash L. Dilated Virchow Robin spaces in multiple sclerosis – a generalised marker of disease? *eBioMedicine*. (2023) 94:104708. doi: 10.1016/j.ebiom.2023.104708

185. Carotenuto A, Cacciaguerra L, Pagani E, Preziosa P, Filippi M, Rocca MA. Glymphatic system impairment in multiple sclerosis: relation with brain damage and disability. *Brain*. (2022) 145:2785–95. doi: 10.1093/brain/awab454

186. Rohr SO, Greiner T, Joost S, Amor S, Valk Pvd, Schmitz C, et al. Aquaporin-4 expression during toxic and autoimmune demyelination. *Cells*. (2020) 9:2187. doi: 10.3390/cells9102187

187. Peng S, Liu J, Liang C, Yang L, Wang G. Aquaporin-4 in glymphatic system, and its implication for central nervous system disorders. *Neurobiol Dis*. (2023) 179:106035. doi: 10.1016/j.nbd.2023.106035

188. He Y, Rajantie I, Ilmonen M, Makinen T, Karkkainen MJ, Haiko P, et al. Preexisting Lymphatic Endothelium but not Endothelial Progenitor Cells Are Essential for Tumor Lymphangiogenesis and Lymphatic Metastasis. *Cancer Res*. (2004) 64:3737–40. doi: 10.1158/0008–5472.CAN-04–0088

189. He Y, Rajantie I, Pajusola K, Jeltsch M, Holopainen T, Yla-Herttuala S, et al. Vascular endothelial cell growth factor receptor 3–mediated activation of lymphatic endothelium is crucial for tumor cell entry and spread via lymphatic vessels. *Cancer Res*. (2005) 65:4739–46. doi: 10.1158/0008–5472.CAN-04–4576

190. Zumsteg A, Baeriswyl V, Imaizumi N, Schwendener R, Rüegg C, Christofori G. Myeloid cells contribute to tumor lymphangiogenesis. *PloS One*. (2009) 4:e7067. doi: 10.1371/journal.pone.0007067

191. Kerjaschki D. The crucial role of macrophages in lymphangiogenesis. *J Clin Invest*. (2005) 115:2316–9. doi: 10.1172/JCI26354

192. Kooij G, Kopplin K, Blasig R, Stuiver M, Koning N, Goverse G, et al. Disturbed function of the blood–cerebrospinal fluid barrier aggravates neuro-inflammation. *Acta Neuropathol (Berl)*. (2014) 128:267–77. doi: 10.1007/s00401–013-1227–1

193. Lopes Pinheiro MA, Kooij G, Mizee MR, Kamermans A, Enzmann G, Lyck R, et al. Immune cell trafficking across the barriers of the central nervous system in multiple sclerosis and stroke. *Biochim Biophys Acta BBA - Mol Basis Dis*. (2016) 1862:461–71. doi: 10.1016/j.bbadis.2015.10.018

194. Mempel TR, Henrickson SE, Von Andrian UH. T-cell priming by dendritic cells in lymph nodes occurs in three distinct phases. *Nature*. (2004) 427:154–9. doi: 10.1038/nature02238

195. Furtado GC, Marcondes MCG, Latkowski J-A, Tsai J, Wensky A, Lafaille JJ. Swift entry of myelin-specific T lymphocytes into the central nervous system in spontaneous autoimmune encephalomyelitis. *J Immunol Baltim Md 1950*. (2008) 181:4648–55. doi: 10.4049/jimmunol.181.7.4648

196. van Zwam M, Huizinga R, Heijmans N, van Meurs M, Wierenga-Wolf AF, Melief M-J, et al. Surgical excision of CNS-draining lymph nodes reduces relapse severity in chronic-relapsing experimental autoimmune encephalomyelitis. *J Pathol*. (2009) 217:543–51. doi: 10.1002/path.2476

197. Podkowa A, Miller RJ, Motl RW, Fish R, Oelze ML. Focused ultrasound treatment of cervical lymph nodes in rats with EAE: A pilot study. *Ultrasound Med Biol*. (2016) 42:2957–64. doi: 10.1016/j.ultrasmedbio.2016.08.007

198. Ruiz-Riquelme A, Lau HHC, Stuart E, Goczi AN, Wang Z, Schmitt-Ulms G, et al. Prion-like propagation of β-amyloid aggregates in the absence of APP overexpression. *Acta Neuropathol Commun*. (2018) 6:26. doi: 10.1186/s40478-018-0529-x

199. McGinley MP, Goldschmidt CH, Rae-Grant AD. Diagnosis and treatment of multiple sclerosis: A review. *JAMA*. (2021) 325:765. doi: 10.1001/jama.2020.26858

200. Murphy DD, Ravina B. Brain banking for neurodegenerative diseases. *Curr Opin Neurol*. (2003) 16:459–63. doi: 10.1097/00019052-200308000-00003

201. Griffin CP, Paul CL, Alexander KL, Walker MM, Hondermarck H, Lynam J. Postmortem brain donations vs premortem surgical resections for glioblastoma research: viewing the matter as a whole. *Neuro-Oncol Adv*. (2022) 4:vdab168. doi: 10.1093/noajnl/vdab168

202. Ferrer I, Martinez A, Boluda S, Parchi P, BarraChina M. Brain banks: benefits, limitations and cautions concerning the use of post-mortem brain tissue for molecular studies. *Cell Tissue Bank*. (2008) 9:181–94. doi: 10.1007/s10561–008-9077–0

203. Dawson TM, Golde TE, Lagier-Tourenne C. Animal models of neurodegenerative diseases. *Nat Neurosci*. (2018) 21:1370–9. doi: 10.1038/s41593–018-0236–8

204. Jucker M. The benefits and limitations of animal models for translational research in neurodegenerative diseases. *Nat Med*. (2010) 16:1210–4. doi: 10.1038/nm.2224

205. Marin-Moreno A, Canoyra S, Fernández-Borges N, Espinosa JC, Torres JM. Transgenic mouse models for the study of neurodegenerative diseases. *Front Biosci Landmark Ed*. (2023) 28:21. doi: 10.31083/j.fbl2801021

206. Yeo XY, Cunliffe G, Tang J, Gigg J, Li Z, Jung S. *Preclinical Modeling of Alzheimer's disease - Success and Limitations*. Alzheimer's Disease and Treatment (2021). pp. 1–29.

207. Oberheim NA, Wang X, Goldman S, Nedergaard M. Astrocytic complexity distinguishes the human brain. *Trends Neurosci*. (2006) 29:547–53. doi: 10.1016/j.tins.2006.08.004

208. Götz J, Bodea L-G, Goedert M. Rodent models for Alzheimer disease. *Nat Rev Neurosci*. (2018) 19:583–98. doi: 10.1038/s41583–018-0054–8

209. Franco R, Cedazo-Minguez A. Successful therapies for Alzheimer's disease: why so many in animal models and none in humans? *Front Pharmacol*. (2014) 5:146. doi: 10.3389/fphar.2014.00146

210. Taoka T, Masutani Y, Kawai H, Nakane T, Matsuoka K, Yasuno F, et al. Evaluation of glymphatic system activity with the diffusion MR technique: diffusion tensor image analysis along the perivascular space (DTI-ALPS) in Alzheimer's disease cases. *Jpn J Radiol*. (2017) 35:172–8. doi: 10.1007/s11604-017-0617-z

211. James ML, Fulton RR, Henderson DJ, Eberl S, Meikle SR, Thomson S, et al. Synthesis and *in vivo* evaluation of a novel peripheral benzodiazepine receptor PET radioligand. *Bioorg Med Chem*. (2005) 13:6188–94. doi: 10.1016/j.bmc.2005.06.030

212. Boutin H, Chauveau F, Thominiaux C, Grégoire M-C, James ML, Trebossen R, et al. 11C-DPA-713: a novel peripheral benzodiazepine receptor PET ligand for *in vivo* imaging of neuroinflammation. *J Nucl Med Off Publ Soc Nucl Med*. (2007) 48:573–81. doi: 10.2967/jnumed.106.036764

213. Kalita M, Park JH, Kuo RC, Hayee S, Marsango S, Straniero V, et al. PET imaging of innate immune activation using ^{11}C radiotracers targeting GPR84. *JACS Au*. (2023) 3:3297–310. doi: 10.1021/jacsau.3c00435

214. Chaney AM, Cropper HC, Jain P, Wilson E, Simonetta F, Johnson EM, et al. PET imaging of TREM1 identifies CNS-infiltrating myeloid cells in a mouse model of multiple sclerosis. *Sci Transl Med*. (2023) 15:eabm6267. doi: 10.1126/scitranslmed.abm6267

215. Stevens MY, Cropper HC, Lucot KL, Chaney AM, Lechtenberg KJ, Jackson IM, et al. Development of a CD19 PET tracer for detecting B cells in a mouse model of multiple sclerosis. *J Neuroinflamm*. (2020) 17:275. doi: 10.1186/s12974–020-01880–8

216. Guglielmetti C, Levi J, Huynh TL, Tiret B, Blecha J, Tang R, et al. Longitudinal imaging of T cells and inflammatory demyelination in a preclinical model of multiple sclerosis using 18F-FAraG PET and MRI. *J Nucl Med Off Publ Soc Nucl Med*. (2022) 63:140–6. doi: 10.2967/jnumed.120.259325

217. Moses WW. Fundamental limits of spatial resolution in PET. *Nucl Instrum Methods Phys Res Sect Accel Spectrometers Detect Assoc Equip*. (2011) 648 Supplement 1:S236–40. doi: 10.1016/j.nima.2010.11.092

218. Hong S, Rhee S, Jung KO. *In vivo* molecular and single cell imaging. *BMB Rep*. (2022) 55:267–74. doi: 10.5483/BMBRep.2022.55.6.030

219. Guilarte TR, Rodichkin AN, McGlothan JL, Acanda de la Rocha AM, Azzam DJ. Imaging neuroinflammation with TSPO: A new perspective on the cellular sources and subcellular localization. *Pharmacol Ther*. (2022) 234:108048. doi: 10.1016/j.pharmthera.2021.108048

220. Largeau B, Dupont A-C, Guilloteau D, Santiago-Ribeiro M-J, Arlicot N. TSPO PET imaging: from microglial activation to peripheral sterile inflammatory diseases? *Contrast Media Mol Imaging*. (2017) 2017:6592139. doi: 10.1155/2017/6592139

221. Nutma E, Ceyzériat K, Amor S, Tsartsalis S, Millet P, Owen DR, et al. Cellular sources of TSPO expression in healthy and diseased brain. *Eur J Nucl Med Mol Imaging*. (2021) 49:146–63. doi: 10.1007/s00259–020-05166–2

222. Mortensen KN, Sanggaard S, Mestre H, Lee H, Kostrikov S, Xavier ALR, et al. Impaired glymphatic transport in spontaneously hypertensive rats. *J Neurosci Off J Soc Neurosci*. (2019) 39:6365–77. doi: 10.1523/JNEUROSCI.1974–18.2019

223. Pinto E. Blood pressure and ageing. *Postgrad Med J*. (2007) 83:109–14. doi: 10.1136/pgmj.2006.048371

224. Laurent S, Boutouyrie P. Arterial stiffness and hypertension in the elderly. *Front Cardiovasc Med*. (2020) 7:544302. doi: 10.3389/fcvm.2020.544302

225. Carey RM, Moran AE, Whelton PK. Treatment of hypertension: A review. *JAMA*. (2022) 328:1849–61. doi: 10.1001/jama.2022.19590

226. Formolo DA, Yu J, Lin K, Tsang HWH, Ou H, Kranz GS, et al. Leveraging the glymphatic and meningeal lymphatic systems as therapeutic strategies in Alzheimer's disease: an updated overview of nonpharmacological therapies. *Mol Neurodegener*. (2023) 18:26. doi: 10.1186/s13024–023-00618–3

227. Lilius TO, Blomqvist K, Hauglund NL, Liu G, Stæger FF, Bærentzen S, et al. Dexmedetomidine enhances glymphatic brain delivery of intrathecally administered drugs. *J Controlled Release*. (2019) 304:29–38. doi: 10.1016/j.jconrel.2019.05.005

228. Liu Y, Liu X, Sun P, Li J, Nie M, Gong J, et al. rTMS treatment for abrogating intracerebral hemorrhage-induced brain parenchymal metabolite clearance dysfunction in male mice by regulating intracranial lymphatic drainage. *Brain Behav*. (2023) 13:e3062. doi: 10.1002/brb3.3062

229. Murdock MH, Yang C-Y, Sun N, Pao P-C, Blanco-Duque C, Kahn MC, et al. Multisensory gamma stimulation promotes glymphatic clearance of amyloid. *Nature*. (2024) 627:149–56. doi: 10.1038/s41586–024-07132–6

230. Zhang H, Cao S, Xu Y, Sun X, Fei M, Jing Q, et al. Landscape of immune infiltration in entorhinal cortex of patients with Alzheimer's disease. *Front Pharmacol*. (2022) 13:941656. doi: 10.3389/fphar.2022.941656

231. Garofalo S, Cocozza G, Bernardini G, Savage J, Raspa M, Aronica E, et al. Blocking immune cell infiltration of the central nervous system to tame Neuroinflammation in Amyotrophic lateral sclerosis. *Brain Behav Immun*. (2022) 105:1–14. doi: 10.1016/j.bbi.2022.06.004

232. Kong Y, Liu K, Hua T, Zhang C, Sun B, Guan Y. PET imaging of neutrophils infiltration in alzheimer's disease transgenic mice. *Front Neurol*. (2020) 11:523798. doi: 10.3389/fneur.2020.523798

233. Hammond MD, Ambler WG, Ai Y, Sansing LH. α4 integrin is a regulator of leukocyte recruitment after experimental intracerebral hemorrhage. *Stroke*. (2014) 45:2485–7. doi: 10.1161/STROKEAHA.114.005551

234. Knier B, Hiltensperger M, Sie C, Aly L, Lepennetier G, Engleitner T, et al. Myeloid-derived suppressor cells control B cell accumulation in the central nervous system during autoimmunity. *Nat Immunol*. (2018) 19:1341–51. doi: 10.1038/s41590–018-0237–5

235. Nichols JM, Kummari E, Sherman J, Yang E-J, Dhital S, Gilfeather C, et al. CBD suppression of EAE is correlated with early inhibition of splenic IFN-γ + CD8+ T cells and modest inhibition of neuroinflammation. *J Neuroimmune Pharmacol*. (2021) 16:346–62. doi: 10.1007/s11481–020-09917–8

236. Pardridge WM. CSF. blood-brain barrier, and brain drug delivery. *Expert Opin Drug Delivery*. (2016) 13:963–75. doi: 10.1517/17425247.2016.1171315

237. Bryniarski MA, Ren T, Rizvi AR, Snyder AM, Morris ME. Targeting the choroid plexuses for protein drug delivery. *Pharmaceutics*. (2020) 12:963. doi: 10.3390/pharmaceutics12100963

238. Dragunow M. Meningeal and choroid plexus cells–novel drug targets for CNS disorders. *Brain Res*. (2013) 1501:32–55. doi: 10.1016/j.brainres.2013.01.013

239. Asano H, Hasegawa-Ishii S, Arae K, Obara A, Laumet G, Dantzer R, et al. Infiltration of peripheral immune cells into the olfactory bulb in a mouse model of acute nasal inflammation. *J Neuroimmunol*. (2022) 368:577897. doi: 10.1016/j.jneuroim.2022.577897

240. Ye D, Yuan J, Yang Y, Yue Y, Hu Z, Fadera S, et al. Incisionless targeted adeno-associated viral vector delivery to the brain by focused ultrasound-mediated intranasal administration. *eBioMedicine*. (2022) 84:104277. doi: 10.1016/j.ebiom.2022.104277

241. Chen H, Yang GZX, Getachew H, Acosta C, Sierra Sánchez C, Konofagou EE. Focused ultrasound-enhanced intranasal brain delivery of brain-derived neurotrophic factor. *Sci Rep*. (2016) 6:28599. doi: 10.1038/srep28599

242. Jung I-W, Han H-K. Effective mucoadhesive liposomal delivery system for risedronate: preparation and *in vitro*/*in vivo* characterization. *Int J Nanomedicine*. (2014) 9:2299–306. doi: 10.2147/IJN.S61181

243. Chiou C-J, Tseng L-P, Deng M-C, Jiang P-R, Tasi S-L, Chung T-W, et al. Mucoadhesive liposomes for intranasal immunization with an avian influenza virus vaccine in chickens. *Biomaterials*. (2009) 30:5862–8. doi: 10.1016/j.biomaterials.2009.06.046

frontiers | Frontiers in Immunology

TYPE Original Research
PUBLISHED 12 June 2024
DOI 10.3389/fimmu.2024.1400641

OPEN ACCESS

EDITED BY
Philipp Albrecht,
Heinrich Heine University of Düsseldorf, Germany

REVIEWED BY
Martin S. Weber,
University Medical Center Göttingen, Germany
Veit Rothhammer,
Department of Neurology University Hospital FAU Erlangen Nuernberg, Germany

*CORRESPONDENCE
Klaus Lehmann-Horn
klaus.lehmann-horn@tum.de

†PRESENT ADDRESSES
Jolien Diddens,
Department of Behavioural Neurobiology, Max Planck Institute for Biological Intelligence, Seewiesen, Germany
Verena Friedrich,
Institute of Medical Microbiology, Immunology and Hygiene, TUM School of Medicine and Health, Technical University of Munich, Munich, Germany

‡These authors have contributed equally to this work

RECEIVED 13 March 2024
ACCEPTED 08 May 2024
PUBLISHED 12 June 2024

CITATION
Georgieva T, Diddens J, Friedrich V, Lepennetier G, Brand RM and Lehmann-Horn K (2024) Single-cell profiling indicates a high similarity between immune cells in the cerebrospinal fluid and in meningeal ectopic lymphoid tissue in experimental autoimmune encephalomyelitis. *Front. Immunol.* 15:1400641. doi: 10.3389/fimmu.2024.1400641

Single-cell profiling indicates a high similarity between immune cells in the cerebrospinal fluid and in meningeal ectopic lymphoid tissue in experimental autoimmune encephalomyelitis

Tanya Georgieva‡, Jolien Diddens†‡, Verena Friedrich†, Gildas Lepennetier, Rosa Margareta Brand and Klaus Lehmann-Horn*

Department of Neurology, TUM School of Medicine and Health, Technical University of Munich, Munich, Germany

Background and objectives: B cell depleting anti-CD20 monoclonal antibodies (aCD20 mAbs) are highly effective in treatment of multiple sclerosis (MS) but fail to halt the formation of meningeal ectopic lymphoid tissue (mELT) in the murine model experimental autoimmune encephalomyelitis (EAE). While mELT can be examined in EAE, it is not accessible *in vivo* in MS patients. Our key objectives were to compare the immune cells in cerebrospinal fluid (CSF), which is accessible in patients, with those in mELT, and to study the effects of aCD20 mAbs on CSF and mELT in EAE.

Methods: Applying single cell RNA sequencing, we compared gene expression profiles in immune cells from (1) CSF with mELT and (2) aCD20 mAbs treated with control treated mice in a spontaneous 2D2xTh EAE model.

Results: The immune cell composition in CSF and mELT was very similar. Gene expression profiles and pathway enrichment analysis revealed no striking differences between the two compartments. aCD20 mAbs led not only to a virtually complete depletion of B cells in the CSF but also to a reduction of naïve CD4+ T cells and marked increase of macrophages. No remarkable differences in regulated genes or pathways were observed.

Discussion: Our results suggest that immune cells in the CSF may serve as a surrogate for mELT in EAE. Future studies are required to confirm this in MS patients. The observed increase of macrophages in B cell depleted CSF is a novel finding and requires verification in CSF of aCD20 mAbs treated MS patients. Due to unresolved technical challenges, we were unable to study the effects of aCD20 mAbs on mELT. This should be addressed in future studies.

KEYWORDS

multiple sclerosis, single-cell sequencing, experimental autoimmune encephalomyelitis, B cells, anti-CD20 treatment, ectopic lymphoid tissue

Introduction

Anti-CD20 monoclonal antibodies (aCD20 mAbs), depleting B cells, are very efficient in treatment of relapsing-remitting forms of multiple sclerosis (MS) (1, 2). Studies have also shown moderate beneficial effects in treatment of progressive MS (PMS), particularly in progression independent of relapse activity (PIRA) in early relapsing-remitting MS and in active primary PMS (3, 4). B cell-rich inflammatory cellular infiltrates in the meninges have been observed in patients with MS and in its murine model, experimental autoimmune encephalomyelitis (EAE). We designated these structures as meningeal ectopic lymphoid tissue (mELT). The presence of mELT in MS patients correlates with an earlier disease onset, a more rapid disease progression, and subpial cortical damage (5–10). mELT resembles secondary lymphoid organs (SLO) (11) to varying degrees and previous studies suggest that it may have similar functions, particularly germinal center activity (12–14). Interestingly, the B cells compartments in peripheral blood and CSF of MS patients are clonally related and exchange across the blood brain barrier (BBB) (15).

Based on the paradigm that 1) mELT contributes to progression in MS by facilitating smoldering inflammation in the central nervous system (CNS) behind the BBB and 2) assuming that B cells are an integral and pivotal component of mELT, we investigated the effects of aCD20 mAbs on mELT in a previous study (16). Applying murine aCD20 mAbs in a spontaneous chronic EAE model that has myelin oligodendrocyte glycoprotein (MOG) specific B and T cells (2D2/TCRMOG × Th/IgHMOG mice) and features mELT in the spinal cord (17, 18), we could confirm previous findings that aCD20 mAbs do not alter the disease course in this particular model (19). One possible explanation for this is, that large amounts of MOG-binding antibodies, which are present even after sustained B cell depletion, in collaboration with TCRMOG 2D2 T cells, are sufficient to induce and maintain EAE. Like in a case in which rituximab depleted B cells from cerebral perivascular spaces (20), we could demonstrate in our previous study that aCD20 mAbs depleted virtually all B cells from the meningeal compartment in EAE. The surprising finding, however, was that mELT forms anyway, despite the absence of B cells to a comparable extent (16). This raises important questions regarding the function of mELT in CNS autoimmunity and whether mELT even without B cells may have a role in MS. If mELT devoid of B cells still contributes to EAE pathogenesis, this may provide an alternative explanation why B cell depleted EAE mice develop EAE like B cell competent control animals and, potentially, why we observe disease progression in MS patients treated with aCD20 mAbs. Thus, a primary objective of this study was to address potential differences and common features of mELT with or without B cells. To address this question, the 2D2xTh EAE model is suitable, even though it does not respond to B cell depletion clinically.

Studying mELT functionally relies predominantly on experimental models. Extracting or otherwise accessing mELT in MS patients is challenging and can be reasonably achieved only in post-mortem tissue. Since cerebrospinal fluid (CSF) is in a spatial relationship with the meningeal compartment and can be readily and routinely obtained in patients, the second objective was to examine similarities and differences between the mELT and CSF compartments in respect to their immune cell composition and phenotype.

In the present study, we applied single cell RNA sequencing to investigate how B cell depletion by aCD20 mAb changes the cellular composition and immune cell phenotypes in mELT and CSF. We here fore used the same murine EAE model introduced above. We compared the immune cell composition in mELT and CSF in B cell competent conditions. Due to technical challenges, which precluded us from obtaining sufficient data from one experimental condition, the aCD20 mAb-treated mELT compartment, we could only approach our primary objective indirectly. After confirming that the immune profile of CSF and mELT in B cell competent mice was quite similar, we used the CSF compartment as a surrogate for mELT when examining the effects of aCD20 mAbs on the meningeal compartment. Our study revealed that the cellular composition and gene expression profiles of mELT and CSF are very similar. aCD20 mAbs efficiently depleted CSF B cells and concomitantly led to a reduction of naïve CD4+ T cells and increase of macrophages.

Materials and methods

2D2xTh mice

2D2xTh EAE mice – which develop spontaneous chronic EAE and meningeal inflammatory lesions in the spinal cord - were generated, held and clinically assessed as previously described (16–18). All animal procedures were approved by the standing committee for experimentation with laboratory animals of the administration of Upper Bavaria (ROB-55.2-2532.Vet_02-16-100).

Anti-CD20 treatment and B cell depletion

Six mice were initially used in the current experiment. Mice were randomly assigned to either the treatment or control group. The treatment was initiated when a mouse reached an EAE score ≥ 3 and was conducted as previously described (16). In brief, B cell depletion was achieved by weekly injection of 100 µg murine aCD20 mAbs (clone 18B12, provided by Roche). *In vivo* grade mouse IgG2a kappa isotype control (Crown bio, Cat: C0006) was used in the control group. One mouse from the treated group was excluded from further analysis due to insufficient effect of the aCD20 treatment. Figure 1A shows the experimental design. Table 1 lists the clinical characteristics of the 5 mice included in the final analyses and Figure 1B their clinical disease course.

Sample collection and single-cell preparation

Mice from both groups were sacrificed 30-35 days after the first injection. Animals were first anesthetized, after which CSF was obtained by puncture of the cisterna magna and stored on ice.

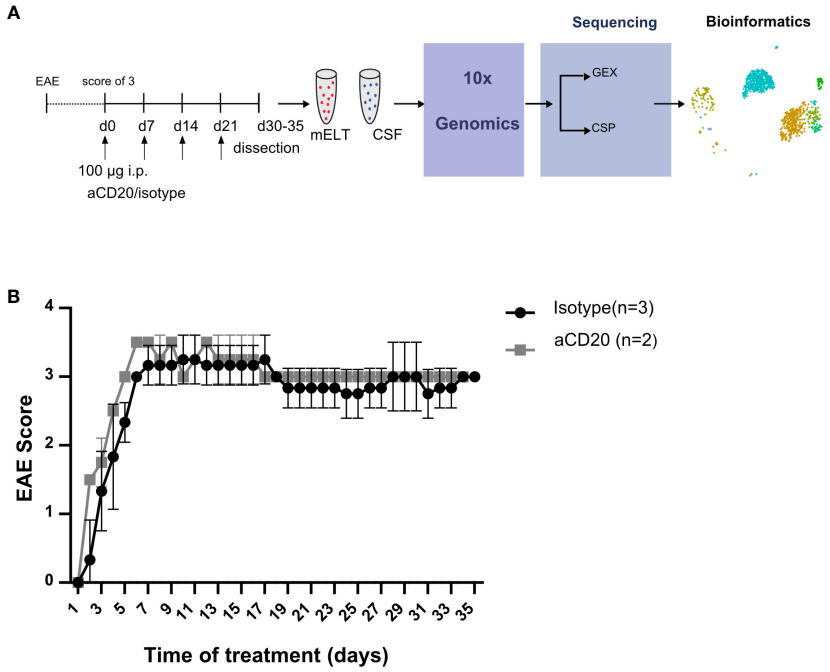

FIGURE 1
Study design and EAE score. **(A)** Mice were treated with a weekly dose of 100 µg of aCD20 mAb (n = 2) or isotype control (n = 3). On day 30-35, mice were dissected, and cell surface protein (CSP) and gene expression (GEX) libraries prepared and sequenced using 10x Genomics technology before bioinformatics analyses. **(B)** Daily evaluated EAE scores over the experimental period. Error bars show +/- SEM for the control group only.

Subsequently mice were sacrificed. After thorough perfusion with ice cold PBS, the spinal cord was dissected. A small test piece was cut from the thoracolumbar part of the spinal cord, which was used to histologically confirm the presence of mELT. Meninges were gently separated from the spinal cord in a petri dish with PBS and, using fine forceps, cut into small pieces under a dissection microscope. Subsequently meninges were digested in 600 µl digestion mix consisting of 4µl DNase, 60µl Collagenase IV and 536µl RPMI Medium for 30 minutes at 37°C on a shaker. Cells were isolated from the digested meninges by passing through 30 µl cell strainers, and washed. Cells from meninges and CSF were finally centrifuged (450xg, 5 min, 4 degrees) and resuspended in 100 µl FACS Buffer.

A brief incubation (10 min, 4°C) with Fc Block reagent was performed to block nonspecific antibody binding. Next, samples were labelled with DNA barcoded TotalSeq antibodies against mouse CD4, CD8a, CD19, Ly6G, and NK1.1, as previously described (11). At the same time, samples were incubated with 2 different TotalSeq Hashtag antibodies, in order to allow pooling samples per two: CSF und meningeal cells were incubated (20 minutes at 4° in the dark) with TotalSeq-C 0301 anti-mouse #1 (clone M1/42; 30-F11, Biolegend, dilution 1:400 in FACS buffer) and TotalSeq anti-mouse 0302 #2 (clone M1/42;30-F11, Biolegend, dilution 1:400 in FACS buffer), respectively. The incubation was followed by 3 wash steps with FACS Buffer and cell counting

TABLE 1 Characteristics of all mice utilized in the experiment.

Sex	treatment	Age at sacrifice (days)	Tissues analyzed	Age at disease onset (days)	disease duration (days)	Max. EAE Score	Mean EAE score	EAE score at sacrifice
female	aCD20	66	mELT, CSF	32	34	3	2,9	2,5
female	aCD20	77	mELT, CSF	46	31	3	2,6	3
female	Isotype	64	mELT, CSF	32	32	3,5	3,1	3
female	Isotype	61	mELT, CSF	31	30	3	2,7	2,5
male	Isotype	66	mELT, CSF	31	35	3	3	3

(Cellometer Auto 2000, Nexcelom Bioscience). Ultimately, the cell concentration was adjusted to $1x10^3$ cells/µl in RPMI/10% FCS, and CSF and meningeal cells were pooled together in a 1:4 ratio per mouse.

Library preparation and sequencing

Cells were loaded onto 10x Genomics Chromium Next GEM Chip G and the Chromium Controller was run according to the manufacturer's instructions (10x Genomics, USA) with a targeted cell recovery of 10,000 cells. Library preparation of Cell Surface Protein Library (CSP Library) and Gene Expression Library (GEX Library) was performed using Chromium Next GEM Single Cell V (D)J Reagent Kits v1.1, following the 10x Genomics protocol CG000208. The quality of library preparation was assessed using the Agilent 2100 Bioanalyzer.

Library quantification and single cell RNA-seq

Real-Time PCR was performed to quantify the libraries. All single cell gene expression, BCR and cell surface protein (CSP) libraries were multiplexed and sequenced using Illumina NovaSeq 6000 (S2 Flow cell), to obtain 26 x 91 bp paired-end reads for gene expression, cell surface protein and BCR libraries, taking into account the differences in read depth requirements. Novaseq sequencing was performed at the Helmholtz Zentrum München (HMGU) by the Genomics Core Facility.

Bioinformatical analysis

Single cell data processing and batch correction

Data processing and batch correction were done on all 5 samples as described before (11). In order to exclude dead/dying cells and reduce potential doublets, we kept only cells with >200 and <2,000 genes, >100 and <10,000 read count, <5% of reads mapping to mitochondrial genes and hemoglobin genes. 33.9% of the cells were removed by this quality filtering to obtain 17,226 cells at the end.

Cluster annotation

Gene markers for each cluster were defined using FindAllMarkers function (Seurat R library) (v 4.0.0). Each cluster was annotated automatically using CIPR (version 0.1.0) based on the "immgen" database. In order to confirm cluster annotation and, detect specific cell types that did not exist in the database, we used Nebulosa (version 1.0.0) to display gene expression density for several gene markers. Plasma cells could not be detected by the annotation of the clusters using CIPR, we therefore used the *Sdc1* and *Tnfrsf17* gene markers to annotate those cells. Glial cells and CD8+ T cells were annotated using the same approach using the *Slc1a2* gene and *Cd8a* gene respectively. After extracting the gene markers for each cluster and inspecting them visually, we decided to name the "Pre-T cell" group "T cell", as it fits better the biological reality.

Cell surface protein data processing and doublet filtering

TotalSeq antibody barcodes were processed in 2 separate assays: one for the tissue of origin and one for the cell type. We used the centred log-ratio (CLR) normalization method, then the HTODemux function (Seurat) was used to label each cell. Unfortunately, hashtag oligo (HTO), indicating the tissue of origin, for mELT had a relatively lower expression and yielded only 5% of the total cells, as compared to 31% cells labeled as CSF. In addition, 54% of the cells were HTO-negative. To improve the yield and differentiate between tissues, we used a 1.5-fold difference in HTO expression per cell. This approach allowed us to rescue mELT cells not labeled because of the low expression of the mELT tag compared to the CSF tag. Using this approach, we could label 44% of cells as CSF origin and 33% as mELT (77% HTO-positive), with 23% still unknown (HTO-negative) for a total of 17,226 cells. The HTO-negative cells were removed.

The cell type specific CSP antibody barcodes defined by HTODemux yielded 3% CD19, 17% CD4, 2% CD8a, 2% Ly6G, 2% NK, 60% unknown (putative doublet) and 14% negative cells. We did not filter out these putative doublets, because of the low confidence in the CSP-data, instead we used the DoubletFinder R package (v2.0.3) to identify doublets that were not filtered in the previous steps based on the gene expression.

We used the CSP information to remove cells that were confidently labelled as one cell type but clustering with a different cell cluster (Example: cells tagged with the antibody for NK cells but found in the B cell cluster). In addition, we also used the BCR-sequencing information to remove cells having B cell information but not in the plasma cell or B cell cluster. Contaminating glia cells, oligodendrocytes and erythroid cells were removed. The remaining 9,585 cells, annotated in 11 cell types, were used for the differential gene expression analysis, that was performed when a condition had at least 50 cells.

Differential gene expression

Differential gene expression was analyzed as described before (11). Clusters comprising fewer than 50 cells were excluded from the analysis. Significant genes (adjusted p-value <0.05) were ranked based on their average log2FC values. The genes mentioned in the text are the 10 most upregulated and 10 most downregulated genes in both comparisons (CSF aCD20 vs CSF isotype and mELT isotype vs CSF isotype).

Pathway enrichment analysis

Using the web-based analytical resource Metascape, we identified significant differences in biological pathways between mELT and CSF, as well as between aCD20-treated and untreated mice (21). We utilized the December 18, 2021 version of Metascape and employed mouse data as input, which was analyzed as if it were human data. The following pathway types were chosen for analysis: GO-Biological processes, WikiPathways, Reactome, and KEGG Pathways.

Enrichment analysis was conducted against a custom background gene list, containing all genes considered in the differential gene expression analysis. Pathways with an adjusted p-value <0.001 were considered. Ribosomal genes were excluded from the analysis.

Results

Immune cells in CSF and mELT form 11 clusters

We aimed to examine and compare the immune cell composition of CSF and mELT. Furthermore, we aimed to analyze the cellular differences in these tissues between the aCD20 treated (B cell depleted) and the control treated (B cell competent) mice. After filtering out low quality cells and corrections using "harmony" library, we obtained the transcriptome from a total of 9,585 single cells: 5,445 cells from mELT and 4,140 cells from CSF. We performed clustering and, in this way, classified the cells into 11 final cell clusters (Figure 2). Based on a combination of automatic cluster annotation (CIPR version 0.1.0, "immgen" database) and marker gene expression (see Methods section), we identified the following 11 cell types: T cells (*Cd3e*), more specifically naïve CD4+ T cells (*Cd4*, *Ccr7, Sell*), activated CD4+ T cells (*Cd4*, *Rora, Pdcd1, Il2*), CD8+ T cells (*Cd8a*), and regulatory T cells (*Foxp3*), B cells (*Cd79a, Cd19*) and plasma cells (*Sdc1, Tnfrsf17*), a cluster containing natural killer (NK) cells and NKT cells (*Klrb1c, Klrk1*), myeloid lineage cells, separated into dendritic cells (DC) (*Flt3*), macrophages (*Cd68*, *Adgre1*), monocytes (*Cd68*), and granulocytes (*S100a8* and *S100a9*). Erythroid cells (*Hbb-bt*) and

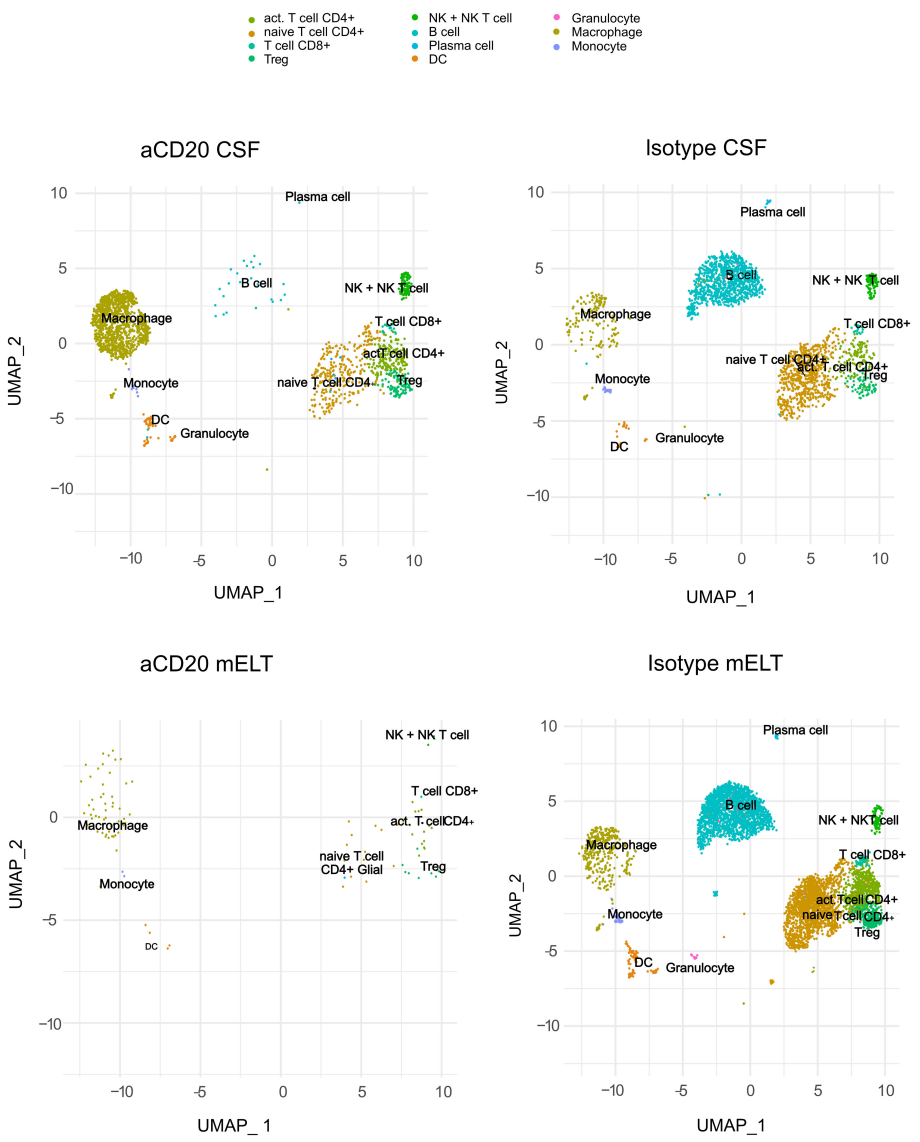

FIGURE 2
Uniform manifold approximation and projection (UMAP) plot representing 11 color-coded cell clusters identified in using single cell sequencing, split per tissue (CSF and mELT) and per treatment (aCD20 treated mice and control treated mice).

10.3389/fimmu.2024.1400641

oligodendrocytes (*Olig1*), probably coming from blood or CNS contamination respectively, were not considered in further analyses.

mELT and CSF have a similar cellular composition

Figure 3 and Table 2 illustrate the cell composition of mELT and CSF from control treated (B cell competent) mice. Both CSF and mELT consist mainly of B and CD4+ T lymphocytes. Their relative numbers (percentage) were comparable in both tissues (Table 2). Other cell types like monocytes, plasma cells, NK cells, macrophages and granulocytes are also equally represented in both CSF and mELT from control treated mice. Overall, regarding the immune cell composition, CSF and mELT were closely related in control treated 2D2xTh EAE mice.

CSF from aCD20 treated mice contains less B cells and naïve CD4+ T cells but more macrophages

As previously shown (16), aCD20 treatment did not alter the EAE course (Figure 1B). The cellular composition of B cell depleted, aCD20 treated CSF seems to be considerably different compared to the B cell competent control group. Due to insufficient data for the mELT aCD20 condition (Table 2), we compared CSF from aCD20 treated versus control treated mice as a surrogate (Figure 4,

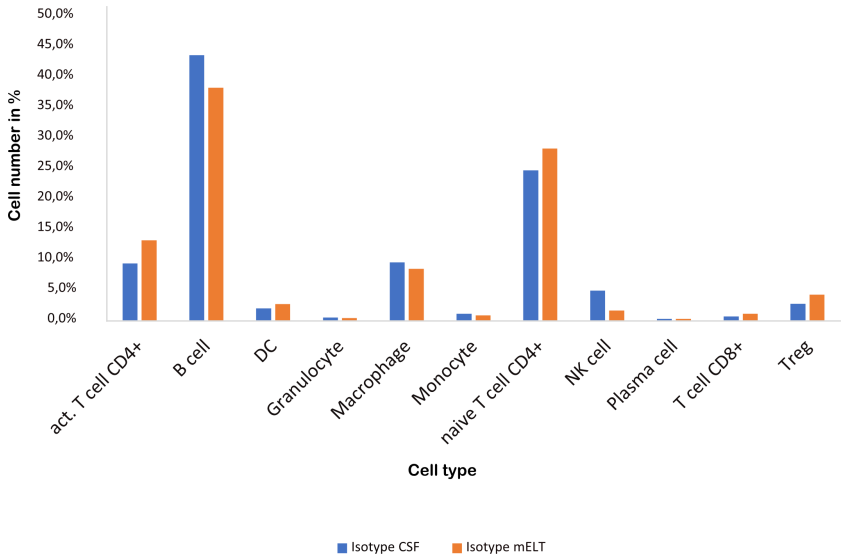

FIGURE 3
Cell numbers in CSF from control treated mice vs. mELT in control treated mice are similar. The percentage of the respective cell types is shown.

TABLE 2 Cell composition per tissue.

Cell Type	aCD20 CSF	aCD20 mELT	Isotype CSF	Isotype mELT
Activated CD4+ T cell	243 (11,9%)	19 (17,9%)	223 (9,4%)	784 (13,3%)
B cell	27 (1,3%)	0 (0%)	1031 (43,6%)	2266 (38,3%)
DC	52 (2,6%)	5 (4,7%)	49 (2,1%)	163 (2,8%)
Granulocyte	1 (0,01%)	0 (0%)	13 (0,6%)	27 (0,5%)
Macrophage	1277 (62,5%)	57 (53,8%)	227 (9,6%)	507 (8,6%)
Monocyte	7 (0,3%)	2 (1,9%)	28 (1,2%)	53 (0,9%)
Naive CD4+ T cell	230 (11,3%)	12 (11,3%)	584 (24,7%)	1674 (28,3%)
NK cell	103 (5%)	2 (1,9%)	118 (5%)	101 (1,7%)
Plasma cell	1 (0,1%)	0 (0%)	8 (0,3%)	21 (0,4%)
CD8+ T cell	20 (1%)	1 (0,9%)	17 (0,7%)	69 (1,2%)
Treg	82 (4%)	8 (7,6%)	66 (2,8%)	254 (4,3%)

Total number of cells (over all mice), as well as the percentage of cells per cell type are given for each tissue.

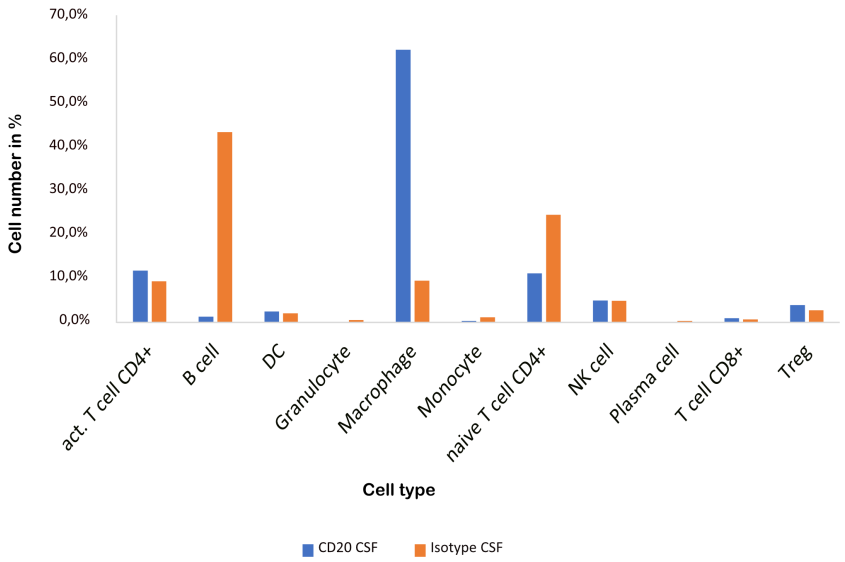

FIGURE 4
CSF from aCD20 treated mice has less B cells and naïve CD4+ T cells, but more macrophages than CSF from control treated mice. The percentage of the respective cell types is shown.

Table 2). Like previously shown for mELT (16), aCD20 treatment depleted virtually all B cells from CSF. In addition, aCD20 treated CSF contained less naïve CD4+ T-cells. Similarly, we observed a reduction of monocytes, granulocytes, and plasma cells, but their number was relatively low overall. Interestingly, we observed a substantial increase of macrophages in CSF samples from the aCD20 treated group when compared to the control treated group (1,277 vs. 227 cells; 62,5% vs. 9,6%). Numbers of activated CD4+ T cells, NK cells, Tregs, CD8+ T cells were similar in both conditions.

aCD20 treatment results in heterogeneous up- and downregulation of proinflammatory genes

In order to identify differences in gene expression in CSF between the aCD20 and isotype conditions, a differential gene expression analysis was conducted for each cell cluster within the respective tissue samples. Only those cell types were included in the analysis, where >50 cells were available in both conditions. Figure 5 illustrates the 10 genes with highest fold change among the significant upregulated and downregulated genes in CSF from aCD20 treated mice compared to the control treated group. A full list of significant genes can be found in Supplementary Table 1.

Differential gene expression analysis showed that the majority of differentially regulated genes was upregulated in the aCD20 treated group in comparison to the control group (Figure 6). One of the most differentially expressed genes, upregulated in the aCD20 treated group in each of the examined cell types, was Ferritin Heavy Chain 1 (*Fth1*), which has a major function in iron storage. Studies have demonstrated an upregulation of the *Fth1* gene in brain tissue of patients with MS lesions (22). However, an association with upregulated *Fth1* gene in immune cells of CSF is currently unknown. Another highly upregulated gene in all examined cell types was *Mbp*. The *Mbp* gene encodes for the myelin basic protein, which is a structural component of myelin sheath. Thus, Mbp expression in our data may represent contamination by myelin. However, according to Marty et al, Mbp expression is detected in T cells isolated from lymph nodes and spleen (23). Several variations in the *Mbp* gene have been associated with an increased susceptibility to developing MS and its clinical course (24). Furthermore, we observed a significant upregulation of the *Pfn1* gene in all immune cell populations. Even though no association with MS has been observed yet, studies have shown that excessive *Pfn1* activity can result in the immune system targeting the body's own cells resulting in other autoimmune diseases (25). *Apoe* was among the top 10 upregulated genes in activated and naïve CD4+ T cells. *Apoe* exhibits notable immunomodulatory properties by attenuating immune activation through downregulation of immune stimulatory proteins on antigen-presenting cells. Multiple scientific investigations have established a potential association between *Apoe* and autoimmune conditions, including MS (26–28). Interestingly, both *Apoe* and *Mbp* also showed higher expression in mELT than in spleen and lymph nodes in many immune celltypes in our previous study, comparing mELT with secondary lymphoid organs (11). Macrophages in CSF of B cell depleted mice exhibited upregulated expression of *Atf3*. *Atf3* correlates with macrophages infiltration and plays a role in inflammation, cell division, and apoptosis (29). Additionally, we observed an upregulation of the *Junb* gene in immune cells from aCD20 treated mice. *Junb* has been identified as a significant contributor to the activation of T cells and the differentiation and proliferation of Tregs (30). In addition, several subunits of cytochrome c oxidase (*Cox5a*, *Cox5b*, *Cox8a*, *Cox6a1*), which play an important role in regulation of ATP synthesis via oxidative

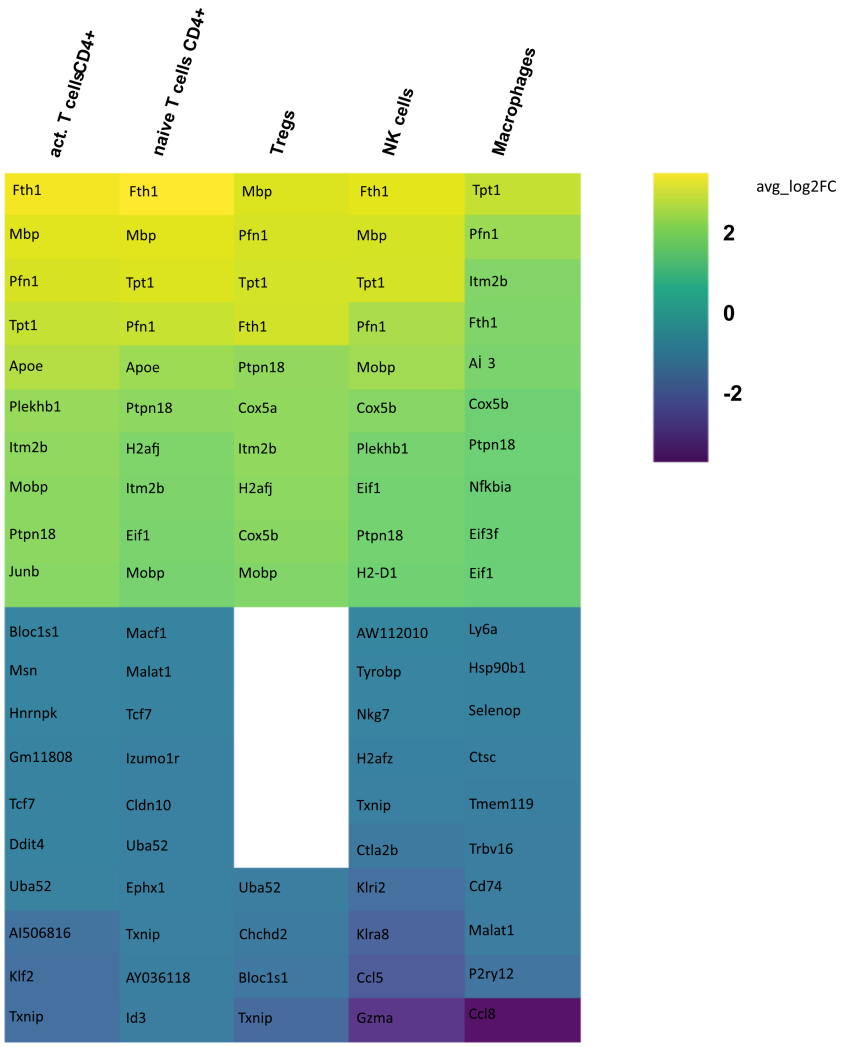

FIGURE 5
Heatmap representing differentially expressed genes (DEGs) between CSF from aCD20 treated and CSF from isotype treated mice for each cell type. Gene expression analysis was conducted only for cell counts >50. Thus, not all cell types are shown. The top 10 up- and downregulated genes are shown, ranked according to average log2 fold-change (avg_log 2FC). Positive avg_log 2FC represent upregulated genes in CSF from aCD20 treated mice, negative values correspond to downregulated genes.

phosphorylation (OXPHOS) (31), were found to be upregulated after CD20 treatment in all studied cell types. Typically, resting lymphocytes generate energy through oxidative phosphorylation and fatty acid oxidation, whereas activated lymphocytes rapidly shift to glycolysis (32). Finally, also translation initiation factors including *Eif1*, and *Eif3f*, were upregulated by CD20 treatment in all studied cell types. Interestingly, another translation initiation factor has been found to play a role in MS development (33). aCD20 mAb treatment leads to an increased expression of proinflammatory chemokines CCL3 and CCL4 in macrophages, which can lead to the attraction of more macrophages and monocytes. In addition, also CXCL14 and CCRL2 were increased in aCD20 mAb-treated CSF samples.

While genes upregulated after aCD20 treatment show more consistency across the different cell types, there is more variability observed in downregulated genes between different cell types. Among the genes found to be downregulated in the CSF after aCD20 treatment was *Txnip*, which was downregulated in activated CD4+ T cells, naive CD4+ T cells, Tregs, and NK cells. The *Txnip* gene has been investigated for its role in inflammatory activation and its implication in neurodegenerative disorders (34). In NK cells, the *Gzma* gene is downregulated in CSF from aCD20 treated mice. The *Gzma* gene, also known as Granzyme A, encodes a serine protease enzyme that is primarily found in the granules of cytotoxic T lymphocytes (CTLs) and NK cells. *Gzma* has been associated with immune activation and promotion of inflammation (35). A downregulated gene in macrophages is the *Ccl8* (C-C Motif Chemokine Ligand 8) gene. *Ccl8* has been linked to a severe disease course in MS (36). Furthermore, *Ccl8* is also known for its role in the induction of inflammation and is highly expressed in tumor-associated macrophages (37).

Although some of the top downregulated genes seemed to be related to inflammation and some of the top upregulated genes are related to regulation of inflammation, overall, gene

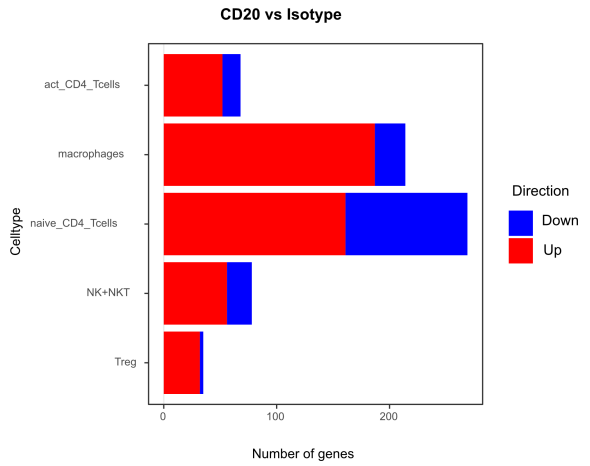

FIGURE 6
Number of genes that exhibit upregulation or downregulation in aCD20 treated mice compared to control treated mice.

expression analyses comparing CSF immune cells of B cell depleted and non-depleted mice did not show a uniform pro- or anti-inflammatory pattern.

The majority of differentially expressed genes were downregulated in mELT compared to CSF

Secondly, we compared the gene expression profiles of immune cells in mELT with CSF in control treated, B cell competent EAE mice. In mELT compared to CSF, overall, more genes were downregulated than upregulated (Figures 7, 8). A full list of significant genes is in Supplementary Table 2.

However, there was an overlap between the top 10 upregulated genes when comparing mELT versus CSF in the control treatment condition (Figure 7) with CSF in aCD20 treatment versus CSF in control treatment (Figure 5). Among the top 10 upregulated genes were once again *Mbp*, *Mobp*, *Fth1*, and *Tpt1*. These genes have been consistently associated with crucial biological processes, including myelin formation (*Mbp*, *Mobp*), iron homeostasis (*Fth1*), and cellular stress response (*Tpt1*). The expression of *Mbp*, *Mobp* and *Plp1*, which is also among the top 10 upregulated genes in the naïve CD4+ T cell dataset, could possibly represent myelin contamination in mELT. In B cells, the expression of immediate early genes (IEGs) such as *Egr1*, *Jund*, and *Fos*, which are rapidly induced in response to antigen receptor or cytokine stimulation (38), exhibited higher levels of expression in mELT compared to CSF. Interestingly, we found IEG also to be higher expressed in mELT compared to lymph nodes and spleen in our previous study (11). It is noteworthy that one of the most upregulated genes in B cells was *Fos*. Previous studies have associated *Fos* with MS (39).

The majority of genes was downregulated in mELT compared to CSF, including the *Klf2* gene, also referred to as Krüppel-like factor 2, downregulated in activated CD4+ T cells and NK cells, naïve CD4+ T cells and B cells. *Klf2* is recognized as a negative regulator of EAE-induced neuroinflammation through the inhibition of pro-inflammatory factors. It has been demonstrated that the absence of *Klf2* exacerbates neurological dysfunction and neuroinflammation (40). Furthermore, in mELT of control-treated mice, there were additional downregulated genes that seem noteworthy - *Hspa8* (all cell types), and *Gzma* (NK cells). *Gzma* has been introduced above. *Hspa8* belongs to the *Hsp70* family of chaperones and exhibits a protective potential in neurodegenerative diseases (41). Additionally, *Hsp70* serves as a marker for inflammatory processes in MS. It has been demonstrated that patients with MS have an elevated level of *Hsp70* in their serum. Specifically, clinically isolated syndrome and relapsing-remitting MS are associated with higher serum concentrations of *Hsp70* compared to progressive MS (42).

In summary, gene downregulation outweighed upregulation in control treated mELT compared to CSF – a finding that remains difficult to interpret.

Pathway enrichment analysis suggests that B cell depletion from CSF has little effect on immune-related pathways in remaining cells

Pathway enrichment analysis was used to identify differentially regulated pathways among differentially expressed genes (both up and downregulated) from 1) the CSF in the aCD20 vs. control treated conditions and 2) B cell competent immune cells between mELT and CSF.

For the first analysis, the top 5 pathways per cell type are shown in Figure 9. The most relevant seem to be T cell activation (in naïve T cells), antigen processing and presentation of exogenous peptide antigen and cytokine signaling in immune system (both macrophages). Moreover, oxidative phosphorylation, which is known to be important for many immune cell functions (32), was among the top pathways for all cell types. Yet, the majority of regulated pathways seem not to be primarily linked to inflammation. Overall, this analysis suggests that the absence of B cells in the CSF does not significantly change the inflammatory state of the remaining immune cells, whereas the phenotype (cell type composition) is clearly different.

Comparing B cell competent immune cells between mELT and CSF (Figure 10), we found an enrichment of relevant immune-related pathways, for example response to cytokine stimulus/signaling in activated CD4+ T cells, adaptive immune system response in B cells and naïve CD4+ T cells, and activation, cell-cell recognition and TCR signaling in naïve T cells.

Discussion

Based on our previously published observation, that aCD20 mAbs efficiently deplete B cells from mELT in spontaneous EAE but do not prevent or inhibit mELT formation, we set out to compare mELT that contained B cells with mELT in which B cells were depleted by single cell RNA sequencing. Unfortunately, due to

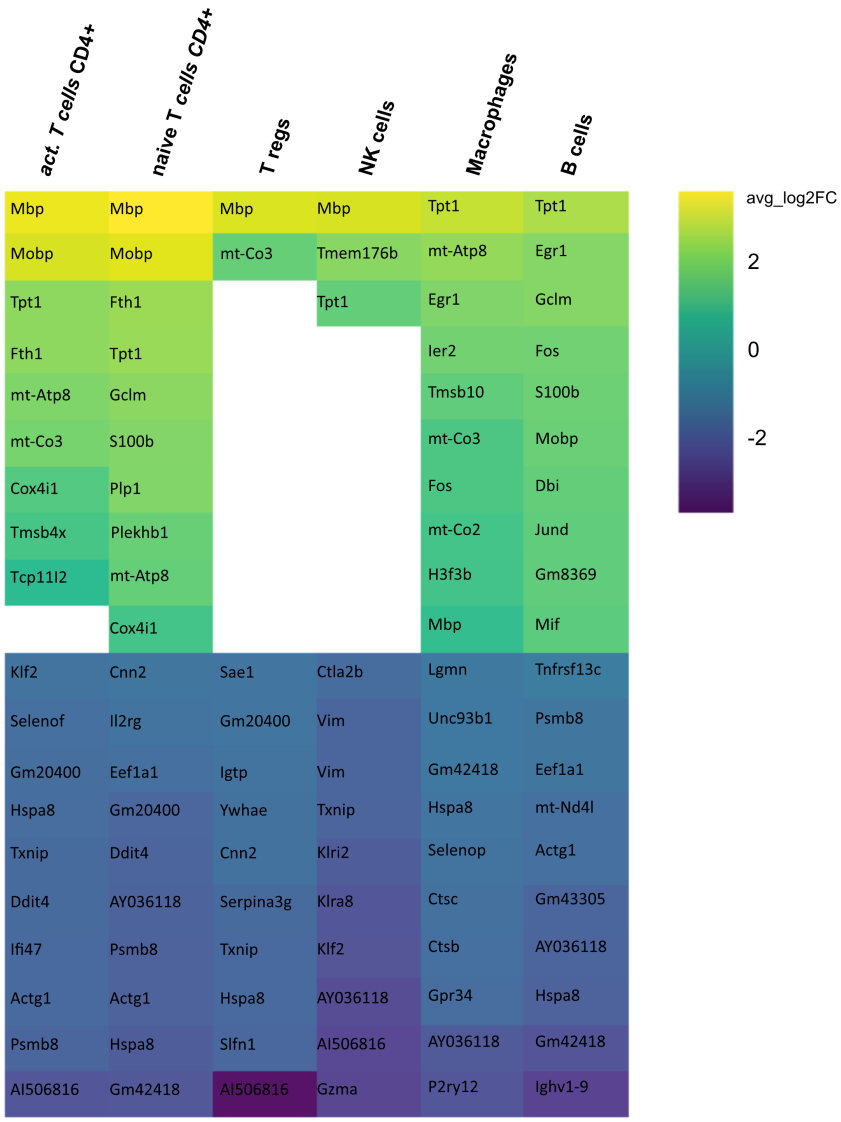

FIGURE 7
Heatmap representing differentially expressed genes (DEGs) between mELT from control treated and CSF from control treated mice for each cell type. Gene analysis was conducted only for cell counts >50. Thus, not all cell types are shown. The top 10 up- and downregulated genes in mELT from control treated mice when compared to CSF from control treated mice are shown. Genes were ranked according to average log2 fold-change (avg_log 2FC). Positive avg_log 2FC represent upregulated genes in mELT from control treated mice (green), negative values correspond to downregulated genes (blue).

unresolved technical challenges, we were unable to obtain, process and analyze enough cells from mELT in aCD20 mAbs treated mice to generate meaningful results in this condition. However, sufficient data could be obtained from control treated (B cell competent) mELT and from the CSF of aCD20 mAbs treated and control treated mice. Thus, we addressed our second objective first: whether the CSF and mELT compartment are related. Our data suggest that the immune cell composition, and to some degree gene expression profile, in the CSF mirrors that in mELT in B cell competent spontaneous EAE mice. Both, CSF and mELT, are predominated by B and CD4+ T lymphocytes. While other studies have highlighted certain aspects of the cellular composition of mELT, mostly based on morphological and immunohistochemical features (6, 16), our previous study has established mELT as a tertiary lymphoid organ closely resembling secondary lymphoid organs (11). Our current report is the first to study murine CSF in EAE by single cell RNA sequencing and comparing it with mELT. The cellular composition and immune phenotype of CSF cells in MS patients and healthy individuals has been studied quite intensively. While the CSF of healthy individuals contains < 5 leukocytes per µl, which are predominantly CD4+ T lymphocytes and fewer monocytes (43), CSF in MS patients may feature mild pleocytosis and a substantial

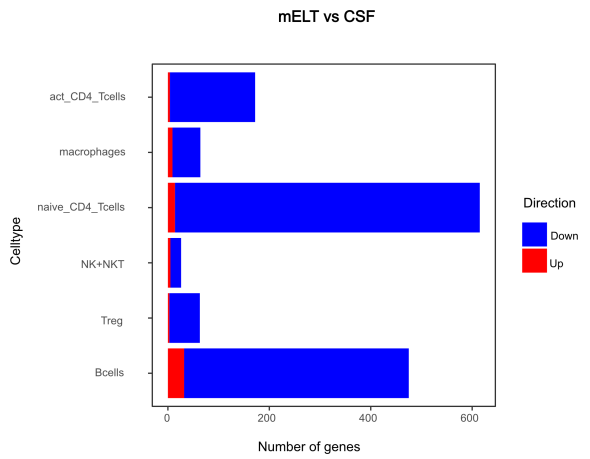

FIGURE 8
Number of genes that exhibit upregulation or downregulation in mELT in comparison to their expression levels in CSF.

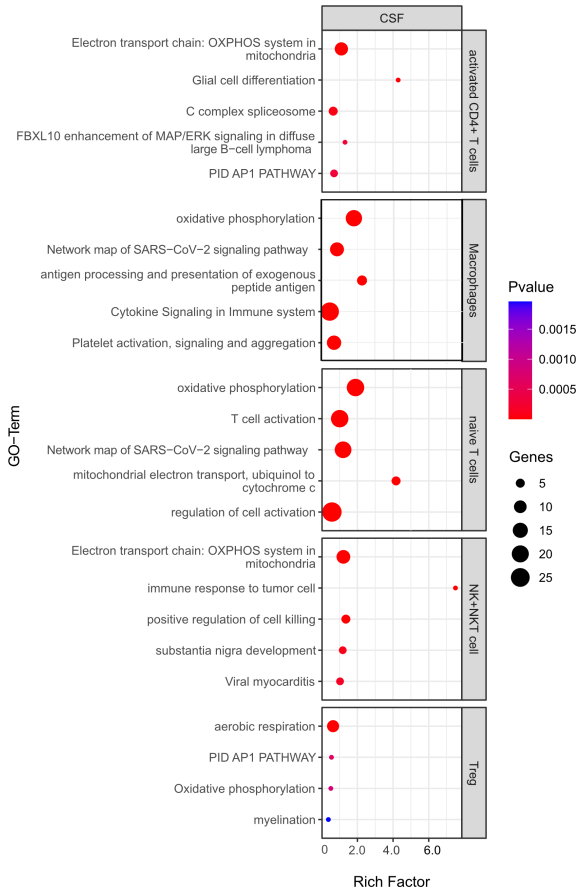

FIGURE 9
Functional enrichment analysis for genes differentially expressed between CSF from aCD20 treated mice and CSF from control treated mice using Metascape. The top 5 GO-terms are shown (For Tregs, only four pathways were significant). For similar gene ontology (GO) terms, only the top-ranked GO term was shown. The dot size reflects the number of genes enriched in the GO term and its color the corresponding statistical significance (p-value). Rich factor is the ratio of differentially expressed gene numbers annotated in this GO-term to all gene numbers annotated in this GO term.

increase in B cells (44). The cellular composition of murine CSF has not been described, to our knowledge. Our data suggests that CSF cells may serve as a surrogate for mELT in our model.

Analyzing the effects of aCD20 mAbs on the CSF compartment revealed, as expected, near complete depletion of B cells. We have previously demonstrated virtually complete B cell depletion from mELT by aCD20 mAbs in the same model using immunohistochemistry (16). Another study demonstrated that aCD20 mAbs could deplete B cells from the meninges, in a model that does not feature mELT (45). Interestingly, we observed a concomitant decrease of naïve CD4+ T cells in the absence of B cells in the CSF. It seems possible that a fraction of CSF T cells, that expressed CD20 on their cell surface, may directly be depleted by aCD20 mAbs (46). Monocytes, plasma cells and granulocytes were also decreased. In contrast, macrophages were markedly increased. This increase exceeded a mere relative, compensatory increase of other cell types in the absence of B cells but seems to be a distinct finding. Our previous study has suggested that macrophages in mELT may stimulate the recruitment of other immune cells to the inflamed CNS (11). We speculate that similar mechanisms may apply to the CSF. Peripheral blood CD11b+ monocytes/macrophages in B cell depleted patients have a more pro-inflammatory phenotype compared to B cell competent patients (47). Possibly, this altered phenotype favors accumulation of those myeloid cells in the CSF. In line with our data, studies have demonstrated that B cell depletion by aCD20 mAbs like rituximab and ocrelizumab in MS patients led to a strong reduction of CSF B cells and, to a lesser degree, T cells (48–50). To our knowledge, no data regarding CSF macrophages in B cell depleted CSF has been published.

Gene expression and pathway enrichment analyses comparing B cell competent mELT with CSF immune cells on the one hand and aCD20 mAbs versus control treated CSF on the other hand did not reveal striking differences with regard to immune cell phenotypes. Despite minor variations, no overarching theme directing any of the conditions in a specific way, either pro- or anti-inflammatory, could be identified. Given the remarkable efficacy of B cell depleting mAbs in treatment of MS, one could have expected a less inflammatory profile in B cell depleted CSF. This may be a limitation of the model we used, as it does not respond to aCD20 mAbs clinically.

This study faced other challenges and limitations. We discussed above how we were unable to obtain sufficient cells from B cell depleted mELT. We did not expect this challenge, since we knew from our previous study that mELT forms under B cell depleted conditions. However, B cell depleted mELT is less dense and structured. Thus, we speculate that this may have caused our difficulties in dissecting enough cells. Another major limitation was that we had to exclude one mouse from the aCD20 treated group due to insufficient B cell depletion after aCD20 mAbs treatment, and CSF cells could not be obtained from one control treated mouse. This prevented statistical analyses. For cost reasons, this study was planned with 3 mice per group, which is also a limitation to the study. Another

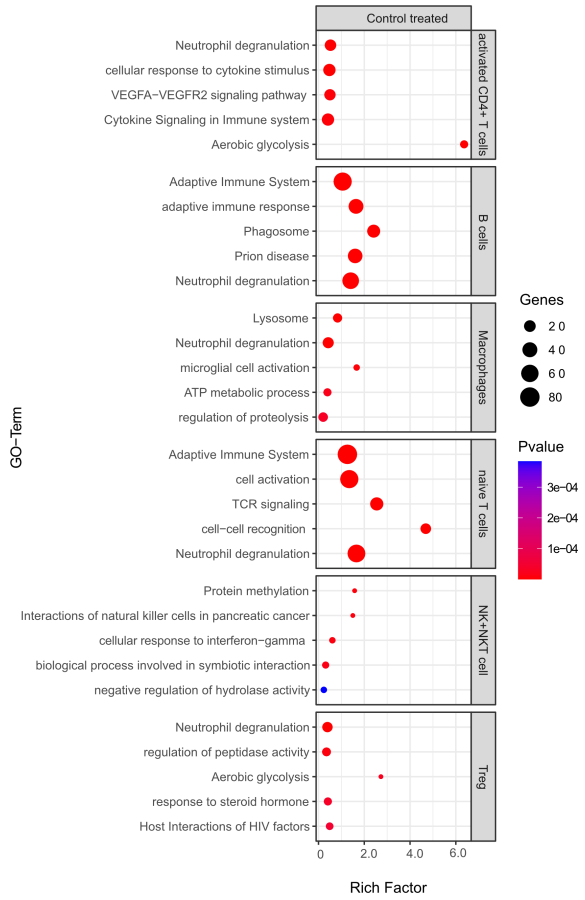

FIGURE 10
Functional enrichment analysis for genes differentially expressed between mELT from control treated mice and CSF from control treated mice using Metascape. The top 5 GO-terms are shown. For similar gene ontology (GO) terms, only the top-ranked GO term was shown. The dot size reflects the number of genes enriched in the GO term and its color the corresponding statistical significance (p-value). Rich factor is the ratio of differentially expressed gene numbers annotated in this GO term to all gene numbers annotated in this GO term.

limitation of our study is that we isolated immune cells from the entire meninges. Therefore, it is possible that, next to immune cells from mELT, our mELT samples may also contain immune cells present in the meningeal compartment outside of mELT.

In summary, one major finding of our study was that the immune cells in the CSF closely resemble those in mELT in 2D2xTh EAE mice. This included particularly the cellular composition and, to some degree, gene expression profiles. Given the relatively easy accessibility of CSF in MS patients, it would be helpful to be able to use CSF as a surrogate for mELT in MS. Future studies will have to verify this finding in humans. Another major finding was the increase of macrophages in the CSF that we observed when B cells were depleted. This also needs to be investigated in CSF of aCD20 mAb treated MS patients. While PIRA remains a challenge in the B cell depletion treatment era in MS, understanding the essential mechanisms of smoldering CNS inflammation, including in mELT and the CSF, is of great importance. It remains to be seen if Bruton's tyrosine kinase (BTK) inhibitors or other novel agents will be able to stop smoldering inflammation in the CNS, e.g. by inhibiting the formation of mELT.

Data availability statement

The names of the repository/repositories and accession number (s) can be found below: GEO repository, https://www.ncbi.nlm.nih.gov/geo/, GSE181506.

Ethics statement

The animal study was approved by standing committee for experimentation with laboratory animals of the administration of Upper Bavaria (ROB-55.2-2532.Vet_02-16-100). The study was conducted in accordance with the local legislation and institutional requirements.

Author contributions

TG: Conceptualization, Data curation, Formal analysis, Validation, Writing – original draft, Investigation, Visualization. JD: Data curation, Formal analysis, Investigation, Validation, Visualization, Supervision, Writing – review & editing. VF: Formal analysis, Investigation, Supervision, Validation, Writing – review & editing, Conceptualization. GL: Formal analysis, Writing – review & editing, Data curation, Software, Visualization. RB: Formal analysis, Writing – review & editing, Investigation. KL-H: Formal analysis, Writing – review & editing, Conceptualization, Data curation, Funding acquisition, Resources, Supervision, Validation, Writing – original draft.

Funding

The author(s) declare financial support was received for the research, authorship, and/or publication of this article. KL-H received research support from the Deutsche Forschungsgemeinschaft (SFB-TR-128, projects A4 and A12, and LE 3079/3-1), the Hertie Foundation (MyLab program), and the US National Multiple Sclerosis Society (NMSS) (G-1508-07064).

Acknowledgments

The authors would like to thank Monika Pfaller, Francesca Romana de Frachis, Melina Pekic Hajdarbasic, Beatrix Lunk (all TUM) for excellent technical assistance. The authors acknowledge

support from F. Hoffmann-La Roche for providing the anti-mouse CD20 antibody 18B12. RB is a fellow of the Hertie Foundation (medMS Doctoral Program). Sequencing was performed at the Helmholtz Zentrum München (HMGU) by the Genomics Core Facility.

Conflict of interest

KL-H has received research support to TUM from Novartis and honoraria and compensation for travel expenses from Novartis, FHLR, Biogen, Teva, Hexal, Bayer, and Merck Serono.

The remaining authors declare that the research was conducted in the absence of any commercial or financial relationships that could be constructed as a potential conflict of interest.

Publisher's note

Supplementary material

The Supplementary Material for this article can be found online at: https://www.frontiersin.org/articles/10.3389/fimmu.2024.1400641/full#supplementary-material

References

1. Hauser SL, Waubant E, Arnold DL, Vollmer T, Antel J, Fox RJ, et al. B-cell depletion with rituximab in relapsing-remitting multiple sclerosis. *N Engl J Med*. (2008) 358:676–88. doi: 10.1056/NEJMoa0706383

2. Hauser SL, Bar-Or A, Comi G, Giovannoni G, Hartung HP, Hemmer B, et al. Ocrelizumab versus interferon beta-1a in relapsing multiple sclerosis. *N Engl J Med*. (2017) 376:221–34. doi: 10.1056/NEJMoa1601277

3. Kappos L, Wolinsky JS, Giovannoni G, Arnold DL, Wang Q, Bernasconi C, et al. Contribution of relapse-independent progression vs relapse-associated worsening to overall confirmed disability accumulation in typical relapsing multiple sclerosis in a pooled analysis of 2 randomized clinical trials. *JAMA Neurol*. (2020) 77:1132–40. doi: 10.1001/jamaneurol.2020.1568

4. Montalban X, Hauser SL, Kappos L, Arnold DL, Bar-Or A, Comi G, et al. Ocrelizumab versus placebo in primary progressive multiple sclerosis. *N Engl J Med*. (2017) 376:209–20. doi: 10.1056/NEJMoa1606468

5. Serafini B, Rosicarelli B, Magliozzi R, Stigliano E, Aloisi F. Detection of ectopic B-cell follicles with germinal centers in the meninges of patients with secondary progressive multiple sclerosis. *Brain Pathol*. (2004) 14:164–74. doi: 10.1111/j.1750-3639.2004.tb00049.x

6. Magliozzi R, Howell O, Vora A, Serafini B, Nicholas R, Puopolo M, et al. Meningeal B-cell follicles in secondary progressive multiple sclerosis associate with early onset of disease and severe cortical pathology. *Brain*. (2007) 130:1089–104. doi: 10.1093/brain/awm038

7. Howell OW, Reeves CA, Nicholas R, Carassiti D, Radotra B, Gentleman SM, et al. Meningeal inflammation is widespread and linked to cortical pathology in multiple sclerosis. *Brain*. (2011) 134:2755–71. doi: 10.1093/brain/awr182

8. Lucchinetti CF, Popescu BF, Bunyan RF, Moll NM, Roemer SF, Lassmann H, et al. Inflammatory cortical demyelination in early multiple sclerosis. *N Engl J Med*. (2011) 365:2188–97. doi: 10.1056/NEJMoa1100648

9. Choi SR, Howell OW, Carassiti D, Magliozzi R, Gveric D, Muraro PA, et al. Meningeal inflammation plays a role in the pathology of primary progressive multiple sclerosis. *Brain*. (2012) 135:2925–37. doi: 10.1093/brain/aws189

10. Reali C, Magliozzi R, Roncaroli F, Nicholas R, Howell OW, Reynolds R. B cell rich meningeal inflammation associates with increased spinal cord pathology in multiple sclerosis. *Brain Pathol*. (2020) 30:779–93. doi: 10.1111/bpa.12841

11. Diddens J, Lepennetier G, Friedrich V, Schmidt M, Brand RM, Georgieva T, et al. Single-cell profiling indicates a proinflammatory role of meningeal ectopic lymphoid tissue in experimental autoimmune encephalomyelitis. *Neurol Neuroimmunol Neuroinflamm*. (2024) 11:e200185. doi: 10.1212/NXI.0000000000200185

12. Lehmann-Horn K, Wang SZ, Sagan SA, Zamvil SS, von Budingen HC. B cell repertoire expansion occurs in meningeal ectopic lymphoid tissue. *JCI Insight*. (2016) 1: e87234. doi: 10.1172/jci.insight.87234

13. Pikor NB, Prat A, Bar-Or A, Gommerman JL. Meningeal tertiary lymphoid tissues and multiple sclerosis: A gathering place for diverse types of immune cells during CNS autoimmunity. *Front Immunol*. (2015) 6:657. doi: 10.3389/fimmu.2015.00657

14. Jones GW, Jones SA. Ectopic lymphoid follicles: inducible centres for generating antigen-specific immune responses within tissues. *Immunology*. (2016) 147:141–51. doi: 10.1111/imm.12554

15. Greenfield AL, Dandekar R, Ramesh A, Eggers EL, Wu H, Laurent S, et al. Longitudinally persistent cerebrospinal fluid B cells can resist treatment in multiple sclerosis. *JCI Insight*. (2019) 4. doi: 10.1172/jci.insight.126599

16. Brand RM, Friedrich V, Diddens J, Pfaller M, Romana de Franchis F, Radbruch H, et al. Anti-CD20 depletes meningeal B cells but does not halt the formation of meningeal ectopic lymphoid tissue. *Neurol Neuroimmunol Neuroinflamm*. (2021) 8. doi: 10.1212/NXI.0000000000001012

17. Krishnamoorthy G, Lassmann H, Wekerle H, Holz A. Spontaneous opticospinal encephalomyelitis in a double-transgenic mouse model of autoimmune T cell/B cell cooperation. *J Clin Invest*. (2006) 116:2385–92. doi: 10.1172/JCI28330

18. Bettelli E, Baeten D, Jager A, Sobel RA, Kuchroo VK. Myelin oligodendrocyte glycoprotein-specific T and B cells cooperate to induce a Devic-like disease in mice. *J Clin Invest*. (2006) 116:2393–402. doi: 10.1172/JCI28334

19. Kinzel S, Lehmann-Horn K, Torke S, Hausler D, Winkler A, Stadelmann C, et al. Myelin-reactive antibodies initiate T cell-mediated CNS autoimmune disease by opsonization of endogenous antigen. *Acta Neuropathol*. (2016) 132:43–58. doi: 10.1007/s00401-016-1559-8

20. Martin Mdel P, Cravens PD, Winger R, Kieseier BC, Cepok S, Eagar TN, et al. Depletion of B lymphocytes from cerebral perivascular spaces by rituximab. *Arch Neurol*. (2009) 66:1016–20. doi: 10.1001/archneurol.2009.157

21. Zhou Y, Zhou B, Pache L, Chang M, Khodabakhshi AH, Tanaseichuk O, et al. Metascape provides a biologist-oriented resource for the analysis of systems-level datasets. *Nat Commun*. (2019) 10:1523. doi: 10.1038/s41467-019-09234-6

22. Hametner S, Wimmer I, Haider L, Pfeifenbring S, Bruck W, Lassmann H. Iron and neurodegeneration in the multiple sclerosis brain. *Ann Neurol*. (2013) 74:848–61. doi: 10.1002/ana.23974

23. Marty MC, Alliot F, Rutin J, Fritz R, Trisler D, Pessac B. The myelin basic protein gene is expressed in differentiated blood cell lineages and in hemopoietic progenitors. *Proc Natl Acad Sci U.S.A*. (2002) 99:8856–61. doi: 10.1073/pnas.122079599

24. Zhou Y, Simpson SJr., Charlesworth JC, van der Mei I, Lucas RM, Ponsonby AL, et al. Variation within MBP gene predicts disease course in multiple sclerosis. *Brain Behav*. (2017) 7:e00670. doi: 10.1002/brb3.670

25. Naneh O, Avcin T, Bedina Zavec A. Perforin and human diseases. *Subcell Biochem*. (2014) 80:221–39. doi: 10.1007/978-94-017-8881-6_11

26. Zhang HL, Wu J, Zhu J. The immune-modulatory role of apolipoprotein E with emphasis on multiple sclerosis and experimental autoimmune encephalomyelitis. *Clin Dev Immunol*. (2010) 2010:186813. doi: 10.1155/2010/186813

27. Bonacina F, Coe D, Wang G, Longhi MP, Baragetti A, Moregola A, et al. Myeloid apolipoprotein E controls dendritic cell antigen presentation and T cell activation. *Nat Commun*. (2018) 9:3083. doi: 10.1038/s41467-018-05322-1

28. Tenger C, Zhou X. Apolipoprotein E modulates immune activation by acting on the antigen-presenting cell. *Immunology*. (2003) 109:392–7. doi: 10.1046/j.1365-2567.2003.01665.x

29. Gilchrist M, Henderson WRJr., Morotti A, Johnson CD, Nachman A, Schmitz F, et al. A key role for ATF3 in regulating mast cell survival and mediator release. *Blood*. (2010) 115:4734–41. doi: 10.1182/blood-2009-03-213512

30. Katagiri T, Kameda H, Nakano H, Yamazaki S. Regulation of T cell differentiation by the AP-1 transcription factor JunB. *Immunol Med*. (2021) 44:197–203. doi: 10.1080/25785826.2021.1872838

31. Cunatova K, Reguera DP, Houstek J, Mracek T, Pecina P. Role of cytochrome c oxidase nuclear-encoded subunits in health and disease. *Physiol Res*. (2020) 69:947–65. doi: 10.33549/physiolres

32. Iwasaki Y, Takeshima Y, Fujio K. Basic mechanism of immune system activation by mitochondria. *Immunol Med.* (2020) 43:142–7. doi: 10.1080/25785826.2020.1756609

33. Zahoor I, Haq E, Asimi R. Multiple sclerosis and EIF2B5: A paradox or a missing link. *Adv Exp Med Biol*. (2017) 958:57–64. doi: 10.1007/978-3-319-47861-6_5

34. Tsubaki H, Tooyama I, Walker DG. Thioredoxin-interacting protein (TXNIP) with focus on brain and neurodegenerative diseases. *Int J Mol Sci*. (2020) 21. doi: 10.3390/ijms21249357

35. Metkar SS, Menaa C, Pardo J, Wang B, Wallich R, Freudenberg M, et al. Human and mouse granzyme A induce a proinflammatory cytokine response. *Immunity*. (2008) 29:720–33. doi: 10.1016/j.immuni.2008.08.014

36. Vyshkina T, Sylvester A, Sadiq S, Bonilla E, Perl A, Kalman B. CCL genes in multiple sclerosis and systemic lupus erythematosus. *J Neuroimmunol*. (2008) 200:145–52. doi: 10.1016/j.jneuroim.2008.05.016

37. Zhang X, Chen L, Dang WQ, Cao MF, Xiao JF, Lv SQ, et al. CCL8 secreted by tumor-associated macrophages promotes invasion and stemness of glioblastoma cells *via* ERK1/2 signaling. *Lab Invest*. (2020) 100:619–29. doi: 10.1038/s41374-019-0345-3

38. Gururajan M, Simmons A, Dasu T, Spear BT, Calulot C, Robertson DA, et al. Early growth response genes regulate B cell development, proliferation, and immune response. *J Immunol*. (2008) 181:4590–602. doi: 10.4049/jimmunol.181.7.4590

39. Shang Z, Sun W, Zhang M, Xu L, Jia X, Zhang R, et al. Identification of key genes associated with multiple sclerosis based on gene expression data from peripheral blood mononuclear cells. *PeerJ*. (2020) 8:e8357. doi: 10.7717/peerj.8357

40. Shi H, Sheng B, Zhang C, Nayak L, Lin Z, Jain MK, et al. Myeloid Kruppel-like factor 2 deficiency exacerbates neurological dysfunction and neuroinflammation in a murine model of multiple sclerosis. *J Neuroimmunol*. (2014) 274:234–9. doi: 10.1016/j.jneuroim.2014.06.023

41. Zatsepina OG, Evgen'ev MB, Garbuz DG. Role of a heat shock transcription factor and the major heat shock protein hsp70 in memory formation and neuroprotection. *Cells*. (2021) 10. doi: 10.3390/cells10071638

42. Lechner P, Buck D, Sick L, Hemmer B, Multhoff G. Serum heat shock protein 70 levels as a biomarker for inflammatory processes in multiple sclerosis. *Mult Scler J Exp Transl Clin*. (2018) 4:2055217318767192. doi: 10.1177/2055217318767192

43. de Graaf MT, de Jongste AH, Kraan J, Boonstra JG, Sillevis Smitt PA, Gratama JW. Flow cytometric characterization of cerebrospinal fluid cells. *Cytometry B Clin Cytom*. (2011) 80:271–81. doi: 10.1002/cyto.b.20603

44. Eggers EL, Michel BA, Wu H, Wang SZ, Bevan CJ, Abounasr A, et al. Clonal relationships of CSF B cells in treatment-naive multiple sclerosis patients. *JCI Insight*. (2017) 2. doi: 10.1172/jci.insight.92724

45. Lehmann-Horn K, Kinzel S, Feldmann L, Radelfahr F, Hemmer B, Traffehn S, et al. Intrathecal anti-CD20 efficiently depletes meningeal B cells in CNS autoimmunity. *Ann Clin Trans Neurol*. (2014) 1:490–6. doi: 10.1002/acn3.71

46. Ochs J, Nissimov N, Torke S, Freier M, Grondey K, Koch J, et al. Proinflammatory CD20(+) T cells contribute to CNS-directed autoimmunity. *Sci Transl Med*. (2022) 14:eabi4632. doi: 10.1126/scitranslmed.abi4632

47. Lehmann-Horn K, Schleich E, Hertzenberg D, Hapfelmeier A, Kumpfel T, von Bubnoff N, et al. Anti-CD20 B-cell depletion enhances monocyte reactivity in neuroimmunological disorders. *J Neuroinflamm*. (2011) 8:146. doi: 10.1186/1742-2094-8-146

48. Stuve O, Cepok S, Elias B, Saleh A, Hartung HP, Hemmer B, et al. Clinical stabilization and effective B-lymphocyte depletion in the cerebrospinal fluid and peripheral blood of a patient with fulminant relapsing-remitting multiple sclerosis. *Arch Neurol*. (2005) 62:1620–3. doi: 10.1001/archneur.62.10.1620

49. Cross AH, Stark JL, Lauber J, Ramsbottom MJ, Lyons JA. Rituximab reduces B cells and T cells in cerebrospinal fluid of multiple sclerosis patients. *J Neuroimmunol*. (2006) 180:63–70. doi: 10.1016/j.jneuroim.2006.06.029

50. Cross AH, Gelfand JM, Thebault S, Bennett JL, von Budingen HC, Cameron B, et al. Emerging cerebrospinal fluid biomarkers of disease activity and progression in multiple sclerosis. *JAMA Neurol*. (2024) 81:373–83. doi: 10.1001/jamaneurol.2024.0017

frontiers | Frontiers in Immunology

TYPE Original Research
PUBLISHED 27 September 2024
DOI 10.3389/fimmu.2024.1426975

OPEN ACCESS

EDITED BY
James William Neal,
Swansea University Medical School,
United Kingdom

REVIEWED BY
Andre Ortlieb Guerreiro Cacais,
Karolinska Institutet (KI), Sweden
Fabrícia Lima Fontes-Dantas,
Rio de Janeiro State University, Brazil

*CORRESPONDENCE
Sarah A. DeVries
sdevries@bu.edu

RECEIVED 02 May 2024
ACCEPTED 28 August 2024
PUBLISHED 27 September 2024

CITATION
DeVries SA, Dimovasili C, Medalla M, Moore TL and Rosene DL (2024) Dysregulated C1q and CD47 in the aging monkey brain: association with myelin damage, microglia reactivity, and cognitive decline. *Front. Immunol.* 15:1426975. doi: 10.3389/fimmu.2024.1426975

Dysregulated C1q and CD47 in the aging monkey brain: association with myelin damage, microglia reactivity, and cognitive decline

Sarah A. DeVries [1*], Christina Dimovasili [1], Maria Medalla [2,3], Tara L. Moore [3,4] and Douglas L. Rosene [1,3]

[1]Laboratory for Cognitive Neurobiology, Dept of Anatomy & Neurobiology, Chobanian and Avedisian School of Medicine, Boston University, Boston, MA, United States, [2]Laboratory of Neural Circuits and Ultrastructure, Dept of Anatomy & Neurobiology, Chobanian and Avedisian School of Medicine, Boston University, Boston, MA, United States, [3]Center for Systems Neuroscience, Boston University, Boston, MA, United States, [4]Laboratory of Interventions for Cortical Injury and Cognitive Decline, Dept of Anatomy & Neurobiology, Chobanian and Avedisian School of Medicine, Boston University, Boston, MA, United States

Normal aging, though lacking widespread neurodegeneration, is nevertheless characterized by cognitive impairment in learning, memory, and executive function. The aged brain is spared from neuron loss, but white matter is lost and damage to myelin sheaths accumulates. This myelin damage is strongly associated with cognitive impairment. Although the cause of the myelin damage is not known, microglia dysregulation is a likely contributor. Immunologic proteins interact with microglial receptors to modulate microglia-mediated phagocytosis, which mediates myelin damage clearance and turn-over. Two such proteins, "eat me" signal C1q and "don't eat me" signal CD47, act in opposition with microglia. Both C1q and CD47 have been implicated in Multiple Sclerosis, a demyelinating disease, but whether they play a role in age-related myelin pathology is currently unknown. The present study investigates C1q and CD47 in relation to age-related myelin degeneration using multilabel immunofluorescence, RNAscope, and confocal microscopy in the cingulum bundle of male and female rhesus monkeys across the lifespan. Our findings showed significant age-related elevation in C1q localized to myelin basic protein, and this increase is associated with more severe cognitive impairment. In contrast, CD47 localization to myelin decreased in middle age and oligodendrocyte expression of *CD47* RNA decreased with age. Lastly, microglia reactivity increased with age in association with the changes in C1q and CD47. Together, these results suggest disruption in the balance of "eat me" and "don't eat me" signals during normal aging, biasing microglia toward increased reactivity and phagocytosis of myelin, resulting in cognitive deficits.

KEYWORDS

innate immune system, complement system, neurodegeneration, white matter, microglia, C1q, CD47

Introduction

Advancing age is the largest risk factor for the development of many diseases, including neurodegenerative diseases such as Alzheimer's disease (AD) (1). Beginning in the third decade, decline of several cognitive domains including processing speed, memory, learning, and executive function begins and continues to deteriorate linearly across the lifespan (2–5). This progressive decline manifests as noticeable cognitive deficits with advancing age, and despite the absence of pathology indicative of neurodegeneration or AD, severe cognitive impairment affects 30% of the aged population and interferes with activities of daily living (3). With the population over 65 years increasing, it is important to identify the underlying mechanisms driving age-related cognitive decline so therapeutic interventions targeting them can be developed. In contrast to neurodegenerative diseases like AD or Parkinson's, neuron loss does not occur with normal aging (6). Nevertheless, neurons in the aging brain exhibit pathological changes that likely interfere with normal connectivity. Namely, breakdown of white matter occurs with age and correlates with cognitive decline (7–9). This myelin damage is evidenced by loss of white matter volume and decreased myelin integrity shown with increasing white matter hyperintensities, particularly in frontal white matter tracts such as the corpus callosum and cingulum bundle (10, 11).

Little is known about the mechanisms underlying myelin degradation with age. However, ultrastructural studies of the rhesus monkey model of normal human aging have shed light on the specific defects aging myelin exhibits. Due to their long lifespans, age-related cognitive decline, and comparable white matter tracts to humans (12–16) our monkey model enables the investigation of how normal aging affects myelin in white matter tracts such as the corpus callosum and cingulum bundle with high translatability to human aging white matter and associated cognitive impairment. Electron microscopy studies in our laboratory show significant myelin degeneration with age in frontal white matter areas including myelin loss or thinning as well as structural changes such as sheath splitting, the presence of less compact myelin, redundant myelin sheaths, and myelin balloons filled with degenerating cytoplasm or fluid (17, 18). Further, loss of myelinated axons have been found in the white matter tracts of aging monkeys (19, 20). An accumulation of these myelin defects with age likely results in axons becoming at least partially demyelinated, causing action potential failures and/or decreased conduction velocity, leading to disrupted cortical communication (21, 22).

Although the cause of myelin pathology is not known, microglia are likely contributors as they play an important role in removing myelin debris that inhibits remyelination (23), a process which becomes dysregulated with age (24). Microglia become overburdened with degenerating myelin, and failure to clear the debris results in accumulation of damaged myelin that blocks remyelination and proper myelin maintenance (23). Moreover, the aging brain is characterized by chronic inflammation (25–27), which is especially elevated in white matter regions (28). This neuroinflammation puts microglia into a cycle of contributing to inflammation while also responding to proinflammatory signaling (29, 30). Chronic neuroinflammation heightens microglia-mediated elimination of cellular components, which may become misdirected with excess pro-inflammatory signaling. The timing and precision of microglia-mediated debris removal is regulated by immunologic proteins that either initiate or inhibit phagocytosis. Two such proteins are the "eat me" classical complement initiator, C1q, and the "don't eat me" immune-regulatory protein, CD47 (31). Dysregulation in both C1q and CD47 have been implicated in age-related diseases such as Multiple Sclerosis (MS), a chronic demyelinating disease (32, 33), synapse removal (34, 35), and normal aging (36). Our previous study showed that C1q and CD47 expression are dysregulated in aging gray matter, likely contributing to age-related synapse loss (37). Changes in C1q and CD47 in aging white matter may direct microglia towards chronic phagocytosis and inflammation and hinder efficient debris clearance and myelin maintenance. However, studies in white matter have mainly focused on either "eat me" or "don't eat me" proteins and not both, so the interaction between the two in white matter remains unknown even though both C1q and CD47 bind to myelin (38, 39) and proper balance between the two molecules is critical for phagocytosis (40). Since these signals have not been studied in aging white matter tracts in relation to myelin damage and related cognitive impairment, the present study aimed to assess changes in the balance of C1q and CD47 in the white matter of the aging cingulum bundle in cognitively assessed nonhuman primates. We hypothesized that aging myelin would express less CD47 and more tagging by C1q, which would be robustly increased in the age-related inflammatory environment. Together this would promote phagocytic and inflammatory microglia response, making myelin more vulnerable to phagocytosis. To assess this, RNAscope and multilabel immunofluorescence (IF) were used to analyze age-related changes in the amount of C1q and CD47 as well as their colocalization with myelin and microglia phenotypes in the monkey brain across normal aging.

Methods

Subjects

Brain tissue and CSF samples came from 36 male and female rhesus monkeys ranging from 7-32 years old (Figures 1A, B). Tissue from 32 of these animals was used in a previous aging study investigating C1q and CD47 in gray matter (37). All monkeys were behaviorally tested on a battery of tasks to assess learning, memory, and executive function. Testing was done each day prior to once daily feeding of rationed chow, fruit, vegetables, and forage feed. Water was available *ad libitum*. Subjects were maintained in the Animal Science Center on Boston University Medical Campus (BUMC), which is fully accredited by AAALAC and managed by a licensed veterinarian and trained staff. All procedures conformed to the NIH Guide for the Care and Use of Laboratory Animals and were approved by the Boston University Institutional Animal Care and Use Committee (IACUC; protocol number 201800053).

10.3389/fimmu.2024.1426975

A

	ID	Age	CII	Sex	IHC	RNAscope	ELISA
Young	AM222	7.4	0.871	M	+	+	
	AM280	8.1	1.244	M	+	+	+
	AM358	8.4	0.247	F	+	+	+
	AM367	8.5	3.500	M			+
	AM299	8.6	0.850	F	+	+	+
	AM296	8.7	0.774	M	+	+	+
	AM368	8.9	0.933	M	+		+
	AM289	9.0	0.325	M	+	+	+
	AM255	9.5	0.123	F	+	+	
	AM294	9.6	2.215	F	+		+
	AM295	10.8	1.523	M	+		+
Middle	AM291	13.7	1.172	F	+		+
	AM353	14.5	1.053	M	+		+
	AM303	15.2	1.168	M	+		+
	AM288	16.0	3.148	M	+		+
	AM378	16.8	4.115	M	+		
	AM297	18.0	1.152	F	+		+
	AM274	18.3	2.284	M	+		+
	AM300	19.0	0.804	F	+		+
	AM293	19.6	2.097	F	+		+
	AM372	20.8	2.853	M	+		
Old	AM287	21.2	2.407	F	+	+	+
	AM286	22.4	1.429	F	+		+
	AM242	23.5	2.099	M	+		
	AM356	24.8	2.471	M	+	+	+
	AM398e	26.0	N/A	M			+
	AM283	26.4	2.847	M	+		+
	AM371	26.6	1.966	F	+	+	
	AM306	26.7	5.323	F	+	+	
	AM298	26.7	1.279	M	+	+	
	AM369	27.0	3.193	F	+	+	+
	AM370	27.5	1.074	F	+	+	+
	AM355	28.3	3.905	M	+	+	
	AM373	30.2	4.971	M	+	+	+
	AM410	31.5	7.357	M			+
	AM402	32.9	0.660	M			+

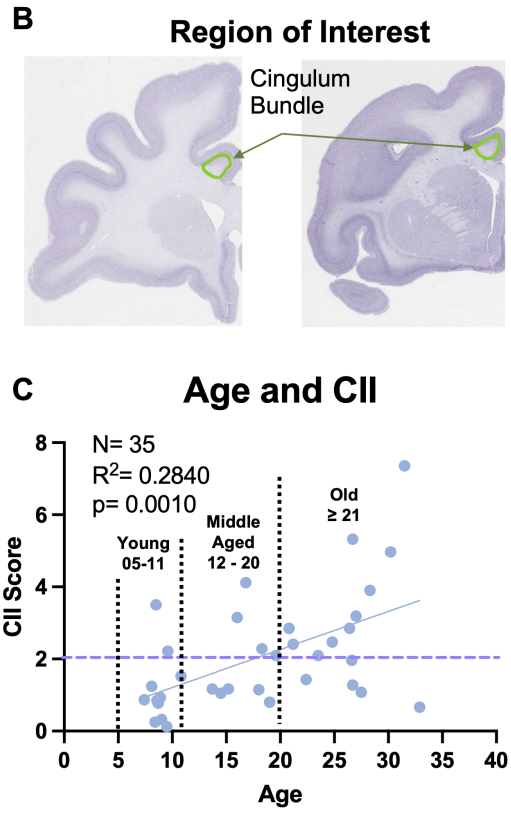

FIGURE 1
Summary of subject information and experimental parameters. **(A)** Table detailing subject ID, age, sex, and CII score for this study's cohort of monkeys and defining which samples from each monkey were used for experiments. **(B)** Histological sections showing the cingulum bundle region of interest. **(C)** Graph showing the distribution of cognitive impairment index (CII) score for all 36 animals. Linear regression analysis revealed significant cognitive impairment with age. Stratification of age groups is shown on the graph, where young are aged 5-11, middle age 12-20, and old are >21 years old. Purple dashed line indicates the cut off for cognitive impairment, with scores above 2.0 considered severely impaired and scores below considered cognitively spared.

Cognitive testing

A battery of cognitive tests was administered to all monkeys assessing rule learning, recognition memory, working memory capacity, and executive function. Specific tasks included the delayed non-match to sample (DNMS) acquisition and 120-second delay, the spatial modality of delayed recognition span task (DRST-spatial), and the category set shifting task (CSST). Procedures for these tasks are summarized below but details can be found elsewhere (14, 41–45). Each behavioral task is analyzed individually, but to characterize overall cognitive status of each monkey, a cognitive impairment index (CII) is also calculated by converting scores from DNMS acquisition and 120-second delay and DRST-spatial to z scores relative to a reference group of 29 young adults so that higher scores reflect greater impairments (41). Monkeys with CII scores <2.0 are classified as cognitively spared while those with scores >2.0 are considered cognitively impaired (14). The spread of CII scores for this cohort of monkeys shows significant cognitive impairment with age (Figure 1C).

Delayed non-match to sample

DNMS assesses rule learning and recognition memory. During the acquisition phase, subjects first learn to correctly identify a novel object from a familiar object presented 10 seconds prior. Once correct identification reaches a criterion of 90% correct responses over 100 trials, subjects transition to DNMS-120 second delay. This introduces a 120 second delay between initial sample presentation and choice to assess the recognition of the novel object.

Delayed recognition span task

DRST-spatial assesses working memory capacity by requiring the subject to identify a new position among an increasing number of spatial locations. For this task, subjects are presented with identical objects for all trials. With each trial, one additional object is added to a novel location among previously presented locations. Subjects must remember the location of all previously

presented items and correctly identify the object at the novel location. Scoring is based on the number of locations chosen correctly prior to an error.

Category set shifting task

This task is an adaptation of the human Wisconsin Card Sorting task and measures aspects of executive function including cognitive set shifting, abstraction, and perseveration. For this task, subjects learn to respond to a certain stimulus property (color or shape), and once the rule is learned, they must learn to shift to a new stimulus category without warning to receive reward (43, 44). CSST provides numerous outcome measures, but we chose to analyze the total number of perseverative errors and broken sets out of total errors based on previous research in our laboratory showing these measures are sensitive to age-related changes (43, 44, 46).

Cerebrospinal fluid collection

Immediately prior to euthanasia, cerebrospinal fluid (CSF) was extracted from the cisterna magna with the monkey sedated with 10mg/kg Ketamine. The sample was frozen immediately at -80°C for long term storage.

Euthanasia and brain harvesting

After completing cognitive assessment, subjects were euthanized and perfused with a two-step protocol that allows both fresh and fixed brain tissue to be harvested, as described (47, 48). Monkeys were deeply anesthetized with Sodium Pentobarbital (25 mg/kg to effect) and euthanized by exsanguination during transcardial perfusion fixation of the brain. Once the animal is deeply anesthetized, the chest cavity is opened, and 4°C Krebs buffer is transcardially perfused via the ascending aorta to flush vasculature and rapidly cool the brain during which the left hemisphere is removed and cut into 2mm thick slabs in a brain matrix and promptly frozen at -80°C to limit proteolysis. Once the left hemisphere is removed, the perfusate is switched to 4% paraformaldehyde (PF) at 37°C for 10 minutes to ensure full fixation. The fixed hemisphere is blocked in situ in the coronal plane, postfixed overnight in 4% PF at 4°C, and cryoprotected in 10% and then 20% glycerol with 2% DMSO and 0.1M buffer (47) before being flash frozen in isopentane at -75°C and stored at -80°C until it is cut into 10 interrupted series of 30µm sections. These sections are collected into a buffer with 15% glycerol and stored at -80°C until removed for processing, which preserves integrity for histochemical processing (48). One series is stored with the addition of 1% PF to ensure optimal RNA preservation for RNAscope studies.

Immunofluorescence

To assess the amount of myelin, C1q, and CD47 present in the cingulum bundle, as well as colocalization of both C1q and CD47 to myelin, immunofluorescence (IF) was performed. Antibodies against C1q and CD47 were used in addition to myelin basic protein (MBP) as a myelin marker. MBP was chosen as it accounts for 30% of myelin composition and mediates tight lamination between myelin lamellae (49) Additionally, IF was used to assess the morphology of microglia using the pan-microglia marker Iba1 and microglia expression of phagocytic protein Galectin-3 (Gal-3) and complement protein C1q. Gal-3 is required for phagocytosis in microglia, is upregulated during aging and neurodegeneration, and may be involved in myelin debris clearance (50). Together, these experiments aimed to reveal changes in C1q and CD47 in relation to myelin loss and increased microglia reactivity.

For IF, fixed tissue from 32 animals was removed from -80°C storage, thawed, and batch processed. For each animal, 3 tissue slices containing the anterior cingulum bundle spaced 2400µm apart were used (Figure 1B). To begin, sections were washed in 0.05M TBS (pH 7.60) for 3x5 min to remove storage buffer. This was followed by antigen retrieval treatment with 10mM sodium citrate buffer (pH 6.0) in a microwave tissue processor (PELCO Biowave, Ted Pella, Inc. Redding, CA) for 5 min at 550W and 50°C to break cross links that may have formed during fixation. After tissue returned to room temperature, sections were blocked in 10% normal goat serum (NGS; Sigma-Aldrich) and 0.4% Triton-X (Tx) in TBS for 1 hr at room temperature. Tissue was then incubated in 2% NGS and 0.2% Tx in TBS along with appropriate mixtures of the following primary antibodies: chicken MBP (1:400; Millipore Sigma, cat# AB9348), mouse C1q (1:400; Abcam, cat# ab71940), rabbit CD47 (1:500; Abcam, cat# ab218810), rabbit Iba1 (1:500; Wako cat# 019-19741), and rat Gal-3 (1:400; ThermoFisher, cat# 14-5301-82) for 72 hrs at 4°C. To enhance antibody penetration, tissue in primary antibody solution was treated in the microwave tissue processor at 150W, 30°C for 2x5 min and allowed to return to room temperature for 1 hr prior to placing in 4°C. To ensure specificity, additional sections were run as needed omitting primary antibodies. On day two, tissue was rinsed with 0.05M TBS and incubated in 2% NGS and 0.2% Tx solution with AlexaFluor 488 goat anti-chicken IgY (1:500; Thermo Fisher Scientific, MA), AlexaFluor 568 goat anti-mouse IgG2b (1:500), AlexaFluor 647 goat anti-rabbit IgG (1:500), AlexaFluor 488 goat anti-rabbit IgG (1:500), and AlexaFluor 647 goat anti-rat IgG (1:500) for 2 hrs at room temperature. Sections were mounted, coverslipped with antifading polyvinyl alcohol DABCO (Sigma-Aldrich, #10981) mounting media, and stored at 4°C until removed for imaging.

Images were acquired on a Zeiss LSM 710 NLO confocal microscope with a 40X oil-immersion objective lens. A 0.5mm^2 tilescan was captured in the center of the cingulum bundle and a grid was overlaid onto the tilescan using ImageJ and images were systematically randomized for analysis. Selected images were thresholded to the same numbers for each channel, then the global % area in the cingulum bundle was measured on ImageJ and colocalization was analyzed using the Colocalization Threshold plugin on ImageJ. One animal was excluded from all analyses for poor antibody penetration across all channels. The density of Iba1+ microglia displaying ramified and hypertrophic morphologies were marked in Neurolucida software (MBF Biosciences) and cells were further marked as C1q+, Gal3+, C1q+Gal3+, or C1q-Gal3-. The proportion of each classification was calculated.

RNAscope

A subset of 16 male and female subjects were stratified according to age as young (<11 years; n=7) or old (>20 years; n=9) and cognitive characterization regardless of age as spared (<2.0) or cognitively impaired (>2.0) as shown in Figure 1A for RNAscope analysis. RNAscope hybridization protocols were carried out using the RNAscope Multiplex Fluorescent Manual Assay kit from Advanced Cell Diagnostics (ACD) according to the manufacturer's instructions. Using one section per subject from the series saved in 15% glycerol with 1% PF, the cingulum bundle was dissected out and the sections were treated with H_2O_2 for 10 min at room temperature, then mounted on SuperFrost Plus microscope slides (Fisher Scientific, MA). After tissue dried and adhered to the slide, target antigen retrieval was performed using Target Retrieval reagent (ACD, CA) at 95°C for 5 min in addition to a 30 min incubation in Protease Plus (ACD, CA) at 40°C in the HybEZ II oven. Tissue was incubated in primary probes *C1qA* (ref# 1200891-C1; ACD, CA), *CD47* (ref# 1200901-C2; ACD, CA), and *Olig2* (ref# 1203071-C1; ACD, CA) for 2 hours at 40°C and stored in 5x SCC hybridization buffer at room temperature overnight. The following day, tissue was incubated in three probe amplification steps (AMP 1-3) and fluorophores Opal 690 (1:300 in TSA buffer; Akoya Biosciences, MA) and Opal 570 (1:750; Akoya Biosciences, MA) were conjugated at 40°C. Two additional slices of tissue were incubated with appropriate ACD probe mixes for a positive control (custom cocktail of #521081, 461341, 457711 housekeeping probes) and a negative control (mix # 320871).

Immediately after RNAscope, tissue was processed for IF with 100% Superblock (Thermo Fisher Scientific, MA) at 40°C for 1 hr, and then incubated in TBS with 0.5% Superblock and 0.3% Tx along with rabbit Iba1 primary antibody (1:250; Wako, cat# 019-19741) for 1 hr at 40°C. Tissue was treated with AlexaFluor 488 donkey anti-rabbit fluorescent secondary for 1 hr at 40°C, followed by treatment with DAPI for 30 sec. Finally, slides were coverslipped with Prolong Gold Mounting Medium (Thermo Fisher Scientific, MA).

Images were acquired in a tilescan on a Zeiss LSM 710 NLO confocal microscope using a 40X oil immersion objective lens. Images were analyzed manually by first identifying 130-140 Iba1+ or Olig2+ cells and then counting the *C1qA* or *CD47* RNA puncta located within the DAPI-labelled soma.

Enzyme-linked immunosorbent assay

To measure MBP in CSF samples (Figure 1A), an ELISA was run across age groups. Previous research has shown increased levels of MBP in the CSF in disease states as an indication of increased damaged myelin in the brain which gets removed via clearance into CSF (51, 52). The ELISA was performed according to manufacturer's instructions for MBP (ANSH Labs, cat# AL108). All CSF samples were thawed from -80°C while on ice and diluted to a concentration of 1:4 with ultrapure water. All reagents, calibrators, and controls were thawed, and the assay was performed at room temperature. All MBP calibrators and controls were reconstituted with 1mL of deionized water each, and all calibrators, controls, and CSF samples were plated in duplicate. Samples were incubated for 1 hr on an orbital microplate shaker at 600rpm. Solution was removed and each well was washed 5 times with wash solution. Following this, the MBP Antibody-Biotin Conjugate Solution was incubated for 1 hr while agitated at 600rpm, after which solution was removed and washed as above. Then Streptavidin Conjugate was added and incubated for 30 min shaking at 600rpm, wells were washed, and TMB chromogen was incubated for 10 min while covered. Finally, stop solution was added, and the absorbance of the solution in the wells was read on a microplate reader (BioRad, Berkeley, California, USA) at a 450nm wavelength.

Statistics

All analyses were performed with the experimenter blinded to subject identity. Data were analyzed using GraphPad Prism (Version 10.1.1) with an $\alpha \leq 0.05$. IF data were analyzed by linear regression with age and cognitive impairment (CII score, CSST total broken sets, and CSST perseverative errors/total shift errors) as independent variables and % area of MBP, C1q, CD47, colocalization, and microglia phenotypes as dependent variables. Further analysis between age groups and cognitive impairment classification were analyzed with one-way analysis of variance (ANOVA) followed with Tukey's *post hoc* test to control for multiple comparisons. Sex and sex by age interaction were analyzed with a two-way ANOVA and Tukey's *post hoc* test. RNAscope data were analyzed between age groups and cognitive status. Data are shown as box plots and group differences were evaluated with a two-tailed independent samples t-test. Relative concentration of MBP in the CSF was analyzed using a one-way ANOVA with Tukey's *post hoc* test comparing young, middle, and old age groups.

Results

Myelin disruption associated with C1q occurs with age and cognitive impairment

Myelin damage and loss is well documented in frontal white matter areas during aging (17, 18, 53, 54). Here, MBP, a major component of myelin composition (55), was used to identify myelin together with antibodies against C1q and CD47 in the cingulum bundle, as shown in Figure 2A. Two-way ANOVA revealed no sex differences in % area of MBP [$F(1,26)= .1409$, $p=0.7104$] (data not shown), so data from both sexes was pooled and analyzed together across age in all subsequent analyses. Subject AM299 and AM283 were identified as outliers using the ROUT test on GraphPad prism and were excluded from MBP and C1q analyses, respectively. Results show a significant linear decrease in myelin marked by MBP with age [$F(1,28)= 9.488$, $R^2 = 0.2531$, $p=0.0046$] (Figure 2B).

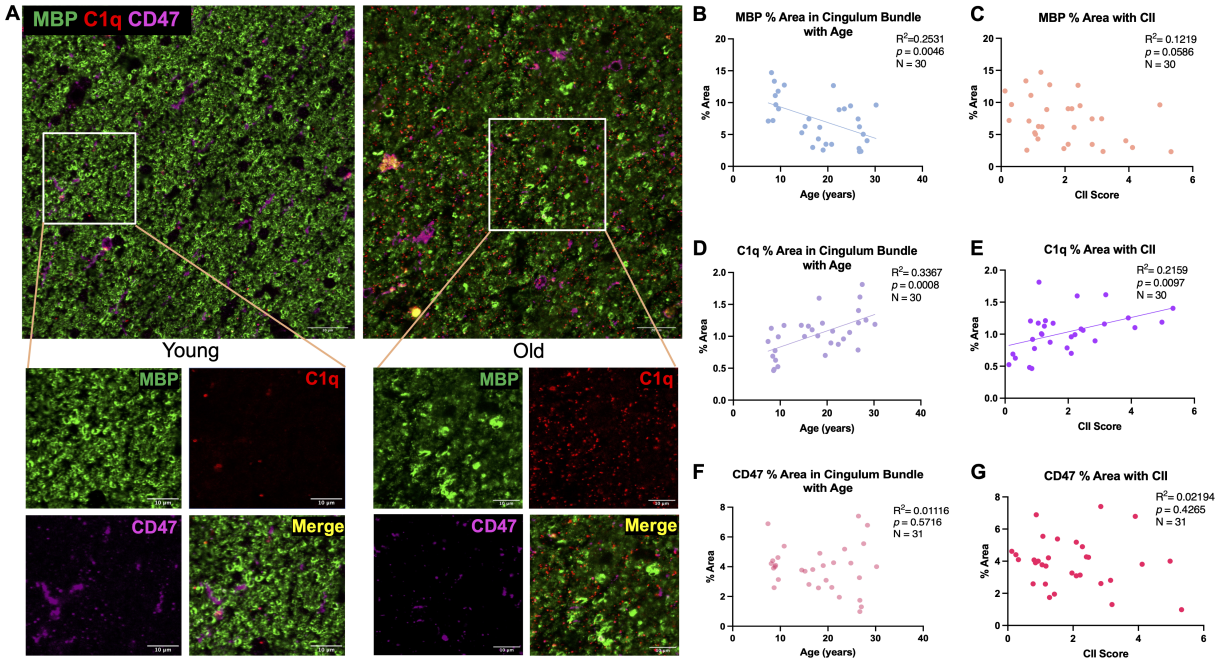

FIGURE 2
Changes in MBP, C1q, and CD47 in the cingulum bundle with age and CII score. **(A)** Representative immunofluorescent images for MBP, C1q, and CD47 in a young and old animal. **(B)** Significant decrease in % area of MBP was found with age that also correlated with **(C)** cognitive impairment. C1q was significantly increased with **(D)** age and **(E)** CII score but % area of CD47 remained stable with both **(F)** age and **(G)** higher CII score. Scale bars represent 20μm in zoomed out images and 10μm for close-up images.

The decreases in MBP levels were also associated with increasing cognitive impairment index (CII) score but only approached significance [$F(1,28)= 3.888$, $R^2 = 0.1219$, $p=0.0586$] (Figure 2C). Coincident with this, the levels of C1q increased with age [$F(1,28)= 14.21$, $R^2 = 0.3367$, $p=0.0008$] (Figure 2D) that was associated with higher CII score [$F(1,28)= 7.711$, $R^2 = 0.2159$, $p=0.0097$] (Figure 2E). The % area of MBP and C1q did not correlate with CSST total broken sets or with perseverative errors/total errors (data not shown). Finally, the % area of CD47 did not change with age [$F(1,29)= 0.3274$, $R^2 = 0.01116$, $p=0.5716$] (Figure 2F) nor was it related to CII [$F(1,29)= 0.6505$, $R^2 = 0.02194$, $p=0.4265$] (Figure 2G). These results confirm previous findings that the myelin is lost in the cingulum bundle with age in addition to structural defects observed (18, 19) and suggest that the increase in C1q may indicate an inflammatory environment priming microglia for phagocytosis.

Colocalization of C1q with MBP in the cingulum bundle

To determine if age-related changes in C1q and CD47 targeted white matter specifically, colocalization of C1q and CD47 with MBP as a marker of myelin was analyzed, as shown in Figure 3A. Indeed, results from linear regression analysis revealed a significant increase in C1q-MBP colocalization with age [$F(1,27)= 12.13$, $R^2 = 0.3100$, $p=0.0017$] (Figure 3B) that also correlated with CII score [$F(1,27)= 11.15$, $R^2 = 0.2922$, $p=0.0025$](Figure 3C). In contrast to C1q, there was no linear correlation between CD47-MBP colocalization and age [$F(1,29)= 0.1342$, $R^2 = 0.0046$, $p=0.7168$] or CII score [$F(1,29)=0.00903$, $R^2 = 0.000311$, $p=0.9249$] (Figures 3D, E).

To further analyze when these changes occur, we grouped monkeys according to young (<11), middle aged (12-20), and old (21-32) and compared across these age groups. One-way ANOVA with multiple comparison Tukey's *post-hoc* analyses revealed a significant increase in C1q-MBP colocalization in old monkeys relative to both young (Main effect $p=0.0005$; Tukey's *post-hoc* $p=0.0040$) and middle-aged (*post-hoc* $p=0.0011$). We then assessed these variables relative to cognitive impairment by comparing cognitively spared and cognitively impaired groups across all animals regardless of age. One-way ANOVA revealed higher C1q-MBP colocalization in cognitively impaired animals (CII>2.0) ($p<0.0001$; Figures 3F, G). Animals AM283 and AM369 were identified as an outlier using the ROUT test on GraphPad prism and were excluded from C1q-MBP analyses. For CD47-MBP, when discrete age groups were compared with one-way ANOVA, a significant decrease was found in middle-age compared to young ($p= 0.0111$) and old ($p=0.0245$; Figure 3H). One-way ANOVA comparison between cognitive classification revealed there was no differences between cognitively spared and impaired animals ($p=0.5927$; Figure 3I). Neither % area of C1q-MBP nor % area of CD47-MBP was correlated with CSST total broken sets or perseverative errors (data not shown). Results suggest significant increase in myelin being tagged for phagocytosis by C1q with age, while CD47 expression specifically decreases in middle age, perhaps in response to myelin damage to facilitate repair and remyelination by accelerating myelin debris clearance.

10.3389/fimmu.2024.1426975

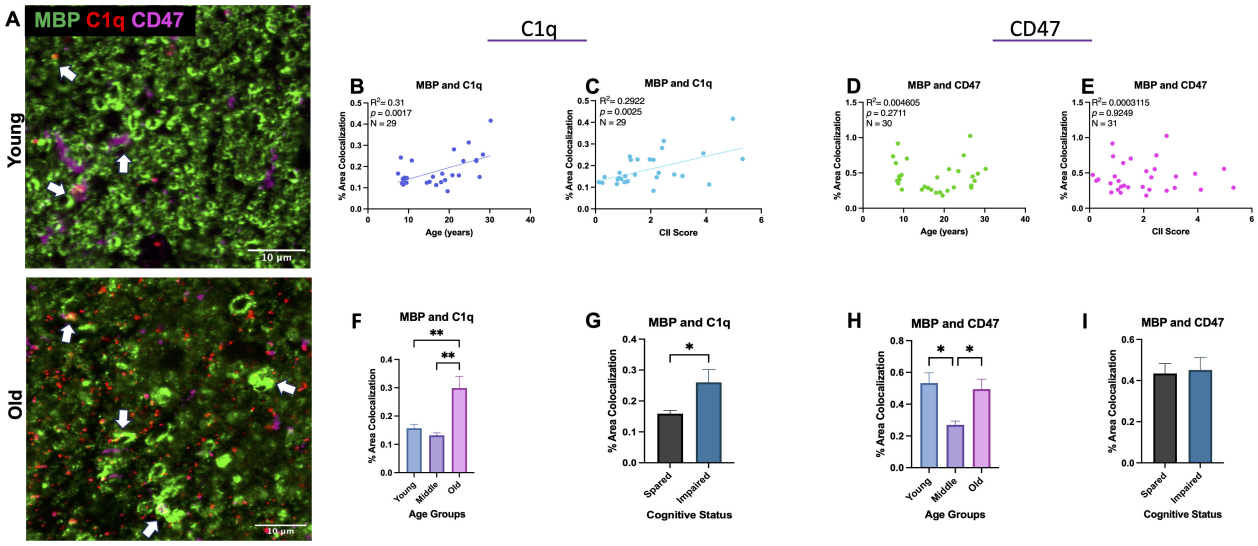

FIGURE 3
Colocalization of C1q and CD47 with MBP during aging and related cognitive impairment. **(A)** Representative immunofluorescent images of C1q, CD47, and MBP. Colocalization is marked with white arrows. **(B)** C1q and MBP colocalization increased with age and **(C)** CII score but **(D, E)** CD47 colocalized with MBP did not change linearly with age or CII score. **(F, G)** Analysis into age and cognition group differences revealed increased C1q-MBP colocalization in old age compared to young and middle age as well as in cognitively impaired compared to spared. **(H)** Analysis into age groups revealed significant decrease in CD47 localized with MBP in middle age compared to young and old age. **(I)** CD47-MBP colocalization did not correlate with cognitive impairment. Young <10, Old >21; cognitively spared <2.0, cognitively impaired >2.0.

Microglia exhibit a phagocytic and inflammatory phenotype with age

To investigate whether microglia in the cingulum bundle exhibit phenotypic changes in response to changes in C1q and CD47, IF was used with Iba1 to visualize morphology together with expression of the phagocytic marker Gal-3 and inflammatory marker C1q. Microglia were classified according to Karperien's (56) morphological categories where ramified microglia are considered homeostatic/surveillant and hypertrophic microglia are phagocytic. We therefore used multilabel IF to classify microglia based on Gal-3 and C1q expression and by morphology as follows: Gal3+ramified, Gal3+hypertrophic, C1q+ramified, C1q +hypertrophic, C1q+Gal3+ramified, C1q+Gal3+hypertrophic, C1q-Gal3-ramified, and C1q-Gal3-hypertrophic. Examples of homeostatic and hypertrophic microglia along with Gal3+ and C1q+ staining are shown in Figures 4A, B and proportions of phenotypes with age are shown in Figures 4C–E. In young monkeys about 50% of the microglia are ramified and Gal3- and C1q-. Interestingly, compared to young, middle aged monkeys had a 4-fold increase and old monkeys a 10-fold increase in the proportion of Gal3+ hypertrophic microglia, indicating increased phagocytosis. This was not the case for C1q+ microglia, which were found in somewhat equivalent proportions across all ages: 29% in young, 25% in middle-aged, and 33% in old.

With age, we found a significant decrease in the ratio of ramified to hypertrophic microglia [$F(1,30)= 71.96$; $R^2 = 0.7058$, $p<0.0001$] (Figure 4F), indicating increasing numbers of microglia exhibiting a hypertrophic morphology. Furthermore, results showed a significant increase in the density of Gal3+ cells [$F(1,30)= 15.66$, $R^2 = 0.3429$, $p=0.0004$] but no significant change in density of C1q+ cells [$F(1,30)= 2.218$, $R^2 = 0.06886$, $p=0.1468$] with age (Figures 4G, H). Interestingly, both ramified Gal3+ ($p<0.0001$) and hypertrophic Gal3+ ($p<0.0001$) microglia increased with age, but C1q+ ramified decreased with age ($p<0.0001$) and hypertrophic C1q+ microglia did not change with age ($p=0.7369$). Furthermore, the density of C1q+Gal3+ hypertrophic ($p=0.0062$) and hypertrophic C1q-Gal3- microglia ($p= 0.0023$) increased with age. Importantly, there were no changes in the density of total Iba1+ microglia (Figure 4I). The decreased ratio of ramified:hypertrophic microglia correlated with higher CII score [$F(1,30)= 10.34$; $R^2 = 0.2564$, $p=0.0031$] (Figure 4J) and the increased density of Gal3+ cells approached significant correlation with CII score [$F(1,30)=3.263$, $R^2 = 0.09810$, $p=0.0809$] but density of C1q+ cells did not correlate with cognitive impairment [$F(1,30)= 0.1048$, $R^2 = 0.003482$, $p=0.7484$] (data not shown). The changes in distribution of morphology and protein expression with CII are presented in Figures 4K, L. In sum, microglia change from a majority showing ramified morphology that were C1q- and Gal-3- in young age (Figure 4C) to more hypertrophic morphology with increased Gal-3 protein expression with old age (Figure 4E). Interestingly, middle aged subjects show intermediary profiles suggesting the transition of microglia into more phagocytic and inflammatory phenotypes (Figure 4D). Taken together, increased shift to phagocytic and inflammatory microglia phenotypes in the cingulum bundle with age are associated with increased C1q expression on myelin and with more severe cognitive impairment.

10.3389/fimmu.2024.1426975

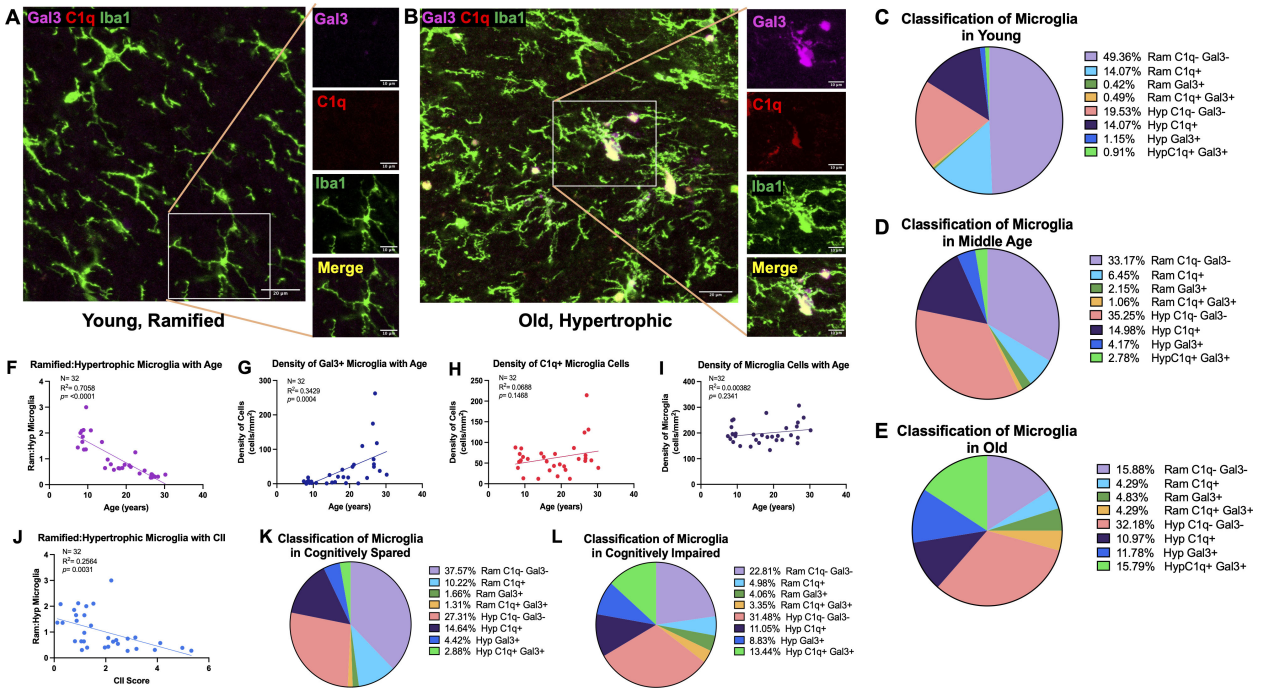

FIGURE 4
Increased proportion and density of phagocytic and inflammatory microglia with age and cognitive impairment. **(A)** Representative image of Iba1+ microglia in a young animal largely expressing ramified morphology without C1q or Gal-3, as shown on zoomed in image, in contrast to **(B)** old animals with more Iba1+ cells exhibiting hypertrophic morphology with C1q and Gal-3 expression. The proportion of microglia cells classified according to ramified or hypertrophic morphology and expression of C1q and Gal-3 are displayed in **(C)** young **(D)** middle aged **(E)** and old animals. The proportion of ramified: hypertrophic microglia significantly decreased with **(F)** age **(J)** and CII score, indicating an increase in hypertrophic microglia. **(G)** Density of Gal3+ cells increased with age, **(H)** while there were no significant age-related changes in the density of C1q+ cells. **(I)** There was no change in density of total microglia. Proportion of microglia morphology and C1q/Gal3 expression in **(K)** cognitively spared animals and in **(L)** cognitively impaired are also shown. Scale bars represent 20μm in zoomed out images and 10μm for close-up images.

Increased microglial C1qA mRNA expression and decreased oligodendrocyte CD47 mRNA expression in the cingulum bundle with age

While there was an age-related increase in C1q protein within the cingulum bundle neuropil, we did not observe age-related differences in microglia expression of C1q protein. Indeed, while C1q+ microglia are associated with immune activation in disease models, there is evidence of diverse interactions between C1q+ production, the downstream receptors, and feedback signaling that can promote both pro- and anti-inflammatory microenvironments (57). Thus, we wanted to assess a part of this dynamic process, by looking at RNA expression of genes for C1q in the cingulum bundle. RNAscope was used with a probe for *C1qA*, a subunit ubiquitously found in all C1q molecules (58, 59). RNA expression was analyzed with age and cognitive impairment groups defined as young (<11) or old (>20) and cognitively spared (<2.0) or impaired (>2.0). *C1qA* mRNA puncta were counted inside of immunofluorescent labeled Iba1+ cells, as shown in Figures 5A, B. Results showed a significant increase in microglial *C1qA* in old (125.5% increase, p= 0.0014; Figure 5C) and in cognitively impaired subjects (74.5% increase p= 0.038; Figure 5D). These results suggest that microglial production of *C1qA* is increased in the aging cingulum bundle.

Given that we see age-related differences in MBP interactions with immune proteins, we then wanted to assess changes in the expression of CD47 RNA within oligodendrocytes, which form and maintain myelin. We hypothesized that oligodendrocytes are less protected by CD47 with age and may be targeted for elimination, leading to disrupted myelination. Another possibility is that oligodendrocytes with less CD47 would produce myelin with less CD47, leaving it more vulnerable to phagocytosis. Here, *CD47* puncta were counted in *Olig2*+ cells as shown in Figures 5E, F. Results showed a significant decrease in *CD47* in the old age group (38.7% decrease, p= 0.0019; Figure 5G) and with cognitive impairment (34.3% decrease, p= 0.027; Figure 5H). These results suggest that oligodendrocytes are less efficient at producing *CD47* with age.

Elevated levels of MBP in the CSF with age

It has been reported that the accumulation of myelin damage in the brain overburdens microglia cells so they can no longer keep up with the demand of breaking down the cholesterol-rich molecules (53). Thus, myelin debris that is not engulfed by microglia may be cleared into the CSF with age. To test this, an ELISA for MBP was run on CSF samples from 27 animals. One animal was excluded

10.3389/fimmu.2024.1426975

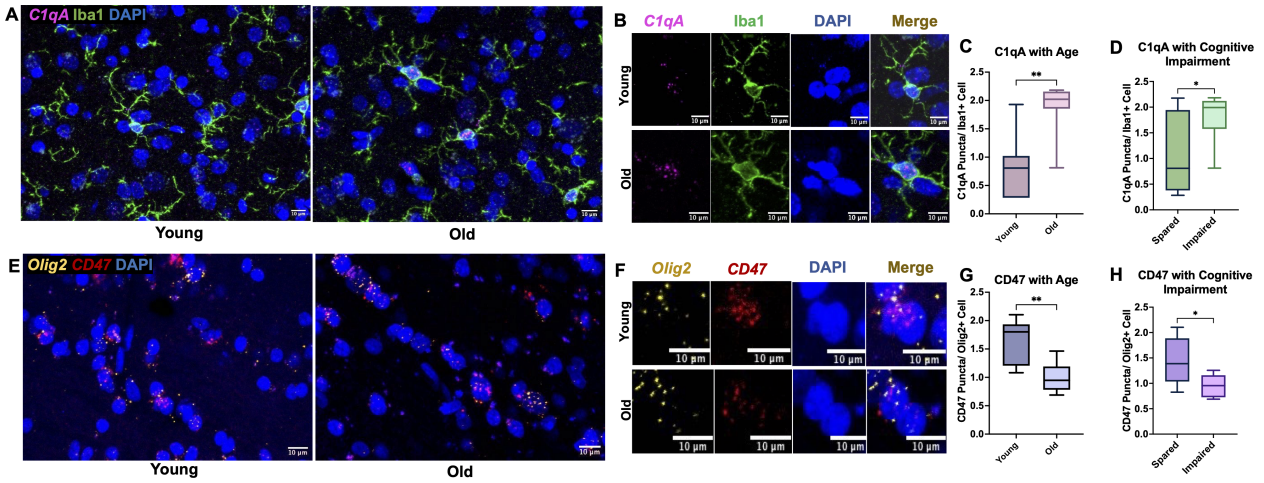

FIGURE 5
C1qA RNA expression increases in microglia cells while *CD47* RNA expression decreases in oligodendrocytes. **(A)** Representative RNAscope images of *C1qA* and DAPI with IF for Iba1 captured in young vs old animals with **(B)** zoomed examples show *C1qA* RNA puncta within single microglia cells. Results show significant increase in *C1qA* RNA expression with **(C)** age and **(D)** with cognitive impairment. **(E)** Example RNAscope images of *Olig2* and *CD47* probes with DAPI in the cingulum bundle of young and old animals. **(F)** Zoomed in images of *Olig2*+ oligodendrocytes expressing *CD47* puncta within DAPI labeled nuclei. **(G)** Decreased *CD47* RNA expression in oligodendrocytes was found in old animals and **(H)** in cognitively impaired animals. *p<0.05; **p<0.01; N=16.

from analysis due to concentration below the manufacturer's range and 3 animals were excluded after they were identified as outliers on the ROUT outlier test on GraphPad Prism. One-way ANOVA results show significant change in MBP in CSF with age [$F(2,20) = 10.24$, p=0.0009]. Specifically, Tukey's *post hoc* test revealed significant increase of MBP in the CSF of old animals compared to both young (p= 0.0008) and middle-aged animals (p= 0.0279), as shown in Figure 6A. This is consistent with the hypothesis that myelin breakdown and clearance into the CSF increases with age. No change was found comparing young and middle-aged animals (p= 0.2847; Figure 6A). Linear regression analyzing the % area of MBP in the brain and concentration of MBP in the CSF revealed significant correlation, where less MBP in the brain was associated with more MBP in the CSF [$F(1,15) = 4.56$, $R^2 = 0.2331$, p=0.0496] (Figure 6B). Together, these suggest that elevated myelin damage in the brain is cleared through the CSF across the lifespan, with highest levels of damage in the old age group.

Discussion

Summary of results

While the root cause of myelin pathology that occurs with age remains unknown, a likely candidate is microglia that become reactive and dysregulated with age-related inflammation. Here, we investigated changes in immunologic proteins C1q and CD47 that modulate microglia phagocytosis of cellular material relative to age-

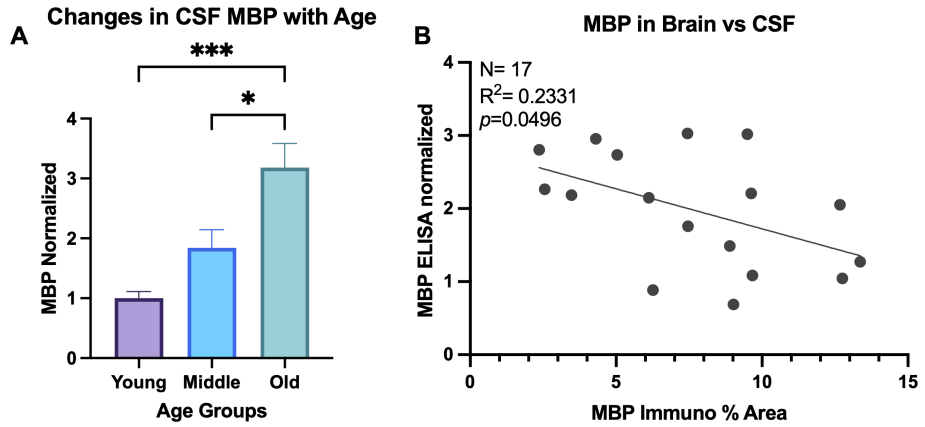

FIGURE 6
MBP in CSF increases with age. **(A)** ELISA was run for MBP in CSF samples and concentrations normalized to the young age group. One-way ANOVA analysis revealed MBP increases in old animals compared to both young and middle-aged animals. **(B)** Linear regression comparing the % area of MBP in the brain compared to the normalized concentration of MBP in the CSF of the same animals. *p<0.05; *** p<0.001.

related myelin damage. Our main findings demonstrate that in the normal aging monkey brain, the "eat me" signal C1q, is increased both in the cingulum bundle microenvironment and specifically localized to myelin, which it may be tagging for phagocytosis. Of particular interest, the "don't eat me" protein CD47 that could mitigate C1q effects decreased in middle age, which would effectively increase myelin vulnerability. However, this was followed by a paradoxical increase of CD47 in old age. *In situ* hybridization showed that CD47 RNA expression decreased in oligodendrocytes with age. Further, we found that with age, microglia take on more reactive phenotypes along with increased expression of C1q RNA. Finally, these changes in C1q, CD47, and microglia phenotypes correlate with more severe cognitive impairment. Together, these results suggest that both C1q and CD47 are dysregulated with age and likely contribute to both the increase in microglia reactivity and vulnerability of myelin to phagocytosis that is associated with cognitive impairment.

Oligodendrocyte and microglia roles in myelin damage

Oligodendrocytes and microglia work together to maintain myelin homeostasis and our observed immune dysregulation makes both likely contributors to age-related myelin deterioration. Mature oligodendrocytes capable of myelinating differentiate from oligodendrocyte precursor cells (OPCs) to maintain myelin across the lifespan (60). Mature oligodendrocytes accumulate damage with age and are particularly vulnerable to oxidative stress byproducts after long periods of time under the extreme metabolic demand required to maintain myelin (60). Thus, myelination by mature aged oligodendrocytes results in the production of abnormal myelin (58). We showed loss of MBP in the cingulum bundle, which not only indicates loss of myelin but also the inability of oligodendrocytes to produce compact myelin with tight lamination as MBP facilitates adhesion of myelin surfaces (49).

Our data show that CD47 RNA expression was decreased in oligodendrocytes with age, suggesting a down-regulation of the "don't eat me" signal. Furthermore, we have recently reported that aged OPC numbers do not change but OPCs exhibit impaired ability to differentiate into mature myelinating oligodendrocytes, likely resulting in less myelin production and ultimately myelin loss (61). Previous work demonstrates OPCs contribute to remyelination by differentiating into mature, myelinating oligodendrocytes (62). Thus, OPCs that fail to differentiate cannot replace the damaged aged oligodendrocytes. Therefore, defective myelin would continue to be produced, making the cause for this OPC differentiation failure an important question to be addressed.

Microglia directly signal to OPCs to promote proliferation, differentiation, and subsequent remyelination (63). During demyelination, regenerative or "M2" microglia drive oligodendrocyte differentiation to facilitate efficient remyelination (64). Additionally, efficient microglia clearance of myelin debris is critical for remyelination (23). However, we demonstrated that microglia reactivity increases with age, suggesting microglia may not be able to polarize into a regenerative phenotype that facilitates OPC differentiation required for remyelination. Further, with age, microglia become overburdened with myelin debris (53) resulting in the accumulation of myelin debris which has been shown to obstruct OPC proliferation (65). Moreover, aged microglia upregulate C1q, which has been shown to directly inhibit OPC differentiation into mature oligodendrocytes via the Wnt signaling pathway in a cuprizone model of MS and myelin pathology (66). Here, we found increased C1q in aging white matter, which may also be inhibiting OPC differentiation. Thus, rather than promoting remyelination, microglia contribute to the inhibition of remyelination during aging by increasing C1q levels, which could lead to increased phagocytosis of myelin and obstruct OPC differentiation as well as ineffectively clearing myelin debris.

C1q and CD47 signaling in disease states

Dysregulation of C1q and CD47 may play an active role in microglia phagocytosis dysregulation and worsening of subsequent pathology during aging. C1q is a pattern recognition receptor (PRR) that directly binds to structures releasing disease associated molecular patterns (DAMPs) associated with cellular damage or debris (57). C1q binding initiates the classical complement cascade of downstream molecule recruitment that ultimately activates innate immune cell response to remove the selected structure (67, 68). Chronic upregulation of C1q occurs in age-related diseases such as AD and MS in association with excess microglia phagocytosis (69). Excessive C1q-stimulated phagocytosis exacerbates disease pathophysiology such as synapse loss in AD and demyelination in MS that contributes to cognitive and neurologic impairment (70–72). In mice, microglia mediate forgetting in a complement dependent manner (73), and elevated C1q in normal aging monkeys and rodents is associated with cognitive impairment (34, 36, 37, 74). The present results confirm elevated C1q with age in white matter tracts where it may contribute to the pro-inflammatory environment and myelin damage. Further, we demonstrate here, along with our previous study in gray matter (37), the association of both microglia reactivity and elevated C1q levels with poorer cognitive performance. Our results show that there is a significant increase in C1q localized to myelin during aging, suggesting that more myelin is targeted by this "eat me" signal which could exacerbate myelin pathology and associated age-related cognitive impairment. Taken together, this suggests aberrant C1q expression and microglia reactivity may underly age-related cognitive decline in learning and memory.

The inhibitory signal, CD47, is a neuroimmune regulatory protein (NIReg) involved in suppressing the duration of inflammation and promoting tissue recovery (32, 33). CD47 binds with receptor signal regulatory protein (SIRPα) located on microglia cells to reduce unnecessary phagocytosis of structures such as myelin (35, 39, 75). Loss of proper CD47-SIRPα interactions has been shown to contribute to progression of neurodegenerative disease including stroke, AD, and MS (32). CD47 reduction is associated with active MS lesions and toxic amyloid beta activity in AD (76–78). The results reported here

suggest that CD47 may be similarly involved in the myelin damage of normal aging. We report that levels of CD47 did not change in the cingulum bundle with age, but that colocalization with myelin decreases in middle age at onset of myelin damage but paradoxically increases again with age when our earlier studies have shown that myelin damage increases (18, 19, 79). From our results, it is unclear how CD47 levels remain stable in the cingulum bundle with age while there is decreased expression of CD47 mRNA in oligodendrocytes. Interestingly, recent work has demonstrated that neuronal SIRPα plays a role in regulating microglia phagocytosis by modulating microglial interaction with CD47 during synaptic refinement and in neurodegeneration (80, 81). Thus, it is possible that the dynamic between CD47 and neuronal SIRPα is altered with aging and should be investigated in future studies. Further, the role of CD47 in disease pathogenesis is less understood and appears to be conflicting. For instance, CD47 may become detrimental in disease states where swift debris clearance and inflammatory response are needed, but the absence of CD47 promotes inflammation and phagocytosis (32). In an EAE model of CD47, blocking of CD47 at disease initiation attenuated disease progression while blocking CD47 at peak demyelination worsened disease states (76). The same is true regarding myelin where deletion of CD47 results in quicker and faster myelin clearance following acute peripheral nerve damage (82), but CD47 knockout accelerates myelin disruption and dismantling by myelin producing Schwann cells (82). As in disease states, our results suggest that CD47 similarly plays nuanced roles in myelin degeneration.

Microglia-mediated myelin phagocytosis in aging

Normal myelin turnover involves the balance between myelin degradation and remyelination which is crucial for myelin homeostasis in the adult brain (83, 84). Disruption of this process, whether by excess myelin phagocytosis or inefficient myelin clearance has severe consequences including triggering inflammation, accumulation of toxic debris, blockage of remyelination, and ultimately worse myelin damage (83), as seen during aging. While aged microglia are still able to phagocytose myelin, their engulfing capacity decreases (85). Further, microglia exhibit difficulty degrading lipid-rich myelin, and these fragments form insoluble inclusions resembling lipofuscin within microglial lysosomal compartments, impeding efficient breakdown (53). Our data show that microglia become more reactive with age as more microglia exhibit a hypertrophic morphology and express C1q and Gal-3. As reported by Safaiyan et al. (86), distinct microglia phenotypes emerge specific to white matter tracts during normal aging reflecting overburdening and chronic degradation of myelin. These microglia, known as white matter associated microglia (WAM), exhibit downregulation of homeostatic genes and upregulation of genes related to lipid metabolism, lysosomal activity, phagocytosis, and major histocompatibility complex class II (MHC-II) (86). Gal-3 is a prominent feature of the WAM signature (86) and may be neurotoxic and involved in myelin debris clearance (86 &87). Indeed, we report the increased proportion of Gal-3 hypertrophic microglia was associated with increased cognitive impairment, which corroborates previous work from our lab (87). Studies of MS in humans demonstrate similar shifts in microglia phenotype from homeostatic to reactive genes. For example, microglia gene expression during active demyelinating lesions for phagocytosis, oxidative injury, and antigen presentation is upregulated (88).

Overall, our data show the heterogeneity of microglial populations that mediate complex interactions within phagocytic signaling (89), which likely have distinct roles in age-related myelin damage clearance. We hypothesized that if myelin debris is accumulating beyond the capacity with which microglia can phagocytose it, excess debris would be cleared into the CSF with age, which is supported by our results. It is important to note that microglia do not act alone in myelin phagocytosis, as astrocytes show limited capability to phagocytose myelin debris, although this may be a compensatory mechanism when microglia become dysfunctional (83, 90). Nevertheless, our results show that microglia become phagocytic and inflammatory with age as myelin damage increases and the “eat me/don’t eat me” signaling becomes dysregulated.

Limitations and pitfalls

Unlike rodent models, monkey frontal white matter tracts have dense white matter, making reliable quantification of myelin difficult using myelin staining, and electron microscopy was not available for the cases used here so quantification of myelin damage was not possible. However, immunolabeling of MBP in the cingulum bundle enabled the quantification of % area of signal with age as surrogate for degree of myelin damage. Furthermore, we measured MBP in the CSF to assess the amount of myelin cleared into the CSF as a potential marker for myelin damage and found that it increased with age. The use of the rhesus monkey is a highly valuable model as these primates have cytoarchitecture highly similar to the human brain, including dense white matter tracts, and similar age-related cognitive impairment despite being spared from AD. Thus, we can extrapolate cellular changes during age-related cognitive decline without the confound of neuron loss in AD. Despite the necessarily correlative nature of the data presented here, the association of cellular changes affecting myelin and cognitive impairment provides valuable insights into potential therapeutic targets.

Conclusions

The observations presented here show that both C1q and CD47 are dysregulated during normal aging in the primate brain in association with myelin breakdown in white matter and cognitive decline. Here, we showed an increase in C1q in the cingulum bundle and specifically on myelin, where it potentially acts as an “eat me” signal to microglia to facilitate myelin phagocytosis. Concurrently, microglia exhibited a higher frequency of reactive phenotypes with age, providing evidence of microglia phagocytic activity coinciding

with complement colocalization to myelin. Additionally, the mitigation of C1q effects by the "don't eat me" molecule CD47 is reduced in aging as CD47 colocalization to myelin decreased in middle age and oligodendrocyte CD47 mRNA expression decreased with old age. Together, this leaves myelin and oligodendrocytes vulnerable to tagging by C1q and phagocytosis by microglia. We believe the changes in C1q and CD47 reported here are detrimental to white matter during aging as they are correlated with worsening cognitive impairment. Our findings lay the foundation for future work investigating the mechanisms by which both "eat me" and "don't eat me" signals contribute to age-related myelin damage, microglia reactivity, and cognitive decline. While C1q and CD47 are just two molecules in a large cascade of signals, they should be considered as potential targets for therapeutic interventions aimed at slowing cognitive aging.

Data availability statement

The raw data supporting the conclusions of this article will be made available by the authors, without undue reservation.

Ethics statement

The animal study was approved by Boston University Institutional Animal Care and Use Committee (IACUC). The study was conducted in accordance with the local legislation and institutional requirements.

Author contributions

SD: Writing – review & editing, Writing – original draft, Methodology, Investigation, Formal analysis, Conceptualization. CD: Writing – review & editing, Methodology. MM: Writing – review & editing, Methodology. TM: Writing – review & editing, Methodology. DR: Writing – review & editing, Supervision, Resources, Funding acquisition, Conceptualization.

Funding

The author(s) declare financial support was received for the research, authorship, and/or publication of this article. This research was supported by NIH/NIA grants 1RF1AG062831, 2RF1AG043640, 1R01 AG075727, 2R01-AG042512, R01 AG078460.

Acknowledgments

We would like to thank Karen Slater, Ashley Fair, and Bryce Conner for their highly appreciated technical assistance and Penny Schultz for her invaluable behavioral testing contribution.

Conflict of interest

The authors declare that the research was conducted in the absence of any commercial or financial relationships that could be construed as a potential conflict of interest.

Publisher's note

References

1. Hung CW, Chen YC, Hsieh WL, Chiou SH, Kao CL. Ageing and neurodegenerative diseases. *Ageing Res Rev*. (2010) 9:S36–46. doi: 10.1016/j.arr.2010.08.006

2. Park DC, Reuter-Lorenz P. The adaptive brain: aging and neurocognitive scaffolding. *Annu Rev Psychol Annu Rev Psychol 60. Palo Alto: Annu Reviews*. (2009) 60:173–96. doi: 10.1146/annurev.psych.59.103006.093656

3. Harada CN, Love MCN, Triebel KL. Normal cognitive aging. *Clinics Geriatr Med*. (2013) 29:737–+. doi: 10.1016/j.cger.2013.07.002

4. Salthouse TA. When does age-related cognitive decline begin? *Neurobiol Aging*. (2009) 30:507–14. doi: 10.1016/j.neurobiolaging.2008.09.023

5. Salthouse TA. Selective review of cognitive aging. *J Int Neuropsychol Society*. (2010) 16:754–60. doi: 10.1017/S1355617710000706

6. Freeman SH, Kandel R, Cruz L, Rozkalne A, Newell K, Frosch MP, et al. Preservation of neuronal number despite age-related cortical brain atrophy in elderly subjects without Alzheimer disease. *J Neuropathol Exp Neurol*. (2008) 67:1205–12. doi: 10.1097/NEN.0b013e31818fc72f

7. Marner L, Nyengaard JR, Tang Y, Pakkenberg B. Marked loss of myelinated nerve fibers in the human brain with age. *J Comp Neurol*. (2003) 462:144–52. doi: 10.1002/cne.10714

8. Liu HJ, Wang LX, Geng ZJ, Zhu QF, Song ZH, Chang RT, et al. A voxel-based morphometric study of age- and sex-related changes in white matter volume in the normal aging brain. *Neuropsychiatr Dis Treat*. (2016) 12:453–65. doi: 10.2147/NDT.S90674

9. Guttmann CRG, Jolesz FA, Kikinis R, Killiany RJ, Moss MB, Sandor T, et al. White matter changes with normal aging. *Neurology*. (1998) 50:972–8. doi: 10.1212/WNL.50.4.972

10. Salat DH, Tuch DS, Greve DN, van der Kouwe AJW, Hevelone ND, Zaleta AK, et al. Age-related alterations in white matter microstructure measured by diffusion tensor imaging. *Neurobiol Aging*. (2005) 26:1215–27. doi: 10.1016/j.neurobiolaging.2004.09.017

11. Head D, Buckner RL, Shimony JS, Williams LE, Akbudak E, Conturo TE, et al. Differential vulnerability of anterior white matter in nondemented aging with minimal acceleration in dementia of the Alzheimer type: Evidence from diffusion tensor imaging. *Cereb Cortex*. (2004) 14:410–23. doi: 10.1093/cercor/bhh003

12. Dyke B, Gage TB, Mamelka PM, Goy RW, Stone WH. A demographic-analysis of the wisconsin-regional-primate-center rhesus colony, 1962-1982. *Am J Primatol*. (1986) 10:257–69. doi: 10.1002/ajp.1350100306

13. Tigges J, Gordon TP, McClure HM, Hall EC, Peters A. Survival rate and life-span of rhesus-monkeys at the yerkes-regional-primate-research-center. *Am J Primatol*. (1988) 15:263–73. doi: 10.1002/ajp.1350150308

14. Moss MB, Moore TL, Schettler SP, Killiany R, Rosene D. *Successful vs. unsuccessful aging in the rhesus monkey. Brain aging: Models, methods, and*

mechanisms. Frontiers in neuroscience. Boca Raton, FL, US: CRC Press/Routledge/Taylor & Francis Group (2007) p. 21–38.

15. Peters A, Rosene DL, Moss MB, Kemper TL, Abraham CR, Tigges J, et al. Neurobiological bases of age-related cognitive decline in the rhesus monkey. *J Neuropathol Exp Neurol*. (1996) 55:861–74. doi: 10.1097/00005072-199608000-00001

16. Peters A, Rosene DL. In aging, is it gray or white? *J Comp Neurol*. (2003) 462:139–43. doi: 10.1002/cne.10715

17. Peters A, Sethares C. Aging and the myelinated fibers in prefrontal cortex and corpus callosum of the monkey. *J Comp Neurol*. (2002) 442:277–91. doi: 10.1002/cne.10099

18. Bowley MP, Cabral H, Rosene DL, Peters A. Age changes in myelinated nerve fibers of the cingulate bundle and corpus callosum in the rhesus monkey. *J Comp Neurol*. (2010) 518:3046–64. doi: 10.1002/cne.22379

19. Peters A. The effects of normal aging on myelin and nerve fibers: A review. *J Neurocytol*. (2002) 31:581–93. doi: 10.1023/A:1025731309829

20. Peters A. The effects of normal aging on myelinated nerve fibers in monkey central nervous system. *Front Neuroanatomy*. (2009) 3:10. doi: 10.3389/neuro.05.011.2009

21. de Lange AMG, Bråthen ACS, Grydeland H, Sexton C, Johansen-Berg H, Andersson JLR, et al. White matter integrity as a marker for cognitive plasticity in aging. *Neurobiol Aging*. (2016) 47:74–82. doi: 10.1016/j.neurobiolaging.2016.07.007

22. Kohama SG, Rosene DL, Sherman LS. Age-related changes in human and non-human primate white matter: from myelination disturbances to cognitive decline. *Age*. (2012) 34:1093–110. doi: 10.1007/s11357-011-9357-7

23. Kotter MR, Li WW, Zhao C, Franklin RJM. Myelin impairs CNS remyelination by inhibiting oligodendrocyte precursor cell differentiation. *J Neurosci*. (2006) 26:328–32. doi: 10.1523/JNEUROSCI.2615-05.2006

24. Shields SA, Gilson JM, Blakemore WF, Franklin RJM. Remyelination occurs as extensively but more slowly in old rats compared to young rats following gliotoxin-induced CNS demyelination. *Glia*. (1999) 28:77–83. doi: 10.1002/(ISSN)1098-1136

25. Abraham J, Jang S, Godbout JP, Chen J, Kelley KW, Dantzer R, et al. Aging sensitizes mice to behavioral deficits induced by central HIV-1 gp120. *Neurobiol Aging*. (2008) 29:614–21. doi: 10.1016/j.neurobiolaging.2006.11.002

26. Franceschi C, Capri M, Monti D, Giunta S, Olivieri F, Sevini F, et al. Inflammaging and anti-inflammaging: A systemic perspective on aging and longevity emerged from studies in humans. *Mech Ageing Dev*. (2007) 128:92–105. doi: 10.1016/j.mad.2006.11.016

27. Jin R, Chan AKY, Wu JS, Lee TMC. Relationships between inflammation and age-related neurocognitive changes. *Int J Mol Sci*. (2022) 23:20. doi: 10.3390/ijms232012573

28. Raj D, Yin ZR, Breur M, Doorduin J, Holtman IR, Olah M, et al. Increased white matter inflammation in aging- and Alzheimer's disease brain. *Front Mol Neurosci*. (2017) 10:18. doi: 10.3389/fnmol.2017.00206

29. Norden DM, Godbout JP. Review: Microglia of the aged brain: primed to be activated and resistant to regulation. *Neuropathol Appl Neurobiol*. (2013) 39:19–34. doi: 10.1111/j.1365-2990.2012.01306.x

30. Di Benedetto S, Muller L, Wenger E, Duzel S, Pawelec G. Contribution of neuroinflammation and immunity to brain aging and the mitigating effects of physical and cognitive interventions. *Neurosci Biobehav Rev*. (2017) 75:114–28. doi: 10.1016/j.neubiorev.2017.01.044

31. Brown GC, Neher JJ. Microglial phagocytosis of live neurons. *Nat Rev Neurosci*. (2014) 15:209–16. doi: 10.1038/nrn3710

32. Gheibihayat SM, Cabezas R, Nikiforov NG, Jamialahmadi T, Johnston TP, Sahebkar A. CD47 in the brain and neurodegeneration: an update on the role in neuroinflammatory pathways. *Molecules*. (2021) 26:15. doi: 10.3390/molecules26133943

33. Griffiths M, Neal JW, Gasque P. Innate immunity and protective neuroinflammation: New emphasis on the role of neuroimmune regulatory proteins. *Neuroinflamm Neuronal Death Repair*. (2007) 82:29–55. doi: 10.1016/S0074-7742(07)82002-2

34. Stephan AH, Madison DV, Mateos JM, Fraser DA, Lovelett EA, Coutellier L, et al. A dramatic increase of C1q protein in the CNS during normal aging. *J Neurosci*. (2013) 33:13460–74. doi: 10.1523/JNEUROSCI.1333-13.2013

35. Lehrman EK, Wilton DK, Litvina EY, Welsh CA, Chang ST, Frouin A, et al. CD47 protects synapses from excess microglia-mediated pruning during development. *Neuron*. (2018) 100:120–+. doi: 10.1016/j.neuron.2018.09.017

36. Datta D, Leslie SN, Morozov YM, Duque A, Rakic P, van Dyck CH, et al. Classical complement cascade initiating C1q protein within neurons in the aged rhesus macaque dorsolateral prefrontal cortex. *J Neuroinflamm*. (2020) 17:15. doi: 10.1186/s12974-019-1683-1

37. DeVries SA, Conner B, Dimovasili C, Moore TL, Medalla M, Mortazavi F, et al. Immune proteins C1q and CD47 may contribute to aberrant microglia-mediated synapse loss in the aging monkey brain that is associated with cognitive impairment. *Geroscience*. (2024) 46:2503–19. doi: 10.1007/s11357-023-01014-x

38. Johns TG, Bernard CCA. Binding of complement component Clq to myelin oligodendrocyte glycoprotein: A novel mechanism for regulating CNS inflammation. *Mol Immunol*. (1997) 34:33–8. doi: 10.1016/S0161-5890(97)00005-9

39. Gitik M, Liraz-Zaltsman S, Oldenborg PA, Reichert F, Rotshenker S. Myelin down-regulates myelin phagocytosis by microglia and macrophages through interactions between CD47 on myelin and SIRP alpha (signal regulatory protein-alpha) on phagocytes. *J Neuroinflamm*. (2011) 8:10. doi: 10.1186/1742-2094-8-24

40. Oldenborg PA, Gresham HD, Lindberg FP. CD47-signal regulatory protein alpha (SIRP alpha) regulates Fc gamma and complement receptor-mediated phagocytosis. *J Exp Med*. (2001) 193:855–61. doi: 10.1084/jem.193.7.855

41. Herndon JG, Moss MB, Rosene DL, Killiany RJ. Patterns of cognitive decline in aged rhesus monkeys. *Behav Brain Res*. (1997) 87:25–34. doi: 10.1016/S0166-4328(96)02256-5

42. Moss MB, Rosene DL, Peters A. Effects of aging on visual recognition memory in the rhesus-monkey. *Neurobiol Aging*. (1988) 9:495–502. doi: 10.1016/S0197-4580(88)80103-9

43. Moore TL, Killiany RJ, Herndon JG, Rosene DL, Moss MB. Impairment in abstraction and set shifting in aged Rhesus monkeys. *Neurobiol Aging*. (2003) 24:125–34. doi: 10.1016/S0197-4580(02)00054-4

44. Moore TL, Killiany RJ, Herndon JG, Rosene DL, Moss MB. A non-human primate test of abstraction and set shifting: An automated adaptation of the Wisconsin Card Sorting Test. *J Neurosci Methods*. (2005) 146:165–73. doi: 10.1016/j.jneumeth.2005.02.005

45. Killiany RJ, Moss MB, Rosene DL, Herndon J. Recognition memory function in early senescent rhesus monkeys. *Psychobiology*. (2000) 28:45–56. doi: 10.3758/BF03330628

46. Moore TL, Killiany RJ, Herndon JG, Rosene DL, Moss MB. Executive system dysfunction occurs as early as middle-age in the rhesus monkey. *Neurobiol Aging*. (2006) 27:1484–93. doi: 10.1016/j.neurobiolaging.2005.08.004

47. Rosene DL, Roy NJ, Davis BJ. A cryoprotection method that facilitates cutting frozen-sections of whole monkey brains for histological and histochemical processing without freezing artifact. *J Histochem Cytochem*. (1986) 34:1301–15. doi: 10.1177/34.10.3745909

48. Estrada LI, Robinson AA, Amaral AC, Giannaris EL, Heyworth NC, Mortazavi F, et al. Evaluation of long-term cryostorage of brain tissue sections for quantitative histochemistry. *J Histochem Cytochem*. (2017) 65:153–71. doi: 10.1369/0022155416686934

49. Boggs JM. Myelin basic protein: a multifunctional protein. *Cell Mol Life Sci*. (2006) 63:1945–61. doi: 10.1007/s00018-006-6094-7

50. García-Revilla J, Boza-Serrano A, Espinosa-Oliva AM, Soto MS, Deierborg T, Ruiz R, et al. Galectin-3, a rising star in modulating microglia activation under conditions of neurodegeneration. *Cell Death Dis*. (2022) 13:11. doi: 10.1038/s41419-022-05058-3

51. Martinsen V, Kursula P. Multiple sclerosis and myelin basic protein: insights into protein disorder and disease. *Amino Acids*. (2022) 54:99–109. doi: 10.1007/s00726-021-03111-7

52. Whitaker JN. Myelin basic protein in cerebrospinal fluid and other body fluids. *Multiple Sclerosis J*. (1998) 4:16–21. doi: 10.1177/135245859800400105

53. Safaiyan S, Kannaiyan N, Snaidero N, Brioschi S, Biber K, Yona S, et al. Age-related myelin degradation burdens the clearance function of microglia during aging. *Nat Neurosci*. (2016) 19:995–8. doi: 10.1038/nn.4325

54. Bartzokis G. Age-related myelin breakdown: a developmental model of cognitive decline and Alzheimer's disease. *Neurobiol Aging*. (2004) 25:5–18. doi: 10.1016/j.neurobiolaging.2003.03.001

55. Kister A, Kister I. Overview of myelin, major myelin lipids, and myelin-associated proteins. *Front Chem*. (2023) 10:9. doi: 10.3389/fchem.2022.1041961

56. Karperien A, Ahammer H, Jelinek HF. Quantitating the subtleties of microglial morphology with fractal analysis. *Front Cell Neurosci*. (2013) 7:18. doi: 10.3389/fncel.2013.00003

57. Bohlson SS, O'Conner SD, Hulsebus HJ, Ho MM, Fraser DA. Complement, C1q, anc C1 q-related molecules regulate macropnage polarization. *Front Immunol*. (2014) 5:7. doi: 10.3389/fimmu.2014.00402

58. Reid KBM, Porter RR. Subunit composition and structure of subcomponent Clq of 1st component of human complement. *Biochem J*. (1976) 155:19–&. doi: 10.1042/bj1550019

59. Fonseca MI, Chu SH, Hernandez MX, Fang MJ, Modarresi L, Selvan P, et al. Cell-specific deletion of C1qa identifies microglia as the dominant source of C1q in mouse brain. *J Neuroinflamm*. (2017) 14:15. doi: 10.1186/s12974-017-0814-9

60. French HM, Reid M, Mamontov P, Simmons RA, Grinspan JB. Oxidative stress disrupts oligodendrocyte maturation. *J Neurosci Res*. (2009) 87:3076–87. doi: 10.1002/jnr.22139

61. Dimovasili C, Fair AE, Garza IR, Batterman KV, Mortazavi F, Moore TL, et al. Aging compromises oligodendrocyte precursor cell maturation and efficient remyelination in the monkey brain. *Geroscience*. (2023) 45:249–64. doi: 10.1007/s11357-022-00621-4

62. Franklina R, Frisen J, Lyons D. Revisiting remyelination: Towards a consensus on the regeneration of CNS myelin. *Semin IN Cell Dev Biol*. (2021) 116:3–9. doi: 10.1016/j.semcdb.2020.09.009

63. Giera S, Luo R, Ying YQ, Ackerman SD, Jeong SJ, Stoveken HM, et al. Microglial transglutaminase-2 drives myelination and myelin repair via GPR56/ADGRG1 in oligodendrocyte precursor cells. *Elife*. (2018) 7:e33385. doi: 10.7554/eLife.33385

64. Miron VE, Boyd A, Zhao JW, Yuen TJ, Ruckh JM, Shadrach JL, et al. M2 microglia and macrophages drive oligodendrocyte differentiation during CNS remyelination. *Nat Neurosci*. (2013) 16:1211–U75. doi: 10.1038/nn.3469

65. Lampron A, Larochelle A, Laflamme N, Préfontaine P, Plante MM, Sánchez MG, et al. Inefficient clearance of myelin debris by microglia impairs remyelinating processes. *J Exp Med*. (2015) 212:481–95. doi: 10.1084/jem.20141656

66. Gao ZX, Zhang C, Feng ZW, Liu ZQ, Yang YR, Yang KX, et al. C1q inhibits differentiation of oligodendrocyte progenitor cells via Wnt/beta-catenin signaling activation in a cuprizone-induced mouse model of multiple sclerosis. *Exp Neurol*. (2022) 348:14. doi: 10.1016/j.expneurol.2021.113947

67. Yednock T, Fong DS, Lad EM. C1q and the classical complement cascade in geographic atrophy secondary to age-related macular degeneration. *Int J Retina Vitreous*. (2022) 8:14. doi: 10.1186/s40942-022-00431-y

68. Kanmogne M, Klein RS. Neuroprotective versus neuroinflammatory roles of complement: from development to disease. *Trends Neurosci*. (2021) 44:97–109. doi: 10.1016/j.tins.2020.10.003

69. Zhang WJ, Chen Y, Pei H. C1q and central nervous system disorders. *Front Immunol*. (2023) 14. doi: 10.3389/fimmu.2023.1145649

70. Qin Q, Wang M, Yin YS, Tang Y. The specific mechanism of TREM2 regulation of synaptic clearance in Alzheimer's disease. *Front Immunol*. (2022) 13:7. doi: 10.3389/fimmu.2022.845897

71. Hansen DV, Hanson JE, Sheng M. Microglia in Alzheimer's disease. *J Cell Biol*. (2018) 217:459–72. doi: 10.1083/jcb.201709069

72. Propson NE, Gedam M, Zheng H. Complement in neurologic disease. *Annu Rev Pathol: Mech Dis*. (2021) 16:16:277–98. doi: 10.1146/annurev-pathol-031620-113409

73. Wang C, Yue HM, Hu ZC, Shen YW, Ma J, Li J, et al. Microglia mediate forgetting via complement-dependent synaptic elimination. *Science*. (2020) 367:688–+. doi: 10.1126/science.aaz2288

74. Reichwald J, Danner S, Wiederhold KH, Staufenbiel M. Expression of complement system components during aging and amyloid deposition in APP transgenic mice. *J Neuroinflamm*. (2009) 6:12. doi: 10.1186/1742-2094-6-35

75. Zhang HY, Li FW, Yang YY, Chen J, Hu XM. SIRP/CD47 signaling in neurological disorders. *Brain Res*. (2015) 1623:74–80. doi: 10.1016/j.brainres.2015.03.012

76. Han MH, Lundgren DH, Jaiswal S, Chao M, Graham KL, Garris CS, et al. Janus-like opposing roles of CD47 in autoimmune brain inflammation in humans and mice. *J Exp Med*. (2012) 209:1325–34. doi: 10.1084/jem.20101974

77. Koning N, Bö L, Hoek RM, Huitinga I. Downregulation of macrophage inhibitory molecules in multiple sclerosis lesions. *Ann Neurol*. (2007) 62:504–14. doi: 10.1002/ana.21220

78. Miller TW, Isenberg JS, Shih HB, Wang YC, Roberts DD. Amyloid-β Inhibits no-cGMP signaling in a CD36-and CD47-dependent manner. *PloS One*. (2010) 5:10. doi: 10.1371/journal.pone.0015686

79. Wisco JJ, Killiany RJ, Guttmann CRG, Warfield SK, Moss MB, Rosene DL. An MRI study of age-related white and gray matter volume changes in the rhesus monkey. *Neurobiol Aging*. (2008) 29:1563–75. doi: 10.1016/j.neurobiolaging.2007.03.022

80. Jiang DY, Burger CA, Akhanov V, Liang JH, Mackin RD, Albrecht NE, et al. Neuronal signal-regulatory protein alpha drives microglial phagocytosis by limiting microglial interaction with CD47 in the retina. *Immunity*. (2022) 55:26. doi: 10.1016/j.immuni.2022.10.018

81. Ding X, Wang J, Huang MX, Chen ZP, Liu J, Zhang QP, et al. Loss of microglial SIRPα promotes synaptic pruning in preclinical models of neurodegeneration. *Nat Commun*. (2021) 12:17. doi: 10.1038/s41467-021-22301-1

82. Gitik M, Elberg G, Reichert F, Tal M, Rotshenker S. Deletion of CD47 from Schwann cells and macrophages hastens myelin disruption/dismantling and scavenging in Schwann cells and augments myelin debris phagocytosis in macrophages. *J Neuroinflamm*. (2023) 20:16. doi: 10.1186/s12974-023-02929-0

83. Xu TT, Liu C, Deng SY, Gan L, Zhang ZJ, Yang GY, et al. The roles of microglia and astrocytes in myelin phagocytosis in the central nervous system. *J Cereb Blood Flow Metab*. (2023) 43:325–40. doi: 10.1177/0271678X221137762

84. Harry Jean G, Toews AD. "Myelination, dysmyelination, and demyelination", In *Handbook of Developmental Neurotoxicology*. (1998), 87–115. doi: 10.1016/B978-012648860-9.50007-8

85. Thomas AL, Lehn MA, Janssen EM, Hildeman DA, Chougnet CA. Naturally-aged microglia exhibit phagocytic dysfunction accompanied by gene expression changes reflective of underlying neurologic disease. *Sci Rep*. (2022) 12:19471. doi: 10.1038/s41598-022-21920-y

86. Safaiyan S, Besson-Girard S, Kaya T, Cantuti-Castelvetri L, Liu L, Ji H, et al. Article White matter aging drives microglial diversity. *Neuron*. (2021) 109:29. doi: 10.1016/j.neuron.2021.01.027

87. Shobin E, Bowley MP, Estrada LI, Heyworth NC, Orczykowski ME, Eldridge SA, et al. Microglia activation and phagocytosis: relationship with aging and cognitive impairment in the rhesus monkey. *Geroscience*. (2017) 39:199–220. doi: 10.1007/s11357-017-9965-y

88. Zrzavy T, Hametner S, Wimmer I, Butovsky O, Weiner H, Lassmann H. Loss of 'homeostatic' microglia and patterns of their activation in active multiple sclerosis. *BRAIN*. (2017) 140:1900–13. doi: 10.1093/brain/awx113

89. Paolicelli RC, Sierra A, Stevens B, Tremblay ME, Aguzzi A, Ajami B, et al. Microglia states and nomenclature: A field at its crossroads. *Neuron*. (2022) 110:3458–83. doi: 10.1016/j.neuron.2022.10.020

90. Clarke LE, Liddelow SA, Chakraborty C, Münch AE, Heiman M, Barres B. Normal aging induces A1-like astrocyte reactivity. *Proc Natl Acad Sci U States A*. (2018) 115:E1896–E905. doi: 10.1073/pnas.1800165115

frontiers | Frontiers in Immunology

TYPE Original Research
PUBLISHED 19 November 2024
DOI 10.3389/fimmu.2024.1454102

OPEN ACCESS

EDITED BY
Shashank Kumar Maurya,
University of Delhi, India

REVIEWED BY
Meghraj Singh Baghel,
Johns Hopkins University, United States
Anamika Anamika,
University of Delhi, India

*CORRESPONDENCE
Hi-Joon Park
acufind@khu.ac.kr
Myung Sook Oh
msohok@khu.ac.kr

RECEIVED 24 June 2024
ACCEPTED 28 October 2024
PUBLISHED 19 November 2024

CITATION
Kim JH, Choi Y, Kim JS, Lee H, Ju IG, Yoo NY, La S, Jeong DH, Na C, Park H-J and Oh MS (2024) Stimulation of microneedles alleviates pathology of Parkinson's disease in mice by regulating the CD4+/CD8+ cells from the periphery to the brain.
Front. Immunol. 15:1454102.
doi: 10.3389/fimmu.2024.1454102

Stimulation of microneedles alleviates pathology of Parkinson's disease in mice by regulating the CD4+/CD8+ cells from the periphery to the brain

Jin Hee Kim[1], Yujin Choi[1], Jin Se Kim[1], Hanbyeol Lee[1], In Gyoung Ju[2], Na Young Yoo[3], Sookie La[3], Do Hyeon Jeong[3], Changsu Na[4], Hi-Joon Park[5,6]* and Myung Sook Oh[1,2]*

[1]Department of Biomedical and Pharmaceutical Sciences, Kyung Hee University, Seoul, Republic of Korea, [2]Department of Oriental Pharmaceutical Science and Kyung Hee East-West Pharmaceutical Research Institute, College of Pharmacy, Kyung Hee University, Seoul, Republic of Korea, [3]Raphas Co. Ltd., Seoul, Republic of Korea, [4]Department of Acupoint and Meridian, Korean Medical College, Dongshin University, Naju, Republic of Korea, [5]Department of Science in Korean Medicine, College of Korean Medicine, Kyung Hee University, Seoul, Republic of Korea, [6]Acupuncture and Meridian Science Research Center (AMSRC), Kyung Hee University, Seoul, Republic of Korea

Introduction: Immune dysfunction is a major cause of neuroinflammation and accelerates the progression of Parkinson's disease (PD). Numerous studies have shown that stimulation of specific acupuncture points (acupoints) can ameliorate PD symptoms. The purpose of this study was to investigate whether attaching microneedles to acupoints would improve PD pathology by recovering immune dysfunction.

Methods: The PD mouse model was induced by intrastriatal injection of 6-hydroxydopamine (6-OHDA), and microneedle patches (MPs) or sham patches (SPs) were attached to GB20 and GB34, representative acupoints for treating PD for 14 days.

Results: First, the behavioral experiment showed that motor disorders induced by 6-OHDA were significantly improved by MP. Simultaneously, 6-OHDA-induced dopaminergic neuronal death and brain neuroinflammation decreased. Conversely, SP had no effect on behavioral disorders, neuronal death, or neuroinflammation. Measurement results from flow cytometry of immune cells in the brain and blood revealed a disruption in the CD4+/CD8+ ratio in the 6-OHDA group, which was significantly restored in the MP group. The brain mRNA expression of cytokines was significantly increased in the 6-OHDA group, which was significantly decreased by MP.

Discussion: Overall, our results suggest that the attachment of MPs to GB20 and GB34 is a new method to effectively improve the pathology of PD by restoring peripheral and brain immune function.

KEYWORDS

Parkinson's disease, microneedle, acupuncture point, peripheral immune, neuroinflammation

1 Introduction

Parkinson's disease (PD) is the second most common neurodegenerative disease, which is characterized by the primary symptoms of behavioral disorders, such as stiffness and tremors (1, 2). A reduction in dopamine levels caused by the death of dopaminergic neurons in the striatonigral circuit is a prominent pathological feature of PD (3, 4). Several mechanisms can contribute to this process, and among the mechanisms identified to date, neuroinflammation is recognized as a common pathophysiology in PD (5, 6). Neuroinflammation is a component of the immune system that protects the brain by eliminating or suppressing pathogens. This may exert beneficial effects by promoting tissue repair or disposal of cellular debris. However, persistent neuroinflammatory responses can contribute to neuronal death (6–8).

Immune dysregulation occurs both centrally and peripherally in patients with PD (5, 9). According to previous studies, immune cell dysfunction occurs in both the brain and blood of patients with PD, and damage to CD4+ T cells and hyperactivity of CD8+ T cells among lymphocytes have consistently been reported (10, 11). In this situation, the cytokines released by aberrant immune cells directly influence neuronal death and exacerbate disease progression (12). Therefore, reducing neuroinflammation by normalizing immune system regulation is a key approach for suppressing neuronal death in the treatment of PD.

Acupuncture points (acupoints) are traditionally believed to reflect the condition of organs at specific points under the skin surface (13, 14). Acupuncture and moxibustion, which stimulate specific acupoints, have long been used as treatment methods. The acupoints known to have therapeutic effects on PD include ST36, GB34, GB20 (GV16), and GV20 (15). In previous clinical studies, stimulation of these acupoints was found to significantly improve the unified PD rating scale in patients with PD (16, 17). Among these, GB34 and GB20 have been reported to suppress neuroinflammation and enhance neurogenesis, and their anti-PD effects have been demonstrated in a previous meta-analysis (16, 18, 19).

Recently, microneedle patches (MPs) have emerged as a new method for effectively stimulating acupoints (20). MPs comprise a micron-scale array of needles with a length of 25 to 2,000 μm, and has the advantage of being non-invasive, causing less pain, being easier to use, and reducing the risk of infection (21, 22). In an unpublished study, we found that the attachment of MPs to the acupoints GB34 and GB20 improved motor disorders in 1-methyl-4-phenyl-1,2,3,6-tetrahydropyridine-induced PD mice by regulating neurotransmitters and heme oxygenase-1(HO-1)/nuclear factor erythroid-2-related factor 2(Nrf2) signaling in the brain. In one prior study, Zhang et al. investigated the effects of thymopentin-containing MPs by attaching acupoints and non-acupoints to immunosuppressed mice (20). The spleens of the group with MPs attached to the acupoints showed a better immunomodulatory effect, confirming the effect of the acupoints. Based on previous studies, we hypothesized that the attachment of MPs to GB20 and GB34 would effectively stimulate acupoints and regulate immunity to improve PD pathology.

In this context, the aim of this study was to investigate whether stimulation of acupoints GB34 and GB20 using MPs could regulate the immune system from the periphery to the brain and improve the pathology of PD in PD mice. We assessed the effects of MPs attached to acupoints on behavioral disorders and histological changes in a mouse model of PD injected with 6-hydroxydopamine (6-OHDA). We further performed flow cytometry of the brain and blood to evaluate the peripheral and central immune systems.

2 Materials and methods

2.1 Materials

6-OHDA, hydrogen peroxide, bovine serum albumin (BSA), tribromoethanol, phosphate buffered saline (PBS), paraformaldehyde (PFA) and sucrose were purchased from Sigma Aldrich (St Louis, MO, United States). Rabbit anti-ionized calcium-binding adapter molecule-1 (Iba-1) was purchased from Fujifilm Wako (Chuo-Ku, Osaka, Japan). 3,3-diaminobenzidine (DAB), rabbit anti-tyrosine hydroxylase (TH) were purchased from Merck Millipore (Burlington, MA, United States). Rabbit anti-Bcl-2–associated X protein (Bax) antibody and rabbit anti-Nrf2 antibody were purchased from Abcam (Cambridge, UK). Rabbit anti-Bcl-2 antibody, mouse horseradish peroxidase (HRP)-conjugated β-actin antibody and goat anti-Glial fibrillary acidic protein (GFAP) were purchased from Santa Cruz Biotechnology (Temecula, CA, USA). Biotinylated goat anti-rabbit antibody, avidin–biotin complex (ABC), normal goat serum, streptavidin-Alexa 594 and Alexa 488 were purchased from Vector

Labs (Burlingame, CA, United States). Anti-rabbit HRP secondary antibodies and rabbit anti-HO-1 antibody were purchased from Enzo Life Science, Inc. (Farmingdale, NY, USA).

2.2 Animals

Seven-week-old male ICR mice were purchased from Daehan Biolink (Eumseong, Republic of Korea). Mice were accommodated at a maintained condition (temperature: 23 ± 1°C, humidity: 60 ± 10% a 12 h light/dark cycle, and water and food ad libitum). All animal studies were performed in accordance with the "Guide for the Care and Use of Laboratory Animals, 8th edition" (National Institutes of Health, 2011) and approved by the "Animal Care and Use Guidelines" of Kyung Hee University, Seoul, Republic of Korea (Approval number: KHSASP-23-536).

2.3 Preparation of MPs

The MN patches were provided by Raphas Co. Ltd. (Seoul, Republic of Korea) and manufactured using a previously reported method (23, 24). Biocompatible microneedles were fabricated using the droplet extension method. A pharmaceutical-grade hyaluronic acid solution was dried on top of a hydrocolloid patch to form five arrays with a 1 mm base width and 350 μm height. A viscous biocompatible polymer was dropped onto the bottom layer of the patch, followed by contact with the other substrates. The two substrates were then separated by a certain distance to stretch the contacting polymer materials. After the tensioning process, drying was conducted to set the shape in the stretched state. Finally, the central part was removed to form identical microneedles on the two substrates. As a Sham patch (SP), only a patch without microneedles was used.

2.4 Surgical procedure for 6-OHDA injection

The injection of 6-OHDA was performed in accordance with previous studies (25, 26). Mice were anesthetized with tribromoethanol (312.5 mg/kg, i.p.) and placed on a stereotaxic apparatus. Each mouse received a unilateral injection of 2 μL vehicle (saline with 0.1% ascorbic acid, for sham-operated mice) or 6-OHDA (8 μg/μL) into the right striatum (ST) (coordinates with respect to bregma in mm: AP 0.5, ML 2.0, DV−3.0), according to the stereotaxic atlas of mouse brain (Franklin and Paxinos, 2013). 6-OHDA was delivered by a microinjection pump at an injection rate of 0.5 μl per min, and the cannula was left in place for 4 min after the end of injection.

2.5 Experimental design

Sixty-four male mice were used for immunohistochemistry and western blot. The mice were randomly divided into four groups as follows: 1) SHAM group (n = 17), 2) 6-OHDA group (6-OHDA-injected, n = 16), 3) SPs group (6-OHDA-injected plus attachment of SPs, n = 15), 4) MPs group (6-OHDA-injected plus attachment of MPs, n = 16). Seven to nine mice per group were sacrificed for immunohistochemistry, and the remaining mice were sacrificed for western blot. Forty male mice were used for flow cytometry and quantitative reverse transcription-polymerase chain reaction (qRT-PCR). The mice were randomly divided into four groups as follows: 1) SHAM group (n = 9), 2) 6-OHDA group (6-OHDA-injected, n = 9), 3) SPs group (6-OHDA-injected plus attachment of SPs, n = 9), 4) MPs group (6-OHDA-injected plus attachment of MPs, n = 9). Five mice per group were sacrificed for flow cytometry, and the remaining mice were sacrificed for mRNA extraction. Before 6-OHDA surgery, the acupoint area was shaved to attach the patches. In the SPs or MPs group, patches were attached to the GB20 and GB34 areas for a total of 14 days, starting one day after 6-OHDA injection (Figure 1). The patch was attached for 2 h, and behavioral experiments or sacrifice were conducted 1 hour after the patch was removed.

2.6 Behavioral tests

2.6.1 Pole test

Pole test was performed on mice for immunohistochemistry and western blot analyses. Prior to the test, the mice underwent a single training session. During the test, each mouse was placed at the top of a pole (diameter = 8 mm, height = 55 cm, rough surface) facing upward. The times required for head down (T-turn) and landing (T-LA) were recorded. If a mouse failed to descend and fell immediately, a maximum time of 60 s was assigned. Three trials were conducted for each mouse, and the average of these trials was calculated (27).

2.6.2 Rotarod test

Rotarod test was performed on mice for immunohistochemistry and western blot analyses. The rotarod device contained a rotating spindle (30 mm in diameter) and five separate compartments for the simultaneous examination of five mice. The rotarod tests were performed for 3 min at a constant speed between 10 and 12 rpm. The training was conducted by placing the mouse on a spindle whenever it fell on the ground. During the test session, the test was performed at the same rotational speed as that of the training. The time that remained on the rotating spindle until the first drop (latency time) was recorded. If no fall occurred, a maximum time of 180 s was assigned. The test was repeated three times, and the average latency time was calculated (27, 28).

2.6.3 Cylinder test

Cylinder test was performed as previously study on mice for immunohistochemistry and western blot analyses (29). Brifly, each mouse was placed in a clear cylinder (8.5 cm diameter, 12 cm height) for 5 min without any habituation prior to recording. The use of the ipsilateral forelimb, contralateral forelimb, or both forelimbs during rat rearing was recorded by a blinded examiner. The results are presented in terms of the ratio of contralateral

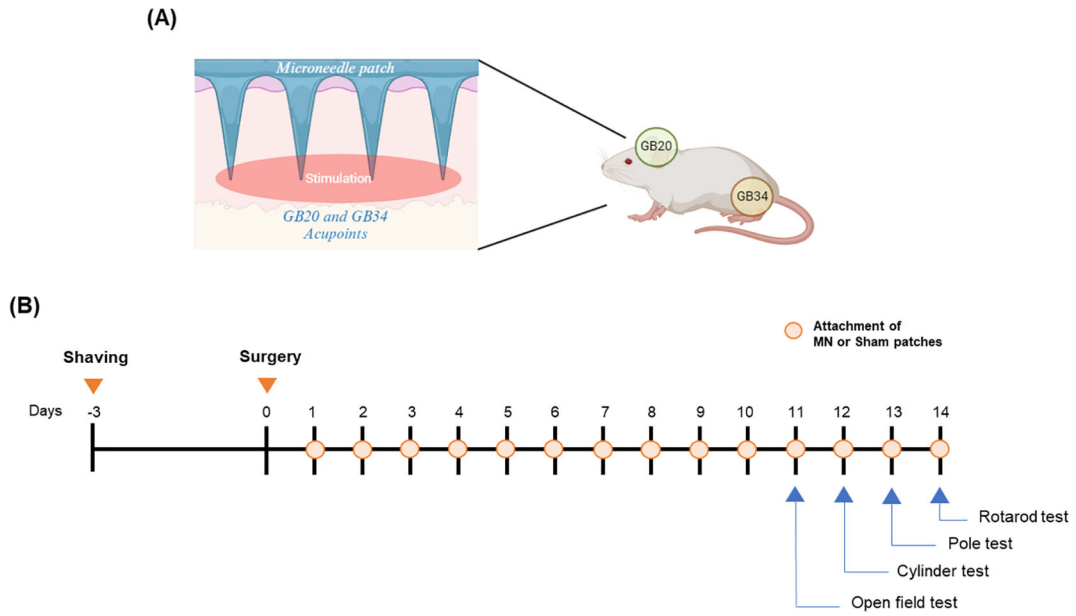

FIGURE 1
Overview of experimental procedure. Attachment points of patches on a mouse **(A)** and overall experimental schedule **(B)**.

forelimb (left) wall touches relative to the number of touches by ipsilateral forelimb (right).

2.6.4 Open field test

OFT was performed on mice flow cytometry and qRT-PCR. For the OFT, the mice were placed in a box (45 × 45 × 45 cm). The central area of the box measured 15 cm × 15 cm. After placing the mouse in the box, the first 5 min was not recorded, and then the position of the mouse was analyzed using an automated computer analysis system (Biobserve, Bonn, Germany) during the 10 min test (30).

2.7 Tissue preparation

On day 14 of SP and MP attachment, mice were anesthetized 1 h after patch removal. Mice for immunohistochemistry were transcardially perfused with 0.05 M PBS, and subsequently fixed with pre-chilled 4% PFA in 0.1 M phosphate buffer. Whole brain tissues were post-fixed with 4% PFA overnight, immersed in a solution containing 30% sucrose in 0.05 M PBS, and stored at 4°C until sectioning. The frozen brains were coronally sectioned on a cryostat at 25 µm, after which they were stored in a storage solution at 4°C. The mice for western blot and qRT-PCR were decapitated, and the ST and substantia nigra (SN) in their vehicle or 6-OHDA injected right hemisphere was isolated and stored at – 80°C until. All tissues used were from the hemisphere injected with 6-OHDA or vehicle only. Half of the ST was used as tissue for measuring dopamine levels, and the other half was used for western blot.The mice used for flow cytometry were anesthetized, and blood was collected from the heart. The right hemisphere of the brain was prepared and injected with vehicle or 6-OHDA. Flow cytometry was performed immediately on the fresh tissue.

2.8 Immunohistochemistry

Brain sections were rinsed in 0.05 M PBS and incubated with 1% hydrogen peroxide (H_2O_2) in 0.05 M PBS for 15 min. Subsequently, sections were replaced with anti-TH antibody (Cat no.: AB152, 1:1000) or anti-DAT antibody (Cat no.: MAB369, 1:1000) in 0.3% Triton X-100, 1% normal goat serum in 0.05 M PBS overnight at 4°C. They were subsequently incubated in an ABC solution with biotinylated anti-rabbit immunoglobulin G (IgG) or anti-rat IgG antibodies (Cat no.: BA-1000, BA-4000, 1:500). For immunofluorescence staining, brain sections were rinsed with 0.05 M PBS, and subsequently incubated with blocking buffer (0.05 M PBS containing 1% BSA, 3% normal goat serum, and 0.4% Triton X-100) for 1 h at room temperature (RT). The sections were incubated with the anti-Iba-1 antibody (Cat no.: 019-19741, 1:1000) or anti-GFAP antibody (Cat no.: SC-6170, 1:2000) overnight at 4°C in the blocking buffer. After rinsing with 1X PBS, cells were visualized with anti-goat Alexa Fluor 594 (Cat no.: A21468, for GFAP) or anti-rabbit Alexa Fluor 488 (Cat no.: A11008, for Iba-1) diluted in blocking buffer (1:500) for 1 h at RT. Images were captured using a microscope (K1-Fluo confocal microscope (Nanoscope Systems, Daejeon, Korea) or Olympus BX51 Fluorescence Microscope (Olympus, Tokyo, Japan). The areas or numbers of TH-, DAT-, Iba-1-, and GFAP-positive cells were analyzed using ImageJ software (National Institutes of Health, Bethesda, MD, USA). All values were calculated by averaging three tissue sections per mouse.

2.9 Western blot

SN tissues were lysed in RIPA buffer containing a protease/phosphatase inhibitor cocktail. Proteins were separated using sodium dodecyl sulfate-polyacrylamide gel electrophoresis and transferred

onto polyvinylidene fluoride membranes. The membranes were blocked with 5% BSA for 30 min, then incubated at 4°C with primary antibody diluted in 1% BSA overnight (TH (Cat no.: AB152) 1:1000; Bcl-2 (Cat no.: SC-783) 1:500; Bax (Cat no.: AB7977) 1:500; Nrf2 (Cat no.: AB31163) 1:500; HO-1 (Cat no.: ADI-SPA-895-F) 1:500; β-actin-HRP (Cat no.: SC-47778HRP) 1:3000). After washing with Tris-buffered saline (10 mM Tris-HCl, 150 mM NaCl, pH 7.5) containing 0.1% Tween 20, the membrane was incubated with a secondary antibody (Cat no.: ADI-SAB-300, 1:3000) at room temperature for 1 h. Proteins were detected using ECL reagent, and visualization and quantification of bands were performed using Image Lab Software (Bio-Rad, CA, USA).

2.10 Measurement of dopamine level

Dopamine levels were measured using a dopamine kit (KA3838, Abnova, Taipei, Taiwan) in half of the ST samples. Tissues were homogenized in 1 mM EDTA and 4 mM sodium metabisulfite to measure dopamine. Subsequently, samples were centrifuged at 12,000 rpm for 20 min and the supernatant was collected for subsequent DA measurements, performed according to the manufacturer's instructions. This assay involved three key steps: extraction, acylation, and enzymatic analysis. Initially, dopamine was extracted from the cell lysate by adding samples to the wells of an extraction plate along with ultrapure water and TE buffer, followed by incubation at room temperature for 60 min with shaking at approximately 600 rpm. After rinsing the plate to remove excess TE buffer, acylation was performed by adding the acylation buffer and reagent to the dried extraction plate and incubating for 15 min at room temperature. The plate was then washed with wash buffer and blotted prior to adding hydrochloric acid to each well, followed by a 10 min incubation at room temperature with shaking. Next, the acylated samples were transferred to new wells, and an enzyme solution was added. The plate was incubated at 37°C for 2 h on a shaker. After this incubation, the supernatant was moved to precoated dopamine microtiter strips, and dopamine antiserum was added to each well. The plate was incubated at 2 to 8°C for 20 h, then washed thoroughly with wash buffer. The enzyme conjugate was added to all wells and incubated for 30 min with shaking. Following another wash, a substrate solution was introduced to the wells and incubated for 25 min. Finally, a stop solution was added, and absorbance due to dye development was measured at 450 nm with a reference wavelength of 630 nm using a microplate reader (31).

2.11 Flow cytometry

Cells from the brain were isolated for flow cytometry as previously described (32). The experimental method for preparing cells from blood for flow cytometry was as follows: fresh blood exceeding 0.6 ml was immediately placed in a heparin tube and reacted on a shaker for 20 min. Subsequently, the suspension was filled with 0.05M PBS up to 1 ml and then slowly dispensed onto the pre-dispensed histopaque. After centrifuging at 400xg for 30 min, the separated peripheral blood mononuclear cell layer was carefully obtained. To this, 200 ul of 2% FBS was added and centrifuged again at 400xg for 10 min to remove the supernatant. Then, 900 μL of red blood cell lysis buffer was added to the remaining pellet, which was reacted for 6 min, and centrifuged at 400xg for 4 min. After removing the supernatant, cells were washed with FACS buffer (containing 1% BSA and 1mM EDTA in sterile 1×PBS) at 400×g for 5 min at 4°C. Cells isolated from the brain and blood were stained with rat anti-mouse CD45R/B220, CD4, CD8a, or CD3. After incubation for 1 h at 4°C, fluorescence data were collected on a Cyto FLEX (Beckman Coulter, Brea, CA, USA) using CytExpert software (Beckman Coulter).

2.12 mRNA extraction and qRT-PCR analysis

Total RNA from tissues was extracted following a previously described method (33). Briefly, Trizol was added to the tissue to lyse and dissolve the cell and nuclear membranes. Following this, chloroform to the mixture, which was then centrifuged to achieve phase separation. The upper aqueous phase, containing the RNA, was carefully collected. RNA precipitation was induced by the addition of isopropanol, followed by a 75% ethanol wash to purify the RNA. The purified RNA was used to synthesize cDNA with TOPscript™ RT DryMIX (Enzynomics, Republic of Korea) for qRT-PCR. RT-PCR was performed using TOPreal™ qPCR 2X PreMIX (SYBR Green; Enzynomics, Republic of Korea), and the CFX Connect Real-Time PCR System (Bio-Rad Laboratories, USA). Primers, synthesized at Cosmo Genetech (Republic of Korea), were as follows: interleukin (IL)-6: forward, 5-CCGGAGAGGAG ACTTCACAG-3, reverse, 5-TTGCCATTGCACAACTCTTT-3; IL-1β: forward, 5-CCCAAGCAATACCCAAAGAA-3, reverse, 5-GCTTGTGCTCTGCTTGTGAG-3; IL-2: forward, 5-AGGAACC TGAAACTCCCCAG-3, reverse, 5-AAATCCAGAACATGCCG CAG-3; IL-4: 5-TCTCGAATGTACCAGGAGCC-3, reverse, 5-ACCTTGGAAGCCCTACAGAC-3; IL-17a: forward, 5-GCCCT CAGACTACCTCAACC-3, reverse, 5-ACACCCACCAGCA TCTTCTC-3.

2.13 Statistical analysis

Differences among the groups were analyzed statistically by one-way analysis of variance (ANOVA) followed by Dunnett's *post-hoc* test or student's *t* test using GraphPad Prism 8.0.1 software (GraphPad Software Inc., USA). All values are presented as mean ± standard error of the mean (S.E.M.). The differences were considered statistically significant at $p < 0.05$ and are expressed in each figure.

3 Results

3.1 MP attachment to acupoints attenuate 6-OHDA-induced PD symptoms in mice

The OFT, pole test, rotarod test, and cylinder test were performed to investigate the effect of MPs attached to acupoints

10.3389/fimmu.2024.1454102

on PD behavioral disorders. In all behavioral experiments, motor impairment was significantly induced by 6-OHDA injection. In the OFT, track length (*p < 0.05), center zone duration (p = 0.76), and number of center zone entries (p = 0.12), and velocity (p = 0.09) increased in the MPs group compared to the 6-OHDA group (Figures 2A–E). In the MPs group, both T-turn (***p < 0.001) and T-LA (*p < 0.05) were significantly decreased compared to those in the 6-OHDA group in the pole test (Figures 2F, G). In the rotarod test, the latency time was decreased by 6-OHDA and significantly increased in the MPs group (*p < 0.05; Figure 2H). In the cylinder test, the use of impaired paws was significantly higher in the MPs group than in the 6-OHDA group (*p < 0.05; Figure 2I). However, in all behavioral experiments, the SPs group showed no significant improvement in behavioral disorders.

3.2 MP attachment to acupoints protects dopaminergic neurons in SN of 6-OHDA-induced PD mice

To evaluate the protective effect of acupoint-attached MPs against dopaminergic neuron loss, immunohistochemistry was performed to measure the optical density of DAT and TH in the ST and the number of TH + cells in the SN (Figure 3A). First, 6-OHDA injection significantly induced the loss of dopaminergic neurons in the ST (DAT, ***p < 0.001; TH, **p < 0.01) and SN (TH, ***p < 0.001). The optical densities of DAT and TH in the ST region showed no significant change owing to the attachment of SP (DAT, p = 0.86; TH, p = 0.99) or MPs (DAT, p = 0.48; TH, p = 0.99; Figures 3B, C). However, the number of TH+ cells measured in the SN increased in the only MPs group compared to the 6-OHDA group ($p < 0.05 in Student's *t*-test; Figure 3D). These results were consistent with the protein levels in the SN (Figure 3E). There were no significant differences in any of the values between the SPs and 6-OHDA groups. However, the protein level of TH was reduced by 6-OHDA injection, whereas MPs enhanced it (p = 0.33; Figure 3F). Moreover, the ratio of Bax and Bcl-2, factors related to apoptosis, increased in the 6-OHDA group and was significantly lowered by MP attachment (*p < 0.05; Figure 3G). The expression levels of Nrf2 and HO-1, which are involved in cell survival through regulation of the oxidative stress response, remained unchanged following 6-OHDA injection but were significantly enhanced by the attachment of MPs to acupoints (*p < 0.05; Figures 3H, I). Finally, measurement of the dopamine contents in the ST revealed decreases induced by 6-OHDA, which tended to increase in the MPs group (p = 0.44; Figure 3J).

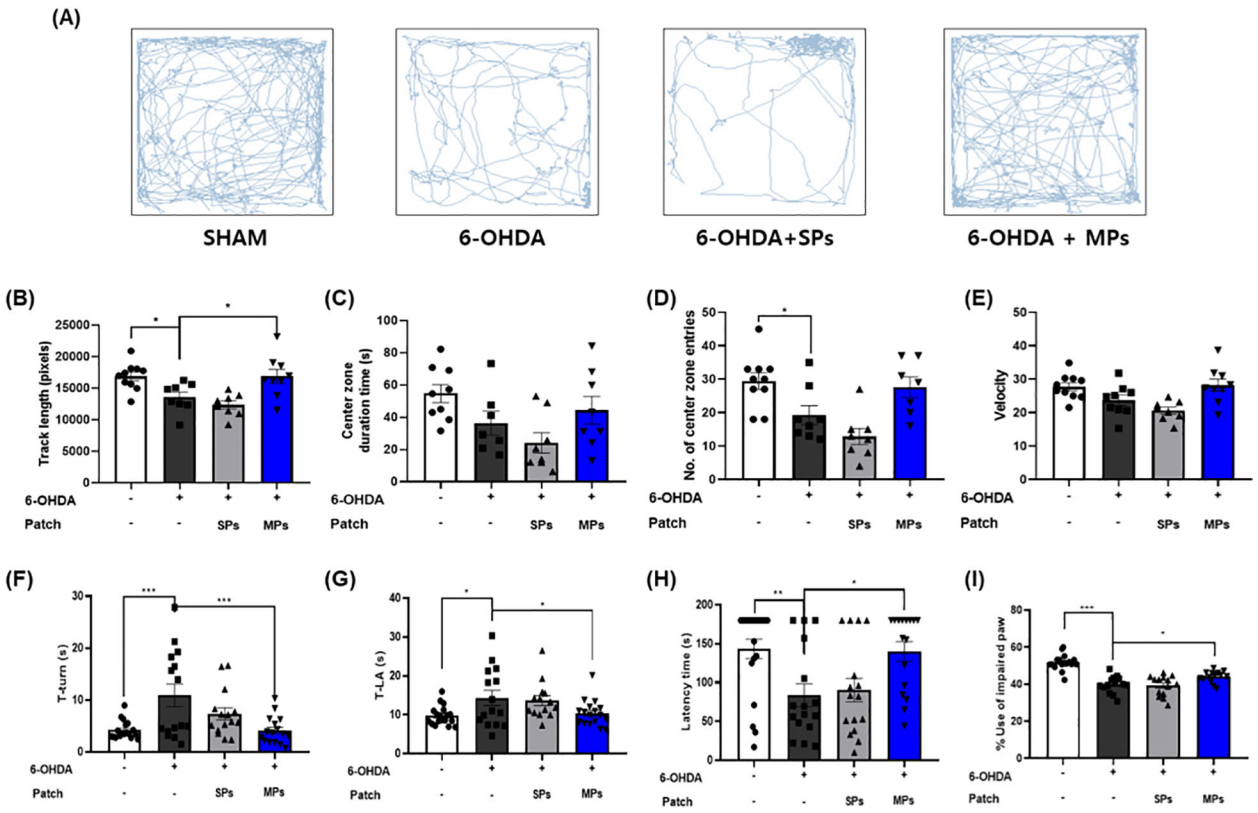

FIGURE 2
Effects of MPs attached to acupoints on PD symptoms in 6-OHDA-injected mice. Behavioral disorders were assessed using the OFT, pole test, rotarod test, and cylinder test. Representative images of the OFT are shown in **(A)**, track length **(B)**, center zone duration time **(C)**, number of center zone entries **(D)**, and velocity **(E)** were measured. T-turn and T-LA in the pole test **(F, G)**, latency time in the rotarod test **(H)**, and impaired paw usage rate in the cylinder **(I)** test were measured. Values are given as the mean ± S.E.M. Data were analyzed by One-way ANOVA followed by *post hoc* Dunnett's multiple comparisons test. *$p < 0.05$, **$p < 0.01$ and ***$p < 0.001$ compared to the 6-OHDA group.

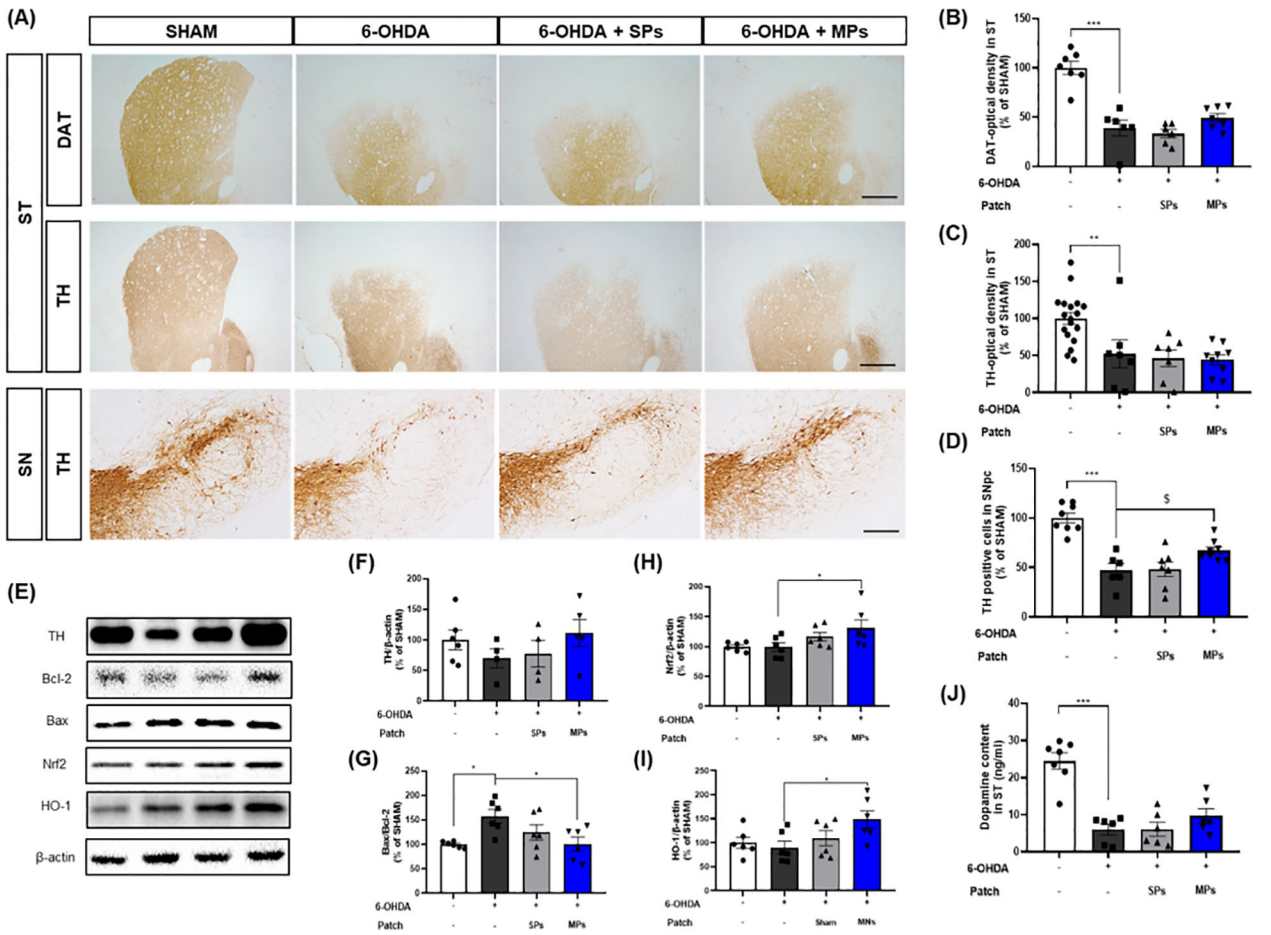

FIGURE 3
Effects of MPs attached to acupoints on dopaminergic neurons in ST and SN of 6-OHDA-injected mice. Representative images of DAT in ST (scale bar = 500 μm) and TH in ST (scale bar = 500 μm) and SN (scale bar = 200 μm) are shown in **(A)**. Graphs were represented as optical density of DAT-immunoreactivity in ST **(B)**, TH-immunoreactivity in ST **(C)** and SN **(D)**. Representative band images of TH, Bcl-2, Bax, Nrf2, and HO-1 in SN are shown in **(E)**. Graphs were represented as expression of TH **(F)**, Bcl-2/Bax ratio **(G)**, Nrf2 **(H)**, and HO-1 **(I)** in SN and dopamine content in ST **(J)**. Values are given as the mean ± S.E.M. Data were analyzed by One-way ANOVA followed by *post hoc* Dunnett's multiple comparisons test or Student's *t*-test. **p* < 0.05, ***p* < 0.01 and ****p* < 0.001 compared to the 6-OHDA group; $*p* < 0.05 using student's *t*-test.

3.3 MP attachment to acupoints reduced neuroinflammation in the brain of 6-OHDA-induced PD mice

The inhibitory effect of the attachment of MPs to acupoints on neuroinflammation was evaluated through immunofluorescence for Iba-1 and GFAP, which are markers of microglia and astrocytes, in the SN and ST. First, Iba-1 staining revealed that the area of Iba-1+ cells was elevated in the 6-OHDA group (SN, *p <0.05; ST, $p< 0.05 in Student's *t*-test). The area of Iba-1+ cells was significantly decreased in the MPs group compared to the 6-OHDA group in both the SN ($p< 0.05 in Student's *t*-test) and ST ($p< 0.05 in Student's *t*-test). Consistent with the results for Iba-1, the area of GFAP+ cells in the SN (**p < 0.01) and ST (***p < 0.001) increased in the 6-OHDA group, and the MPs group showed a significant reduction in GFAP+ cell area compared to the 6-OHDA group (SN and ST, $p< 0.05 in Student's *t*-test). No significant neuroinflammatory effects were observed in the SPs group (Figure 4).

3.4 MP attachment to acupoints balancing central immune system in the brain of 6-OHDA-induced PD mice

Immunity in PD has primarily been investigated in relation to T cells (34). Increased CD3+ T cells infiltration into the brain and a decreased CD4+/CD8+ ratio have been observed in postmortem brain tissue (10). B cells in the brain have only recently begun to be investigated in PD; however, it is believed that they may contribute to neuroinflammation because they are activated by T cells. In addition, the 6-OHDA-induced mouse model used in the present study is recognized for exhibiting an impaired blood-brain barrier (BBB) and a compromised immune system (35, 36). Therefore, to assess the effect of MPs attached to acupoints on the central immune system, we evaluated several key immune markers, including B220 and CD3+, and the CD4 +/CD8 + ratio in the hemisphere injected with 6-OHDA. First, the percentage of B220, a B cell marker, decreased in the MPs group compared to that in the

10.3389/fimmu.2024.1454102

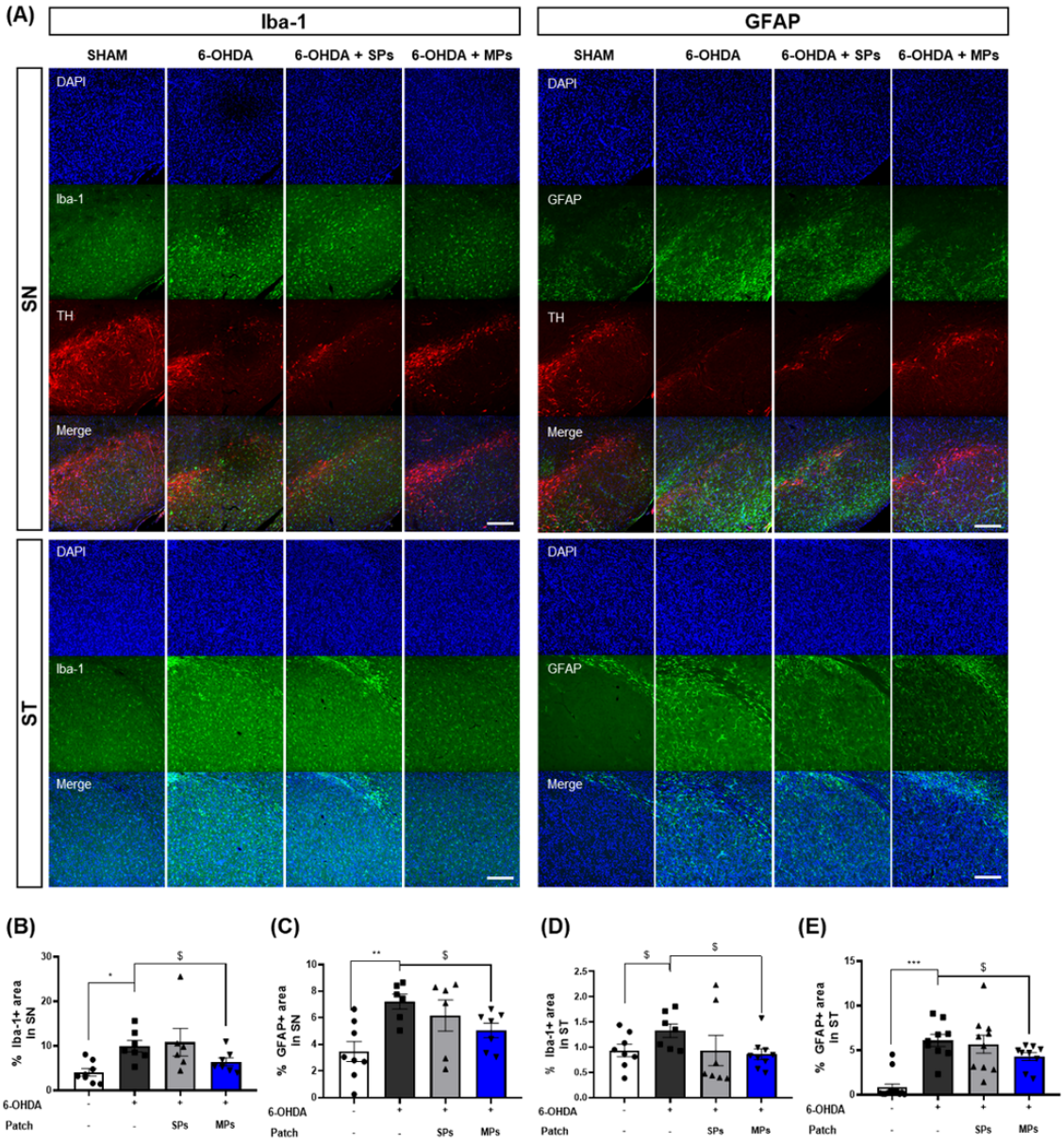

FIGURE 4
Effects of MPs attached to acupoints on expression of Iba-1 and GFAP in ST and SN of 6-OHDA-injected mice. Representative images of Iba-1 and GFAP in SN and ST (scale bar = 200 μm) are shown in **(A)**. Graphs were represented as % Iba-1+ area in SN **(B)** and ST **(D)**. Graphs were represented as % GFAP+ area in SN **(C)** and ST **(E)**. Values are given as the mean ± S.E.M. Data were analyzed by One-way ANOVA followed by *post hoc* Dunnett's multiple comparisons test or Student's *t*-test. **p* < 0.05, ***p* < 0.01 and ****p* < 0.001 compared to the 6-OHDA group using One-way ANOVA; $*p* < 0.05 using student's *t*-test.

6-OHDA group (p = 0.36), although the difference was not significant. In addition, CD3+ T cells, which are the co-receptors of T cells, were investigated. The percentage of CD3+ T cells was elevated in the 6-OHDA group (**p < 0.01) and significantly lower in the MPs group than in the 6-OHDA group (***p < 0.001). Finally, the ratios of helper and killer T cells to T cells were measured. The injection of 6-OHDA significantly reduced the CD4+/CD8+ ratio (**p < 0.01), which was restored by the attachment of MPs to acupoints ($p< 0.05 in Student's *t*-test; Figure 5). Therefore, we surmised that the attachment of MPs to acupoints restored the central immune system disturbed by 6-OHDA injection.

3.5 MP attachment to acupoints modulating mRNA expressions of cytokines in the ST and SN of 6-OHDA-induced PD mice

Cytokines contributing to the differentiation and activation of immune cells are also associated with neuronal death (37). Therefore,

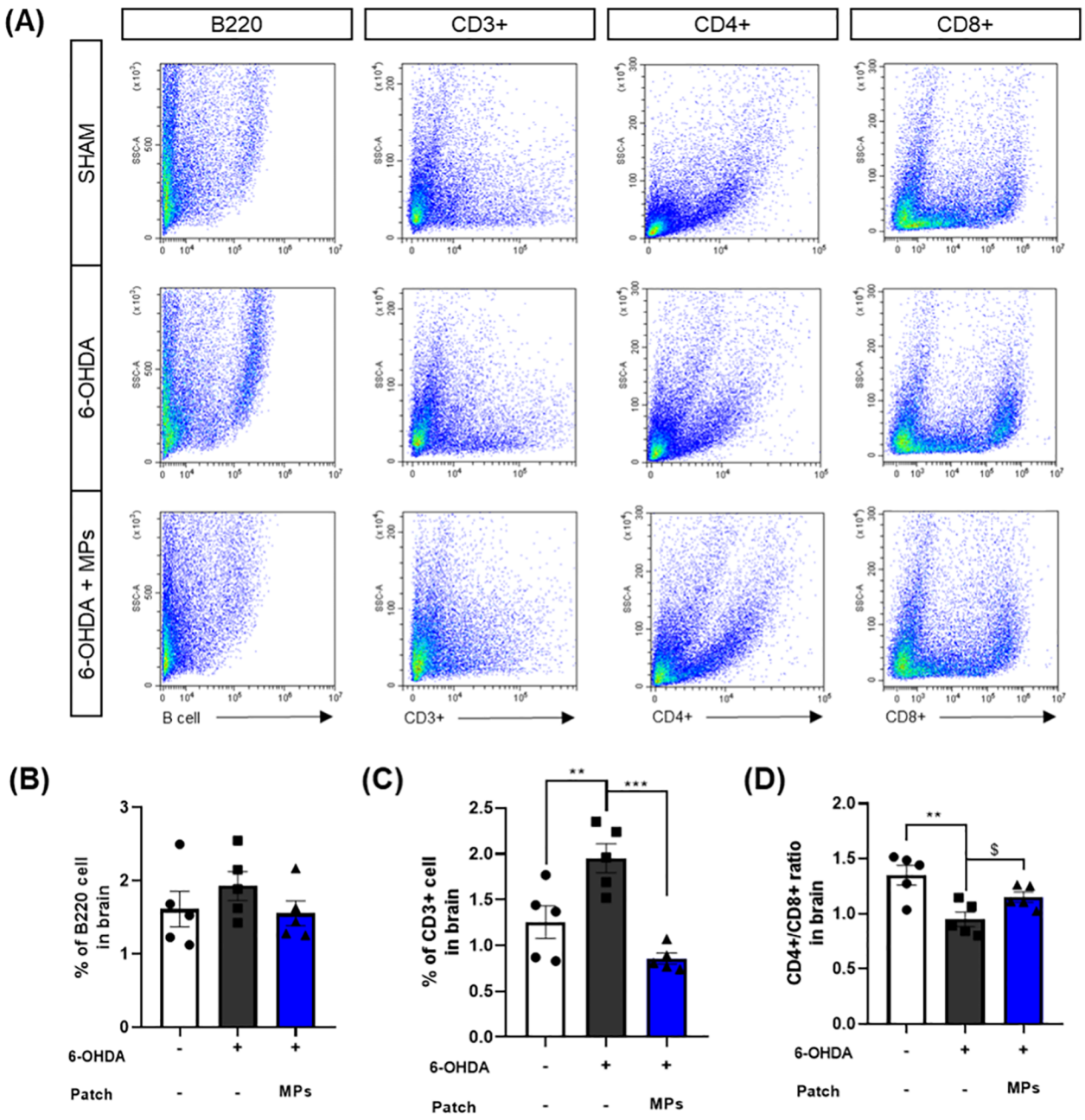

FIGURE 5
Effects of MPs attached to acupoints on % of B220, CD3+, CD4+, and CD8+ cells in the brain of 6-OHDA-injected mice. Representative flow cytometry plots of B220, CD3+, CD4+ and CD8+ cells in brain are shown in **(A)**. Graphs were represented as % of B220 **(B)**, CD3+ **(C)** and CD4+/CD8+ ratio **(D)** in brain. Values are given as the mean ± S.E.M. Data were analyzed by One-way ANOVA followed by *post hoc* Dunnett's multiple comparisons test or Student's *t*-test. $^{**}p < 0.01$ and $^{***}p < 0.001$ compared to the 6-OHDA group using One-way ANOVA; $\$p < 0.05$ using student's *t*-test.

we assessed the mRNA expression of cytokines associated with B and T cells in the ST and SN. In both ST and SN, the mRNA expression levels of IL-6 (ST, **p < 0.01; SN, *p < 0.05), IL-1β (ST, p = 0.1; SN, p = 0.08), IL-2 (ST, **p < 0.01; SN, *p < 0.05), IL-4 (ST, *p < 0.05; SN, p = 0.05), and IL-17a (ST, p = 0.16; SN, p = 0.32)were increased by 6-OHDA injection. In contrast, in the MPs group, the levels of all cytokines were lower than those in the 6-OHDA group. In particular, the decreases in IL-6 (ST, **p < 0.01; SN, *p < 0.05), IL-1β (ST, *p < 0.05; SN, p = 0.09), IL-2 (ST, **p < 0.01; SN, *p < 0.05) and IL-4 (ST, *p < 0.05; SN, p = 0.09) in the ST and IL-6 and IL-2 in the SN were significant (IL-17a: ST, p = 0.11; SN, p = 0.42; Figure 6).

3.6 MP attachment to acupoints balancing peripheral immune system in the blood of 6-OHDA-induced PD mice

We further measured the number of immune cells in the blood to investigate whether the same effect was observed in the peripheral immune system connected to the skin where the MPs were attached. Changes in the T and B cells in the periphery of patients with PD have been reported in many cases (11, 38). The previously mentioned CD3+, CD4+, and CD8+ T cells enter the brain from the periphery when the BBB collapses. In addition, B

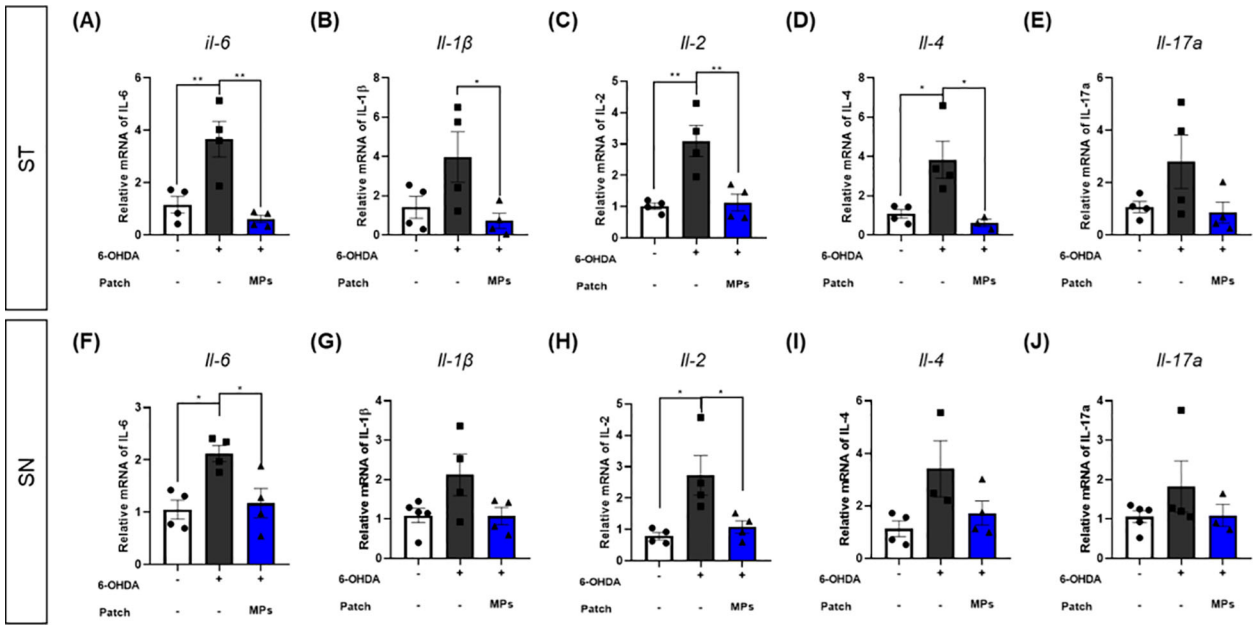

FIGURE 6
Effects of MPs attached to acupoints on mRNA expressions of cytokines in the brain of 6-OHDA-injected mice. The mRNA expressions of IL-6, IL-1β, IL-2, IL-4 and IL-17a in ST **(A–E)** and SN **(F–J)** were measured by qRT-PCR. Values are given as the mean ± S.E.M. Data were analyzed by One-way ANOVA followed by *post hoc* Dunnett's multiple comparisons test. *$p < 0.05$ and **$p < 0.01$ compared to the 6-OHDA group using One-way ANOVA.

cells activated in the periphery due to α-synuclein can induce the secretion of antibodies that are deposited in the center nervous system (39). Therefore, the normalization of peripheral immune cells in PD may have a direct effect on neuroinflammation within the brain.

As in the brain, the percentages of B220 B cells and CD3+ T cells, and the CD4+/CD8+ ratio were assessed in the blood. Injection of 6-OHDA was found to increase the percentages of B220 ($p = 0.44$) and CD3+ ($p = 0.43$) cells, and a decreased CD4+/CD8+ ratio in the blood ($$p < 0.01$ in Student's *t*-test), similar to the results in the brain. This suggests that the intrastriatal injection of 6-OHDA disrupts the peripheral immune system. In the MPs group, the percentages of B220 ($p = 0.29$) and CD3+ ($p = 0.11$) cells were lower and the ratio of CD4+/CD8+ cells was higher ($*p < 0.05$) in the blood than in the 6-OHDA group (Figure 7). These results suggest that MPs attached to acupoints restore the central and peripheral immune systems.

4 Discussion

In this study, we demonstrated that the attachment of MPs to GB20 and GB34 restored the immune system from the periphery to the brain, further inhibiting neuroinflammation and dopaminergic damage in the brain. Additionally, these tissue changes improved the behavioral disorders caused by 6-OHDA injection. We found that the attachment of MPs normalized the percentages of B220 and CD3+ cells and the ratio of CD4+ helper T cells/CD8+ killer T cells in the blood and brain, thus regulating cytokine levels in the brain. Furthermore, MPs attached to acupoints have been shown to inhibit the activation of microglia and astrocytes in the brain and regulate Bcl2/Bax and Nrf2/HO-1. These results indicate that the attachment of MPs to GB20 and GB34 could be a new treatment method for effectively improving PD pathology by mediating the immune system.

Acupoints have been identified in humans, and numerous studies have explored their corresponding locations in animals to facilitate effective research. Various studies have demonstrated that many acupoints in humans correspond to locations in mice (40, 41). Among these points, GB20 is located near the skull, close to the cervical nerves that connect the brainstem and upper spinal cord, and is known to regulate upper nervous system functions (42). Conversely, GB34 is situated at the junction of muscles and tendons and is involved in controlling lower body movement (42). Previous studies have also shown that simultaneous stimulation of both GB20 and GB34 is more effective than stimulating either point alone (43, 44). Based on this evidence, we selected GB20 and GB34 for microneedle stimulation in our study.

According to various studies, immune system dysfunction is prominent in PD, and is closely associated with neuroinflammation, a major pathology of PD (9, 45). It has been reported that aging, the primary risk factor for developing PD, leads to an increase in immune cells, but a decrease in their function (5). Among the variety of related immune cells, the most notable immune change in PD is a decrease in the CD4/CD8 ratio within T cells. In our study, 6-OHDA injection resulted in a decrease in the CD4+/CD8+ ratio in the brain and blood, as well as an increase in T and B cells. Additionally, we observed an increase in cytokine levels and the activation of microglia and astrocytes in the brain. This finding suggests that the 6-OHDA injection model is suitable for evaluating

10.3389/fimmu.2024.1454102

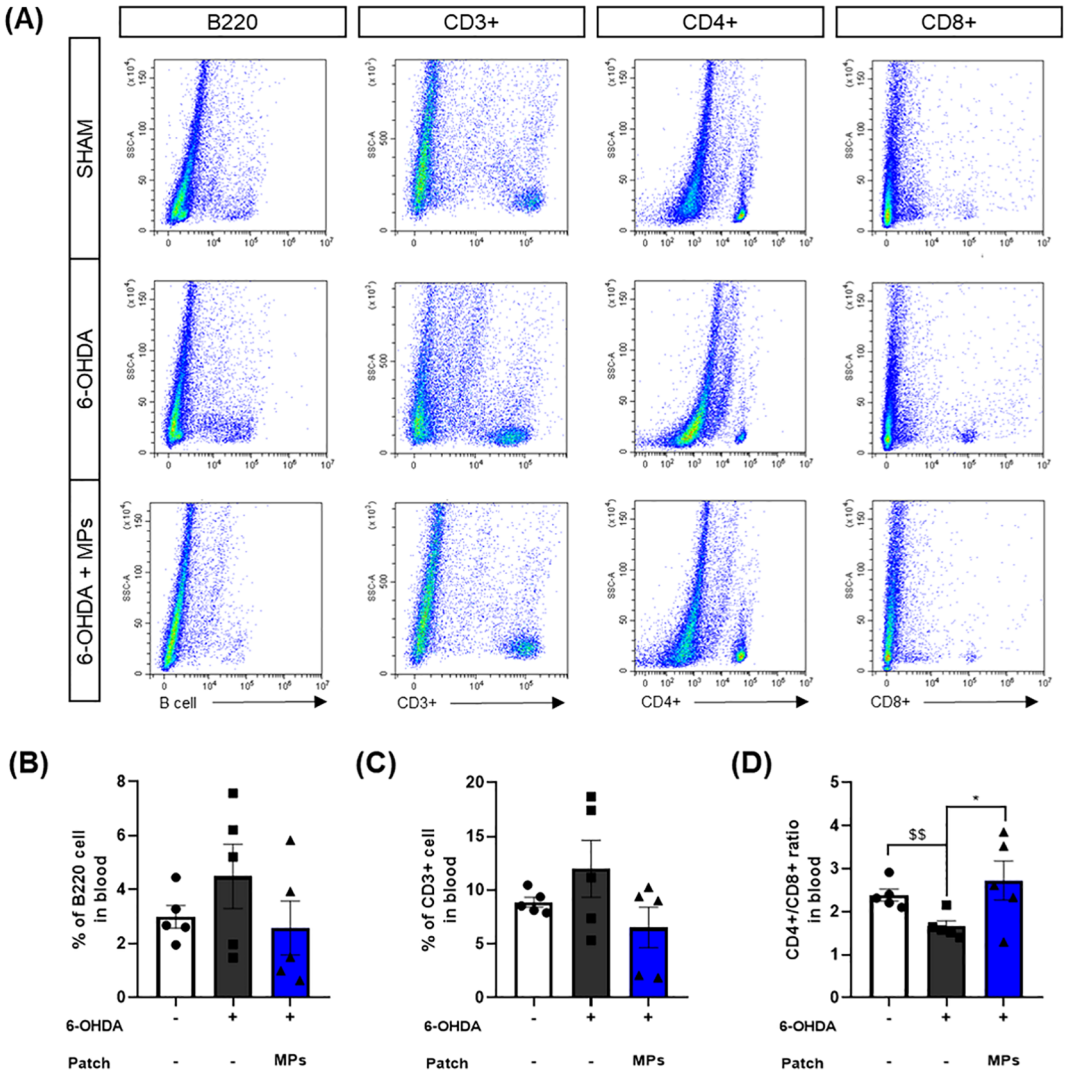

FIGURE 7
Effects of MPs attached to acupoints on % of B220, CD3+, CD4+ and CD8+ cells in the blood of 6-OHDA-injected mice. Representative flow cytometry plots of B220, CD3+, CD4+ and CD8+ cells in blood are shown in **(A)**. Graphs were represented as % of B220 **(B)**, CD3+ **(C)** and CD4+/CD8+ ratio **(D)** in blood. Values are given as the mean ± S.E.M. Data were analyzed by One-way ANOVA followed by *post hoc* Dunnett's multiple comparisons test or Student's *t*-test. *$p < 0.05$ compared to the 6-OHDA group using One-way ANOVA; $$$p < 0.01$ using student's *t*-test.

the effects of inflammation caused by immune disorders in patients with PD.

Additionally, our study demonstrated that the attachment of MPs to GB20 and GB34 normalized the levels of cytokines, B220, and CD3+, and the CD4+/CD8+ ratio caused by 6-OHDA injection in the blood and brain. The MPs attached to the skin at GB20 and GB34 are expected to cause changes in the peripheral immune system, which can further affect the immune system in the brain. Under normal circumstances, the peripheral and central immune systems are separate; however, in PD, the breakdown of the BBB leads to a mingling of the central and peripheral immune systems (39). Therefore, the regulation of peripheral immune cells can affect the brain more easily. This suggests that under normal conditions, the attachment of MPs does not cause significant changes to the brain immune system, and only has a significant effect under pathological conditions. In addition, MP-induced immune normalization reduces cytokine levels and suppresses the activation of microglia and astrocytes in the brain. Therefore, our results suggested that MPs suppress neuroinflammation in the brain via immune regulation.

Further, the current study showed that attachment of MPs to GB20 and GB34 prevented 6-OHDA-induced death of dopaminergic neurons specifically in the SN rather than the ST. In our study, 6-OHDA was injected into the ST, where terminal regions of dopaminergic neurons vulnerable to damage were clustered (46). As such, damage to the ST is more fatal, and recovery takes longer period of time. In our findings, there was no change in TH-optical density in the ST of the MPs group compared to that of the 6-OHDA group, but dopamine levels and DAT-optical density tended to increase in the MPs group. These results indicate that MPs may not have an effect on dopaminergic neurons in the ST, but that they might recover if MPs are applied for a longer period of time.

We found that the PD symptom improvement, dopaminergic neuron protection, and neuroinflammation inhibition effects observed in the MPs group did not occur in the SPs group. This result disproves that the PD improvement effect occurs due to microneedle acupoint stimulation rather than other effects. Our results suggest that MPs can effectively stimulate acupoints, which are key locations for traditional treatments. Therefore, this study is a new attempt to combine traditional and modern technologies.

This study had several limitations. First, it is unclear how MPs attached to the skin alter the peripheral immune system. Previous studies have further shown that acupuncture stimulation of acupoints activates mast cells, resulting in an immune cell response (47, 48). We expect that the immune response to acupuncture occurs similarly to the attachment of MPs, and we plan to analyze the mechanism through further study. Second, this study only selected GB20 and GB34 among many acupoints, and did not compare them with other acupoints. In addition to the GB20 and GB34 acupoints that we selected, other acupoints have been shown to be effective in treating PD, and comparative studies are needed.

Collectively, our results reveal that the attachment of MPs to GB20 and GB34 regulates the immune system from the periphery to the brain, suppressing neuroinflammation and protecting dopaminergic neurons in the brain. Therefore, the stimulation of acupoints using MPs has great potential as a candidate treatment for various diseases, including PD.

Data availability statement

The raw data supporting the conclusions of this article will be made available by the authors, without undue reservation.

Ethics statement

All animal studies were performed in accordance with the "Guide for the Care and Use of Laboratory Animals, 8th edition" (National Institutes of Health, 2011) and approved by the "Animal Care and Use Guidelines" of Kyung Hee University, Seoul, Republic of Korea (Approval number: KHSASP-23-536). The study was conducted in accordance with the local legislation and institutional requirements.

Author contributions

JHK: Conceptualization, Investigation, Methodology, Validation, Writing – original draft, Writing – review & editing. YC: Methodology, Validation, Writing – review & editing. JSK: Investigation, Validation, Writing – review & editing. HL: Validation, Writing – review & editing. IGJ: Writing – review & editing. NYY: Resources, Writing – review & editing. SL: Resources, Writing – review & editing. DHJ: Resources, Writing – review & editing. CN: Funding acquisition, Writing – review & editing. H-JP: Conceptualization, Funding acquisition, Project administration, Writing – review & editing. MSO: Conceptualization, Funding acquisition, Project administration, Supervision, Writing – review & editing.

Funding

The author(s) declare financial support was received for the research, authorship, and/or publication of this article. This research was supported by grants from the National Research Foundation of Korea, funded by the Korean government (grant number 2022M3A9B6017813).

Conflict of interest

Authors NYY, SL, and DHJ were employed by the company Raphas Co. Ltd.

The remaining authors declare that the research was conducted in the absence of any commercial or financial relationships that could be construed as a potential conflict of interest.

Publisher's note

References

1. Barros-Santos T, Clarke G. Gut-initiated neuroprotection in Parkinson's disease: When microbes turn the tables in the battle against neuroinflammation. *Brain Behav Immun*. (2023) 108:350–2. doi: 10.1016/j.bbi.2022.12.016

2. Huh E, Choi JG, Choi Y, Ju IG, Noh D, Shin DY, et al. 6-shogaol, an active ingredient of ginger, improves intestinal and brain abnormalities in proteus mirabilis-induced parkinson's disease mouse model. *Biomol Ther (Seoul)*. (2023) 31:417–24. doi: 10.4062/biomolther.2023.098

3. Morris HR, Spillantini MG, Sue CM, Williams-Gray CH. The pathogenesis of Parkinson's disease. *Lancet*. (2024) 403:293–304. doi: 10.1016/S0140-6736(23)01478-2

4. Balestrino R, Schapira AHV. Parkinson disease. *Eur J Neurol*. (2020) 27:27–42. doi: 10.1111/ene.14108

5. Tansey MG, Wallings RL, Houser MC, Herrick MK, Keating CE, Joers V. Inflammation and immune dysfunction in Parkinson disease. *Nat Rev Immunol*. (2022) 22:657–73. doi: 10.1038/s41577-022-00684-6

6. Li C, Ke B, Chen J, Xiao Y, Wang S, Jiang R, et al. Systemic inflammation and risk of Parkinson's disease: A prospective cohort study and genetic analysis. *Brain Behav Immun*. (2024) 117:447–55. doi: 10.1016/j.bbi.2024.02.013

7. Boo KJ, Gonzales EL, Remonde CG, Seong JY, Jeon SJ, Park YM, et al. Hycanthone inhibits inflammasome activation and neuroinflammation-induced depression-like behaviors in mice. *Biomol Ther (Seoul)*. (2023) 31:161–7. doi: 10.4062/biomolther.2022.073

8. Regensburger M, Rasul Chaudhry S, Yasin H, Zhao Y, Stadlbauer A, Buchfelder M, et al. Emerging roles of leptin in Parkinson's disease: Chronic inflammation,

neuroprotection and more? *Brain Behav Immun*. (2023) 107:53–61. doi: 10.1016/j.bbi.2022.09.010

9. Cossu D, Hatano T, Hattori N. The role of immune dysfunction in parkinson's disease development. *Int J Mol Sci*. (2023) 24:16766. doi: 10.3390/ijms242316766

10. Contaldi E, Magistrelli L, Comi C. T lymphocytes in parkinson's disease. *J Parkinsons Dis*. (2022) 12:S65–74. doi: 10.3233/JPD-223152

11. Lauritsen J, Romero-Ramos M. The systemic immune response in Parkinson's disease: focus on the peripheral immune component. *Trends Neurosci*. (2023) 46:863–78. doi: 10.1016/j.tins.2023.07.005

12. Marogianni C, Sokratous M, Dardiotis E, Hadjigeorgiou GM, Bogdanos D, Xiromerisiou G. Neurodegeneration and inflammation-an interesting interplay in parkinson's disease. *Int J Mol Sci*. (2020) 21:8421. doi: 10.3390/ijms21228421

13. Jang JH, Yeom MJ, Ahn S, Oh JY, Ji S, Kim TH, et al. Acupuncture inhibits neuroinflammation and gut microbial dysbiosis in a mouse model of Parkinson's disease. *Brain Behav Immun*. (2020) 89:641–55. doi: 10.1016/j.bbi.2020.08.015

14. Sun L, Yong Y, Wei P, Wang Y, Li H, Zhou Y, et al. Electroacupuncture ameliorates postoperative cognitive dysfunction and associated neuroinflammation via NLRP3 signal inhibition in aged mice. *CNS Neurosci Ther*. (2022) 28:390–400. doi: 10.1111/cns.13784

15. Pereira CR, MaChado J, Rodrigues J, de Oliveira NM, Criado MB, Greten HJ. Effectiveness of acupuncture in parkinson's disease symptoms-A systematic review. *Healthcare (Basel)*. (2022) 10. doi: 10.3390/healthcare10112334

16. Lee SH, Lim S. Clinical effectiveness of acupuncture on Parkinson disease: A PRISMA-compliant systematic review and meta-analysis. *Med (Baltimore)*. (2017) 96:e5836. doi: 10.1097/MD.0000000000005836

17. Zhao Y, Zhang Z, Qin S, Fan W, Li W, Liu J, et al. Acupuncture for parkinson's disease: efficacy evaluation and mechanisms in the dopaminergic neural circuit. *Neural Plast*. (2021) 2021:9926445. doi: 10.1155/2021/9926445

18. Zhou M, Pang F, Liao D, He X, Yang Y, Tang C. Electroacupuncture at Fengchi (GB20) and Yanglingquan(GB34) Ameliorates Paralgesia through Microglia-Mediated Neuroinflammation in a Rat Model of Migraine. *Brain Sci*. (2023) 13. doi: 10.3390/brainsci13040541

19. Wen X, Li K, Wen H, Wang Q, Wu Z, Yao X, et al. Acupuncture-related therapies for parkinson's disease: A meta-analysis and qualitative review. *Front Aging Neurosci*. (2021) 13:676827. doi: 10.3389/fnagi.2021.676827

20. Zhang Q, Xu C, Lin S, Zhou H, Yao G, Liu H, et al. Synergistic immunoreaction of acupuncture-like dissolving microneedles containing thymopentin at acupoints in immune-suppressed rats. *Acta Pharm Sin B*. (2018) 8:449–57. doi: 10.1016/j.apsb.2017.12.006

21. Ruan S, Zhang Y, Feng N. Microneedle-mediated transdermal nanodelivery systems: a review. *Biomater Sci*. (2021) 9:8065–89. doi: 10.1039/D1BM01249E

22. Dixon RV, Skaria E, Lau WM, Manning P, Birch-Machin MA, Moghimi SM, et al. Microneedle-based devices for point-of-care infectious disease diagnostics. *Acta Pharm Sin B*. (2021) 11:2344–61. doi: 10.1016/j.apsb.2021.02.010

23. Lee KH, Kim JD, Jeong DH, Kim SM, Park CO, Lee KH. Development of a novel microneedle platform for biomarker assessment of atopic dermatitis patients. *Skin Res Technol*. (2023) 29:e13413. doi: 10.1111/srt.13413

24. Kim JD, Kim M, Yang H, Lee K, Jung H. Droplet-born air blowing: novel dissolving microneedle fabrication. *J Control Release*. (2013) 170:430–6. doi: 10.1016/j.jconrel.2013.05.026

25. Eo H, Kwon Y, Huh E, Sim Y, Choi JG, Jeong JS, et al. Protective effects of DA-9805 on dopaminergic neurons against 6-hydroxydopamine-induced neurotoxicity in the models of Parkinson's disease. *BioMed Pharmacother*. (2019) 117:109184. doi: 10.1016/j.biopha.2019.109184

26. Ham HJ, Yeo IJ, Jeon SH, Lim JH, Yoo SS, Son DJ, et al. Botulinum toxin A ameliorates neuroinflammation in the MPTP and 6-OHDA-induced parkinson's disease models. *Biomol Ther (Seoul)*. (2022) 30:90–7. doi: 10.4062/biomolther.2021.077

27. Sedelis M, Schwarting RK, Huston JP. Behavioral phenotyping of the MPTP mouse model of Parkinson's disease. *Behav Brain Res*. (2001) 125:109–25. doi: 10.1016/S0166-4328(01)00309-6

28. Zhang QS, Heng Y, Mou Z, Huang JY, Yuan YH, Chen NH. Reassessment of subacute MPTP-treated mice as animal model of Parkinson's disease. *Acta Pharmacol Sin*. (2017) 38:1317–28. doi: 10.1038/aps.2017.49

29. Magno LAV, Collodetti M, Tenza-Ferrer H, Romano-Silva MA. Cylinder test to assess sensory-motor function in a mouse model of parkinson's disease. *Bio Protoc*. (2019) 9:e3337. doi: 10.21769/BioProtoc.3337

30. Goodnough CL, Montoya J, Cartusciello EB, Floranda EL, Gross ER. Nicotinamide adenine dinucleotide does not improve anesthetic recovery in rodents. *Res Sq*. (2024). doi: 10.21203/rs.3.rs-4515123/v1

31. Magalingam KB, Somanath SD, Md S, Haleagrahara N, Fu JY, Selvaduray KR, et al. Tocotrienols protect differentiated SH-SY5Y human neuroblastoma cells against 6-hydroxydopamine-induced cytotoxicity by ameliorating dopamine biosynthesis and dopamine receptor D2 gene expression. *Nutr Res*. (2022) 98:27–40. doi: 10.1016/j.nutres.2021.09.003

32. Kim N, Ju IG, Jeon SH, Lee Y, Jung MJ, Gee MS, et al. Inhibition of microfold cells ameliorates early pathological phenotypes by modulating microglial functions in Alzheimer's disease mouse model. *J Neuroinflamm*. (2023) 20:282. doi: 10.1186/s12974-023-02966-9

33. Chomczynski P, Sacchi N. Single-step method of RNA isolation by acid guanidinium thiocyanate-phenol-chloroform extraction. *Anal Biochem*. (1987) 162:156–9. doi: 10.1016/0003-2697(87)90021-2

34. Bhatia D, Grozdanov V, Ruf WP, Kassubek J, Ludolph AC, Weishaupt JH, et al. T-cell dysregulation is associated with disease severity in Parkinson's Disease. *J Neuroinflamm*. (2021) 18:250. doi: 10.1186/s12974-021-02296-8

35. Theodore S, Maragos W. 6-Hydroxydopamine as a tool to understand adaptive immune system-induced dopamine neurodegeneration in Parkinson's disease. *Immunopharmacol Immunotoxicol*. (2015) 37:393–9. doi: 10.3109/08923973.2015.1070172

36. Carvey PM, Zhao CH, Hendey B, Lum H, Trachtenberg J, Desai BS, et al. 6-Hydroxydopamine-induced alterations in blood-brain barrier permeability. *Eur J Neurosci*. (2005) 22:1158–68. doi: 10.1111/j.1460-9568.2005.04281.x

37. Liu Z, Qiu AW, Huang Y, Yang Y, Chen JN, Gu TT, et al. IL-17A exacerbates neuroinflammation and neurodegeneration by activating microglia in rodent models of Parkinson's disease. *Brain Behav Immun*. (2019) 81:630–45. doi: 10.1016/j.bbi.2019.07.026

38. Munoz-Delgado L, Macias-Garcia D, Perinan MT, Jesus S, Adarmes-Gomez AD, Bonilla Toribio M, et al. Peripheral inflammatory immune response differs among sporadic and familial Parkinson's disease. *NPJ Parkinsons Dis*. (2023) 9:12. doi: 10.1038/s41531-023-00471-7

39. Weiss F, Labrador-Garrido A, Dzamko N, Halliday G. Immune responses in the Parkinson's disease brain. *Neurobiol Dis*. (2022) 168:105700. doi: 10.1016/j.nbd.2022.105700

40. Yin CS, Jeong HS, Park HJ, Baik Y, Yoon MH, Choi CB, et al. A proposed transpositional acupoint system in a mouse and rat model. *Res Vet Sci*. (2008) 84:159–65. doi: 10.1016/j.rvsc.2007.04.004

41. Sung-Tae Koo S-KK, Kim E-H. Jae-Hyo Kim, Dae-Hwan Youn,Bong-Hyo Lee, Youn-Byoung Chae, Il-Hwan Choi, Sun-Mi Choi, Acupuncture point locations for experimental animal studies in rats and mice. *Korean J acupuncture*. (2010) 27:67–78.

42. Lyu RY, Wen ZL, Tang WC, Yang XM, Wen JL, Wang B, et al. Data mining-based detection of the clinical effect on motion style acupuncture therapy combined with conventional acupuncture therapy in chronic neck pain. *Technol Health Care*. (2022) 30:521–33. doi: 10.3233/THC-228048

43. Xu X, Liu L, Zhao L, Li B, Jing X, Qu Z, et al. Effect of electroacupuncture on hyperalgesia and vasoactive neurotransmitters in a rat model of conscious recurrent migraine. *Evid Based Complement Alternat Med*. (2019) 2019:9512875. doi: 10.1155/2019/9512875

44. Liu L, Xu XB, Qu ZY, Zhao LP, Zhang CS, Li ZJ, et al. Determining 5HT(7)R's involvement in modifying the antihyperalgesic effects of electroacupuncture on rats with recurrent migraine. *Front Neurosci*. (2021) 15:668616. doi: 10.3389/fnins.2021.668616

45. Tan EK, Chao YX, West A, Chan LL, Poewe W, Jankovic J. Parkinson disease and the immune system - associations, mechanisms and therapeutics. *Nat Rev Neurol*. (2020) 16:303–18. doi: 10.1038/s41582-020-0344-4

46. Afonso-Oramas D, Cruz-Muros I, Castro-Hernandez J, Salas-Hernandez J, Barroso-Chinea P, Garcia-Hernandez S, et al. Striatal vessels receive phosphorylated tyrosine hydroxylase-rich innervation from midbrain dopaminergic neurons. *Front Neuroanat*. (2014) 8:84. doi: 10.3389/fnana.2014.00084

47. Li Y, Yu Y, Liu Y, Yao W. Mast cells and acupuncture analgesia. *Cells*. (2022) 11. doi: 10.3390/cells11050860

48. Chen LZ, Kan Y, Zhang ZY, Wang YL, Zhang XN, Wang XY, et al. Neuropeptide initiated mast cell activation by transcutaneous electrical acupoint stimulation of acupoint LI4 in rats. *Sci Rep*. (2018) 8:13921. doi: 10.1038/s41598-018-32048-3

frontiers | Frontiers in Immunology

TYPE Opinion
PUBLISHED 16 December 2024
DOI 10.3389/fimmu.2024.1519032

OPEN ACCESS

EDITED BY
Rajnikant Mishra,
Banaras Hindu University, India

REVIEWED BY
Roberto Crocchiolo,
Niguarda Ca' Granda Hospital, Italy
Norbert Ahrens,
Amedes MVZ for Laboratory Diagnostics Raubling GmbH, Germany
Suryanarayan Biswal,
Central University of Punjab, India
Vishal Gupta,
National Cancer Institute at Frederick (NIH), United States

*CORRESPONDENCE
Yandy Marx Castillo-Aleman
yandy.castillo@adscc.ae

RECEIVED 29 October 2024
ACCEPTED 30 November 2024
PUBLISHED 16 December 2024

CITATION
Castillo-Aleman YM and Krystkowiak PC (2024) Extracorporeal photopheresis in stiff person syndrome.
Front. Immunol. 15:1519032.
doi: 10.3389/fimmu.2024.1519032

Extracorporeal photopheresis in stiff person syndrome

Yandy Marx Castillo-Aleman[1]*
and Pierre Christophe Krystkowiak[2]

[1]Department of Immunology, Abu Dhabi Stem Cells Center (ADSCC), Abu Dhabi, United Arab Emirates, [2]Department of Neurology, Specialized Rehabilitation Hospital/Capital Health, Abu Dhabi, United Arab Emirates

KEYWORDS

extracorporeal photopheresis, immunomodulation, movement disorders, neuroimmunomodulation, stiff person syndrome

1 Introduction

Stiff person spectrum disorders (SPSDs) are a rare group of neuroimmunological disorders characterized by progressive rigidity and triggered painful spasms of the limb muscles. Despite the first description by Moersch and Woltman in 1956 of the formerly coined "stiff man syndrome" (1) or as a gender-neutral term of "stiff person syndrome (SPS)," (2) this condition has a clinical spectrum that includes not only classical SPS but also other SPS variants, such as progressive encephalomyelitis with rigidity and myoclonus (PERM) (3).

Classical SPS is the predominant clinical form and presents as an insidious onset with rigidity and stiffness of the trunk muscles, which advance to joint deformities, impaired posturing, and abnormal gait (1, 3). Patients may also develop painful generalized muscle spasms triggered by unexpected stimuli and may be associated with other autoimmune disorders (3, 4). The clinical features of SPS variants include focal or segmental SPS ("stiff limb syndrome"), jerky SPS, SPS with epilepsy, SPS with dystonia, cerebellar, and paraneoplastic variants (3–5).

In addition to axial and limb muscle stiffness and diffuse myoclonus, patients with PERM ("SPS-plus syndrome") exhibit relapsing–remitting brain stem symptoms, breathing issues, and prominent autonomic dysfunction (6).

Despite significant advances in the treatment of SPSDs, the prognosis remains unpredictable, with an inadequate response in many patients, leading to severe disability and sudden death (5, 7). Moreover, most patients receiving standard-of-care medications may require progressively higher doses, leading to intolerable adverse events (5), among other limitations of pharmacological interventions discussed later. Therefore, there is a need to identify innovative therapies in which we describe the potential use of extracorporeal photopheresis (ECP) as a rational approach for patients with SPSDs, specifically classical SPS. Of note, there are no case reports, patient cohorts, or clinical trials have been reported on the use of ECP in SPS yet. Accordingly, this study aims to propose ECP as a potential treatment for SPS by analyzing the current evidence supporting its clinical application.

2 Etiopathophysiology

SPSDs are associated with high titers of autoantibodies to different antigens of inhibitory synapses, generating low level of synthesis and release of γ-aminobutyric acid (GABA) on presynaptic or postsynaptic neuronal junctions within the central nervous system (CNS), resulting in impaired functioning (3, 8).

Glutamic acid decarboxylase (GAD), a cytoplasmic enzyme with two isoforms (GAD67 and GAD65) that transforms glutamate into GABA, has been widely recognized as a primary target identified in classical SPS, predominately anti-GAD65 antibodies (3, 8).

However, other autoantibodies have also been reported, and various correlations with SPSD variants have been established, including antibodies against GABA receptor-associated protein and dipeptidyl-peptidase-like protein-6 (DPPX) in classical SPS, amphiphysin and gephyrin in paraneoplastic variants, and glycine receptor associated with PERM (3, 9).

The classical SPS etiopathophysiology has been explained by the B cell-mediated inhibition of GABAergic neurons and their synapses, whereas GAD65-specific T cells accumulated in the CNS could drive the intrathecal GAD65 IgG production (3, 10). T cell-mediated cytotoxicity has also been reported in SPS, as GAD65-specific T cells can initiate cytotoxic immune responses (11).

Despite evidence suggesting that GAD65-specific T cells are likely to be scarce and mainly confined to the naïve repertoire in blood (10), there is a systemic and oligoclonal immune response mediated by stable B cell clones (12) leading to serum titers that are 50-fold higher than cerebrospinal fluid (CSF) titers (4).

Interestingly, the serum and CSF anti-GAD antibodies first reported by Solimena et al. in a patient with SPS, diabetes mellitus, and epilepsy (13) were not consistently correlated with the clinical fluctuations of the disease (4, 11). These autoantibodies are directed to GAD65 intracellular antigens and have been postulated to interact with peptide fragments during GABA exocytosis on neuronal surfaces, exerting a change in the synaptic transmission by blocking either GAD function or synthesis (14).

GAD65-specific memory T cells could enter the CNS and mount effector responses against GAD65-expressing neurons, including infiltrating $CD8^+$ T cells (11) detected in the spinal cord of deceased patients with SPS, along with neuronal loss and axonal swelling (15).

3 Current therapies

SPS treatment includes drugs that increase the GABAergic tone in combination with immunomodulating or immunosuppressant agents (4, 5).

At the onset of SPS symptoms or appropriate diagnosis, diazepam or other benzodiazepines (GABA agonists) are commonly used as the cornerstone of symptomatic therapies. However, other drugs, including muscle relaxants, botulinum toxin injections, and centrally acting agents, are also used (11).

SPS immunotherapies are usually the first-line treatment and include corticosteroids, therapeutic plasma exchange, high-dose intravenous immunoglobulins (IVIg), and subcutaneous immunoglobulins (SCIg) (11).

Anti-B cell therapies have recently been proposed as a rational approach in second-line therapies, along with mycophenolate mofetil, azathioprine, or a combination of therapies (4, 5, 11). Treatment with autologous anti-CD19 chimeric antigen receptor (CAR) T cells has also been successfully reported in a patient with refractory SPS (16). Third-line therapies include cyclophosphamide or a combination of therapies (e.g., IVIg and rituximab or mycophenolate mofetil) (11).

Autologous non-myeloablative hematopoietic stem cell transplantation (HSCT) in disabled patients with SPS has also been reported, despite its variable beneficial effects (fourth-line therapies) (11, 17).

Commonly, SPS pharmacological treatment is combined with nonpharmacological interventions (e.g., selective physical therapy, deep tissue massage techniques, heat therapy, osteopathic and chiropractic manipulation, and acupuncture) in a multifaceted approach (11). Nevertheless, current pharmacological interventions lead to heterogeneous clinical responses and pose various limitations (Table 1), which support exploring further strategies, such as ECP, that might be added to the SPS therapeutic armamentarium.

4 Rationale supporting ECP

ECP is a leukapheresis-based immunotherapy in which autologous leukocytes are exposed to a photosensitizing agent and ultraviolet-A (UVA) irradiation before being reinfused. The photosensitizing agent 8-methoxypsoralen (8-MOP) conjugates with the DNA of leukocytes upon UVA photoactivation, resulting in the inhibition of DNA synthesis and cell division and the induction of apoptosis, generating a cascade of events (18).

It has been approved for the palliative treatment of cutaneous T cell lymphoma, and many other indications have been successfully explored, including graft-versus-host disease, rejection of solid organ transplantation, and a few autoimmune diseases (18).

During a regular ECP procedure, nearly 5%–10% of the total blood-circulating mononuclear cells are drawn and exposed to 8-MOP and UVA, and the susceptibility to ECP-induced apoptosis varies from cell to cell (18, 19). For instance, B and T cells are highly susceptible to 8-MOP/UVA exposure, whereas monocytes and regulatory T cells (Tregs) are more resistant to ECP (18).

ECP exerts "direct effects," including apoptosis of treated leukocytes, followed by phagocytosis, which trigger cascades of downstream "indirect effects." (20) Many cell interactions initiate a cascade of immunological changes, differentiation of monocytes into dendritic cells (DCs), and successive presentation of antigens

TABLE 1 Potential limitations of SPS pharmacological interventions (4, 5, 9, 11, 15).

Category	Examples	Potential limitations
Symptomatic therapy	- Benzodiazepines - Baclofen - Botulinum toxin	- Heterogeneity of clinical outcomes - Treatment response per phenotype - Differences in individual tolerability - Adverse events (e.g., respiratory depression) - Symptomatic withdrawal or rebound after treatment discontinuation (e.g., if malfunctioning baclofen pumps) - Combination of symptomatic therapies often required
First-line immunotherapy	- Corticosteroids - IVIg/SCIg - Plasma exchange	- Adverse events (e.g., increased risk of developing diabetes, infusion reactions, risk of thrombosis, renal dysfunction, stroke, aseptic meningitis) - Treatment response per phenotype - Long-term maintenance treatment is needed - Logistical and financial issues
Second-line immunotherapy	- Rituximab - Mycophenolate mofetil - Azathioprine	- Heterogeneity of clinical outcomes with subtherapeutic responses - Long-term maintenance treatment is needed - Adverse events (e.g., severe immunosuppression)
Third-line immunotherapy	- Cyclophosphamide - Combination of therapies	- Heterogeneity of clinical outcomes with subtherapeutic responses - Predictors of response are poorly defined - Adverse events (e.g., severe immunosuppression)
Fourth-line immunotherapy	- CAR-T cells - Autologous HSCT	- Heterogeneity of clinical outcomes with subtherapeutic responses - Predictors of response are poorly defined - Logistical and financial issues

IVIg/SCIg, intravenous/subcutaneous immunoglobulins; CAR-T, chimeric antigen receptor (CAR) T cells; HSCT, hematopoietic stem cell transplantation.

(18). ECP-treated cells also recruit other modulators, such as phagocytes, via soluble and membrane-bound "find me" signals (21). The "indirect effects" of ECP include the eradication of (pathogenic) clonal cells, a shift in antigen-presenting cell (APC) populations, changes in cytokine secretion, and modulation of Tregs and regulatory B cells (Bregs) (20, 22).

4.1 Blood–brain barrier: An objection for ECP?

Although the CNS has been considered an immunoprivileged site, current evidence shows the effective recruitment of immune cells across the blood–brain barrier (BBB) into perivascular and parenchymal spaces (23).

T cell responses targeting CNS antigens are initiated in secondary lymphoid organs, and not in the CNS (10). In fact, activated T cells may penetrate the BBB, regardless of their specificity, and intrathecally are retained those T cells which encounter their cognate antigen (24).

In this regard, Skorstad et al. indicated that GAD65-specific T cells may first be activated in the periphery and later accumulate in the CNS, including proliferation and promotion of B cell differentiation into GAD65 IgG-producing plasma cells within the intrathecal compartment of patients with SPS (10).

Compared with serum anti-GAD65 antibodies, the CSF antibodies of patients with SPS exhibit a 10-fold higher binding avidity, indicating intrathecal synthesis by clonally restricted GAD65-specific B cells driven by local antigens within the confines of the BBB (4, 10).

Additionally, DCs involved in both primary and secondary immune responses can migrate not only into the perivascular space under degeneration and neuroinflammation (23), but also into the CSF-drained spaces of the CNS, even in the absence of neuroinflammation (25, 26). Furthermore, DCs can traffic to peripheral lymphoid organs (e.g., cervical lymph nodes) and present CNS antigens to T cells in the periphery (26).

Therefore, although the BBB may diminish the effects of ECP, the periphery–CNS trafficking of immune cells and anti-GAD65 antibody production can justify its investigational use in preclinical models and, eventually, in clinical trials.

4.2 Weighing the ECP pros and cons

Unlike standard immunosuppressive therapies, ECP does not cause general immunosuppression; instead, it appears to exert complex specific effects (27) across different immune pathways (22).

Analyzing the various immune specificities in the variations of the clinical phenotypes of SPSDs, we herein describe some potential mechanisms and caveats of ECP to be considered in the context of classical SPS.

4.2.1 Arguments in favor of ECP feasibility for SPS

4.2.1.1 Postulated ECP mechanisms in classical SPS

– Considering the pathophysiology of SPS and the presence of GAD65-specific T cells in the CNS that drive intrathecal production of GAD65 IgG (10), the indirect effects of ECP may be preponderant in SPS.

- ECP induces apoptosis that first appears in activated lymphocytes (e.g., affinity-maturated B cell clones), which are more sensitive to apoptosis than other cells (28).
- Despite the intrathecal synthesis of GAD65 antibodies indicating that T cells from CSF cells can be more relevant than those from blood in SPS (9), there is also persistent systemic oligoclonal production of GAD65-specific IgG (12).
- Apoptotic GAD65-specific B and T cells may be phagocytosed by DCs that present antigens to T-helper ($CD4^+$) cells, consequently raising specific tolerance to the clonal T cell population (29).
- ECP increases $CD4^+$ $CD25^+$ $Foxp3^+$ Tregs induced by a tolerogenic phenotype of DCs in contact with apoptotic cells in the periphery (23, 30, 31), which can also gain access to the CNS during neuroinflammatory autoimmunity events (23).
- Activated T cells of any specificity can penetrate the BBB; however, only those reactivated in the CNS are intrathecally retained (10).
- Following the increase of Tregs induced by ECP, the CSF-drained spaces of the CNS are eventually accessed by such activated cells, even in a non-neuroinflammatory environment (25).
- Before the blood-derived leukocytes enter the CSF, they first pass-through fenestrated capillaries and accumulate in the choroid plexus parenchyma, in which resident DCs can skew immune cells (25). ECP-induced apoptotic (GAD65-specific) cells can induce a tolerogenic phenotype of such unique DCs.
- Blood-borne cytokines that cross the BBB and enter the CSF and interstitial fluid spaces of the CNS may also favor this immune regulation (30).
- Circulant GAD65-specific T and B cells may undergo immunogenic cell death and serve as the major sources of subsequent GAD65 antigen processing and presentation (32).
- Similarly, other SPS immune-modulating therapies can tackle the peripheral compartment (e.g., therapeutic plasma exchange (33), high-dose IVIg (34), B cell depletion (16, 35), and autologous non-myeloablative HSCT (17)).
- Substantial Th2 cytokine levels drive a T cell–B cell collaboration and may drive intrathecal production of oligoclonal IgG in SPS (10). In this regard, ECP may restore the Th1/Th2 balance and induce tolerance (19).
- Furthermore, ECP can decrease the pro-inflammatory T cell subset of Th17 cells that commonly cross epithelial blood–CSF barriers (19).

4.2.1.2 Additional elements to be considered

- Adequate safety profile of ECP (36).
- Different immune specificities may exist within the same patient with SPS (11), and he/she may still benefit from ECP.
- The coexistence of nuclear and cytoplasmic autoantibodies that reflect immune responses to multiple CNS and other tissue-specific antigens (4) would also be addressed by ECP.
- The clonal pattern of GAD65 antibodies in the CSF remains stable for several years (9).
- ECP may be feasible in the case of certain concomitant autoimmune diseases with SPS (e.g., type 1 diabetes mellitus, ClinicalTrials.gov identifier NCT05413005, an ongoing clinical trial in our center) (37).
- Previous and ongoing ECP-based clinical trials on other immune-mediated CNS disorders (e.g., multiple sclerosis – MS, NCT05168384, which is also active in our hospital) (38).

Previous clinical experience with ECP has been documented in other immune-mediated CNS disorders, such as MS, in which a few case reports and small clinical trials verified the safety of ECP, but the results were inconclusive in terms of efficacy (39, 40). For instance, Besnier et al. reported that ECP transiently modified the course of severe secondary chronic progressive MS with a rebound after treatment discontinuation (41), and Cavaletti et al. reported evidence of adequate efficacy in a subgroup of patients with MS not responsive to or ineligible for standard immunomodulating treatments (42).

Regarding the use of photopheresis in patients with classical SPS, our group has proposed to execute the termed OPTION study, a pilot open-label trial using ECP as an add-on investigational intervention (NCT06703333) comprised of one ECP cycle (two consecutive days) every other week for three months, followed by one ECP cycle every month for additional three months. This trial will evaluate safety outcomes as the primary endpoints, but the efficacy will be preliminarily assessed through changes in the Distribution of Stiffness Index (DSI) and Heightened Sensitivity Score (HSS) (43).

Figures 1A, B summarize the main etiopathophysiological CNS events and postulated mechanisms of ECP in SPS, respectively.

4.2.2 Caveats and limitations of ECP feasibility in SPS

- The peripheral blood (main ECP direct target) is separated from the diseased organ by the BBB.
- GAD65-specific T cells are likely to be scarce in peripheral blood, and the intrathecal synthesis of GAD65 antibodies indicates that CSF T cells can be more relevant than blood T cells (9).

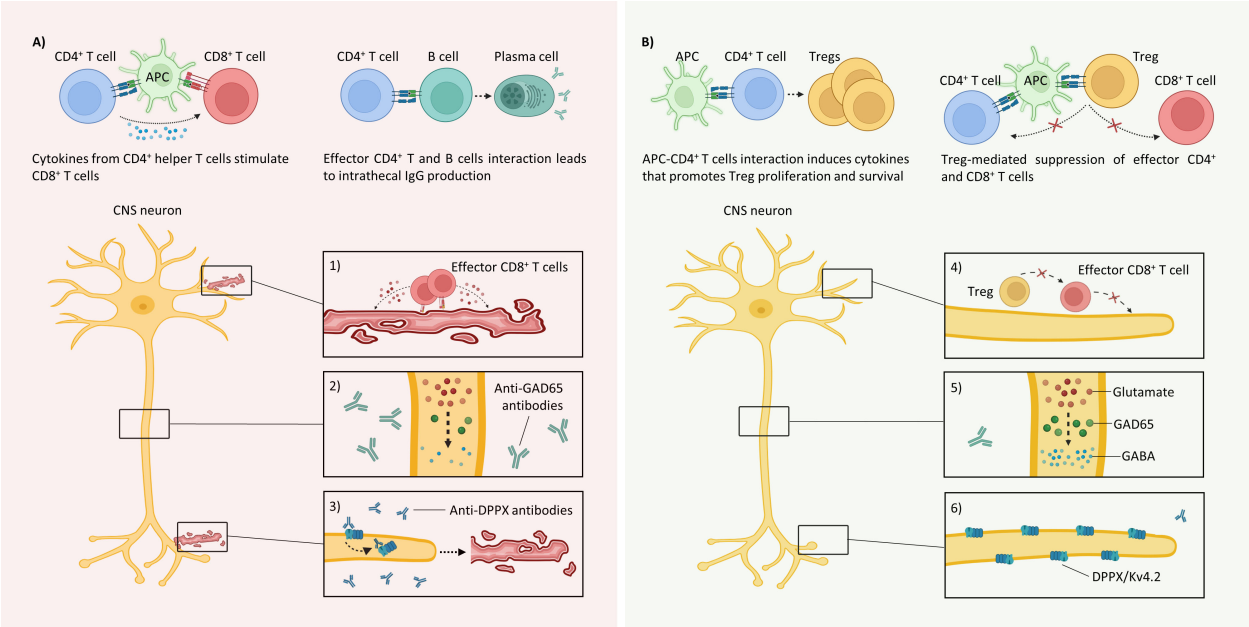

FIGURE 1
Immunopathology of classical SPS and the postulated mechanisms of ECP **(A)** Various peripherally circulating cells recognizing GAD65 peptides can traffic to the CNS and mount immune responses, leading to dysfunctional synapses because of the following: *1) CD8⁺ T cell-mediated cytotoxicity:* The GAD65 epitopes presented in the MHC-I molecules recognized by autoreactive T cells initiate cytotoxic immune responses by releasing perforin and granzyme **(B)** *2) Loss of inhibitory signals:* Although neurons do not internalize GAD65 antibodies, they recognize linear epitopes and limit GABA synthesis. *3) Antibody-mediated neuronal hyperexcitability and cytotoxicity:* Anti-DPPX antibodies initiate the internalization of the accessory proteins DPPX and KV4.2 (left), which produce hyperexcitability and cytotoxicity (right). *B)* The following postulated mechanisms of ECP may result in homeostasis in classical SPS: *4) Tolerance to GAD65-expressing neurons: Treg*-mediated suppression of effector GAD65-specific CD4⁺ and CD8⁺ T cells. *5) Inhibitory signal restoration:* Decreases in intrathecal GAD65 IgG production may regulate inhibitory interneurons. *6) Membrane surface stabilization:* The decrease in anti-DPPX antibodies reduces the internalization of both DPPX and Kv4.2 and stabilizes neuron membranes. APC, antigen-presenting cell; DPPX, dipeptidyl-peptidase-like protein-6; GABA, γ-aminobutyric acid; MHC-I, major histocompatibility complex class I. Created with BioRender.com.

- Serological markers are not commonly correlated with clinical severity, and the systemic synthesis of GAD65 antibodies may be insufficient for mediating SPS (44, 45).
- Different epitope specificity between serum and the CSF may reduce the potential efficacy of ECP (9).
- ECP may be a rational approach for certain disorders of the spectrum (e.g., classical SPS) but it is not feasible for all SPSDs (e.g., paraneoplastic variants).
- Lack of controlled clinical trials due to the low prevalence of SPS.
- Potential ECP-induced immune regulation may not be clinically relevant.
- The availability of ECP providers may also be challenging, including logistical and financial issues, vascular access needs (which, in the case of poor peripheral venous accesses, may eventually require the insertion of a central venous catheter), potential adverse events, and the uncertain ECP schedule and duration, which ultimately depend on the treatment response.

With the aforementioned pieces of evidence, being a well-tolerated and safe procedure with long-term effects in approved indications, ECP might overcome various gaps faced with current SPS treatments, which commonly provide a shorter duration of clinical improvement or variable beneficial effects (5, 7, 16, 17). For instance, instead of the therapeutic approach of controlling disease symptoms (e.g., benzodiazepines and muscle relaxants), targeting some of the critical cells involved in the etiopathophysiology (e.g., anti-B cell therapies) or even "rebooting" the immune system (autologous HSCT), ECP possesses established immunologic effects that, in combination with those treatments, may gradually modulate the dysregulated immune response observed in SPS.

5 Conclusions

Although the exact mechanism of action of ECP remains unclear and requires further studies in SPS, its wide-ranging immunomodulatory effects may be beneficial in this disabling disorder. By exploring the effect of ECP in preclinical models and formal clinical trials, this approach may also foster its use in SPS and potentially in other neuroimmunological diseases.

Author contributions

YMCA: Conceptualization, Data curation, Formal analysis, Investigation, Methodology, Resources, Supervision, Validation, Visualization, Writing – original draft, Writing – review & editing. PCK: Investigation, Methodology, Resources, Supervision, Validation, Writing – review & editing.

Funding

The author(s) declare that no financial support was received for the research, authorship, and/or publication of this article.

Acknowledgments

The authors gratefully acknowledge the team of ADSCC physicians, nurses, scientists, and other stakeholders for supporting our ECP services.

Conflict of interest

The authors declare that the research was conducted in the absence of any commercial or financial relationships that could be construed as a potential conflict of interest.

Generative AI statement

The author(s) declare that no Generative AI was used in the creation of this manuscript.

Publisher's note

References

1. Moersch FP, Woltman HW. Progressive fluctuating muscular rigidity and spasm ("stiff-man" syndrome); report of a case and some observations in 13 other cases. *Proc Staff Meet Mayo Clin.* (1956) 31:421–7.

2. Asher R. A woman with the stiff-man syndrome. *Br Med J.* (1958) 1:265–6. doi: 10.1136/bmj.1.5065.265

3. Muranova A, Shanina E. Stiff person syndrome. In: *StatPearls*. StatPearls Publishing, Treasure Island (FL (2023).

4. Rakocevic G, Floeter MK. Autoimmune stiff person syndrome and related myelopathies: understanding of electrophysiological and immunological processes. *Muscle Nerve.* (2012) 45:623–34. doi: 10.1002/mus.23234

5. Baizabal-Carvallo JF, Jankovic J. Stiff-person syndrome: insights into a complex autoimmune disorder. *J Neurol Neurosurg Psychiatry.* (2015) 86:840–8. doi: 10.1136/jnnp-2014-309201

6. Grech N, JP CG, Pace A. Progressive encephalomyelitis with rigidity and myoclonus (PERM). *Pract Neurol.* (2022) 22:48–50. doi: 10.1136/practneurol-2021-003087

7. Mitsumoto H, Schwartzman MJ, Estes ML, Chou SM, La Franchise EF, De Camilli P, et al. Sudden death and paroxysmal autonomic dysfunction in stiff-man syndrome. *J Neurol.* (1991) 238:91–6. doi: 10.1007/BF00315688

8. Ciccotto G, Blaya M, Kelley RE. Stiff person syndrome. *Neurol Clin.* (2013) 31:319–28. doi: 10.1016/j.ncl.2012.09.005

9. Holmøy T, Geis C. The immunological basis for treatment of stiff person syndrome. *J Neuroimmunol.* (2011) 231:55–60. doi: 10.1016/j.jneuroim.2010.09.014

10. Skorstad G, AL H, Vartdal F, Holmøy T. Cerebrospinal fluid T cell responses against glutamic acid decarboxylase 65 in patients with stiff person syndrome. *J Autoimmun.* (2009) 32:24–32. doi: 10.1016/j.jaut.2008.10.002

11. Newsome SD, Johnson T. Stiff person syndrome spectrum disorders; more than meets the eye. *J Neuroimmunol.* (2022) 369:577915. doi: 10.1016/j.jneuroim.2022.577915

12. Skorstad G, AL H, Torjesen P, Alvik K, Vartdal F, Vandvik B, et al. GAD65 IgG autoantibodies in stiff person syndrome: clonality, avidity and persistence. *Eur J Neurol.* (2008) 15:973–80. doi: 10.1111/j.1468-1331.2008.02221.x

13. Solimena M, Folli F, Denis-Donini S, Comi GC, Pozza G, De Camilli P, et al. Autoantibodies to glutamic acid decarboxylase in a patient with stiff-man syndrome, epilepsy, and type I diabetes mellitus. *N Engl J Med.* (1988) 318:1012–20. doi: 10.1056/NEJM198804213181602

14. Dinkel K, HM M, KM J, Karges W, Richter W. Inhibition of gamma-aminobutyric acid synthesis by glutamic acid decarboxylase autoantibodies in stiff-man syndrome. *Ann Neurol.* (1998) 44:194–201. doi: 10.1002/ana.410440209

15. Dade M, Berzero G, Izquierdo C, Giry M, Benazra M, Delattre JY, et al. Neurological syndromes associated with anti-GAD antibodies. *Int J Mol Sci.* (2020) 21:3701. doi: 10.3390/ijms21103701

16. Faissner S, Motte J, Sgodzai M, Geis C, Haghikia A, Mougiakakos D, et al. Successful use of anti-CD19 CAR T cells in severe treatment-refractory stiff-person syndrome. *Proc Natl Acad Sci U S A.* (2024) 121:e2403227121. doi: 10.1073/pnas.2403227121

17. Burt RK, Balabanov R, Han X, Quigley K, Arnautovic I, Helenowski I, et al. Autologous hematopoietic stem cell transplantation for stiff-person spectrum disorder: A clinical trial. *Neurology.* (2021) 96:e817–30. doi: 10.1212/WNL.0000000000011338

18. Vieyra-Garcia PA, Wolf P. Extracorporeal photopheresis: A case of immunotherapy ahead of its time. *Transfus Med Hemother.* (2020) 47:226–35. doi: 10.1159/000508479

19. Webb C. Extracorporeal photopheresis in conditions of autoimmunity. *Transfus Apher Sci.* (2023) 62:103678. doi: 10.1016/j.transci.2023.103678

20. Knobler R, Berlin G, Calzavara-Pinton P, Greinix H, Jaksch P, Laroche L, et al. Guidelines on the use of extracorporeal photopheresis. *J Eur Acad Dermatol Venereol.* (2014) 28 Suppl 1:1–37. doi: 10.1111/jdv.12311

21. Maniati E, Potter P, NJ R, Morley BJ. Control of apoptosis in autoimmunity. *J Pathol.* (2008) 214:190–8. doi: 10.1002/path.2270

22. Cho A, Jantschitsch C, Knobler R. Extracorporeal photopheresis-an overview. *Front Med (Lausanne).* (2018) 5:236. doi: 10.3389/fmed.2018.00236

23. Sagar D, Foss C, El Baz R, MG P, ZK K, Jain P. Mechanisms of dendritic cell trafficking across the blood-brain barrier. *J Neuroimmune Pharmacol.* (2012) 7:74–94. doi: 10.1007/s11481-011-9302-7

24. Hickey WF, BL H, Kimura H. T-lymphocyte entry into the central nervous system. *J Neurosci Res.* (1991) 28:254–60. doi: 10.1002/jnr.490280213

25. Lopes Pinheiro MA, Kooij G, MR M, Kamermans A, Enzmann G, Lyck R, et al. Immune cell trafficking across the barriers of the central nervous system in multiple sclerosis and stroke. *Biochim Biophys Acta.* (2016) 1862:461–71. doi: 10.1016/j.bbadis.2015.10.018

26. Ousman SS, Kubes P. Immune surveillance in the central nervous system [published correction appears in Nat Neurosci. *Nat Neurosci.* (2012) 15:1096–101. doi: 10.1038/nn.3161

27. Arora S, Setia R. Extracorporeal photopheresis: Review of technical aspects. *Asian J Transfus Sci.* (2017) 11:81–6. doi: 10.4103/ajts.AJTS_87_16

28. Heshmati F. Updating ECP action mechanisms. *Transfus Apher Sci.* (2014) 50:330–9. doi: 10.1016/j.transci.2014.04.003

29. Dupont E, Craciun L. UV-induced immunosuppressive and anti-inflammatory actions: mechanisms and clinical applications. *Immunotherapy.* (2009) 1:205–10. doi: 10.2217/1750743X.1.2.205

30. Capuano M, Sommese L, Pignalosa O, Parente D, Fabbricini R, Nicoletti GF, et al. Current clinical applications of extracorporeal photochemotherapy. *Ther Apher Dial.* (2015) 19:103–10. doi: 10.1111/1744-9987.12245

31. Lamioni A, Parisi F, Isacchi G, Giorda E, Di Cesare S, Landolfo A, et al. The immunological effects of extracorporeal photopheresis unraveled: induction of tolerogenic dendritic cells *in vitro* and regulatory T cells *in vivo*. *Transplantation*. (2005) 79:846–50. doi: 10.1097/01.tp.0000157278.02848.c7

32. Hannani D. Extracorporeal photopheresis: tolerogenic or immunogenic cell death? Beyond current dogma. *Front Immunol*. (2015) 6:349. doi: 10.3389/fimmu.2015.00349

33. Czempik PF, Gawryluk J, Wiórek A, Krzystanek E, Krzych ŁJ. Efficacy and safety of therapeutic plasma exchange in stiff person syndrome. *Open Med (Wars)*. (2021) 16:526–31. doi: 10.1515/med-2021-0220

34. Dalakas MC, Fujii M, Li M, Lutfi B, Kyhos J, McElroy B. High-dose intravenous immune globulin for stiff-person syndrome. *N Engl J Med*. (2001) 345:1870–6. doi: 10.1056/NEJMoa01167

35. Dalakas MC. Invited article: inhibition of B cell functions: implications for neurology. *Neurology*. (2008) 70:2252–60. doi: 10.1212/01.wnl.0000313840.27060.bf

36. Alfred A, PC T, Dignan F, El-Ghariani K, Griffin J, Gennery AR, et al. The role of extracorporeal photopheresis in the management of cutaneous T-cell lymphoma, graft-versus-host disease and organ transplant rejection: a consensus statement update from the UK Photopheresis Society. *Br J Haematol*. (2017) 177:287–310. doi: 10.1111/bjh.14537

37. US National Library of Medicine. *ClinicalTrials.gov* (2024). Available online at: https://clinicaltrials.gov/study/NCT05413005 (Accessed October 29, 2024).

38. US National Library of Medicine. *ClinicalTrials.gov* (2024). Available online at: https://clinicaltrials.gov/study/NCT05168384 (Accessed October 29, 2024).

39. Poehlau D, Rieks M, Postert T, Westerhausen R, Busch S, Hoffmann K, et al. Photopheresis–a possible treatment of multiple sclerosis?: report of two cases. *J Clin Apher*. (1997) 12:154–5. doi: 10.1002/(sici)1098-1101(1997)12:3<154::aid-jca9>3.0.co;2-9

40. Rostami AM, Sater RA, Bird SJ, Galetta S, Farber RE, Kamoun M, et al. A double-blind, placebo-controlled trial of extracorporeal photopheresis in chronic progressive multiple sclerosis. *Mult Scler*. (1999) 5:198–203. doi: 10.1177/135245859900500310

41. Besnier DP, Chabannes D, JM M, Dupas B, Esnault VL. Extracorporeal photochemotherapy for secondary chronic progressive multiple sclerosis: a pilot study. *Photodermatol Photoimmunol Photomed*. (2002) 18:36–41. doi: 10.1034/j.1600-0781.2002.180106.x

42. Cavaletti G, Perseghin P, Dassi M, Cavarretta R, Frigo M, Caputo D, et al. Extracorporeal photochemotherapy: a safety and tolerability pilot study with preliminary efficacy results in refractory relapsing-remitting multiple sclerosis. *Neurol Sci*. (2006) 27:24–32. doi: 10.1007/s10072-006-0561-7

43. US National Library of Medicine. *ClinicalTrials.gov* (2024). Available online at: https://clinicaltrials.gov/study/NCT06703333 (Accessed November 26, 2024).

44. Dalakas MC. Stiff-person syndrome and GAD antibody-spectrum disorders: GABAergic neuronal excitability, immunopathogenesis and update on antibody therapies. *Neurotherapeutics*. (2022) 19:832–47. doi: 10.1007/s13311-022-01188-w

45. Rakocevic G, Raju R, Dalakas MC. Anti-glutamic acid decarboxylase antibodies in the serum and cerebrospinal fluid of patients with stiff-person syndrome: correlation with clinical severity. *Arch Neurol*. (2004) 61:902–4. doi: 10.1001/archneur.61.6.902

frontiers | Frontiers in Immunology

TYPE Original Research
PUBLISHED 08 January 2025
DOI 10.3389/fimmu.2024.1508974

OPEN ACCESS

EDITED BY
Estela Maris Muñoz,
Institute of Histology and Embryology of Mendoza Dr. Mario H. Burgos (IHEM)-UNCuyo-CONICET, Argentina

REVIEWED BY
Claudia Cantoni,
Barrow Neurological Institute (BNI), United States
Herena Eixarch,
Vall d'Hebron Research Institute (VHIR), Spain

*CORRESPONDENCE
Cecilia Simonini
ceciliasimonini24@gmail.com

†These authors have contributed equally to this work

RECEIVED 10 October 2024
ACCEPTED 16 December 2024
PUBLISHED 08 January 2025

CITATION
Zucchi E, Banchelli F, Simonini C, De Biasi S, Martinelli I, Gianferrari G, Lo Tartaro D, Cossarizza A, D'Amico R and Mandrioli J (2025) Tregs levels and phenotype modifications during Amyotrophic Lateral Sclerosis course.
Front. Immunol. 15:1508974.
doi: 10.3389/fimmu.2024.1508974

Tregs levels and phenotype modifications during Amyotrophic Lateral Sclerosis course

Elisabetta Zucchi[1,2†], Federico Banchelli[2†], Cecilia Simonini[2*†], Sara De Biasi[3], Ilaria Martinelli[2], Giulia Gianferrari[1,2], Domenico Lo Tartaro[3], Andrea Cossarizza[3,4], Roberto D'Amico[3,5] and Jessica Mandrioli[2,6] on behalf of RAP-ALS study group

[1]Neuroscience PhD Program, University of Modena and Reggio Emilia, Modena, Italy, [2]Department of Neurosciences, Ospedale Civile di Baggiovara, Azienda Ospedaliero-Universitaria di Modena, Modena, Italy, [3]Department of Medical and Surgical Sciences for Children and Adults, University of Modena and Reggio Emilia, Modena, Italy, [4]National Institute for Cardiovascular Research, Bologna, Italy, [5]Unit of Statistical and Methodological Support to Clinical Research, Azienda Ospedaliero-Universitaria, Modena, Italy, [6]Department of Biomedical, Metabolic and Neural Sciences, University of Modena and Reggio Emilia, Modena, Italy

Introduction: T regulatory cells (Tregs) inversely correlate with disease progression in Amyotrophic Lateral Sclerosis (ALS) and fast-progressing ALS patients have been reported to exhibit dysfunctional, as well as reduced, levels of Tregs. This study aimed to evaluate the longitudinal changes in Tregs among ALS patients, considering potential clinical and biological modifiers of their percentages and concentrations. Additionally, we explored whether measures of ALS progression, such as the decline over time in the revised ALS Functional Rating Scale (ALSFRS-r) or forced vital capacity (FVC) correlated Treg levels and whether Treg phenotype varied during the course of ALS.

Methods: Total Tregs (detected by CD3, CD4, FoxP3, CD25, and CD127) were quantified at five time points over 54 weeks in 21 patients in the placebo arm of the RAP-ALS trial; next they were characterized for the expression of surface markers including CD38, CD39, CXCR3, and PD1. Repeated measures mixed models were used to analyze the longitudinal course of Tregs, considering potential associations with other clinical and laboratory characteristics. Correlations between ALSFRS-r or FVC and Tregs over time were similarly investigated.

Results: Our study showed that Treg levels did not change significantly on average during the observation period in our ALS cohort. However, PD1+Tregs decreased and CD39+Tregs increased over time. Male sex and cholesterol levels were associated with increasing Tregs (%) over time, while monocytes positively affected Treg concentrations. Treg concentrations showed a modesty association with FVC decline but were not associated with ALSFRS-r decline.

Discussion: Treg levels remained stable during the ALS observation period and were not significantly associated with ALSFRS-r variations, suggesting that Treg numbers alone may have limited utility as a pharmaco-dynamic biomarker for ALS trials. However the observed changes in Treg phenotypes, such as the decrease in PD1+Tregs, indicate that phenotypic variations may warrant further investigation for their potential role in ALS progression and therapeutic targeting.

KEYWORDS

ALS, T regulatory cell, ALSFRS-r, FVC (forced vital capacity), cholesterol, monocyte

1 Introduction

Amyotrophic Lateral Sclerosis (ALS) is a rare neurogenerative disorder affecting the upper and lower motor neurons, with a global lifetime risk of approximately one in 350 people (1, 2). Notwithstanding death or permanent ventilation results in three to five years since the onset of disease, there is wide heterogeneity in clinical presentation, and different phenotypes, with prognostic repercussions, are recognized in ALS (2). While the mechanisms beneath the motor neuronal degeneration have not been fully elucidated, multiple lines of evidence point to non-cell autonomous processes contributing to the damage to the motor neurons (3).

Crucial to the neuroinflammatory modulation, T regulatory cells (Tregs), a subset of T cells characterized by expression of CD4+, FoxP3+, CD25+, are known as potential modifiers of disease progression in Amyotrophic Lateral Sclerosis (ALS) (4). Tregs are central to immune homeostasis, by regulating the delicate equilibrium between immune activation and tolerance (5), with specific roles in preventing autoimmune conditions (6), controlling systemic inflammation (7) and contrasting immunosurveillance for tumor expansion (8). In SOD1-mutated mice with ALS, increased concentrations of Tregs were observed during the early phases of the disease and later decreased, consistent with an M1-like toxic microglia environment switch into the spinal cord; in this model passive transfer of functional Tregs prolonged survival (9). Moreover, in fast-progressing patients with ALS, reduced (9, 10) and dysfunctional Tregs (11) were found compared to slowly progressing patients, and FoxP3 expression, their master regulator, inversely correlated with disease progression and survival.

Based on this evidence, several trials have attempted to expand Tregs and restore their function as a targetable mechanism for slowing the course of ALS (12–14), by tuning down the pro-inflammatory systemic immune background detected in most ALS patients (4). While some randomized controlled trials (RCTs) are currently ongoing, setting as a primary objective to increase Tregs or FoxP3 expression compared to baseline values (14), many of the completed trials could not reach this biological outcome.

However, while some preliminary data from SOD1-mutated mice highlighted a disease progression-dependent decrease in peripheral Tregs during active phases of ALS (9), longitudinal studies assessing Tregs number in ALS patients are lacking, and interpretation of Treg variations compared to placebo in clinical trials might be challenging. In line with the continuously growing knowledge about more complex Treg phenotypes, tissues of origin, or capabilities to adapt to different inflammatory challenges, other demographic or biological factors may modify Treg number or functions and should be considered for the sake of efficacy analysis in the design of clinical trials for ALS therapy.

The primary objective of this study was to evaluate the longitudinal trajectories of Tregs in patients with ALS, including possible modifiers of their percentages or concentrations. Secondly, the relationship between the decline in ALSFRS-r or forced vital capacity (FVC) with Tregs and the longitudinal trajectories of Treg subpopulations, as defined by expression of specific surface markers, was explored in ALS patients.

2 Methods

2.1 Study participants

For this study, we considered patients who were enrolled in the RAP-ALS clinical trial and allocated to placebo arm. These patients (21 subjects) were treated with Riluzole but were not on other experimental drugs and underwent the study procedures which included serial serum sampling from baseline to week 54 as previously reported (15). The study design, subject selection, and participants in RAP-ALS clinical trial have been reported elsewhere (15, 16). Briefly, 63 patients with definite, clinically probable or probable with laboratory support ALS according to revised El Escorial Criteria, within 18 months since onset of motor symptoms were recruited from 2017 through 2020. Regularly scheduled visits at week 4, 8, 12, 18, 30, 42 and 54 were performed with blood samples collection at week 8, 18, 30, 42 and 54.

The revised form of the ALS Functional Rating Scale (ALSFRS-r), weight, body mass index (BMI), vital parameters, neurological examination and forced vital capacity (FVC) were assessed at baseline (week 0), and at weeks 4, 8, 12, 18, 24, 30, 42, 54.

Weight change was calculated as the actual weight recorded at each visit minus the weight before the onset of disease.

2.2 Standard protocol approvals, registrations, and patient consents

Ethical approval was obtained by Ethical Committee of the coordinating center (Comitato Etico Provinciale di Modena) in May 2017 (file number 95/17) and written informed consent was obtained from all the participants.

2.3 Tregs and other laboratory assessments

All the biological procedures related to RAPALS study, including Tregs number and function assessment, have been previously reported (15, 16). In brief, immunophenotype of Treg cell subpopulations were performed by polychromatic flow cytometry at baseline and week 8, 18, 30, 54 as shown in (Figure 1). Freshly isolated PBMC were washed and stained with commercially available monoclonal antibodies (mAb) directly conjugated with different fluorochromes. For T regulatory cells phenotype, the following markers, besides viability marker (AQUA Live Dead) were used: anti-CD3-Pe-Cy5, -CD4-AF700, CD8-APC-Cy7, CD25-PE, CD127-APC-Cy7, HLA-DR-PE-Cy7, CXCR3-BV421, CD38-BV605, PD-1-BV605, CD39-BV421. Treg cells were identified as FoxP3+, CD25++, CD127- cells within CD3 +CD4+ T cells. A first activation/homing panel was set with the following markers for CD4+ and CD8+ T cells, Tregs included: CD38 and CXCR3. CD38 was included for its role in modulating immune suppression and its association with NAD+ metabolism (17), which could influence Treg function in the inflammatory environment. CXCR3 is noted for its involvement in Treg migration to inflamed tissues (18).

A second metabolic/exhaustion/activation panel was similarly set for Tregs and CD4+, CD8+ T cells according to the expression of PD1 and CD39 (Figure 1). CD39 is a key ectoenzyme contributing to the generation of adenosine, an anti-inflammatory molecule, potentially reflecting a compensatory mechanism in response to neuroinflammation (19). PD-1 is mentioned as a marker of Treg exhaustion, whose decrease over time may indicate a loss of immunosuppressive capacity (20).

Tregs and their subpopulations were expressed as percentages over total Tregs in the case of Tregs subpopulations, and as percentages over total CD4 T cells, as assessed by flow cytometric analysis at the central University lab, or as concentrations (number of cells per microliter), in the case of total Tregs. These concentrations were obtained by calculating the proportion of Treg/total CD4 T cells from the percentage obtained at the University lab by the gating strategy and the total number of lymphocytes as assessed by standard labs of each MND center.

We were unable to include five measurements for all patients due to dropouts during the RAP-ALS trial (15). Additionally, logistical challenges in collecting and processing fresh samples, such as the limited availability of biological material, further affected our ability to obtain five measurements for every patient.

Neurofilament heavy chain (NfH) and light chain (NfL) were analyzed in plasma by Ella Automated Immunoassay System (Simple Plex Human NF Cartridge, R&D System, Minneapolis, MN), according to the manufacturer's instructions and as already reported (21, 22).

Standard blood exams including hematology, biochemistry (creatinine, urea, uric acid, total cholesterol, LDL cholesterol, triglycerides, ALT, AST, GGT) and urinalysis were performed by certified local laboratories at week 4, 8, 12, 18, 24, 30, 42 and 54.

2.4 Model design for Tregs variations

To explain the variations of Tregs during time, the effect of several demographic, clinical and laboratory variables was assessed by considering all these explanatory variables: time since onset of disease, ALSFRS-r, FVC, age at onset of disease, site of onset (bulbar vs spinal), weight loss since onset of disease, sex, BMI, albumin, creatinine, C-reactive protein (CRP), uric acid, total cholesterol, triglycerides, monocytes, neutrophil-to-lymphocytes ratio (NLR), and serum neurofilament light (NfL). ALSFRS-r and FVC were chosen to investigate if their decline could explain Tregs variations over time. Since Tregs may be affected by sexual hormones, adiposity and aging, we included sex, BMI, weight change, which is also a prognostic factor for ALS (23), and age at onset, as other explanatory variables. The site of onset, besides being a crucial independent prognostic factor for ALS, was added to correct for different trajectories of ALSFRS-r or FVC decline, as bulbar onset or bulbar phenotype patients might show steeper declines during the early phases of ALS or have more difficulties in performing functional respiratory tests (24). Regarding lab values, we chose CRP as a general marker of systemic inflammation, monocytes and NLR to investigate other aspects of systemic inflammation with novel roles recently linked to ALS progression (25–28), albumin to account for nutritional status, creatinine as a marker of renal function and a known biomarker of progression in ALS (29), total cholesterol and triglycerides as markers of lipid metabolism possibly related to Treg cells (30), uric acid for protein metabolism, serum NfL to investigate possible relations between the pace of neurodegeneration with Tregs variations.

2.5 Statistical methods

Characteristics of patients were described using mean, standard deviation and range for numerical variables and using absolute and percentage frequencies for categorical variables.

The association between the candidate explanatory variables (demographics, anthropological measures, clinical characteristics, neurofilaments, and laboratory values over time) and the outcomes of interest (Tregs percentages and concentrations, ALSFRS-r and FVC) measured at each time point was assessed using generalized linear mixed models. Since Tregs percentages and concentrations

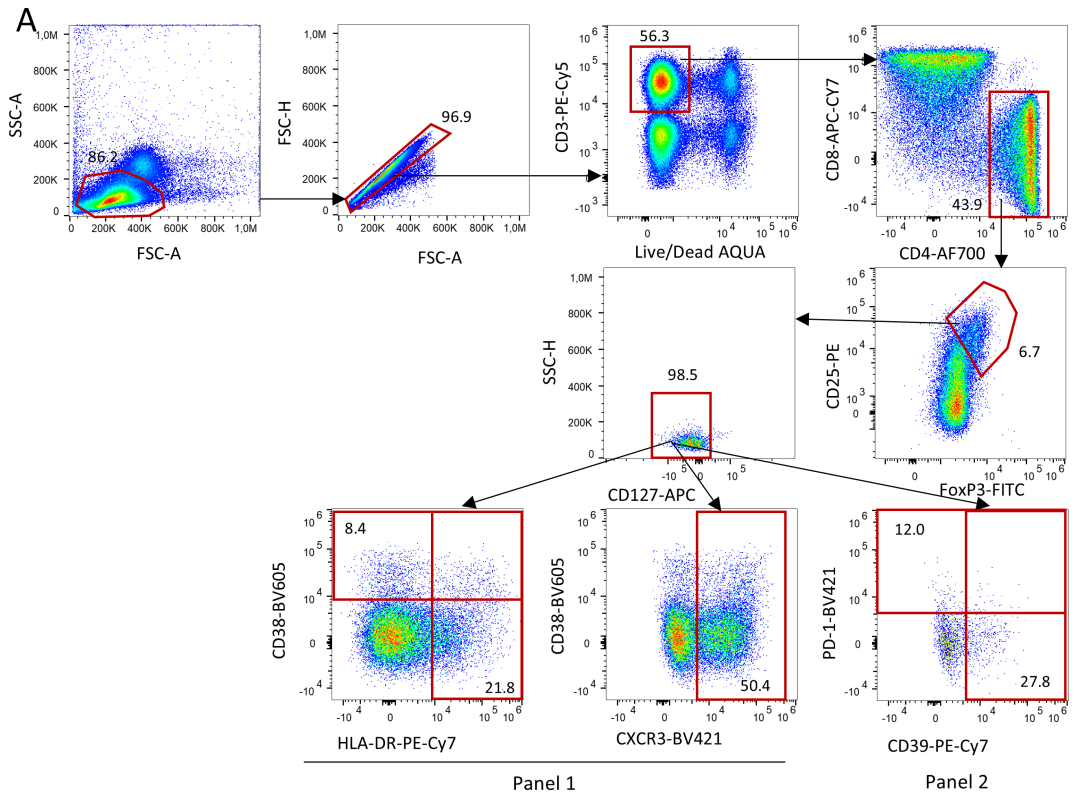

B

Panel 1

Marker	Fluorochrome	Brand	Cat	Titer (ml)
Live Dead	AQUA	ThermoFisher	L34957	1.25
CD3	PE-CY5	Biolegend	300410	0.6
CD4	AF700	Biolegend	300526	0.6
CD8	APC-CY7	Biolegend	301016	0.6
CD127	APC	Biolegend	351316	0.6
CD25	PE	Biolegend	302606	3.75
FoxP3	FITC	Biolegend	320106	3.75
CD38	BV605	Biolegend	303532	1.25
HLA-DR	PE-CY7	Biolegend	307616	0.6
CXCR3	BV421	Biolegend	353716	0.6

Panel 2

PD-1	BV605	Biolegend	329924	2.5
CD39	PE-CY7	Biolegend	328212	0.6

FIGURE 1
Gating strategy used to identify Tregs and their subpopulations. **(A)** Lymphocytes were identified by physical parameters, doublets were removed and alive CD3+ T cells were selected accordingly. In this population, CD4+ T were selected and within this, those who were CD25++, FoxP3+ and CD127- were defined as Tregs. In this population, by using two different panels (which shared the same backbone, such as Live Dead, CD3, CD4, CD8, CD127, CD25,FoxP3; all reported in **(B)**, Tregs expressing HLA-DR, CD38, CXCR3, PD-1 and CD39 were identified.

may explain different immunological effects, they were considered as separate outcome variables during the analyses.

Firstly, unadjusted models including time from onset as the only independent variable were estimated, to describe the observed linear trend over time of Tregs, ALSFRS-r and FVC. Secondly, multivariable models including all candidate independent variables were estimated, to describe which demographic, clinical and laboratory characteristics were associated with the outcomes.

All independent variables were time-varying except for age, sex, and site of onset. When analyzing ALSFRS-r and FVC as the dependent variables, albumin, CRP, uric acid, total cholesterol, monocytes, creatinine, triglycerides and NLR were not considered as independent variables.

An individual random intercept term was included in all models to allow the average value of the outcome to vary between patients. To allow the outcome slope to vary over time between patients, a

random slope term was included in all unadjusted models and, if it improved the Bayesian information criterion (BIC) value, also in multivariable models.

Thirdly, we investigated if other specific Treg subpopulations could be influenced by ALSFRS-r, FVC and the other individual characteristics measured at each time point. The following cell markers were used to classify Treg subpopulations: CD38, CXCR3, CD39, PD1.These markers of Treg activity were considered as additional dependent variables, all measured as percentage over total Tregs, percentage over CD4 T cells or concentration.

Tregs percentages and concentration (including Tregs subpopulation) were analyzed using a multiplicative effect generalized linear mixed model with gamma distribution and log link function, whereas ALSFRS-r and FVC were analyzed using an additive effect linear mixed model with gaussian distribution and identity link function. The choice of the models was based on the BIC comparing several alternative models (including gaussian, log-gaussian, inverse gaussian, gamma and beta models with additive or multiplicative effects), as well as on goodness-of-fit measures and on visual inspection of the shape and skewness of the outcomes distributions.

Results for multiplicative effect models were reported as the mean ratio (MR), whereas results for additive effect models were expressed as the mean difference (MD). Uncertainty in estimated was reported as the 95% confidence interval (CI).

Missing values in the laboratory explanatory variables were imputed for each patient by using the linear trend criterion, bounded within the minimum and maximum observed values for that individual. For all models, listwise deletion was applied for records with missing values in the other independent variables.

Analyses were performed with R 4.3.2 (The R Foundation for Statistical Computing, Wien). Statistical significance was set at $p < 0.05$, and results with $p < 0.10$ were considered of potential interest.

3 Results

3.1 Tregs natural history in ALS patients

All 21 patients who were allocated to the placebo arm in the RAP-ALS trial were included in this analysis. Their clinical features are summarized in Table 1 and the baseline values of total Treg counts,

TABLE 1 Clinical features of ALS patients included in the analysis of Tregs longitudinal variations.

Clinical features	Females (n=8)	Males (n=13)	Total (n=21)
Age at baseline (years)	59.30 (10.05)	53.25 (14.23)	55.55 (12.88)
Age at onset (years)	58.39 (10.09)	52.18 (14.03)	54.54 (12.78)
Spinal site of onset	4 (50.0%)	11 (84.6%)	15 (71.4%)
Weight at baseline (kg)	59.88 (9.30)	78.24 (9.56)	71.24 (12.98)
BMI at baseline (kg/m^2)	24.16 (3.16)	24.85 (2.21)	24.59 (2.56)
Weight loss at baseline (kg)	2.00 (2.73)	0.53 (3.80)	1.09 (3.44)
Time since first ALS symptom (months)	10.5 (4.41)	12.38 (4.15)	11.67 (4.25)
ALSFRS-r score at baseline	38.63 (5.40)	38.62 (5.56)	38.62 (5.36)
Disease progression rate at baseline	1.28 (1.28)	0.84 (0.66)	1.00 (0.94)
FVC at baseline (%)	91.05 (19.49)	97.5 (13.16)	95.04 (15.72)
Kings' staging at baseline	1.75 (0.46)	1.77 (0.44)	1.76 (0.44)
Albumin at baseline (g/dL)	4.69 (0.70)	4.52 (0.34)	4.58 (0.50)
CRP at baseline (mg/dL)	0.79 (1.34)	0.66 (0.77)	0.71 (1.00)
Uric acid at baseline (mg/dL)	3.84 (0.82)	5.47 (1.12)	4.85 (1.28)
Total cholesterol at baseline (mg/dL)	251.00 (39.79)	196.46 (20.86)	217.24 (39.39)
Monocytes at baseline (counts/mm^3)	0.49 (0.13)	0.52 (0.14)	0.51 (0.13)
Creatinine at baseline (mg/dL)	0.70 (0.10)	0.79 (0.16)	0.75 (0.15)
Triglycerides at baseline (mg/dL)	95.38 (28.69)	110.46 (43.72)	104.71 (38.62)
NLR at baseline	2.99 (1.37)	2.12 (0.53)	2.45 (1.01)
Serum NfL at baseline (pg/ml)	194.88 (70.8)	142.17 (152.41)	163.25 (126.48)

Continuous variables were presented as means (standard deviations) while categorical variables as absolute numbers (percentages). Disease progression rate at baseline was calculated as the difference between presumed maximal ALSFRS-r score before onset of ALS (31) minus ALSFRS-r score at baseline, divided by time in months from onset to baseline. *data on serum NfL for one male patient is missing.

ALSFRS-r, Amyotrophic Lateral Sclerosis Functional Rating Scale-revised; FVC, forced vital capacity; BMI, body mass index; CRP, C-reactive protein; NLR, neutrophil-to-lymphocytes ratio; NfL, neurofilament light chain.

together with Tregs identified by phenotypic markers, are described in Supplementary Table 1. Female patients experienced more severe weight loss at baseline, compared to the weight before the onset of the disease, and were more likely to present with bulbar onset.

Nine out of 750 laboratory or anthropometric measurements were imputed (1.2%). Overall, 75 measurements were included in the main analysis, collected in a period starting from 5 months, until 30 months, since the onset of disease. Tregs subpopulations analyses were carried out on a lower number of participants due to missing data. In detail, CD38 and CXCR3 markers were measured for 15 patients with 51 measurements, whereas CD39 and PD1 markers for 16 patients with 55 measurements (Supplementary Table 2). Missing values resulted from challenges posed by COVID-19 pandemic and logistical issues in the collection and processing of fresh samples, including limitations in the availability of biological material.

When considering the time since onset of first motor symptoms of ALS, the unadjusted average monthly variation in Tregs % resulted in a -0.3% decrease (MR=0.997, 95%CI 0.984;1.010, p=0.598). Setting Treg cell count as the dependent variable resulted in a similar non-significant average yearly decrease of -0.8% (MR=0.992, 95%CI 0.975,1.009, p=0.344). Graphical representations of the average trends in Tregs since disease onset with individual variations are provided in Figure 2.

3.2 Influence of clinical and laboratory variables in Tregs variations in ALS patients

To describe Tregs variations during time, the effect of several demographic, clinical, and laboratory variables was tested by multivariable generalized linear mixed models, in an attempt to account for the clinical heterogeneity of the cohort. Table 2 shows the mean ratios for each explanatory variable in the multivariable analysis.

When corrected for all the explanatory variables, time since onset of the disease as well as ALSFRS-r and FVC did not modify Treg percentages or cell counts. Among demographic characteristics, being a male was associated with increased Tregs, especially when considering their percentages over total CD4 T cells (MR = 1.701, 95%CI 1.021;2.832, p= 0.041). Other metabolic markers such as total cholesterol positively correlated with Tregs both when measured as percentages over CD4 T cells and as cell counts, whereas albumin seemed to have positive, though non-significant, association with Tregs (%) (MR=1.179, 95%CI 0.994;1.398, p=0.059). When considering markers of peripheral inflammation, we observed that monocyte counts positively affected Treg cell counts (MR=1.112, 95%CI 1.031;1.200, p=0.006) but not percentages, while NLR negatively correlated with Tregs cell count: for each one-unit increase in the log of this ratio, Treg concentrations decreased on average of 27.5% (MR=0.725, 95%CI 0.557;0.944, p= 0.017). Neither neurofilaments nor CRP modified Tregs.

3.3 Effect of Tregs variations over ALSFRS-R and FVC during ALS course

Next, we wanted to investigate whether Treg number, expressed as percentages over total CD4 T cells or as concentrations, could influence ALSFRS-r or FVC. In the unadjusted analysis, ALSFRS-R declined on average of 1.244 points per month (95%CI -1.636;-0.851, p<0.001) while FVC of 1.873% per month (95%CI -3.078;-0.668, p=0.002) (Figure 3). Since the site and age of onset, BMI, weight loss, and neurofilaments are all known prognostic factors for ALS, they were all included as explanatory variables in the models; sex was also included as a covariate. Two separate models including Treg expressed as percentages over total CD4 T cells and as concentrations were run, to investigate which unit of measure

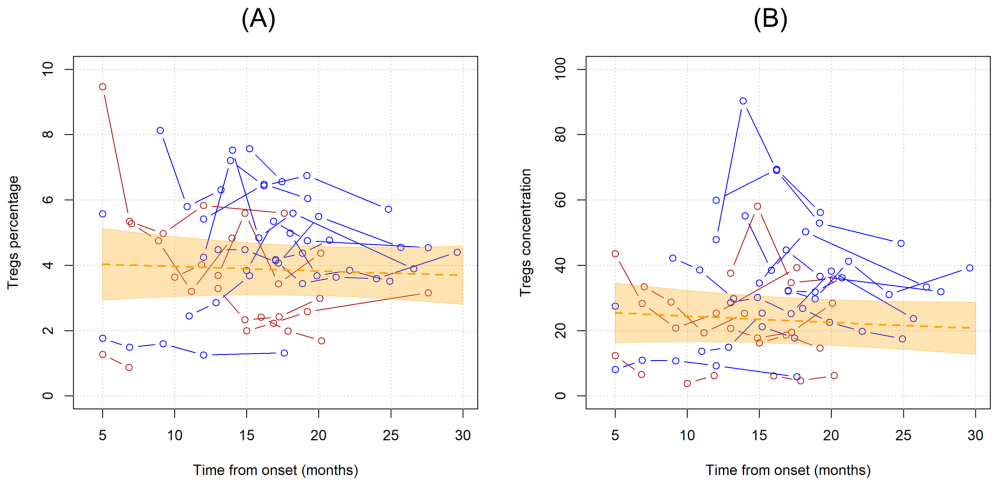

FIGURE 2
Unadjusted linear trends over time of Tregs percentages over total CD4 T cells **(A)** and Tregs concentrations **(B)**. Continuous lines represent observed trajectories for each single patient with ALS. Female patients' Tregs trajectories are depicted in red color, while males' ones in blue. Dotted orange line represents the average linear variation in Tregs percentage **(A)** and concentration **(B)** over time, expressed in months since onset of disease, with 95% confidence interval depicted by the yellow-shaded area. Tregs concentrations are expressed as cell count per microliter.

10.3389/fimmu.2024.1508974

TABLE 2 Multivariable model for variations in Tregs, expressed as Tregs percentages (over total CD4 T cells) or Tregs concentrations (cell count/ul).

Variable		Tregs percentage (over total CD4 T cells)			Tregs concentration (cell count/uL)		
		MR	95% CI	p-value	MR	95% CI	p-value
Time from onset	+ 30 days	1.003	0.984; 1.022	0.766	0.997	0.974; 1.022	0.832
ALSFRS-R	- 5 points	0.987	0.913; 1.067	0.738	0.992	0.900; 1.093	0.869
FVC	- 10%	0.976	0.937; 1.016	0.237	0.985	0.935; 1.038	0.573
Site of onset	Bulbar vs Spinal	0.884	0.538; 1.452	0.625	0.630	0.355; 1.121	0.116
BMI	+ 1 kg/m²	0.988	0.905; 1.078	0.783	0.983	0.885; 1.092	0.753
Weight change	- 10 kg	0.865	0.598; 1.250	0.439	0.943	0.601; 1.480	0.799
Age at onset	+ 10 years	0.990	0.835; 1.173	0.906	0.982	0.807; 1.196	0.859
Sex	M vs F	**1.701**	**1.021; 2.832**	**0.041**	1.622	0.897; 2.933	0.110
Albumin	+ 1 g/dL	1.179	0.994; 1.398	0.059	1.175	0.951; 1.452	0.136
CRP	+ 1 (log scale)	1.071	0.972; 1.180	0.164	1.085	0.958; 1.229	0.199
Uric acid	+ 1 mg/dL	0.988	0.904; 1.081	0.799	1.025	0.916; 1.148	0.666
Total cholesterol	+ 100 mg/dL	**1.339**	**1.008; 1.780**	**0.044**	**1.472**	**1.034; 2.095**	**0.032**
Monocytes	+ 0.1 cell/mm³	1.038	0.975; 1.105	0.244	**1.112**	**1.031; 1.200**	**0.006**
Creatinine	+ 1 mg/dL	0.954	0.881; 1.032	0.240	0.944	0.853; 1.045	0.266
Triglycerides	+ 1 (log scale)	0.853	0.695; 1.047	0.129	0.994	0.766; 1.289	0.962
NLR	+ 1 (log scale)	1.219	0.981; 1.515	0.075	**0.725**	**0.557; 0.944**	**0.017**
Serum NfL	+ 1 (log scale)	0.957	0.796; 1.152	0.645	0.964	0.764; 1.216	0.757

Multiplicative effect generalized linear mixed model with gamma distribution and log link function were employed to study Tregs (%) and Treg concentrations variations over time. Mean ratios (MR) with 95% confidence interval (CI) are reported to explain the effect of each variable on Treg % or Treg concentrations, respectively. Significance is set with p-values < 0.05, which are reported in bold character. The mean ratio represents the ratio between average Tregs percentage or concentrations, whichever the dependent variable is. A mean ratio equal to one implies the explanatory variable has an estimated average 0% effect on Tregs; any increase or decrease in the mean ratio over one suggests there is an average percentage increase or decrease in Tregs compared to reference values.

ALSFRS-r, Amyotrophic Lateral Sclerosis Functional Rating Scale-revised; FVC, forced vital capacity; BMI, body mass index; CRP, C-reactive protein; NLR, neutrophil-to-lymphocytes ratio; NFL, neurofilament light chain.

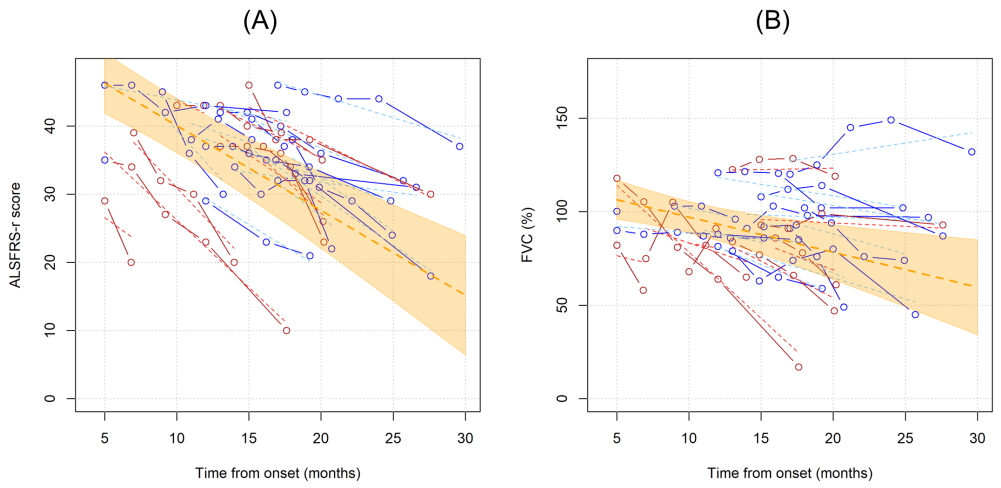

FIGURE 3
Unadjusted linear trends over time of ALSFRS-r **(A)** and FVC percentages **(B)**. Continuous lines represent observed trajectories for each single patient with ALS, while dotted lines depict predicted trajectories. Female patients' Tregs trajectories are depicted in red color, while males' ones in blue. Dotted orange line represents the average linear variation in ALSFRS-r **(A)** and FVC (%) **(B)** over time, expressed in months since onset of disease, with 95% confidence interval depicted by the yellow-shaded area. Predicted values were calculated from an additive effect multivariable linear mixed model which considers clinical and laboratory characteristics as the independent variables.

10.3389/fimmu.2024.1508974

TABLE 3 Multivariable model for variations in ALSFRS-r and FVC.

ALSFRS-r							
Variable		Tregs percentage*			Tregs concentration*		
		MD	95% CI	p-value	MD	95% CI	p-value
Time from onset	+ 30 days	**-0.900**	**-1.288; -0.513**	**<0.001**	**-0.928**	**-1.357; -0.499**	**<0.001**
FVC	-10%	**-1.186**	**-1.939; -0.433**	**0.002**	**-1.204**	**-1.971; -0.437**	**0.002**
Tregs	+1 unit *	0.114	-0.662; 0.890	0.773	-0.026	-0.112; 0.060	0.553
Site of onset	Bulbar vs Spinal	2.364	-5.433; 10.160	0.552	1.926	-5.722; 9.573	0.622
BMI	+ 1 kg/m²	-0.947	-2.419; 0.525	0.207	-1.062	-2.522; 0.398	0.154
Weight change	- 10 kg	-5.026	-11.370; 1.318	0.121	-5.543	-11.969; 0.883	0.091
Age at onset	+ 10 years	1.429	-1.275; 4.133	0.300	1.472	-1.153; 4.096	0.272
Sex	M vs F	3.622	-4.075; 11.318	0.356	4.126	-3.284; 11.535	0.275
Serum NfL	+ 1 (log scale)	-0.361	-2.952; 2.229	0.785	-0.521	-3.043; 2.001	0.686
FVC (%)							
Variable		Tregs percentage*			Tregs concentration*		
		MD	95% CI	p-value	MD	95% CI	p-value
Time from onset	+ 30 days	-0.366	-1.636; 0.904	0.573	-0.294	-1.569; 0.982	0.652
ALSFRS-r	- 5 points	**-6.809**	**-10.428; -3.190**	**<0.001**	**-7.108**	**-10.574; -3.642**	**<0.001**
Tregs	+1 unit *	0.929	-1.728; 3.585	0.493	0.291	-0.019; 0.601	0.066
Site of onset	Bulbar vs Spinal	-6.136	-23.533; 11.260	0.489	-3.323	-18.708; 12.061	0.672
BMI	+ 1 kg/m²	1.651	-1.566; 4.869	0.315	1.411	-1.630; 4.453	0.363
Weight change	- 10 kg	2.753	-14.278; 19.785	0.751	5.041	-12.376; 22.458	0.571
Age at onset	+ 10 years	2.472	-3.660; 8.604	0.429	1.763	-3.433; 6.959	0.506
Sex	M vs F	7.246	-10.176; 24.667	0.415	4.499	-11.010; 20.009	0.570
Serum NfL	+ 1 (log scale)	2.230	-5.666; 10.127	0.580	1.585	-5.635; 8.804	0.667

Additive effect linear mixed models were used to investigate ALSFRS-R and FVC variations over time. Mean differences (MD) with 95% confidence interval (CI) are reported to explain the effect of each variable on ALSFRS-R and FVC. Four models were analyzed. In the upper section of the table, two models were constructed with ALSFRS-R variation over time as the dependent variable, and the independent variables listed in the first column. Among these independent variables, Tregs were included as percentages in the upper left portion of the table and as concentrations in the upper right portion.

In the lower section of the table, two additional models were constructed with FVC% variation over time as the dependent variable, and the independent variables listed in the first column. Similarly, Tregs were included as percentages in the lower left portion of the table and as concentrations in the lower right portion.

Significance is set with p-values < 0.05, which are reported in bold characters. A positive mean difference implies that the variation in the explanatory variable is associated to an increase in ALSFRS-r or FVC scores, whichever the dependent variable is, whereas a negative sign in the mean difference suggests that the variation in the explanatory variable is associated to a decrease in ALSFRS-r or FVC scores.

*for both ALSFRS-r and FVC, the effect of Tregs in the first model is related to a 1% increase, whereas in the second model to a 1 cell count/uL increase.

ALSFRS-r, Amyotrophic Lateral Sclerosis Functional Rating Scale-revised; FVC, forced vital capacity; BMI, body mass index; NFL, neurofilament light chain.

better reflects ALSFRS-r or FVC decline. Table 3 shows the results of the four multivariable mixed models.

FVC and ALSFRS-r decline were tightly connected: for each 10% decrease in FVC, ALSFRS-r score declines on average by 1.204 points (95%CI -1.971;-0.4374, p= 0.002, when Treg concentrations were considered in the model, see upper right portion of the Table 3), and vice versa, every 5 points drop in ALSFRS-r corresponds to an average decline of 7.1081% in FVC (95%CI -10.574;-3.642, p<=0.0001, see lower right portion of the Table 3), independently of the decline due to the time course of the disease. Similar results were observed when Tregs percentages instead of concentrations were included in the model (left portion of Table 3).

Notably, Treg percentage variations did not influence either ALSFRS-r or FVC decline, while Treg cell counts had a positive, though non-significant effect, on FVC scores: every single Treg cell count decrease over one microliter corresponded to an average drop of 0.291% of FVC (95%CI -0.601;0.019, p=0.066). This effect was replicated when running a more simplified model including only time since onset of the disease and Treg variations. Among all the explanatory variables included in the multivariable models, only weight loss slightly affected ALSFRS-r decline, though without reaching statistical significance (every 10 kilograms loss corresponded to an average decline of 5.543 points when Treg concentrations were accounted, 95%CI-11.969;0.883, p= 0.091). All

the other explanatory variables, serum NfL included, were not independently associated with ALSFRS-r or FVC declines over time.

3.4 Tregs phenotype modifies during ALS course

CD38, CXCR3, CD39, PD1 markers were employed to characterize Tregs. In the first analysis, the unadjusted linear trends of these subpopulations were investigated (Figure 4). Notably, PD1+ Tregs significantly declined over time when considered as percentages over total CD4 T cells (MR= 0.956, 95%CI 0.921;0.993, p=0.019), while when measured as percentages over Tregs and as concentrations this trend did not reach statistical significance (Supplementary Table 2). CD39+Tregs, when measured as percentages over total Tregs, showed a non-significant linear increase over time (MR=1.029, 95%CI 0.989;1.070, p=0.159).

Next, we run multivariable models including all the abovementioned variables, whose results are summarized in Table 4 and Supplementary Tables 3-6.

When considering each subpopulation in percentages over total Tregs (Table 4), an opposite trend could be observed between CD39 + and PD1+Tregs, with the former increasing every month since onset of the disease by an average 11% (MR= 1.112, 95%CI 1.046;1.183, p=0.001) and the latter decreasing on average by 6% (MR= 0.939, 95%CI 0.894;0.987, p=0.013). Similarly, the decline in ALSFRS-r resulted in opposite effects on these two subpopulations still when assuming time since onset of the disease, with CD39 +Tregs decreasing for each 5-point loss in ALSFRS-r while PD1+ increased, though without reaching statistical significance (MR= 1.219, 95% CI 0.987;1.506, p=0.067).

Moreover, in the adjusted multivariable models, CD38+Treg counts showed a significant increase over time (accounted as months since onset of the disease) (Supplementary Table 3). Regarding other clinical variables associated with ALS, weight loss was an independent

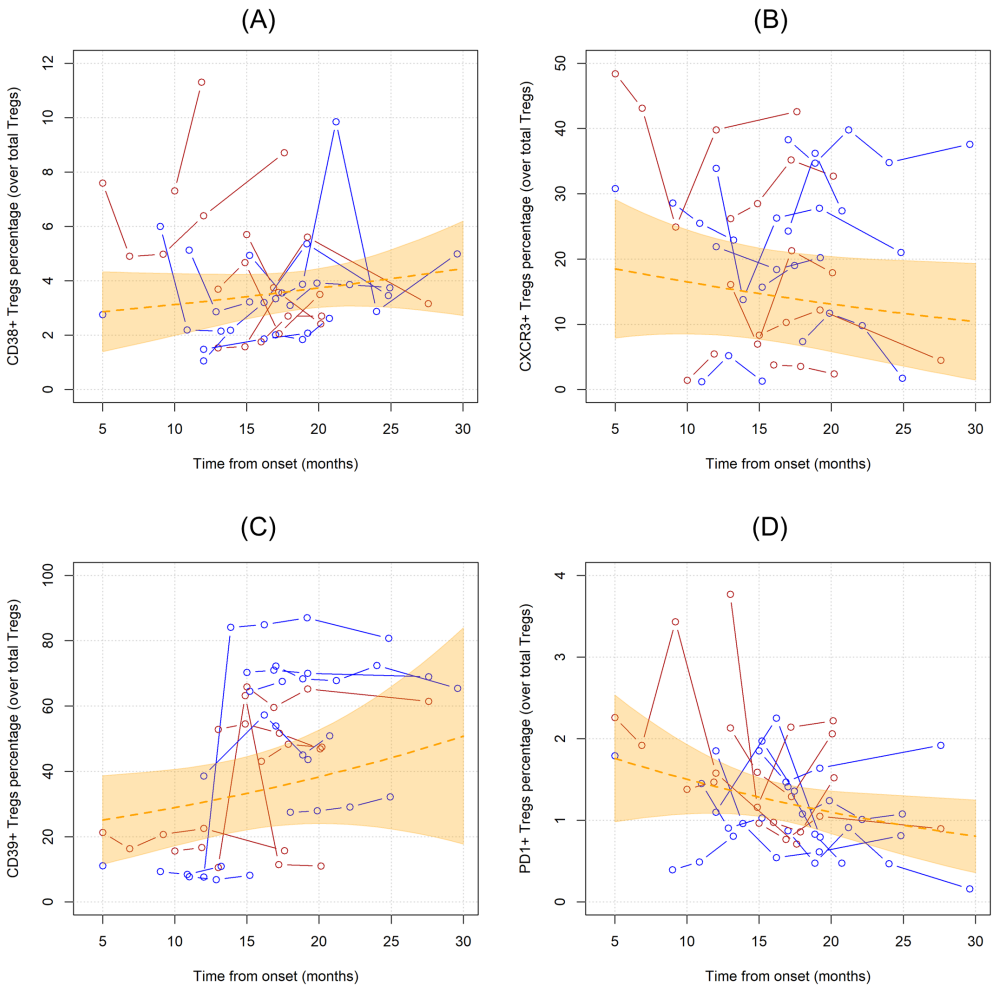

FIGURE 4
Unadjusted linear trends over time of CD38+ **(A)**, CXCR3+ **(B)**, CD39+ **(C)**, and PD1+ **(D)** Tregs subpopulations expressed in percentages over total Tregs. Continuous lines represent observed trajectories for each single patient with ALS. Female patients' Tregs trajectories are depicted in red color, while males' ones in blue. Dotted orange line represents the average linear variation in CD38+ Tregs **(A)**, CXCR3+ Tregs **(B)**, CD39+ Tregs **(C)**, and PD1+ Tregs **(D)** over time, expressed in months since onset of disease, with 95% confidence interval depicted by the yellow-shaded area. Tregs subpopulations are expressed as the percentage over total Tregs.

10.3389/fimmu.2024.1508974

TABLE 4 Multivariable model for variations in Tregs subpopulations defined by expression of markers CD38, CD39, CXCR3, PD1, expressed as percentages over total Tregs.

Variable		CD38+ Tregs			CXCR3+ Tregs		
		MR	95% CI	p-value	MR	95% CI	p-value
Time from onset	+ 30 days	1.023	0.986; 1.062	0.220	1.024	0.960; 1.092	0.476
ALSFRS-R	- 5 points	0.868	0.712; 1.059	0.163	0.815	0.603; 1.101	0.183
FVC	- 10%	**1.142**	**1.031; 1.264**	**0.011**	1.046	0.899; 1.218	0.559
Site of onset	Bulbar vs Spinal	0.941	0.651; 1.360	0.747	0.624	0.213; 1.828	0.390
BMI	+ 1 kg/m²	0.961	0.843; 1.097	0.559	0.896	0.651; 1.235	0.503
Weight change	- 10 kg	0.739	0.381; 1.434	0.371	0.785	0.176; 3.501	0.751
Age at onset	+ 10 years	1.113	0.958; 1.293	0.163	0.797	0.539; 1.179	0.256
Sex	M vs F	1.004	0.569; 1.772	0.989	1.919	0.493; 7.474	0.348
Albumin	+ 1 g/dL	1.512	0.730; 3.132	0.265	**0.286**	**0.106; 0.773**	**0.014**
CRP	+ 1 (log scale)	**1.330**	**1.033; 1.712**	**0.027**	1.275	0.809; 2.012	0.296
Uric acid	+ 1 mg/dL	1.007	0.837; 1.212	0.938	1.306	0.890; 1.915	0.173
Total cholesterol	+ 100 mg/dL	**1.968**	**1.203; 3.221**	**0.007**	**3.058**	**1.226; 7.626**	**0.017**
Monocytes	+ 0.1 mm³	0.969	0.877; 1.071	0.543	0.995	0.838; 1.183	0.957
Creatinine	+ 1 mg/dL	1.078	0.956; 1.216	0.220	0.888	0.656; 1.203	0.444
Triglycerides	+ 1 (log scale)	0.720	0.430; 1.203	0.210	0.876	0.427; 1.796	0.718
NLR	+ 1 (log scale)	1.098	0.722; 1.668	0.662	1.075	0.596; 1.937	0.811
NFL in serum	+ 1 (log scale)	**0.696**	**0.515; 0.940**	**0.018**	0.891	0.539; 1.473	0.653
Variable		CD39+ Tregs			PD1+ Tregs		
		MR	95% CI	p-value	MR	95% CI	p-value
Time from onset	+ 30 days	**1.112**	**1.046; 1.183**	**0.001**	**0.939**	**0.894; 0.987**	**0.013**
ALSFRS-R	- 5 points	**0.707**	**0.552; 0.907**	**0.006**	1.219	0.987; 1.506	0.067
FVC	- 10%	1.055	0.926; 1.201	0.423	0.960	0.860; 1.072	0.468
Site of onset	Bulbar vs Spinal	0.589	0.330; 1.050	0.073	0.771	0.322; 1.851	0.561
BMI	+ 1 kg/m²	0.953	0.783; 1.159	0.627	1.075	0.833; 1.386	0.580
Weight change	- 10 kg	0.480	0.200; 1.151	0.100	1.233	0.419; 3.628	0.703
Age at onset	+ 10 years	**1.251**	**1.026; 1.526**	**0.027**	1.164	0.855; 1.583	0.335
Sex	M vs F	0.996	0.440; 2.252	0.992	0.632	0.206; 1.942	0.423
Albumin	+ 1 g/dL	0.778	0.338; 1.791	0.556	1.214	0.583; 2.529	0.604
CRP	+ 1 (log scale)	1.098	0.785; 1.534	0.585	1.186	0.837; 1.681	0.337
Uric acid	+ 1 mg/dL	1.191	0.831; 1.705	0.341	0.880	0.692; 1.120	0.299
Total cholesterol	+ 100 mg/dL	0.878	0.427; 1.808	0.725	0.771	0.388; 1.532	0.458
Monocytes	+ 0.1 mm³	1.040	0.910; 1.188	0.568	0.881	0.768; 1.011	0.072
Creatinine	+ 1 mg/dL	0.954	0.811; 1.122	0.568	1.189	0.969; 1.459	0.098
Triglycerides	+ 1 (log scale)	1.810	0.897; 3.654	0.098	**1.789**	**1.066; 3.001**	**0.028**
NLR	+ 1 (log scale)	1.242	0.742; 2.078	0.410	1.230	0.788; 1.920	0.362
NFL in serum	+ 1 (log scale)	**1.548**	**1.000; 2.395**	**0.050**	1.372	0.920; 2.045	0.121

Multiplicative effect generalized linear mixed model with gamma distribution and log link function were employed to study each Treg subpopulation variation. Mean ratios (MR) with 95% confidence interval (CI) are reported to explain the effect of each variable on Treg % or Treg concentrations, respectively. Significance is set with p-values < 0.05, which are reported in bold character. The mean ratio represents the ratio between each subpopulation's average Tregs percentage.

ALSFRS-r, Amyotrophic Lateral Sclerosis Functional Rating Scale-revised; FVC, forced vital capacity; BMI, body mass index; CRP, C-reactive protein; NLR, neutrophil-to-lymphocytes ratio; NFL, neurofilament light chain.

factor in decreasing CD38+Treg concentrations (MR=0.404, 95%CI 0.188-0.869,p=0.020), while age at onset influenced CD39+Tregs(%) over total Tregs (MR=1.251,95%CI 1.026;1.526, p=0.027). Total cholesterol species determined a rise over time of CD38+ and CXCR3+Tregs (Supplementary Tables 3, 5), while triglycerides acted more on PD1+Tregs, by opposing their longitudinal trend towards a decrease over time. Albumin affected CXCR3+Tregs by decreasing their levels in every unit of measure they were considered.

Finally, by incorporating serum NfL in the multivariable model, we could observe an opposite effect of this marker of neurodegeneration on Treg subpopulations: while decreasing CD38+Tregs (MR= 0.696, 95%CI 0.515;0.940, p=0.018 for CD38+Tregs/total Tregs), each log unit increase in serum NfL increased PD1+Tregs (MR=1.495, 95%CI 1.010-2.213, p=0.044 for PD1+Tregs/total CD4) and CD39+Treg, though the latter with minimal statistical significance when considered as CD39 +Tregs/total Tregs (MR=1.548, 95%CI 1.000-2.395, p=0.050).

4 Discussion

In this explorative longitudinal study, we suggest that Tregs number does not change over time in ALS patients; lipid and in particular cholesterol metabolism, peripheral inflammation, and gender might impact Treg fluctuations during the natural history of ALS and should be considered when designing and interpreting clinical trials in which Treg levels are used as biomarkers. The characterization of Tregs phenotype by analysis of the four surface markers (CD38, CXCR3, CD39, PD1) was limited to the percentage of Tregs expressing each marker at the time, without considering distinct or overlapping subpopulations. However, when phenotyping within the Treg population, this preliminary analysis showed PD1+Tregs might change during ALS course with a decrease over time, while CD39 +Tregs may tend to expand, especially when ALSFRS-r score does not vary over time. PD1+ Tregs decreasing over time since onset of the disease might suggest a progressive decline in their immunoregulatory capacity, potentially contributing to the heightened inflammation observed in ALS. On the other hand, the expansion of CD39+ Tregs could represent a compensatory mechanism attempting to counteract neuroinflammation through enhanced adenosine production, which has anti-inflammatory effects. However, given the small sample size in our study and lack of supportive functional studies, the observed trend require confirmation in larger cohorts before definitive conclusions can be drawn about their role in ALS pathophysiology.

This study also meant to attempt to explain part of the intricate relationship between Tregs and other variables as sex, age, cholesterol, and inflammation, during ALS clinical course. The advantage of such an approach is to synthesize all variables at once considering their variations in time; however, we recognize these findings merely "scratch the surface" of a much more complicated and dynamic balance between biological phenomena and the validation of the relation of each explanatory variable with Tregs would require a whole set of functional experiments per se. Besides, the incorporation of all these explanatory variables in a multivariable model could be subject to statistical bias given the limited sample size of our study, and the lack of a validation cohort; however, the results of the regression coefficients for each variable were fairly consistent across all the multivariable models run for every dependent variable when measured in different units of measure.

With these limits in mind, the association between Tregs and cholesterol metabolism has been already described in genetic hyperlipidemias, where excess circulating cholesterol species are sensed by Tregs and impair their function and proliferative capacities (32). In the general population, HDL was found to positively associated with Tregs (33), and rosuvastatin administration decreased the number of peripheral Tregs in normocholesterolemic subjects (34). In familial hypercholesterolemia patients, increased Treg frequencies were found, though their suppressive capacities were impaired and impacted atherosclerosis progression (35). On the other hand, recent trials on autologous Tregs transplantation in ALS patients indicate oxidized-LDL species decreased following this intervention (36), suggesting that functional Tregs may act on the reverse on circulating lipid species attenuating overall oxidative stress mediated by them. In our study, the positive association between total cholesterol and Tregs was particularly evident for CD38+ and CXCR3+ subsets, probably reflecting a switch to a more metabolically active profile with higher homing capacities.

When looking at all the explanatory variables for Tregs variations concerning inflammation, the abovementioned inherent limits of our observational work may hold, along with the risk of reverse causation, and the necessity of further functional experiments to clarify the sequential regulation of each immunological player during the ALS clinical course.

NLR, a known marker of all-cause mortality in the general population as well as in ALS patients (25, 27) in our study seemed to modify Tregs. Not surprisingly, CRP, a known marker of systemic inflammation, predicted higher levels of metabolically activated CD38+ and PD1+Tregs without affecting total Treg concentrations or percentages over total CD4 T cells. Besides, in our analysis, we could observe a positive association between Tregs and monocytes in multivariable analysis, suggesting an independent role of this variable. Interestingly, monocytes were proven to longitudinally increase over time in ALS patients (37). Other works have explored the role of activated monocytes in driving ALS progression (26, 28, 38, 39).

Males seem to have increased Tregs, especially metabolically active CD38-positive, during the ALS course. This is in line with previous works in which Treg frequencies were found to be increased in healthy male subjects (40, 41). Sex-specific differences in ALS prognosis dictated by peripheral blood cell counts have been recently uncovered spanning several immune cells, from neutrophils to natural killer cells (25, 42), raising the possibility of an interplay between sexual hormones and immune regulation in ALS.

More recently, the balance between activated and resting Tregs in contrast with the proportion of T effector cells have been described to have opposite effects on survival, with protective or noxious consequences respectively (43). PD1 surface expression within T cells could be associated to exhaustion only when co-expression of other markers and *in vivo* tests of cytokine production are performed, otherwise the effects downstream this receptor-ligand interaction could be so multifaced it would be reductive to tag as "exhausting" Tregs those expressing PD1 (44). In previous studies on multiple sclerosis, PD1+Tregs were found to be altered compared to healthy controls (45), and disease-modifying treatments could enhance the

surface expression of PD1 on Tregs (46). In our study, though we limited our analysis to the surface expression of this marker, PD1 +Tregs seemed to decrease with ALS course since the onset of the disease with an inverse correlation with ALSFRS-r decline. Conversely, CD39-expressing Tregs identify a subpopulation of Tregs with enhanced suppressive capacities due to the ATPase activity of this membrane protein (47) and that was found to be increased over time since the start of symptoms in our ALS cohort, especially when the ALSFRS-r score did not decrease as expected. These data may suggest that, though total Tregs do not longitudinally modify because of ALS clinical course, their phenotype might change. Intriguingly, serum NfL, which could reflect the neurodegenerative pace, affects only certain markers-expressing Tregs, in particular CD38+Tregs, which decreased for each increase in serum NfL, and CD39+ or PD1+Treg, which on the other hand, expanded upon NfL increase.

In the authors' opinion, the prognostic implications of such observations deserve further research and could be interesting markers for monitoring the disease progression.

The relation between Treg levels with ALSFRS-r decline was not supported by our study. In this setting, however, FVC could be more sensitive than ALSFRS-R to Treg concentrations increase, and the instrumental monitoring of respiratory function in ALS efficiently predicts the disease evolution towards support procedures (48). Longitudinal models of ALSFRS-r or FVC decline in our cohort confirmed the strong relation between these two clinical measures of ALS one to the other, independently of time, as already reported in other studies (31). The other clinical and biological variables did not seem to account for variations in ALSFRS-r and FVC, highlighting that the decline in these measures may be mainly related to time and not to other individual characteristics.

The importance of including several clinical and demographic variables besides time in regression models for explaining the variations of Tregs numbers during the ALS course is paramount to understanding how intricate the relation between T regulatory cells and immune homeostasis in patients is. Limiting our observations for time wouldn't have allowed us to predict Tregs fluctuations and, above all, would have misled us to the hypothesis Tregs number does not vary over time in ALS and might be used as an efficient pharmacodynamic marker for ALS. Our analysis is limited by the analysis of a single cohort, with restricted sample size and number of observations; besides, due to the small number of observations per subject, it was not possible to include several random slopes in mixed models to account for individual variations of each independent variable's effect on the outcomes. Moreover, the findings of our study are limited to the ALS course period ranging from about 5 to 30 months from disease onset.

Notwithstanding these inherent limitations, our findings should prompt further longitudinal studies in larger and multiple cohorts of ALS patients, collecting more Tregs assessments over time per subject, to validate these results.

5 Conclusions

In conclusion, though Treg number appears to be constant over the disease course and does not affect ALSFRS-r decline, our study suggests that Tregs widely fluctuate and may differently vary in response to contingencies, such as inflammatory or metabolic (especially lipidic) triggers, or in a sex-specific manner, though these results should be confirmed in other cohorts and larger studies. This should be considered and possibly discourages choosing Treg levels as pharmaco-dynamic markers for ALS clinical trial data interpretation.

Furthermore, the characterization of Treg phenotypic activity through the analysis of surface marker expression has offered the opportunity to better explain some of the variations in Tregs during the course of ALS since the onset of symptoms and has shed light on PD1+ and CD39+Tregs, which tend to vary and positively correlate with markers of neurodegeneration. This preliminary insight on how Tregs might vary in phenotype with disease progression should be the subject of broader functional investigations.

Data availability statement

The raw data supporting the conclusions of this article will be made available by the authors to external researchers who provide scientific proposals and whose proposed use of the data has been approved by an independent review committee identified for this purpose.

Ethics statement

The studies were approved by Comitato Etico Provinciale di Modena. The studies were conducted in accordance with the local legislation and institutional requirements. The participants provided their written informed consent to participate in this study.

Author contributions

EZ: Conceptualization, Data curation, Funding acquisition, Investigation, Writing – original draft. FB: Data curation, Formal analysis, Investigation, Methodology, Visualization, Writing – original draft. CS: Conceptualization, Data curation, Methodology, Writing – original draft. SDB: Investigation, Methodology, Visualization, Writing – review & editing. IM: Data curation, Investigation, Methodology, Writing – review & editing. GG: Data curation, Formal analysis, Writing – review & editing. DLT: Formal analysis, Methodology, Writing – review & editing. AC: Investigation, Methodology, Supervision, Writing – review & editing. RD'A: Formal analysis, Methodology, Writing – review & editing. JM: Conceptualization, Funding acquisition, Investigation, Methodology, Resources, Supervision, Validation, Writing – review & editing.

Funding

The author(s) declare financial support was received for the research, authorship, and/or publication of this article. The study was supported by ARISLA (Fondazione Italiana di Ricerca per la

SLA) (FGCR02/2015 to JM) and the Italian Ministry of Health (Bando PNRR-2023) (NRR-MCNT2-2023-12378140, to EZ and JM). The funders of the study were not involved in protocol design, data collection, statistical analysis, data interpretation, writing of the report, and the decision to submit this article.

Acknowledgments

The authors acknowledge the other members of RAP-ALS Study Group that contributed to data collection within the RAP-ALS study (Supplementary Table 7).

Conflict of interest

The authors declare that the research was conducted in the absence of any commercial or financial relationships that could be construed as a potential conflict of interest.

Generative AI statement

The author(s) declare that no Generative AI was used in the creation of this manuscript.

Publisher's note

Supplementary material

The Supplementary Material for this article can be found online at: https://www.frontiersin.org/articles/10.3389/fimmu.2024.1508974/full#supplementary-material

References

1. Wolfson C, Gauvin DE, Ishola F, Oskoui M. Global prevalence and incidence of amyotrophic lateral sclerosis: A systematic review. *Neurology*. (2023) 101:e613–23. doi: 10.1212/WNL.0000000000207474

2. Feldman EL, Goutman SA, Petri S, Mazzini L, Savelieff MG, Shaw PJ, et al. Amyotrophic lateral sclerosis. *Lancet*. (2022) 400:1363–80. doi: 10.1016/S0140-6736(22)01272-7

3. Van Harten ACM, Phatnani H, Przedborski S. Non-cell-autonomous pathogenic mechanisms in amyotrophic lateral sclerosis. *Trends Neurosci*. (2021) 44:658–68. doi: 10.1016/j.tins.2021.04.008

4. Appel SH, Beers DR, Zhao W. Amyotrophic lateral sclerosis is a systemic disease: peripheral contributions to inflammation-mediated neurodegeneration. *Curr Opin Neurol*. (2021) 34:765–72. doi: 10.1097/WCO.0000000000000983

5. Contreras-Castillo E, García-Rasilla VY, García-Patiño MG, Licona-Limón P. Stability and plasticity of regulatory T cells in health and disease. *J Leukoc Biol*. (2024) 116:33–53. doi: 10.1093/jleuko/qiae049

6. Malek TR, Yu A, Vincek V, Scibelli P, Kong L. CD4 regulatory T cells prevent lethal autoimmunity in IL-2Rbeta-deficient mice. Implications for the nonredundant function of IL-2. *Immunity*. (2002) 17:167–78. doi: 10.1016/s1074-7613(02)00367-9

7. Hu W, Wang ZM, Feng Y, Schizas M, Hoyos BE, van der Veeken J, et al. Regulatory T cells function in established systemic inflammation and reverse fatal autoimmunity. *Nat Immunol*. (2021) 22:1163–74. doi: 10.1038/s41590-021-01001-4

8. Glasner A, Plitas G. Tumor resident regulatory T cells. *Semin Immunol*. (2021) 52:101476. doi: 10.1016/j.smim.2021.101476

9. Beers DR, Henkel JS, Zhao W, Wang J, Huang A, Wen S, et al. Endogenous regulatory T lymphocytes ameliorate amyotrophic lateral sclerosis in mice and correlate with disease progression in patients with amyotrophic lateral sclerosis. *Brain*. (2011) 134:1293–314. doi: 10.1093/brain/awr074

10. Henkel JS, Beers DR, Wen S, Rivera AL, Toennis KM, Appel JE, et al. Regulatory T-lymphocytes mediate amyotrophic lateral sclerosis progression and survival. *EMBO Mol Med*. (2013) 5:64–79. doi: 10.1002/emmm.201201544

11. Beers DR, Zhao W, Wang J, Zhang X, Wen S, Neal D, et al. ALS patients' regulatory T lymphocytes are dysfunctional, and correlate with disease progression rate and severity. *JCI Insight*. (2017) 2:e89530. doi: 10.1172/jci.insight.89530

12. Thonhoff JR, Beers DR, Zhao W, Pleitez M, Simpson EP, Berry JD, et al. Expanded autologous regulatory T-lymphocyte infusions in ALS: A phase I, first-in-human study. *Neurol Neuroimmunol Neuroinflamm*. (2018) 5:e465. doi: 10.1212/NXI.0000000000000465

13. Thonhoff JR, Berry JD, Macklin EA, Beers DR, Mendoza PA, Zhao W, et al. Combined regulatory T-lymphocyte and IL-2 treatment is safe, tolerable, and biologically active for 1 year in persons with amyotrophic lateral sclerosis. *Neurol Neuroimmunol Neuroinflamm*. (2022) 9:e200019. doi: 10.1212/NXI.0000000000200019

14. Li X, Bedlack R. Evaluating emerging drugs in phase II & III for the treatment of amyotrophic lateral sclerosis. *Expert Opin Emerg Drugs*. (2024) 29:93–102. doi: 10.1080/14728214.2024.2333420

15. Mandrioli J, D'Amico R, Zucchi E, De Biasi S, Banchelli F, Martinelli I, et al. Randomized, double-blind, placebo-controlled trial of rapamycin in amyotrophic lateral sclerosis. *Nat Commun*. (2023) 14:4970. doi: 10.1038/s41467-023-40734-8

16. Mandrioli J, D'Amico R, Zucchi E, Gessani A, Fini N, Fasano A, et al. Rapamycin treatment for amyotrophic lateral sclerosis: Protocol for a phase II randomized, double-blind, placebo-controlled, multicenter, clinical trial (RAP-ALS trial). *Med (Baltimore)*. (2018) 97:e11119. doi: 10.1097/MD.0000000000011119

17. Kar A, Mehrotra S, Chatterjee S. CD38: T cell immuno-metabolic modulator. *Cells*. (2020) 9:1716. doi: 10.3390/cells9071716

18. Hoerning A, Koss K, Datta D, Boneschansker L, Jones CN, Wong IY, et al. Subsets of human CD4(+) regulatory T cells express the peripheral homing receptor CXCR3. *Eur J Immunol*. (2011) 41:2291–302. doi: 10.1002/eji.201041095

19. Mandapathil M, Lang S, Gorelik E, Whiteside TL. Isolation of functional human regulatory T cells (Treg) from the peripheral blood based on the CD39 expression. *J Immunol Methods*. (2009) 346:55–63. doi: 10.1016/j.jim.2009.05.004

20. Zinselmeyer BH, Heydari S, Sacristán C, Nayak D, Cammer M, Herz J, et al. PD-1 promotes immune exhaustion by inducing antiviral T cell motility paralysis. *J Exp Med*. (2013) 210:757–74. doi: 10.1084/jem.20121416

21. Simonini C, Zucchi E, Bedin R, Martinelli I, Gianferrari G, Fini N, et al. CSF heavy neurofilament may discriminate and predict motor neuron diseases with upper motor neuron involvement. *Biomedicines*. (2021) 9:1623. doi: 10.3390/biomedicines9111623

22. Martinelli I, Zucchi E, Simonini C, Gianferrari G, Bedin R, Biral C, et al. SerpinA1 levels in amyotrophic lateral sclerosis patients: An exploratory study. *Eur J Neurol*. (2024) 31:e16054. doi: 10.1111/ene.16054

23. Janse van Mantgem MR, van Eijk RPA, van der Burgh HK, Tan HHG, Westeneng HJ, van Es MA, et al. Prognostic value of weight loss in patients with amyotrophic lateral sclerosis: a population-based study. *J Neurol Neurosurg Psychiatry*. (2020) 91:867–75. doi: 10.1136/jnnp-2020-322909

24. Ortholand J, Pradat PF, Tezenas du Montcel S, Durrleman S. Interaction of sex and onset site on the disease trajectory of amyotrophic lateral sclerosis. *J Neurol*. (2023) 270:5903–12. doi: 10.1007/s00415-023-11932-7

25. Grassano M, Manera U, De Marchi F, Cugnasco P, Matteoni E, Daviddi M, et al. The role of peripheral immunity in ALS: a population-based study. *Ann Clin Transl Neurol*. (2023) 10:1623–32. doi: 10.1002/acn3.51853

26. Mcgill RB, Steyn FJ, Ngo ST, Thorpe KA, Heggie S, Henderson RD, et al. Monocyte CD14 and HLA-DR expression increases with disease duration and severity in amyotrophic lateral sclerosis. *Amyotroph Lateral Scler Frontotemporal Degener*. (2022) 23:430–7. doi: 10.1080/21678421.2021.1964531

27. Leone MA, Mandrioli J, Russo S, Cucovici A, Gianferrari G, Lisnic V, et al. Neutrophils-to-lymphocyte ratio is associated with progression and overall survival in amyotrophic lateral sclerosis. *Biomedicines*. (2022) 10:354. doi: 10.3390/biomedicines10020354

28. Yildiz O, Schroth J, Lombardi V, Pucino V, Bobeva Y, Yip PK, et al. The expression of active CD11b monocytes in blood and disease progression in amyotrophic lateral sclerosis. *Int J Mol Sci*. (2022) 23:3370. doi: 10.3390/ijms23063370

29. Holdom CJ, Janse van Mantgem MR, van Eijk RPA, Howe SL, van den Berg LH, McCombe PA, et al. Venous creatinine as a biomarker for loss of fat-free mass and disease progression in patients with amyotrophic lateral sclerosis. *Eur J Neurol*. (2021) 28:3615–25. doi: 10.1111/ene.15003

30. Berod L, Friedrich C, Nandan A, Freitag J, Hagemann S, Harmrolfs K, et al. *De novo* fatty acid synthesis controls the fate between regulatory T and T helper 17 cells. *Nat Med*. (2014) 20:1327–33. doi: 10.1038/nm.3704

31. Daghlas SA, Govindarajan R, Pooled Resource Open-Access ALS Clinical Trials Consortium. Relative effects of forced vital capacity and ALSFRS-R on survival in ALS. *Muscle Nerve*. (2021) 64:346–51. doi: 10.1002/mus.27344

32. Pinzon Grimaldos A, Bini S, Pacella I, Rossi A, Di Costanzo A, Minicocci I, et al. The role of lipid metabolism in shaping the expansion and the function of regulatory T cells. *Clin Exp Immunol*. (2022) 208:181–92. doi: 10.1093/cei/uxab033

33. Schmitz T, Freuer D, Linseisen J, Meisinger C. Associations between serum cholesterol and immunophenotypical characteristics of circulatory B cells and Tregs. *J Lipid Res*. (2023) 64:100399. doi: 10.1016/j.jlr.2023.100399

34. Karmaus PW, Shi M, Perl S, Biancotto A, Candia J, Cheung F, et al. Effects of rosuvastatin on the immune system in healthy volunteers with normal serum cholesterol. *JCI Insight*. (2019) 4:e131530. doi: 10.1172/jci.insight.131530

35. Bonacina F, Martini E, Svecla M, Nour J, Cremonesi M, Beretta G, et al. Adoptive transfer of CX3CR1 transduced-T regulatory cells improves homing to the atherosclerotic plaques and dampens atherosclerosis progression. *Cardiovasc Res*. (2021) 117:2069–82. doi: 10.1093/cvr/cvaa264

36. Beers DR, Thonhoff JR, Faridar A, Thome AD, Zhao W, Wen S, et al. Tregs attenuate peripheral oxidative stress and acute phase proteins in ALS. *Ann Neurol*. (2022) 92:195–200. doi: 10.1002/ana.26375

37. Cui C, Ingre C, Yin L, Li X, Andersson J, Seitz C, et al. Correlation between leukocyte phenotypes and prognosis of amyotrophic lateral sclerosis. *Elife*. (2022) 11: e74065. doi: 10.7554/eLife.74065

38. Du Y, Zhao W, Thonhoff JR, Wang J, Wen S, Appel SH. Increased activation ability of monocytes from ALS patients. *Exp Neurol*. (2020) 328:113259. doi: 10.1016/j.expneurol.2020.113259

39. Zhao W, Beers DR, Hooten KG, Sieglaff DH, Zhang A, Kalyana-Sundaram S, et al. Characterization of gene expression phenotype in amyotrophic lateral sclerosis monocytes. *JAMA Neurol*. (2017) 74:677–85. doi: 10.1001/jamaneurol.2017.0357

40. Robinson GA, Peng J, Peckham H, Butler G, Pineda-Torra I, Ciurtin C, et al. Investigating sex differences in T regulatory cells from cisgender and transgender healthy individuals and patients with autoimmune inflammatory disease: a cross-sectional study. *Lancet Rheumatol*. (2022) 4:e710–24. doi: 10.1016/S2665-9913(22)00198-9

41. Singh RP, Bischoff DS. Sex hormones and gender influence the expression of markers of regulatory T cells in SLE patients. *Front Immunol*. (2021) 12:619268. doi: 10.3389/fimmu.2021.619268

42. Murdock BJ, Zhao B, Pawlowski KD, Famie JP, Piecuch CE, Webber-Davis IF, et al. Peripheral immune profiles predict ALS progression in an age- and sex-dependent manner. *Neurol Neuroimmunol Neuroinflamm*. (2024) 11:e200241. doi: 10.1212/NXI.0000000000200241

43. Yazdani S, Seitz C, Cui C, Lovik A, Pan L, Piehl F, et al. T cell responses at diagnosis of amyotrophic lateral sclerosis predict disease progression. *Nat Commun*. (2022) 13:6733. doi: 10.1038/s41467-022-34526-9

44. Pauken KE, Wherry EJ. Overcoming T cell exhaustion in infection and cancer. *Trends Immunol*. (2015) 36:265–76. doi: 10.1016/j.it.2015.02.008

45. Sambucci M, Gargano F, De Rosa V, De Bardi M, Picozza M, Placido R, et al. FoxP3 isoforms and PD-1 expression by T regulatory cells in multiple sclerosis. *Sci Rep*. (2018) 8:3674. doi: 10.1038/s41598-018-21861-5

46. Wu Q, Mills EA, Wang Q, Dowling CA, Fisher C, Kirch B, et al. Siponimod enriches regulatory T and B lymphocytes in secondary progressive multiple sclerosis. *JCI Insight*. (2020) 5:e134251. doi: 10.1172/jci.insight.134251

47. Borsellino G, Kleinewietfeld M, Di Mitri D, Sternjak A, Diamantini A, Giometto R, et al. Expression of ectonucleotidase CD39 by Foxp3+ Treg cells: hydrolysis of extracellular ATP and immune suppression. *Blood*. (2007) 110:1225–32. doi: 10.1182/blood-2006-12-064527

48. Andrews JA, Meng L, Kulke SF, Rudnicki SA, Wolff AA, Bozik ME, et al. Association between decline in slow vital capacity and respiratory insufficiency, use of assisted ventilation, tracheostomy, or death in patients with amyotrophic lateral sclerosis. *JAMA Neurol*. (2018) 75:58–64. doi: 10.1001/jamaneurol.2017.3339

frontiers | Frontiers in Immunology

TYPE Original Research
PUBLISHED 08 January 2025
DOI 10.3389/fimmu.2024.1494842

OPEN ACCESS

EDITED BY
Wassim Elyaman,
Columbia University, United States

REVIEWED BY
Hanane Touil,
Columbia University, United States
Abeer Obaid,
AbbVie, United States

*CORRESPONDENCE
Laure Michel
laure.michel@chu-rennes.fr

RECEIVED 11 September 2024
ACCEPTED 03 December 2024
PUBLISHED 08 January 2025

CITATION
Rodriguez S, Couloume L, Ferrant J, Vince N, Mandon M, Jean R, Monvoisin C, Leonard S, Le Gallou S, Silva NSB, Bourguiba-Hachemi S, Laplaud D, Garcia A, Casey R, Zephir H, Kerbrat A, Edan G, Lepage E, Thouvenot E, Ruet A, Mathey G, Gourraud P-A, Tarte K, Delaloy C, Amé P, Roussel M and Michel L (2025) Blood immunophenotyping of multiple sclerosis patients at diagnosis identifies a classical monocyte subset associated to disease evolution.
Front. Immunol. 15:1494842.
doi: 10.3389/fimmu.2024.1494842

Blood immunophenotyping of multiple sclerosis patients at diagnosis identifies a classical monocyte subset associated to disease evolution

Stéphane Rodriguez[1,2], Laura Couloume[1], Juliette Ferrant[1,2], Nicolas Vince[3], Marion Mandon[1,2], Rachel Jean[1,2], Celine Monvoisin[1], Simon Leonard[1], Simon Le Gallou[1,2], Nayane S. B. Silva[3,4], Sonia Bourguiba-Hachemi[3], David Laplaud[3,5], Alexandra Garcia[3], Romain Casey[6,7,8,9], Helene Zephir[10], Anne Kerbrat[11], Gilles Edan[11], Emmanuelle Lepage[11], Eric Thouvenot[12,13], Aurelie Ruet[14,15], Guillaume Mathey[16,17], Pierre-Antoine Gourraud[3,5], Karin Tarte[1,2], Celine Delaloy[1], Patricia Amé[1,2], Mikael Roussel[1,2] and Laure Michel[1,2,8]*on behalf of OFSEP investigators

[1]Institut National de la Santé et de la Recherche Médicale (INSERM), Unité Mixte de Recherche U1236, Université Rennes, Etablissement Français du Sang Bretagne, LabEx IGO, Rennes, France, [2]Pole Biologie-Centre Hospitalier Universitaire (CHU) Rennes, Rennes, France, [3]Institut National de la Santé et de la Recherche Médicale (INSERM), Centre Hospitalier Universitaire (CHU) Nantes, Nantes University, Center for Research in Transplantation and Translational Immunology, UMR 1064, Nantes, France, [4]São Paulo State University, Molecular Genetics and Bioinformatics Laboratory, School of Medicine, Botucatu, Brazil, [5]Service de Neurologie, Centre Hospitalier Universitaire (CHU) Nantes, CRC-SEP Pays de la Loire, CIC 1413, Nantes, France, [6]Lyon University, University Claude Bernard Lyon 1, Lyon, France, [7]Hospices Civils de Lyon, Neurology Department, Sclérose en Plaques, Pathologies de la Myéline et Neuro-Inflammation, Bron, France, [8]Observatoire Français de la Sclérose en Plaques, Centre de Recherche en Neurosciences de Lyon, INSERM 1028 and CNRS UMR 5292, Lyon, France, [9]EUGENE DEVIC EDMUS Foundation against Multiple Sclerosis, State-Approved Foundation, Bron, France, [10]Lille University, Inserm U1172, Lille University Hospital, Lille, France, [11]Neurology Department, Rennes Clinical Investigation Centre, Rennes University Hospital-Rennes University-Institut National de la Santé et de la Recherche Médicale (INSERM), Rennes, France, [12]Department of Neurology, Nimes University Hospital, Nimes, France, [13]Institut de Génomique Fonctionnelle, UMR5203, Inserm 1191, Université de Montpellier, Montpellier, France, [14]Neurocentre Magendie, Institut National de la Santé et de la Recherche Médicale (INSERM) U1215, Bordeaux, France, [15]CHU de Bordeaux, Department of Neurology, Bordeaux, France, [16]Department of Neurology, Nancy University Hospital, Nancy, France, [17]Université de Lorraine, Inserm, INSPIIRE, Nancy, France

Introduction: Myeloid cells trafficking from the periphery to the central nervous system are key players in multiple sclerosis (MS) through antigen presentation, cytokine secretion and repair processes.

Methods: Combination of mass cytometry on blood cells from 60 MS patients at diagnosis and 29 healthy controls, along with single cell RNA sequencing on paired blood and cerebrospinal fluid (CSF) samples from 5 MS patients were used for myeloid cells detailing.

10.3389/fimmu.2024.1494842

Results: Myeloid compartment study demonstrated an enrichment of a peculiar classical monocyte population in 22% of MS patients at the time of diagnosis. Notably, this patients' subgroup exhibited a more aggressive disease phenotype two years post-diagnosis. This monocytic population, detected in both the CSF and blood, was characterized by CD206, CD209, CCR5 and CCR2 expression, and was found to be more frequent in MS patients carrying the HLA-DRB1*15:01 allele. Furthermore, pathways analysis predicted that these cells had antigen presentation capabilities coupled with pro-inflammatory phenotype.

Discussion: Altogether, these results point toward the amplification of a specific and pathogenic myeloid cell subset in MS patients with genetic susceptibilities.

KEYWORDS

multiple sclerosis, cerebrospinal fluid, classical monocyte, disability, antigen presentation

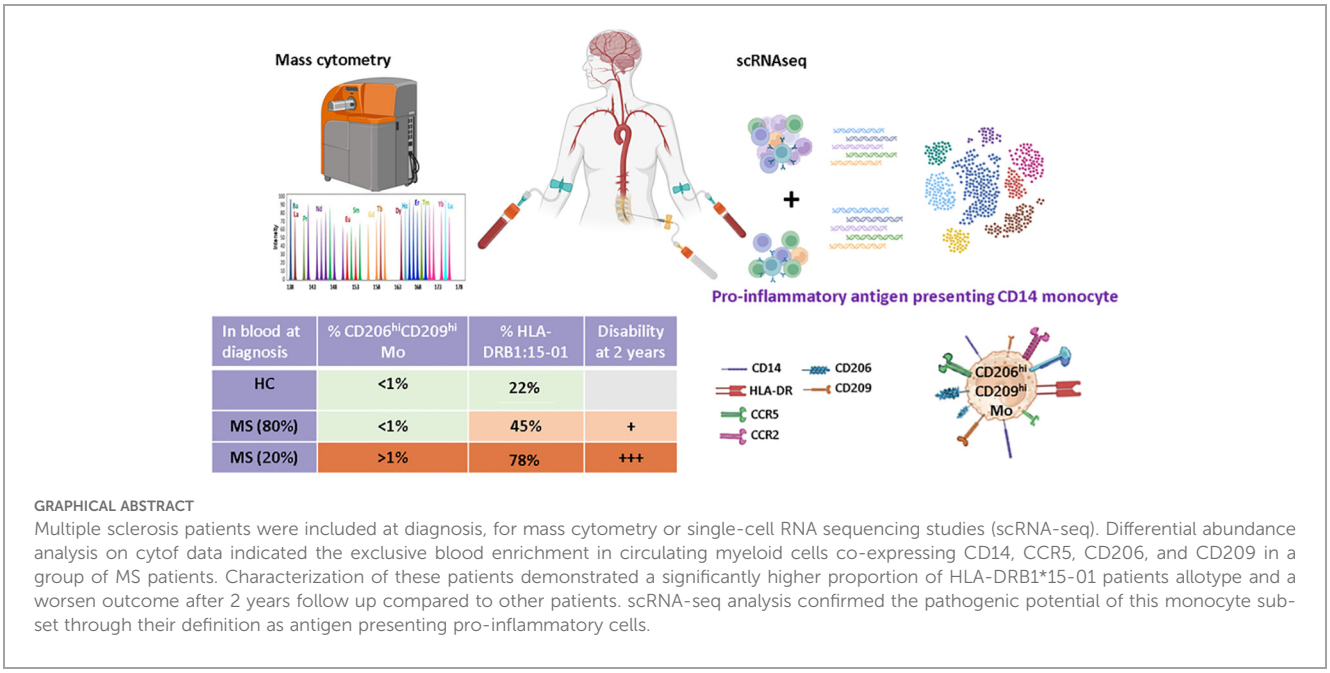

In blood at diagnosis	% CD206^{hi}CD209^{hi} Mo	% HLA-DRB1:15-01	Disability at 2 years
HC	<1%	22%	
MS (80%)	<1%	45%	+
MS (20%)	>1%	78%	+++

GRAPHICAL ABSTRACT
Multiple sclerosis patients were included at diagnosis, for mass cytometry or single-cell RNA sequencing studies (scRNA-seq). Differential abundance analysis on cytof data indicated the exclusive blood enrichment in circulating myeloid cells co-expressing CD14, CCR5, CD206, and CD209 in a group of MS patients. Characterization of these patients demonstrated a significantly higher proportion of HLA-DRB1*15-01 patients allotype and a worsen outcome after 2 years follow up compared to other patients. scRNA-seq analysis confirmed the pathogenic potential of this monocyte subset through their definition as antigen presenting pro-inflammatory cells.

Introduction

Relapsing-remitting multiple sclerosis (RRMS) is a demyelinating autoimmune disease characterized by chronic inflammation of the central nervous system (CNS). A complex interplay between immune cells both outside (1–3) and locally within the CNS (4, 5) dictates immune cells' capacity to infiltrate the CNS and to polarize them into pathogenic pro-inflammatory cells. This is well illustrated with blood myeloid cells infiltrating the CNS and especially monocytes. Monocyte is a heterogeneous subset usually defined by CD14 and CD16 surface molecule expression comprising CD14^{++} CD16^{-}classical monocytes (cMo), CD14^{++} CD16^{++} intermediate monocytes (intMo), and CD14^{-} CD16^{++} non-classical monocytes (ncMo). All these subsets can traffic to tissue lesions (6, 7) while microglial cells and the border-associated macrophages (BAMs) are associated with tissue-derived myeloid cells in human CSF (8). Infiltrating monocytes can acquire the dendritic cell marker CD209 following transmigration across a blood-brain barrier (BBB) model (9). Although data about human monocytes fate in MS CNS are limited, they are more abundant in the experimental autoimmune encephalomyelitis (EAE) mice model of MS. Beyond subsets mentioned earlier, tissue-infiltrating monocytes were demonstrated to alternatively differentiate in monocyte-derived dendritic cells (moDC) (10), macrophages (moMac) (11, 12), or monocytic

myeloid-derived suppressor cells (m-MDSC) (13) once reaching the CNS, having either a detrimental (14) or protective role (15). There, the capacity of monocyte-derived cells to impact disease course lay on their antigen presentation propensity, their secretome profile, and phagocytic capacity (11, 16, 17), making them a valuable therapeutic target. In line, the blockade of myeloid cells trafficking from the periphery to the CNS, specifically through targeting Ninjurin-1 or more broadly through anti-VLA-4 usage, demonstrated efficacy in controlling EAE and RRMS CNS inflammation (18, 19).

Given the demonstrated role of monocytes in RRMS and their peripheral origin, many have tried to study them by standard flow cytometry within peripheral blood mononuclear cells (PBMCs). Although most studies report an increase in cMo frequency in RRMS patients, it is more controversial concerning ncMo (20–24). These discrepancies may be related to the cohorts used, the markers assessed, and/or the analysis method, pointing to the lack of robust and exhaustive characterization of the peripheral myeloid compartment in RRMS patients. Finally, although m-MDSCs abundance and monocyte/lymphocyte ratios in patients at diagnosis were correlated to higher disability overtime (25, 26) few carefully assessed the link between myeloid compartment composition at the early disease stage and individual outcome.

In this study, we took advantage of a highly characterized cohort of RRMS patients to perform mass cytometry on PBMCs sampled at diagnosis. Unsupervised analysis on the myeloid compartment allowed us to identify a specific population of classical monocytes expressing CD209 and CD206 enriched in some MS patients. This increased frequency defined a patient's subgroup highly enriched in HLA-DRB1*15:01 individuals who displayed a poorer outcome 2 years post-diagnosis. Characterization of an equivalent monocytic population by scRNA-seq on paired CSF and blood cells from unrelated MS patients together with pathway enrichment analysis indicated that these cells are present in both CSF and blood, have a proinflammatory profile, and have a higher propensity to process and present antigens compared to other classical monocytes.

Material and methods

Cohorts

This study was registered and approved by the Ethics Committee of Rennes Hospital (notice n° 20.05). MS patients included in this work were extracted from the OFSEP (Observatoire Français de la Sclérose en Plaques) MS French registry (27–30), www.ofsep.org. All participants provide written informed consent for participation. In accordance with the French legislation, OFSEP was approved by both the French data protection agency (*Commission Nationale de l' Informatique et des Libertés* [CNIL]; authorization request 914066v3) and a French ethical committee (*Comité de Protection des Personnes* [CPP]: reference 2019-A03066-51), and the present study was declared compliant to the MR-004 (*Méthodologie de reference 004*) of the CNIL.

Participating centers were Rennes, Lille, Nancy, Nimes, and Bordeaux. Inclusion criteria were: (i) age > 18 years old, (ii) MS diagnosis according to McDonald 2017 criteria at the last visit (31), (iii) sampled during their first neurological episode, and (iv) with at least one visit/year during the follow-up. Progressive MS patients were excluded. At the time of PBMC or CSF sampling, all MS patients included were drug-naïve and so had never been treated by disease-modifying therapy (DMT). Blood samples were obtained from 65 early RRMS patients and 29 age- and sex-paired healthy controls (HCs).

Clinical details of patients enrolled in mass cytometry cohort or of the scRNA-seq study are summarized in Tables 1, 2, respectively.

Blood samples processing

Blood was collected in heparin tubes for a total of 30 to 50 mL. The same volume of phosphate buffered saline (PBS) was added to the blood and diluted blood was then gently deposited on 20 mL Lymphoprep (Eurobio scientific, Ref: CMSMSL01-0U), followed by 20 min centrifugation at 1000 g with no brakes. Lymphocytes ring was then collected, washed, plaquettes were removed (two centrifugations 10 min, 200 g, 4°C with no brakes), and red blood cells were lysed by the use of Easylyse (Dako) (10 min at room temperature). Peripheral blood mononuclear cells (PBMCs) were then counted and viability assessed by trypan blue staining. An average of 40 million cells was obtained per donor and banked in Foetal Calf Serum (FCS) 10% dimethylsulfoxide in two cryovials containing 20 million cells each and stored in liquid nitrogen for subsequent usage. When PBMC samples were thawed for experimentation purposes, cell viability and cell count were obtained by the use of a Nucelocounter NC-200 (Chemotec, 3450 Allerod, Denmark) device. Cell viability ranged from 85% to 96%.

Plasma collection

Heparin blood tubes were pooled, and 20 mL of blood was used to get plasma. Blood was centrifugated (680 g, 5 min) and plasma collected for banking at −80°C.

CSF samples processing

Five milliliter of CSF was obtained by lumbar puncture; samples were immediately processed by centrifugation (450 g, 5 min), and the supernatant was stored at −80°C while cells were counted and cell viability assessed by trypan blue staining. Cell viability ranged from 90% to 98%. On average, 25,000 cells were obtained per donor. Cells were then immediately used for scRNA-seq experiments.

Mass cytometry

Frozen PBMCs from MS patients and sex- and age-matched HC were processed for cytofin staining as previously described (32, 33). A minimum of 2 million cells were used for staining. Antibodies used for cell staining and listed in Supplementary Table S1 were purchased in either metal-labeled (Fludigm antibodies) or

TABLE 1 Detailed clinical parameters from healthy controls and multiple sclerosis cohorts: (HC) healthy controls, (MS) multiple sclerosis, (EDSS) expanded disability status scale, (Gd) gadolinium lesions positivity, (SC) spinal cord lesions, (CIS) clinically isolated syndrome, (CSF) cerebrospinal fluid.

Baseline variable	HC		MS						
	Total	%	Total	%	MS wo CD206^{hi} CD209^{hi} Mo (CD206^{hi} CD209^{hi} Mo < 1%)		MS w CD206^{hi} CD209^{hi} Mo (CD206^{hi} CD209^{hi} Mo ≥ 1%)		*p*-value*
					N	%	N	%	
Total	**29**		**60**		**47**	***78.3***	**13**	***21.7***	
Sex									**0.947**
Men	10	*34.5*	19	*31.6*	15	*31.9*	4	*44.4*	
Women	19	*65.5*	41	*68.4*	32	*68.1*	9	*55.6*	
Age [median (Q1–Q3)]									**0.829**
	30 [25.5–45.5]		31 [24–37.7]		31 [24–40]		31 [24–35.5]		
Delay relapse onset/sampling (days)									**0.869**
Mean ± SD	NA	NA	60.9 ± 56		58.6 ± 55		69.1 ± 60.9		
Median [Q1–Q3]	NA	NA	42.5 [14.2–93.7]		40 [15–82]		56 [5–133]		
EDSS									**0.869**
Mean ± SD	NA	NA	1.3 ± 1.3		1.3 ± 1.1		1.5 ± 1.4		
Median [Q1–Q3]	NA	NA	1.5 [0–2]		1 [0–2]		1.5 [0–2.5]		
T2 lesions number ≥ 9									**0.527**
Yes	NA	NA	35	*58.3*	26	*55.3*	9	*69.2*	
No	NA	NA	25	*41.7*	21	*44.7*	4	*30.8*	
Gd lesions									**0.7582**
Yes	NA	NA	31	*51.7*	25	*53.2*	6	*46.1*	
No	NA	NA	29	*48.3*	22	*46.8*	7	*53.85*	
SC lesions									**0.758**
Yes	NA	NA	39	*65*	30	*63.8*	9	*69.2*	
No	NA	NA	21	*35*	17	*36.2*	4	*30.8*	
CIS type									**0.737**
Motor-Brainstem	NA	NA	19	*31.6*	14	*29.8*	5	*38.5*	
Sensitive-optical nerve	NA	NA	41	*68.4*	33	*70.2*	8	*62.5*	
CSF oligoclonal bands (15NA)			**45**		**33**		**12**		**0.741**
Yes	NA	NA	40	*88.9*	29	*87.9*	11	*91.6*	
No	NA	NA	5	*11.1*	4	*12.1*	1	*8.4*	

When indicated, the mean and standard deviations (SD) are displayed as well as the median with Q1-Q3 interquartile in brackets. *p-values: correspond to Mann-Whitney statistical test p-value. NA, not applicable. Percentage are in italic and values in bold.

uncoupled format. Antibody conjugation to a metal with the Maxpar Antibody Labeling Kit (Fluidigm) and subsequent titration were done prior to the staining procedure and according to manufacturer protocol. Briefly, cells from frozen PBMCs were counted, and Cisplatin cell ID staining was done to assess cell viability. In the next step, membrane markers of interest were labeled with a cocktail of dedicated antibodies, while subsequent cell fixation and permeabilization with Fix Perm Buffer (Miltenyi Ref: 130093142) allowed the assessment of intracellular marker expression. Intra-cellular staining was therefore done, followed by iridium labeling to discriminate singlets from doublets during analysis. Finally, suspensions of fixed cells were banked at −80°C until acquisition on the Helios™ System (Fluidigm) from the CyPS plateform (Paris Pitié Salpêtrière).

TABLE 2 Detailed clinical parameters from scRNAseq cohort: *(HC)* healthy controls, *(MS)* multiple sclerosis, *(EDSS)* expanded disability status scale, *(Gd)* gadolinium lesions positivity, *(SC)* spinal cord lesions, *(CIS)* clinically isolated syndrome, *(CSF)* cerebrospinal fluid.

Baseline variable	RRMS	
	Total	%
Total	**5**	
Sex		
Men	1	*20*
Women	4	*80*
Age [median (Q1-Q3)]		
	35 [24–43]	
Delay relapse onset/sampling (days)		
Mean ± SD	56.8 ± 32.76	
Median [Q1–Q3]	45 [28.5–91]	
EDSS		
Mean ± SD	1.5 ± 0.58	
Median [Q1–Q3]	1.5 [1–2]	
T2 lesions number ≥ 9		
Yes	2	*40*
No	3	*60*
Gd lesions		
Yes	4	*80*
No	1	*20*
SC lesions (1NA)		
Yes	2	*50*
No	2	*50*
CIS type		
Motor-Brainstem	2	*40*
Sensitive-Optical nerve	3	*60*
CSF oligoclonal bands		
Yes	5	*100*
No	0	*0*

When indicated, the mean and standard deviations (SDs) are displayed as well as the median with Q1–Q3 interquartile in brackets. Percentage are in italic and values in bold.

Cytof data analysis

FCS files obtained from the platform were first processed for bead-based normalization on EQ-Beads (Fluidigm) through the use of the R package premessa (https://github.com/ParkerICI/premessa). Such normalized FCS then served as input for sample cleaning from debris and doublets (DNA1 vs. DNA2), from dead cells (DNA1 vs. Cisplatin), and beads (Ce140D1 vs. DNA1) within the Cytobank cloud-based platform (Cytobank, Inc). Dimensional reduction was performed on each file separately according to the viSNE algorithm and settings defined previously (34) (perplexity = 30; iterations = 5000; theta = 0.45). Clusters corresponding to myeloid cells were delineated based on lineage marker expression ($CD45^+CD3^-CD19^-CD36^+HLA\text{-}DR^+$) and then exported for deep analysis with the help of the Catalyst package on R (https://rdrr.io/bioc/CATALYST). In total, more than 11 million myeloid cells were analyzed, ranging from 278 to 312,260 cells retrieved per patient. The cell clustering process was done with all markers except those used for lineage discrimination through the FlowSOM algorithm and with the following parameters: self-organizing map = 20 × 20 and maxK = 30 (maximum number of meta clusters to evaluate). Each FlowSOM-defined cluster was evaluated and either kept untouched for further analysis, merged with phenotypically similar clusters, or removed when related to other cell lineage residual contamination. Retained clusters were highlighted on UMAP dimensional reduction based on the same markers as those used for FlowSOM clustering. Differential frequencies of major monocyte subsets were assessed through the Mann and Whitney test. Clusters' differential abundances between individual groups were analyzed through a generalized linear mixed model (GLMM) and Benjamini-Hochberg adjustment, while differential marker expression between HC, $CD206^{hi}$, and $CD209^{hi}$ cMo-enriched patients and not-enriched patients was tested with multiple ANOVA and a Tukey *post hoc* test. Results were considered significant when adj $p < 0.05$.

scRNA-seq sequencing

Paired CSF and blood collected from MS patients at their first neurological episode were used for scRNA-seq experiments. Although CSF cells were processed freshly, PBMCs get a freezing/thawing cycle before use. A mean of 25,000 cells from CSF (corresponding to all cells) and the equivalent amount of paired PBMCs were loaded in the Chromium 10× (10× Genomics, Pleasanton, CA, USA) for single-cell capture and barcoding. Libraries were prepared according to the manufacturer's protocol with the 10× 5' kit (Chromium Next Gem Single Cell 5' reagent kit v1.1). Libraries were processed using NovaSeq 6000 (Illumina, San Diego, CA), with a depth of 50,000 reads/cell and a paired sequencing of 28 nucleotides in R1 and 91 in R2. Sequenced were then aligned with Cellranger v6.1.1 in intron inclusion mode on the Human GRCh38 scRNA-seq optimized transcriptomic reference v1.0 as in Pool et al. (35) The median number of genes retrieved per cell ranged from 1.651 to 1.981 in CSF while it varied from 812 to 3,014 in peripheral blood. Quality controls were done on each sample individually, and cells displaying either several genes lower than 400 or higher than 4,000, several UMI over 15,000, a mitochondrial cell read ratio higher than 10%, or a ribosomal gene's frequency lower than 8% were filtered out, as clusters predicted to comprise mainly doublets through singleCellTK package v2.8.0.

scRNA-seq data processing

Filtered datasets from each sample were merged and log normalized before data integration with the FindIntegrationAnchors

and IntegrateData functions from Seurat v4.3.0 on the first 20 correlation components. Immunoglobulin and T-cell receptor genes were removed for the integration step only. PCA analysis was then done on an integrated dataset and used for UMAP processing and cell clustering (20 nearest neighbors, resolution 0.4). Cell subset labeling resulted from the concordance between several analyses. Briefly, differentially expressed genes between clusters were obtained through the FindAllMarkers function from the Seurat package with test.use set to "wilcox." These lists were then used in EnrichR to predict cell type. In addition, gene signature characteristics from cell lineage and obtained from literature (36) were used to assess the enrichment score of these signatures in all clusters previously defined via the ModuleScore function from Seurat. Finally, SingleR v2.0.0 was used to automatically assign labels to either cells or clusters based on signatures managed by celldex package v1.8.0. Reference index tested were HumanPrimaryCellAtlasData, BlueprintEncodeData, DatabaseImmuneCellExpressionData, MonacoImmuneData and NovershternHematopoieticData. The same strategy was used to label clusters at any step.

Once cell lineage subsets were defined, myeloid cells were sorted, and the newly generated dataset was integrated according to the Harmony algorithm from the Harmony package v0.1.1. Newly defined clusters (15 nearest neighbors, resolution = 0.15), were then labeled as previously detailed, and this whole process was repeated to retrieve classical monocyte populations (15 nearest neighbors, resolution = 0.5). $CD206^{hi}$ $CD209^{hi}$ cMo signature scoring resulted from Module Score function processing. To decipher specific pathways characterizing the different clusters comprised among classical monocytes, pathways from MSigDB Hallmark and Kegg were used to assess specific pathway enrichment at the single cell level with the use of the AUCell and GSEABase packages v1.20.2 and 1.60.0, respectively. Differential enrichments in gene signatures were appreciated following a comparison of CSF and blood compartments. Finally, an interactome study was done on CSF cell subsets through the use of CellChat package v1.6.1.

Genotyping, imputation, and scoring

DNA was extracted from PBMCs obtained from 50 patients from the mass cytometry cohort. The samples underwent genotyping using the Affymetrix PMRA chip array. Standard quality controls on individuals and SNPs were performed using Plink (37). From 852,860 SNPs, quality control resulted in a remainder of 414,387 SNPs. SNPs were excluded based on the following criteria: non-autosomal (N = 34,049), deviation from Hardy-Weinberg equilibrium (N = 1,800), low genotyping (N = 11,848), and low frequency [minor allele frequency (MAF) < 0.01, N = 344,210]. Some SNPs were below both genotyping and frequency thresholds. We then performed SNP imputation. First, we converted plink files into vcf files using bcftools (38), next, we used Topmed to impute our dataset using default parameters (imputation.biodatacatalyst.nhlbi.nih.gov) (39). We obtained 9,073,739 high-confidence (>0.8) SNPs after imputation.

From these imputed SNPs, we calculated the MSGB (MS Genetic Burden) (40). This polygenic MS risk score follows a log-additive model: . MSGB was calculated with 195 SNPs extracted from the latest published GWAS on MS (41).

In addition, we performed *HLA* imputation using the HIBAG R package (42) and our in-house reference panel built with the 1000 Genomes projects data (43, 44). This allowed us to determine which patient carried the *HLA-DRB1*15:01* allele.

Global age-related multiple sclerosis severity

gARMMS was calculated through EDSS scores ranking based on the patient's age at the time of assessment (45), in this study: 24 months following diagnosis. The frequency of patients with a gARMSS score higher than 5 was calculated among the patient's groups. Mann-Whitney test was done to assess significant differences between patients' groups.

Neurofilaments, cytokines, and chemokines

Neurofilament light chain (R-PLEX F217X-3), sIL2RA, IL-15, CXCL10, CCL2, CCL20, and CXCL12 (U-PLEX biomarkers group 1 custom) content in plasma samples was assessed with a QuickPlex SQ 120MM Reader (Society Meso Scale Discovery, Rockville, MD). Undiluted samples were deposited on dedicated coated plates, and the standard procedure was followed according to the manufacturers' protocol. Mann-Whitney test was done to assess significant differences between patients' groups.

Statistical analysis

Unless specified, statistical analyses were done using GraphPad Prism software, version 8.4. A two-tailed Mann-Whitney test was performed to compare two independent groups or more than two independent groups. P-values ≤ 0.05 were considered significant. A Fisher exact test was used to test proportional differences; p-values ≤ 0.05 were considered significant.

Data accessibility

Data are deposited on EGA on accession number: EGA50000000296.

Results

Blood of RRMS patients is enriched in a specific subset of myeloid cells

To explore patients' myeloid phenotypes, PBMCs from 60 highly characterized RRMS patients (MS) sampled at diagnosis together with 29 samples from age- and sex-matched HCs were processed for

mass cytometry and unsupervised analysis (Table 1). viSNE visualization of high-dimensional single-cell data based on the t-Distributed Stochastic Neighbor Embedding (t-SNE) algorithm of each sample eased the delineation of myeloid cells among circulating cells based on lineage markers CD19, CD16, CD36, and CD3 expression (Supplementary Figure S1A). From these, no differences in frequencies of CD3 T, B lymphocytes, or myeloid cells were observed between MS and HC donors (Supplementary Figure S1B). To further detail myeloid population composition, a myeloid subset from each sample was isolated and processed with FlowSOM algorithm to cluster these cells, and then specific identities were assigned to each cluster based on their associated cell phenotype. Eight clusters were considered using this strategy and plotted on Uniform Manifold Approximation and Projection (UMAP) (Figure 1A). Among these clusters and according to their respective CD14/CD16 expression (Figure 1B), cMo, intMo, and ncMo were identified. Interestingly, in addition to these prototypical phenotypes, we highlighted two subsets of monocytes: CD206^{hi} CD209^{hi} Mo and CD206^{int} CD209^{int} Mo that expressed CD14 but not CD16 and clustered separately from cMo due to their strong expression of specific markers (Figure 1B). In addition, conventional dendritic cells (cDC) were defined through the expression of CD11c in the absence of CD14 and CD16 expression, plasmacytoid dendritic cells (pDC) were distinguished by high CD123 expression, while remaining cells (others) were characterized through the poor expression of most of the markers assessed but intermediate levels of CD11c, CD11b, and high levels of PD-L1. When frequencies of the different monocytic clusters were compared between HC and MS patients, significant differences were observed with a decreased intMo frequency in MS patients (mean HC vs. MS: 5.74% ± 3.23 vs. 3.6% ± 2.52, $p = 0.027$), while CD206^{hi} CD209^{hi} Mo (mean HC vs. MS: 0.06% ± 0.16 vs. 4.52% ± 12.1, $p = 0.01$) and CD206^{int} CD209^{int} Mo (mean HC vs. MS: 0.21% ± 0.51 vs. 2.79% ± 12.1, $p = 0.0014$) were increased (Figure 1C).

Enriched myeloid cells display characteristics of activated and tissue-trafficking classical monocyte

To confirm CD206^{hi} CD209^{hi} Mo enrichment in MS patients, differential myeloid cluster abundance was tested by a generalized linear mixed model. In line with frequencies analysis, CD206^{hi} CD209^{hi} Mo abundancy was significantly associated with MS status (p = 8.7e-07) as CD206^{int} CD209^{int} Mo to a lesser extent (p = 1.6e-03), while intMo were more abundant in HC ($p = 0.035$) (Figure 2A). A closer look at CD206^{hi} CD209^{hi} Mo frequency indicated that such enrichment was occurring in only a part of MS patients while being virtually absent from HC (Figure 2A). Accordingly, a 1% threshold of CD206^{hi} CD209^{hi} Mo frequency among myeloid cells allowed to discriminate HC from MS patients, and among MS patients, those with CD206^{hi} CD209^{hi} Mo enrichment: frequency ≥ 1% (MS wo CD206^{hi} CD209^{hi} Mo) from those with no enrichment: frequency < 1% (MS wo CD206^{hi} CD209^{hi} Mo) (Figure 1C, lower left panel: dashed line illustrates the 1% threshold and Supplementary Figure S2A: illustrative myeloid composition according to the donors' status). To get insights about CD206^{hi} CD209^{hi} Mo enrichment in MS patients regarding the other myeloid subsets, we performed a correlation analysis on myeloid population frequencies in HC and MS patients. Correlation matrix patterns between HC and MS donors were found to be highly different, with a strong and significant anti-correlation between CD206^{hi} CD209^{hi} Mo and cMo frequencies in MS patients that was absent from HC (Figure 2B), suggesting that cMo and CD206^{hi} CD209^{hi} Mo subsets were intimately related. Further, the high HLA-DR, CD86, and CD45RA expression by CD206^{hi} CD209^{hi} Mo together with high levels of CCR5, CCR2, and CD106 markers compared to cMo cells (Figure 1B) pointed out an active pro-inflammatory profile (46, 47) associated with trafficking abilities toward inflamed tissues (3, 7). In addition to these markers, CD206^{hi} CD209^{hi} Mo cells intriguingly expressed CD206 (MMR/MRC1) and CD209 (DC-SIGN), while these molecules are more classically found on monocyte-derived tissue resident cells (9, 48). To ascertain the co-expression of these markers, we assessed the percentage of cells expressing these discriminating molecules within their related cluster and confirmed that CD206^{hi} and CD209^{hi} Mo cells were a pure population co-expressing CD206 and CD209 together with the mentioned markers (Supplementary Figure S2B). Altogether, these results demonstrated that CD206^{hi} CD209^{hi} Mo are monocytes that differed from the classical monocyte archetypical phenotype via the upregulation of inflammatory and trafficking markers. Therefore, whether CD206^{hi} CD209^{hi} Mo amplification reflects a shift of monocytic cell phenotype or a disease-linked expansion of this subset remained to be determined since no significant increase in cMo frequency was observed (mean = 82.92% ± 9.31 vs. 86.55% ± 8.17, $p = 0.0673$) (Supplementary Figure S3A). To know whether this phenotypic change was associated with the modulation of plasmatic cytokines/chemokines concentrations, we seek for differences in sIL2RA, IL-15, CXCL10, CCL2, CCL20, and CXCL12 plasmatic content between MS patients with CD206^{hi} CD209^{hi} Mo and MS patients without CD206^{hi} CD209^{hi} Mo. No significant differences were found between MS groups (Supplementary Figure S3B).

MS patients with CD206^{hi} CD209^{hi} Mo cells present a poorer prognosis

Next, considering that only 22% of our MS cohort displayed an enrichment in CD206^{hi} CD209^{hi} Mo cell frequency, we decided to study patients' profiles according to CD206^{hi} CD209^{hi} Mo cell enrichment. At baseline, no significant differences on clinical and demographical variables were observed between MS patients with CD206^{hi} CD209^{hi} Mo and MS patients with CD206^{hi} CD209^{hi} Mo (Table 1). However, after 2 years of follow-up, a significantly higher percentage of MS patients with CD206^{hi} CD209^{hi} Mo experienced inflammatory activity (relapses and/or new T2 lesions on magnetic resonance imaging) compared to MS patients wo CD206^{hi} CD209^{hi} Mo (71% vs. 88%; $p < 0.01$) (Figure 3A), and significantly more MS patients with CD206^{hi}

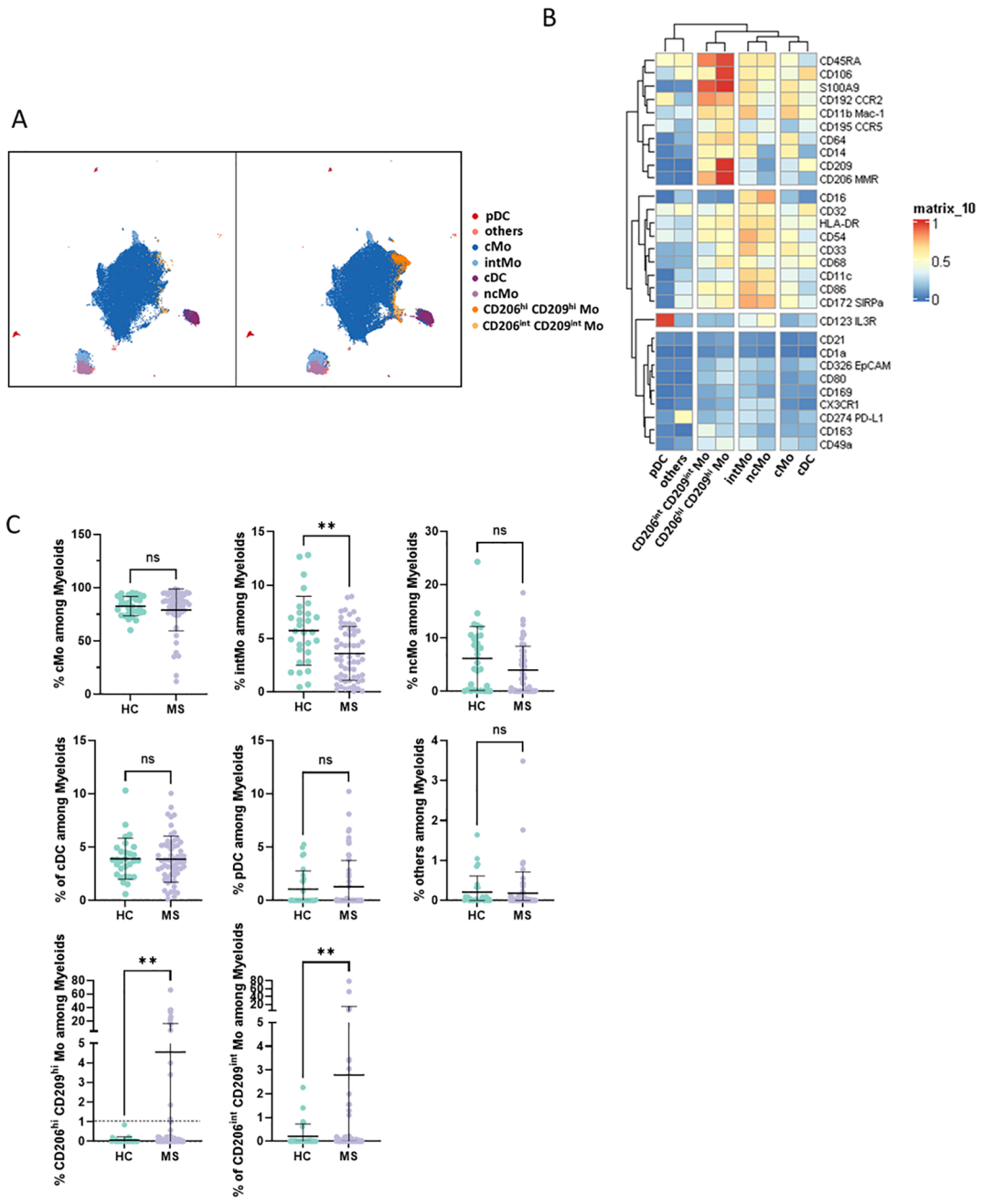

FIGURE 1
(A) UMAPs illustrating the myeloid clusters retrieved following FlowSOM unsupervised analysis in HC (left) and MS donors (right). **(B)** Heatmap summarizing markers expression scaled by row among clusters defined through unsupervised analysis. **(C)** Dotplots illustrating myeloid subsets frequencies among myeloid cells. Mann-Whitney test was used to determine statistical differences with ns: not significant, $^{**}p < 0.01$.

CD209^{hi} Mo presented an EDSS score ≥2 compared to MS patients wo CD206^{hi} CD209^{hi} Mo (32% vs. 55%; $p < 0.01$) (Figure 3B, left). Corroborating these results, we found a significantly higher proportion of patients displaying an age-related multiple sclerosis severity (ARMSS) (45) score higher than five among MS patients with CD206^{hi} CD209^{hi} Mo two years following diagnosis ($p = 0.018$) (Figure 3B, right), while no correlation between CD206^{hi} CD209^{hi} Mo frequency and donor age was observed (Supplementary Figure S3C). Further, although no differences were noticed between groups in plasmatic neurofilament light chain (Nfl) concentration (Supplementary Figure S4), nor in patients' burden in genes at risk (MSGB), using the most recent associated SNPs set from the International Multiple Sclerosis Genetics Consortium (41) (Figure 3C, left), we found that 75% of MS patients with CD206^{hi} CD209^{hi} Mo carry either HLA-DRB1*15:01 and/or HLA-DQB1*06:02 compared to 45% in MS patients with CD206^{hi} CD209^{hi} Mo ($p < 0.001$) (Figure 3C, right). Altogether, these results point out a potential role of these cells in disease severity and a potential role of HLA-DRB1*15:01 haplotype in CD206^{hi} CD209^{hi} Mo higher frequency.

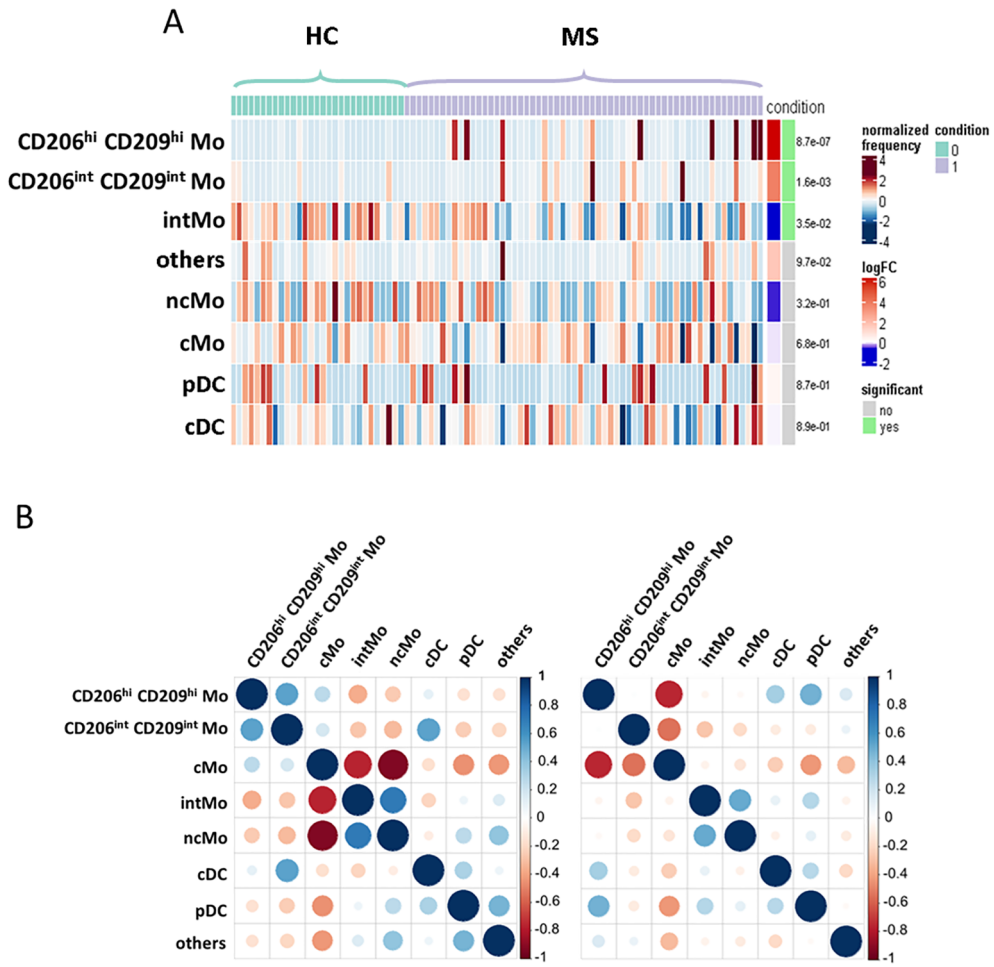

FIGURE 2
Enriched myeloid cells display characteristics of activated and tissue resident classical monocyte. **(A)** Heatmap figuring cluster differential abundance between HC and MS donors, with each bar within a cluster representing a donor and color is depending on differential enrichment. Differential abundance significance was tested through generalized linear mixed model and *p*-values for each cluster are indicated on the right. **(B)** Correlation matrix depicting correlation between myeloid subsets frequencies among HC donors (left) and MS patients (right).

CD206^{hi} CD209^{hi} Mo-like cells infiltrate RRMS patients' CSF at diagnosis

In an attempt to get further insights into CD206^{hi} CD209^{hi} Mo cell specificities and potential role in MS pathogenicity, we explored data from paired CSF and blood scRNA-seq from RRMS patients sampled at diagnosis (n = 5) (Table 2). More than 55,000 cells were recovered and analyzed for gene expression. Cell clustering based on differential gene expression allowed to discriminate major cell lineages and annotate them based on characteristic gene expression, supported by SingleR-assisted labeling while cells with an undefined identity were not represented (Figure 4A). This strategy allowed us to isolate myeloid cells from other circulating cells and to retrieve 2232 and 7840 myeloid cells from CSF and blood, respectively (Figure 4B). In line with literature (49–51), the myelocytic composition of CSF differed from the blood one, with a differential enrichment when comparing median frequencies in both cDC (22.24% of myeloid CSF cells retrieved vs. 2.18% of blood myeloid cells), pDC (18.42% vs. 1.44%), as well as in ncMo expressing CD16 (21.41% in CSF vs. 11.21% in the blood) in CSF concomitant to a decreased frequency of CD14 expressing cMo cells (29.02% in CSF vs. 84.2% in the blood) (Figure 4C). Considering that CD206^{hi} CD209^{hi} Mo cells express CD14 but not CD16, we first isolated cMo from other myeloid cells and performed a subset clustering. Two (cMo2 and cMo3) out of the three clusters recapitulating the cMo population were found in both CSF and blood, while the cMo1 subset was observed in the blood compartment only (Figure 4D, upper panels). To identify CD206^{hi} CD209^{hi} Mo among clusters, we then looked for events co-expressing the two discriminating markers: CD206 and CD209 (*MRC1* and *DC-SIGN*, respectively) at the transcript level. Although few events were strictly co-expressing *MRC1* and *DC-SIGN* (Figure 4D middle and lower panels), cMo clustering indicated that they were found almost exclusively in one CSF cluster: cMo3. Importantly, such events were observed in four out of five CSF samples (Supplementary Figure S5), avoiding individual bias. To exclude microglial contamination and confirm the monocytic identity of detected CD206^{hi} CD209^{hi} Mo-like cells, we tested through gene set enrichment analysis their transcriptomic proximity with human CNS myeloid cell subsets as defined in

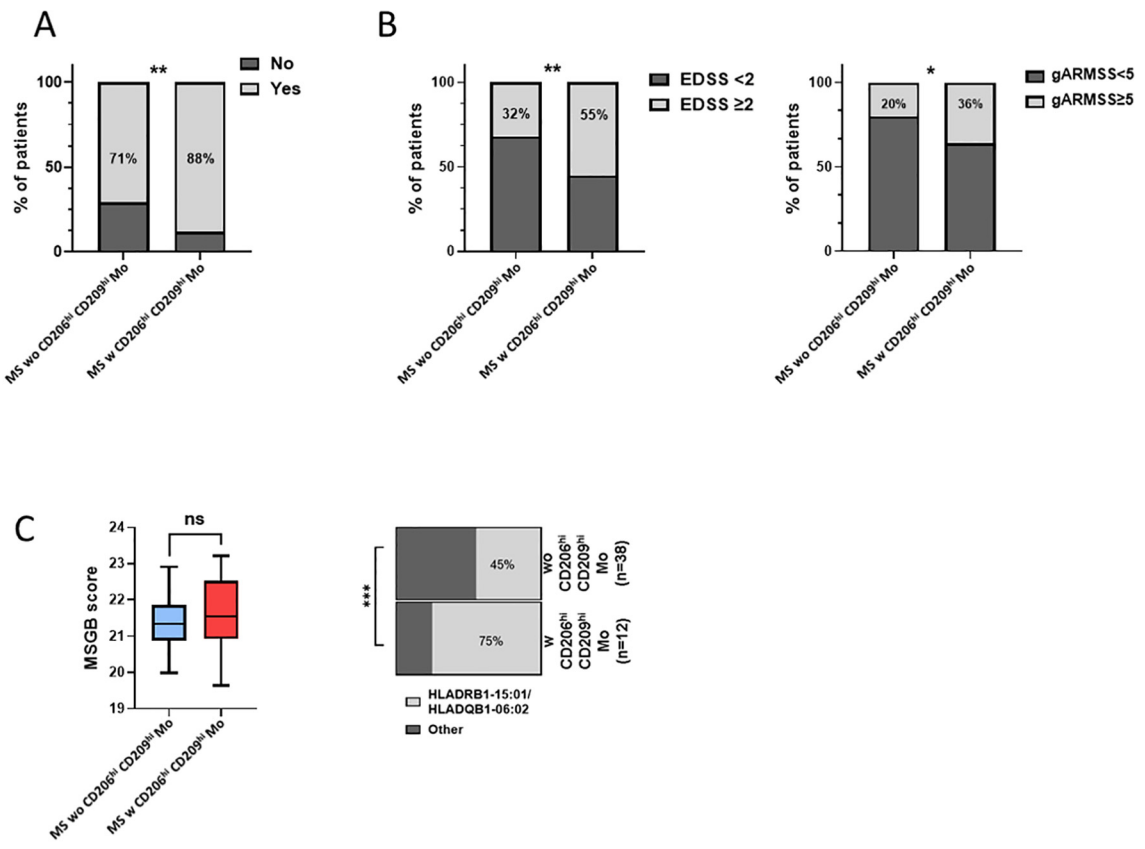

FIGURE 3
MS patients w CD206^{hi} CD209^{hi} Mo have a peculiar profile. **(A)** Histogram plot illustrating radio-clinic activity in patients displaying low (MS wo CD206^{hi} CD209^{hi} Mo) or high (MS w CD206^{hi} CD209^{hi} Mo) CD206^{hi} CD209^{hi} Mo cells frequency. Significance is based on Mann and Whitney test with $^{**}p < 0.01$. **(B)** percentage of patients with EDSS ≥2 at 2 years (left). Significance is based on Mann and Whitney test with $^{*}p < 0.05$ and $^{**}p < 0.01$. Histogram plot depicting ARMSS score ≥5 frequency among MS wo CD206^{hi} CD209^{hi} Mo and MS w CD206^{hi} CD209^{hi} Mo, 2 years following diagnosis (right). Significance is based on Fisher's exact test with $p = 0.0178$. **(C)** Boxplot indicating MSGB patients' score. Mann and Whitney test demonstrated no significant differences between groups (ns) (left). Histogram plot illustrating the frequency of patients HLA-DRB1*15:01 and HLA-DQB1*06:02 genes (right). Fisher's exact test demonstrated highly significant difference with $^{***}p < 0.001$.

literature (8). CD206^{hi} CD209^{hi} Mo-like cells were found enriched in genes belonging to monocytic lineage (adjusted *p*-value = 9,78E-23) rather than BAMs (EMP3, adjusted *p*-value = 1.39E-11) or microglial cells (MG TREM2: negative enrichment score or MG CCL2, MG CX3CR1: adjusted *p*-value > 0.05) (Figure 4E). They were also discriminated from CD1c mDC considering *CD14* expression by CD206^{hi} CD209^{hi} Mo-like cells. Therefore, CD206^{hi} CD209^{hi} Mo-like cells are predicted as originating from circulating rather than resident myeloid cells from the CNS, in line with their presence in the peripheral bloodstream. To better quantify CD206^{hi} CD209^{hi} Mo-like cell frequency in the different compartments and to refine their identification at the RNA level despite transcript drop-out, we selected, among the best-expressed transcripts, *CCR5* as an additional CD206^{hi} CD209^{hi} Mo marker to the CD206^{hi} CD209^{hi} Mo-like gene signature (*MRC1, DC-SIGN, CCR5*). Signature scores for each event plotted on the UMAPs were retrieved, and the number of cells with positive scores (Figure 4F UMAPs dark dots) was assessed. A significant enrichment in our dataset of CD206^{hi} CD209^{hi} Mo-like cells was highlighted in CSF while few events were found in peripheral blood (Figure 4F higher panels), indicating that CD206^{hi} CD209^{hi} Mo-like cells can be observed in both CSF and blood. The presence of CD206^{hi} CD209^{hi} Mo in both blood and CSF compartments was additionally assessed in two publicly available datasets (50, 51) following the same strategy. In line with our findings, although cMo frequency was strongly decreased in CSF compared to blood in these other datasets (Figure 4F middle panels: Esaulova et al. dataset, lower panels: Ramesh et al. dataset), CD206^{hi} CD209^{hi} Mo-like can be identified in both compartments. Nevertheless, CD206^{hi} CD209^{hi} Mo-like cell frequency was found higher in CSF than in blood, similarly in all the datasets tested (Figure 4F right panels). Altogether, these demonstrated that cells with close similarities to CD206^{hi} CD209^{hi} Mo cells as *CD14, MRC1, DC-SIGN*, and *CCR5* transcript expression can be found in both peripheral blood and CSF from RRMS patients by scRNA-seq data. These are enriched in a specific monocyte cluster, and their higher frequency in CSF may suggest either (i) their higher migration capacities, (ii) their better retention/survival in CSF, (iii) and/or an increased monocyte polarization in CSF.

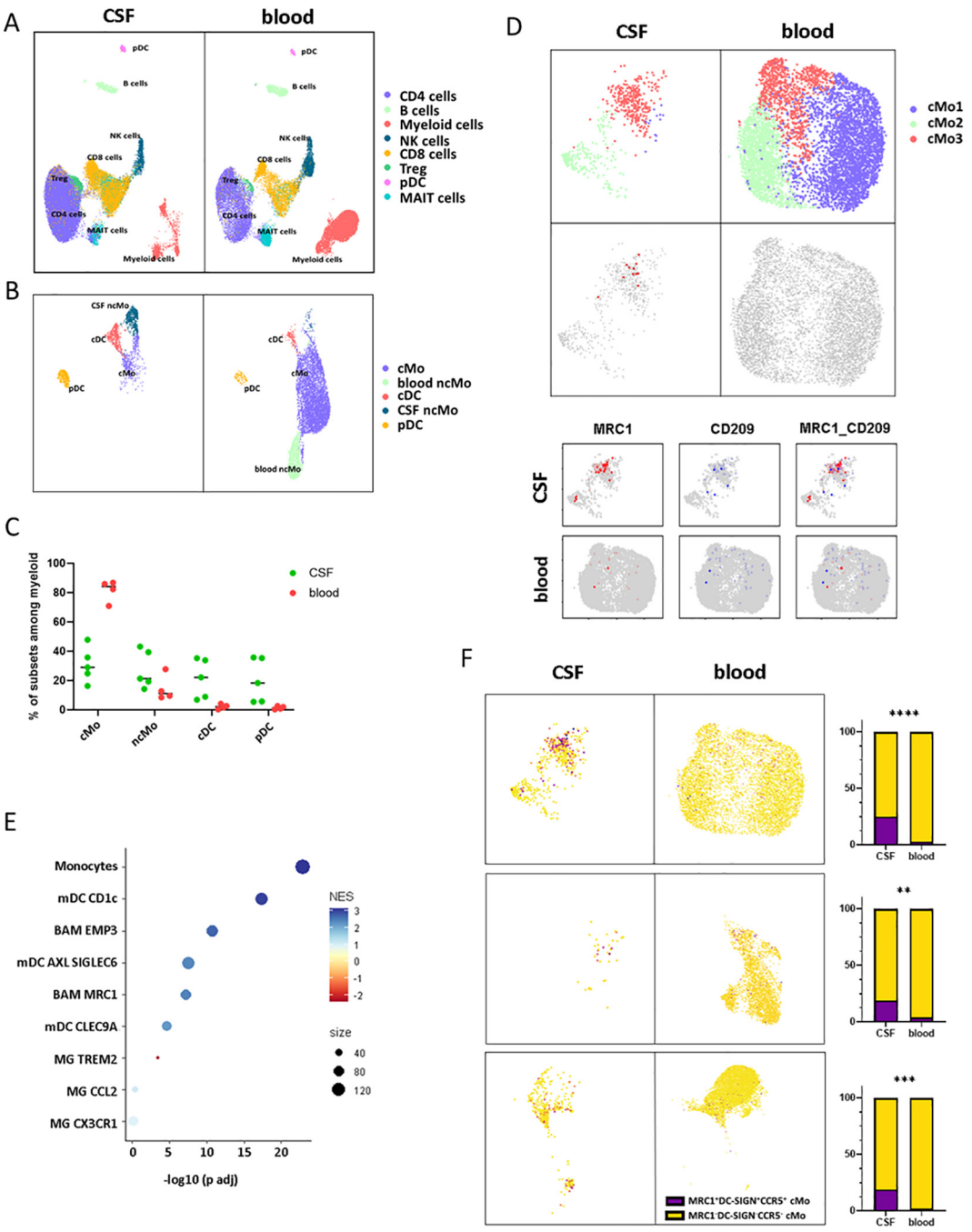

FIGURE 4
CD206^{hi} CD209^{hi} Mo-like cells can be found in RRMS CSF at diagnosis. **(A)** UMAPs representing immune cells retrieved and analyzed from scRNA-seq cohort in blood and CSF of MS patients following integration and unidentified cells removal. Clusters are labeled with cell identities according to genes expression. **(B)** UMAPS illustrating myeloid cell compartment in both CSF and blood with cluster labeling according to genes signatures. **(C)** Circle diagram displaying cell subset proportions among myeloid cells in CSF and blood with bars as median. **(D)** UMAPs depicting classical monocytes major clusters (upper panels). UMAPs illustrating *MRC1/DC-SIGN* co-expressing events in CSF and blood (middle panels). UMAPs figuring classical monocytes events expression of *MRC1*/CD206 (red) and *DC-SIGN*/CD209 (blue) transcripts in CSF and blood (lower panels). **(E)** Circle diagram displaying CD206^{hi} CD209^{hi} Mo-like cell proximity to the related myeloid subset gene signatures through GSEA. Circle color depicts normalized enrichment score and circle size: CD206^{hi} CD209^{hi} Mo-like cells/associated subset signatures overlap. **(F)** (left panels) UMAPs figuring CD206^{hi} CD209^{hi} Mo signature scoring (*CCR5, MRC1, DC-SIGN*) among classical monocyte events from our dataset (up), Esaulova dataset (middle), Ramesh dataset (lower). (Right panels) UMAP associated histogram plots depicting CD206^{hi} CD209^{hi} Mo signature positive cells frequency among classical monocytes in CSF and PB. Significance is based on Mann and Whitney test with $^{**}p < 0.01$, $^{***}p < 0.001$, $^{****}p < 0.001$.

CD206^{hi} CD209^{hi} Mo-like cells' phenotypic characterization at the transcriptomic level

To decipher CD206^{hi} CD209^{hi} Mo-like cells' properties, we first considered this population defined at the cluster level according to Figure 4D and sought for their specifically active pathways in comparison to the other classical monocyte clusters. Cluster analysis indicated that cMo3, the cluster comprising CD206^{hi} CD209^{hi} Mo-like events, was characterized by cells displaying high *HLA* molecule expression together with higher *CD74* (Figure 5A). Querying events displaying antigen processing and presentation properties according to the Kegg database confirmed that the cMo3 cluster had a greater propensity to process and present antigens (Figure 5B, Kegg database signature-enriched events plotted in red). This capacity was also found to be significantly higher (p = 0.0004) when we performed prospective gene set enrichment analysis comparing the CSF cMo3 cluster to its peripheral blood counterpart (Figure 5C), supported by significantly higher *HLA* expression in the CSF cluster compared to the blood one (Figure 5D). In addition, pathways related to immune cell activation (Figure 5C, red labels) were found overactivated in CSF migrating cells compared to their blood counterpart, reflecting their

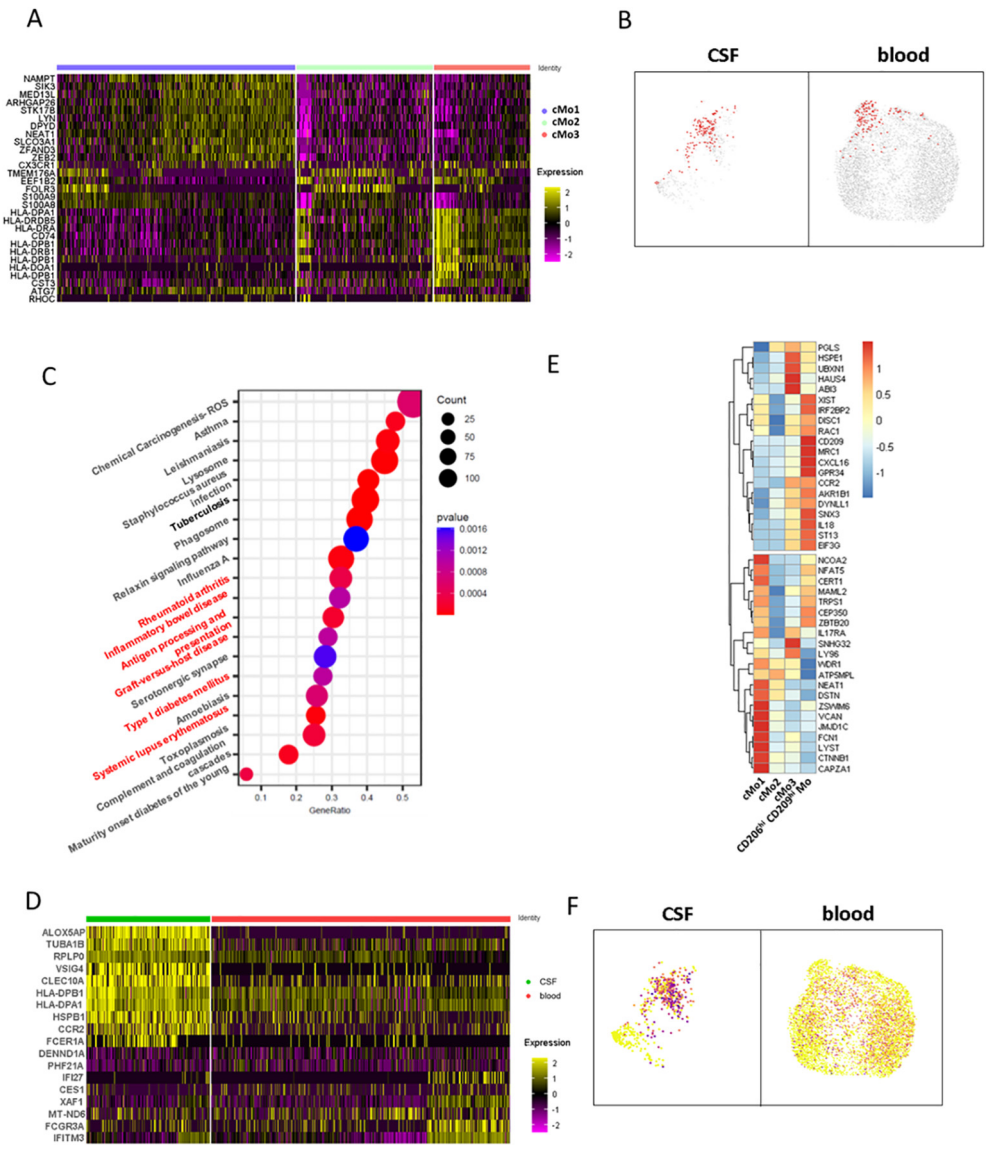

FIGURE 5
CD206^{hi} CD209^{hi} classical monocyte-like cells phenotypic characterization at the gene level. **(A)** Heatmap depicting differentially expressed genes characterizing classical monocytes major clusters defined in Figure 4D upper panels. **(B)** UMAPs illustrating cells enriched in the genes signature belonging to the antigen processing and presentation pathway from the Kegg database. Enriched cells are figured as red dots in CSF (left) and blood (right). **(C)** Circle diagram illustrating CSF cMo3 cluster comparison to its peripheral blood counterpart through GSEA analysis. Enriched pathways are depicted, with signature overlap with cMo3 CSF versus blood differentially upregulated genes illustrated through circle size and p-value as color gradient. Pathways related to immune cells activation are labeled in red. **(D)** Heatmap displaying differentially expressed genes between CSF cMo3 cluster and its peripheral blood counterpart. **(E)** Heatmap displaying top regulated genes among CD206^{hi} CD209^{hi} Mo-like cells with CD206^{hi} CD209^{hi} Mo-like cells defined by MRC1/CD209 expression in comparison to previously defined classical monocyte clusters cMo1, cMo2, and cMo3. **(F)** UMAPs illustrating CCR2 expression among classical monocytic cells.

proinflammatory phenotype. These data therefore suggest that the cMo3 cluster corresponds to a monocyte subset with antigen presentation with enhanced proinflammatory properties once in the CSF. To strengthen our findings and regarding that cMo3 cluster may comprise CD206^{hi} CD209^{hi} Mo unrelated cells, we looked at CD206^{hi} CD209^{hi} Mo-like cells strictly defined through their gene co-expression and assessed their differential gene expression regarding other CSF monocyte clusters (Figure 5E, mean expression of most differentially expressed genes). This confirmed the proinflammatory polarization of CD206^{hi} CD209^{hi} Mo-like cells, illustrated by higher expression of related markers such as *IL18* and *CCR2*, with CCR2 cells being highly predominant in the CNS (Figure 5F) as previously described in EAE model (7). Altogether, these data indicated that CD206^{hi} CD209^{hi} Mo-like cells, once reaching the CNS, may have a pathogenic role partly through antigen presentation, fueling local inflammation.

Discussion

Myeloid cells play a key role in the MS course. Although their infiltration inside the CNS contributes to inflammation, some protective subsets have also been described. Using mass cytometry and scRNA-seq analysis, we highlighted here an enrichment of a peculiar classical monocyte subset (i.e., CD206^{hi} CD209^{hi} Mo cells) in some RRMS patients' blood at diagnosis, defining a patients' subgroup displaying a poorer prognosis 2 years following diagnosis. Single-cell RNA-seq analysis pointed out the potential pathological role of this myeloid subset through their CSF enrichment, underlying specific trafficking, and their propensity to process and present antigen.

CD206^{hi} CD209^{hi} Mo cells can be distinguished from other classical monocytes through their high expression of CD206 and CD209, two markers classically expressed by tissue-infiltrating monocyte-derived cells. CD206 and CD209 markers strict co-expression was not described previously in circulating cells; however, monocyte-derived macrophages treated with IL-3 demonstrate an upregulation of Dectin-1, CD206, and in 10% of them, CD209 (52). This phenotype was associated with an increased phagocytosis capacity. Phagocytosis is an important process for antigen processing and presentation to CD4 T cells; in lymph nodes, monocytic cells expressing CD14, CD206, and CD209 have been described as specifically located in the T-cell area and display antigen presentation capacities (53). This is in line with the CD206^{hi} CD209^{hi} Mo-like cell phenotype described in our scRNA-seq dataset, with a high propensity to process and present antigens. Focusing on CD209-expressing CD14 monocytes, it was demonstrated that they are enriched within an inflamed microenvironment where they participate in MS disease activity by supporting CD4 T-cell activation (9) and in rheumatoid arthritis and psoriatic arthritis patients through secretion of pro-inflammatory cytokines (54).

On the other hand, CD206-expressing monocytic cells are classically associated with an anti-inflammatory phenotype, as described for *in vitro* differentiated regulatory macrophages (55) or infiltrating CD14^{+} CD206^{+} tumor monocytes, which specifically express Arginase-1, IL-10, and TGFβ (56). Importantly, it was demonstrated that macrophages found at the center of MS brain demyelinating lesions can express both CD206 and the pro-inflammatory marker iNOS. In their settings, iNOS/CD206 co-expression may represent cells transiting from a pro-inflammatory to a non-inflammatory phenotype (48). Recruitment of CD206/iNOS co-expressing macrophages was also described in the lungs of patients with chronic obstructive pulmonary disease, and these cells are associated with disease severity (57). In the same way, blood circulating CD206-expressing CD14 monocytes are observed in patients with more severe idiopathic membranous nephropathy (58). These apparently conflicting results about the polarization of CD206 monocytes highlight their highly plastic phenotype, which may be controlled by environmental cues and interacting cells. In both murine models and *in vitro* experiments, it was observed that polarization of endothelial cells from the BBB may regulate iNOS and Arginase-1 expression in interacting macrophages. Specifically, inflamed barriers were found to trigger the expression of iNOS (59).

Our data suggest potential interactions between CD206^{hi} CD209^{hi} Mo and BBB endothelial cells, illustrated by the presence of CD206^{hi} CD209^{hi} Mo-like cells in the CSF, along with elevated expression of both VCAM-1 and CCR5 expression. Even if VCAM-1 expression is poorly described on monocytes, its upregulation by blood classical monocytes in co-culture with endothelial cells has been reported (60), supporting CD206^{hi} CD209^{hi} Mo interaction with the BBB. Further, CCR5 is found to be expressed by 70% of CD14^{+} monocytic cells infiltrating the CSF regardless of CNS pathology, while only 20% of blood circulating monocytes are expressing it (61). The CCR5/CCL5 axis has also been demonstrated critical in the recruitment of pathological monocytes within the CNS of EAE mice model (3). Importantly, although CNS microenvironment imprinting was observed about CSF CD206^{hi} CD209^{hi} Mo-like cells (*CX3CR1*, *CLEC10A*), these were found transcriptionally closer to monocytes than to BAMs, while being highly different from microglial subsets, indicating that CD206^{hi} CD209^{hi} Mo-like cells are from peripheral origin.

Therefore, considering (i) CD206^{hi} CD209^{hi} Mo cells blood enrichment at diagnosis in patients with a worse outcome, (ii) CD206^{hi} CD209^{hi} Mo-like cells' peripheral origin and presence in CSF, (iii) CD206^{hi} CD209^{hi} Mo and CD206^{hi} CD209^{hi} Mo-like cells expression of proteins and transcripts involved in antigen presentation and cell co-stimulation, and (iv) CD206^{hi} CD209^{hi} Mo expression of pro-inflammatory and trafficking markers at the protein (CD45RA (47), VCAM-1, CCR2, CCR5) and transcripts level (*CCR2, IL18*)—prompted us to suggest that CD206^{hi} CD209^{hi} Mo cells represent an activated and pathogenic subset of classical monocyte population that had experienced tissue trafficking. Whether these cells observed by mass cytometry indeed represent a blood recirculating fraction defining CD206^{hi} CD209^{hi} Mo enriched patients nevertheless still has to be confirmed.

Interestingly, we found that patients carrying the MS-associated susceptibility alleles HLA-DRB1*15:01 and HLA-DQB1*06:02 were more frequent among CD206^{hi} and CD209^{hi} Mo patients. The frequency of the HLA-DRB1*15:01 haplotype in MS patients compared to the general population has already been shown to be overrepresented among the MS population (50,48% vs. 24.14% in

controls) (62). Although we found several HLA-DRB1*15:01 positive individuals among the MS patients wo CD206^{hi} CD209^{hi} Mo in line with literature regarding the MS population (45%), we observed that 75% of MS patients w CD206^{hi} CD209^{hi} Mo carry this susceptibility gene. We may therefore wonder whether this specific haplotype favors CD206^{hi} CD209^{hi} Mo proliferation and/or survival, partly explaining their specific enrichment in MS. Although B cells and myeloid cells share an overlapping immunopeptidome, HLA-DRB1*15:01-derived self-peptides presentation involved in autoreactive T-cell amplification seems restricted to B cells (63). Nevertheless, CD206^{hi} CD209^{hi} Mo/T-cell interaction through other myelin-derived peptide presentations may participate in disease evolution/relapses as highlighted in mice model (64) and in line with the higher propensity of CCR2 circulating myeloid cells to contact tissue lesions infiltrating T cells in EAE mice (16). Over HLA-DRB1*15:01 expression in monocytes compared to other haplotypes is linked to the specific hypomethylation of the HLA-DRB1*15:01 exon 2 DNA sequence, linking epigenetic HLA-DRB1*15:01 expression and MS risk (65). Whether this mechanism is involved in monocyte/T-cell enhanced interaction supporting T-cell pathological activity or whether demethylation of this gene impacts related genes expression (66) contributing to monocyte pathogenicity hence has to be studied.

Altogether, the combination of (i) leading-edge techniques such as mass cytometry and scRNA-seq performed on (ii) a highly detailed cohort of patients at diagnosis who (iii) benefit from a cautious annual follow-up, allowed us to proceed to an unprecedented description of a circulating myeloid population associated to the patients 'outcome. However, although the number of patients was enough to draw robust conclusions, this study was highly descriptive, and the lack of a validation cohort to confirm our findings is a limitation of this work. Assessing more patients and controls over a longer period should help in the estimation of CD206^{hi} CD209^{hi} Mo's contribution to patients' outcomes, independently of treatments and other confounding factors. A study of patients benefiting from anti-VLA4 treatment would be of particular interest in this context. Further, many conclusions are gene-based as the supportive role of CD206^{hi} CD209^{hi} Mo cells toward T cells has thus to be specifically tested on sorted cells as their potential contribution to pathogenesis through cytokines production. We believe that getting more insight into this cell subset, for example, by blocking their polarization, their trafficking to the CNS, or their antigen presentation process, should be considered as therapeutic strategies.

Data availability statement

The datasets analyzed for this study can be found in the European Genome-Phenome Archive: EGAD50000000445.

Ethics statement

This study was registered and approved by the Ethics Committee of Rennes Hospital (notice n° 20.05). MS patients included in this work were extracted from the OFSEP (Observatoire Français de la Sclérose en Plaques) MS French registry, www.ofsep.org. All participants provide written informed consent for participation. In accordance with the French legislation, OFSEP was approved by both the French data protection agency (Commission Nationale de l' Informatique et des Libertés (CNIL); authorization request 914066v3) and a French ethical committee (Comité de Protection des Personnes (CPP): reference 2019-A03066-51), and the present study was declared compliant to the MR-004 (Méthodologie de reference 004) of the CNIL. The studies were conducted in accordance with the local legislation and institutional requirements. The participants provided their written informed consent to participate in this study.

Author contributions

SR: Conceptualization, Data curation, Formal analysis, Funding acquisition, Investigation, Methodology, Project administration, Software, Supervision, Validation, Writing – original draft, Writing – review & editing. LC: Writing – review & editing, Data curation, Formal analysis, Investigation, Methodology. JF: Methodology, Validation, Writing – review & editing. NV: Data curation, Formal analysis, Investigation, Methodology, Software, Validation, Writing – review & editing. MM: Writing – review & editing, Data curation, Investigation. RJ: Writing – review & editing, Data curation, Investigation. CM: Writing – review & editing, Investigation, Methodology. SL: Writing – review & editing, Data curation, Methodology, Software, Validation. SLG: Writing – review & editing, Methodology. NS: Investigation, Methodology, Writing – review & editing, Data curation, Formal analysis. SB-H: Writing – review & editing, Project administration. DL: Investigation, Writing – review & editing. AG: Writing – review & editing, Data curation, Formal analysis, Investigation, Methodology. RC: Writing – review & editing, Resources. HZ: Writing – review & editing, Resources. AK: Writing – review & editing, Resources. GE: Writing – review & editing, Resources. EL: Writing – review & editing, Resources. ET: Writing – review & editing, Resources. AR: Writing – review & editing, Resources. GM: Writing – review & editing, Resources. P-AG: Resources, Writing – review & editing. KT: Supervision, Validation, Writing – review & editing. CD: Writing – review & editing. PA: Writing – review & editing. MR: Methodology, Validation, Writing – review & editing. LM: Conceptualization, Funding acquisition, Methodology, Project administration, Resources, Supervision, Validation, Writing – original draft, Writing – review & editing, Investigation.

OFSEP contributors

The following contributors, who are listed in alphabetical order, contributed to the work of Observatoire Français de la Sclérose en Plaques:

OFSEP investigators

CISCO project:

List of OFSEP investigators (Steering Committee, Principal investigators, Biology group, Imaging group)

Steering Committee

RC, PhD, Observatoire français de la sclérose en plaques (OFSEP), Centre de coordination national, Lyon/Bron, France; François Cotton, MD, Hospices civils de Lyon, Hôpital Lyon sud, Service d'imagerie médicale et interventionnelle, Lyon/Pierre-Bénite, France; Jérôme De Sèze, MD, Hôpitaux universitaire de Strasbourg, Hôpital de Hautepierre, Service des maladies inflammatoires du système nerveux – neurologie, Strasbourg, France; Pascal Douek, MD, Union pour la lutte contre la sclérose en plaques (UNISEP), Ivry-sur-Seine, France; Francis Guillemin, MD, CIC 1433 Epidémiologie Clinique, Centre hospitalier régional universitaire de Nancy, Inserm et Universitéde Lorraine, Nancy, France; DL, MD, Centre hospitalier universitaire de Nantes, Hôpital nord Laennec, Service de neurologie, Nantes/Saint-Herblain, France; Christine Lebrun-Frenay, MD, Centre hospitalier universitaire de Nice, UniversitéNice Côte d'Azur, Hôpital Pasteur, Service de neurologie, Nice, France; Lucilla Mansuy, Hospices civils de Lyon, Département de la recherche clinique et de l'innovation, Lyon, France; Thibault Moreau, MD, Centre hospitalier universitaire Dijon Bourgogne, Hôpital François Mitterrand, Service de neurologie, maladies inflammatoires du système nerveux et neurologie générale, Dijon, France; Javier Olaiz, PhD, Université Claude Bernard Lyon 1, Lyon ingéniérie projets, Lyon, France; Jean Pelletier, MD, Assistance publique des hôpitaux de Marseille, Centre hospitalier de la Timone, Service de neurologie et uniténeuro-vasculaire, Marseille, France; Claire Rigaud-Bully, Fondation Eugène Devic EDMUS contre la sclérose en plaques, Lyon, France; Bruno Stankoff, MD, Assistance publique des hôpitaux de Paris, Hôpital Saint-Antoine, Service de neurologie, Paris, France; Sandra Vukusic, MD, Hospices civils de Lyon, Hôpital Pierre Wertheimer, Service de neurologie A, Lyon/Bron, France; HZ, MD, Centre hospitalier universitaire de Lille, Hôpital Salengro, Service de neurologie, Lille, France.

Investigators

Romain Marignier, MD, Hospices civils de Lyon, Hôpital Pierre Wertheimer, Service de neurologie A, Lyon/Bron, France; Marc Debouverie, MD, Centre hospitalier reǵional universitaire de Nancy, Hôpital central, Service de neurologie, Nancy, France; GE, MD, Centre hospitalier universitaire de Rennes, Hôpital Pontchaillou, Service de neurologie, Rennes, France; Jonathan Ciron, MD, Centre hospitalier universitaire de Toulouse, Hôpital Purpan, Service de neurologie inflammatoire et neuro-oncologie, Toulouse, France; AR, MD, Centre hospitalier universitaire de Bordeaux, Hôpital Pellegrin, Service de neurologie, Bordeaux, France; Nicolas Collongues, MD, Hôpitaux universitaire de Strasbourg, Hôpital de Hautepierre, Service des maladies inflammatoires du système nerveux – neurologie, Strasbourg, France; Catherine Lubetzki, MD, Assistance publique des hôpitaux de Paris, Hoôpital de la Pitie-'Salpeêtrière, Service de neurologie, Paris, France; HZ, MD, Centre hospitalier universitaire de Lille, Hôpital Salengro, Service de neurologie, Lille, France; Pierre Labauge, MD, Centre hospitalier universitaire de Montpellier, Hôpital Gui de Chauliac, Service de neurologie, Montpellier, France; Gilles Defer, MD, Centre hospitalier universitaire de Caen Normandie, Service de neurologie, Hôpital Côte de Nacre, Caen, France; Mikaël Cohen, MD, Centre hospitalier universitaire de Nice, Université Nice Côte d'Azur, Hôpital Pasteur, Service de neurologie, Nice, France; Agnès Fromont, MD, Centre hospitalier universitaire Dijon Bourgogne, Hôpital François Mitterrand, Service de neurologie, maladies inflammatoires du système nerveux et neurologie générale, Dijon, France; Sandrine Wiertlewsky, MD, Centre hospitalier universitaire de Nantes, Hôpital nord Laennec, Service de neurologie, Nantes/Saint-Herblain, France; Eric Berger, MD, Centre hospitalier régional universitaire de Besançon, Hôpital Jean Minjoz, Service de neurologie, Besançon, France; Pierre Clavelou, MD, Centre hospitalier universitaire de Clermont-Ferrand, Hôpital Gabriel-Montpied, Service de neurologie, Clermont-Ferrand, France; Bertrand Audoin, MD, Assistance publique des hôpitaux de Marseille, Centre hospitalier de la Timone, Service de neurologie et uniténeuro-vasculaire, Marseille, France; Claire Giannesini, MD, Assistance publique des hôpitaux de Paris, Hôpital Saint-Antoine, Service de neurologie, Paris, France; Olivier Gout, MD, Fondation Adolphe de Rothschild de l'oeil et du cerveau, Service de neurologie, Paris, France; ET, MD, Centre hospitalier universitaire de Nîmes, Hôpital Carémeau, Service de neurologie, Nîmes, France; Olivier Heinzlef, MD, Centre hospitalier intercommunal de Poissy Saint-Germain-en-Laye, Service de neurologie, Poissy, France; Abdullatif Al-Khedr, MD, Centre hospitalier universitaire d'Amiens Picardie, Site sud, Service de neurologie, Amiens, France; Bertrand Bourre, MD, Centre hospitalier universitaire Rouen Normandie, Hôpital Charles-Nicolle, Service de neurologie, Rouen, France; Olivier Casez, MD, Centre hospitalier universitaire Grenoble-Alpes, Site nord, Service de neurologie, Grenoble/La Tronche, France; Philippe Cabre, MD, Centre hospitalier universitaire de Martinique, Hôpital Pierre Zobda-Quitman, Service de Neurologie, Fort-de-France, France; Alexis Montcuquet, MD, Centre hospitalier universitaire Limoges, Hôpital Dupuytren, Service de neurologie, Limoges, France; Alain Créange, MD, Assistance publique des hôpitaux de Paris, Hôpital Henri Mondor, Service de neurologie, Créteil, France; Jean-Philippe Camdessanché, MD, Centre hospitalier universitaire de Saint-étienne, Hôpital Nord, Service de neurologie, Saint-étienne, France; Justine Faure, MD, Centre hospitalier universitaire de Reims, Hôpital Maison-Blanche, Service de neurologie, Reims, France; Aude Maurousset,MD,Centre hospitalier reǵional universitaire de Tours, Hôpital Bretonneau, Service de neurologie, Tours, France; Ivania Patry, MD, Centre hospitalier sud francilien, Service de neurologie, Corbeil-Essonnes, France; Karolina Hankiewicz, MD, Centre hospitalier de Saint-Denis, Hôpital Casanova, Service de neurologie, Saint-Denis, France; Corinne Pottier, MD, Centre hospitalier de Pontoise, Service de neurologie, Pontoise, France; Nicolas Maubeuge, MD, Centre hospitalier universitaire de Poitiers, Site de la Milétrie, Service de neurologie, Poitiers, France; Céline Labeyrie, MD,

Assistance publique des hôpitaux de Paris, Hôpital Bicêtre, Service de neurologie, Le Kremlin-Bicêtre, France; Chantal Nifle, MD, Centre hospitalier de Versailles, Hôpital André-Mignot, Service de neurologie, Le Chesnay, France;

Biology group

Patrick Gelé, CRB/CIC1403, Centre de Biologie Pathologie Génétique, Lille, France; Mireille Desille-Dugast, CRB, Laboratoire de Cytogénétique et Biologie Cellulaire, CHU Pontchaillou, Rennes, France; Céline Loiseau, CRB, Laboratoire de cytogénétique, CHU de Nîmes, Nîmes, France; Julien Jeanpetit, Centre de Ressources Biologiques Plurithématique (CRB-P), Bordeaux Biothèques Santé (BBS), Pôle de Biologie et de Pathologie, CHU de Bordeaux, Bordeaux, France; Sandra Lomazzi, CRB Lorrain- CHRU Nancy, Vandoeuvre-les-Nancy, France; DL, Centre hospitalier universitaire de Nantes, Hôpital nord Laennec, Service de neurologie, Nantes/Saint-Herblain, France; ET, Centre hospitalier universitaire de Nîmes, Hopital Carémeau, Service de neurologie, Nîmes, France; Guillaume Brocard, Observatoire français de la sclérose en plaques (OFSEP), Centre de coordination national, Lyon/Bron, France; RC, Observatoire français de la sclérose en plaques (OFSEP), Centre de coordination national, Lyon/Bron, France; Nathalie Dufay, NeuroBioTec, Hôpital Neurologique Pierre Wertheimer, Hospices Civils de Lyon, Lyon/Bron, France; Caroline Barau, Laboratoire de la PRB, Centre d'Investigation Clinique (CIC), Groupe Hospitalier Henri Mondor, Créteil, France; Shaliha Bechoua, Etablissement Français du Sang, Service Biothèque-CRB, Dijon, France; Gilda Belrose, Centre de Ressources Biologiques de la Martinique (CeRBiM), CHU de Martinique Pierre ZOBDA-QUITMAN, Fort-de-France, France; Juliette Berger, CRB Auvergne - CHU Estaing, Clermont- Ferrand, France; Marie-Pierrette Chenard, CRB, UF 6337, Département de Pathologie, Hôpital de Hautepierre, Hôpitaux Universitaires de Strasbourg, Strasbourg, France; Esther Dos Santos, Service de Biologie médicale, Poissy, France; Arianna Fiorentino, CRB HUEP-SU, Faculté de médecine site Saint Antoine, Paris, France; Sylvie Forlani, Banque ADN & Cellules-ICM U1127, PRB, GH Pitie´ Salpetrière, Paris, France; Géraldine Gallot, CRB, UF 7296, CHU de Nantes, Hôtel Dieu, Institut de biologie, Nantes, France; Michèle Grosdenier, EFS, CHU de Poitiers, Poitiers, France; Yves-Edouard Herpe, Biobanque de Picardie - CHU Amiens-Picardie, Amiens, France; Caroline Laheurte, Etablissement Français du Sang, Besançon, France; Hélène Legros, CHU Caen Normandie, Caen, France; Sylvain Lehmann, CHU Saint Eloi, IRMB, Biochimie Protéomique Clinique, Montpellier, France; Philippe Lorimier, Centre de Ressources Biologiques, Institut de Biologie et de Pathologie, CHU Albert Michallon, Grenoble, France; Mikael Mazighi, Fondation Ophtalmologique Adolphe de Rothschild, Centre de Ressources Biologiques, Paris, France; Samantha Montagne, CHRU Bretonneau, CRB, EFS, Tours, France. Bénédicte Razat, CRB Toulouse Bio Ressources, Toulouse, France; Noémie Saut, Service d'Hématologie Biologique, CHU Timone adultes, Marseille, France; Emilie Villeger, CRBIoLim, CHU Dupuytren, Limoges, France; Kevin Washetine, CHU de Nice, Hôpital Pasteur 1, Nice, France.

Imaging group

Olivier Outteryck, MD, CHRU Lille, Consultations de neurologie D, Lille, France; Jean-Pierre Pruvo, MD, CHRU Lille, Service de radiologie, Lille, France; Elise Bannier, PHD Institut de Recherche en Informatique et Systèmes Aléatoires, Rennes, France; Jean-Christophe Ferre, MD, CHU Rennes, Service de radiologie, Rennes, France; Thomas Tourdias, MD, CHU Bordeaux, Service de radiologie, Bordeaux, France; Vincent Dousset, MD, CHU Bordeaux, Service de radiologie, Bordeaux, France; Rene Anxionnat, MD, CHU Nancy, Service de radiologie, Nancy, France; Roxana Ameli, MD, Hospices civils de Lyon, Service de radiologie, Lyon, France; Arnaud Attye, MD, CHU de Grenoble, Service de radiologie, Grenoble, France; Douraied Bensalem, MD, CHU Brest, Service de radiologie, Brest, France; Marie-Paule Boncoeur-Martel, MD, CHU Limoges, Service de radiologie, Limoges, France; Fabrice Bonneville, MD, CHU Toulouse Purpan, Service de radiologie, Toulouse, France; Claire Boutet, MD, CHU Saint-Etienne, Service de radiologie, Saint-Etienne, France; Jean-Christophe Brisset, PHD Median technologies, Valbonne, France; Frédéric Cervenanski, PHD CREATIS, Villeurbanne, France; Béatrice Claise, MD, CHU Clermont-Ferrand, Service de radiologie, Clermont-Ferrand, France; Olivier Commowick, I PHD NRIA, Rennes, France; Jean-Marc Constans, MD, CHU Amiens – Picardie, Service de radiologie, Amiens, France; Pascal Dardel, MD, CH Chambéry, Service de radiologie, Chambéry, France; Hubert Desal, MD, CHU Nantes, Service de radiologie, Nantes, France; Françoise Durand-Dubief, MD, Hospices civils de Lyon, Service de Neurologie, Lyon, France; Alina Gaultier, MD, CHU Nantes, Service de radiologie, Nantes, France; Emmanuel Gerardin, MD, CHU Rouen, Service de radiologie, Rouen, France; Tristan Glattard, PHD CREATIS, Villeurbanne, France; Sylvie Grand, MD, CHU de Grenoble, Service de radiologie, Grenoble, France; Thomas Grenier, PHD CREATIS, Villeurbanne, France; Rémy Guillevin, MD, CHR Poitiers, Service de radiologie, Poitiers, France; Charles Guttmann, MD, Harvard Medical School, Boston, USA; vAlexandre Krainik, MD, CHU Grenoble Alpes, Service de radiologie, Grenoble, France; Stéphane Kremer, MD, CHU Strasbourg, Service de radiologie, Strasbourg, France; Stéphanie Lion, Centre de coordination national de l'OFSEP, Lyon/Bron, France; Nicolas Menjot de Champfleur, MD, CHU Montpellier, Service de radiologie, Montpellier, France; Lydiane Mondot, MD, CHU Nice, Service de radiologie, Nice, France; Nadya Pyatigorskaya, MD, ICM, Service de radiologie, Paris, France; Sylvain Rabaste, MD, Hospices civils de Lyon, Service de radiologie, Lyon, France; Jean-Philippe Ranjeva, MD, APHM - CHU Marseille Timone, Service de radiologie, Marseille, France; Jean-Amédée Roch, MD, Hôpital privéJean Mermoz, Service de radiologie, Lyon, France; Jean Claude Sadik, MD, Fondation A. de Rothschild, Service de radiologie, Paris, France; Dominique Sappey-Marinier, MD, Hospices civils de Lyon, Service de radiologie, Lyon, France; Julien Savatovsky, MD, Fondation A. de Rothschild, Service de radiologie, Paris, France; Jean-Yves Tanguy, MD, CH Angers, Service de radiologie, Angers, France; Ayman Tourbah, MD, Hôpital Raymond Poincaré, Service de Neurologie, Garches, Fr.

Funding

The author(s) declare financial support was received for the research, authorship, and/or publication of this article. This study was supported by ARSEP and INCR.

Acknowledgments

The authors are thankful to the CyPS platform (Cytometry Core CyPS, Sorbonne University, Pitie-Salpetriere Hospital, Paris, France). This work was conducted using data from the Observatoire Français de la Sclérose en plaques (OFSEP) which is granted by the French State and handled by the "Agence Nationale de la Recherche," within the framework of the "France 2030" programme, under the reference ANR-10-COHO-002, Observatoire Français de la Sclérose en Plaques (OFSEP), by the Eugène Devic EDMUS Foundation against MS and by the ARSEP Foundation. The authors are also grateful to the Rennes University Hospital as to the ARSEP foundation and the INCR (Institut des Neurosciences Clinique de Rennes) for their unvaluable support in this study.

Conflict of interest

The authors declare that the research was conducted in the absence of any commercial or financial relationships that could be construed as a potential conflict of interest.

Publisher's note

Supplementary material

The Supplementary Material for this article can be found online at: https://www.frontiersin.org/articles/10.3389/fimmu.2024.1494842/full#supplementary-material

References

1. van Langelaar J, Rijvers L, Janssen M, Wierenga-Wolf AF, Melief M-J, Siepman TA, et al. Induction of brain-infiltrating T-bet–expressing B cells in multiple sclerosis. *Ann Neurol.* (2019) 86:264–78. doi: 10.1002/ana.25508

2. Schnell A, Huang L, Singer M, Singaraju A, Barilla RM, Regan BML, et al. Stem-like intestinal Th17 cells give rise to pathogenic effector T cells during autoimmunity. *Cell.* (2021) 184:6281–6298.e23. doi: 10.1016/j.cell.2021.11.018

3. Shi K, Li H, Chang T, He W, Kong Y, Qi C, et al. Bone marrow hematopoiesis drives multiple sclerosis progression. *Cell.* (2022) 185:2234–2247.e17. doi: 10.1016/j.cell.2022.05.020

4. Amorim A, De Feo D, Friebel E, Ingelfinger F, Anderfuhren CD, Krishnarajah S, et al. IFNγ and GM-CSF control complementary differentiation programs in the monocyte-to-phagocyte transition during neuroinflammation. *Nat Immunol.* (2022) 23:217–28. doi: 10.1038/s41590-021-01117-7

5. McGinley AM, Sutton CE, Edwards SC, Leane CM, DeCourcey J, Teijeiro A, et al. Interleukin-17A serves a priming role in autoimmunity by recruiting IL-1β-producing myeloid cells that promote pathogenic T cells. *Immunity.* (2020) 52:342–356.e6. doi: 10.1016/j.immuni.2020.01.002

6. Waschbisch A, Schröder S, Schraudner D, Sammet L, Weksler B, Melms A, et al. Pivotal role for CD16+ Monocytes in immune surveillance of the central nervous system. *J Immunol.* (2016) 196:1558–67. doi: 10.4049/jimmunol.1501960

7. Mildner A, Mack M, Schmidt H, Brück W, Djukic M, Zabel MD, et al. CCR2+Ly-6Chi monocytes are crucial for the effector phase of autoimmunity in the central nervous system. *Brain.* (2009) 132:2487–500. doi: 10.1093/brain/awp144

8. Ostkamp P, Deffner M, Schulte-Mecklenbeck A, Wünsch C, Lu I-N, Wu GF, et al. A single-cell analysis framework allows for characterization of CSF leukocytes and their tissue of origin in multiple sclerosis. *Sci Transl Med.* (2022) 14:eadc9778. doi: 10.1126/scitranslmed.adc9778

9. Ifergan I, Kébir H, Bernard M, Wosik K, Dodelet-Devillers A, Cayrol R, et al. The blood–brain barrier induces differentiation of migrating monocytes into Th17-polarizing dendritic cells. *Brain.* (2008) 131:785–99. doi: 10.1093/brain/awm295

10. Zozulya AL, Ortler S, Lee J, Weidenfeller C, Sandor M, Wiendl H, et al. Intracerebral dendritic cells critically modulate encephalitogenic versus regulatory immune responses in the CNS. *J Neurosci.* (2009) 29:140–52. doi: 10.1523/JNEUROSCI.2199-08.2009

11. Monaghan KL, Zheng W, Hu G, Wan ECK. Monocytes and monocyte-derived antigen-presenting cells have distinct gene signatures in experimental model of multiple sclerosis. *Front Immunol.* (2019) 10:2779. doi: 10.3389/fimmu.2019.02779

12. Locatelli G, Theodorou D, Kendirli A, Jordão MJC, Staszewski O, Phulphagar K, et al. Mononuclear phagocytes locally specify and adapt their phenotype in a multiple sclerosis model. *Nat Neurosci.* (2018) 21:1196–208. doi: 10.1038/s41593-018-0212-3

13. Moliné-Velázquez V, Cuervo H, Vila-del Sol V, Ortega MC, Clemente D, de Castro F. Myeloid-derived suppressor cells limit the inflammation by promoting T lymphocyte apoptosis in the spinal cord of a murine model of multiple sclerosis. *Brain Pathol.* (2011) 21:678–91. doi: 10.1111/j.1750-3639.2011.00495.x

14. Ajami B, Bennett JL, Krieger C, McNagny KM, Rossi FMV. Infiltrating monocytes trigger EAE progression, but do not contribute to the resident microglia pool. *Nat Neurosci.* (2011) 14:1142–9. doi: 10.1038/nn.2887

15. White MPJ, Webster G, Leonard F, La Flamme AC. Innate IFN-γ ameliorates experimental autoimmune encephalomyelitis and promotes myeloid expansion and PDL-1 expression. *Sci Rep.* (2018) 8:259. doi: 10.1038/s41598-017-18543-z

16. Jordão MJC, Sankowski R, Brendecke SM, Sagar Locatelli G, Tai Y-H, Tay TL, et al. Single-cell profiling identifies myeloid cell subsets with distinct fates during neuroinflammation. *Science.* (2019) 363:eaat7554. doi: 10.1126/science.aat7554

17. Engel S, Jolivel V, Kraus SHP, Zayoud M, Rosenfeld K, Tumani H, et al. Laquinimod dampens IL-1β signaling and Th17-polarizing capacity of monocytes in patients with MS. *Neurol - Neuroimmunol Neuroinflammation.* (2021) 8:1–10. doi: 10.1212/NXI.0000000000000908

18. Polman CH, O'Connor PW, Havrdova E, Hutchinson M, Kappos L, Miller DH, et al. A randomized, placebo-controlled trial of natalizumab for relapsing multiple sclerosis. *N Engl J Med.* (2006) 354:899–910. doi: 10.1056/NEJMoa044397

19. Ifergan I, Kebir H, Terouz S, Alvarez JI, Lécuyer M-A, Gendron S, et al. Role of ninjurin-1 in the migration of myeloid cells to central nervous system inflammatory lesions. *Ann Neurol.* (2011) 70:751–63. doi: 10.1002/ana.22519

20. Haschka D, Tymoszuk P, Bsteh G, Petzer V, Berek K, Theurl I, et al. Expansion of neutrophils and classical and nonclassical monocytes as a hallmark in relapsing-remitting multiple sclerosis. *Front Immunol.* (2020) 11:594. doi: 10.3389/fimmu.2020.00594

21. Lee CH, Jiang B, Nakhaei-Nejad M, Barilla D, Blevins G, Giuliani F. Cross-sectional analysis of peripheral blood mononuclear cells in lymphopenic and non-lymphopenic relapsing-remitting multiple sclerosis patients treated with dimethyl fumarate. *Mult Scler Relat Disord.* (2021) 52:103003. doi: 10.1016/j.msard.2021.103003

22. D'Amico E, Zanghì A, Parrinello NL, Romano A, Palumbo GA, Chisari CG, et al. Immunological subsets characterization in newly diagnosed relapsing–remitting multiple sclerosis. *Front Immunol.* (2022) 13:819136. doi: 10.3389/fimmu.2022.819136

23. Monteiro A, Rosado P, Rosado L, Fonseca AM, Coucelo M, Paiva A. Alterations in peripheral blood monocyte and dendritic cell subset homeostasis in relapsing-remitting multiple sclerosis patients. *J Neuroimmunol.* (2021) 350:577433. doi: 10.1016/j.jneuroim.2020.577433

24. Gjelstrup MC, Stilund M, Petersen T, Møller HJ, Petersen EL, Christensen T. Subsets of activated monocytes and markers of inflammation in incipient and

progressed multiple sclerosis. *Immunol Cell Biol*. (2018) 96:160–74. doi: 10.1111/imcb.1025

25. Ortega MC, Lebrón-Galán R, Machín-Díaz I, Naughton M, Pérez-Molina I, García-Arocha J, et al. Central and peripheral myeloid-derived suppressor cell-like cells are closely related to the clinical severity of multiple sclerosis. *Acta Neuropathol (Berl)*. (2023) 146:263–82. doi: 10.1007/s00401-023-02593-x

26. Palavra F, Geria L, Jorge A, Marques M, dos Santos CS, Amaral J, et al. Neutrophil/lymphocyte and monocyte/lymphocyte indexes as potential predictors of relapse at 1 year after diagnosis of pediatric multiple sclerosis: a single-center, exploratory and proof-of-concept study. *Front Neurosci*. (2024) 17:1305176. doi: 10.3389/fnins.2023.1305176

27. Vukusic S, Casey R, Rollot F, Brochet B, Pelletier J, Laplaud D-A, et al. Observatoire Français de la Sclérose en Plaques (OFSEP): A unique multimodal nationwide MS registry in France. *Mult Scler J*. (2020) 26:118–22. doi: 10.1177/1352458518815602

28. Brocard G, Casey R, Dufay N, Marignier R, Michel L, Hisbergues M, et al. The biological sample collection of the OFSEP French MS registry: An essential tool dedicated to researchers. *Mult Scler Relat Disord*. (2023) 77:104872. doi: 10.1016/j.msard.2023.104872

29. Confavreux C, Compston DA, Hommes OR, McDonald WI, Thompson AJ. EDMUS, a European database for multiple sclerosis. *J Neurol Neurosurg Psychiatry*. (1992) 55:671–6. doi: 10.1136/jnnp.55.8.671

30. Brisset JC, Kremer S, Hannoun S, Bonneville F, Durand-Dubief F, Tourdias T, et al. New OFSEP recommendations for MRI assessment of multiple sclerosis patients: Special consideration for gadolinium deposition and frequent acquisitions. *J Neuroradiol*. (2020) 47:250–8. doi: 10.1016/j.neurad.2020.01.083

31. Thompson AJ, Banwell BL, Barkhof F, Carroll WM, Coetzee T, Comi G, et al. Diagnosis of multiple sclerosis: 2017 revisions of the McDonald criteria. *Lancet Neurol*. (2018) 17:162–73. doi: 10.1016/S1474-4422(17)30470-2

32. Ferrant J, Le Gallou S, Manson G, Genebrier S, Mourcin F, Tarte K, et al. High-dimensional phenotyping of human myeloid-derived suppressor cells/tumor-associated macrophages in tissue by mass cytometry. *Methods Mol Biol Clifton NJ*. (2021) 2236:57–66. doi: 10.1007/978-1-0716-1060-2_6

33. Roussel M, Ferrant J, Reizine F, Le Gallou S, Dulong J, Carl S, et al. Comparative immune profiling of acute respiratory distress syndrome patients with or without SARS-CoV-2 infection. *Cell Rep Med*. (2021) 2:100291. doi: 10.1016/j.xcrm.2021.100291

34. Couloume L, Ferrant J, Le Gallou S, Mandon M, Jean R, Bescher N, et al. Mass cytometry identifies expansion of T-bet+ B cells and CD206+ Monocytes in early multiple sclerosis. *Front Immunol*. (2021) 12:653577. doi: 10.3389/fimmu.2021.653577

35. Pool AH, Poldsam H, Chen S, Thomson M, Oka Y. Recovery of missing single-cell RNA-sequencing data with optimized transcriptomic references. *Nat Methods*. (2023) 20:1506–15. doi: 10.1038/s41592-023-02003-w

36. Monaco G, Lee B, Xu W, Mustafah S, Hwang YY, Carré C, et al. RNA-seq signatures normalized by mRNA abundance allow absolute deconvolution of human immune cell types. *Cell Rep*. (2019) 26:1627–1640.e7. doi: 10.1016/j.celrep.2019.01.041

37. Chang CC, Chow CC, Tellier LC, Vattikuti S, Purcell SM, Lee JJ. Second-generation PLINK: rising to the challenge of larger and richer datasets. *GigaScience*. (2015) 4:7. doi: 10.1186/s13742-015-0047-8

38. Danecek P, Bonfield JK, Liddle J, Marshall J, Ohan V, Pollard MO, et al. Twelve years of SAMtools and BCFtools. *GigaScience*. (2021) 10:giab008. doi: 10.1093/gigascience/giab008

39. Taliun D, Harris DN, Kessler MD, Carlson J, Szpiech ZA, Torres R, et al. Sequencing of 53,831 diverse genomes from the NHLBI TOPMed Program. *Nature*. (2021) 590:290–9. doi: 10.1038/s41586-021-03205-y

40. Gourraud PA, McElroy JP, Caillier SJ, Johnson BA, Santaniello A, Hauser SL, et al. Aggregation of multiple sclerosis genetic risk variants in multiple and single case families. *Ann Neurol*. (2011) 69:65–74. doi: 10.1002/ana.22323

41. International Multiple Sclerosis Genetics Consortium, . Multiple sclerosis genomic map implicates peripheral immune cells and microglia in susceptibility. *Science*. (2019) 365. doi: 10.1126/science.aav7188

42. Zheng X, Shen J, Cox C, Wakefield JC, Ehm MG, Nelson MR, et al. HIBAG–HLA genotype imputation with attribute bagging. *Pharmacogenomics J*. (2014) 14:192–200. doi: 10.1038/tpj.2013.18

43. 1000 Genomes Project Consortium, Auton A, Brooks LD, Durbin RM, Garrison EP, Kang HM, Korbel JO, Marchini JL, et al. A global reference for human genetic variation. *Nature*. (2015) 526:68–74. doi: 10.1038/nature15393

44. Douillard V, Castelli EC, Mack SJ, Hollenbach JA, Gourraud P-A, Vince N, et al. Approaching genetics through the MHC lens: tools and methods for HLA research. *Front Genet*. (2021) 12:774916. doi: 10.3389/fgene.2021.774916

45. Manouchehrinia A, Westerlind H, Kingwell E, Zhu F, Carruthers R, Ramanujam R, et al. Age Related Multiple Sclerosis Severity Score: Disability ranked by age. *Mult Scler J*. (2017) 23:1938–46. doi: 10.1177/1352458517690618

46. Beyer M, Mallmann MR, Xue J, Staratschek-Jox A, Vorholt D, Krebs W, et al. High-resolution transcriptome of human macrophages. *PloS One*. (2012) 7:e45466. doi: 10.1371/journal.pone.0045466

47. Nagasawa T, Kobayashi H, Aramaki M, Kiji M, Oda S, Izumi Y. Expression of CD14, CD16 and CD45RA on monocytes from periodontitis patients. *J Periodontal Res*. (2004) 39:72–8. doi: 10.1111/j.1600-0765.2004.00713.x

48. Giles DA, Washnock-Schmid JM, Duncker PC, Dahlawi S, Ponath G, Pitt D, et al. Myeloid cell plasticity in the evolution of central nervous system autoimmunity. *Ann Neurol*. (2018) 83:131–41. doi: 10.1002/ana.25128

49. Schafflick D, Xu CA, Hartlehnert M, Cole M, Schulte-Mecklenbeck A, Lautwein T, et al. Integrated single cell analysis of blood and cerebrospinal fluid leukocytes in multiple sclerosis. *Nat Commun*. (2020) 11:247. doi: 10.1038/s41467-019-14118-w

50. Esaulova E, Cantoni C, Shchukina I, Zaitsev K, Bucelli RC, Wu GF, et al. Single-cell RNA-seq analysis of human CSF microglia and myeloid cells in neuroinflammation. *Neurol - Neuroimmunol Neuroinflammation*. (2020) 7:1–11. doi: 10.1212/NXI.0000000000000732

51. Ramesh A, Schubert RD, Greenfield AL, Dandekar R, Loudermilk R, Sabatino JJ, et al. A pathogenic and clonally expanded B cell transcriptome in active multiple sclerosis. *Proc Natl Acad Sci*. (2020) 117:22932–43. doi: 10.1073/pnas.2008523117

52. Cardone M, Ikeda KN, Varano B, Belardelli F, Millefiorini E, Gessani S, et al. Opposite regulatory effects of IFN-β and IL-3 on C-type lectin receptors, antigen uptake, and phagocytosis in human macrophages. *J Leukoc Biol*. (2014) 95:161–8. doi: 10.1189/jlb.0313168

53. Angel CE, Chen CJJ, Horlacher OC, Winkler S, John T, Browning J, et al. Distinctive localization of antigen-presenting cells in human lymph nodes. *Blood*. (2009) 113:1257–67. doi: 10.1182/blood-2008-06-165266

54. Marzaioli V, Canavan M, Floudas A, Flynn K, Mullan R, Veale DJ, et al. CD209/CD14+ Dendritic cells characterization in rheumatoid and psoriatic arthritis patients: activation, synovial infiltration, and therapeutic targeting. *Front Immunol*. (2022) 12:722349. doi: 10.3389/fimmu.2021.722349

55. Martinez FO, Gordon S, Locati M, Mantovani A. Transcriptional profiling of the human monocyte-to-macrophage differentiation and polarization: new molecules and patterns of gene expression1. *J Immunol*. (2006) 177:7303–11. doi: 10.4049/jimmunol.177.10.7303

56. Takahashi H, Sakakura K, Kudo T, Toyoda M, Kaira K, Oyama T, et al. Cancer-associated fibroblasts promote an immunosuppressive microenvironment through the induction and accumulation of protumoral macrophages. *Oncotarget*. (2016) 8:8633–47. doi: 10.18632/oncotarget.14374

57. Bazzan E, Turato G, Tinè M, Radu CM, Balestro E, Rigobello C, et al. Dual polarization of human alveolar macrophages progressively increases with smoking and COPD severity. *Respir Res*. (2017) 18:40. doi: 10.1186/s12931-017-0522-0

58. Hou J, Zhang M, Ding Y, Wang X, Li T, Gao P, et al. Circulating CD14+CD163+CD206+ M2 monocytes are increased in patients with early stage of idiopathic membranous nephropathy. *Mediators Inflamm*. (2018) 2018:5270657. doi: 10.1155/2018/5270657

59. Ivan DC, Walthert S, Locatelli G. Central nervous system barriers impact distribution and expression of iNOS and arginase-1 in infiltrating macrophages during neuroinflammation. *Front Immunol*. (2021) 12:666961. doi: 10.3389/fimmu.2021.666961

60. Tso C, Rye KA, Barter P. Phenotypic and functional changes in blood monocytes following adherence to endothelium. *PloS One*. (2012) 7:e37091. doi: 10.1371/journal.pone.0037091

61. Trebst C, Lykke Sørensen T, Kivisäkk P, Cathcart MK, Hesselgesser J, Horuk R, et al. CCR1+/CCR5+ Mononuclear phagocytes accumulate in the central nervous system of patients with multiple sclerosis. *Am J Pathol*. (2001) 159:1701–10. doi: 10.1016/S0002-9440(10)63017-9

62. Creary LE, Mallempati KC, Gangavarapu S, Caillier SJ, Oksenberg JR, Fernández-Viña MA. Deconstruction of HLA-DRB1*04:01:01 and HLA-DRB1*15:01:01 class II haplotypes using next generation sequencing in European Americans with multiple sclerosis. *Mult Scler Houndmills Basingstoke Engl*. (2019) 25:772–82. doi: 10.1177/1352458518770019

63. Wang J, Jelcic I, Mühlenbruch L, Haunerdinger V, Toussaint NC, Zhao Y, et al. HLA-DR15 molecules jointly shape an autoreactive T cell repertoire in multiple sclerosis. *Cell*. (2020) 183:1264–1281.e20. doi: 10.1016/j.cell.2020.09.054

64. Rasouli J, Casella G, Ishikawa LLW, Thome R, Boehm A, Ertel A, et al. IFN-β Acts on monocytes to ameliorate CNS autoimmunity by inhibiting proinflammatory cross-talk between monocytes and th cells. *Front Immunol*. (2021) 12:679498. doi: 10.3389/fimmu.2021.679498

65. Kular L, Liu Y, Ruhrmann S, Zheleznyakova G, Marabita F, Gomez-Cabrero D, et al. DNA methylation as a mediator of HLA-DRB1*15:01 and a protective variant in multiple sclerosis. *Nat Commun*. (2018) 9:2397. doi: 10.1038/s41467-018-04732-5

66. HLA-DRB1*15:01 and the MERTK gene interact to selectively influence the profile of MERTK-expressing monocytes in both health and MS. *Neurol Neuroimmunol Neuroinflamm*. (2024) 11(2):1–12. doi: 10.1212/NXI.0000000000200190

frontiers | Frontiers in Immunology

TYPE Review
PUBLISHED 29 January 2025
DOI 10.3389/fimmu.2025.1531068

OPEN ACCESS

EDITED BY
Estela Maris Muñoz,
Institute of Histology and Embryology of Mendoza Dr. Mario H. Burgos (IHEM)-UNCuyo-CONICET, Argentina

REVIEWED BY
Barbara Rossi,
University of Verona, Italy
Massimiliano Castellazzi,
University of Ferrara, Italy
Rejane Rua,
INSERM U1104 Centre d'immunologie de Marseille-Luminy (CIML), France

*CORRESPONDENCE
Olga L. Rojas
olga.rojas@uhn.ca

RECEIVED 19 November 2024
ACCEPTED 10 January 2025
PUBLISHED 29 January 2025

CITATION
Patel PU, Regmi A, Dass AI and Rojas OL (2025) Immune conversations at the border: meningeal immunity in health and disease. *Front. Immunol.* 16:1531068. doi: 10.3389/fimmu.2025.1531068

Immune conversations at the border: meningeal immunity in health and disease

Preya U. Patel[1,2], Aryan Regmi[1,2], Angelina I. Dass[1,2] and Olga L. Rojas[1,2]*

[1]Department of Immunology, University of Toronto, Toronto, ON, Canada, [2]Krembil Research Institute, University Health Network, Toronto, ON, Canada

The brain and spinal cord, collectively known as the central nervous system, are encapsulated by an overlapping series of membranes known as the meninges. Once considered primarily a physical barrier for central nervous system protection, the bordering meninges are now recognized as highly immunologically active. The meninges host diverse resident immune cells and serve as a critical interface with peripheral immunity, playing multifaceted roles in maintaining central nervous system homeostasis, responding to pathogenic threats, and neurological disorders. This review summarizes recent advancements in our understanding of meningeal immunity including its structural composition, physiological functions, and role in health and disease.

KEYWORDS

meningeal anatomy, meningeal immunity, central nervous system, immune cells - dura mater, CNS diseases

1 Introduction

The central nervous system (CNS), formed by the brain and spinal cord, is a highly specialized and sensitive system protected by the blood-brain barrier (BBB), a semipermeable microvessel system which restricts molecular, microbial, and immunological access to the CNS from peripheral circulation. Growing evidence in the field shows how the BBB is not the only interface involved as a barrier system in the CNS. The CNS is encapsulated by a three-layered membrane system called the meninges and further protected by the vertebrae or the skull (1). In addition to providing structural support, it has become abundantly clear that the meninges are areas with high immunological activity. Meningeal immunity encompasses a complex and dynamic system that includes a wide repertoire of immune cells, lymphatics, permeable vasculature, and cytokine signaling pathways. Under steady-state conditions, meningeal lymphoid and myeloid populations provide immune surveillance and primary defense against pathogens, while also supporting cognitive and behavioral functions (2–5). Advanced imaging techniques and single-cell sequencing technologies have offered

unprecedented insight into the specialized architecture and immune landscape of the meninges. It was initially thought that meningeal lymphocytes were exclusively derived from the periphery, but recent evidence has shown that the bone marrow of the skull calvaria is an important source of meningeal immune cells (6–8). Furthermore, organized lymphoid structures within the meninges at steady-state that may support the development of immune cells and facilitate local antigen-presentation in the meninges have been recently identified (9). Differences in the meningeal immune milieu have been described with aging as well as with neurological diseases like multiple sclerosis, viral infections, and neurodegenerative diseases, further suggesting the meninges are a unique immune niche within the CNS. This review provides an updated understanding of meningeal immunity, covering its roles in health and disease. A summary of key anatomical features of the meningeal compartment is first provided, followed by a detailed description of the immune cell subsets involved in the meninges at homeostasis, and emerging evidence about their spatial organization. We further discuss changes in meningeal immunity during various neurological conditions, concluding with research gaps and future directions.

2 Anatomy of the meninges and contribution to mobilization of immune cells

The meninges are composed of three structurally distinct layers: the dura mater, arachnoid mater and pia mater (Figure 1). Together, these layers were thought to exist to provide structural support to the brain; however, a growing body of evidence supports the idea that the meninges play critical roles in immune surveillance and homeostatic functions of the CNS.

The outermost layer of the meninges, the dura mater, is a dense, collagenous, and highly vascularized membrane. The dura mater is composed of the periosteal layer that lies adjacent to the skull, and the meningeal layer. The periosteal layer contains fibroblasts and osteoblasts which secrete copious amounts of collagen, providing the dura with strength (10). The two layers of the dura are mostly fused, but they separate to give way to large dural sinuses including the superior sagittal, transverse, and occipital sinuses that are essential to drain blood and cerebrospinal fluid (CSF) from the brain back into systemic circulation (1). Intracranial bridging veins that drain blood from the brain also empty into the dural venous sinuses (1) (Figure 1). The blood supply of the dura derives mainly from the meningeal arteries in both humans and mice, and the dural vasculature is connected to the skull bone marrow through bone encased vascular channels, referred to as osseous channels (6, 7, 11). The blood vessels in the dura are unique compared to the other vessels in the CNS, as they are fenestrated and lack tight junctions, permitting the movement of relatively large molecules from the blood into the dura mater (12). Furthermore, recent work has characterized an extensive *bona fide* dural lymphatic vessel network in the dorsal and basal part of the skull that drain CSF and meningeal immune cells into the deep cervical lymph nodes (dCLNs), and partly the superficial cervical lymph nodes (13–15). Dural lymphatic vessels, also referred to as meningeal lymphatic vessels (MLV), in mice are characterized by the expression of classical endothelial markers, including Prospero homeobox protein 1 (Prox1), lymphatic vessel endothelial hyaluronan receptor 1 (Lyve1), Podoplanin (gp38), and vascular endothelial growth factor receptor (VEGFR) (14, 15). Interestingly, dorsal and basal meningeal lymphatic vessels (MLVs) differ morphologically. Basal MLVs have blunt-ended capillaries and lymphatic valves–features that, along with their position near the underlying subarachnoid mater, make them better suited for CSF uptake and drainage than dorsal MLVs (14). Similar structures have been identified in humans through the use of magnetic resonance imaging (16). While a deeper characterization of drainage pathways from the meninges to the cervical lymph nodes in humans is still required, it appears that in contrast to mice, CSF drainage in humans occurs primarily through the dorsal MLVs near the dural sinuses (15–17). The efflux of CSF to the dura mater is not only important for the drainage of waste, but also for the presentation of brain-derived antigens to dural immune cells and communication with the adjacent skull bone marrow (4, 13–15, 18).

Beneath the dura mater lies the arachnoid mater, a thin fibrous membrane named for its spider web-like appearance (19). This membrane consists of layers of flattened epithelial cells bound by tight junctions and is separated from the underlying pia mater by the subarachnoid space (SAS) (20) (Figure 1). The SAS is filled with CSF that provides buoyancy and support to the brain by regulating cerebral blood flow and facilitating the drainage of waste (14, 21–23). CSF in the SAS can be drained to the cervical lymph nodes by meningeal lymphatics located in the dural layer or may enter the dural sinuses through arachnoid granulations (24). Fibroblast-like cells and collagenous projections produced by cells of the arachnoid mater called arachnoid trabeculae, anchor the arachnoid mater to the pia mater, allowing CSF to circulate within the SAS (25) (Figure 1). By using transgenic mice to delineate arachnoid barrier cells, microscopy techniques, and fluorescent tracers to track CSF movement, researchers recently demonstrated gaps in the arachnoid membrane around cerebral bridging veins. These gaps, termed arachnoid cuff exit (ACE) points, may enable the bulk movement of CSF and molecules directly between the dura and the SAS (26) (Figure 1).

The innermost meningeal layer, the pia mater, is a delicate membrane composed of endothelial and fibroblast-like cells that adheres tightly to the surface of the brain and spinal cord (1, 27). Arteries in the SAS extend through the pia mater, forming arterioles that can penetrate the brain parenchyma (28) (Figure 1). These blood vessels are surrounded by fluid-filled space, known as the perivascular space or Virchow-Robin space, acting as conduits of the glymphatic system which is postulated to facilitate exchange of CSF and brain interstitial fluid and enable waste clearance including at capillary level (27, 29, 30). The pia envelopes most of the blood vessels traversing through the SAS, and the lack of tight junctions within the pia mater allows for the movement of molecules and fluid between the pia, perivascular space and the SAS, enabling communication between all three compartments (29, 31). Astrocyte projections line the underside of the pial membrane, forming another CNS barrier known as the glial limitans (32) (Figure 1).

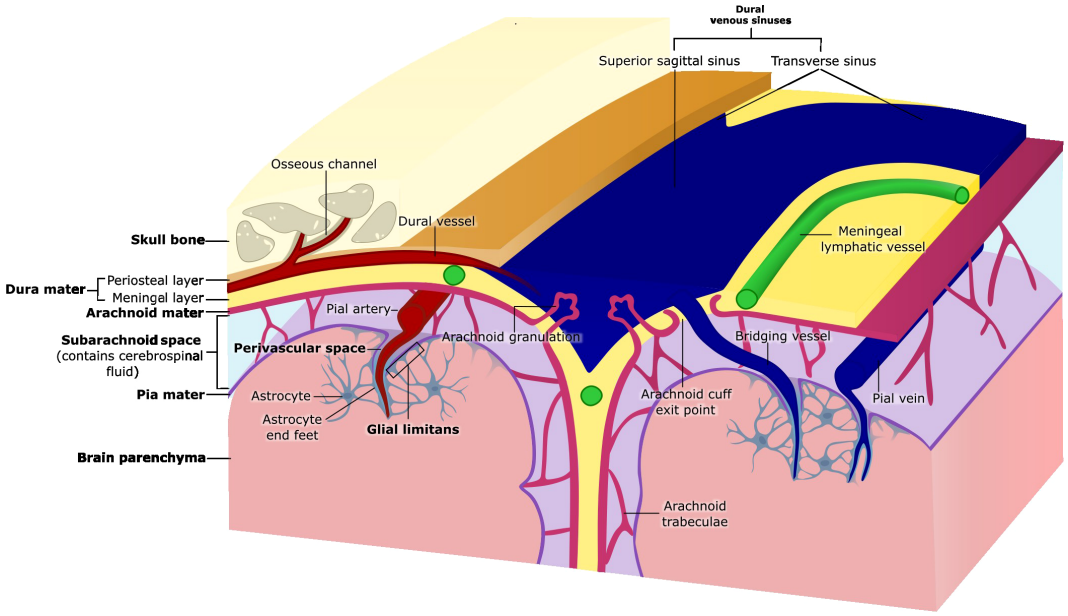

FIGURE 1
Anatomy of the meninges. The meninges are three membranous layers that cover the brain and spinal cord. The dura mater, the outermost layer, consists of a periosteal layer and a meningeal layer, which separate to form the dural venous sinuses (e.g., superior sagittal and transverse sinuses). Beneath the dura lies the arachnoid mater, a thin tissue layer which forms the arachnoid granulations that protrude into the dura mater, and arachnoid trabeculae that traverse the subarachnoid space and attach to the pia mater. The subarachnoid space contains cerebrospinal fluid (CSF) and is crossed by bridging vessels that supply the brain as well as drain blood from the brain into the dural venous sinuses. Arachnoid cuff exit points are openings that form where bridging vessels cross the arachnoid mater into the subarachnoid space. The pia mater, the innermost meningeal layer, adheres closely to the surface of the brain. The glial limitans is a thin layer of astrocytic end feet connected by tight junctions that lies directly beneath the pia mater. The perivascular space surrounding pial blood vessels is also lined by pia mater (coverage not shown), that then becomes continuous with the glial limitans as the vessels penetrate the brain parenchyma.

Similarly, these astrocytes end-feet wrap all parenchyma-permeating blood vessels. The function of this barrier is to further regulate the movement of molecules from the CSF into the CNS parenchyma (29, 32, 33). Together, the pia mater and the arachnoid mater form the leptomeninges, which are considerably thinner than the dura and cover the brain and spinal cord's surface (1, 34).

3 Immune composition of the meninges at steady-state

Due to its distinctive fenestrated vasculature and lymphatic system, the dura mater harbors a substantial population of immune cells within the meninges during homeostatic conditions (Figure 2A). In wild-type young adult mice at steady-state, dural CD45+ immune cells isolated by mechanical dissociation consist of neutrophils (43.7%), B cells (26.3%), T cells (3.2% double negative, 2.8% $CD8^+$, and 1.7% $CD4^+$), monocytes (2.5% $Ly6C^+$, 1.2% $Ly6C^-$), natural killer cells (1.6%), macrophages (1.3%), mast cells (1.1%), plasmacytoid dendritic cells (pDCs) (1%), classical dendritic cells (cDCs) (0.9%), type 2 innate lymphoid cells (ILC2) (0.4%), and plasma cells (0.3%) (7) (Figure 2A). It is important to highlight that enzymatic tissue dissociation of the dura has been associated with small differences in the immune cell composition, including an increased frequency of neutrophils, mast cells, and DCs (35). Meningeal immune cells are distributed throughout the meningeal layers, with a notable tendency to localize around the dural venous sinuses under steady-state conditions (4, 5, 7, 9, 35). Recent research has demonstrated that some immune cells form organized clusters along the dural sinuses, known as dural-associated lymphoid tissues (DALT) (4, 5, 9) (Figure 2B). In contrast to the dura, the leptomeninges feature tight junctions and low expression of adherence molecules under homeostasis to tightly regulate leukocyte trafficking (1, 34). The leptomeninges hosts unique macrophage and dendritic cell (DC) subsets, as well as a few lymphoid cells, but considerably less B cells than the dura (36, 37) (Figure 2A). While leptomeninges are implicated in neurological diseases such as meningitis and MS, their role in meningeal immunity under homeostatic conditions remains poorly understood (38, 39). Below we highlight what is known in the literature about the most prominent adaptive and innate immune cells in the meningeal compartment under steady-state conditions, and our understanding of the spatial organization of select meningeal lymphocyte populations.

3.1 T cells

While T cells are mostly absent from the brain parenchyma, they are readily detected in the murine meninges during steady state (4). Whole-mount immunohistochemistry and two-photon imaging in a live mouse revealed that T cells are not evenly distributed throughout the dural tissue but are highly localized to

10.3389/fimmu.2025.1531068

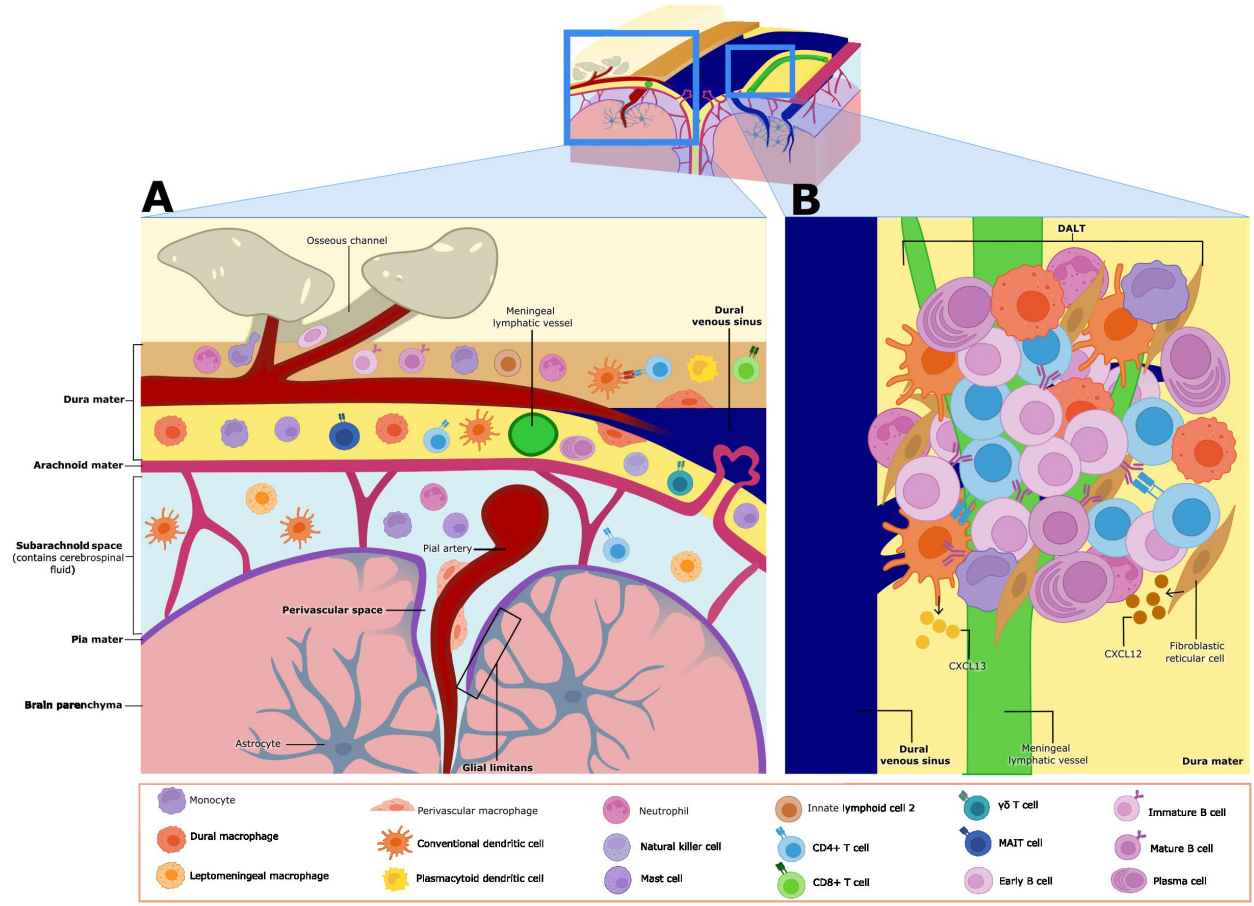

FIGURE 2
Meningeal immune cell niche at homeostasis. **(A)** The meninges contain various subsets of immune cells during homeostasis. γδ, CD8, CD4, and MAIT T cells are found in the dura mater and the leptomeninges (made up of the arachnoid membrane, subarachnoid space, and the pia mater–leptomeningeal cells are shown only in the subarachnoid space in this figure). Monocytes, conventional dendritic cells (cDCs), natural killer (NK) cells and type 2 innate lymphoid cells (ILC2s) are also found in both the dura mater and leptomeninges. Neutrophils, plasma cells, plasmacytoid dendritic cells (pDCs), and dural macrophages (dmMφ) have only been described in the dura mater. Leptomeningeal macrophages (mMφ) and perivascular macrophages are found in leptomeninges and the perivascular Virchow-Robin space respectively. Mature B cells are found in both regions, but immature and early B cells have only been described in the dura mater. Meningeal cells play key roles in immune surveillance and some subsets influence brain function and behavior through cytokine secretion. **(B)** Closer view of dural-associated lymphoid tissue (DALT). DALTs are immune cell aggregates found along the dural venous sinuses, and they contain activated B cells and plasma cells. DALTs also contain other immune subsets, such as conventional dendritic cells (cDCs), monocytes, neutrophils, and $CD4^+$ T cells. Stromal cells like fibroblastic reticular cells and follicular dendritic cells, provide structural support to DALT, as well as release chemoattractants such as CXCL13 and potentially CXCL12, which may contribute to the formation, activation and expansion of these structures. DALTs are strategically positioned around the dural venous sinuses and ACE points, likely to mount rapid and robust immune responses against pathogens.

regions around the dural sinuses (4). Parabiotic studies have indicated that $CD4^+$ and $CD8^+$ T cells are continuously replaced in the homeostatic dural meninges from peripheral blood (4, 40). There was preferential infiltration of circulating T cells from the dural sinuses, and to a lesser extent along cerebral veins projecting into the sinus (4). Endothelial cells forming the dural sinus vasculature expressed lower amounts of tight junction proteins and high amounts of integrins which favored T cell adherence and extravasation (4). The dural stromal composition—including endothelial cells, mural cells, fibroblast-like cells, and stroma-derived chemokines—further promoted homeostatic T cell recruitment and retention (4). For example, *Cxcl12* and *Cxcl16* were highly expressed in the meninges and involved in the recruitment of circulating CXCR4 and CXCR6-expressing leukocytes (4). Following resection of the dCLNs, wild-type mice had substantially greater accumulation of $CD4^+$ T cells in the meninges, suggesting that draining lymph nodes represent a critical exit point for these cells (40). Dural $CD4^+$ T cells are polarized towards Th1, Th2, Th17 and regulatory T (T_{reg}) cell subsets, which suggests that a balance between pro- and anti-inflammatory subsets exists at homeostasis (Table 1) (4).

Several subsets of meningeal T cells have been shown to play critical roles in cognitive function and neurogenic development, likely representing an evolutionary link between the nervous and immune systems. The Morris Water Maze (MWM) test is widely used in neuroscience research to evaluate spatial learning and memory in mice. In wild-type mice, the performance of the MWM test led to the accumulation of meningeal interleukin (IL)-4-producing $CD4^+$ T cells (2). Pharmacological depletion of meningeal T cells or using IL-4 deficient mice resulted in learning

TABLE 1 Key immune cell subsets in the meninges of central nervous system during homeostasis.

Immune Cell subset	Location	Origin	Role	References
T cells (CD4, CD8, MAIT cell, γδ T cell)	Dura (4-7.7%) Leptomeninges (3%)	Peripheral circulation	Cognition and behavior Immune surveillance	(33–39) (4, 51, 171)
B cells and plasma cells	Dura (7-27%) Leptomeninges (1%)	Skull bone marrow Peripheral circulation	Immune surveillance and dural-associated lymphoid tissue structure Regulate stress-like behavior	(5, 7, 8, 51, 52) (45)
Leptomeningeal Macrophages (mMφ)	Leptomeninges	Embryonic Yolk Sac (development) Self-Renewal (adulthood)	Immune surveillance Monitoring and filtering the CSF	(46) (68)
Dural Macrophages (dmMφ)	Dura	Embryonic Yolk Sac (development) Blood Monocytes (adulthood)	Immune surveillance	(46)
Perivascular Macrophages (pvMφ)	Virchow–Robin Spaces	Postnatal seeding by mMφ (development) Self-Renewal (adulthood)	Immune surveillance Monitoring and filtering the CSF Regulate endothelial permeability? Regulation of systemic immunity Regulation of lipid and glucose metabolism within the CNS	(46) (68–71) (72, 73) (74–76) (77, 78)
Dendritic Cells (DCs)	Dura (1.9-19%) Leptomeninges (2.6%)	Skull bone marrow Peripheral circulation	Antigen presentation to T cells	(4, 7, 51, 78)
Neutrophils	Dura (12-43.7%)	Skull bone marrow Peripheral circulation	Immune surveillance Production of ROS, enzymes and chemoattractants	(6, 7, 51, 78) (81)
Mast Cells	Dura (1.1-2%)	Skull bone marrow Peripheral circulation	Cognition and glial cell function	(7, 51, 84, 85)
Innate lymphoid cells (ILCs)	Dura (0.4%)	Skull bone marrow Peripheral circulation	Motor and psychiatric function	(7, 86, 87)
Natural Killer Cells (NKs)	Dura (1.6-4%) Leptomeninges (1%)	Skull bone marrow Peripheral circulation	IFNγ expression to astrocytes	(7, 51, 86, 93, 94)

deficits that could be reversed with intraperitoneal injection of wild-type, but not IL-4-deficient, $CD4^+$ T cells (2). Meningeal T cell release of IL-4 may support learning by promoting hippocampal brain-derived neurotrophic factor (BDNF) release and neurogenesis (41). Specifically, this effect may be mediated by astrocytes which border the meninges and can respond to meningeal cytokine release. Indeed, IL-4-treated astrocytes *in vitro* produced more BDNF and hippocampi from mice tested using memory and cognition tasks had increased BDNF mRNA, which was absent in IL-4-deficient mice (2, 41). However, the direct application of IL-4 inhibited adult hippocampal neural stem cell proliferation *in vitro* (42). Work by Radjavi A et al. suggested that T cell antigen specificity may be required to support learning and cognition (40). Mice with a limited $CD4^+$ T cell repertoire restricted to reactivity against chicken egg ovalbumin antigen (OTII mice) had impaired hippocampal neurogenesis and memory despite elevated CNS IL-4 levels (42, 43). However, the transfer of T cells reactive to a common CNS antigen into OTII mice improved performance in the MWM test (43). In support, resection of the dCLNs, which likely limited brain-derived antigen sampling, impaired learning and memory function in wild-type mice subjected to the MWM test despite a greater accumulation of $CD4^+$ T cells in the meninges (40). Together, these studies indicate that homeostatic levels of $CD4^+$ T cell cytokines, including IL-4, that is lost in mice with limited T cell repertoires may be required to support hippocampal-based memory and learning functions. While $CD4^+$ T cells directed against CNS-derived self-antigen may be sufficient to rescue MWM task performance at least in animals with clonally restricted T cell repertoires, this does not preclude the requirement of other antigenic specificities of $CD4^+$ T cell populations, and the nuances of T cell specificity to support cognitive functions remains largely unknown (40).

Furthermore, interferon-gamma (IFN-γ) production by meningeal T cells has been linked to regulating social behavior in mice (44). There is a high frequency of T cells in the healthy meninges that produce IFN-γ. Infiltrating meningeal T cells may use the integrin VLA-4 to cross vasculature and enter the meningeal space (44). The administration of anti-VLA-4 antibody partially depleted meningeal T cells during steady-state, and this was sufficient to impair social behavior in mice measured using the three-chamber sociability test. Mice that were IFN-γ- deficient ($IFN\text{-}\gamma^{-/-}$) exhibited similar social deficits, further highlighting that T cell-derived IFN-γ supports social behavior (44). Social interactions are required for the survival of a species, but they also increase the likelihood of pathogen transmission. Therefore, it is plausible that this aspect of pathogen defense in the meninges, mediated by IFN-γ, may have coevolved with social behavior to provide mutual benefits (44).

Additionally, IL-17a-secreting meningeal γδ (γδ17) T cells, have been implicated in controlling short-term memory and anxiety-like behavior during steady-state in mice (45, 46). Located along the dural sinuses, γδ17 T cells are reported to produce about 90% of IL-

17a that is found within the meninges during steady-state conditions (46). These cells originate in the fetal-thymus and populate the meninges shortly after birth in a CXCR6-dependent manner (45, 46). Notably, these cells are self-renewing and not replenished by contributions from the periphery (46). The production of IL-17a by meningeal γδ17 T cells was first implicated in the promotion of short-term memory through increasing glutamatergic synaptic plasticity of the hippocampal neurons (45). Short-term memory, as assessed by the Y maze, was impaired in full-body IL-17a or γδ-deficient mice, bone marrow chimeras mostly devoid of meningeal γδ17 T cells, as well as when meningeal IL-17a was blocked with an antibody administered into the CSF (45). This effect was linked to IL-17a-driven BDNF production by glial cells that enhanced hippocampal neuronal synaptic plasticity to support short-term memory (45). Shortly after, another study demonstrated that the administration of anti-T cell receptor γδ antibodies into the CSF to deplete γδ17 meningeal cells improved performance in the elevated plus maze and open field tests, which was interpreted as reduced anxiety behavior, but did not alter memory function (46). The IL-17a receptor is expressed in cortical glutamatergic neurons, and accordingly its deletion increased anxiety-like behavior in mice (46). Notably, researchers were not able to replicate the previous finding of γδ17 T cell function in short-term memory function, and owing to the limitations in specific ablation of meningeal γδ17 T cells, the exact role of these cells in CNS homeostasis remains unclear. Overall, given the fact that IL-17a has been highly conserved throughout the evolution of the vertebrate immune system and plays key roles in host defense at barrier sites, IL-17a expression by meningeal γδ17 T cells may represent an evolutionary link that serves to protect at barrier sites against pathogens, but also increase the alertness of an animal in new environments conferring survival benefits (46).

While studies have demonstrated a role for meningeal T cell-derived cytokines such as IL-4, IFN-γ, and IL-17 at influencing behavior and cognition, it is currently unclear how these cytokines traverse the meningeal layers and reach the brain. Cytokines in the CSF may reach the brain parenchyma through the glymphatic system along perivascular channels, where they influence neurons through direct receptor signaling (47, 48). Alternatively, in an indirect route, glial cells may first detect the cytokines within the CSF and then release other cytokines, which subsequently impact neuronal activity (2, 42, 48).

3.2 B cells

Although B cells comprise a substantial proportion of dural immune cells at steady-state, B cell origin and diversity in the meninges during homeostasis has been explored less extensively than T cells and myeloid cells (7, 37, 49, 50). During steady state in young adult wild-type mice, most meningeal B cells are located within the dura, particularly in the extravascular compartment around blood and lymphatic vessels adjacent to the dural venous sinuses (7, 37, 50). Similarly, within post-mortem human meningeal samples from individuals without inflammatory disease, B cells were often found in the perivascular areas near dural sinuses (7). The dural B cell population in mice is predominantly comprised of the B2 subtype, displaying heterogeneity comparable to that observed in the skull bone marrow but distinct from circulating blood (7, 50). This diverse population included early B cells ($IgD^{-}CD21^{-}CD23^{-}IgM^{lo}CD24^{+}CD43^{+}IL7R^{+}CD93^{+}$), immature B cells ($IgD^{lo}CD22^{lo}CD21^{lo}CD23^{lo}CD24^{+}$), and mature B cells ($MHC\text{-}II^{+}IgM^{+}IgD^{+}$) (7). This pattern reflected the calvarial origin of meningeal B cells and migration into the dura through osseous channels in the skull bone independent of systemic circulation (7, 37, 50). Many early dural B cells expressed the chemokine receptor *Cxcr4*, and dural fibroblast-like cells had a high expression of its ligand *Cxcl12* (7). Although it remains to be functionally validated, the CXCR4-CXCL12 axis may represent the migratory axis implicated in calvaria-derived B cell homing to the meninges (7). Moreover, dural B cells showed slow turnover and long-term tissue residency, with the dural lymphatic system offering opportunity for exit from the CNS (7, 37, 50). A similar trajectory of developing B cells was identified in a non-human primate, suggesting evolutionary conservation in meningeal B cell development (50). Using a fluorescent reporter system of B cell activation by self-antigens, researchers demonstrated that transitional and mature meningeal B cells have functional B cell receptors (BCRs) (7). Furthermore, transgenic mice with B cells reactive against a myelin oligodendrocyte glycoprotein, a common CNS-epitope, were significantly reduced in the dura compared to other lymphoid and peripheral tissue (7, 50). Collectively, these results suggest that early B cells, supplied by the calvaria, complete their maturation in the dura which provides a local source of CNS epitopes for negative selection. Interestingly, parabiosis studies revealed that unlike early developing B cells, mature dural B cells are capable of exchanging with blood (50). This suggests that the meninges may serve as an additional site of negative selection against peripherally derived B cells that escaped negative selection (Table 1) (50).

Meningeal B cells have indirectly been implicated in regulating anxiety-like behavior through myeloid cell activation (51). Chronically stressed mice exhibited a marked decrease in B cells in both the dura and the leptomeninges, but an increase in meningeal myeloid cells (Table 1) (51). The transcriptional program of meningeal B cells changed significantly during stressed conditions, with the induction of innate immune transcriptional programs and antimicrobial production genes that likely enable communication with meningeal myeloid cells (51). However, the exact mechanism underlying why meningeal B cells decrease during stress, and their functional impacts on myeloid cell activation within the meninges is yet to be elucidated (51).

During homeostasis, both mouse and human meninges have also been found to contain immunoglobulin-A (IgA^{+}) plasma cells, which are terminally differentiated B cells that secrete large amounts of antibodies (5, 37). Sequencing of the B cell receptor (BCR sequencing) revealed that a large portion of these meningeal IgA^{+} cells originated in the intestines. Accordingly, IgA^{+} plasma cells were scarce in the meninges of germ-free mice, but their numbers were restored following gut microbiome re-colonization (5). Interestingly, the composition of the microbiome influenced the repopulation dynamics, with microbiomes derived from two

different healthy human donors or a wild-type mouse leading to differences in both plasma cell numbers and the antibody isotype they secreted (5). These results suggest that the composition and variation of the intestinal microbiome can strongly affect the phenotype of meningeal plasma cells during steady-state conditions (5). Given the substantial person-to-person variability in intestinal microbiome profiles, further research in this area will be required to understand how these differences shape the meningeal plasma cell compartment and its functional role in immune surveillance.

3.3 Border associated macrophages

The meninges contain distinct populations of tissue-resident macrophages, collectively known as CNS-associated macrophages (CAMs), also referred to as meningeal or border-associated macrophages (52, 53). The distinct characteristics of each meningeal layer create unique niches that shape resident myeloid populations, influencing their transcriptional profiles and creating distinct populations of CAMs within the meninges. Furthermore, regions such as the perivascular space and choroid plexus also contain populations of resident macrophages. The most well-characterized CAMs include leptomeningeal macrophages (mMφ), dural macrophages (dmMφ), perivascular macrophages (pvMφ), and choroid plexus macrophages (cpMφ) (35, 36, 54–58). Additional heterogeneity exists within these populations; for example, cpMφ comprise of distinct stromal cpMφ and epiplexus Kolmer cells (cpepiMφ), while dmMφ and stromal cpMφ CAMs further divide into major histocompatibility complex class II (MHC-II)^{low} and MHC-II^{high} subsets (35, 36, 55).

Tissue-resident macrophages exhibit ontogenetic distinction, originating from either embryonic source, such as the yolk sac and fetal liver, or from circulating bone marrow-derived monocytes during postnatal development (59–65). Fate mapping of embryonically derived macrophages using a tamoxifen-inducible *Cx3cr1*^{CreERT2} model showed that CAMs originate from erythro-myeloid progenitors (EMPs) of the fetal yolk sac, with no contribution of definitive hematopoiesis during development (56, 57, 66, 67). By embryonic day 10.5 (E10.5), the CNS is colonized by progenitor macrophages that give rise to CAMs and microglia (57, 58). Originally, it was believed that CD206^{+} progenitors gave rise to macrophages and CD206^{-} to microglia, but a recent study has shown that CD206^{+} progenitors can give rise to both cell types (57, 58). Embryonic studies in mice show that by E12.5, meningeal CAMs are present, however pvMφ are only seen at post-natal day 10 (P10), suggesting a postnatal origin for pvMφ. After the development of the perivascular space postnatally, it is seeded by mMφ, which then diverge into pvMφ as the niche matures (57, 58). During adulthood, CAM subsets exhibit heterogeneity in terms of their method of replenishment (35, 56). mMφ, pvMφ, and cp^{epi}Mφ exhibit long-term self-renewal with non-significant seeding from blood monocytes (35, 56). On the other hand, dmMφ and stromal cpMφ are largely replenished by blood monocytes (Table 1) (49, 51, 56). This suggests that CAMs in permeable brain regions like the dura and choroid plexus stroma undergo replenishment by bone marrow monocytes, while deeper regions rely on long term self-renewal.

Much like microglia, the development of CAMs is dependent on the transcription factors *Pu.1* (SFPI) and *Irf8* but independent of *Myb* (35, 56, 62). Knocking out *Pu.1* leads to a lack of pvMφ, mMφ, and cpMφ, due to a reduction in yolk sac progenitor cells from which CAMs arise. *Irf8* is demonstrated to be a master regulator of CAMs and critical for the divergence of microglia and CAMs (56, 57, 62, 68). In *Irf8* deficient mice, there is a reduction in the number of mMφ at E14.5 (56). Postnatally, *Irf8* is required for expansion of mMφ and pvMφ (58). While the numbers of stromal cpMφ were originally shown to be unaltered in *Irf8*-deficient mice, further studies using macrophage specific *Irf8* deletion showed altered composition of the transcriptional profile of stromal cpMφ without *Irf8*, keeping them in the MHC-II^{low} state and failing to transition into mature MHC-II^{high} cpMφ (35, 56). TGF-βR signaling is dispensable for CAMs but not for microglia development (57, 69). Similarly, transcription factors such as *Batf3* and *Nr4a1* are not required for CAM development (56). As mentioned earlier, pvMφ are derived postnatally at the same time as the perivascular space develops. pvMφ reside within the Virchow–Robin space, where vascular smooth muscle cells (VSMCs) are found (58). VSMCs depend on *Notch3* for development and homeostasis, and in mice lacking *Notch3*, there is a strong reduction in pvMφ. Other CAM subsets are unaffected in *Notch3* knockouts (58). pvMφ also exhibit the need for integrin signaling via *Tln1* and depend on *c-Maf*, a transcriptional factor key for vascular macrophages (58).

CAMs were initially thought to be distinguishable from microglia by their high CD45 expression, whereas microglia are characterized by intermediate CD45 levels (69, 70). However, the discovery of CAM subsets with low CD45 expression in mice highlighted the need for more specific CAM markers (55). Subsequent studies identified CD206, CD36, and Lyve1 as markers specific to CAMs within the CNS (54–56). MHC-II and CD38 are also markers used to identify CAMs while CCR2 helps distinguish dmMφ and stromal cpMφ, as these subsets are replenished by blood monocytes (35, 55, 56). At steady state, CAMs can be identified by a core gene signature consisting of CD206, platelet factor 4 (Pf4), carbonyl reductase 2 (Cbr2), Ms4a7 and Stab1 (36). Additional studies have added Apoe, Ms4a6c, Lyz2 and Tgfbi as universal CAM gene signatures (35). This raises two points of interest: 1) MHC-II^{low} and MHC-II^{high} CAMs are distinct transcriptionally, and 2) cp^{epi}Mφ do not exhibit the universal CAM gene signature, rather being more akin to microglial signatures (35). CAMs can also be further distinguished by their lack of α4-integrin and CD44 expression, markers of peripheral monocytes and immune cells respectively (36, 55, 71, 72).

Although significant research has focused on the ontogeny and identity of CAMs, their physiological roles remain poorly understood due to high variability. Positioned at the borders of the CNS, mMφ, dmMφ, and pvMφ contribute to barrier functions and assist in the surveillance and filtering of antigens and metabolic products within the CSF (52, 53). Through receptors like CD206 and the scavenger receptor CD163, pvMφ can uptake exogenous dyes introduced into the CSF, demonstrating their capacity to

scavenge and filter this fluid (Table 1) (73–75). Recently, CAMs were also shown to be able to uptake peripheral compounds, with MHC-II$^+$ CAMs displaying a greater ability to do so (76). In peripheral tissues, vascular macrophages are known to regulate endothelial permeability, suggesting that pvMφ may play a similar role in regulating the BBB (77, 78).

pvMφ also exhibit roles in the regulation of systemic immune responses (79–81). When stimulated by systemic IL-1 and lipopolysaccharide, pvMφ secrete prostaglandin E2, which activates the hypothalamic-pituitary-adrenal axis, ultimately leading to glucocorticoid production and suppression of immune responses (79). The response of pvMφ to systemic IL-1 requires the expression of IL-1 receptors on endothelial cells, indicating a close relationship between these cell types (80, 81). Interestingly, the ablation of CAMs in mice showed that pvMφ can exert direct anti-inflammatory effects on endothelial cells (79).

Using high-fat diet conditions in mice, pvMφ have been shown to induce GLUT1 expression in CNS endothelial cells via the secretion of vascular endothelial growth factor (VEGF) (82). Under similar conditions, pvMφ have been found to contain lipid particles. pvMφ in adipose tissue have been shown to play a crucial role in the regulation of metabolic syndrome, further supporting the notion that pvMφ can play an important role in lipid and glucose metabolism/circulation within the CNS (83).

Future research should focus on CAM ontogeny, plasticity and functionality. This includes investigating the timing, signaling cues, and unique environmental niches that support targeted localization of CAM subsets across meningeal regions. Another important direction is to explore the potential for movement of CAMs between different meningeal regions and if they can assume location specific functions. If CAMs can indeed relocate and take on distinct functions, it would suggest a remarkable functional plasticity and diversity among subsets. Uncovering the precise functional roles of CAMs remains essential, as their contributions to immune surveillance, homeostasis, and responses to injury or disease are not yet fully understood. Research into the transcriptional and molecular diversity within CAM subsets could reveal whether there is redundancy in function or whether these cells are specialized based on their meningeal location, ultimately clarifying the roles CAMs play in maintaining CNS health and responding to pathology.

3.4 Dendritic cells

Dendritic cells, characterized as Flt3$^+$ and Fcgr1$^-$ make up approximately 19% of immune cells found in the healthy dura mater after enzymatic dissociation of the tissue and include conventional type 1 (cDC1) and type 2 (cDC2) subsets, as well as migratory DCs (migDCs), and plasmacytoid DCs (pDCs) expressing Siglech, Ccr9, and Pacsin1 genes (35). Monocyte-dendritic cell progenitors (MDPs) were identified in the skull bone marrow by flow cytometry, indicating local seeding of this antigen-presenting cell (APC) niche by adjacent CNS compartments (Table 1) (8). DCs in the meninges are responsible for capturing antigens in proximity to the dural sinuses and presenting them to patrolling T cells (4). Dural sinus-associated conventional type 2 DCs (cDC2s) were found to predominantly take up intra-cisterna magna-administered OVA antigen over the intravenous route, indicating their selective presentation of CNS/CSF-derived antigens (4). Indeed, cDC2s were also found to take up CSF-derived antigens including amyloid-beta (Aβ) peptides, Aβ1-40 and Aβ1-42 (4).

3.5 Neutrophils

As for the innate immune system, neutrophils expressing Ly6g, Ngp, Camp, and S100a9 genes, make up approximately 12% of immune cells found in the healthy dura mater after enzymatic tissue dissociation (35). By using spectrally resolved *in vivo* cell labeling in the murine skull, recent literature has evidenced that dural neutrophils are mainly being supplied by the skull bone marrow and not from the periphery after injury (6). Since their discovery in the dura mater and leptomeninges, neutrophils have been identified as key players in brain diseases including ischemic stroke, Alzheimer's disease (AD) and MS (84, 85). In both the Middle Cerebral Artery Occlusion stroke mouse model and human post-mortem tissue from patients with ischemic stroke, neutrophils were found in the leptomeninges surrounding the infarcted region of the brain (85). Through their production of reactive oxygen species (ROS), proteases, peptidases like MMP-9 that disrupt the BBB, and cytokines that attract other immune cells, these meningeal neutrophils may have a significant influence on the immune landscape in stroke (Table 1) (86).

3.6 Mast cells

Regarding meningeal mast cells, this population of innate immune cells makes up approximately 2% of immune cells found in the healthy dura mater of mice after enzymatic tissue dissociation (35). Meningeal mast cells have been found to disrupt CNS vascular integrity which is linked to neutrophil recruitment in neuroinflammation (Table 1) (87). These cells were further found to influence stroke pathology, as mast cell deficient Kit$^{W/Wv}$ mice had smaller infarcts and reduced brain swelling compared to wild-type controls after stroke (88). However, the role of mast cells in the CNS borders has been more substantially explored in the pathophysiology of migraine. Mast cell degranulation has been found to induce nociception in a calcitonin gene-related peptide (CGRP)-dependent manner (89). Interestingly, there has been recent evidence suggesting that endogenous acetylcholine contributes to migraine pathology mainly through activation of meningeal mast cells (89). Studies in the 5xFAD model of AD pathology have also found routes of communication between the brain and meningeal compartments in the context of mast cells, describing their ability to scan CSF contents for brain antigens and initiate the expression of genes for immune-related effector proteins (90). This may have functional consequences for brain immunity, as an increase in the frequency of disease-associated microglia (DAM) clusters has been described in mast cell-deficient 5xFAD mice (90). However, the exact nature of communication between meningeal mast cells and brain-resident microglia is not yet fully understood.

3.7 Innate lymphoid cells and natural killer cells

Innate lymphoid cells (ILCs) and natural killer (NK) cells have also been identified as key players in meningeal immunity (91). From all subsets of ILCs, ILC2s are the predominant subtype in the meninges and localize primarily around the dural venous sinuses (91). Meningeal ILC2s were found to become activated in an IL-33-dependent manner in response to spinal cord injury (SCI) and traumatic brain injury (TBI) (Table 1) (91, 92). Nevertheless, their functional implications in disease have not been clearly assessed. However, a beneficial effect on recovery after SCI was indeed observed after addition of wild-type lung-derived ILC2s into the meningeal space (91). In TBI, activation of the metabolic regulator AMP-activated protein kinase (AMPK) led to an increase in IL-13- and IL-5-producing ILC2s, as well as an increase in a distinct IL-10-producing subset of ILC2s in the meninges (92). AMPK-regulated expansion of meningeal ILC2s after TBI was further associated with suppression of pro-inflammatory ILC1 and ILC3 subsets and improvements in motor and psychiatric function in mice (92). ILC2s in the meninges were also found to moderately increase in aging, with a more substantial increase observed in the choroid plexus, and intracerebroventricular transfer of activated ILC2s was associated with enhanced cognitive function of aged mice (93). However, ILC subsets were found to have a contrasting role in the HSV-IL-2 model of MS, as mice lacking ILC2, but not ILC1s or ILC3s, were protected from CNS demyelination (94). This research has come to light despite reports of meningeal ILC1 and ILC3 subsets supporting pro-inflammatory processes in the CNS, indicating the need for closer functional analyses of ILC subsets in the meninges to better understand their complex roles in neuroinflammatory conditions (95–97).

NK cells, a subset of ILC1s, are found to make up approximately 4% of immune cells found in the healthy dura mater after enzymatic tissue dissociation and showed expression of Klrb1c, Ncr1, Eomes and Gzma genes (Table 1) (35). Resident NK cells and ILC1s in the meningeal dura have been found to regulate the behavior of adult mice through IFN-γ production (98). Additionally, the production of IFN-γ by meningeal NK cells in a gut microbiome-dependent manner limited CNS inflammation through supporting $LAMP1^{+}TRAIL^{+}$ astrocyte induction of T cell apoptosis (99). However, the exact physiological functions of NK cells in the CNS meninges, and how their production of IFN-γ is involved in mediating these functions is poorly understood.

4 Spatial organization of immune cells in the dura mater

Although meningeal immune cells are distributed diffusely across the three meningeal layers, several clusters of immune cells have been observed to localize along the dural venous sinuses during steady-state conditions revealing a previously unappreciated level of immune organization in the meninges (4, 5). Comprehensive imaging and single-cell RNA sequencing (RNA-Seq) studies of the dura in naive mice have recently expanded our understanding of the composition and function of these immune clusters, termed the DALT (9) (Figure 2B). The largest immune aggregate identified was located in the rostral-rhinal confluence of the sinuses (9). The rostral-rhinal hub contained various immune cells, including $CD11c^{+}$ myeloid cells, T follicular helper cells, T follicular regulatory cells, various B cell subsets (developing, naive, and germinal center), fibroblastic reticular cells, and a complex network of lymphatic vessels and fenestrated vessels (9). Stromal cells within the hub were a source of B and T cell chemoattractant CXCL13. It is plausible other chemokines like CXCL12 are secreted by the stromal cells within DALT, given its key role in lymphocyte migration to the meninges (4, 7). Other cells found in the meninges such as neutrophils, ILC2, monocytes, and macrophages were part of the hub, as well (9) (Figure 2B, Table 1). Additionally, it was shown that naive B cells could be recruited to the DALT structure from peripheral circulation, but once they were locally activated by T cell interactions within the DALT, a germinal center response could be maintained as evidenced by class-switching and plasma cell differentiation, without further input from circulating immune cells (9) (Figure 2B). It is unclear as of yet whether DALT structures can support negative selection of B cells that was previously reported to occur within the dura (7, 50). Similar lymphoid aggregates containing B and T cells have been observed in human dural samples near the base of skull, just above the cribriform plate (9).

The mechanisms governing DALT formation and lymphocyte recirculation within the DALT are yet to be elucidated, as well as the relationship between DALT and responses to aging and different neurological conditions (9). Under homeostatic conditions, these neuroimmune hubs likely serve as regions of immune surveillance. Indeed, with infection and challenge they are seen to grow and respond, as will be discussed later. This lymphoid structure was present in early post-natal animals but expanded in number with age (9). Interestingly, the meninges have been recently identified to play a critical role in promoting CNS tolerance through the expression of CNS-derived autoantigens on APCs, mainly $CD11b^{+}$ $CD11c^{-}$ macrophages (Table 1) (18). Particularly, the meninges are enriched in their expression of various myelin-basic protein-derived peptides, including peptides which maintain regulatory populations of T cells in the CNS under homeostatic conditions (Table 1) (18). It is unknown if there is a link between DALT structures and tolerance induction in the dura, but plausible as APCs are present within the DALT and dural sinuses are enriched in brain-derived antigen carried in through CSF influx (4, 9).

5 Meningeal immunity in disease

5.1 Multiple sclerosis

Multiple sclerosis (MS) is a chronic demyelinating CNS disorder that affects over 2.5 million individuals worldwide (100). MS is characterized by the accumulation of myelin autoreactive immune cells and subsequent damage of the myelin, impairing motor and cognitive function. The etiology of the disease remains unknown but is thought to result from a complex interplay of genetic and environmental risk factors (100). Current treatments

consist mainly of disease-modifying therapies to control inflammation. Although most of the tissue damage is found within the parenchyma, several studies in humans and animal models have implicated meningeal inflammation playing a critical role in MS pathology (39, 100, 101).

Studies in the widely used experimental autoimmune encephalomyelitis (EAE) animal model of MS-like pathology offer more insight into the role of meningeal inflammation in MS development and progression. EAE can be induced by adoptive transfer of autoreactive T cells (passive EAE) or immunization with myelin antigens (active EAE). After active EAE in SJL mice, meningeal inflammation precedes widespread CNS inflammation, and is characterized by the accumulation of neutrophils, DCs, macrophages, and T cells (102, 103) (Figure 3). Similarly, autoreactive T cells are detected in the meninges in early stages of passive EAE (104, 105). Recent findings have highlighted differential contributions of the meningeal layers in cell infiltration during autoimmunity. In both passive and active models of EAE in mice and rats, as well as human post-mortem MS tissue, myeloid and T cell infiltration occurred predominantly in the leptomeninges of the spinal cord and brain compared to the dura (104) (Figure 3). The meninges undergo extracellular matrix remodeling and dural and arachnoid fibroblasts show an enrichment of immune functions which promote the migration and retention of immune cells (26). However, transcriptomic analysis suggests that dural vasculature expresses relatively lower levels of adhesion factors which may reduce endothelial cell interactions between effector T cells, as compared to the leptomeninges (104). Furthermore, there is a downregulation of SEMA3A in the leptomeninges, which may further support trafficking of neutrophils, T cells and myeloid cells at ACE points (26) (Figure 2A). Imaging of the spinal cord during passive EAE has shown that incoming effector T cells from the periphery crawl and traverse the leptomeningeal vessels in an integrin-dependent manner, appearing in the SAS just one day after adoptive transfer (106–108). The accumulation of encephalitogenic T cells in the leptomeninges is promoted by chemokine signaling through the CXCR3-CCR5 axis and contact with leptomeningeal macrophages through integrin receptors and antigenic stimulation (107). Together, these results demonstrate that the meninges are a critical checkpoint for leukocyte and autoreactive T cell entry into the CNS during neuroinflammation. Effector T cells within the dura and leptomeninges must be reactivated by APCs presenting self-cognate antigen, including macrophages and DCs, before they can invade the CNS parenchyma (36, 37, 109–111) (Figure 3). As with cell recruitment, effector T cell reactivation varies across meningeal layers. In a rat model of EAE, leptomeningeal APCs were capable of spontaneously reactivating effector T cells, while dural APCs could present antigen to T cells but required additional autoantigen supplementation to fully stimulate them (104). In a model of passive EAE, single-cell RNA-Seq of

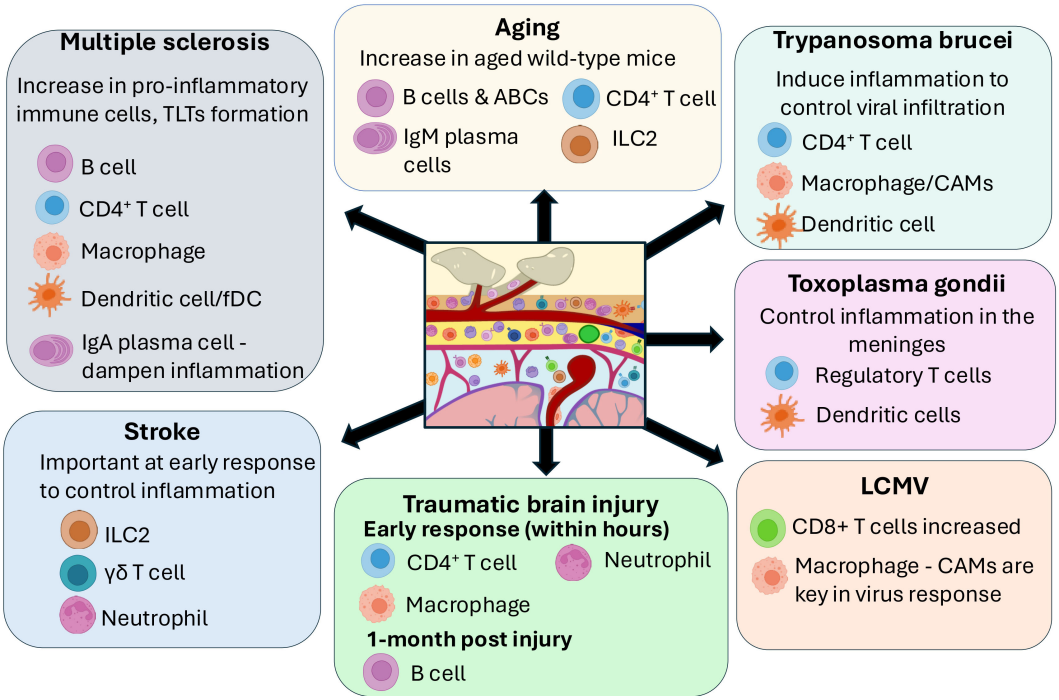

FIGURE 3
Role of meningeal immune cells in the brain in disease. The importance of different meningeal immune cells subsets in different brain diseases is summarized in this figure. In autoimmune diseases such as Multiple Sclerosis, an increase in proinflammatory immune cells including B cells, T cells, macrophages and DC in the meninges has been described, including formation of Tertiary Lymphoid tissue (TLTs) in the meninges. On the other hand, accumulation of IgA Plasma cells in the dura mater might play a role in dampening inflammation. Stroke and Traumatic brain injury show an important role of innate immune cells such as Type 2 innate lymphoid cells (ILC2) and neutrophils/macrophages in the meninges. Pathogenic brain infections such as Trypanosoma, Toxoplasma and *Lymphocytic choriomeningitis mammarenavirus* (LCMV) have shown an important role of meningeal T cells, dendritic cells and macrophages. On the other hand, aged wild type mice have shown a significant increase of T cells, B cells, Aged-associated B cells (ABCs) and IgM plasma cells in the meninges.

myeloid cells identified several neuroinflammation-associated monocyte-derived populations in the leptomeninges. Interestingly, these peripherally derived CD11c$^+$ APCs within the leptomeninges (as well as other areas of the CNS) were found to play a larger role in effector T cell activation and disease induction compared to CNS-resident myeloid populations (36). Indeed, high-throughput single cell sequencing on CD45$^+$cells isolated from different CNS compartments such as the leptomeninges, parenchyma and choroid plexus have unraveled the CNS myeloid landscape during neuroinflammation (36). Furthermore, there are contrasting results regarding the role of MLVs and draining lymph nodes in effector T cell reactivation during EAE (13, 104, 112, 113). The pharmacological ablation of MLVs and surgical resection of the dCLNs both attenuated EAE severity, likely through limiting antigen sampling and reactivation of T cells (13, 112, 113). Transcriptional profiling of antigen-specific T cells in draining cervical lymph nodes following EAE induction in mice with ablated MLVs compared to EAE mice without lymphatic manipulation showed a reduced inflammatory response of brain-reactive T cells, suggesting that lymphatic drainage in the meninges is critical to fully reactivate antigen-specific T cells in the lymph nodes (13). However, when dorsal and skull base lymphatic vessels were genetically ablated using adenoviral vector expressing vascular endothelial growth factor (VEGF) C/D that blocks essential lymphatic vessel growth factors, no changes in effector T cell infiltration and overall immune cell recruitment to the meninges or EAE severity was observed (104). Overall, the inflamed meningeal milieu in MS supports effector T cell retention and activation that promotes their ability to invade the CNS parenchyma.

The leptomeninges are often sites of tertiary lymphoid tissues (TLT), which are ectopic immune aggregates resembling secondary lymphoid tissues, and are frequently associated with cortical demyelination, axonal atrophy and more severe forms of (39, 114–116). Meningeal TLTs in MS and EAE are B cell-rich, but also contain T cells, plasma cells, DCs and macrophages (102) (Figure 3). Infiltrating CD4$^+$ T cells expressing IL-17 and Podoplanin were shown to play critical roles in driving the formation of meningeal tertiary lymphoid structures in EAE through stromal cell remodeling to produce extracellular matrix proteins and chemoattractants that promote cell retention (102, 117). In fact, T cells were shown to populate meningeal TLTs first, followed by B cells and other cell types (102). In EAE models, meningeal stromal cells and follicular DCs contribute to the formation of TLT by producing lymphoid-homing chemokines such as CXCL13 and BAFF, which parallels findings in MS patients (102, 118, 119). Infiltrating meningeal neutrophils may also promote the accumulation of B cells in TLTs in an integrin VLA-4-dependent manner (120, 121).

Meningeal TLTs are thought to promote local antigen-specific immune responses that exacerbate chronic disease in MS (122– 124). TLTs have been linked with epitope spreading of myelin-specific T cell responses (122). Additionally, stromal cells that support TLT integrity interact with encephalogenic T cells to produce cytokines that further sustain their responses (102). Several antigen-experienced B cell clones are shared between meningeal TLTs and corresponding brain parenchyma infiltrates in some MS patients (123). The IgH[MOG] transgenic mouse model, which possesses a B cell repertoire biased to recognizing myelin antigen, provides additional insights into the role of B cells within tertiary lymphoid structures in EAE (121, 124). When EAE is actively induced in IgH[MOG] mice, the animals develop severe disease that is characterized by meningeal TLTs (124). The production of IL-23 from meningeal and CNS-infiltrating autoreactive B cells within TLTs promoted inflammation through the maintenance of effector CD4$^+$ T cells in the CNS (124).

Meningeal ILCs and mast cells also interact with autoreactive T cells to propagate autoimmunity. Specifically, a subset of T-bet-dependent ILCs localized to the meninges have been shown to support CNS infiltration of myelin-reactive T cells by secreting pro-inflammatory cytokines and matrix metalloproteases (95). Additionally, meningeal mast cells become activated early in EAE and secrete tumor necrosis factor (TNF)-α and IL-1β, aiding in neutrophil recruitment that facilitates BBB dysfunction and inflammatory cytokine production by T cells (87, 105, 125). In mice, the absence of mast cells prevents effector T cell accumulation in the meninges conferring protection from EAE, and reconstitution of meningeal mast cells can restore disease (105, 126). Furthermore, mast cell colocalization with T cells has been observed in post-mortem tissue of some MS patients, reinforcing the idea of interaction between the two subsets (105).Interestingly, meningeal NK cells have been implicated in dampening disease through by IFN-γ production in a gut microbiome-dependent manner. IFN-γ production limited CNS inflammation through supporting astrocyte-mediated effector T cell apoptosis (99).

Overall, a growing body of evidence suggests that meningeal immunity plays a crucial role in the regulation of CNS inflammation and immune surveillance during MS and in animal models of MS pathology. The meninges not only serve as a pathway for autoreactive T cells other effector leukocyte populations to enter the CNS, but also as a route for draining CNS antigens and immune cells. They are also the site of TLT formation which is associated with epitope spreading and sustaining encephalitogenic T cell activity. However, several questions about the immune reactions within the meninges to promote neuroinflammation in EAE and MS remain. While there is a contribution of peripherally derived B cells to the inflamed meninges, recent discoveries demonstrate calvaria-derived B cells develop and undergo negative selection against CNS-derived epitopes locally within the meninges, and B cell-rich DALT structures can sustain local germinal center responses. Further research will be required to clarify the contributions of locally derived B cells compared to peripherally derived B cells in EAE and MS (7, 9, 50, 121, 127). Moreover, a better understanding of the mechanisms guiding tolerance to self-antigens in these spaces under normal conditions, and how this process is disrupted in autoimmune diseases like MS, could offer valuable insights for future therapeutic interventions. Additionally, ectopic tertiary lymphoid structures likely play a key role in supporting immune processes during MS and EAE (39, 102). Understanding processes that govern tertiary lymphoid structure formation better, if they are related to DALT structures present during homeostasis, and how the structures evolve across disease course will be critical to manipulating the balance between

anti- and pro-inflammatory reactions within the meninges during neuroinflammation.

5.2 Immunity against pathogens

The meninges function as a gateway for neurotropic pathogens targeting the brain parenchyma. CNS interfaces have multiple entry points, enabling immune cells to access the CNS for viral clearance while also serving as sites for pathogen infiltration. This role of the meninges as a critical entry point for pathogens is evident in infections like zika virus (ZIKV) and human immunodeficiency virus (HIV).

Postmortem examinations of neonates with ZIKV showed lymphocytic inflammation and the presence of viral antigens in the meninges (128, 129). Another study found that meningeal inflammation from ZIKV occurred independently of brain parenchymal infection, with meningeal involvement often observed without any corresponding infection in the brain (130). This provided compelling evidence that the meninges serve as a key entry point for ZIKV infection in the CNS. Characterization of the cell infiltrates in the meninges and perivascular space after ZIKV infection revealed elevated levels of macrophages, $CD4^+$ and $CD8^+$ T cells, and NK cells, along with an increase in cytokine expression, highlighting the meninges as a significant site of immune activation during ZIKV infection (128).

HIV has long been recognized for its ability to infect the CNS and cause neurocognitive disorders, such as HIV-associated dementia. However, the precise mechanisms and timing of its entry into the brain parenchyma remained unclear, with early theories suggesting that HIV infiltrated the brain via monocyte trafficking during the initial stages of infection (131, 132). Post-mortem analysis of human tissues has since shown that the HIV antigen p24 is localized with pvMφ at the CNS interface well before it is detected within the brain parenchyma, suggesting the meningeal immune cells as critical for early viral presence and potential entry into the brain (131–134). In fact, pvMφ have been shown to express CCR5, the necessary co-receptor, required for HIV entry into macrophages (135). Using bioinformatic and phylogenetic analyses to trace viral gene flow, it was determined that HIV not only migrates from the meninges into the CNS parenchyma but also travels from the meninges to peripheral tissues. This bidirectional movement underscores the meninges' role as both a reservoir and a conduit for viral dissemination within and beyond the CNS (133).

5.2.1 Lymphocytic choriomeningitis virus

Lymphocytic choriomeningitis virus (LCMV) is a pathogen known to cause meningitis in both humans and rodents (136). Previous studies have investigated the immune response to LCMV through intracerebral or intracranial inoculation methods. In these models, LCMV was found to replicate within CAMs and DCs before spreading to peripheral tissues, where it triggers a $CD8^+$ T cell response. The resulting pathology and edema in the brain arise when $CD8^+$ T cells migrate into the meninges, leading to immune-mediated damage (137) (Figure 3). Notably, depleting $CD8^+$ T cells before LCMV infection reduces the incidence of CNS disease, yet mice lacking effector pathways commonly employed by antiviral $CD8^+$ T cells (such as granzyme, FasL, and IFN-γ) exhibit increased mortality (137). This indicates that $CD8^+$ T cells do not induce immune-mediated pathology through direct cytotoxic actions. Instead, it has been demonstrated that the infiltrating antiviral $CD8^+$ T cells undergo reactivation in the meninges via both antigen-dependent and independent mechanisms (38), leading to increased release of CCL3, 4 and 5 to attract monocytes and neutrophils from the bloodstream (137). These cells are directly responsible for the vascular pathology associated with LCMV infections. Subsequent studies established that CAMs are infected, activated and killed during LCMV infections, eventually being replaced by blood monocytes. Interestingly, the replacement of blood monocytes decreases the ability for the meningeal immune compartment to responds to secondary microbial challenges, shown to be due to alterations in cholinergic receptor expression (138). Recently, using a peripheral LCMV infection model, it was demonstrated that CAMs play a crucial role in protecting the meninges from LCMV infection, primarily through IFNAR signaling pathways (76).

5.2.2 *Trypanosoma brucei*

Trypanosoma brucei (*T. brucei*), the parasite responsible for human sleeping sickness (African trypanosomiasis) and diseases in other animals, induces inflammation in the choroid plexus and meninges in both rodent and primate models (139–141). Intravital imaging in rodents revealed that following infection, T cells and DCs accumulate in the meninges, with both immune cells and parasites remaining confined to the dura around 40 days post-infection (142). A more recent study demonstrated that *T. brucei* infiltrates the CNS in a stepwise manner–beginning with the meninges, progressing to the choroid plexus, then the CSF, and ultimately reaching the brain parenchyma (143). During this process, monocytes are recruited into the meningeal layers and choroid plexus, while CAMs undergo proliferation. Fate mapping and single-cell RNA-Seq approaches reveal distinct transcriptional signatures between recruited monocytes in the choroid plexus and the cpMφ, suggesting a divergence in the roles of the two cell populations during infection based on ontogeny (Figure 3). Depletion of CAMs at early stages of *T. brucei* infection using a $Cx3cr1^{CreER}$:R26-DTR mice (depletion due to diphtheria toxin receptor present on embryonically derived macrophages) led to an increased parasitic load in the meninges (143). However, depletion at later stages of the disease did not result in a similar rise in parasitic burden. This suggests that CAMs play a critical role in the early stages of infection, helping to control the initial parasite load and limiting its entry into the CNS borders. The fact that depletion at later stages did not exacerbate the infection indicates that functional redundancies exist between CAMs and infiltrating myeloid cells, somewhat contradicting the transcriptomic findings. Quite interestingly, as *T. brucei* infection resolves, microglia return to a steady state like transcriptomic signature, whilst CAMs sustain an inflammatory signature and exhibit lasting transcriptomic alterations (143).

5.2.3 Toxoplasma gondii

Toxoplasma gondii (*T. gondii*) is a protozoan parasite that can cause chronic CNS infections. T_{reg} cells have been shown to localize to the meninges during toxoplasmic encephalitis in mice and are largely absent from the brain parenchyma (144). These T_{reg} cells utilize the chemokine receptor CXCR3 to remain within the meninges during infection, allowing effector T cells to carry out parasite control within the brain parenchyma (144). A recent study found that during chronic *T. gondii* infection, there was increased activation and expansion of DCs within the dural meninges (145). These DCs were increasingly mature at chronic stages of infection, with the cDC1 subset specifically upregulating markers such as CD80, CD86, and MHC-II. These DCs were also able to capture antigens from the CSF and transport them along local lymphatic vessels to the dCLNs, where they activated both $CD4^+$ and $CD8^+$ T cells (145). These studies highlight an important role of the meningeal immunity and lymphatic networks at connecting and presenting antigens in the CLN to control of *T. gondii* (Figure 3).

5.2.4 *Streptococcus pneumoniae*

Streptococcus pneumoniae (*S. pneumoniae*) is a well-known cause of bacterial meningitis, leading to significant damage through both pathogen-specific virulence factors and host-driven immunopathology. In mice, mMφ and pvMφ have been shown to play a protective role in *S. pneumoniae*-induced meningitis (3). A recent study has also shown an interaction between dural nociceptors and meningeal immunity during *S. pneumoniae*-induced meningitis (146). During infection, *S. pneumoniae* can stimulate these nociceptors, resulting in the release of CGRP within the meninges. CGRP acts to suppress CAM activity, diminishing cytokine production and impairing the recruitment of additional immune cells to the CNS, ultimately exacerbating disease pathology (146). These results not only underscore the complex interactions between the nervous and immune systems in meningitis, but also highlight the need to further explore how neuroimmune signaling modulates immune responses within the meninges during infection.

As discussed previously, the meninges, particularly the dura mater, have been shown to contain B cells and plasma cells, serving as a site for B cell development and selection (5, 9) In mice, the dural sinuses are populated by gut microbiota-dependent IgA^+ plasma cells. Following intravenous infection with *Candida albicans*, a fungus capable of causing meningoencephalitis in neonates and adults, there is an expansion of B cells and IgA^+ plasma cells within the dura. These IgA^+ plasma cells help trap the fungus, and in mice deficient in IgA or lacking meningeal plasma cells, the fungus spreads to the brain parenchyma (5). A more recent study discovered an intricate DALT within the rostral confluence of the sinuses, referred to as the rostral-rhinal venolymphatic hub, and other sites along the dural venous sinuses (9). Intravenously administered antigens accumulated within the DALT resulting in increased numbers of CD45+ and activated B cells within the structure. Furthermore, in response to nasal infection with vesicular stomatitis virus (VSV), the rostral-rhinal venolymphatic hub showed germinal center expansion and somatic hypermutation reactions resulting in the production of antigen-specific B cells and plasma cells (9). The strategic location of DALT along the dural sinuses may help fortify immune surveillance along vulnerable ACE points, where pathogens from the dura may easily access the SAS below. Together, these studies demonstrate the importance of the dural meninges in providing a humoral defense against fungal and viral infections and serving as a key interface between the brain and the body. Future research should investigate how the dynamic variability of the intestinal microbiome shapes humoral immunity in the meninges and influences susceptibility to infectious diseases.

Despite advances in understanding the role of meningeal immune cells, the precise effector mechanisms meningeal immune cells use to fight off pathogens locally remain unclear. There is limited knowledge of whether meningeal immune cells exhibit specialized responses compared to their peripheral counterparts, and little is known about the potential functional heterogeneity of immune cells across the different layers of the meninges in response to pathogens. Future research should focus on uncovering these unique immune dynamics to better understand how the meninges contribute to CNS defense in the context of infection.

6 Meningeal immunity in neurodegenerative diseases and brain injury

6.1 Stroke

During the acute phase of ischemic stroke (within 24h), innate immune cells are mobilized into the CNS through the production of damage associated molecular patterns (DAMPs), pro-inflammatory cytokines and binding proteins by necrotic cells and activated microglia in the region of the infarcted tissue (147). Inflammatory mediators including TNF, IL-2, CCL2, IL-6, and IL-17 are found to be upregulated in the brain and peripheral blood within hours after ischemia (148, 149). In addition to attracting peripheral immune cells, circulating DAMPs and cytokines cause BBB disruption that allow peripheral immune cells to enter the brain parenchyma and contribute to the inflammatory environment (147). This is followed by significant immunodepression that can leave individuals more susceptible to infectious disease in the days-to-weeks post-stroke (147). In the cervical lymph nodes, into which MLVs drain, higher levels of brain-derived antigens, including MAP2 and myelin basic protein, were found in patients with acute stroke (150). In addition to harboring brain-derived antigens that may be presented to B and T cells, the meningeal lymphatics is an important drainage pathway for CSF that may contribute to the accumulation of neuroinflammatory products in the brain if disrupted after ischemic stroke (151).

Leukocytes in the meninges also respond differently after stroke than those in the brain. A temporary site-specific increase in granulocytes and ILC2s was observed in the dura mater at 24h post-ischemia, as well as a decrease in DCs, NK cells and macrophage subsets and no changes in B cells despite these cells

showing an increase in the brain (152). However, neutrophils are more significantly increased in leptomeningeal vessels within hours after experimental stroke (153). CD163$^+$ border-associated macrophages participate in granulocyte recruitment, favor the expression of vascular endothelial growth factor and contribute to neurological dysfunction in a focal brain ischemia rat model (154). More recently described IL-17a-secreting γδ17 T cells, which are pro-inflammatory but also implicated in regulating neuronal signaling and cognition in the meninges, are found to be upregulated in the meningeal tissue in ischemic stroke through processes modulated by the intestinal microbiota (149) (Figure 3). This sheds light onto some promising research into dietary interventions that may improve post-stroke outcomes by modulation of IL-17a production by γδ17 T cells in the meninges (149). The efficacy of other immunomodulatory therapeutics, including inflammation-mediating minocycline and fingolimod as well as therapeutics that increase T_{reg} expression, are currently being evaluated in clinical trials (155, 156).

6.2 Traumatic brain injury

Altered meningeal immunity in TBI is another emerging area of interest that is being explored in human cases and experimental models (157). Immediately post-injury, BBB disruption occurs, and an inflammatory response is initiated through release of DAMPs by damaged neurons and glial cells as well as an influx of neutrophils to the damaged tissue (158). Circulating DAMPs bind to Pattern Recognition Receptors (PRRs) on activated glial cells and macrophages initiating pro-inflammatory cytokines and ROS release, as well as the migration of pro-inflammatory macrophages to the dCLNs to present antigens to naïve T cells and further adaptive responses (159). Traumatic Meningeal Enhancement, associated with meningeal injury and inflammation, has been described in a small sub-cohort of 13% (n=4) of patients with moderate TBI, and 6% (n=2) of patients with severe TBI out of 30 study participants up to 1-year post-injury (160). Studies in mice found severe deficits in the meningeal lymphatic system after TBI that lasted up to 1-month post-injury, and rejuvenation of meningeal lymphatic drainage with viral delivery of VEGF-C was able to ameliorate TBI-induced gliosis (161). In the K14-VEGFR3-Ig model that lack MLVs, a significant reduction in infiltrating CD4$^+$ T cells was observed in the brain, suggesting the involvement of MLVs in the neuroimmune response after brain injury (162).

Regarding immune cellular responses in the post-TBI meninges, death of meningeal macrophages was observed within 30 mins of compression injury in mice, followed by infiltration of myelomonocytic cells (monocytes/neutrophils) into the meningeal tissue that scavenge dead cells in a similar manner to neutrophils in the injured brain (47). Pro-inflammatory cytokines IL-1α and IL-1β were found to be elevated in the meninges 6h – 1 day after meningeal compression injury in mice (163). High-throughput RNA-Seq further demonstrated an upregulation of genes related to macrophage and T cell responses at 7 days post-injury, including CD4$^+$ Th2 and Th17 cells, CD8$^+$ T cells, and NKT cells (164, 165). Increased B cell and IFN gene signatures, including five sub-clusters of B cells, were also observed at 1-month post-injury in the dural meninges of aged mice (164, 165). A neuroprotective effect of meningeal macrophages was also observed through their clearance of extravascular fibrinogen and production of MMP-2 during wound repair post-injury (163) (Figure 3).

Given the known role of adaptive immunity in TBI, therapeutics that target inflammatory responses in the injured CNS are currently being investigated. In mice, exogenous administration of IL-33 was found to reduce glial activation and improve the drainage of MLVs to the dCLNs (166). Immunomodulatory therapies have shown efficacy in pre-clinical studies of TBI but failed to improve disease outcomes in larger clinical trials (167). More insight into the contribution of the meninges in seeding immune cells into the brain post-injury, the role of meningeal immunity in long-term recovery, and the effect of aging on this compartment is required to improve the efficacy of immunomodulatory therapies for TBI.

6.3 Neurodegenerative diseases and aging

Age-associated changes in meningeal immunity have not been extensively explored in Parkinson's Disease (PD) and Alzheimer's Disease (AD). Dynamic contrast-enhanced magnetic resonance imaging of the MLVs in idiopathic PD patients revealed significantly reduced flow of CSF compared to normal controls and patients with atypical Parkinsonian disorders (168). In mice treated with α-synuclein (α-syn) preformed fibrils, blocking MLV flow increased α-synuclein pathology and worsened motor and memory deficits (168). Emergence of α-syn pathology was associated with delayed meningeal lymphatic drainage, significant increases in meningeal macrophages with strong phosphorylated α-syn immunoreactivity, and increased expression of inflammatory cytokines IL-1, IL-6, IFN-γ and TNF-α (168). Singe-cell RNA-Seq and depletion studies in mice further implicated specific subsets of border-associated macrophages (BAMs) in mediating α-syn related neuroinflammation, with these cells playing a role in immune cell recruitment, infiltration and antigen presentation to CD4$^+$ T cells (169). BAMs were further identified in human postmortem brain tissues from PD patients in close proximity to T cells (169) (Figure 3).

In AD patients and animal models, there has been further evidence implicating the intricate communication networks between innate and adaptive and immune cells in the brain and meningeal layers. Exacerbated glial activation is a hallmark of later stages of AD, as well as vascular damage which together may promote the influx of adaptive and innate cells into the various CNS compartments (170). Impaired meningeal lymphatic drainage was found to be associated with aging, and disruption of MLVs in mouse models of AD promoted the accumulation of amyloid β in the meninges and brain parenchyma (171). Interestingly, near-infrared light was found to modulate lymphatic drainage in mouse models of AD, resulting in improved cognition and alleviation of AD-associated pathology including neuroinflammation (172). A recent study in aged mice demonstrated that IFN-γ production by T cells accumulated in the meninges was a driver of lymphatic

impairment, connecting the cellular response to meningeal lymphatic dysfunction seen in aging (173). Evidence for increased numbers of meningeal T and B cells, increased expression of pro-inflammatory cytokines, and increased function such as engulfment in macrophages and other myeloid cells was also uncovered by RNA-Seq in aged mice (174). In particular, a specific population of border-associated macrophages expressing high levels of CD163 and LYVE1 are involved at regulating arterial motion and subsequently regulate CSF flow dynamics, implicated in brain clearance in aging and AD (175). Brain perivascular macrophages located in the perivascular space are involved at increasing oxidative stress and neurovascular dysfunction induced by amyloid beta accumulation in mice (176). Increased expression of border-associated ILC2s was further evidenced in aged mice, mostly accumulated in the choroid plexus, and transfer of *ex-vivo* expanded and activated ILC2s into the brain of aged mice by intracerebroventricular injection was found to alleviated age-associated cognitive decline (93). However, meningeal mast cells were associated with cognitive deficits, and depletion of mast cells in 5xFAD mice elevated the expression of neuroprotective microglia and reduced astrocyte reactivity (90). BAMs in the aged meninges also expressed more AD GWAS genes than other cell types, further highlighting the importance of meningeal immunity in AD development (177).

The dura mater of aged wild type mice harbors a unique population of blood-derived B cells resembling age-associated B cells (ABCs), which have been previously described in the spleen, and had a higher amount of IgM^+ plasma cells in the dura (7). The amount of IgA^+ plasma cells do not change when comparing young and old mice (7). The accumulation of ABCs and IgM^+ plasma cells in the dura with age may endanger the specialized immune environment of the CNS during aging, but their definitive role remains to be defined (7). Furthermore, recent literature has shown how B cells increase in the meninges at early stages of amyloid beta pathology in 5xFAD mice and may exhibit protective effects on AD-like neuropathology by producing the anti-inflammatory cytokine IL-35. However, these cells showed a decline with age (178). In humans, gene microarray analysis of the choroid plexus from postmortem brain tissues of AD patients and normal controls also demonstrated increased expression of EBI3 in AD, a subunit of IL-35, and single-cell RNA-seq data from peripheral blood mononuclear cells further revealed increased variability in B cell expression in human AD as well as the expression of several subtypes of B regulatory cells (178). On the other hand, MHC-II-associated invariant peptide (CLIP)-positive $CD19^+$ B cells were expanded in the meninges of aged 5xFAD mice, and antagonizing CLIP was sufficient to reduced CLIP+ B cells and improved both brain pathology and behavioral deficit (179).

In other models of aging, the number of meningeal mucosal-associated invariant T (MAIT) cells increased with age. Single-cell RNA-Seq revealed MAIT cells were enriched in antioxidant defense genes compared to meningeal $CD4^+$ and $CD8^+$ cells (180). Adult (7-month) MAIT-deficient *Mr1*$^{-/-}$ mice had decreased expression of tight junction proteins in the leptomeninges and loss of meningeal barrier function that was attributed to an accumulation of ROS in the leptomeninges (180). The loss of barrier function led to microglia activation and hippocampal microgliosis that correlated with impaired spatial learning and memory (180). Interestingly, this phenotype was not observed in young (5-week-old) *Mr1*$^{-/-}$ mice, highlighting an age-related homeostatic function of MAIT cells, and the existence of potentially compensatory antioxidant systems in younger mice (180).

Despite this evidence of the emerging role of meningeal immunity in aging diseases, many questions remain surrounding the exact mechanisms used by meningeal immune cells to influence processes in the aging brain (Figure 3). Elucidating the interplay between reduced meningeal lymphatic drainage and increased activation of meningeal immune cells may help clarify these questions and contribute to the development of new therapeutic targets for age-associated neuroinflammation.

7 Discussion and conclusion

Over the last decade, numerous studies have demonstrated that meninges play a critical role in the CNS that goes beyond mechanical protection. The meninges represent a rich immune microenvironment within the CNS that is populated by immune cells derived from embryonic precursors, the adjacent skull bone marrow, and peripheral circulation. The meninges and their immune cells act as a dynamic immunological barrier, shielding the brain from foreign antigens while also mediating tolerance through sampling of brain-derived antigens, and influencing cognition and behavior through the secretion of cytokines. These functional distinctions highlight the unique role of meningeal immunity in maintaining CNS homeostasis and responding to injury or disease, therefore serving as an active immunological site in health and disease.

The recent anatomical discoveries of the glymphatic and meningeal lymphatic systems has provided a clear rationale for the influx and efflux of immune cells within the meningeal layers and the periphery, ultimately draining into the CLNs. A clearer understanding of meningeal anatomy and composition has also shed light onto the complex network involved in the modulation, activation, and migration of immune cells within the skull, meninges and brain. Part of this network also involves complex interactions between resident immune cells and the non-immune cellular components of the meninges, such as stromal cells, fibroblasts, and endothelial cells. For example, the secretion of CXCL13 and CXCL12 by stromal cells in the meninges is crucial to drive the migration and retention of B and T cells within the compartment. Further research is essential to uncover the mechanisms around how non-immune cells contribute to the maintenance and regulation of meningeal immunity and how molecular, metabolic, and genetic cues within the meningeal immune and non-immune cells can define the meningeal immune niche. Additionally, understanding whether certain immune cell interactions within the meningeal niche are redundant, synergistic, or antagonistic could provide insight into the hierarchical structure of meningeal immunity.

As explored in this review, meningeal immune cells dynamically respond to changes, becoming particularly active during disease states such as neuroinflammation, infection, neurodegeneration,

and brain injury. There is substantial, yet largely untapped potential in targeting these meningeal immune cells for therapeutic purposes. Therapeutic strategies could involve modulating how these cells respond under pathological conditions or, alternatively, preconditioning them during steady-state conditions to promote a protective response when disease arises.

Furthermore, therapeutic targeting does not have to be limited to the resident immune cells in the meninges. Focusing on the signaling pathways and chemokine gradients within the meningeal environment can potentially influence the recruitment and activity of peripheral immune cells to the meninges. For instance, enhancing chemokine signals to recruit protective immune subsets, while diminishing signals that attract pro-inflammatory cells, could help reshape meningeal immunity to favor neuroprotection and mitigate disease progression.

Despite recent advancements, a deeper understanding of the immune interactions within the meninges is still required. Challenges remain in understanding when and by which mechanisms to target specific immune cells in the meninges either originating from within the CNS compartment, the periphery, or both. This increased understanding will allow for leveraging of the distinctive properties of the meningeal immune niche, offering an opportunity to pioneer novel therapies to protect and restore CNS health across various neurological diseases.

Author contributions

PUP: Visualization, Writing – original draft, Writing – review & editing, Data curation, Formal analysis, Investigation. AR: Data curation, Formal analysis, Investigation, Writing – original draft, Writing – review & editing, Conceptualization. AID: Data curation, Formal analysis, Investigation, Writing – original draft, Writing – review & editing, Conceptualization. OLR: Conceptualization, Writing – original draft, Writing – review & editing, Funding acquisition, Resources, Supervision, Visualization.

Funding

The author(s) declare that financial support was received for the research, authorship, and/or publication of this article. This research was supported by a UHN-Krembil start-up grant (#410013711).

Conflict of interest

The authors declare that the research was conducted in the absence of any commercial or financial relationships that could be construed as a potential conflict of interest.

Generative AI statement

The author(s) declare that no Generative AI was used in the creation of this manuscript.

Publisher's note

References

1. Ghannam JY, Al Kharazi KA. Neuroanatomy, cranial meninges, in: *StatPearls* (2024). Treasure Island (FL: StatPearls Publishing. Available online at: http://www.ncbi.nlm.nih.gov/books/NBK539882/ (Accessed 2024 Nov 11).

2. Derecki NC, Cardani AN, Yang CH, Quinnies KM, Crihfield A, Lynch KR, et al. Regulation of learning and memory by meningeal immunity: a key role for IL-4. *J Exp Med.* (2010) 207:1067–80. doi: 10.1084/jem.20091419

3. Polfliet MM, Zwijnenburg PJ, van Furth AM, van der Poll T, Döpp EA, Renardel de Lavalette C, et al. Meningeal and perivascular macrophages of the central nervous system play a protective role during bacterial meningitis. *J Immunol Baltim Md.* (2001) 2001167:4644–50. doi: 10.4049/jimmunol.167.8.4644

4. Rustenhoven J, Drieu A, Mamuladze T, de Lima KA, Dykstra T, Wall M, et al. Functional characterization of the dural sinuses as a neuroimmune interface. *Cell.* (2021) 184:1000–1016.e27. doi: 10.1016/j.cell.2020.12.040

5. Fitzpatrick Z, Frazer G, Ferro A, Clare S, Bouladoux N, Ferdinand J, et al. Gut-educated IgA plasma cells defend the meningeal venous sinuses. *Nature.* (2020) 587:472–6. doi: 10.1038/s41586-020-2886-4

6. Herisson F, Frodermann V, Courties G, Rohde D, Sun Y, Vandoorne K, et al. Direct vascular channels connect skull bone marrow and the brain surface enabling myeloid cell migration. *Nat Neurosci.* (2018) 21:1209–17. doi: 10.1038/s41593-018-0213-2

7. Brioschi S, Wang WL, Peng V, Wang M, Shchukina I, Greenberg ZJ, et al. Heterogeneity of meningeal B cells reveals a lymphopoietic niche at the CNS borders. *Science.* (2021) 373:eabf9277. doi: 10.1126/science.abf9277

8. Cugurra A, Mamuladze T, Rustenhoven J, Dykstra T, Beroshvili G, Greenberg ZJ, et al. Skull and vertebral bone marrow are myeloid cell reservoirs for the meninges and CNS parenchyma. *Science.* (2021) 373:eabf7844. doi: 10.1126/science.abf7844

9. Fitzpatrick Z, Ghabdan Zanluqui N, Rosenblum JS, Tuong ZK, Lee CYC, Chandrashekhar V, et al. Venous-plexus-associated lymphoid hubs support meningeal humoral immunity. *Nature.* (2024) 628:612–9. doi: 10.1038/s41586-024-07202-9

10. Schachenmayr W, Friede RL. The origin of subdural neomembranes. I. Fine structure of the dura-arachnoid interface in man. *Am J Pathol.* (1978) 92:53–68.

11. Cai R, Pan C, Ghasemigharagoz A, Todorov MI, Förstera B, Zhao S, et al. Panoptic imaging of transparent mice reveals whole-body neuronal projections and skull-meninges connections. *Nat Neurosci.* (2019) 22:317–27. doi: 10.1038/s41593-018-0301-3

12. Balin BJ, Broadwell RD, Salcman M, el-Kalliny M. Avenues for entry of peripherally administered protein to the central nervous system in mouse, rat, and squirrel monkey. *J Comp Neurol.* (1986) 251:260–80. doi: 10.1002/cne.902510209

13. Louveau A, Herz J, Alme MN, Salvador AF, Dong MQ, Viar KE, et al. CNS lymphatic drainage and neuroinflammation are regulated by meningeal lymphatic vasculature. *Nat Neurosci.* (2018) 21:1380–91. doi: 10.1038/s41593-018-0227-9

14. Ahn JH, Cho H, Kim JH, Kim SH, Ham JS, Park I, et al. Meningeal lymphatic vessels at the skull base drain cerebrospinal fluid. *Nature.* (2019) 572:62–6. doi: 10.1038/s41586-019-1419-5

15. Louveau A, Smirnov I, Keyes TJ, Eccles JD, Rouhani SJ, Peske JD, et al. Structural and functional features of central nervous system lymphatic vessels. *Nature.* (2015) 523:337–41. doi: 10.1038/nature14432

16. Absinta M, Ha SK, Nair G, Sati P, Luciano NJ, Palisoc M, et al. Human and nonhuman primate meninges harbor lymphatic vessels that can be visualized noninvasively by MRI. *eLife.* (2017) 6:e29738. doi: 10.7554/eLife.29738.018

17. Ringstad G, Eide PK. Cerebrospinal fluid tracer efflux to parasagittal dura in humans. *Nat Commun*. (2020) 11:354. doi: 10.1038/s41467-019-14195-x

18. Kim MW, Gao W, Lichti CF, Gu X, Dykstra T, Cao J, et al. Endogenous self-peptides guard immune privilege of the central nervous system. *Nature*. (2025) 637 (8044):176–83. doi: 10.1038/s41586-024-08279-y

19. Lopes CA, Mair WG. Ultrastructure of the arachnoid membrane in man. *Acta Neuropathol (Berl)*. (1974) 28:167–73. doi: 10.1007/BF00710326

20. Pease DC, Schultz RL. Electron microscopy of rat cranial meninges. *Am J Anat*. (1958) 102:301–21. doi: 10.1002/aja.1001020207

21. Griffiths IR, Pitts LH, Crawford RA, Trench JG. Spinal cord compression and blood flow. I. The effect of raised cerebrospinal fluid pressure on spinal cord blood flow. *Neurology*. (1978) 28:1145–51. doi: 10.1212/WNL.28.11.1145

22. Mortazavi MM, Quadri SA, Khan MA, Gustin A, Suriya SS, Hassanzadeh T, et al. Subarachnoid trabeculae: A comprehensive review of their embryology, histology, morphology, and surgical significance. *World Neurosurg*. (2018) 111:279–90. doi: 10.1016/j.wneu.2017.12.041

23. Decimo I, Fumagalli G, Berton V, Krampera M, Bifari F. Meninges: from protective membrane to stem cell niche. *Am J Stem Cells*. (2012) 1:92–105.

24. Welch K, Friedman V. The cerebrospinal fluid valves. *Brain J Neurol*. (1960), 83:454–69. doi: 10.1093/brain/83.3.454

25. Weller RO. Microscopic morphology and histology of the human meninges. *Morphol Bull Assoc Anat*. (2005) 89:22–34. doi: 10.1016/S1286-0115(05)83235-7

26. Smyth LCD, Xu D, Okar SV, Dykstra T, Rustenhoven J, Papadopoulos Z, et al. Identification of direct connections between the dura and the brain. *Nature*. (2024) 627:165–73. doi: 10.1038/s41586-023-06993-7

27. Hutchings M, Weller RO. Anatomical relationships of the pia mater to cerebral blood vessels in man. *J Neurosurg*. (1986) 65:316–25. doi: 10.3171/jns.1986.65.3.0316

28. Jones EG. On the mode of entry of blood vessels into the cerebral cortex. *J Anat*. (1970) 106:507–20.

29. Hannocks MJ, Pizzo ME, Huppert J, Deshpande T, Abbott NJ, Thorne RG, et al. Molecular characterization of perivascular drainage pathways in the murine brain. *J Cereb Blood Flow Metab Off J Int Soc Cereb Blood Flow Metab*. (2018) 38:669–86. doi: 10.1177/0271678X17749689

30. Hablitz LM, Nedergaard M. The glymphatic system: A novel component of fundamental neurobiology. *J Neurosci Off J Soc Neurosci*. (2021) 41:7698–711. doi: 10.1523/JNEUROSCI.0619-21.2021

31. Ichimura T, Fraser PA, Cserr HF. Distribution of extracellular tracers in perivascular spaces of the rat brain. *Brain Res*. (1991) 545:103–13. doi: 10.1016/0006-8993(91)91275-6

32. Quintana FJ. Astrocytes to the rescue! Glia limitans astrocytic endfeet control CNS inflammation. *J Clin Invest*. (2017) 127:2897–9. doi: 10.1172/JCI95769

33. Horng S, Therattil A, Moyon S, Gordon A, Kim K, Argaw AT, et al. Astrocytic tight junctions control inflammatory CNS lesion pathogenesis. *J Clin Invest*. (2017) 127:3136–51. doi: 10.1172/JCI91301

34. Greenberg RW, Lane EL, Cinnamon J, Farmer P, Hyman RA. The cranial meninges: anatomic considerations. *Semin Ultrasound CT MR*. (1994) 15:454–65. doi: 10.1016/S0887-2171(05)80017-4

35. Van Hove H, Martens L, Scheyltjens I, De Vlaminck K, Pombo Antunes AR, De Prijck S, et al. A single-cell atlas of mouse brain macrophages reveals unique transcriptional identities shaped by ontogeny and tissue environment. *Nat Neurosci*. (2019) 22:1021–35. doi: 10.1038/s41593-019-0393-4

36. Jordão MJC, Sankowski R, Brendecke SM, Sagar, Locatelli G, Tai YH. Single-cell profiling identifies myeloid cell subsets with distinct fates during neuroinflammation. *Science*. (2019) 363:eaat7554. doi: 10.1126/science.aat7554

37. Schafflick D, Wolbert J, Heming M, Thomas C, Hartlehnert M, Börsch AL, et al. Single-cell profiling of CNS border compartment leukocytes reveals that B cells and their progenitors reside in non-diseased meninges. *Nat Neurosci*. (2021) 24:1225–34. doi: 10.1038/s41593-021-00880-y

38. Kang SS, Herz J, Kim JV, Nayak D, Stewart-Hutchinson P, Dustin ML, et al. Migration of cytotoxic lymphocytes in cell cycle permits local MHC I-dependent control of division at sites of viral infection. *J Exp Med*. (2011) 208:747–59. doi: 10.1084/jem.20101295

39. Lucchinetti CF, Popescu BFG, Bunyan RF, Moll NM, Roemer SF, Lassmann H, et al. Inflammatory cortical demyelination in early multiple sclerosis. *N Engl J Med*. (2011) 365:2188–97. doi: 10.1056/NEJMoa1100648

40. Radjavi A, Smirnov I, Derecki N, Kipnis J. Dynamics of the meningeal CD4(+) T-cell repertoire are defined by the cervical lymph nodes and facilitate cognitive task performance in mice. *Mol Psychiatry*. (2014) 19:531–3. doi: 10.1038/mp.2013.79

41. Wolf SA, Steiner B, Akpinarli A, Kammertoens T, Nassenstein C, Braun A, et al. CD4-positive T lymphocytes provide a neuroimmunological link in the control of adult hippocampal neurogenesis. *J Immunol Baltim Md*. (2009) 182:3979–84. doi: 10.4049/jimmunol.0801218

42. Jeon SG, Kim KA, Chung H, Choi J, Song EJ, Han SY, et al. Impaired memory in OT-II transgenic mice is associated with decreased adult hippocampal neurogenesis possibly induced by alteration in th2 cytokine levels. *Mol Cells*. (2016) 39:603–10. doi: 10.14348/molcells.2016.0072

43. Radjavi A, Smirnov I, Kipnis J. Brain antigen-reactive CD4+ T cells are sufficient to support learning behavior in mice with limited T cell repertoire. *Brain Behav Immun*. (2014) 35:58–63. doi: 10.1016/j.bbi.2013.08.013

44. Filiano AJ, Xu Y, Tustison NJ, Marsh RL, Baker W, Smirnov I, et al. Unexpected role of interferon-γ in regulating neuronal connectivity and social behavior. *Nature*. (2016) 535:425–9. doi: 10.1038/nature18626

45. Ribeiro M, Brigas HC, Temido-Ferreira M, Pousinha PA, Regen T, Santa C, et al. Meningeal γδ T cell-derived IL-17 controls synaptic plasticity and short-term memory. *Sci Immunol*. (2019) 4:eaay5199. doi: 10.1126/sciimmunol.aay5199

46. Alves de Lima K, Rustenhoven J, Da Mesquita S, Wall M, Salvador AF, Smirnov I, et al. Meningeal γδ T cells regulate anxiety-like behavior via IL-17a signaling in neurons. *Nat Immunol*. (2020) 21:1421–9. doi: 10.1038/s41590-020-0776-4

47. Roth TL, Nayak D, Atanasijevic T, Koretsky AP, Latour LL, McGavern DB. Transcranial amelioration of inflammation and cell death after brain injury. *Nature*. (2014) 505:223–8. doi: 10.1038/nature12808

48. Alves de Lima K, Rustenhoven J, Kipnis J. Meningeal immunity and its function in maintenance of the central nervous system in health and disease. *Annu Rev Immunol*. (2020) 38:597–620. doi: 10.1146/annurev-immunol-102319-103410

49. Korin B, Ben-Shaanan TL, Schiller M, Dubovik T, Azulay-Debby H, Boshnak NT, et al. High-dimensional, single-cell characterization of the brain's immune compartment. *Nat Neurosci*. (2017) 20:1300–9. doi: 10.1038/nn.4610

50. Wang Y, Chen D, Xu D, Huang C, Xing R, He D, et al. Early developing B cells undergo negative selection by central nervous system-specific antigens in the meninges. *Immunity*. (2021) 54:2784–94. doi: 10.1016/j.immuni.2021.09.016

51. Lynall ME, Kigar SL, Lehmann ML, DePuyt AE, Tuong ZK, Listwak SJ, et al. B-cells are abnormal in psychosocial stress and regulate meningeal myeloid cell activation. *Brain Behav Immun*. (2021) 97:226–38. doi: 10.1016/j.bbi.2021.08.002

52. Kierdorf K, Masuda T, Jordão MJC, Prinz M. Macrophages at CNS interfaces: ontogeny and function in health and disease. *Nat Rev Neurosci*. (2019) 20:547–62. doi: 10.1038/s41583-019-0201-x

53. Prinz M, Erny D, Hagemeyer N. Ontogeny and homeostasis of CNS myeloid cells. *Nat Immunol*. (2017) 18:385–92. doi: 10.1038/ni.3703

54. Zeisel A, Muñoz-ManChado AB, Codeluppi S, Lönnerberg P, La Manno G, Juréus A, et al. Brain structure. Cell types in the mouse cortex and hippocampus revealed by single-cell RNA-seq. *Science*. (2015) 347:1138–42. doi: 10.1126/science.aaa1934

55. Mrdjen D, Pavlovic A, Hartmann FJ, Schreiner B, Utz SG, Leung BP, et al. High-dimensional single-cell mapping of central nervous system immune cells reveals distinct myeloid subsets in health, aging, and disease. *Immunity*. (2018) 48:380–95. doi: 10.1016/j.immuni.2018.01.011

56. Goldmann T, Wieghofer P, Jordão MJC, Prutek F, Hagemeyer N, Frenzel K, et al. Origin, fate and dynamics of macrophages at central nervous system interfaces. *Nat Immunol*. (2016) 17:797–805. doi: 10.1038/ni.3423

57. Utz SG, See P, Mildenberger W, Thion MS, Silvin A, Lutz M, et al. Early fate defines microglia and non-parenchymal brain macrophage development. *Cell*. (2020) 181:557–73. doi: 10.1016/j.cell.2020.03.021

58. Masuda T, Amann L, Monaco G, Sankowski R, Staszewski O, Krueger M, et al. Specification of CNS macrophage subsets occurs postnatally in defined niches. *Nature*. (2022) 604:740–8. doi: 10.1038/s41586-022-04596-2

59. Epelman S, Lavine KJ, Beaudin AE, Sojka DK, Carrero JA, Calderon B, et al. Embryonic and adult-derived resident cardiac macrophages are maintained through distinct mechanisms at steady state and during inflammation. *Immunity*. (2014) 40:91–104. doi: 10.1016/j.immuni.2013.11.019

60. McMenamin PG, Wealthall RJ, Deverall M, Cooper SJ, Griffin B. Macrophages and dendritic cells in the rat meninges and choroid plexus: three-dimensional localization by environmental scanning electron microscopy and confocal microscopy. *Cell Tissue Res*. (2003) 313:259–69. doi: 10.1007/s00441-003-0779-0

61. Schulz C, Gomez Perdiguero E, Chorro L, Szabo-Rogers H, Cagnard N, Kierdorf K, et al. A lineage of myeloid cells independent of Myb and hematopoietic stem cells. *Science*. (2012) 336:86–90. doi: 10.1126/science.1219179

62. Kierdorf K, Erny D, Goldmann T, Sander V, Schulz C, Perdiguero EG, et al. Microglia emerge from erythromyeloid precursors via Pu.1- and Irf8-dependent pathways. *Nat Neurosci*. (2013) 16:273–80. doi: 10.1038/nn.3318

63. Gomez Perdiguero E, Klapproth K, Schulz C, Busch K, Azzoni E, Crozet L, et al. Tissue-resident macrophages originate from yolk-sac-derived erythro-myeloid progenitors. *Nature*. (2015) 518:547–51. doi: 10.1038/nature13989

64. Hagemeyer N, Kierdorf K, Frenzel K, Xue J, Ringelhan M, Abdullah Z, et al. Transcriptome-based profiling of yolk sac-derived macrophages reveals a role for Irf8 in macrophage maturation. *EMBO J*. (2016) 35:1730–44. doi: 10.15252/embj.201693801

65. Molawi K, Wolf Y, Kandalla PK, Favret J, Hagemeyer N, Frenzel K, et al. Progressive replacement of embryo-derived cardiac macrophages with age. *J Exp Med*. (2014) 211:2151–8. doi: 10.1084/jem.20140639

66. Yona S, Kim KW, Wolf Y, Mildner A, Varol D, Breker M, et al. Fate mapping reveals origins and dynamics of monocytes and tissue macrophages under homeostasis. *Immunity*. (2013) 38:79–91. doi: 10.1016/j.immuni.2012.12.001

67. Goldmann T, Wieghofer P, Müller PF, Wolf Y, Varol D, Yona S, et al. A new type of microglia gene targeting shows TAK1 to be pivotal in CNS autoimmune inflammation. *Nat Neurosci*. (2013) 16:1618–26. doi: 10.1038/nn.3531

68. Huang G, Zhang P, Hirai H, Elf S, Yan X, Chen Z, et al. PU.1 is a major downstream target of AML1 (RUNX1) in adult mouse hematopoiesis. *Nat Genet*. (2008) 40:51–60. doi: 10.1038/ng.2007.7

69. Butovsky O, Jedrychowski MP, Moore CS, Cialic R, Lanser AJ, Gabriely G, et al. Identification of a unique TGF-β-dependent molecular and functional signature in microglia. *Nat Neurosci*. (2014) 17:131–43. doi: 10.1038/nn.3599

70. Ford AL, Goodsall AL, Hickey WF, Sedgwick JD. Normal adult ramified microglia separated from other central nervous system macrophages by flow cytometric sorting. Phenotypic differences defined and direct *ex vivo* antigen presentation to myelin basic protein-reactive CD4+ T cells compared. *J Immunol Baltim Md*. (1995) 1995154:4309–21.

71. Ajami B, Samusik N, Wieghofer P, Ho PP, Crotti A, Bjornson Z, et al. Single-cell mass cytometry reveals distinct populations of brain myeloid cells in mouse neuroinflammation and neurodegeneration models. *Nat Neurosci*. (2018) 21:541–51. doi: 10.1038/s41593-018-0100-x

72. Butovsky O, Siddiqui S, Gabriely G, Lanser AJ, Dake B, Murugaiyan G, et al. Modulating inflammatory monocytes with a unique microRNA gene signature ameliorates murine ALS. *J Clin Invest*. (2012) 122:3063–87. doi: 10.1172/JCI62636

73. Kim WK, Alvarez X, Fisher J, Bronfin B, Westmoreland S, McLaurin J, et al. CD163 identifies perivascular macrophages in normal and viral encephalitic brains and potential precursors to perivascular macrophages in blood. *Am J Pathol*. (2006) 168:822–34. doi: 10.2353/ajpath.2006.050215

74. Galea I, Palin K, Newman TA, Van Rooijen N, Perry VH, Boche D. Mannose receptor expression specifically reveals perivascular macrophages in normal, injured, and diseased mouse brain. *Glia*. (2005) 49:375–84. doi: 10.1002/glia.20124

75. Mato M, Ookawara S, Sakamoto A, Aikawa E, Ogawa T, Mitsuhashi U, et al. Involvement of specific macrophage-lineage cells surrounding arterioles in barrier and scavenger function in brain cortex. *Proc Natl Acad Sci U S A*. (1996) 93:3269–74. doi: 10.1073/pnas.93.8.3269

76. Rebejac J, Eme-Scolan E, Arnaud Paroutaud L, Kharbouche S, Teleman M, Spinelli L, et al. Meningeal macrophages protect against viral neuroinfection. *Immunity*. (2022) 55:2103–17. doi: 10.1016/j.immuni.2022.10.005

77. He H, Mack JJ, Güç E, Warren CM, Squadrito ML, Kilarski WW, et al. Perivascular macrophages limit permeability. *Arterioscler Thromb Vasc Biol*. (2016) 36:2203–12. doi: 10.1161/ATVBAHA.116.307592

78. Venero Galanternik M, Castranova D, Gore AV, Blewett NH, Jung HM, Stratman AN, et al. A novel perivascular cell population in the zebrafish brain. *eLife*. (2017) 6:e24369. doi: 10.7554/eLife.24369

79. Serrats J, Schiltz JC, García-Bueno B, van Rooijen N, Reyes TM, Sawchenko PE. Dual roles for perivascular macrophages in immune-to-brain signaling. *Neuron*. (2010) 65:94–106. doi: 10.1016/j.neuron.2009.11.032

80. Matsuwaki T, Eskilsson A, Kugelberg U, Jönsson JI, Blomqvist A. Interleukin-1β induced activation of the hypothalamus-pituitary-adrenal axis is dependent on interleukin-1 receptors on non-hematopoietic cells. *Brain Behav Immun*. (2014) 40:166–73. doi: 10.1016/j.bbi.2014.03.015

81. Vasilache AM, Qian H, Blomqvist A. Immune challenge by intraperitoneal administration of lipopolysaccharide directs gene expression in distinct blood-brain barrier cells toward enhanced prostaglandin E(2) signaling. *Brain Behav Immun*. (2015) 48:31–41. doi: 10.1016/j.bbi.2015.02.003

82. Jais A, Solas M, Backes H, Chaurasia B, Kleinridders A, Theurich S, et al. Myeloid-cell-derived VEGF maintains brain glucose uptake and limits cognitive impairment in obesity. *Cell*. (2016) 165:882–95. doi: 10.1016/j.cell.2016.03.033

83. Mato M, Ookawara S, Sano M, Fukuda S. Uptake of fat by fluorescent granular perithelial cells in cerebral cortex after administration of fat rich chow. *Experientia*. (1982) 38:1496–8. doi: 10.1007/BF01955791

84. Rossi B, Constantin G, Zenaro E. The emerging role of neutrophils in neurodegeneration. *Immunobiology*. (2020) 225:151865. doi: 10.1016/j.imbio.2019.10.014

85. Perez-de-Puig I, Miró-Mur F, Ferrer-Ferrer M, Gelpi E, Pedragosa J, Justicia C, et al. Neutrophil recruitment to the brain in mouse and human ischemic stroke. *Acta Neuropathol (Berl)*. (2015) 129:239–57. doi: 10.1007/s00401-014-1381-0

86. Jickling GC, Liu D, Ander BP, Stamova B, Zhan X, Sharp FR. Targeting neutrophils in ischemic stroke: translational insights from experimental studies. *J Cereb Blood Flow Metab Off J Int Soc Cereb Blood Flow Metab*. (2015) 35:888–901. doi: 10.1038/jcbfm.2015.45

87. Christy AL, Walker ME, Hessner MJ, Brown MA. Mast cell activation and neutrophil recruitment promotes early and robust inflammation in the meninges in EAE. *J Autoimmun*. (2013) 42:50–61. doi: 10.1016/j.jaut.2012.11.003

88. Arac A, Grimbaldeston MA, Galli SJ, Bliss TM, Steinberg GK. Meningeal mast cells as key effectors of stroke pathology. *Front Cell Neurosci*. (2019) 13:126. doi: 10.3389/fncel.2019.00126

89. Kilinc E, Torun IE, Baranoglu Kilinc Y. Meningeal mast cell-mediated mechanisms of cholinergic system modulation in neurogenic inflammation underlying the pathophysiology of migraine. *Eur J Neurosci*. (2024) 59:2181–92. doi: 10.1111/ejn.15888

90. Lin CCJ, Herisson F, Le H, Jaafar N, ChEtal K, Oram MK, et al. Mast cell deficiency improves cognition and enhances disease-associated microglia in 5XFAD mice. *Cell Rep*. (2023) 42:113141. doi: 10.1016/j.celrep.2023.113141

91. Gadani SP, Smirnov I, Wiltbank AT, Overall CC, Kipnis J. Characterization of meningeal type 2 innate lymphocytes and their response to CNS injury. *J Exp Med*. (2017) 214:285–96. doi: 10.1084/jem.20161982

92. Baban B, Braun M, Khodadadi H, Ward A, Alverson K, Malik A, et al. AMPK induces regulatory innate lymphoid cells after traumatic brain injury. *JCI Insight*. (2021) 6:e126766. doi: 10.1172/jci.insight.126766

93. Fung ITH, Sankar P, Zhang Y, Robison LS, Zhao X, D'Souza SS, et al. Activation of group 2 innate lymphoid cells alleviates aging-associated cognitive decline. *J Exp Med*. (2020) 217:e20190915. doi: 10.1084/jem.20190915

94. Hirose S, Jahani PS, Wang S, Jaggi U, Tormanen K, Yu J, et al. Type 2 innate lymphoid cells induce CNS demyelination in an HSV-IL-2 mouse model of multiple sclerosis. *iScience*. (2020) 23:101549. doi: 10.1016/j.isci.2020.101549

95. Kwong B, Rua R, Gao Y, Flickinger J, Wang Y, Kruhlak MJ, et al. T-bet-dependent NKp46+ innate lymphoid cells regulate the onset of TH17-induced neuroinflammation. *Nat Immunol*. (2017) 18:1117–27. doi: 10.1038/ni.3816

96. Steffen J, Ehrentraut S, Bank U, Biswas A, Figueiredo CA, Hölsken O, et al. Type 1 innate lymphoid cells regulate the onset of Toxoplasma gondii-induced neuroinflammation. *Cell Rep*. (2022) 38:110564. doi: 10.1016/j.celrep.2022.110564

97. Hatfield JK, Brown MA. Group 3 innate lymphoid cells accumulate and exhibit disease-induced activation in the meninges in EAE. *Cell Immunol*. (2015) 297:69–79. doi: 10.1016/j.cellimm.2015.06.006

98. Garofalo S, Cocozza G, Mormino A, Bernardini G, Russo E, Ielpo D, et al. Natural killer cells and innate lymphoid cells 1 tune anxiety-like behavior and memory in mice via interferon-γ and acetylcholine. *Nat Commun*. (2023) 14:3103. doi: 10.1038/s41467-023-38899-3

99. Sanmarco LM, Wheeler MA, Gutiérrez-Vázquez C, Polonio CM, Linnerbauer M, Pinho-Ribeiro FA, et al. Gut-licensed IFNγ+ NK cells drive LAMP1+TRAIL+ anti-inflammatory astrocytes. *Nature*. (2021) 590:473–9. doi: 10.1038/s41586-020-03116-4

100. Russi AE, Brown MA. The meninges: new therapeutic targets for multiple sclerosis. *Transl Res J Lab Clin Med*. (2015) 165:255–69. doi: 10.1016/j.trsl.2014.08.005

101. Absinta M, Vuolo L, Rao A, Nair G, Sati P, Cortese ICM, et al. Gadolinium-based MRI characterization of leptomeningeal inflammation in multiple sclerosis. *Neurology*. (2015) 85:18–28. doi: 10.1212/WNL.0000000000001587

102. Pikor NB, Astarita JL, Summers-Deluca L, Galicia G, Qu J, Ward LA, et al. Integration of th17- and lymphotoxin-derived signals initiates meningeal-resident stromal cell remodeling to propagate neuroinflammation. *Immunity*. (2015) 43:1160–73. doi: 10.1016/j.immuni.2015.11.010

103. Walker-Caulfield ME, Hatfield JK, Brown MA. Dynamic changes in meningeal inflammation correspond to clinical exacerbations in a murine model of relapsing-remitting multiple sclerosis. *J Neuroimmunol*. (2015) 278:112–22. doi: 10.1016/j.jneuroim.2014.12.009

104. Merlini A, Haberl M, Strauß J, Hildebrand L, Genc N, Franz J, et al. Distinct roles of the meningeal layers in CNS autoimmunity. *Nat Neurosci*. (2022) 25:887–99. doi: 10.1038/s41593-022-01108-3

105. Russi AE, Walker-Caulfield ME, Guo Y, Lucchinetti CF, Brown MA. Meningeal mast cell-T cell crosstalk regulates T cell encephalitogenicity. *J Autoimmun*. (2016) 2016:100–10. doi: 10.1016/j.jaut.2016.06.015

106. Rothhammer V, Heink S, Petermann F, Srivastava R, Claussen MC, Hemmer B, et al. Th17 lymphocytes traffic to the central nervous system independently of α4 integrin expression during EAE. *J Exp Med*. (2011) 208:2465–76. doi: 10.1084/jem.20110434

107. Schläger C, Körner H, Krueger M, Vidoli S, Haberl M, Mielke D, et al. Effector T-cell trafficking between the leptomeninges and the cerebrospinal fluid. *Nature*. (2016) 530:349–53. doi: 10.1038/nature16939

108. Bartholomäus I, Kawakami N, Odoardi F, Schläger C, Miljkovic D, Ellwart JW, et al. Effector T cell interactions with meningeal vascular structures in nascent autoimmune CNS lesions. *Nature*. (2009) 462:94–8. doi: 10.1038/nature08478

109. Lodygin D, Odoardi F, Schläger C, Körner H, Kitz A, Nosov M, et al. A combination of fluorescent NFAT and H2B sensors uncovers dynamics of T cell activation in real time during CNS autoimmunity. *Nat Med*. (2013) 19:784–90. doi: 10.1038/nm.3182

110. Greter M, Heppner FL, Lemos MP, Odermatt BM, Goebels N, Laufer T, et al. Dendritic cells permit immune invasion of the CNS in an animal model of multiple sclerosis. *Nat Med*. (2005) 11:328–34. doi: 10.1038/nm1197

111. Kivisäkk P, Imitola J, Rasmussen S, Elyaman W, Zhu B, Ransohoff RM, et al. Localizing central nervous system immune surveillance: meningeal antigen-presenting cells activate T cells during experimental autoimmune encephalomyelitis. *Ann Neurol*. (2009) 65:457–69. doi: 10.1002/ana.21379

112. van Zwam M, Huizinga R, Heijmans N, van Meurs M, Wierenga-Wolf AF, Melief MJ, et al. Surgical excision of CNS-draining lymph nodes reduces relapse severity in chronic-relapsing experimental autoimmune encephalomyelitis. *J Pathol*. (2009) 217:543–51. doi: 10.1002/path.v217:4

113. Furtado GC, Marcondes MCG, Latkowski JA, Tsai J, Wensky A, Lafaille JJ. Swift entry of myelin-specific T lymphocytes into the central nervous system in spontaneous

autoimmune encephalomyelitis. *J Immunol Baltim Md.* (2008) 181:4648–55. doi: 10.4049/jimmunol.181.7.4648

114. Howell OW, Reeves CA, Nicholas R, Carassiti D, Radotra B, Gentleman SM, et al. Meningeal inflammation is widespread and linked to cortical pathology in multiple sclerosis. *Brain J Neurol.* (2011) 134:2755–71. doi: 10.1093/brain/awr182

115. Magliozzi R, Howell O, Vora A, Serafini B, Nicholas R, Puopolo M, et al. Meningeal B-cell follicles in secondary progressive multiple sclerosis associate with early onset of disease and severe cortical pathology. *Brain J Neurol.* (2007) Pt 4):1089–104. doi: 10.1093/brain/awm038

116. Serafini B, Rosicarelli B, Magliozzi R, Stigliano E, Aloisi F. Detection of ectopic B-cell follicles with germinal centers in the meninges of patients with secondary progressive multiple sclerosis. *Brain Pathol Zurich Switz.* (2004) 14:164–74. doi: 10.1111/j.1750-3639.2004.tb00049.x

117. Peters A, Pitcher LA, Sullivan JM, Mitsdoerffer M, Acton SE, Franz B, et al. Th17 cells induce ectopic lymphoid follicles in central nervous system tissue inflammation. *Immunity.* (2011) 35:986–96. doi: 10.1016/j.immuni.2011.10.015

118. Magliozzi R, Columba-Cabezas S, Serafini B, Aloisi F. Intracerebral expression of CXCL13 and BAFF is accompanied by formation of lymphoid follicle-like structures in the meninges of mice with relapsing experimental autoimmune encephalomyelitis. *J Neuroimmunol.* (2004) 148:11–23. doi: 10.1016/j.jneuroim.2003.10.056

119. Haugen M, Frederiksen JL, Degn M. B cell follicle-like structures in multiple sclerosis-with focus on the role of B cell activating factor. *J Neuroimmunol.* (2014) 273:1–7. doi: 10.1016/j.jneuroim.2014.05.010

120. Lehmann-Horn K, Sagan SA, Bernard CCA, Sobel RA, Zamvil SS. B-cell very late antigen-4 deficiency reduces leukocyte recruitment and susceptibility to central nervous system autoimmunity. *Ann Neurol.* (2015) 77:902–8. doi: 10.1002/ana.24387

121. Parker Harp CR, Archambault AS, Cheung M, Williams JW, Czepielewski RS, Duncker PC, et al. Neutrophils promote VLA-4-dependent B cell antigen presentation and accumulation within the meninges during neuroinflammation. *Proc Natl Acad Sci U S A.* (2019) 116:24221–30. doi: 10.1073/pnas.1909098116

122. Kuerten S, Schickel A, Kerkloh C, Recks MS, Addicks K, Ruddle NH, et al. Tertiary lymphoid organ development coincides with determinant spreading of the myelin-specific T cell response. *Acta Neuropathol (Berl).* (2012) 124:861–73. doi: 10.1007/s00401-012-1023-3

123. Lovato L, Willis SN, Rodig SJ, Caron T, Almendinger SE, Howell OW, et al. Related B cell clones populate the meninges and parenchyma of patients with multiple sclerosis. *Brain J Neurol.* (2011) 134:534–41. doi: 10.1093/brain/awq350

124. Fazazi MR, Doss PMIA, Pereira R, Fudge N, Regmi A, Joly-Beauparlant C, et al. Myelin-reactive B cells exacerbate CD4+ T cell-driven CNS autoimmunity in an IL-23-dependent manner. *Nat Commun.* (2024) 15:5404. doi: 10.1038/s41467-024-49259-0

125. Sayed BA, Christy AL, Walker ME, Brown MA. Meningeal mast cells affect early T cell central nervous system infiltration and blood-brain barrier integrity through TNF: a role for neutrophil recruitment? *J Immunol Baltim Md.* (2010) 184:6891–900. doi: 10.4049/jimmunol.1000126

126. Secor VH, Secor WE, Gutekunst CA, Brown MA. Mast cells are essential for early onset and severe disease in a murine model of multiple sclerosis. *J Exp Med.* (2000) 191:813–22. doi: 10.1084/jem.191.5.813

127. Bankoti J, Apeltsin L, Hauser SL, Allen S, Albertolle ME, Witkowska HE, et al. In multiple sclerosis, oligoclonal bands connect to peripheral B-cell responses. *Ann Neurol.* (2014) 75:266–76. doi: 10.1002/ana.24088

128. Azevedo RSS, de Sousa JR, Araujo MTF, Martins Filho AJ, de Alcantara BN, Araujo FMC, et al. *In situ* immune response and mechanisms of cell damage in central nervous system of fatal cases microcephaly by Zika virus. *Sci Rep.* (2018) 8:1. doi: 10.1038/s41598-017-17765-5

129. Chimelli L, Melo ASO, Avvad-Portari E, Wiley CA, Camacho AHS, Lopes VS, et al. The spectrum of neuropathological changes associated with congenital Zika virus infection. *Acta Neuropathol (Berl).* (2017) 133:983–99. doi: 10.1007/s00401-017-1699-5

130. Chimelli L, Avvad-Portari E. Congenital Zika virus infection: a neuropathological review. *Childs Nerv Syst ChNS Off J Int Soc Pediatr Neurosurg.* (2018) 34:95–9. doi: 10.1007/s00381-017-3651-3

131. Lamers SL, Fogel GB, Singer EJ, Salemi M, Nolan DJ, Huysentruyt LC, et al. HIV-1 Nef in macrophage-mediated disease pathogenesis. *Int Rev Immunol.* (2012) 31:432–50. doi: 10.3109/08830185.2012.737073

132. Lamers SL, Rose R, Ndhlovu LC, Nolan DJ, Salemi M, Maidji E, et al. The meningeal lymphatic system: a route for HIV brain migration? *J Neurovirol.* (2016) 22:275–81. doi: 10.1007/s13365-015-0399-y

133. Lamers SL, Gray RR, Salemi M, Huysentruyt LC, McGrath MS. HIV-1 phylogenetic analysis shows HIV-1 transits through the meninges to brain and peripheral tissues. *Infect Genet Evol J Mol Epidemiol Evol Genet Infect Dis.* (2011) 11:31–7. doi: 10.1016/j.meegid.2010.10.016

134. Thompson KA, Cherry CL, Bell JE, McLean CA. Brain cell reservoirs of latent virus in presymptomatic HIV-infected individuals. *Am J Pathol.* (2011) 179:1623–9. doi: 10.1016/j.ajpath.2011.06.039

135. Hattler JB, Irons DL, Luo J, Kim WK. Downregulation of CCR5 on brain perivascular macrophages in simian immunodeficiency virus-infected rhesus macaques. *Brain Behav.* (2023) 13:e3126. doi: 10.1002/brb3.v13.8

136. Kang SS, McGavern DB. Lymphocytic choriomeningitis infection of the central nervous system. *Front Biosci J Virtual Libr.* (2008) 13:4529–43. doi: 10.2741/3021

137. Kim JV, Kang SS, Dustin ML, McGavern DB. Myelomonocytic cell recruitment causes fatal CNS vascular injury during acute viral meningitis. *Nature.* (2009) 457:191–5. doi: 10.1038/nature07591

138. Rua R, Lee JY, Silva AB, Swafford IS, Maric D, Johnson KR, et al. Infection drives meningeal engraftment by inflammatory monocytes that impairs CNS immunity. *Nat Immunol.* (2019) 20:407–19. doi: 10.1038/s41590-019-0344-y

139. Schmidt H. The pathogenesis of trypanosomiasis of the CNS. Studies on parasitological and neurohistological findings in trypanosoma rhodesiense infected vervet monkeys. *Virchows Arch A Pathol Anat Histopathol.* (1983) 399:333–43. doi: 10.1007/BF00612951

140. Poltera AA, Hochmann A, Rudin W, Lambert PH. Trypanosoma brucei brucei: a model for cerebral trypanosomiasis in mice–an immunological, histological and electronmicroscopic study. *Clin Exp Immunol.* (1980) 40:496–507.

141. Quan N, Mhlanga JD, Whiteside MB, McCoy AN, Kristensson K, Herkenham M. Chronic overexpression of proinflammatory cytokines and histopathology in the brains of rats infected with Trypanosoma brucei. *J Comp Neurol.* (1999) 414:114–30. doi: 10.1002/(SICI)1096-9861(19991108)414:1<114::AID-CNE9>3.0.CO;2-G

142. Coles JA, Myburgh E, Ritchie R, Hamilton A, Rodgers J, Mottram JC, et al. Intravital imaging of a massive lymphocyte response in the cortical dura of mice after peripheral infection by trypanosomes. *PloS Negl Trop Dis.* (2015) 9:e0003714. doi: 10.1371/journal.pntd.0003714

143. De Vlaminck K, Van Hove H, Kancheva D, Scheyltjens I, Pombo Antunes AR, Bastos J, et al. Differential plasticity and fate of brain-resident and recruited macrophages during the onset and resolution of neuroinflammation. *Immunity.* (2022) 55:2085–2102.e9. doi: 10.1016/j.immuni.2022.09.005

144. O'Brien CA, Overall C, Konradt C, O'Hara Hall AC, Hayes NW, Wagage S, et al. CD11c-expressing cells affect regulatory T cell behavior in the meninges during central nervous system infection. *J Immunol Baltim Md.* (2017) 198:4054–61. doi: 10.4049/jimmunol.1601581

145. Kovacs MA, Cowan MN, Babcock IW, Sibley LA, Still K, Batista SJ, et al. Meningeal lymphatic drainage promotes T cell responses against Toxoplasma gondii but is dispensable for parasite control in the brain. *eLife.* (2022) 11:e80775. doi: 10.7554/eLife.80775.sa2

146. Pinho-Ribeiro FA, Deng L, Neel DV, Erdogan O, Basu H, Yang D, et al. Bacteria hijack a meningeal neuroimmune axis to facilitate brain invasion. *Nature.* (2023) 615:472–81. doi: 10.1038/s41586-023-05753-x

147. Zera KA, Buckwalter MS. The local and peripheral immune responses to stroke: implications for therapeutic development. *Neurother J Am Soc Exp Neurother.* (2020) 17:414–35. doi: 10.1007/s13311-020-00844-3

148. Iadecola C, Buckwalter MS, Anrather J. Immune responses to stroke: mechanisms, modulation, and therapeutic potential. *J Clin Invest.* (2020) 130:2777–88. doi: 10.1172/JCI135530

149. Piepke M, Jander A, Gagliani N, Gelderblom M. IL-17A-producing γδ T cells: A novel target in stroke immunotherapy. *Eur J Immunol.* (2024) 13:e2451067. doi: 10.1002/eji.202451067

150. Planas AM, Gómez-Choco M, Urra X, Gorina R, Caballero M, Chamorro Á Brain-derived antigens in lymphoid tissue of patients with acute stroke. *J Immunol Baltim Md.* (2012) 188:2156–63. doi: 10.4049/jimmunol.1102289

151. Wang YJ, Sun YR, Pei YH, Ma HW, Mu YK, Qin LH, et al. The lymphatic drainage systems in the brain: a novel target for ischemic stroke? *Neural Regener Res.* (2023) 18:485–91. doi: 10.4103/1673-5374.346484

152. Beuker C, Schafflick D, Strecker JK, Heming M, Li X, Wolbert J, et al. Stroke induces disease-specific myeloid cells in the brain parenchyma and pia. *Nat Commun.* (2022) 13:945. doi: 10.1038/s41467-022-28593-1

153. Otxoa-de-Amezaga A, Gallizioli M, Pedragosa J, Justicia C, Miró-Mur F, Salas-Perdomo A, et al. Location of neutrophils in different compartments of the damaged mouse brain after severe ischemia/reperfusion. *Stroke.* (2019) 50:1548–57. doi: 10.1161/STROKEAHA.118.023837

154. Pedragosa J, Salas-Perdomo A, Gallizioli M, Cugota R, Miró-Mur F, Briansó F, et al. CNS-border associated macrophages respond to acute ischemic stroke attracting granulocytes and promoting vascular leakage. *Acta Neuropathol Commun.* (2018) 6:76. doi: 10.1186/s40478-018-0581-6

155. Zhao K, Wang P, Tang X, Chang N, Shi H, Guo L, et al. The mechanisms of minocycline in alleviating ischemic stroke damage and cerebral ischemia-reperfusion injury. *Eur J Pharmacol.* (2023) 955:175903. doi: 10.1016/j.ejphar.2023.175903

156. Malone K, Shearer JA, Waeber C, Moore AC. The impact of fingolimod on Treg function in brain ischemia. *Eur J Immunol.* (2023) 53:e2350370. doi: 10.1002/eji.202350370

157. Mokbel AY, Burns MP, Main BS. The contribution of the meningeal immune interface to neuroinflammation in traumatic brain injury. *J Neuroinflammation.* (2024) 21:135. doi: 10.1186/s12974-024-03122-7

158. Needham EJ, Helmy A, Zanier ER, Jones JL, Coles AJ, Menon DK. The immunological response to traumatic brain injury. *J Neuroimmunol.* (2019) 332:112–25. doi: 10.1016/j.jneuroim.2019.04.005

159. Braun M, Vaibhav K, Saad NM, Fatima S, Vender JR, Baban B, et al. White matter damage after traumatic brain injury: A role for damage associated molecular patterns. *Biochim Biophys Acta Mol Basis Dis.* (2017) 1863:2614–26. doi: 10.1016/j.bbadis.2017.05.020

160. Rizk T, Turtzo LC, Cota M, van der Merwe AJ, Latour L, Whiting MD, et al. Traumatic microbleeds persist for up to five years following traumatic brain injury despite resolution of other acute findings on MRI. *Brain Inj.* (2020) 34:773–81. doi: 10.1080/02699052.2020.1725835

161. Bolte AC, Dutta AB, Hurt ME, Smirnov I, Kovacs MA, McKee CA, et al. Meningeal lymphatic dysfunction exacerbates traumatic brain injury pathogenesis. *Nat Commun.* (2020) 11:4524. doi: 10.1038/s41467-020-18113-4

162. Wojciechowski S, Virenque A, Vihma M, Galbardi B, Rooney EJ, Keuters MH, et al. Developmental dysfunction of the central nervous system lymphatics modulates the adaptive neuro-immune response in the perilesional cortex in a mouse model of traumatic brain injury. *Front Immunol.* (2020) 11:559810. doi: 10.3389/fimmu.2020.559810

163. Russo MV, Latour LL, McGavern DB. Distinct myeloid cell subsets promote meningeal remodeling and vascular repair after mild traumatic brain injury. *Nat Immunol.* (2018) 19:442–52. doi: 10.1038/s41590-018-0086-2

164. Buenaventura RG, Harvey AC, Burns MP, Main BS. Traumatic brain injury induces an adaptive immune response in the meningeal transcriptome that is amplified by aging. *Front Neurosci.* (2023) 17:1210175. doi: 10.3389/fnins.2023.1210175

165. Bolte AC, Shapiro DA, Dutta AB, Ma WF, Bruch KR, Kovacs MA, et al. The meningeal transcriptional response to traumatic brain injury and aging. *eLife.* (2023) 12:e81154. doi: 10.7554/eLife.81154

166. Liu M, Huang J, Liu T, Yuan J, Lv C, Sha Z, et al. Exogenous interleukin 33 enhances the brain's lymphatic drainage and toxic protein clearance in acute traumatic brain injury mice. *Acta Neuropathol Commun.* (2023) 11:61. doi: 10.1186/s40478-023-01555-4

167. Simon DW, McGeachy MJ, Bayır H, Clark RSB, Loane DJ, Kochanek PM. The far-reaching scope of neuroinflammation after traumatic brain injury. *Nat Rev Neurol.* (2017) 13:171–91. doi: 10.1038/nrneurol.2017.13

168. Ding XB, Wang XX, Xia DH, Liu H, Tian HY, Fu Y, et al. Impaired meningeal lymphatic drainage in patients with idiopathic Parkinson's disease. *Nat Med.* (2021) 27:411–8. doi: 10.1038/s41591-020-01198-1

169. Schonhoff AM, Figge DA, Williams GP, Jurkuvenaite A, Gallups NJ, Childers GM, et al. Border-associated macrophages mediate the neuroinflammatory response in an alpha-synuclein model of Parkinson disease. *Nat Commun.* (2023) 14:3754. doi: 10.1038/s41467-023-39060-w

170. DeTure MA, Dickson DW. The neuropathological diagnosis of Alzheimer's disease. *Mol Neurodegener.* (2019) 14:32. doi: 10.1186/s13024-019-0333-5

171. Da Mesquita S, Louveau A, Vaccari A, Smirnov I, Cornelison RC, Kingsmore KM, et al. Functional aspects of meningeal lymphatics in ageing and Alzheimer's disease. *Nature.* (2018) 560:185–91. doi: 10.1038/s41586-018-0368-8

172. Wang M, Yan C, Li X, Yang T, Wu S, Liu Q, et al. Non-invasive modulation of meningeal lymphatics ameliorates ageing and Alzheimer's disease-associated pathology and cognition in mice. *Nat Commun.* (2024) 15:1453. doi: 10.1038/s41467-024-45656-7

173. Rustenhoven J, Pavlou G, Storck SE, Dykstra T, Du S, Wan Z, et al. Age-related alterations in meningeal immunity drive impaired CNS lymphatic drainage. *J Exp Med.* (2023) 220:e20221929. doi: 10.1084/jem.20221929

174. Neutzner M, Kohler C, Frank S, Killer HE, Neutzner A. Impact of aging on meningeal gene expression. *Fluids Barriers CNS.* (2023) 20:12. doi: 10.1186/s12987-023-00412-9

175. Drieu A, Du S, Storck SE, Rustenhoven J, Papadopoulos Z, Dykstra T, et al. Parenchymal border macrophages regulate the flow dynamics of the cerebrospinal fluid. *Nature.* (2022) 611:585–93. doi: 10.1038/s41586-022-05397-3

176. Park L, Uekawa K, Garcia-Bonilla L, Koizumi K, Murphy M, Pistik R, et al. Brain perivascular macrophages initiate the neurovascular dysfunction of Alzheimer Aβ Peptides. *Circ Res.* (2017) 121:258–69. doi: 10.1161/CIRCRESAHA.117.311054

177. Kearns NA, Iatrou A, Flood DJ, De Tissera S, Mullaney ZM, Xu J, et al. Dissecting the human leptomeninges at single-cell resolution. *Nat Commun.* (2023) 14:7036. doi: 10.1038/s41467-023-42825-y

178. Feng W, Zhang Y, Ding S, Chen S, Wang T, Wang Z, et al. B lymphocytes ameliorate Alzheimer's disease-like neuropathology via interleukin-35. *Brain Behav Immun.* (2023) 108:16–31. doi: 10.1016/j.bbi.2022.11.012

179. Iannucci J, Dominy R, Bandopadhyay S, Arthur EM, Noarbe B, Jullienne A, et al. Traumatic brain injury alters the effects of class II invariant peptide (CLIP) antagonism on chronic meningeal CLIP + B cells, neuropathology, and neurobehavioral impairment in 5xFAD mice. *J Neuroinflammation.* (2024) 21:165. doi: 10.1186/s12974-024-03146-z

180. Zhang Y, Bailey JT, Xu E, Singh K, Lavaert M, Link VM, et al. Mucosal-associated invariant T cells restrict reactive oxidative damage and preserve meningeal barrier integrity and cognitive function. *Nat Immunol.* (2022) 23:1714–25. doi: 10.1038/s41590-022-01349-1

Frontiers in Immunology

Explores novel approaches and diagnoses to treat immune disorders.

The official journal of the International Union of Immunological Societies (IUIS) and the most cited in its field, leading the way for research across basic, translational and clinical immunology.

Discover the latest Research Topics

See more →

Frontiers

Avenue du Tribunal-Fédéral 34
1005 Lausanne, Switzerland
frontiersin.org

Contact us

+41 (0)21 510 17 00
frontiersin.org/about/contact